Dissertation zur Erlangung des Doktorgrades
der Fakultät für Chemie und Pharmazie
der Ludwig-Maximilians-Universität München

The Role of Kindlin-3 in Hematopoietic Stem Cell Homeostasis and Mature Effector Cells

Raphael Hubert Ruppert

aus

Erlangen

Februar 2014

Erklärung

Diese Dissertation wurde im Sinne von §7 Abs. 3 der Promotionsordnung vom 28. November 2011 von Herrn Prof. Dr. Reinhard Fässler betreut.

Ehrenwörtliche Versicherung

Diese Dissertation wurde selbständig, ohne unerlaubte Hilfe erarbeitet.

München, am 25.02.2014

_____

(Raphael Hubert Ruppert)

Dissertation eingereicht am:

1. Gutachter Prof. Dr. Reinhard Fässler
2. Gutachter Prof. Dr. Markus Sperandio

Mündliche Prüfung am 20.05.2014

1. Table of Contents

2. In-text Figures

3. Abbreviations

5-FU	5-Fluoruracil
A-MuLV	Abelson murine leukemia virus
ABC	ATP-binding cassette
Abl	Abelson murine leukemia viral oncogene
AdMIDAS	Adjacent to MIDAS
ADP	Adenosine diphosphate
AGM	Aorta-gonad-mesonephros
ALL	Acute lymphoblastic leukemia
AML	Acute myeloid leukemia
Ang-1	Angiopoietin-1
AP	Accelerated phase
ATP	Adenosine triphosphate
Bcr	Breakpoint cluster region
BM	Bone marrow
BMP	Bone morphogenetic protein
BMT	BM transplantation
BP	Blast phase
BrdU	5-bromo-2'-deoxyuridine
Ca^{2+}	Calcium ions
CAFC	Cobblestone area forming cell
Cal-DAG-GEF	Ca^{2+} and diacylglycerol-regulated guanine nucleotide exchange factor
CAM	Cell adhesion molecule
CaR	Calcium receptor
CAR cells	CXCL12-abundant reticular cells
CBF-1	C-promoter-binding-factor-1
Cbl	Casitas B-lineage lymphoma pro-oncogene protein
CCyR	Cumulative complete cytogenetic response
CFC	Colony forming cell
CFU-S	Spleen colony forming unit
CLL	Chronic lymphocytic leukemia
CLP	Common lymphoid progenitor
CML	Chronic myelogenous (or myeloid) leukemia
CMP	Common myeloid progenitor
c-Myc	MYC v-myc avian myelocytomatosis viral oncogene homolog
CNS	Central nervous system
CP	Chronic phase
Crkl	CRK-like protein
CSC	Cancer stem cell
CXCL12	CXC-motiv-chemokine 12
CXCR4	CXC-motiv-chemokine receptor type 4
DAG	Diacylglycerol
DCs	Dendritic cells
Dkk1	Dickkopf-1
DNA	Deoxyribonucleic acid
E7.5	Embryonic day (E) 7.5
ECM	Extracellular matrix
EGF	Epidermal growth factor
ERK	Extracellular signal-regulated kinase

ESCs	Embryonic stem cells
FACS	Fluorescence activated cell sorting
FAK	Focal adhesion kinase
FERM domain	4.1 protein, ezrin, radixin, moesin domain
FGF-1	Fibroblast growth factor-1
FGFR 1-4	Fibroblast growth factor receptor 1-4
FN	Fibronectin
Frz	Frizzled
G-CSF	Granulocyte colony-stimulating factor
GEF	Guanine nucleotide exchange factor
Gli-1	Glioblastoma-1
GMP	Granulocyte-macrophage progenitor
GPCRs	G protein-coupled receptors
GPVI	Glycoprotein VI
Grb2	Growth factor receptor-bound protein 2
HLA-matched	Human leukocyte antigens-matched
Ho	Hoechst 33342
HSC	Hematopoietic stem cell
HSPC	Hematopoietic stem and precursor cell
ICAM-1	Intercellular adhesion molecule-1
ICM	Inner cell mass
IFN-α	Interferon-α
IP3	Inositol trisphosphate
iPSCs	Induced pluripotent stem cells
IRS1	Insulin receptor substrate 1
JaK	Janus kinase
Lef	Lymphoid enhancer-binding factor
LPS	Lipopolysaccharide
LRP5/6	low-density lipoprotein-receptor-related protein 5/6
LSC	Leukemic stem cell
LT-HSC	Long-term HSC
LTC-IC	Long-term culture-initiating cell
M-Bcr	Major breakpoint cluster region
m-Bcr	Minor breakpoint cluster region
MAdCAM-1	Mucosal addressin cell adhesion molecule-1
MAML-1	Mastermind-like-1
MAPK	Mitogen-activated protein kinase
MDR1	Multidrug resistance-1
MDS	Myelodysplastic syndromes
MEP	Megakaryocyte erythroid progenitor
Mg^{2+}	Magnesium ions
MIDAS	Metal ion-dependent adhesion site
mKL	Membrane-bound kit ligand
MM	Multiple myeloma
MMP	Matrix metalloproteinase
MPL	Myeloproliferative leukemia virus oncogene
MPP	Multipotent progenitor
MSC	Mesenchymal stem cell
MUC-1	Mucin-1
Mx1-Cre	myxovirus (influenza virus) resistance 1
NK	Natural killer cell

OBs	Osteoblasts
OCLs	Osteoclasts
OPN	Osteopontin
PB	Peripheral blood
PECAM-1	Platelet endothelial cell adhesion molecule-1
PCK-ζ	Protein kinase C-zeta
PDGF	Platelet-derived growth factor
Ph chromosome	Philadelphia chromosome
PH-domain	Pleckstrin homology-domain
PI-PLC	Phosphatidylinositol-specific phospholipase C
PI3K	Phosphoinositide-3-kinase
PIP2	Phosphatidylinositol 4,5-bisphosphate or PtdIns(4,5)P_2
PIP3	phosphatidylinositol 3,4,5-trisphosphate or PtdIns(3,4,5)P_3
PIPKI	phosphatidylinositol-4-phosphate 5-kinase
PLC	Phospholipase C
PPR	PTH/PTH-related peptide (PTHrP) receptor
PSGL-1	P-selectin glycoprotein ligand-1
PSI domain	Plexin, Semaphorin and Integrin domain
pSP	Para-aortic splanchnopleurae
PTB domain	Phosphotyrosine-binding domain
Ptch1	Patched
PtdIns	Phosphatidylinositol
PtdIns(3,4,5)P_3	PIP3
PtdIns(4,5)P2	PIP2
PTEN	Phosphatase and tensin homolog
PTH	Parathyroid hormone
PYK-2	Protein tyrosine kinase-2
RACK-1	Receptor for activated C kinase 1
RANKL	Receptor activator of nuclear factor kappa B ligand
RGDS	Arg-Gly-Asp-Ser motif
RIAM	Rap1 interacting adaptor molecule
S1P	Sphingosine-1-phosphate
SCF	Stem cell factor (also known as kit-ligand, KL, or steel factor)
SCID	Severe combined immunodeficiency
SDF-1	Stromal-derived factor-1
SH	Src-homology domain
Shc	SRC homology containing protein
Shh	Sonic hedgehog
SLAM	Signaling lymphocytic activation molecule
Smad	Small mothers against decapentaplegic
Smo	Smoothened
SNO	Spindle-shaped N-cadherin$^+$ osteoblastic
SNS	Sympathic nervous system
Spl	Spleen
SP	Side population
ST-HSC	Sort-term HSC
STAP	Stimulus-triggered acquisition of pluripotency
STAT	Signal transducer and activator of transcription
SyMBS	Synergistic metal ion binding site
Tcf	Transcription factor
TGF-β	Transforming growth factor-β

Tie2	Tyrosine kinase with immunoglobulin-like and EGF-like domains 2
TLR	Toll-like receptor
tm-SCF	Transmembrane-stem cell factor
TPO	Thrombopoietin
trOPN	Thrombin-cleaved osteopontin
TYK 2	Tyrosine kinase 2
UGR	urogenital ridges
UNC-112	Uncoordinated protein 112
VCAM-1	Vascular cell adhesion molecule-1 (CD106)
VLA-4	Very late antigen-4
Wnt	Wingless-type
wt	wild-type
μ-Bcr	Micro breakpoint cluster region

4. List of Publications

This thesis is based on the following publications. The publications are also referred in the text by arabic numbers.

Paper 1: **Ruppert R**, Moser M, Sperandio M, Rognoni E, Orban M, Oostendorp RA, Massberg S, Fässler R. Kindlin-3 controls quiescence of hematopoietic stem cells in mice. Cell Stem Cell 2014 (under revision).

Paper 2: Moser M, Bauer M, Schmid S, **Ruppert R**, Schmidt S, Sixt M, Wang HV, Sperandio M, Fässler R. Kindlin-3 is required for β2 integrin-mediated leukocyte adhesion to endothelial cells. Nat Med. 2009 Mar;15(3):300-5.

Paper 3: Schmidt S, Nakchbandi I, **Ruppert R**, Kawelke N, Hess MW, Pfaller K, Jurdic P, Fässler R, Moser M. Kindlin-3-mediated signaling from multiple integrin classes is required for osteoclast-mediated bone resorption. J Cell Biol. 2011 Mar 7;192(5):883-97.

Paper 4: Moretti F, **Ruppert R**, Fässler R, Moser M. Role of kindlin-3 in T cell progenitor homing and thymocyte development. (manuscript in preparation).

Paper 5: Moretti F, Moser M, Lyck R, Abadier M, **Ruppert R**, Engelhardt B, Faessler R. Kindlin-3 regulates integrin activation and adhesion reinforcement of effector T cells. Proc Natl Acad Sci USA. 2013 Oct 15;110(42):17005-10.

Paper 6: Schmidt S, Moretti F, Zeiler M, **Ruppert R**, Mann M, Sperandio M, Fässler R, Moser M. Platelets and neutrophils require different Kindlin-3 copy numbers to control integrin-mediated functions *in vivo.* J Exp Med 2014. (submitted).

Paper 7: Petzold T, **Ruppert R**, Pandey D, Barocke V, Meyer H, Lorenz M, Zhang L, Siess W, Massberg S, Moser M. β1 integrin-mediated signals are required for platelet granule secretion and hemostasis in mouse. Blood. 2013 Oct 10;122(15):2723-31

Paper 8: Rognoni E, Widmaier M, Jakobson M, **Ruppert R**, Ussar S, Katsougkri D, Böttcher RT, Lai-Cheong JE, Rifkin BD, McGrath J, Fässler R. Kindlin-1 controls cutaneous epithelial stem cell proliferation by modulating Wnt ligand and TGFβ availability. Nat Med. 2014, (in press).

Paper 9: Cantor J, Browne CD, **Ruppert R**, Féral CC, Fässler R, Rickert RC, Ginsberg MH. CD98hc facilitates B cell proliferation and adaptive humoral immunity. Nat Immunol. 2009 Apr;10(4):412-9.

Paper 10: Ye F, Petrich BG, Anekal P, Lefort CT, Kasirer-Friede A, Shattil SJ, **Ruppert R**, Moser M, Fässler R, Ginsberg MH. The Mechanism of Kindlin-Mediated Activation of Integrin αIIbβ3. Curr Biol. 2013 Nov 18;23(22):2288-2295.

Paper 11: Speicher T, Siegenthaler B, Bogorad RL, **Ruppert R**, Petzold T, Padrissa-Altes S, Bachofner M, Anderson DG, Koteliansky V, Fässler R, Werner S. Knock-down and knockout of β1-integrin in hepatocytes impairs liver regeneration through inhibition of growth factor signaling. Nat Commun. 2014 (under revision).

Reprints were made with permission of the publishers.

5. Summary

Integrins are a superfamily of cell adhesion molecules that link the extracellular matrix (ECM) to the cytoskeleton. They mediate the attachment between cells and their environment and transduce signals from the outside into the cell. Integrins require a pre-activation step prior to high affinity ligand binding, which is characterized by a conformational change of the integrin ectodomain and the separataion of the transmembrane and cytoplasmic domains leading to the modulating numerous intracellular signaling pathways such as proliferation, migration or survival. Integrin activation is induced by the binding of two cytoplasmic proteins, talin and kindlin, to the cytoplasmic tail of β subunits. The kindlin protein family studied in this thesis consists of three evolutionarily conserved members, kindlin-1, -2 and -3. Kindlin-1 is expressed in epithelial cells, kindlin-2 widely and kindlin-3 in the hematopoietic system.

Loss of kindlin-3 in mice leads to a lethal phenotype within one week after birth. The mice suffer from severe hemorrhage due to an integrin activation defect on platelets, neutrophelia due to a leukocyte integrin activation defect, severe osteopetrosis due to dysfunctional integrins and an erythrocyte defect caused by an unknown mechanism. Kindlin-3 deficient hematopoietic chimeras ($K3^{-/-}$ chimeras) generated with kindlin-3 null fetal liver cells are unable to generate T cells and show an increased lethality compared to wild-type (wt) control chimeras.

In my thesis work I first investigated the role of kindlin-3 in the regulation and maintenance of hematopoietic stem and precursor cells (HSPCs) (**paper 1**). Adhesion molecules maintain interactions between hematopoietic stem cells (HSCs) and their microenvironment, called niche, in the bone marrow (BM). The increased lethality of the $K3^{-/-}$ chimeras and their severe pancytopenia point to HSC defects. Indeed, I could show that $K3^{-/-}$ HSPCs have a reduced BM homing potential due to an extravasation defect. The $K3^{-/-}$ HSCs found in the BM of recipient mice are unable to enter quiescence and instead are in an active, proliferating state. Furthermore, $K3^{-/-}$ HSPCs have a severe BM retention defect resulting in increased levels of HSPCs in the peripheral blood (PB). These defects exhaust HSCs in old $K3^{-/-}$ chimeras and under situations of hematopoietic stress such as 5-FU treatment or serial transplantations. Finaly, I was able to show that HSPCs have different requierements for kindlin-3. The maintenance of active HSCs and HPCs is dependent on kindlin-3, while quiescent HSCs do not require kindlin-3 but are imidetly lost after activation in the absence of kindlin-3. These results show that kindlin-3 is an essential regulator for HSPCs homeostasis.

In the second study we investigated why $K3^{-/-}$ chimeras exhibit neutrophila (**paper 2**). We found that kindlin-3 is required to activate β2 integrins on leukocytes. Furthermore, we found that the phenotype of the kindlin-3 deficient mice resembles human patients suffering from the autosomal recessive leukocyte adhesion deficiency syndrome type III (LAD-III), which is characterized by severe hemorrhages and a leukocyte extravasation defect. Indeed, LAD-III patients were shown to have null mutations in their *KINDLIN-3* gene.

In **paper 3** I helped analyzing the pronounced osteopetrosis in kindlin-3 deficient mice. We found that kindlin-3 deficient osteoclasts (OCLs) have an adhesion and spreading defect due to defects in the activation of β1, β2, and β3 integrins. By comparing the properties of $K3^{-/-}$ OCLs with OCLs deficient in one, two or all three integrin classes, respectively, we observed that loss of a single intergin class already affects the functions of OCLs, while the loss of all integrin classes resembles the defects of kindlin-3 deficient osteoblasts indicating that kindlin-3 affects the activation of β1, β2 and β3 integrins.

In **paper 4** I participated in the analysis of T cell development in kindlin-3-deficient mice. We observed that they develop progressive thymus atrophy. In transplantation experiments of fetal liver cells into irradiated or RAG-2-null mice we observed that T cell progenitor homing to the adult thymus is kindlin-3 dependent, while homing of kindlin-3 deficient T cell progenitors during early development, i.e. before thymus vascularization has taken place is unaffected and that they can leave the vascular system, migrate towards and enter the thymus primordium, indicating that the initial population of the thymus anlage by T cell progenitors apparently occurs in a kindlin-3 and integrin-independent manner. We also showed that the T cell progenitors, which entered the thymus, show a reduced proliferation due to a weakened crosstalk with the thymus microenvironment but can mature into single $CD4^+$ and $CD8^+$ T cells.

In **paper 5** we tested whether kindlin-3 supports the essential function of β1 integrins in the development of autoimmune diseases such as multiple sclerosis (MS) in humans and experimental autoimmune encephalitis (EAE) in mice. We showed that $K3^{-/-}$ T effector cells were able to extravasate through inflamed endothelial cells with high integrin ligands on their surface into central nervous system (CNS) and induce EAE. T cell extravasation did not occur under naïve conditions where ligand expression was low. This finding was confirmed with *in vitro* assays showing that kindlin-3 in T effector cells is required to induce α4β1 and αLβ2 integrin mediated ligand binding if ligand levels are low, but is less important if ligand levels are high indicating that loss of kindlin-3 is, at least in part, compensated by integrin ligand avidity.

In **paper 6** I helped addressing how much kindlin-3 is needed by hematopoietic cells to fulfill their biological tasks. We observed that mice expressing only 5% and 10% of normal kindlin-3 levels were viable, but were only able to activate a limited number of integrins with the consequence that they had a severe bleeding tendency and a leukocyte adhesion defect. Furthermore, we found that platelets and neutrophils have a similar number of kindlin-3 and talin proteins while the integrin levels differed. Leukocytes have twofold more integrins compared to talin and kindlin-3, while platelets have twofold more kindlin-3 and talin compared to integrins, These findings suggest that platelets need high kindlin-3 levels, while leukocytes require lower level for integrin activation.

In **paper 7** I contributed to an analysis in which we studied the role of β1 integrins and its interaction with kindlin-3 for platelet functions such as granule secretion. While the platelet-specific αIIbβ3 integrin is fundamental for platelet-mediated hemostasis, the relevance of β1 integrins on platelets is controversial. We found that mice lacking β1 integrin or expressing an activation-deficient β1 integrin have prolonged bleeding times due to insufficient activation of Rac-1, actin dynamics, granule secretion, and platelet aggregation. Furthermore, we also observed that hypomorphic mice expressing only 3% of β1 integrins on platelets have normal bleeding times but reduced platelet adhesion. Interestingly, the studies also revealed that integrin outside-in signaling leading to platelet spreading FAK phosphorylation, and platelet aggregation does not require a direct interaction of kindlin-3 with the β1 integrin tail.

Finally, in **paper 8** I was involved in the analysis of mice lacking kindlin-1 in cutaneous epithelial cells. These mice recapitulate Kindler syndrome in human patients and have a hyperactive stem cell compartment leading to hyperthickened epidermis, development of ectopic hair follicle and increased skin tumor susceptibility. Mechanistically, we found that kindlin-1 regulates keratinocyte adhesion through β1 integrins and stem cell homeostasis by balancing on the one hand wingless-type (Wnt)/β-catenin mediated growth-promoting signals through an integrin-independent regulation of Wnt ligand expression and on the other hand growth inhibitory signals through αvβ6 integrin-mediated activation of transforming growth factor-β (TGF-β).

Altogether these findings revealed that kindlins are essential regulators of integrin activation on different cell types, for integrin outside-in signaling and for integrin-independent signaling tasks. The functions of kindlin-3 seem to depend on the type of integrin, type of hematopoietic cell and physiological status of the cell. Many questions are still open; for example, it is unclear how integrin-independent functions are executed at the molecular level

and how outside-in signaling of integrins is achieved. It is also unclear how the crosstalk between kinlins and talin at the cytoplasmic tails of integrins is mediated.

During the time of my Phd thesis I also collaborated with international groups that did not directly relate to my thesis work. In one study I collaborated with Mark Ginsberg (at UCSD) to investigate the role of the CD98 heavy chain (hc) on B cells (**paper 9**). We were able to show that CD98hc facilitates humoral immunity by supporting B cells proliferation, in an integrin-dependent manner. In another study I helped him to study the activation of αIIbβ3 by talin and kindlin-3 (**paper 10**). We observed that kindlin-3 does neither enhance the activation of αIIbβ3 mediated by the talin head domain nor the affinity of purified αIIbβ3. Apparently, kindlins promote αIIbβ3 binding to multivalent but not monovalent ligands and increase the clustering of ligand-occupied αIIbβ3. I also helped Sabine Werner (at ETH Zürich) to examine the role of β1 integins on hepatocytes during liver regeneration (**paper 11**). We found that loss of ß1 integrins on hepatocytes results in a severe liver necrosis and reduced hepatocyte proliferation after partial hepatectomy due to impaired ligand-induced phosphorylation of epidermal growth factor (EGF) and hepatocyte growth factor (HGF) receptors indicating a strong cooperation between β1 integrin signaling and the two growth factor receptor signaling pathways.

6. Introduction

6.1. Stem Cells: The Origin of Life

A single stem cell, the fertilized egg (zygote), gives rise to all cells in a mammalian multicellular organism that consists of more than 240 different cell types. The principle of stem cells was already formulated 1858 by Rudolf Virchow who postulated that all cells in an organism are derived from preexisting cells. He coined the famous sentence "*omnis cellula e cellula*" (all cells come from cells) [1]. Stem cells are undifferentiated cells that have the abilities for unlimited or prolonged self-renewal by generating identical copies of themselves and to give rise to differentiated cell types. Development, tissue repair and cancer, resulting from uncontrolled cell division and additional imbalance of cell differentiation or cell death, are the three major processes in which stem cells play a central role. Stem cells can be classified into four categories with different stem cell potency: the embryonic stem cells (ESCs), the adult or somatic stem cells, induced pluripotent stem cells (iPSCs) and stimulus-triggered acquisition of pluripotency cells (STAP cells) [2-5].

The zygote is a totipotent stem cell that develops into all cell types including the embryonic membranes (amnion, chorion, allantois, and yolk sac). After fertilization, mammalian development starts with several cell divisions until cells are arranged in a solid ball, the morula, which occurs at the 32- to 64-cell stage. These cells called blastomeres at this stage still remain totipotent. In the next stage a hollow ball of cells, termed blastocyst, is formed. Beyond the blastocyst stage, development proceeds with a combination of cell division and cell movements. Cells of the blastocyst's outer layer, the trophoblasts, will form the embryonic membranes and the placenta, while the inner cell mass (ICM) develops into the fetus. The ICM is pluripotent and differentiates into cell types of the three germ layers known as the ectoderm, mesoderm, and endoderm. These three germ layers develop during a process called gastrulation in which the single-layered blastula is reorganized into the trilaminar structure giving rise to the gastrula. The ectoderm emerges first from the outer layer of the blastula, termed epiblast, and is the most exterior layer. It gives rise to the epidermis (skin and associated organs) and the future nervous system. The mesoderm is the middle layer and differentiates to the connective tissue, muscles, bones and blood. The endoderm is the innermost layer and develops into the gastrointestinal tract, the lungs and associated structures. Interestingly, germinal cells from the gonadal or genital ridge, which are the precursor of the gonads, are not derived from any of these three germ layers but rather develop outside the embryo (figure 1).

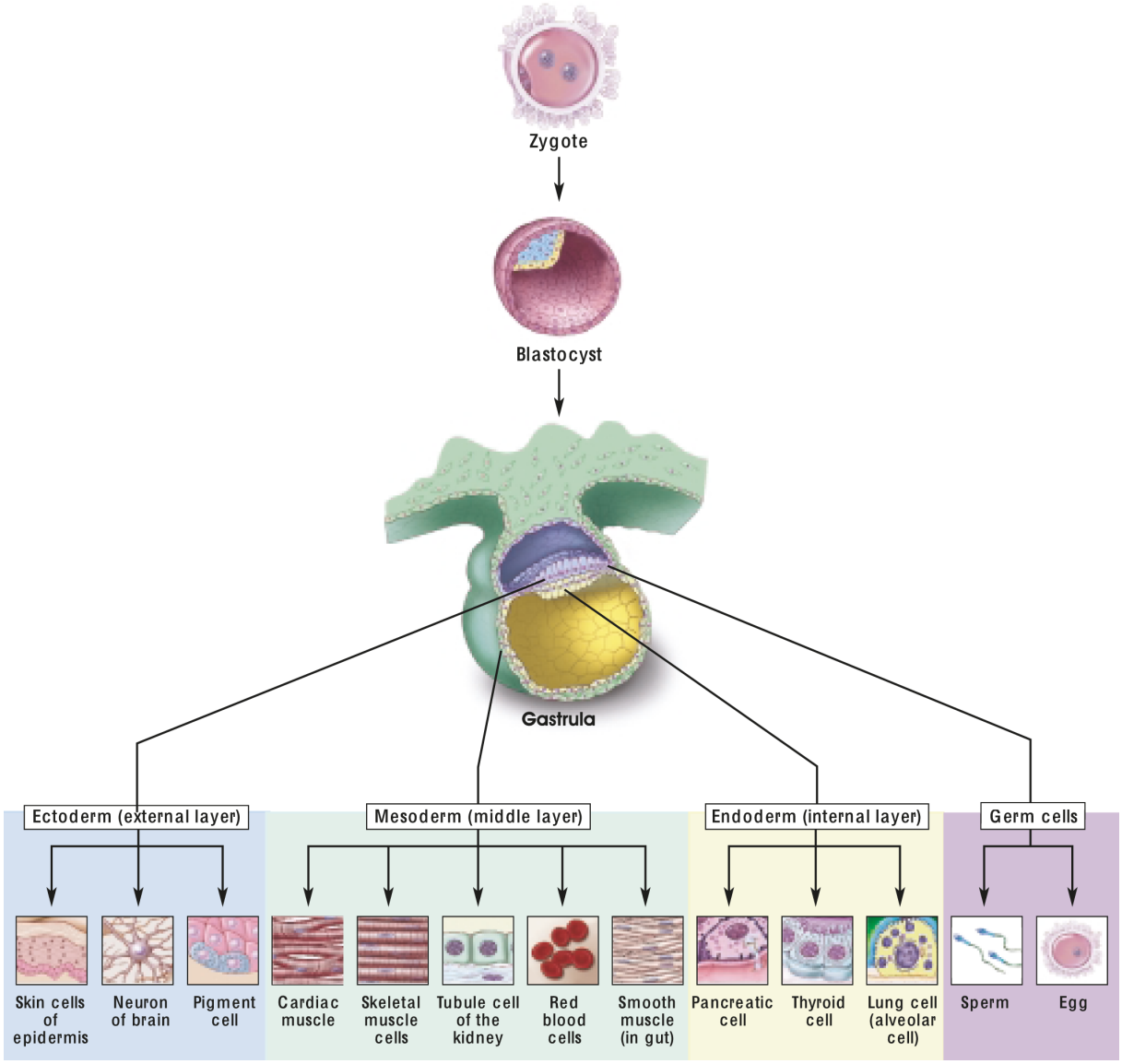

Figure 1: Differentiation from zygote into the specialized tissues during mammalian early development
(picture: © 2001 Terese Winslow, Caitlin Duckwall)

During stem cell fate determination, cells encounter progressive restrictions of their developmental potential for gaining higher specialization. For example, during differentiation of the small intestine epithelium (see figure 2) the initial totipotent zygote undergoes several determination steps to finally become fully specialzed. Some of the ESCs differentiate into multipotent endodermal germ layer stem cell, which have potential to give rise to several different tissues such as gut, pancreatic, thyroid, and lung tissue. The next determination step includes oligopotent lineage stem cells occurring e.g. in yolk sack and gut endoderm. Tissue-determined stem cells such as the quadripotent intestinal progenitor cells can give rise

to mucous, absorptive, neuroendocrine, or paneth cells, which in turn further terminally differentiate in nullipotent mature cells [6].

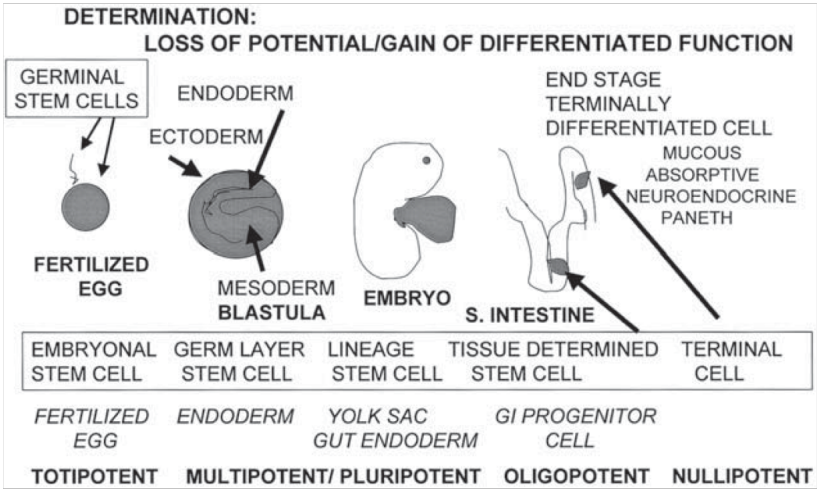

Figure 2: Differentiation potential of stem and progenitor cells in the developing small intestine

During the process of determination the stem cells lose their stem cell potential and gain specialized functions. The differentiation potential ranges from totipotent for the fertilized egg to nullipotent for a terminal differentiated cell (e.g. paneth cell) (adapted from Stem Cells Handbook by Stewart Stell 2004).

During self-renewal (or self-regeneration) and differentiation stem cells use two different mechanisms of cell divisions, a symmetric or asymmetric division (Figure 3).

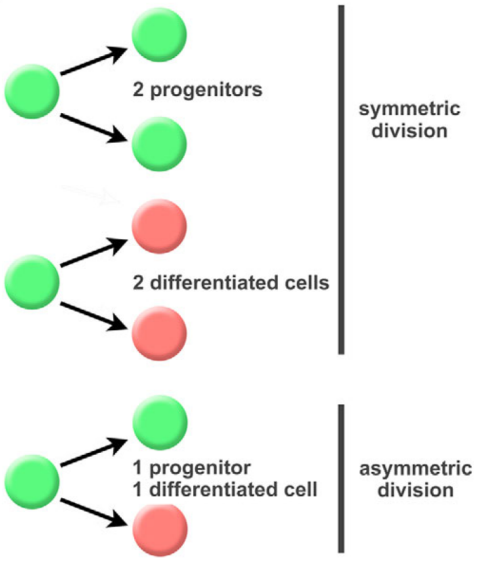

Figure 3 : Symmetric and asymmetric stem cell division

Stem cells can divide symmetrically thereby generating either two stem cells (expansion), or two differentiated cells (depletion). During an asymmetric division a stem cell generates one new stem cell (self-renewal) and one differentiated cell (differentiation) (adapted from Lee et al., 2008) [7].

During self-renewal stem cells divide symmetrically leading to an increased number of daughter stem cells with the same stem cell properties as the origin cells. This type of cell division is not only predominantly observed during very early embryonic developmental stages, but also during wound healing and regeneration. During asymmetric cell division the stem cell divides into one daughter cell with stem-cell fate (self-renewal) while the other daughter cell differentiates. This type of cell division also leads to self-renewal as the symmetric division, but not to an expansion of stem cells [7]. Asymmetric divisions are particularly important later in development when it comes to tissue specification, but also in adult stem cells, e.g. in HSCs. In asymmetric cell divisions the correct orientation of the mitotic spindle can be regulated by either cell intrinsic mechanism such as an asymmetric localization of cell polarity factors and/or the polarized localization of cell fate determinants or by asymmetric exposure of extrinsic cues, represented by the microenvironment, to initially identical daughter cells, resulting in the acquisition of different cell fates [8] see figure 4.

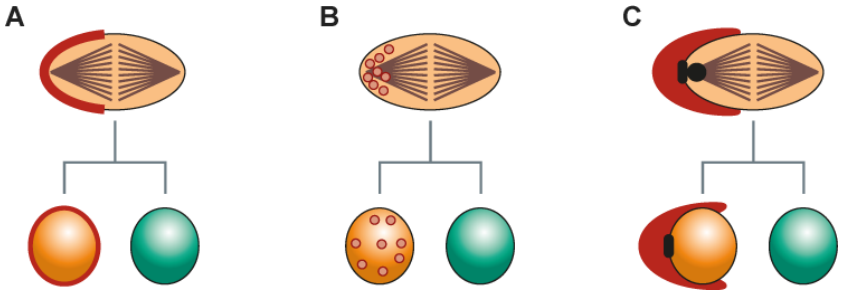

Figure 4: Three different modes of asymmetric division of stem cells

A) Intrinsic asymmetric division mediated by the asymmetric localization of cell polarity factors (red). B) Intrinsic asymmetric division mediated by cell fate determinants (red), which can be associated with the centrosome or the membrane being differentially distributed to the daughter cells or, as shown here, segregated to the cytoplasm of one daughter cell. C) Extrinsic asymmetric division; here, the to daughter cells have the same developmental potential but due to exposure to different stem-cell microenvironments (stem cell niche in red) only one daughter cell becomes essential, extrinsic cues from the environment retaining the stem cell fate, while the other cell is exposed to differentiation factors. Orange: stem cells. Green: differentiated cells (adapted from Morrison et al., 2006).

Stem cells are not only important during development. The somatic stem cells can be found in several types of differentiated tissues and organs such as BM, blood, skin, skeletal muscle, CNS, small intestine, teeth, heart, liver or gut epithelial. Their main functions are the replacement of dying or injured cells and thereby maintenance of the tissue. For somatic stem cells also the potential of transdetermination was described, which defines the differentiation of a stem cell from one adult tissue to another tissue [9] (figure 5). This has to be distinguished from an other type of cell plasticity termed transdifferentiation which occurs when a differentiated cell directly transforms into another differentiated lineage without

dedifferentiation into a stem or precursor cell [10]. Many of the experiments proving the plasticity of somatic stem cells were done with HSCs originated from the mesodermally derived BM showing that they were able to differentiate into other mesodermally derived tissues such as liver [11-13], cardiac muscle [14,15] and skeletal muscle [16,17], or even into tissues from an other germ layer, e.g. into neural tissue, which is derived from the ectoderm [18,19]. The novel possibilities to use the plasticity of somatic stem cells for therapeutic tissue regenerations are controversially discussed, as the yield of plastic differentiation, e.g. with HSCs, is extremely low and, therefore, of questionable therapeutic relevance [20].

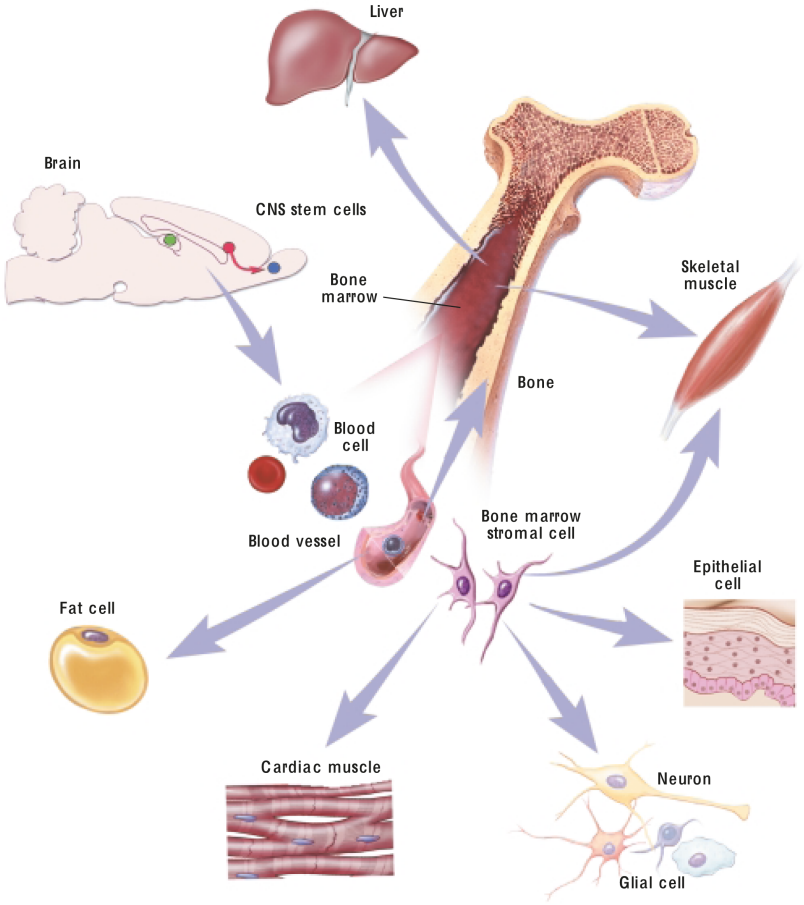

Figure 5: Adult stem cell plasticity

The term plasticity, describes the ability of a stem cell from one adult tissue to generate differentiated cell types of another tissue either, from the same or from a different embryonic germ layer. For example HSCs (derived from mesoderm), have the potential to transdeterminate into skeletal muscle (also derived from mesoderm) or neurons (derived from ectoderm) (adapted from Kumar et al., 2010) [21].

6.2. Hematopoietic Stem Cells

The blood forming system, known as the hematopoietic system, contains more than 10 distinct mature cell types including erythrocytes (red blood cells), platelets, myeloid cells such as granulocytes (neutrophils, basophils and eosinophils), monocytes, dendritic cells (DCs), mast cells and macrophages and lymphocytes such as B and T cells. Many blood cells and certain kinds of epithelial cells have a very short lifetime and hence, have to be continuously replenished. For example human erythrocytes have a lifetime of approximately 120 days. To maintain the homeostasis of blood cells and to ensure survival, an adult human needs to produce approximately one trillion new hematopoietic cells every day [22]. This continuous production of mature blood cells mainly takes place in the BM where a small pool of HSCs resides, which are the ultimate, and only, source of blood cells (figure 6). HSCs are defined primarily by their ability to self-renew and to give rise to all kinds of blood cells. These properties of HSCs makes it possible for a single cell to regenerate the entire hematopoietic system of an organism as shown in transplantation experiments in mice [23]. HSCs are very rare, e.g. in mice only around 1 in 10,000 to 15,000 BM cells are HSCs [24]. In general, two types of HSCs are distinguishable: the long-term HSCs (LT-HSCs), which have the ability to proliferate and self-renew during the entire lifetime of the organism, and sort-term HSCs (ST-HSCs), which show higher proliferation rates but only for a limited time, possibly a few months. In order to maintain the life long survival of LT-HSCs, they are most of the time quiescent [25]. Only around 8-10% of LT-HSCs enter the cell cycle each day [26,27].

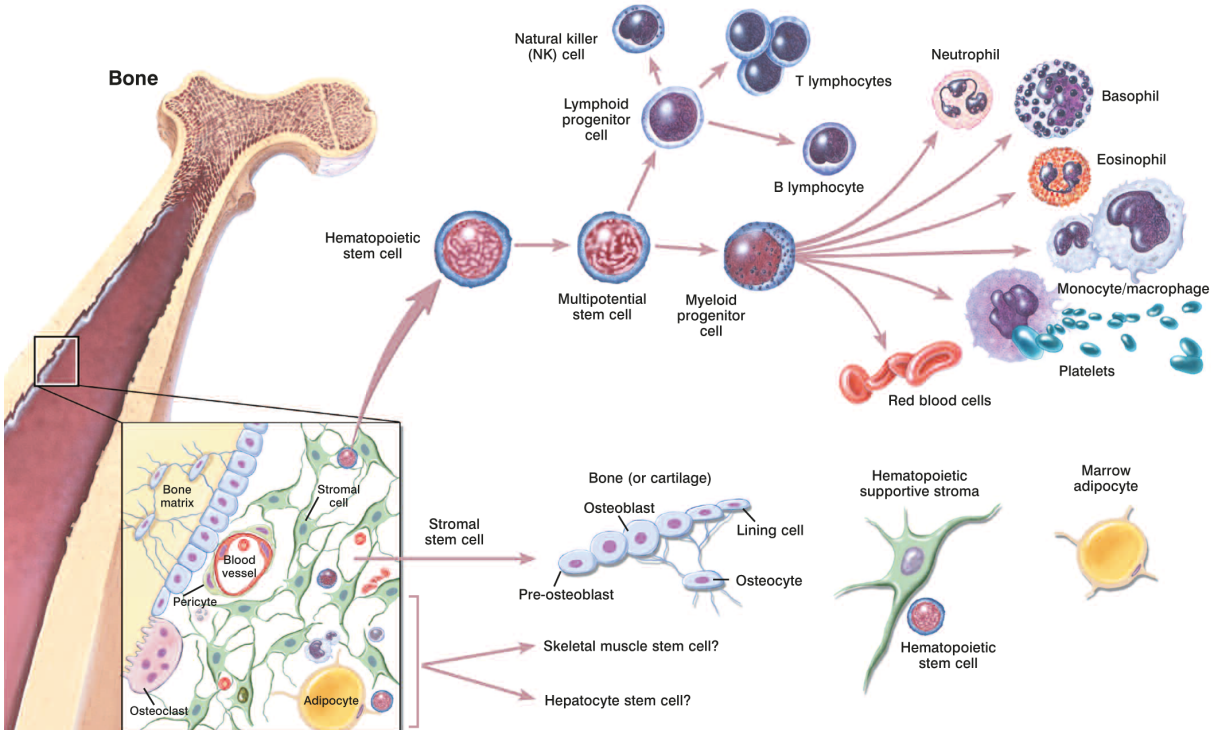

Figure 6: Overview of hematopoietic cell differentiation in the BM

HSC predominantly located close to the dense bone in a specific microenvironment containing stroma cells. All hematopoietic cells can be derived from a single HSC through cell division and differentiation into several intermediate precursor cell stages to the finally terminal differentiated effector cells. A related differentiation and maturation is also observed for stroma cells (picture: © 2001 Terese Winslow, Lydia Kibiuk).

First evidence for the existence of HSCs came from observations of people, which were exposed to high doses of radiation after the Hiroshima and Nagasaki bombings in 1945. Survivors of the atomic bombs had an immune-compromised hematopoietic system and died of normally nonpathogenic infections or an insufficient production of platelets resulting in hemorrhages. In 1949 Jacobsen et al. showed that mice that received a minimal lethal dose of whole body irradiation developed the same radiation syndromes and died from hematopoietic failures approximately two weeks after irradiation. Furthermore, they were able to demonstrate that shielding organs such as single bones or the spleen (Spl), in which hematopoiesis occurs, can prevent the irradiation syndrome [28]. Thereafter, in 1951 transplantation experiments with cells isolated from BM or Spl showed that these cells were able to rescue lethally irradiated animals [29,30]. In the early 1960s, when it was clear that cellular rather than humoral factors are essential for the rescue of lethally irradiated organism, Till and McCulloch further analyzed the cellular composition of the BM to determine the cell type(s) responsible for the reconstitution of the hematopoietic system. They observed the formation of colonies within the spleen composed of myeloid and erythroid cells 8 to 10 or 12 days after transplantation of BM cells into lethally irradiated recipients [31]. Furthermore,

they proved the clonal nature of the Spl colonies by showing that the different cells within one colony were all derived from a single HSPC [32]. Spleen colony forming cells (CFC) were also further transplantable and had the potential to reconstitute the hematopoietic system of lethally irradiated secondary recipients [33]. Although the development of more precise markers for the characterization of HSCs revealed that the Spl colonies are formed by more differentiated myeloid progenitor cells, rather than by HSCs, [34] the discovery of spleen colony forming units (CFU-S) were a milestone in hematopoietic research and immensely contributed to the identification of HSCs.

6.3. Hematopoietic Stem Cell Hierarchy

Although the current understanding of the hematopoietic development is not complete, the hematopoietic system is one of the best-described systems of stem cell development. For the different cell types of the hematopoietic system a hierarchical model has been proposed by arranging stem and progenitor cells according to their lineage differentiation potential (figure 7). At the top of the hierarchy is a small pool of LT-HSCs with an indefinite self-renewal potential. These cells are most of the time quiescent and can give rise to all different hematopoietic cell types on a single cell level throughout the entire lifetime of an organism. Once HSCs commit to differentiation, they cannot revert to a self-renewing state indicating that specific signals, provided by specific factors, seem to be needed to maintain HSCs.

ST-HSCs are derived from LT-HSCs. They are still multipotent but have a restricted self-renewal potential and their reconstitution potential, in a murine system, is restricted to a few months [35]. ST-HSCs give rise to multipotent progenitors (MPPs). These briefly self-renewing cells are pluripotent but have no long-term reconstitution capability [36,37]. The MPPs further differentiate into oligolineage-restricted progenitors that are committed to the lymphoid or myeloid lineages through irreversible maturation steps. The differentiation into common lymphoid progenitors (CLPs) and common myeloid progenitors (CMPs) is the first major branching point of the hematopoietic tree. The CLPs are restricted to give rise to innate lymphoid cells, such as B, T and natural killer (NK) cells, while CMPs first differentiate into granulocyte-macrophage progenitors (GMPs), which in turn give rise to monocytes, macrophages and granulocytes or into megakaryocyte-erythroid progenitors (MEPs), which in turn produce megakaryocytes, platelets and erythrocytes. Once the precursors have become lineage restricted they stop to proliferate and mature, through several

maturation steps, into the different lineage-committed effector cells of the hematopoietic system.

This differentiation pathway is not rigid. Under certain conditions developmental steps can be bypassed as cells of the heterogeneous MPP population can directly give rise to MEPs without passing through CMPs [37]. Furthermore, the fact that both CMPs and CLPs can give rise to DCs [38,39] or that MEPs maintain the potential to differentiate at an extreme low frequency into B cells [40] further suggests the existence of alternative commitment pathways.

The molecular mechanisms regulating lineage commitment within the hematopoietic system is a complex stepwise process combining the alternate expression of specific transcriptional regulators, growth factors, and growth factor receptors, whose combination determines lineage commitment and maturation [41,42].

All of these different stem and progenitor populations, shown in figure 7, can be separated as pure populations by using cell surface markers as described in the next section.

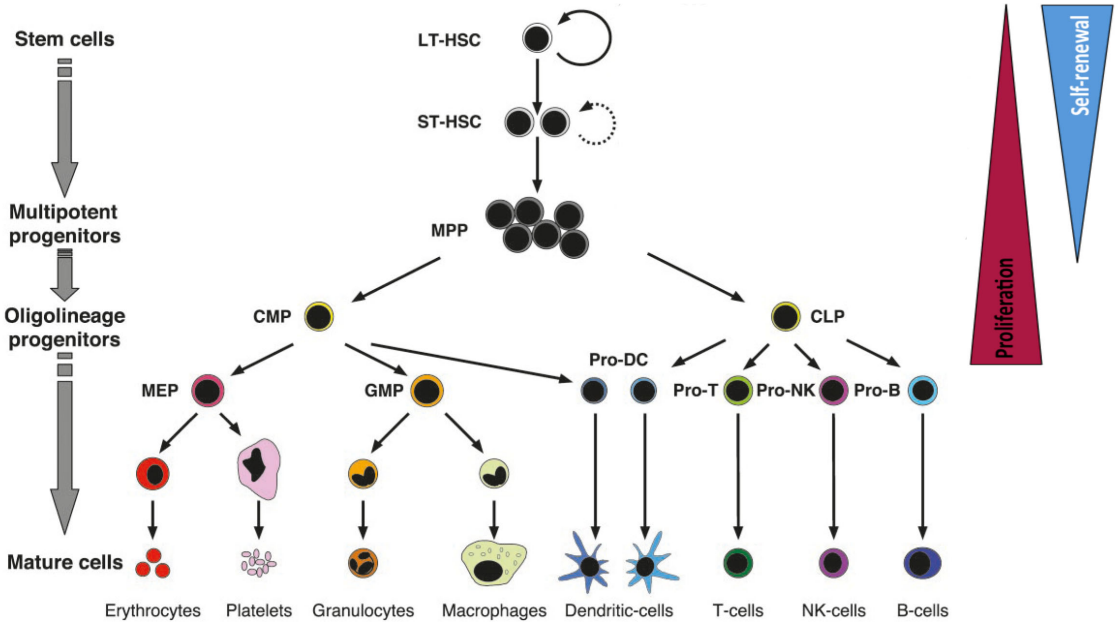

Figure 7: Model of the hematopoietic hierarchy

On top of the hierarchy are highly self-renewing LT-HSCs, which are most of the time quiescent and give rise to all hematopoietic cell types (multipotency). While LT-HSCs have the ability to reconstitute the whole blood system of an organism with a single cell, ST-HSCs have gained a higher proliferative potential and have a limited reconstitution potential, athough they are still multipotent. The ST-HSCs differentiate into multipotent progenitors (MPPs), which are not self-renewing and have no long-term reconstitution capability but are highly proliferating. The MPPs give rise to oligopotent precursors that are committed to the myeloid or lymphoid lineages, the common myeloid progenitor (CMP) or common lymphoid progenitor (CLP). The CLPs can further differentiate into lineage restricted precursors which finally give rise to dendritic, T, NK, or B cells while CMP further differentiate into committed megakaryocyte-erythroid progenitors (MEPs) giving rise to erythrocytes and platelets or granulocyte-macrophage progenitors (GMPs) giving rise to granulocytes and macrophages. Lineage restricted precursors are maturing into the mature effector cells and are not proliferative active (modified from Passegué et al., 2003) [43].

6.4. Hematopoietic Stem Cell Characterization

A major challenge in the hematopoietic research since the 1960s has been the identification, characterization and isolation of HSCs. The identification of HSCs is strenuous for several reasons. First, the number of HSCs in a large mix of several other BM resident populations is very small. Second, HSCs appear and behave similar to other white blood cells in culture, which makes it impossible to identify them only by morphological characteristics, e.g. size and shape. Third, phenotypical and functional characteristics of HSCs are not uniquely consistent, meaning that a HSC population characterized by its specific, homogeneous phenotypic marker expression could contain cells that are heterogenic in other properties such as their longevity, self-renewal or multipotency.

However, the advance in transplantation assays, genetic engineered mouse models, antibody and cell culture technologies in the last 20 years improved the understanding of processes involved in the differentiation of HSCs into progenitor cells and finally mature blood cells and led to further development and improvement of various methods for the characterization of stem and progenitor cell populations that are now available for use in HSC research.

For the immunophenotypical analysis of HSPCs the development of fluorescence activated cell sorting (FACS) has been crucial. The FACS-based methods enable the recognition, quantification and purification of small numbers of HSCs in large mixed populations. The purity of FACS isolated HSC populations has increased in recent years, so that around 50%-96% of the isolated cells in a certain population, depending on the combination of antibodies against specific surface marker that had been used, can give rise to long-term reconstitution after transplantation [44,45]. For mouse HSCs these markers include panels of 8 to 14 different antibodies recognizing cell surface proteins present on differentiated lineages (e.g. macrophages, B and T cells etc.) therefore collectively referred to as “Lin”, as well as the proteins c-kit, Sca-1, CD34, CD150, CD48, CD41, CD135, CD49b, CD127, and CD16/32. The combination of surface markers used for the recognition of human HSPCs differs from this and have been defined by using Lin, CD34, CD38, CD45RA, CD90, CD49f, CD135, CD10, and CD7. While none of these markers alone recognize functional stem cell activity, several cell surface marker combinations of at least 3 different markers, see figure 8, are used to purify near-homogenous populations of HSCs [46,47].

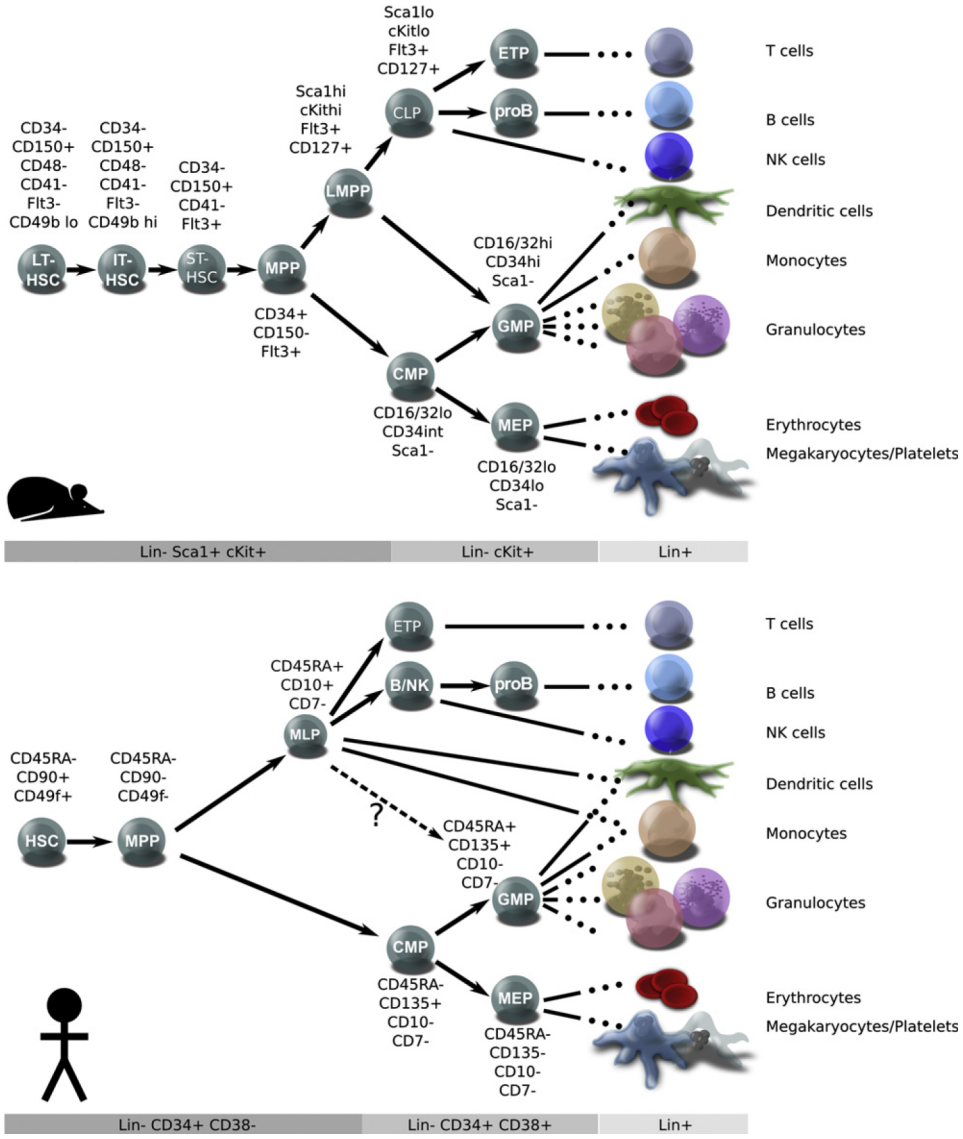

Figure 8: Models of adult mouse and human hematopoietic hierarchies

The major classes of stem and progenitor cell populations defined by cell surface phenotypes in adult mouse (top) and human (bottom). Antibody panels are listed next to each population and in the gray bars below each schematic (adapted from Doulatov et al., 2012) [46].

In addition to antibodies, fluorescent dyes such as rhodamine123, which stains mitochondria, or the DNA-binding dye Hoechst33342 (Ho) have been used to explore the high drug efflux properties of HSCs [48-52]. Both of these dyes are fast released from HSCs due to a high efflux mediated by membrane pumps of the adenosine triphosphate (ATP)-binding cassette (ABC) transporter superfamily, highly expressed in HSCs and can so be distinguished from mature cells, which retain the dyes at a higher intensity [48,51]. With the advancement of this method, the Ho side population (SP) [48] is more commonly used today. Hereby, cells stained with Ho are simultaneously visualized at two wavelengths. The SP cells, a population containing HSPCs, appear in a distinct “tail” profile [48].

However, all of the mentioned phenotypically defined populations are not 100% homogeneous. In theory, the best strategy to dissect this heterogeneity is the analysis of single cells, which is not realistic due to the lack of differentiation criteria. Furthermore, none of the currently used HSC markers are directly linked to an essential HSC function and there are variations of these markers depending on genetic alleles [53], mouse strains [54], developmental stages [55] or activation stages [56,57] as well as differences of markers between species such as humans and mice. Thus, the functional potential of HSCs and progenitors cannot be measured solely based on surface expression markers, which makes additional functional assays absolutely necessary for the identification of HSCs.

For the functional characterization of hematopoietic stem and progenitor cells several *in vitro* and *in vivo* assays with certain advantages but also critical limitations, have been developed and are currently commonly used (figure 9).

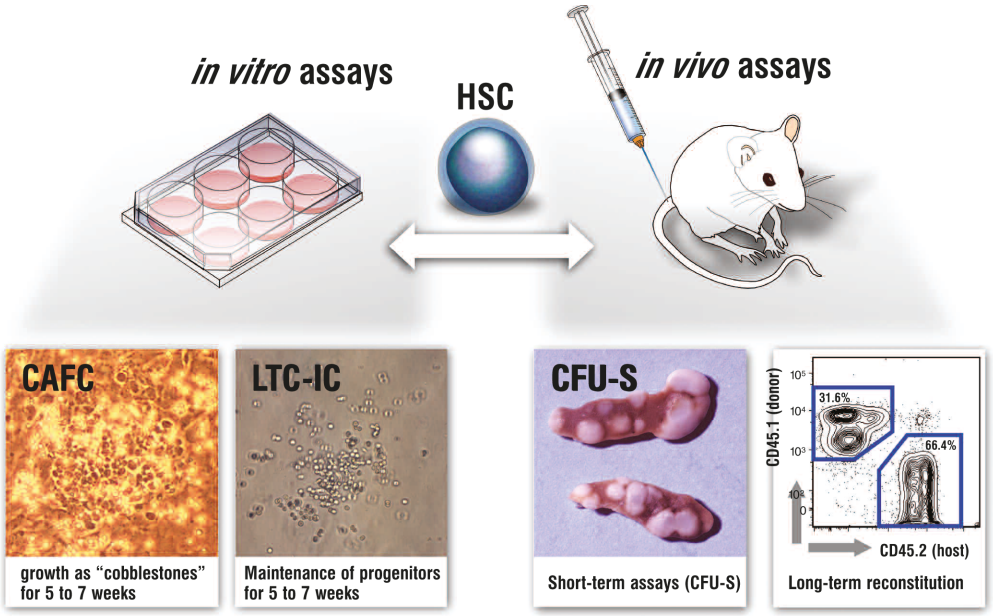

Figure 9: Overview of assays used to detect hematopoietic stem and progenitor cells

The right side shows two *in vivo* assays. In both assays test cells are transplanted into irradiated recipient mice. The spleen colony forming (CFU-S) assay measures the presence of predominantly HPCs in the test cell population by their ability to form colonies in the Spl of the recipient after a certain period of time. Each colony derives from one HPC. The long-term reconstitution assay addresses the ability of HSCs within a test population to mediate long-term engraftment and to produce multilineage effector cells. The left side shows two *in vitro* assays. *In vitro* assays do not have the resolution for identifying HSCs as *in vivo* transplantation assays but are often the only possibility, e.g. to investigate human cell samples. The Cobble-stone Area Forming Cell (CAFC) assay measures the ability of HSCs to grow for up to seven weeks in specific types of colonies under stroma cells, which are easy to identify. In the Long-Term Culture-Initializing Cell (LTC-IC) assay, test cells are plated on a feeder layer for at least 5 weeks. After that time, only HSCs maintain the ability to give rise to progenitor cells with clonogenic potential (adapted from the homepage of National Institutes of Health "Regenerative Medicine 2006").

In vitro, tissue culture based assays are especially important for the investigation of human hematopoietic cells because of the limitation of *in vivo* transplantation assays for human cells. The CFC assay quantifies progenitor cells, but does not quantify HSCs, in a given population. In the process, the test cells are plated in a semisolid agar or methylcellulose culture media supplemented with specific growth factors [58]. The majority of colonies in this assay are derived from oligolineage-restricted progenitors. The colony formation is normally measured 2 weeks after plating. *In vitro* assays for measuring HSCs content in a test population include the long-term culture-initiating cell (LTC-IC) and the cobblestone area forming cell (CAFC) assays [59]. Both assays are co-culture systems that are used to measure HSC frequencies. The LTC-IC assay is based on the ability of HSCs to maintain their clonogenic potential over more than 4 weeks in co-culture compared to progenitor cells. The CAFC assay measures the

ability of HSCs to grow in specific colonies under the stromal feeder layer (so called cobblestone areas) for 5 to 7 weeks after initial plating. Progenitor cells are not able to grow for such a long time period under this culture conditions.

The classical CFU-S assay described by Till and McCulloch's [31] is an *in vivo* assay that measures the ability of progenitor cells, rather than HSCs, to build large colonies in the Spl of recipients, see figure 9, after transplantation into lethally irradiated mice. However, the best assays for analyzing HSC content are *in vivo* reconstitution assays [60,61]. During this process the specific test populations, single pre-purified HSCs or mixed populations in the case of competitive assays, are transplanted into lethally irradiated recipient mice and the overall survival of the recipients or the repopulation potential of the entire hematopoietic system from the test cells is measured. For this kind of assays, especially in competitive transplantation assays, the differentiation between host and donor-derived cells is essential. For this differentiation several types of marker systems are used. For example, the injection of male cells into a female host allows detection of donor cells by the male-cell-specific Y-chromosome. However, the expression of different variations of cell-surface proteins that are recognized by specific monoclonal antibodies such as CD45 is most commonly used (see figure 9). To measure the long-term reconstitution potential of HSCs in mouse models, the recipients have to be monitored at least up to 4 to 6 months after transplantation [62].

In serial transplantations the BM from a previous reconstituted recipient is used as donor cells for the reconstitution of the second generation of lethally irradiated recipients and so on and so forth. This assay should address the lifespan and expansion limits of HSCs but one has to take into account that not only the lifespan but also the transplantability, which can alter under different conditions, influences these result.

Small numbers or frequencies of stem cells in a given hematopoietic population can be addressed in competitive reconstitution assays, in which different amounts of test cells are mixed with a defined population of (mostly total BM) host type cells. The host cells should mediate radioprotection and thereby ensure the survival while the reconstitution potential of the test cell or cells can be determined by the percentage of donor derived effector cells. An example of a competitive reconstitution assays for the quantification of the HSC frequency in a test cell population is shown in figure 10.

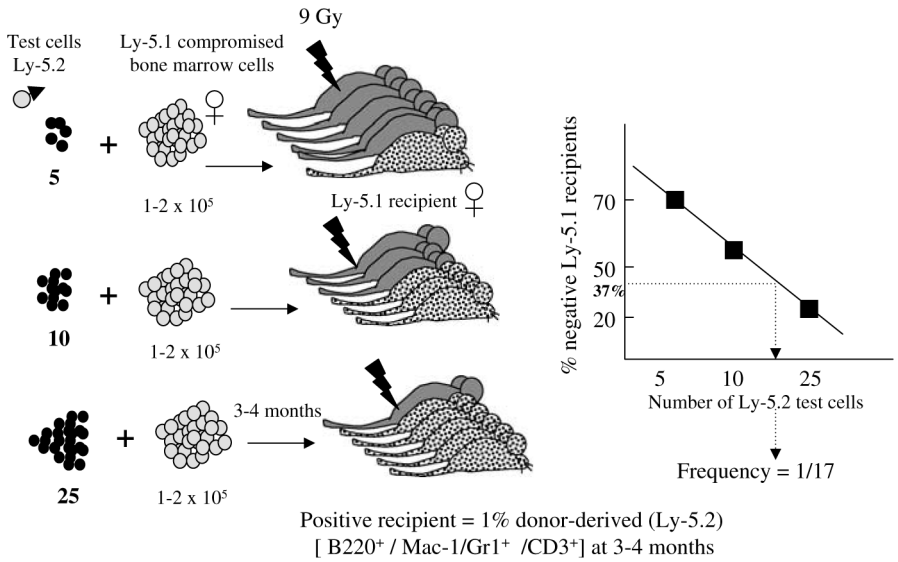

Figure 10: Limiting dilution assay for the quantification of HSCs *in vivo*

Different numbers of test cells are always mixed with the same amount of host type rescue cells and transplanted into lethally irradiated mice. After 3 to 4 months the contribution of donor-derived multilineage cells in the PB is measured. Positive recipients are defined as showing at least 1% donor-derived cells (dotted mice). Because of the linear relationship between the number of injected cells and the proportion of negative recipients, Poisson's statistics can be used to calculate the frequency of HSCs (adapted from Coulombel et al., 2004) [63].

For the investigation of human HSCs in mice several experimental models with immunologically incompetent mice are available including severe combined immunodeficiency (SCID) [64-66], NOD-SCID [67] and Rag-$2^{-/-}C\gamma^{-/-}$ [68] mice. These mutant mice cannot mount an immune response against foreign cells and can therefore be used as recipients for human cells. However, the limitation of this system is that it is not mimicking the natural human environment and that only a fraction of the total lifespan of a human HSC can be measured in mice. Hence, only clinical HSC transplantations can address long-term functions of human HSCs.

There are several factors that have to be considered in all *in vivo* transplantation experiments especially if transgenic mice are investigated; they include the homing properties to the BM, a potentially impaired differentiation of HSCs into hematopoietic lineages, an altered proliferative kinetics of progenitors or defects of HSCs in the interaction with the BM microenvironment [47].

In summary, the ability to obtain highly purified HSCs population combined with functional *in vitro* and *in vivo* assays has greatly facilitated the functional and biochemical characterization of HSCs. However, no definite HSC marker, gene or other criterion has been found so far. Probably the progress in genomic sequencing, genome wide analysis of RNA

expression and protein levels and their comparisons among various types of stem cells may help to identify sets of genes allowing to clearly define “stemness” for HSCs.

6.5. Origin of Hematopoietic Stem Cells: From Hemangioblast to Adult HSCs

HSCs development during embryogenesis is a complex process involving multiple stages that are temporally and anatomically distinct, involving several anatomical sites such as the yolk sac, the aorta-gonad-mesonephros (AGM) region (figure 11), the placenta, the fetal liver and finally the BM (see also figure 12 and 14), thereby requiring unique cellular and molecular regulators. Defining the developmental origins of hematopoiesis is further complicated compared with stationary tissues by the fact that cells of the hematopoietic system circulate, thereby changing their site of “potential” origin.

The conceptus consists of an intra-embryonic compartment that will become part of the fetus and supportive extra-embryonic tissues such as the allantois and the yolk sac. During development multiple waves of hematopoiesis take place at different times and locations involving both compartments. In zebrafish there are at least three distinct phases, while in mammals at least two phases of haematopoietic development exist. The initial wave, referred to as “primitive” phase, takes place in specific areas of the yolk sac called blood islands at embryonic day 7.5 (E7.5) in mice. The primitive hematopoietic system is only transient and is rapidly replaced by the adult-type, also termed ‘‘definitive’’ hematopoiesis. The main site of definitive hematopoiesis is the AGM region [69-72]. The AGM consists of the dorsal aorta surrounded by mesenchyme and the urogenital ridges (UGR) [73] (Figure 11).

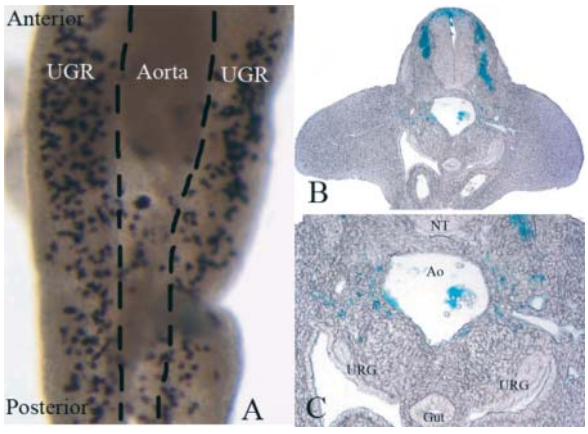

Figure 11: Ventral and sagittal images of the AGM region and the flanking urogenital ridges

(A) Ventral view of the dissected UGR and AGM of an E11 mouse embryo. Germ cells are visualized.

(B) Sagittal section of the UGR/AGM region from an E11.0 embryo. The UGR is ventral to the dorsal aorta, which is ventral to the neural tube. (C) Higher magnification of B. Ao = dorsal aorta, NT = neural tube (adapted from Pietila et al., 2005).

This region develops from the lateral plate mesoderm and is first called para-aortic splanchnopleurae (pSP) before it becomes the AGM. Already at E8.5, before the circulation is established, the pSP contains progenitor cells with myeloid potential [69]. Before the development of HSCs with adult repopulating potential in the AGM at E10.5 [71,72,74,75], not only in the pSP but also in other sites of the mouse conceptus such as the yolk sac, allantois or placenta, cells with hematopoietic potential were found at specific times. Therefore, at least 4 further classes of hematopoietic cells can be defined, before the appearance of adult-definitive HSCs, see figure 12 and 14 [76].

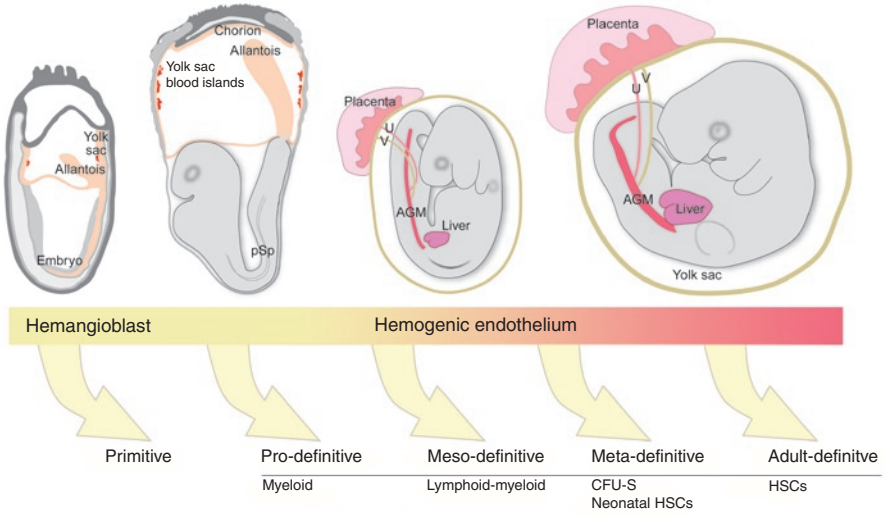

Figure 12: Generation of hematopoietic cells during development of the mouse conceptus

Shown are four different embryonic days from left to right: E7.5, E8.25, E9 and E10.5. The five different classes of hematopoietic cells, defined by their function, are generated at specific time points indicated by arrows. The hematopoietic potential of the different classes of definitive HSCs is indicated by the cell type they can give rise to (below the line). The pro-, meso-, meta- and adult-definitive classes are derived from hematogenic endothelium, while the primitive class is derived from hemangioblasts. At E7.5 and E8.25 the placenta will form by the fusion of the outgrowing allantois and the chorion. At E9 the embryo is enveloped in the yolk sac and the colonization of the fetal liver by hematopoietic progenitors commences. At E10.5 hematopoietic clusters and the first HSCs are found in the dorsal aorta in the AGM region, the vitelline (V) and umbilical (U) arteries (adapted from Dzierzak et al., 2008).

While primitive hematopoietic cells are derived from a hemangioblast, the definitive hematopoietic cells are generated from a hemogenic endothelium. Already long time ago, the hemangioblast was hypothesized as a common origin for primitive hematopoietic and vascular cells because of the close physical association of primitive erythrocytes and endothelial cells in the developing yolk sac [77]. The hemangioblast is a mesodermal precursor whose activity has been detected earliest in the posterior region of the primitive streak [78] from where the cells migrate to the yolk sac (see figure 13). Thus, fate decisions to

become endothelial or hematopoietic cells are already been made before the blood island formation.

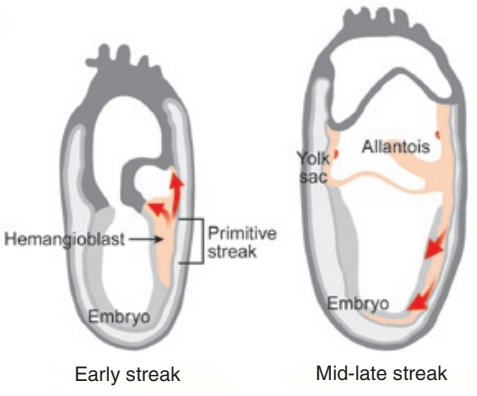

Figure 13: Migration of mesodermal cells during early-streak and mid- to late-steak stage in the mouse
Mesoderm emerging from the primitive streak forms first the extra-embryonic yolk sac and later the allantois in the early-steak stage. Red arrows indicate the emigration of mesoderm cells from the primitive streak. Red dots indicate blood islands derived from mesodermal hemangioblasts (adapted from Dzierzak et al., 2008).

The process from which the definitive classes of hematopoietic progenitors arise, the haemogenic endothelium hypothesis, seems to be related but still distinct to the haemangioblast hypothesis. Discrete subsets of vascular endothelial cells seem to show hemogenic potential during development [79], indicating an endothelial origin for definitive hematopoietic cells. This was further supported by the fact that developing, definitive HSCs have specific properties in common with endothelial cells, such as surface marker expression or the ability to incorporate acetylated low-density lipoprotein [80]. Furthermore, it was possible to visualize in several species cluster of hematopoietic cells budding from the ventral wall into the lumen of the dorsal aorta as well as the vitelline and umbilical arteries [81]. Other studies have suggested that definitive HSCs originate from the mesoderm/mesenchyme adjacent to endothelial cells in the ventral aspect of the dorsal aorta [82] or that mesenchymal cell populations in discrete patches ventral-lateral to the dorsal aorta (subaortic patches) poke through the aorta and bud off HSCs [83]. Individual cells in the subaortic patches, expressing surface marker characteristic for HSCs and displaying reconstitution potential, further confirmed this. While the localization of hematopoietic clusters in the chick aorta is strictly localized to the ventral wall, it was shown that in mice hematopoietic cluster can be found on both the ventral and dorsal endothelium of the dorsal aorta and that both contain hematopoietic progenitors, while fully potent HSCs are restricted to the ventral aspect [75].

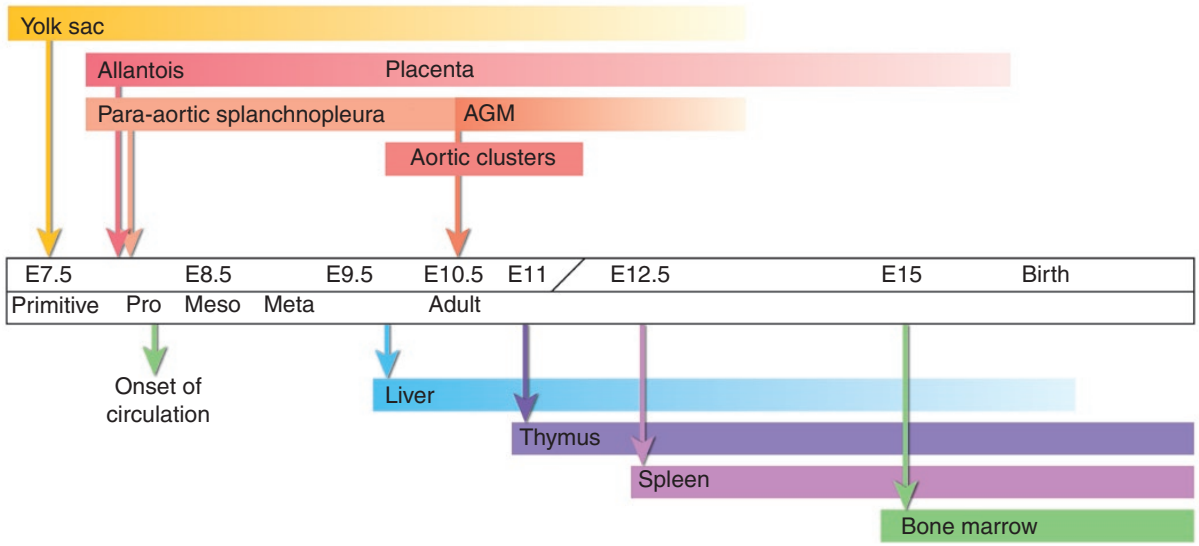

Figure 14: Timeline of hematopoietic development in mice

The arrows above the timeline indicate the onset of hematopoietic cell generation and/or appearance in the specific parts of the mouse conceptus. Organs that are subsequently seeded by HSCs from the locations above at specific time points are shown below the timeline. The circulation is established at 8.25-8.5. Arrows denote the earliest time points of hematopoiesis in the associated tissue or organ; bars represent the duration of hematopoiesis in that tissue or organ (adapted from Dzierzak et al., 2008).

Following the definitive hematopoietic activity in the AGM starting at E10.5, additional activity was detected subsequently in the umbilical artery connecting dorsal aorta to the placenta, the yolk sac and the placenta proper [84-86]. HSCs detected in the yolk sac and the placenta could arise by *de novo* generation or expansion of pre-existing HSC populations coming from the AGM through the circulation, which is established at E8.25-8.5 (figure 14) [87], or both. However, quantitative spatial and temporal analyses of HSCs suggest that both yolk sac and placenta contribute to the pool of HSC in the fetal liver [85,86,88], because the number of HSCs is to high to be derived only by cells coming from the AGM alone. Most likely an additive production of HSCs by AGM, yolk sac and placenta, plus the expansion of HSCs in the fetal liver itself, is responsible for the large number of fetal liver HSCs [85,89]. While the colonization of the fetal liver starts at E9 with myeloerythroid progenitors that generate definitive erythroid cells, the first definitive HSCs appear at E11.5 (see figure 14). After E12.5 the fetal liver is the main hematopoietic organ where massive HSC expansion takes place. By E15.5-16.5 a plateau with the maximum number of around 1000 HSCs is reached and thereafter the HSC number starts to decline [55,85,90].

The definitive hematopoiesis is followed by the colonization of the thymus at E11, the Spl at E12.5 and finally the BM starting at E15 (see figure 14) [76,91,92]. In none of this hematopoietic organs *de novo* HSC generation takes place [93,94]. It is rather believed that a

massive expansion and subsequently differentiation of HSCs occurs, which initially seeds these organs. These processes are specifically supported and controlled by the microenvironment surrounding the HSCs within the different organs.
Interestingly, the population of the thymus might originate from the circulation as well as from direct migration of HSCs through tissues, as it was suggested by experiments in birds showing the migration of progenitors to the thymus along the thoracic duct [95].
Before the colonization of the BM a specific, supportive microenvironment for the HSCs has to be created. The skeletal development commences at E12.5 with mesenchymal cells first giving rise to chondrocytes that create a cartilaginous mold of the skeleton during mesenchymal condensation [96]. Calcified bone is subsequently generated, through endochondral ossification by osteoblasts (OBs) replacing chondrocytes. Invasion of a vascular system into the developing bones facilitates the seeding of hematopoietic cells through the circulation.

6.6. Trafficking of HSCs in the adult organism

As described in the section above, HSC trafficking is absolutely essential during embryonic development for the sequential colonization of different hematopoietic organs to finally build a functional life-long hematopoietic system. However, the trafficking of HSCs is not only restricted to embryogenesis. Migration and circulation of HSCs is also essential in the adult organism during hematopoietic homeostasis [97]. It contributes to innate immune responses, reproduction of mature effector cells after hematopoietic injury [98] and is also crucial for clinical applications such as BM or stem cell transplantations [99]. In adult mice and humans the majority of HSCs reside in the BM. The engraftment of HSCs in the BM during organogenesis, after BM transplantation (BMT) and after treatment with chemotoxic drug or irradiation refers to a complex multistep process, in which transiently circulating cells become resident tissue cells. Furthermore, they refill the entire hematopoietic system by their ability to proliferate, self-renew, differentiate and thereby give rise to multilineage progenitors.
The first step of this process, the specific recruitment of circulating HSCs to the BM, is known as “homing” (see figure 15) and refers to the initial interaction of HSCs with the microvasculature and their consecutive transendothelial migration, called diapedesis. The next step is the interstitial migration of HSCs through the ECM within the marrow, which is an active amoeboid movement that can occur independently of blood flow. For this mode of trafficking the HSCs need to recognize and respond to extravascular guidance cues. Finally, the HSCs lodge in suitable, specific anatomical sites, also termed “niche”, where they

establish complex regulatory interaction with their environment that controls their survival, proliferation and differentiation. This step is widely termed “lodgement”.

Homing of HSPCs into the BM is a fast and efficient process, occurring within minutes or few hours rather than days [100], and involves a multiple adhesion cascade with similarities to the homing process described for mature blood leukocytes into peripheral tissues [101-105] controlled by the actions of cytokines, chemotactic factors and cell adhesion molecules (CAMs). For the homing of HSPCs into the BM, the cells not only have to recognize BM specific endothelial cells in the sinusoids but also have to firmly adhere to them in order to resist the constant hydrodynamic shear resulting from the blood flow. In the initial step of at least three intravascular adhesion steps [101,106], the fast flowing cells tether and then slowly roll along the vascular surface. This slowing down of HSPCs is mediated mainly by the endothelial selectins, P- and E-selectin, as well as vascular cell adhesion molecule-1 (VCAM-1, or CD106), which are expressed on BM microvessels and interact with their counter-receptors P-selectin glycoprotein ligand (PSGL)-1 and low affinity α4β1 (very late antigen-4, VLA-4) expressed on HSPCs [107]. As the specific expression of these three adhesion molecules in a unique side-by-side combination is restricted to the BM [108] and only rarely expressed on endothelial cells outside the BM in the absence of inflammatory stimulation, it seems that they also function as the specific recognition signal for the BM extravasation. Important for this initial binding is a fast binding kinetics, however, their bond lifetime is rather short so that in the next step of the cascade a firm adhesion has to be established. To adhere firmly, the rolling cells must receive an activation signal that leads to conformational changes of integrins, mainly α4β1 but also αLβ2 (lymphocyte function-associated antigen 1, LFA-1), which interact with VCAM-1 and intercellular adhesion molecule-1 (ICAM-1), respectively [109,110]. The most important chemokine, triggering this integrin activation, is the soluble or surface-bound CXCL12 (CXC-motiv-chemokine 12, also known as stromal-derived factor-1; SDF-1), which is sampled by the rolling cells and activates the HSPCs through the Gαi protein-coupled receptor CXCR4 (CXC-motiv-chemokine receptor type 4) [111]. In addition, also signals mediated by Gαs protein-coupled receptor have been shown to be involved in BM homing and engraftment [112]. While the importance of α4β1 during homing is widely accepted, the role of α4β7 is not entirely clear. There are reports implicating α4β7 in HSPC rolling [113] and the expression of its specific ligand mucosal addressin cell adhesion molecule-1 (MAdCAM-1) on BM endothelium [114], while others have not found a role of this pathway during HSPC homing into the BM [109]. Another adhesion molecule contributing to BM

homing of HSPCs is CD44 [115]. It has been shown that CD44 can also bind to E-selectin [115] but the major ligand of CD44 is hyaluronic acid, an anionic ECM glycosaminoglycan expressed on BM endothelial cells and in the interstitium [116,117].

The above-mentioned interaction of CXCL12 with CXCR4 is not only important in homing but also plays a critical role for the retention of HSCs in the BM niche, mobilization (see below) and as guiding cue during interstitial migration towards the stem cell niche. CXCR4 mediated downstream signaling involves the activation of phosphatidylinositol-specific phospholipase C (PI-PLC) and phosphoinositide-3-kinase (PI3K) that activate protein kinase C-zeta (PKC-ζ), which then induces protein tyrosine kinase-2 (Pyk-2) and extracellular signal-regulated kinase (ERK) thereby influencing adhesion and chemotaxis of HSPCs [104,118]. Following firm adhesion, CXCL12 is also responsible for the integrin-dependent diapedesis of HSPCs, although it is believed that also other adhesion molecules such as CD31 (platelet endothelial cell adhesion molecule-1; PECAM-1) or CD99 may be involved [119,120].

As described above, the process of HSPC homing shares several similarities with the multistep process described for leukocytes but there are also notable differences. For example, while E-selectin interacts with α4 integrins during HSC homing, E-selectin closely cooperates with P-selectin in neutrophil recruitment to inflamed sites [121].

Another interesting point is that the BM homing efficiency of transplanted HSCs can also vary according to the cell cycle status of the cell. Several studies showed that the ability of phenotypically identical HSCs to engraft irradiated recipients becomes dramatically decreased if the cells were activated [122,123]. How and at which point the cell cycle status can influence the engraftment process is not yet clear.

A detailed understanding of the process of BM homing is also essential to improve BMT strategies, which is often the only way to treat patients with blood cancers. A successful BMT is in first line dependent on the ability of intravenously injected HSPCs to rapidly traffic to BM niches. Most HSPCs used for transplantations are obtained from cord blood, having the advantage to overcome problems in finding fully human leukocyte antigens (HLA)-matched donors in allogeneic BMT [124-126]. However, a potential disadvantage of cord blood-derived HSPCs is that their homing potential is less effective than that of HSPCs derived from adult BM, increasing the risk of early post-transplant complications. One explanation for this problem is the reduced expression of molecules important for homing on the surface of cord blood HSPCs [127]. To overcome these problems, transplantation of higher numbers of HSPCs is necessary, which is difficult to obtain due to the rare sources of

these cells. Other approaches to overcome these problems include improving the homing potential, as it was shown that a fast migration of HSPCs into the BM is directly correlated with a faster hematopoietic recovery [128]. Therefore, various protocols are used to incubate cord blood HSPCs with different cytokine cocktails to enhance the expression of adhesion molecules before transplantation [127,129].

After HSCs have migrated through the BM intersitium and lodged into their suitable niches they may undergo several symmetrical cell divisions to expand their cell numbers before they turn from the active cycling stage into quiescence, while still retaining a tightly regulated balance between self-renewal and lineage differentiation to maintain the entire hematopoietic system [130].

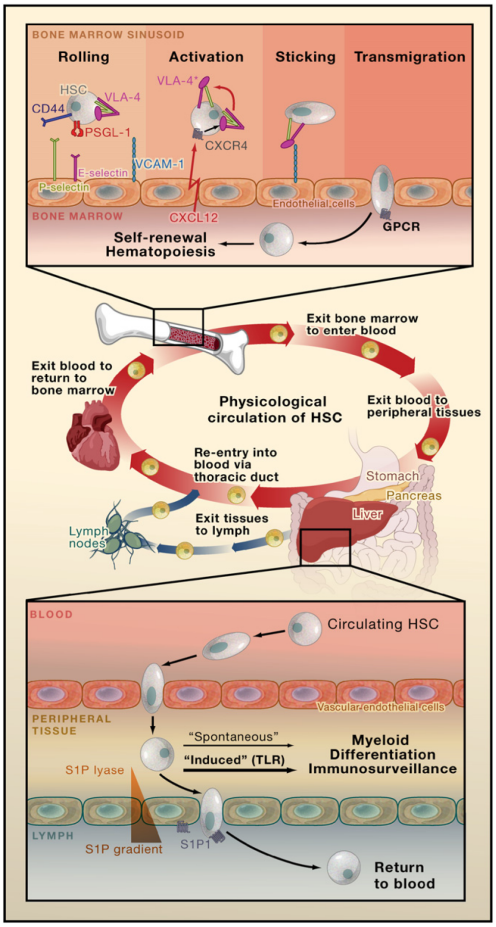

Figure 15: Migration of adult hematopoietic stem and progenitor cells

The top of the figure shows the multistep adhesion cascade of HSPCs homing from the blood into the BM. The middle part illustrates the trafficking of migratory HSPCs under physiological conditions. Some HSPCs are continuously entering the blood circulation from the BM. They then either return to the BM or enter peripheral organs which they exit via lymphatic vessels and return into the blood. HSPCs remain in the circulation only for a few seconds, while in peripheral tissues they can spend more than 36 h before they enter the draining lymphatics in a S1P-dependent manner (shown at the bottom). HSPCs in peripheral tissues can spontaneously or under stress conditions (such as infection or tissue necrosis) via Toll-like receptors (TLRs) differentiate into immune cells (adapted from Laird et al., 2008).

Despite the continuous BM retention signals that HSCs receive from direct and/or indirect interactions with different components of their specific niches (in detail discussed below in section 6.7), there is always a small but significant fraction of HSPCs found in the blood circulation and peripheral tissues (see figure 15) [98,131] indicating that the lodgment into the niche is by no means the final stop in the journey of HSPCs. A previous study using a parabiosis mouse model, in which two mice are surgically joined so that they share a common blood circulation, showed that around 400 HSPCs are constantly circulating in the blood at any given time and have the ability to re-engraft the BM and that other or even the same HSC are newly released into the circulation. This re-engraftment of HSPCs was observed under normal, non-inflammatory, physiological conditions and in the absence of myelosuppressive treatment indicating that a HSPC recirculation is important for the maintenance of the hematopoietic homeostasis [131].

The BM to blood migration, also termed “mobilization” starts with a de-adhesion step of the HSPCs from the BM microenvironment. The process is tightly controlled by specialized signals modulating chemo-attractant cytokines, growth factors and hormones, which are controlling the release from the BM [132,133]. Stromal elements upregulate proteolytic enzymes such as matrix metalloproteinase (MMP)-9 and cysteine protease cathepsin K leading to the proteolytic cleavage of CXCL12, KitL and VCAM-1 [134-137]. In addition, the activation of surface-expressed proteases produced by HSPCs such as the dipeptidase CD26 leads to the increased cleavage of CXCL12 [138], resulting in the loss of adhesive contacts between stromal cells and HSPCs. It has been shown that also certain niche cell types such as OCLs are involved in the release of HSPCs after direct cytokine stimulation [136].

Interestingly, also the sympathic nervous system (SNS) that innervates bone and BM stromal cells has a regulatory influence on the hematopoietic system [139-141]. Previous studies showed that the HSPCs released into the circulation follow a circadian pattern in mice with a peak of blood HSPCs 5 h after onset of light and a nadir 5 h after darkness. This circadian oscillation is regulated by adrenergic signals transduced by the β3 adrenoreceptor, which plays a major role in controlling CXCL12 expression, as it results in down regulation of CXCL12 and thus promotes the HSPC release [142].

Mobilization can also be induced by certain drugs including a variety of cytokines such as granulocyte colony-stimulating factor (G-CSF), chemokines such as IL-3, IL-6, IL-8, Mip-1α or Groβ and small molecules such as the CXCR4 antagonist AMD3100 [137,143,144]. Most commonly used is the mobilization with G-CSF. The G-CSF influences HSPCs trafficking in several ways and may involve several cellular targets. For example, G-CSF induces the

activation of several proteases such as neutrophil elastase and cathepsin G or the release of membrane bound stem cell factor (SCF) through MMP-9 activity [134,135]. It was further shown that signals from the SNS also contribute to G-CSF-induced HSPC mobilization via β-adrenergic stimuli [141] and that G-CSF mobilization can be enhanced when used in combination with AMD3100 [144]. Also antibody-based inhibition of integrins such as α4β1 or β2 have been shown to induce HSPCs mobilization [145,146].

Induced HSC mobilization has an important clinical relevance. For example, HSCs mobilized in the PB greatly facilitates their collection for allogeneic stem cell transplantations, compared to conventional isolation of HSC directly from the BM. Furthermore, mobilizing argents are administered to patients after chemotherapy or BM transplantations to reduce the time required of normalizing the numbers of circulating blood cells [147].

A few years ago, new, additional migration routes of HSPCs have been discovered by showing that BM-derived HSPCs not only travel from the BM into the blood and vice versa but also from the blood into multiple peripheral tissues such as liver, kidneys, and lung, thereafter into the lymph and from the lymph via the thoracic duct, which is the main draining lymph vessel, back into the blood. From the blood they might return into the BM or directly repeat the peripheral migration cycle (see figure 15) [98]. It is still not clear if the HSPCs, which enter this migration cycle are somehow a specialized subpopulation or if all circulating HSPCs have the potential to patrol through peripheral tissues. Furthermore, little is known about the regulatory signals controlling adhesive cascades involved in the homing of HSPCs from the blood into other tissues than the BM. However, the egress of HSPCs from the peripheral tissues seems to depend on sphingosine-1-phosphate (S1P) and S1P receptors, which are also involved in the egress of lymphocyte from secondary lymphoid organs into the lymph [148-150]. However, there are also distinct difference in entering the lymphatic system between HSPCs and mature lymphocytes. While HSPCs enter the system mostly in non-lymphoid tissues via the lymphatic vasculature, mature lymphocytes get access to the lymphatic vasculature by homing to lymphoid organs.

A gradient of S1P exists between the peripheral organs and the lymphatic vessels, with highest concentration in the lymph and lowest in the tissues of peripheral organs [151,152]. This S1P gradient is formed and maintained by the S1P lyase, degrading S1P in the tissues [153]. HSPCs follow this gradient to leave the peripheral organs (see figure 15).

Although the biological reason for this migration of HSPCs through peripheral tissues is not entirely clear, there is evidence that these cells might provide a rapidly recruitable source for local production of immune and inflammatory effector cells. Stress signals mimicking an

inflammation, induced by Toll-like receptor 4 (TLR4) agonists, led to diminished S1P receptor expression on HSPCs resulting in their prolonged retention in peripheral organs providing the necessary time for HSPCs to differentiate into immune cells. Mouse HSPCs express TLRs (e.g. TLR2 and TLR4) [132,154], which can recognize foreign molecules such as the bacterial outer membrane component, lipopolysaccharide (LPS) [155]. Binding of LPS to TLRs on HSPCs leads to their activation shifting them from quiescence into the cell cycle and finally differentiation into myeloid cells including several subsets of monocytes, macrophages, and DCs [156]. In this way the locally generated HSPC-derived leukocytes not only participate in classical innate immune responses but also contribute to the suppression of local infection and elimination of dead cells.

6.7. Hematopoietic stem cell niche

HSCs are the best characterized somatic adult stem cells today and are often used as a paradigm for other types of stem cell. However, despite this knowledge their exact localization within the BM is not fully resolved, which is mainly due to the complex structure of the BM compared to other tissues such as the skin, intestine, muscle or brain, where the localization of stem cells is well identified and described.

The stem cell “niche” is defined as specialized cellular and molecular microenvironment surrounding a stem cell that is together with stem cell autonomous mechanisms involved in the regulation of their functions including a tightly regulated balance between self-renewal, proliferation, differentiation and quiescence as well as the activation of specific cellular programs in response of hematopoietic stress (e.g. bleedings). The concept of the HSC niche was first proposed by Schofield in 1978 [157] and has remained largely undisputed until today, although it markedly evolved. The concept of the niche includes specific anatomically and functionally defined locations with several cell types, soluble molecules, gradients and signaling pathways, as well as physical components, such as shear stress, temperature and oxygen levels, see figure 16 [158-163].

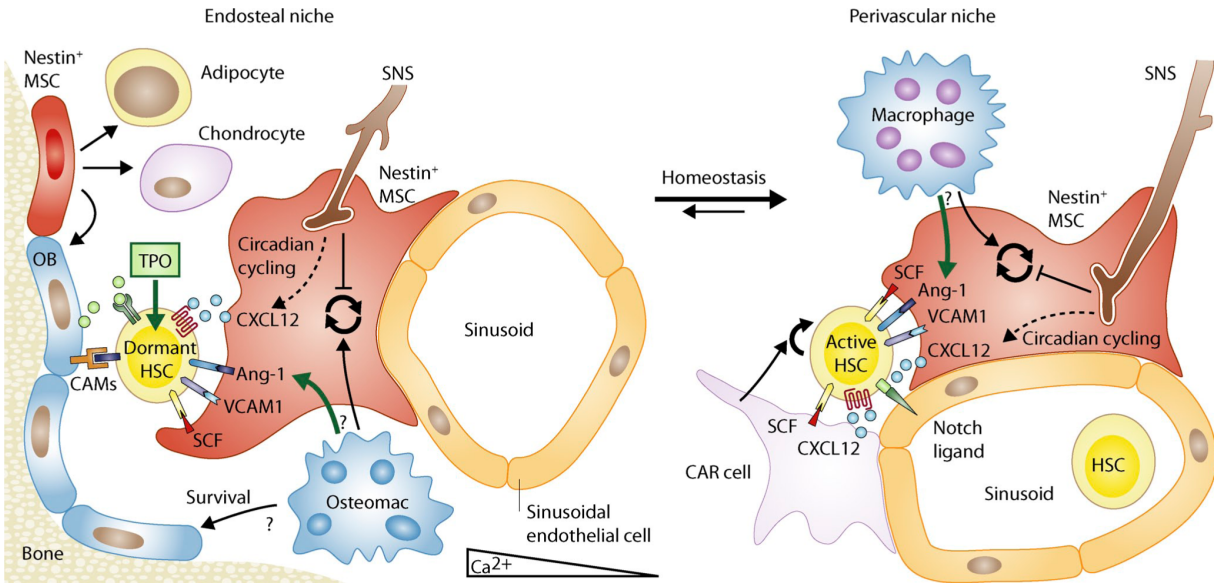

Figure 16: Model showing two localizations for HSCs in the mouse BM interstitium

The left side depicts the endosteal niche harboring quiescent LT-HSCs. The right side shows the perivascular/vascular niche thought to be in more distance to the endosteum and next to sinusoids promoting the self-renewal of active HSCs. For details see the main text (adapted from Ehninger et al., 2011) [164].

Two different areas within the BM are discussed as HSCs niches: the endosteal and vascular niche. The endosteal niche is located near the endosteum in the trabecular or cortical bone. The endosteum is the inner surface of the bone and in immediate proximity to the BM. A cell layer containing mature cells but also precursors, heterogeneous in their degree of differentiation, of bone forming OBs and bone-resorbing OCLs, covers the endosteal surface. In contrast, the vascular niche is located around sinusoids, which are reticular fenestrated venules that predominantly compose the vascular bed of the BM. Although the exact location of HSCs is still controversial [165] (discussed below) there is evidence that single quiescent HSCs are predominantly located in the endosteal niche, while activated HSCs are in closer contact to sinusoids [166].

OBs were one of the first cell types identified as niche components involved in HSC regulation *in vivo* by two independent studies showing that the number of HSCs is increased by the expansion of OBs, thereby enlarging the HSC niche, through the activation of parathyroid hormone/parathyroid-hormone-related peptide (PTH/PTHrP) receptors (PPRs) [167], or through the conditional deletion of the bone morphogenetic protein 1a (BMP1a) receptor [168] in the BM. This indicates that PTH and BMP signaling influence the number of HSCs by regulating the niche size. In addition, the deletion of osteoblastic cells in a transgenic mouse model results in a 3- to 10-fold decrease in primitive hematopoietic cells [169].

Contrary to these studies, other data revealed that OBs are not essential for the function of stem cells. One report showed that biglycan-deficient mice have reduced OBs but no alteration in the numbers of HSCs [170] and the increase of OBs by strontium chloride exposure did not lead to an increase in HSC numbers in mice [171]. A possible explanation for the discrepancy between these studies could be the use of different mouse models or the heterogeneity of OB differentiation stages. It is possible that only a small subpopulation of OBs with a certain degree of differentiation is influencing hematopoiesis and the different OB subtypes have a differential sensitivity to biglycan or strontium.

However, there are several reports indicating that molecules expressed on or secreted from OBs are involved in HSC regulation. Most controversially discussed is the function of N-cadherin in the regulation of HSCs [170,172]. On the one hand, use of 5-bromo-2'-deoxyuridine (BrdU) label-retaining assays indicated that label-retaining, slow-cycling HSCs localized near a specialized subpopulation of OBs expressing N-cadherin, spindle-shaped N-cadherin^{+} osteoblastic (SNO) cells. HSCs also express N-cadherin on their surface, where it interacts and forms a homophilic adhesion complex with β-catenin [171,166][168,173]. Furthermore, transient knock-down of N-cadherin increased cell division of HSPCs in *in vitro* experiments and inhibited long-term engraftment of HSPCs after transplantation [174]. Contrary to these findings, it was not possible to detect N-cadherin by using two commercially available antibodies or by using a N-cadherin$^{lacZ/+}$ gene trap mouse [170]. The same group further showed that the conditional deletion of N-cadherin in hematopoietic cells using the Mx1-Cre^{+}N-cadherin$^{fl/+}$ mouse model did not lead to reduced HSC frequencies. They also observed no defects in the engraftment of HSCs isolated from Mx1-Cre^{+}N-cadherin$^{fl/+}$ mice after N-cadherin deletion [175]. According to these conflicting findings, it is still not clear if N-cadherin plays a critical role in HSC regulation.

Further, it was shown by transplantation experiments with HSCs into tm-SCF deficient mice that the interaction of transmembrane-stem cell factor (tm-SCF), also termed membrane-bound kit ligand (mKL) and its specific receptor c-kit on HSCs are essential for HSCs localization into the endosteal niche [176].

OBs also secrete several factors that are important for the regulation of HSCs in the endosteal niche. The interaction between angiopoietin-1 (Ang-1) expressed on OBs can induce HSC quiescence through the interaction with its specific receptor Tie2 (tyrosine kinase with immunoglobulin-like and EGF-like domains 2) on HSCs and enhance the long-term repopulation capacity of HSCs *in vivo* [177]. The cytokine thrombopoietin (TPO), which is also released from OBs, binds to the myeloproliferative leukemia virus oncogene (MPL)

receptor on HSCs and thereby positively regulates HSC quiescence and survival. HSCs lacking MPL exhaust with time due to overproliferation and loss of quiescence. In addition, blocking of TPO signaling in OBs leads to a reduction of quiescent HSCs, while exogenous TPO inhibits HSC proliferation [178].

The interaction between CXCR4 on HSCs and CXCL12, which is manly secreted from stroma cells in the vascular niche, but also at lower amounts by OBs, is essential for the localization, retention and quiescence of HSCs in the niche [164]. Furthermore, the fibroblast growth factor-1 (FGF-1) secreted by niche cells is involved in the regulation of HSCs by promoting stem cell self-renewal and expansion [179] through FGFR1-4 mediated activation of several signaling pathways such as the mitogen-activated protein kinase (MAPK) pathway, STATs (signal transducer and activator of transcription) and PI3K [180].

Additionally, the ECM molecule osteopontin (OPN) is also produced by OBs. HSCs can interact with OPN through CD44 and β1 integrins and thereby are retained in the endosteal niche. This interaction is suggested to further enhance HSC quiescence as it negatively regulates proliferation and differentiation of HSCs, which was shown by markedly enhanced cycling of HSCs in $Opn^{-/-}$ mice [181]. Another important regulatory factor for HSC in the endosteal niche are extracellular calcium ions (Ca^{2+}), which can be sensed by HSCs through the calcium receptor (CaR). The expression of the CaR on HSCs is important for their localization in the endosteum, probably by regulating the interaction of HSCs with collagen I, as CaR null mice show a defective homing of HSCs to the endosteal niche and reduced *in vivo* long-term engraftment capacity [182]. The MUC-1 mucin can initiate calcium signaling through binding to ICAM-1 [183] and could therefore also play a role in the interaction between HSCs and their niche.

Various cell types other than OBs located in the endosteal niche have also been shown to play a role in HSCs regulation. For example, stimulation of OCLs with receptor activator of nuclear factor kappa B ligand (RANKL) mobilizes HSCs into the PB [136]. However, more recent data indicate that the influence of OCLs on HSCs must be rather indirect, by influencing other niche components such as OBs, as RANKL-deficient mice showed no increased mobilization of HSCs [184]. Furthermore, a specialized group of $F4/80^{+}$ macrophages, termed osteomacs, are located in the endosteal region. Deletion of osteomacs reduced the number of OBs and induced mobilization of HSCs into the PB [185]. Megakaryocytes might also have an indirect influence on HSCs by regulating the development of OBs within the endosteal niche [186]. Adipocytes, located in the endosteal niche, seem to have a negative influence on the HSC function and maintenance [187]. Finally,

input from the SNS influences OBs and seems to be required for HSC attraction to the endosteal niche [141].

The identification of the "SLAM code" (signaling lymphocytic activation molecule) [45,188], which combines the use of antibodies against CD150 (SLAMF1) and CD48 together with commonly used antibodies for the identification of HSCs (described in section 6.4), as novel HSC marker revealed that around 70% of $CD150^{+}CD48^{-}$ HSCs are located to or within 5 cell diameters from endothelial or perivascular cells [188]. This was the first proof for the existence of the vascular niche as supportive microenvironment next to the previously described endosteal niche. Several cell types including perivascular mesenchymal stem cells (MSCs), especially $nestin^{+}$ MSCs, CXCL12-abundant reticular cells (CAR cells) and neuronal cells are essential for the regulation of HSCs in the perivascular space [189-192]. MSCs are thought to give rise to different niche cell types such as OBs, chondrocytes, adipocytes, fibroblasts, and endothelial cells, but are also directly involved in HSC regulation [168,193]. $Nestin^{+}$ MSCs are strictly perivascular but are also found in the endosteum, albeit at lower frequencies and therefore, could also influence the regulation of HSCs in the endosteal niche. $Nestin^{+}$ MSCs express HSC maintenance factors such as CXCL12, SCF, Ang-1, IL-7, VCAM-1 or OPN. Depletion of $Nestin^{+}$ MSCs in mice resulted in a reduced number of HSCs in the BM and also in a diminished homing efficiency of wt HSCs into the BM [189]. CAR cells are found close to sinusoids in the BM and express CD44, VCAM-1, platelet-derived growth factor receptor (PDGFR)-α and PDGFR-β, and secrete SCF and CXCL12. Furthermore, CAR cells can also differentiate into OBs and adipocytes [191]. It is hypothesized that CAR cells regulate the proliferation of HSCs rather than their quiescence as deletion of CAR cells in a mouse model led to a decreased total number of HSCs by reducing the number of cycling HSCs as well as cycling lymphoid and erythroid progenitors [191,192]. It has been shown that not only the stroma cells surrounding the vasculature, but also the BM sinusoidal endothelial cells themselves influence HSCs [194]. Therefore, some reports distinguish a perivascular niche from a pure vascular niche. Recently, it has been shown that the nonmyelinating Schwann glial cells located in the vascular niche are important for HSC quiescence by regulating the activation of latent TGF-β that is critical for the TGF-β/Smad signaling in HSC maintenance [190]. Not only the direct influence from niche components on HSCs is essential for their regulation, but also the crosstalk between different niche cells is important for the regulatory properties of the entire niche: it was shown that $CD169^{+}$ macrophages regulate CXCL12 levels and cross talk with $nestin^{+}$ niche cells promoting the retention of HSCs in the niche [195].

The contradictions within the literature regarding differential functions of the vascular and endosteal niche indicate that the models based on anatomically separated niches are not able to fully explain the complex regulatory influences of the environment on HSCs. Rather, the available data today indicate that a single HSC receives input from multiple, distinct niche cell types at different location at different stages of development and that HSCs may even be able to move quite readily between these locations. Recent real-time 3-dimensional (3D) imaging studies indicated that HSCs reside in a complex meshwork with both vascular and mesenchymal components of the BM indicating that the vascular and endosteal niche components are intimately entwined within trabecular bone, being in a close relationship rather than mutually exclusive [196,197]. However, it seems that the interplay between the vascular and endosteal niche will remain a point of intensive discussion, at least for the near future [165].

Furthermore, it is well accepted that in addition to cell-cell contacts also the interaction with ECM components associated with either niche type regulates HSC functions. ECM proteins secreted from stroma cells build up a 3D network, which includes the above-mentioned OPN and in addition fibronectins, laminins, collagen types I, III, and IV, vitronectin, thrompospondin, hemonectin, hyaluronic acid, and various proteoglycans. Several of these proteins are located in distinct areas of the BM intersitium [198], which is an indication that they might have different regulatory effects for HSCs during homing and lodgment. However, most of the data showing a role of ECM proteins in HSC regulation are based on *in vitro* co-culture experiments with HSC and stroma cells after elution of the BM, which have the disadvantage that they only weakly reflect the complex structure of the BM intersitium. One study showed that the adhesion of HSPCs to fibronectin varied with the cell lineage and the maturation stage of the cells [199]. Further it was shown that the disruption of the interaction between α5β1 and fibronectin results in a decreased engraftment into the BM [200]. Transplantation experiments with HSCs, which were prior treated with hyaluronidase to remove the hyaluronic acid, resulted in alteration in HSC lodgment at the endosteum arguing for a regulatory function of hyaluronic acid, which was further confirmed in *in vitro* experiments [201]. As it is not possible for most ECM components to remove them from the BM *in vivo*, little is known about the function of different ECM proteins on the regulation of HSC quiescence or long-term maintenance.

The niche also protects HSCs from damage by reactive oxygen species, which is important for their long-term survival and repopulation potential [202,203]. It is suggested that the BM intersitium is hypoxic (low oxygen levels) due to low blood perfusion [204]. According to

this theory, the localization of LT-HSCs in hypoxic regions was investigated by their distribution between areas with lower or higher blood perfusion measured with the fluorescent dye Ho after injection into mice. After a certain period of time, cells next to the vasculature with a high blood perfusion, were more stained with Ho than cells in regions with poor blood perfusion. Transplantation experiments into lethally irradiated mice were performed to investigate the properties of HSCs with low or high Ho signal. The results indicated that cells with lowest Ho uptake inferred to be hypoxic had the highest long-term repopulation potential [205]. These and other reports argue that quiescent HSCs are predominantly located in areas containing hypoxic sinusoids within the endosteum [206,207].

The BM niche also expresses several developmental factors, which are important for the regulation of HSC self-renewal, such as components of the Smad, Wnt, sonic hedgehog (Shh), and Notch pathways [208]. The Smad signaling pathway transduces signals from receptor complexes activated by ligands of the TGF-β superfamily, including TGF-β itself, activins, nodal and BMPs. Both, HSCs and niche cells secrete TGF-β. *In vitro* experiments showed that TGF-β is a potent inhibitor of HSPCs proliferation [209]. However, whether TGF-β is a regulator of HSC quiescence under physiological *in vivo* conditions is unclear, as there is an apparent discrepancy between *in vitro* and *in vivo* data. Studies inducing a conditional deletion of TGF-β type I or II receptors using a Mx1-Cre driver line showed no effect on HSPC numbers, their cell-cycle distribution or self-renewal properties [210-212], indicating that TGF-β signaling is not important for the maintenance of HSC quiescence *in vivo*. Furthermore, BMP-4 had no effect on the proliferation of purified murine HSCs [213]. On the other hand, *in vivo* experiments with a conditional deletion of the intracellular mediator Smad 4 impaired the self-renewal properties of HSPCs [214], which was not observed in TGF-β type I or II receptor knock-out mice. This argues for the existence of other ligands and receptors important for the HSC regulation that induce the Smad pathway.

In vitro treatment of HSPCs with Wnt ligands led to their expansion and maintained their immature phenotype [215] indicating that the Wnt/β-catenin pathway is important for HSC maintenance and self-renewal. Wnt signaling can be mediated via a β-catenin-dependent (canonical) pathway or β-catenin-independent (non-canonical) pathway. In HSCs the canonical Wnt pathway mediates the majority of Wnt signaling. Wnt ligands are secreted from niche cells and interact with a receptor complex on HSCs, wich consists of Frizzled (Frz) and two co-receptors, low-density lipoprotein-receptor-related protein 5/6 (Lrp5/6), leading to the stabilization and nuclear transolcation of β-catenin, where it binds the transcription factor (Tcf) and Lymphoid enhancer-binding factor (Lef) to induce the

transcription of target genes such as cyclinD1 and c-Myc. Data from *in vivo* experiments are less clear regarding the role of Wnt signaling for HSC regulation. Constitutive active nuclear β-catenin signaling activated HSCs, increased their proliferation and blocked their differentiation leading to HSC exhaustion [216,217]. More recently it was shown that non-canonical Wnt signaling through the interaction between Flamingo and Frz 8 on HSCs occuring in close proximity to N-cadherin^{+} OBs is important for the maintenance of HSC quiescence [218]. Furthermore, the overexpression of the Wnt-inhibitor Dickkopf-1 (Dkk1) in OBs results in a increased proliferation and reduced *in vivo* repopulating ability of HSCs [219] indicating that Wnt signaling in the niche is crucial to maintain HSC quiescence. These reports argue that the fine-tuning of Wnt/β-catenin activity can have different (positive as well as negative) effects on the maintenance of HSC long-term quiescence [220]. In contrast, there are reports showing in *in vivo* experiments that Wnt signaling is dispensable for adult HSC homeostasis, as conditional deletion of β-catenin or both β-catenin and its homolog γ-catenin in hematopoietic cells failed to affect HSC numbers, their self-renewal or engraftment potential [221,222]. These discrepancies make it difficult to value the importance of the Wnt signaling pathway for the *in vivo* regulation of HSCs.

The importance of the Notch signaling pathway for HSC maintenance is also controversial. First indications that the Notch pathway has a regulatory influence in the development of the hematopoietic system came from mice in which Notch-1, the ligand Jagged-1 or the coactivator protein C-promoter-Binding-Factor-1 (CBF-1) were deleted. The mutant mice had defects in embryonic HSC development [223-225]. It has also been shown that Notch signaling is involved in the regulation of the adult hematopoiesis. In several different *in vitro* experimental settings it was shown that induction of the Notch signaling pathway leads to an expansion of HSPCs [226-228]. The importance of Notch for the maintenance of undifferentiated HSPCs was further supported by *in vivo* data showing that activation of the Notch pathway increases HSC activity and is required for the increased self-renewal upon Wnt activation [229]. Furthermore, expression of activated Notch in HSPCs resulted in enhanced HSC self-renewal and decreased differentiation in recipient mice [230]. In contrast, another report showed that conditional deletion of Jagged-1 alone or together with Notch-1 in hematopoietic cells and/or BM stromal cells had no effect on HSC regulation in mice [231]. Also experiments with mice expressing dominant-negative forms of Notch signaling inhibiting Mastermind-like1 (MAML-1) and CBF-1in hematopoietic cells had no influence on HSC frequency, total numbers or function [232]. Altogether these results postulate a

debatable role of the Notch signaling pathway in the maintenance of adult HSCs by limiting their proliferation and differentiation.

Also the data about Shh signaling for HSCs is controversial. While HSCs cultured *in vitro* with Shh promotes their proliferation [233], *in vivo* data are contradictory. Deletion of the receptor Smoothened (Smo), which is a key signal transducer in the hedgehog signaling pathway, had no defects on the lineage differentiation of HSCs but reduced their reconstitution potential in serial transplantations [234,235]. Deletion of the transcription factors Glioblastoma-1 (Gli-1) increased the HSC pool [236] and decreased expression of the hedgehog receptor Patched (Ptch1) in mice also results in increased numbers of HSPCs due to elevated proliferation and led to a higher short-term but lower long-term reconstitution potential of lin^- cells [237]. These results argue for a function of Shh signaling in maintaining HSC self-renewal but rate under conditions of hematopoietic stress such as serial transplantation than under homeostatic condition. Contrary to this finding, there are reports showing that Shh is not essential for the regulation of HSC maintenance as adult mice with a conditional deletion of Smo in hematopoietic cells had no defects in the HSC compartment during steady-state hematopoiesis, after transplantation, or after induction of hematopoietic stress with a 5-FU treatment [238,239].

The extrinsic cues essential for the regulation of the HSC homeostasis are highly complex and require a bidirectional communication between the HSCs and niche components. The junction between a HSC and its niche cells can also be compared to the complex and tightly regulated processes taking place at a neuronal or immunological synapse. Therefore, in some reports this adhesion and signaling unit is also termed stem-cell–niche synapse [240]. Figure 17 summarizes the most important ligand-receptor interactions between HSCs and niche cells.

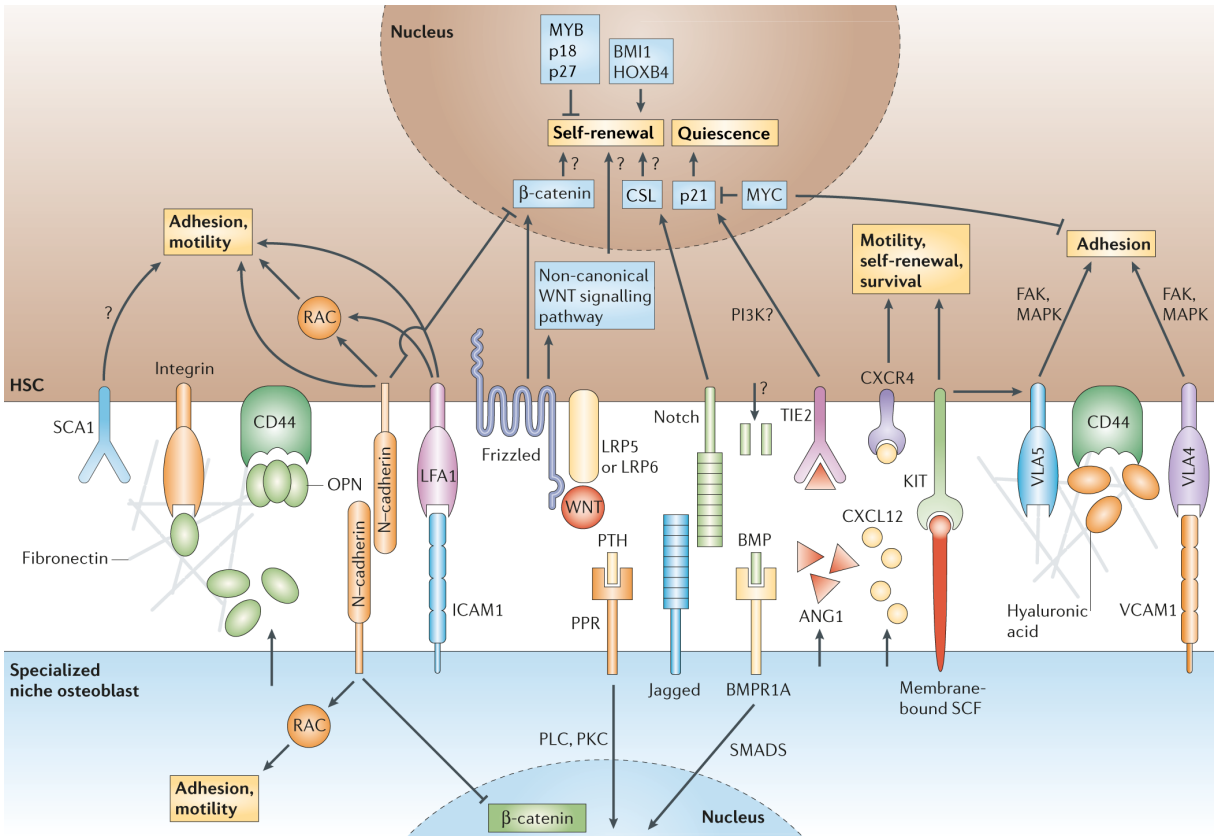

Figure 17: Model of the interaction processes between a HSC and a niche OB

Shown are the most important ligand–receptor interactions, adhesion molecules, soluble cytokines and growth factors as well as signaling pathways, which have been postulated to play a role in the regulation of HSC maintenance by a delicate balance between HSC self-renewal and differentiation. The complexity of the interaction between the HSC and niche cells underlines how important a precise localization with a certain distance to the niche components is for correctly responding to the signals from the niche. It is important to note that the interactions are bidirectional indicating that HSCs can also modulate their microenvironment. For details see the main text (adapted from Wilson et al., 2006).

Regarding this complexity within the stem cell niche it is easily conceivable that the precise positioning of the HSC within the niche is absolutely critical for correct interactions with membrane bound ligands as well as exposure to certain thresholds and gradients of soluble regulatory factors released from niche cells. HSCs express a wide variety of adhesion molecules mediating not only the homing and lodgment of HSCs after transplantation but also by indirectly mediating HSC homeostasis via positioning HSCs in the niche and by directly mediating regulatory signaling pathways. The most important adhesion molecules on HSCs are therefore discussed in the next section.

6.8. Adhesion Molecules on HSCs

To secure an orderly progression of hematopoiesis a tightly coordinated interaction between HSPC and their surrounding microenvironment is absolutely essential. Therefore, HSPCs express a wide variety of adhesion molecules, which mediate cell-cell and cell-ECM interactions required for their homing into the BM interstitium and residence in the BM niche. They further play an important role for HSC survival, death, specific gene expression, proliferation, differentiation and quiescence. Signaling pathways that are regulating HSPC behavior could be either activated directly by the adhesive interactions themselves or by modulating responses to cytokine- or growth factor-dependent signals [241-243]. Vice versa, cytokines and growth factors can modulate the adhesive interactions between HSPCs and their environment, thereby providing a further possibility to influence the hematopoietic system [244]. First evidence for a contact dependent inhibition of the HSPC proliferation came from *in vitro* experiments where $CD34^+$ HSCs were co-cultured with stroma cells. The proliferation of HSCs was inhibited when they were in direct contact with the stroma cells, whereas an increased proliferation occurred when the direct contact was prevented [241,245]. More than 20 different CAMs have been discovered on HSCPs [246] making it difficult to reveal the specific contribution of each single molecule on the regulation of HSPCs as an extensive crosstalk is known to occur between them. CAMs on HSPCs and their microenvironmental cells include members of the integrin family, CD44, selectins, cadherins, sialomucins and the immunoglobulingene superfamily, see figure 18.

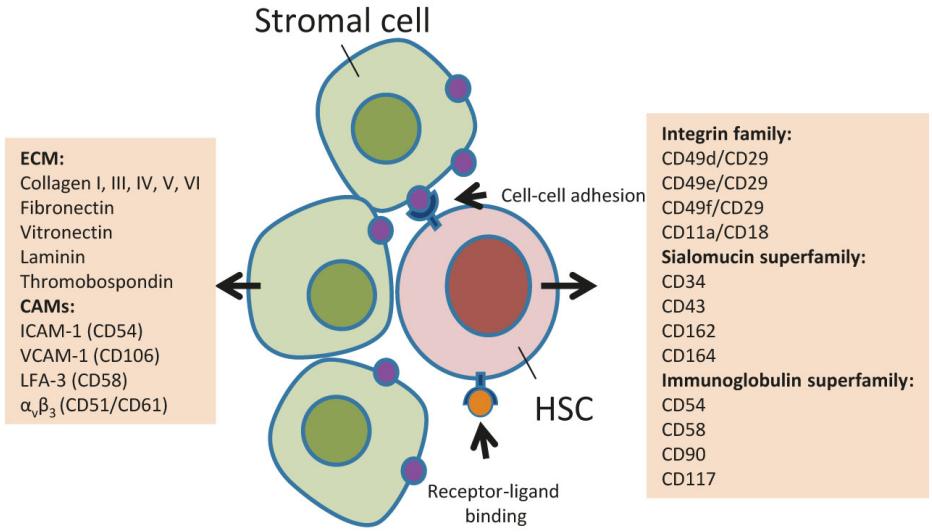

Figure 18: Cell adhesion molecules (CAMs) and ligands expressed on HSCs and stromal cells

$\alpha_4\beta_1$ (VLA-4, CD49d/CD29), $\alpha_5\beta_1$ (VLA-5, CD49e/CD29), $\alpha_6\beta_1$ (CD49f/CD29), $\alpha_L\beta_2$ (LFA-1, CD11a/CD18), Sialophorin (CD43), P-selectin glycoprotein ligand-1 (PSGL-1, CD162), Sialomucin core protein 24 (CD164), Thy-1 (CD90), c-kit (CD117) (modified from Lam et al., 2010) [247].

The classical cadherins namely E-, P-, VE- and N-cadherin are single-pass transmembrane glycoproteins and the major CAMs, mediating Ca^{2+}-dependent cell-cell adhesions in a homophilic manner. The expression pattern of the different cadherins is temporally and spatially restricted during development and in adult tissues. E- and P-cadherin are often co-expressed but they do not co-express with N-cadherin [173]. While the expression of N-cadherin on stromal cells e.g. OBs has been shown [168,218] the expression on adult HSCs as well as the contribution of N-cadherin for the development and maintenance of HSPCs is controversially discussed (see section 6.7) [170,172,173,175].

CD44 binds to hyaluronate and is expressed on almost all hematopoietic cells [248]. The receptor further cooperates with β1-integrins to promote adhesion of HPCs to fibronectin [249].

The family of selectins contains three proteins, E- (endothelial, CD62E), L- (leukocyte, CD62L) and P- (platelet, CD62P) selectins [250]. Selectins predominantly play an essential role in leukocyte trafficking, but there is also evidence that they are important for the homing of HSPCs into the BM. HSPCs express L-selectin [251] but L-selectin$^{-/-}$ mice have no obvious HSC defect [252]. Furthermore, E-selectin$^{-/-}$ and P-selectin$^{-/-}$ mice or different combination of double as well as the triple knock-out mice have no severe HSC phenotype [253,254].

In addition, ten different sialomucins have been found on HSPCs including the stem cell antigen CD34 [251], PSGL-1 [255], CD43 [256], CD164 [257] and CD45RA [258]. The sialomucins are involved in HSPC adhesion to the BM microenvironment thereby negatively regulating their proliferation and/or differentiation. CD34 was the first sialomucin described on HSPCs [259] and might play a role in HSPC adhesion [260]. CD34 deficient mice have a decreased number of HSPCs in the yolk sack and in fetal livers probably due to a premature differentiation [261]. PSGL-1 is the receptor for P-selectin on HSPCs and is involved in the adhesion of HSPCs to endothelial cells during processes such as homing into the BM [262]. In addition, CD164 might have a function during HSPC adhesion and homing, as this receptor is not only expressed on $CD34^+$ and BM stroma cells but also on the endothelium [263]. Engagement of CD164 on $CD34^+$ cells prevents the activation of quiescent HSCs after cytokine stimulation, an indication of a regulatory function for HSPC proliferation [264]. How sialomucin transmit their regulatory signals on HSPCs is not yet clear but additional signaling and/or adaptor proteins must be required as the cytoplasmic tails of sialomucins lack enzymatic activity [265].

HSPCs also express a wide variety of integrins including $\alpha_v\beta_3$, $\alpha_4\beta_1$, $\alpha_2\beta_1$, $\alpha_5\beta_1$, $\alpha_6\beta_1$, $\alpha_L\beta_2$, and $\alpha_9\beta_1$ [266]. An essential role in HSPCs homing to and migration through the BM interstitium

as well as HSPC retention in the BM niche, has been reported for β1 integrins, particularly $\alpha_4\beta_1$ and $\alpha_5\beta_1$, by several groups [111,200,267-270]. The importance of β1 integrins for the development of a normal hematopoietic system has been shown in β1 integrin deficient mice. By injection of β1-deficient ES cells into wt blastocysts it was possible to generate β1-deficient chimeric mice, in which β1-deficient hematopoietic progenitor cells were not able to colonize the fetal liver or to be retained in the fetal liver microenvironment [268]. Furthermore, it was shown that β1-deficient HSPCs were not able to engraft adult mice after irradiation, confirming the importance of β1 integrins for HSPC trafficking [269]. However, if β1 integrins are deleted in HSPCs after the engraftment was completed, no obvious defects in the hematopoietic system were observed under steady state conditions [271], which might be explained by the fact that under normal homeostasis other adhesion molecules, most likely further integrins, are sufficient to maintain normal hematopoiesis. The $\alpha_4\beta_1$ integrin on HSPCs mediates both cell-cell and cell-ECM interactions by binding to VCAM-1 on other cells or by binding to at least three distinct sites on FN [272,273], while $\alpha_5\beta_1$ only binds to the Arg-Gly-Asp-Ser (RGDS) binding domain of FN [274]. Disruption of the $\alpha_5\beta_1$ leads to reduced BM engraftment of HSCs [200]. Homing and engraftment defects were also demonstrated for α4 deficient HSPCs [110,267,275-277], but with reduced severity compared to β1-deficient cells. Furthermore, it was shown that α4-deficient HSPCs were differently located in the BM interstitium after homing compared to wt HSPCs [278], underlining the importance of integrins for a precise HSCs localization in the BM niche. Additionally, it has been shown in several reports that the interaction between β1 integrins and its ligands is important for the regulation of HSPCs mobilization into the PB [275,279-281].

High affinity states of integrins cannot only be transiently induced by direct ligand binding, a process called outside-in signaling (described in section 6.9.2) or by cross talk with activated receptors for cytokines and/or chemokines, a process called inside-out signaling (described in section 6.9.1). It has been shown that TPO, CXCL12, IL-3 and SCF all can activate $\alpha_4\beta_1$, leading to an increased adhesion of HSPCs to BM stroma cells [282].

The integrin-mediated interactions of HSCs with their environment are not only important for HSC localization but also for HSC proliferation, as β1 integrin mediated adhesion to stroma cells inhibits HSPCs proliferation [242,283]. This was also shown by several *in vivo* studies investigating signaling pathways important for maintaining HSC quiescence. For example, quiescence mediating signaling pathways such as Tie2/Ang-1 or MPL/TPO induce upregulation of β1 integrins on LT-HSCs, thereby leading to an increased adhesion of HSC on niche components [177,178]. Furthermore, c-Myc, which is important for controlling the

balance between HSC quiescence and proliferation, regulates the expression of integrins. Forced c-Myc expression in HSCs reduces the expression of integrins. Quiescent HSCs, therefore, express low levels of c-Myc and are retained in the niche by upregulation of integrins. Activated HSCs downregulate their integrin expression, due to increased c-Myc levels, resulting in the departure from the niche [284]. Also the interaction of $\alpha_4\beta_1$ and $\alpha_9\beta_1$ integrins on HSCs with thrombin-cleaved OPN (trOPN) within the endosteal region functions as a chemoattractant for HSCs and is important for the suppression of the HSC proliferation by regulating their lodgment into the BM niche after transplantation [181,285]. This was further confirmed by OPN-deficient mice, in which the lack of OPN results in an impaired retention of HSCs in the endosteal BM niche [266]. These findings indicate that regulation of hematopoiesis may be maintained by the combined effects of cytokines and chemokines together with contact mediated interactions.

There are also reports postulating that β2 and β3 integrins are expressed on HSCs. The interaction of β2 integrins with their specific ligand ICAM-1 might also be involved in mediating adhesion of HSC within the BM niche [286] and during HSPCs mobilization into the blood circulation [287,288]. The β3 integrin was discussed as a potential HSPC marker, as HSPCs with a SP phenotype (explained in section 6.4) also express higher amounts of β3 integrin. However, its function on HSPCs is not clear [289].

Like most adhesion receptors, integrins do not have an intrinsic catalytic activity; therefore recruitment of non-receptor kinases is necessary for the activation of signaling pathways [290]. For signal transduction integrins activate focal adhesion kinase (FAK) or the related PYK-2 [291], which activate adaptor proteins containing a Src-homology domain (SH)-2 and SH-3, thereby activating the PI3K pathway and/or the Ras/MAPK pathway [292]. Both signaling pathways regulate cell growth, proliferation, differentiation and survival. How sialomucins, CD44 and selectins mediate signaling is not that well understood.

6.9. Integrin Structure and Function

Integrins are receptors with dual function mediating both adhesion (cell-cell or cell-matrix adhesion) and signaling, thus enabling the cell to bind and respond to the environment. They are heterodimeric type I transmembrane glycoproteins consisting of non-covalently associated α and β subunits [293]. The integrin protein family is evolutionary highly conserved from sponges to mammals [294]. In mammals there are 18 different α and 8 β subunits, which form at least 24 functional αβ heterodimers [293], see figure 19. Integrins can be grouped in four major classes by their ligand binding properties although there is a significant overlap in

binding e.g. the same ligand can be recognized by several different integrin heterodimers and one integrin heterodimer can bind several different ligands (figure 19) [295]. An additional level of complexity arises from different splice isoformes and distinct developmental and tissue expression profiles [295,296]. For example, the β1D isoform is expressed in muscle and heart, while β1A isoform is expressed in remaining tissues. Therefore, deletion of β1A in mice cannot be compensated by expression of β1D isoform [297].

The name integrins refers to their imminent role in maintaining the cytoskeletal-ECM integrity [298,299]. All integrins link ECM to the actin cytoskeleton with exception of α6β4, which connects ECM to intermediate filaments. Integrins provide a bidirectional connection across the cell membrane thereby linking the cell interior with the extracellular environment. Upon ligand binding integrins can transduce a variety of signaling events to regulate numerous cellular processes such as adhesion, proliferation, survival, apoptosis, cell shape, polarity, motility, gene expression, and differentiation, most of which depends on the ability of integrins to modulate the cytoskeleton [300].

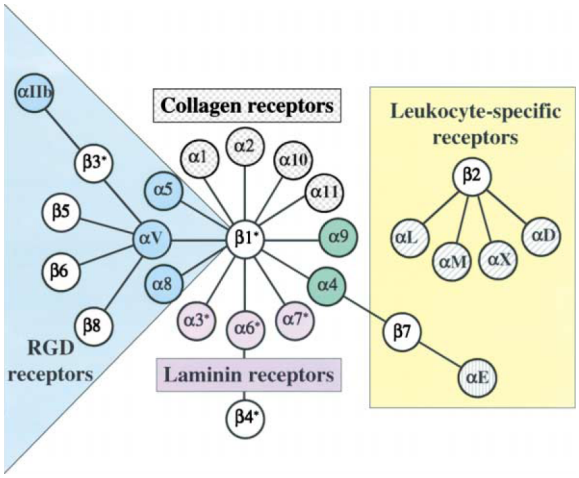

Figure 19: The integrin family

Indicated are 18 α and 8 β subunits that are able to form 24 different integrin heterodimers known to be expressed in mammals. Highlighted are ligands specific for certain integrin subgroups (adapted from Hynes, 2002).

The function of integrins is tightly related to their structure. Each subunit is a type I transmembrane protein with an extracellular domain, consisting of 700 to 900 amino acids, a single transmembrane helix and a cytoplasmic domain, containing 10 to 70 amino acids. The exception is β4 integrin with a 1074 amino acids long cytoplasmic tail [301]. In an inactive heterodimer the α-β subunits are connected via hydrophobic and electrostatic interactions formed between the KπGFFKR sequence (π standing for a conserved apolar amino acid) in the α and the HDR(R/K)E motif in the β subunit [302,303]. It has been postulated that the

arginine residue in the α subunits and the aspartate residue in the β subunits form a salt bridge, at least in some heterodimers [304,305].

The cytoplasmic domain of integrins lacks enzymatic activity as well as actin binding motifs and therefore, depends on the binding of other molecules to mediate processes such as signal transduction and/or coupling to the cytoskeleton. The cytoplasimc tail of the β subunit contains two NPxY motifs, which are part of a canonical recognition sequence for phosphotyrosine-binding (PTB) domains, present in a large number of proteins [306].

Most of our structural knowledge about the transmembrane domains of integrins comes from studies of αIIbβ3 integrin [307]. The β3 transmembrane domain forms a 30 amino acid long α helix, which is longer than the average thickness of membrane lipid bilayer suggesting that this structure is tilted within the membrane. The αIIb transmembrane domain forms a 24 amino acids long α helix followed by a backbone reversal and therefore, does not display the tilt within the membrane [308].

The extracellular domains of α and β subunits in a heterodimer adopt a head on a stalk conformation (figure 20). The αvβ3 and αIIbβ3 crystal structures have been analyzed and serve as a model for other integrin heterodimers [307], however it is not clear if this structure indeed applies to other integrin heterodimers. The extracellular domain of the β subunit is composed of a βA (also named βI) domain inserted into an immunoglobulin (Ig)-like “hybrid” domain, a N-terminal PSI (plexin, semaphorins and integrin) domain, four tandem cysteine-rich EGF-like repeats and a β tail domain (β-TD) with a disulfide bond connecting the PSI and distal EGF domain (figure 20) [293,301]. The extracellular domain of α subunit contains an N-terminal seven bladed propeller domain followed by an Ig-like (thigh) domain, a genu domain, which is a short disulfide-bonded loop with a Ca^{2+}-binding site at which the head-piece folds over its leg when the integrin turns in its bent, inactive conformation (mechanism described below) and two β sandwich domains (calf 1 and calf 2) (figure 20).

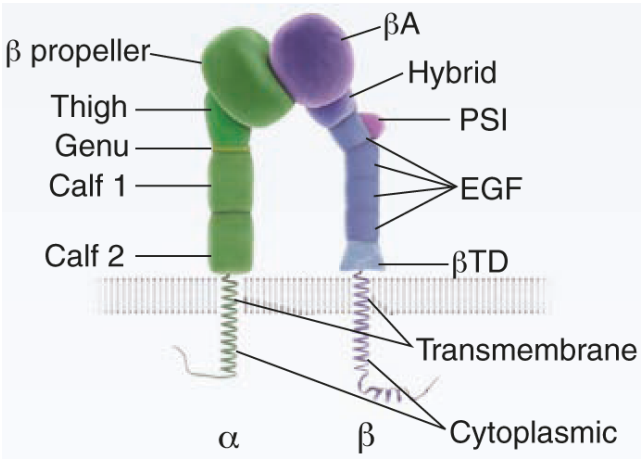

Figure 20: Model of an integrin heterodimer with the different sub-domains

Integrin heterodimer in its activated, extended conformation. The α subunit is shown in green and the β subunit in violet. A detailed description of the different sub-domains is in the main text (modified from Moser et al., 2009).

The head domain represents the ligand binding part of the heterodimer with the extracellular domain of the α subunit determining the ligand specificity of the integrin. The ligand-binding pocket lies at the interface between the β propeller and the βA domain. The interaction of integrins with their ligands also depends on the binding of divalent cations. The head of the α chain contains a Ca^{2+}-binding β-propeller domain. Several heads of α subunits have an inserted domain (I-domain) [309], which has a metal ion-dependent adhesion site (MIDAS) coordinating the binding of magnesium ions (Mg^{2+}) and thereby controlling the ligand binding [310]. The binding of ligands in the head of the β chains is mediated by three binding sites in the βA domain, containing a central Mg^{2+} binding MIDAS flanked by two Ca^{2+} sites termed synergistic metal ion binding site (SyMBS) and adjacent to MIDAS (AdMIDAS), respectively [311].

Unlike most other transmembrane molecules integrins have the ability to transduce signals bidirectionaly across the plasma membrane, meaning from the extracellular environment into the cell (called outside-in signaling) and vice versa, from the intracellular compartment to the cell surface (called inside-out signaling). Both processes are described in the following sections.

6.9.1. Inside-out signaling

Integrins exist in different conformations. Depending on their activation, integrins can assume the low (bent conformation of the extracellular domains), intermediate and high affinity state (extended conformation), for ligand binding, see figure 21.

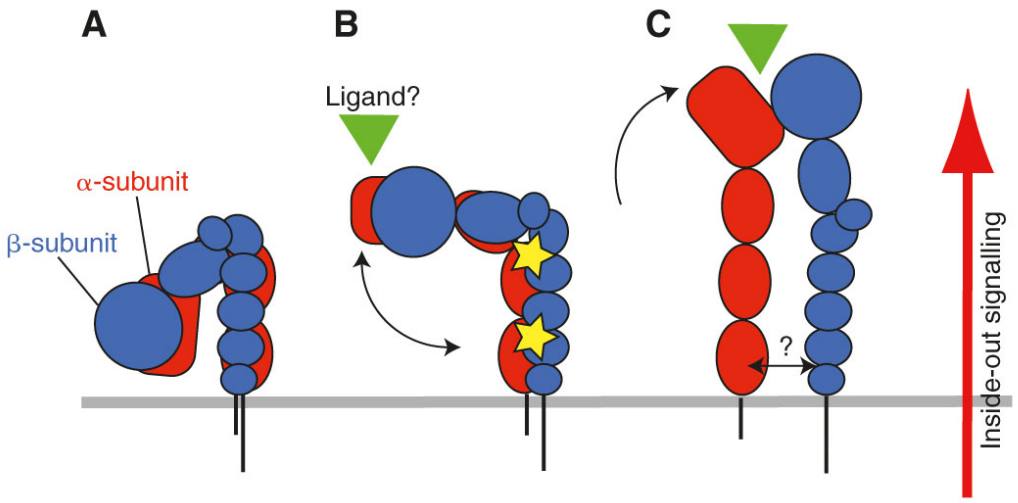

Figure 21: Model of conformational changes during integrin activation

A) The bent conformation of the inactive integrin, in which the α and β extracellular, the transmembrane and cytoplasmic domains are tightly associated. B) The "primed" conformation in which the relaxation in the legs leads to an exposure of epitopes for stimulatory antibodies (yellow stars). The head-piece is still closed but a small outward movement of the hybrid domains might bring the ligand-binding pocket in a conformation necessary to achieve the high-affinity conformation in the next step. C) High affinity, ligand bound conformation with an opened head-piece and separated legs. Green triangle represents the ligand (modified from Askari et al., 2009) [312].

The process of integrin activation occurs through inside-out signaling. It requires the binding of intracellular proteins to the integrin tail, thereby transducing signals to the cell surface through conformational changes within the integrins.

The enormous relevance for a precise regulation of the integrin activation becomes clear if one focuses on integrins expressed on hematopoietic cells. For example leukocytes have to extravasate the blood circulation to migrate towards the inflammatory side in the case of an inflammation. For this process the precise and tight regulation of integrin activation is essential, as defects can lead to severe diseases such as leukocyte adhesion deficiency (LAD). Also HSCs critically depend on integrin activation for the extravasation from blood vessels, homing and BM retention. Alteration in the integrin activation on HSCs can result in hematopoietic defects leading to pancytopenia. Most extensively studied is integrin activation on platelets, which express αIIbβ3 integrin that mediate their aggregation to seal injured blood vessels. Activation defects can prevent platelet aggregation leading to extensive bleedings, while hyper-activation results in pathological platelet aggregation, which can lead to arterial thrombosis and finally cause heart attacks or stroke [313].

Activation of platelets upon vascular injury is driven by signaling events that are triggered by insoluble proteins such as collagen and von Willdebrand factor and soluble factors such as adenosine diphosphate (ADP), thrombin and thromboxane A2 [314]. These factors activate G-protein coupled receptors (GPCRs) or the collagen receptor glycoprotein VI (GPVI), a non-GPCRs, leading to the activation of PLC, which hydrolyzes phosphatidylinositol resulting in the production of the secondary messengers inositoltrisphosphate (IP3) and diacylglycerol (DAG). Consequently, IP3 causes increase of cytoplasmic Ca^{2+}, and DAG activates the protein kinase-C (PKC) and the Rap guanine nucleotide exchange factor (Rap-GEF), a Ca^{2+} and DAG-dependent GEF (Cal-DAG-GEF) for Ras-like small GTPases such as Rap1 [314]. Activated Rap 1, in turn binds to its effector Rap1-interacting adapter molecule (RIAM) allowing its interaction with talin, thereby unmasking talin's integrin binding site and allowing integrin activation, see figure 22 [315]. In addition to talin it has also been shown that kindlin-3 binds β1, β2 and β3 integrin tails and is critically involved in integrin activation, further discussed below [316,317]. It is unclear, however, how kindlin-3 is activated.

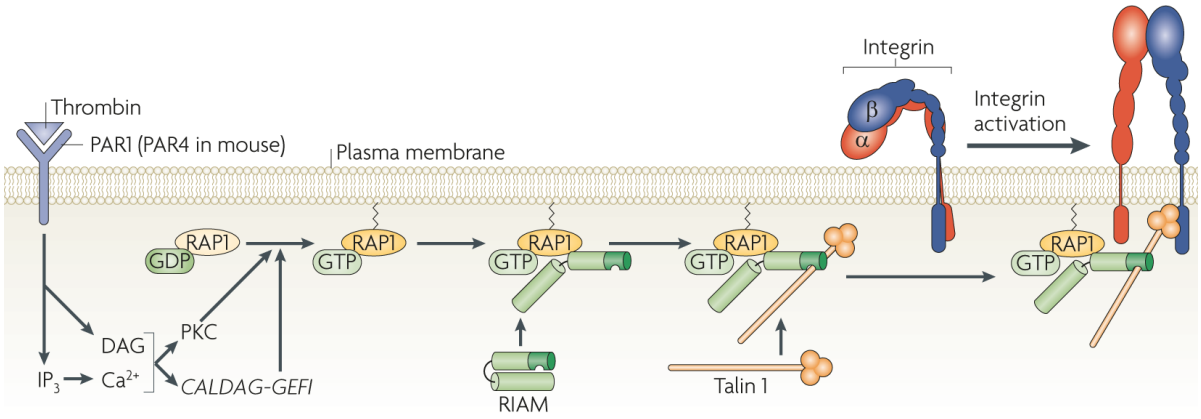

Figure 22: Connection between agonist stimulation (e.g. thrombin binding) and αIIbβ3 activation

Thrombin binding to its receptor leads to phospholipid hydrolysis resulting in the generation of IP_3 and DAG. IP3 causes an increased level of Ca^{2+} in the cytosol, which together with activated protein kinase C (PKC) isoforms activates Rap1 guanine a Ca^{2+} and DAG-dependent GEF (Cal-DAG-GEF). The Cal-DAG-GEF complex converts the GDP-bound form of Rap1 into the active GTP-bound form. Active Rap1 recruits RIAM and talin to the plasma membrane. Unmasking the integrin binding site in the F3 domain of talin enables talin to bind to the β3 integrin tail, leading to integrin activation (adapted from Shattil et al., 2010) [318].

In other cell types such as lymphocytes, chemokines can trigger additional signaling pathways that involve activation of PI3K and small GTPases, RhoA and most likely Rac1, which in turn trigger downstream PtdIns(4,5)P2 and activate kinases such as phosphatidylinositol-4-phosphate 5-kinase (PIPKI). This in turn leads to local increase of

PtdIns(4,5)P2 and activation of talin [319]. A schematic drawing of activation and binding of talin to the β integrin tail is shown in figure 23.

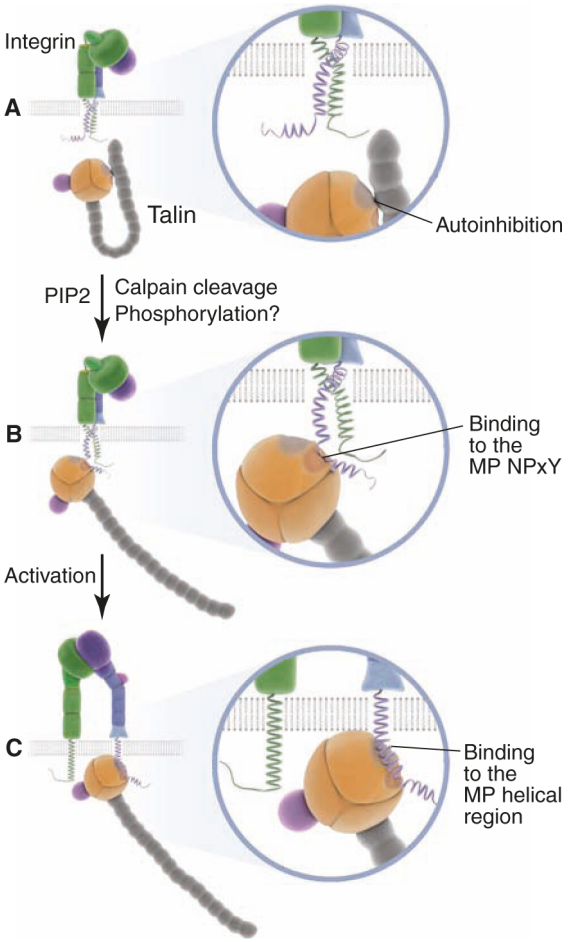

Figure 23: Talin-mediated activation of integrins

A) In an unstimulated cell (e.g. platelets), talin is predominantly localized to the cytoplasm [320] in an autoinhibitory conformation, in which the integrin-binding domain within the head is blocked by its own C-terminal rod [321,322]. B) Signaling via PtdIns(4,5)P2 abrogates the autoinhibition, recruiting talin to the plasma membrane where it binds with its F3 subdomain to the NPxY motive in the β integrin tail. C) Thereafter a talin-specific loop in the F3 subdomain binds a membrane proximal (MP) α helix in the β integrin tail, leading to the separation of the α and β integrin cytoplasmic tails and finally resulting in the active integrin conformation (adapted from Moser et al., 2009).

Next to kindlins, talin is considered a major activator of integrins [323]. It is a cytoskeleton-associated protein present in two isoforms, talin-1 and talin-2 in humans and mice [324]. Functional talin is structured as an antiparallel homodimer of two 270 kDa proteins. Each protein consists of a N-terminal, globular FERM (4.1, ezrin, radixin, moesin) domain and a C-terminal rod with several helical bundles, containing multiple vinculin binding sites, a second integrin-binding site and an F-actin binding site [324]. The FERM domain consists of three subdomains, known as F1, F2 and F3. The F3 subdomain harbors a

PTB motif essential for binding to the cytoplasmic tail of the β integrin subunits, see figure 24.

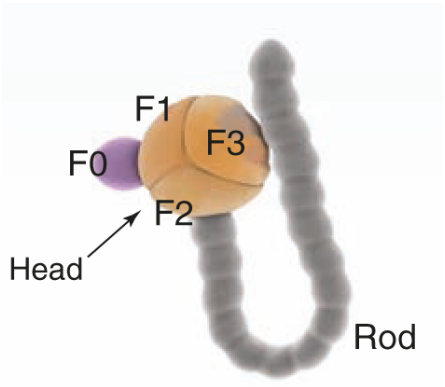

Figure 24: Structural model of talin

The head contains a FERM (4.1, ezrin, radixin, moesin) domain with three subdomains (F1, F2, and F3) and a F0 subdomain (adapted from Moser et al., 2009).

Talin binds the integrin β tail at the membrane-proximal NPxY motif, see figure 25, which allows electrostatic interaction between the positively charged F3 subunit and the polar head groups of lipids in the plasma membrane.

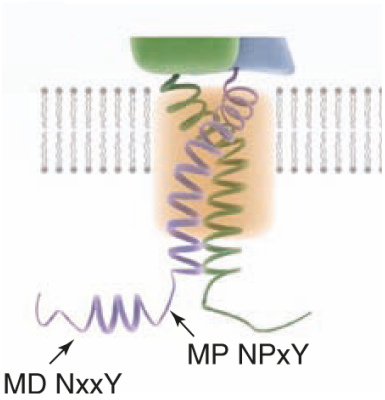

Figure 25: The cytoplasmic tails of α and β integrin subunits

The transmembrane and membrane proximal cytoplasmic domains of the α and β subunits. Indicated are the membrane distal (MD) NxxY and proximal (MP) NPxY binding motifs (modified from Moser et al., 2009).

Binding of talin to both, the membrane proximal and membrane distal NPxY motifs is necessary for integrin tail separation [304,305]. In addition to actin and vinculin binding sites, the talin rod domain contains another integrin binding motif possibly involved in integrin clustering [325] as it has been shown that full length talin is required for the connection of integrins to the cytoskeleton and integrin clustering [326].

However, talin is not the only integrin activator. It was shown that also the kindlin family of proteins is also necessary for this process [316]. A series of *in vivo* and *in vitro* experiments

showed that the conformational shift from the low- to the high-affinity state was only possible in the presence of kindlins [316,327-329]. In contrast to talin, kindlins bind to the distal NxxY motif of β1, β2 and β3 integrin tails (figure 25). In addition, kindlins bind serine/threonine motif, located between two NxxY patches. The integrin interaction site within the kindlin sequence has been mapped in the F3 subdomain of the FERM domain, as the substitution of particular glutamate and tryptophan residues with alanine prevents integrin binding and activation [316,330]. A scheme illustrating the recruitment of kindlin to the β integrin tail is shown in figure 26. For a precise description of the kindlin structure, see section 6.10.1.

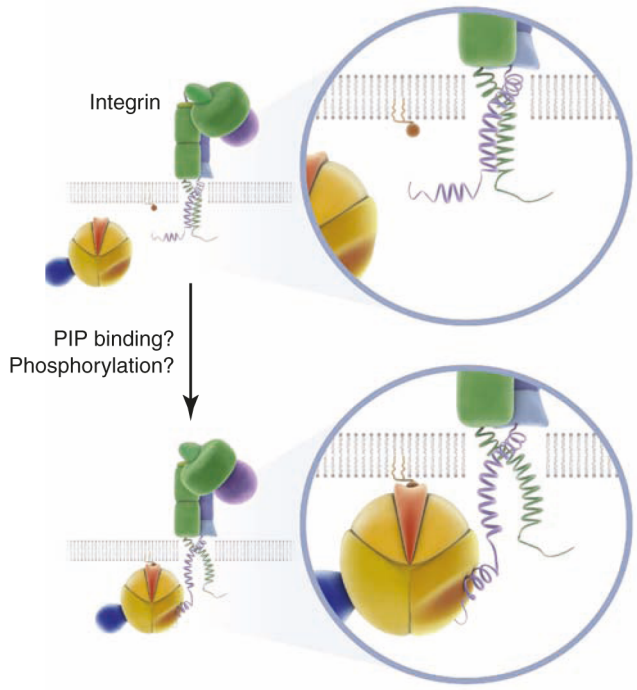

Figure 26: Recruitment of kindlin to the β integrin tails

Kindlins binding to plasma membrane phosphoinositides via their PH domain and/or further phosphorylation might activate kindlins, leading to their interaction with the membrane distal (MD) NxxY motif of the β integrin cytoplasmic tail (adapted from Moser et al., 2009).

Kindlins alone are not sufficient to shift integrins to a high-affinity state but they cooperate with talin, as it was shown that co-expression of kindlin-1 or -2 with the talin-head domain synergistically increase αIIbβ3 activation [331]. Furthermore, overexpression of the talin-head domain failed to increase αIIbβ3 activation in kindlin knock-down CHO cells [332]. These results argue that talin alone is not sufficient to increase the integrin activation and that it requires kindlins. Controversially, recent reports postulate that talin alone is both necessary and sufficient for integrin activation, as it was possible to activate integrins and even a kindlin binding-defective integrin mutant by the talin head domain alone in an *in vitro* experimental setting, using recombinant proteins and membrane lipid nanodiscs [333]. A follow-up study,

investigated the influence of kindlins on the talin recruitment to β integrin tails and vice versa and postulated that kindlins do not promote talin recruitment to the plasma membrane or to αIIbβ3 integrin and that talin does not promote a interaction between kindlins and αIIbβ3 integrin [334]. Furthermore, in neutrophils talin alone is able to induce a conformational shift of the αLβ2 integrin from its inactive to the intermediate conformation but kindlin-3 is essential to acquire the high-affinity conformation [335], arguing for distinct functions of talin and kindlin during integrin activation, which can even differ between different integrin heterodimers.

However, a cooperation of talin and kindlin through their distinct binding sites in the integrin β tail is necessary for full integrin activation *in vivo* and neither of these proteins is sufficient alone [328,336]. Further studies are necessary to elucidate details of their interactions with integrin tails, as it is still unclear whether kindlin and talin bind integrin β tails simultaneously or in a sequential manner. It is possible that both activators bind sequentially, e.g. kindlin first and then facilitates the talin binding. Alternatively, they may bind simultaneously to the β integrin tail, which has recently been show to be possible [337] and together activate integrins, maybe by recruiting further known or unknown proteins. A further possibility is, that one of the two proteins is the primary activator and the other an "enabler" mediating supportive functions such as signaling events leading to the binding of the activator to the β integrin tail or displacing inhibitors from the integrin tails, which prevent the binding of the activator. This interaction between both proteins can occur on the same integrin heterodimer, or involving several integrins so that kindlins and talins are bound to different integrin tails and trans-communicate [318,338], which was recently shown by our group to be rather unlikely [339]. However, it is clear that talin and kindlin binding induces a conformational change of integrin tails. This conformational change is further propagated through the transmembrane domains to the extracellular domains of the integrins.

The exact mechanism of the integrin conformational changes is not fully understood, however, two major models have been proposed. The "switchblade" model states that the conformational changes leading to the extracellular extension starts with the dissociation of the cytoplasmic and the transmembrane domains of the inactive bent integrin. According to this model a salt bridge between the cytoplasmic domains of the integrin heterodimers becomes disrupted. The separation of integrin tails occurs upon binding of kindlin and/or talin. Furthermore, this model states that ligand binding only occurs in the extended, high-affinity state [301,338]. In contrast, the "debolt" model states that integrins do not depend on full extension of their extracellular domain for ligand binding, but rather the

extension occurs only after ligand binding and actomyosin pulling. According to this model the change in the tilt of the transmembrane domain leads to the change in the conformation of the head domain and the exposure of ligand binding sites [301,311,312,340].

6.9.2. Outside-in signaling

Outside-in signaling of integrins is initiated by ligand binding and results in recruitment of further proteins to the integrin cytoplasmic tail [341]. Since integrins do not possess enzymatic activity, they depend on the interaction with a variety of auxiliary proteins to transduce signals. Recent findings demonstrate the presence of more than 245 proteins associated directly or indirectly with the cytoplasmic domains of integrins [342,343] [344]. These proteins can either have a mechanical role linking integrins to the cytoskeleton, mainly F-actin, or a signaling role in diverse signaling pathways controlling processes such as cell spreading, migration, proliferation and apoptosis [323,345,346].

One can distinguish between three temporal stages in integrin downstream signaling, shown in figure 27 [326]. Up-regulation of lipid kinase activity, leading to an increase in the local concentrations of phosphoinositide second messengers such as phosphatidylinositol 4,5-bisphosphate (PtdIns(4,5)P2) and phosphatidylinositol 3,4,5-trisphosphate (PtdIns(3,4,5)P3) as well as rapid phosphorylation of specific proteins, is one of the immediate events downstream of integrin activation. Subsequently, these changes lead to activation of various signaling pathways, within several minutes. The cell adhesion-dependent phosphorylation of FAK and Src kinases is considered a central event in the integrin-mediated signaling. Particularly important is the phosphorylation of FAK at the tyrosine-397, which enables its interaction with Src family kinases, as it creates the docking site for the SH2 domain of Src. Interaction of FAK and Src leads to activation of Src. The resulting activated FAK/Src complex subsequently phosphorylates other focal adhesion proteins such as FAK, paxillin, and p130Cas, leading to the recruitment of intermediate signaling molecules such as the adaptor protein growth factor receptor-bound protein 2 (Grb2). In this way, it leads to the activation of downstream signaling pathways such as the Ras/MAPK pathway. Another important event in downstream integrin signaling is activation of Rho family GTPases and other actin regulatory proteins, which leads to the reorganization of the actin cytoskeleton, changes in cell shape, and initiation of cell migration. Finally, integrin outside-in signaling, on the long-term scale, leads to activation of proliferation pathways as well as the initiation of genetic programs controlling cell morphology [326]. This is mainly achieved by cross talking with GFRs such as EGFR, IGFR, PDGFR, and TGFR. These extensive cross-talks are

regulated on multiple levels and are essential for physiological and pathological conditions [347-350].

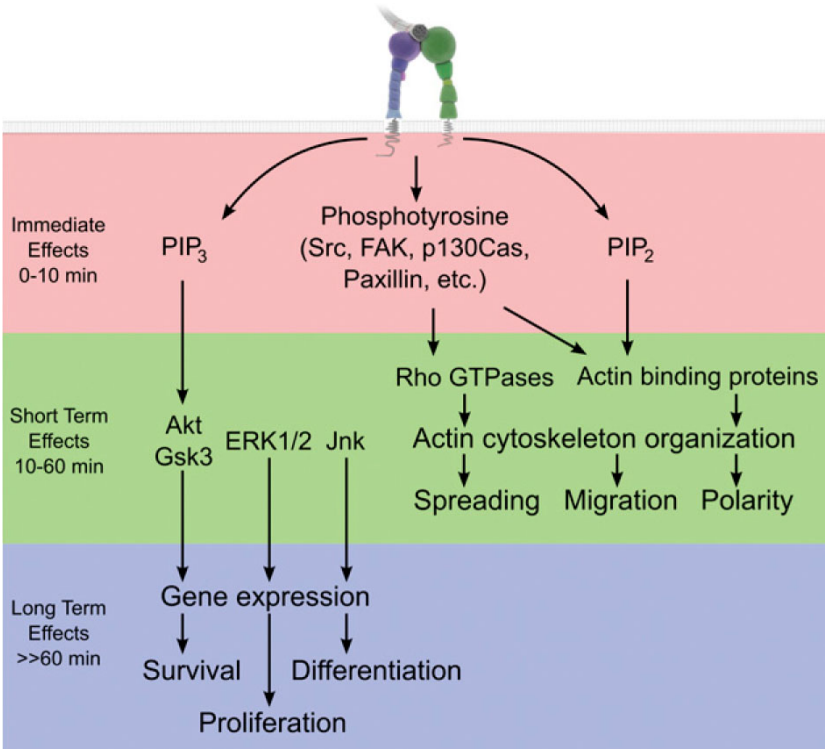

Figure 27: Effects of integrin outside-in signaling

Signaling processes downstream of the activated integrins can be divided into three temporal stages. First, the immediate effects combine the rapid phosphorylation of specific proteins as well as increased lipid kinase activity leading to higher concentrations of PtdIns(4,5)P2 and PtdIns(3,4,5)P3. Second, the short-term effects occur within several minutes and are reflected in activation of signaling pathways as well as of Rho family GTPases and other actin regulatory proteins leading to the reorganization of the actin cytoskeleton. Third, the long-term effects include activation of signaling pathways regulating proliferation and survival as well as induction of genetic programs controlling cell fate (adapted from Legate, Wickström et al., 2009).

6.10. The Kindlin Protein Family

The kindlin protein family consists of three members (kindlin-1, kindlin-2 and kindlin-3) in mice and humans, while *C. elegans* expresses one kindlin ortholog, named uncoordinated protein 112 (Unc-112) and *Drosophila* two, named fermitin-1 and -2. The kindlin family of proteins bears its name after a human autosomal recessive genodermatosis called Kindler syndrome [351].

The kindlin genes are evolutionary conserved with 15 exons in both the human and the murine gene. All three kindlin genes contain the ATG start codon within the second exon. The three kindlin proteins show a high sequence similarity to each other, with 74% similarity

and even 60% identity between Kindlin-1 and -2. Kindlin-3 shows 69% similarity and 53% identity to Kindlin-1 and 67% similarity and 49% identity to Kindlin-2 [352].

6.10.1. Structure of the Kindlin Proteins

All kindlin proteins share the same domain structure with a C-terminal FERM domain and a short N-terminal F0 domain [353]. The FERM domain consists of three subdomains: F1, F2, and F3 (figure 28). The F1 subdomain has an ubiquitin like structure, the F2 subdomain has an α-helix bundle structure harboring a pleckstrin homology (PH) domain, while the F3 subdomain contains a PTB domain, belonging to the PH superfold family [354-356].

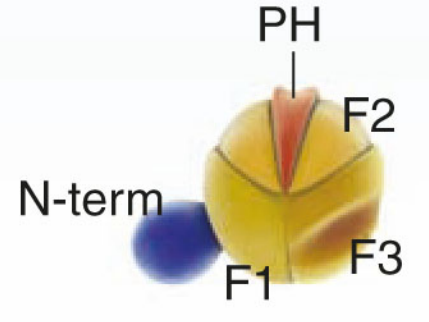

Figure 28: Structural model of kindlin

All kindlins contain a C-terminal FERM domain with the three subdomains F1, F2, F3. The FERM domain is separated into two halves by a pleckstrin homology (PH) domain, which is inserted within the F2 subdomain (adapted from Moser et al., 2009).

The FERM domain is found in a variety of cytosceletal-associated proteins (e.g. talin) and was shown to be involved in the interaction between the membrane and the cytoskeleton. For example, FERM containing proteins are involved in the connection of actin to transmembrane proteins such as integrins, CD43, CD44, ICAM-2 and ICAM-3 [357]. PH/PTB-domains have a common folding structure, with two perpendicular anti-parallel β-sheets followed by a C-terminal α-helix [356,358,359]. Initially this domain was described in the SRC homology 2-containing protein (Shc), a Src homology 2-domain adaptor protein, to serve as interaction site for activated receptor tyrosine kinases. To date, there have been approximately 50 proteins discovered containing PTB domains, one of which is talin. Besides binding phosphorylated NPxpY motif, these proteins can also bind non-phosphorylated NPxY with the same or higher affinity [360,361].

Approximately 250 pleckstrin homology-domain (PH-domain) containing proteins, including protein kinases, guanine nucleotide exchange factors (GEFs), phospholipases and cytoskeletal proteins have been discovered [358,362]. The main function is the binding to

phosphatidylinositol (PtdIns) lipids within cell membranes and therefore recruiting the proteins to cellular membrane structures [362-364]. PtdIns differ in their phosphorylation of the inositol moiety and exhibit a specific spatial and temporal distribution within various cellular membranes, e.g. PtdIns(4,5)P2 is predominantly found in the plasma membrane and steady state Golgi apparatus, while PtdIns(3,4)P2 and PtdIns(3,4,5)P3 are found transiently in the plasma membrane upon receptor stimulation. As various PH domains differ in their ability to bind to distinct PtdIns, they in turn can recruit the PH containing proteins to different sub-cellular compartments. In addition, the phosphorylation and dephosphorylation of PtdIns, executed by kinases (e.g. PI3K) and lipid phosphatases (e.g. phosphatase and tensin homolog (PTEN)) [359], create additional level of distribution regulation for PH containing proteins.

6.10.1.1. Kindlin-1

Kindlin-1 is expressed mainly in epithelial cells. The highest levels of kindlin-1 mRNA are detected in bladder and colon, and lower levels in kidney, stomach, small intestine and skin. Epidermal expression levels are generally much higher than the levels in dermis.

In humans, loss of function mutations in kindlin-1 occur throughout the entire gene and lead to various truncated forms of the protein. The mutations result in skin disease called Kindler syndrome [365]. Patients with Kindler syndrome are suffering from numerous skin pathologies with various severities [366]. Main characteristics of this condition include skin atrophy and trauma induced skin blistering appearing in very young patients and becoming less severe with age. However, Kindler patients also develop increased poikiloderma and photosensitivity with age and have greater predisposition for squamous cell carcinoma [367]. Additionally, cases of ulcerative colitis have been described [365]. The full mechanism of this disease remains unclear, as the defective anchorage of actin cytoskeleton to cellular matrix adhesion sites cannot explain the poikiloderma, photosensitivity and cancer predisposition [368,369]. Similar to humans, kindlin-1 deletion in mice leads to early post-natal lethality due to skin atrophy and ulcerative colitis [329]. Epidermal basal keratinocytes show polarized distribution of kindlin-1 at the dermal-epidermal junction zone between hemidesmosomes. Deletion of kindlin-1 in these cells leads to loss of polarity, reduced proliferation, and increased cell death [329]. Kindlin-1 deficient keratinocytes also demonstrate reduced and undirected migration due to defects in adhesions, actin organizations and loss of polarity [329,353]. Kindlin-1 interacts with β1, β3 and β6 integrin subunits [329] and localizes to integrin mediated adhesion sites in cultured cells.

6.10.1.2. Kindlin-2

Kindlin-2 is almost ubiquitously expressed with the exception of hematopoietic cells. The highest levels are present in striated muscles [328]. In contrast to kindlin-1, kindlin-2 shows higher expression in dermis and low levels in epidermis [352], which could together with the different subcellular localization explain the inability of kindlin-2 to rescue kindlin-1 loss and the symptoms of Kindler patients.

Like kindlin-1, kindlin-2 binds β1 and β3 integrin subunits and localizes to adhesion sites in cultured keratinocytes. In addition, kindlin-2 shows a specific co-localization with E-cadherin and localizes to cell-cell contacts in differentiated keratinocytes [328,332,352]. In cardiomyocytes, kindlin-2 also localizes to actin stress fibers [352] and to α-actinin in Z discs. Interestingly, kindlin-2 contains a nuclear localization sequence in its N-terminus, which would suggest some unknown, nuclear functions. Kindlin-2 nuclear localization was observed in leiomyosarcomas and leiomyomas [370].

Kindlin-2 deletion in mice leads to peri-implantation lethality due to a severe endoderm and epiblast detachment from the basement membrane [328]. Loss of kindlin-2, similar to loss of kindlin-1, leads to defective cell spreading and impaired adhesions [371].

6.10.1.3. Kindlin-3

Kindlin-3 expression is restricted to the hematopoietic system [352], where it can be detected in various hematopoietic cells such as macrophages, monocytes, DCs, neutrophils, erythrocytes, B cells, T cells, platelets, OCLs, megakaryocytes, and HSPCs [352]. Kindlin-3, similar to kindlin-1 and -2, localizes to integrin adhesion structures, where it interacts with the β1, β2 and β3 integrin tail [316,352]. However, unlike keratinocytes and fibroblasts, hematopoietic cells do not adhere to ECM via focal adhesion, but instead form specific structures called podosomes, which contain a central actin core surrounded by a ring of plaque proteins such as talin, vinculin, and paxillin [372,373]. In podosoms kindlin-3 colocalizes with vinculin [352].

Kindlin-3 deficiency in mice leads to an early post natal lethality due to numerous defects including, anemia, severe hemorrhage in the gastrointestinal tract, skin, brain, and bladder [316], see figure 29. The hemorrhages can be detected already during E13 to E17 days of embryonic development, and are similar to the phenotype observed in Glanzmann´s trombasthenia, which occurs due to defective αIIb or β3 integrins.

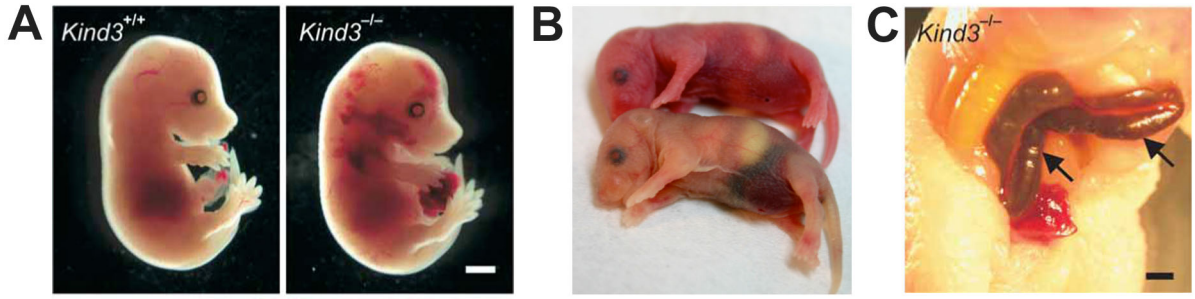

Figure 29: Kindlin-3 deficient mice suffer from severe hemorrhages

A) E15.5 embryos having bleedings at several locations. B) Newborn mice (P2) with severe bleedings in the abdomen. C) The bleedings occur especially in the bladder and intestinal tract (arrows) (modified from Moser et al., 2008).

The hemorrhages in kindlin-3 deficient mice can be explained by impaired platelet function [316]. *In vitro* and *in vivo* assays performed with kindlin-3 deficient platelets revealed a defect in aggregation, adhesion, and spreading, while the platelet maturation and production is unaffected as shown by experiments with fetal liver cell chimeras [316]. The bleeding phenotype of kindlin-3 deficient mice led to the discovery of mutations in the human *KINDLIN*-3 gene causing leukocyte adhesion deficiency syndrome type III (LAD-III, also known as LAD-I variant), a rare autosomal recessive immunodeficiency syndrome [374]. In humans two further types of LAD exists, named according to their chronological discovery LAD-I and LAD-II, which have independent defects from kindlin-3 but share several common phenotypic characteristics such as recurrent bacterial infections and leukocytosis [374]. LAD-I is caused by null mutations in the β2 integrin gene results in an extravasation defect of leukocytes due to impaired firm adhesion [375]. LAD-II is due to impaired posttranslational fucosylation of selectin ligands causing a dramatically reduced leukocyte rolling [376].

Patients suffering of LAD-III show mild immunodeficiency with recurrent fungal and bacterial infections, leukocytosis, and severe hemorrhages similar to Glanzmann's trombasthenia. A list of known mutations in kindlin-3 gene carried by members of 21 families with LAD-III patients has recently been published [377], showing that most of the mutations are nonsense mutations leading to truncated forms of the kindlin-3 protein devoid of the C-terminal integrin binding region. However, kindlin-3 can indirectly interact with integrins via the scaffold protein receptor for activated C kinase-1 (RACK-1) [378], thereby enabling integrin-mediated signaling. This fact could explain the differences in severity of phenotype between LAD-III patients. In addition, some patients show increased bone density [379], similar to the osteopetrosis that has been observed in kindlin-3 deficient mice [380], which

can be explained by the absence of the kindlin-3 protein in the bone resorbing OCLs. These cells adhere less to the bone structure, due to defects in the podosome formation [380].

6.11. Hematopoietic malignancies

Malignant transformation involves the acquisition of one or a series of genetic mutations in HSCs or more mature progenitor cells, disrupting the normal hematopoietic balance between maturation and replenishment. This could lead to increased proliferation rates, decreased apoptosis, enhanced self-renewal, maturational arrest and defective telomere maintenance. For the complete understanding of these processes one needs to resolve both the molecular events underlying the malignant growth as well as the cellular context in which the oncogenic mutations occurs. Hematological malignancies are malignant neoplasms comprising leukemias, lymphomas, myelodysplastic syndromes (MDS), multiple myeloma (MM) and myeloproliferative disorders.

Lymphomas are clonal malignant disorders derived from lymphocytes, either precursors or mature T cells or B cells originating from the lymphoid organs or extranodal tissues. In general, they can be divided into low-grade and high-grade lymphomas. Low-grade lymphomas show a lower cellular proliferation rate and also progress more slowly than high-grade lymphomas, which will, if untreated, cause death relative quickly. Therefore, it is beneficial that high-grade lymphomas are easier to treat than low-grade lymphomas. Additionally, they are divided into two broad categories, the Hodgkin and non-Hodgkin lymphomas. Hodgkin lymphomas are diagnosed histologically by the presence of characteristic mutated B-lineage cells called Reed-Sernberg cells within the appropriate cellular background and are relatively restricted in their pathology compared to non-Hodgkin lymphomas, which are very diverse in nature. Lymphomas were initially thought to be ‘solid’ compared with leukemia being ‘liquid’, where malignant cells are spilling into the PB. However, this differentiation is sometimes blurred as lymphomas often enter a leukemic phase, where malignant lymphoid cells, which were restricted to a particular lymphoid organ, overspill into the blood and BM. Therefore, nowadays the classification, based on the cell of origin and define biological entities e.g. follicular center cells giving rise to follicular lymphoma, is rather used.

Leukemias are first classified according to the cell lineage, which is affected into myeloid or lymphoid leukemias. They are further divided into acute and chronic types. In acute leukemia, the clinical course is rapidly progressive and the leukemic cells are immature blasts, leading to death relatively rapidly if untreated. In contrast, a chronic leukemia has a slow and indolent

clinical course and the tumor cells are mature-looking in lymphoid leukemia and intermediate forms (promyelocytes, myelocytes, and metamyelocytes) in myeloid leukemia. Chronic leukemias are less aggressive and have blasts below 20%. Maturational arrest does not occur in chronic leukemias, although the cells often fail to undergo apoptosis, allowing the malignant cells to accumulate. In lymphomas one does not separate between acute or chronic types, but its clinical course is essentially determined by the maturity of the tumor cells. By combining the four differentiation criteria one can separate four major classes of leukemias. The acute forms include Acute Lymphoblastic Leukemia (ALL) and Acute Myeloid Leukemia (AML) and the chronic forms include Chronic Lymphocytic Leukemia (CLL) and the Chronic Myelogenous Leukemia (CML).

The MDS, also termed 'pre-leukemia', describes a range of heterogeneous diseases restricted to the myeloid lineage. MDS are all disorders of HSCs leading to an increased number of precursors in the BM but accompanied with cytopenia in the PB due to the premature death of the immature cells in the BM. The MM is a malignancy of the lymphoid compartment and associated with the proliferation of malignant plasma cells, which accumulate in the BM leading to myelosuppression and the activation of OCLs. The OCL activity causes breakdown of bone, leading to pathological fractures. In addition, an increased production of monoclonal antibodies occurs, which can damage the kidney if present in the plasma at excessive concentrations. Myeloproliferative disorders is a collective term describing disorders affecting the myeloid lineage leading to an increased proliferation including: the polycythaemia, a increased proliferation of red cell precursors leading to an accumulation of mature red cells in the PB; the myelofibrosis, leading to a increased proliferation of fibroblasts in the BM and thereby modulating the BM microenvironment as well as HSPCs and the essential thrombocythaemia, which is a inappropriate proliferation of megakaryocytes leading to an increased number of platelets [381].

6.11.1. Chronic Myeloid Leukemia (CML)

CML is a clonal multi-lineage myeloproliferative disorder of stem cell origin characterized by the Philadelphia (Ph) chromosome so called after the city in which it was discovered [382]. The course of disease is triphasic, starting with an early chronic phase (CP) in which most of the patient are diagnosed lasting 3 to 6 years without treatment, followed by an accelerated phase (AP) and finally leading to a terminal blast phase (BP) of short duration characterized by a block of cell differentiation leading to an accumulation (more than 30%) of myeloid or lymphoid blast cells in the PB or BM [383]. CML makes around 15 % of all types of leukemia in adults and has an incidence of 1 case per 100000 people per year [384]. The

median age of patients diagnosed with CML is from 45 to 55 years, while 1/3 of the patients are over 60 years old. The high age of the patients is a critical factor for therapeutic strategies such as stem cell transplantation or INF-α treatment, which work well in younger patients, but can have severe side effects in older people. The high age together with limited donor availability, therefore exclude approximately 75% of patients for these treatment strategies [385].

CML was the first human neoplasm explained by a chromosomal abnormality, in which a reciprocal translocation between the long arms of chromosomes 9 and 22, t(9,22)(q34,q11), leads to the shortened Ph chromosome containing the *BCR-ABL* fusion gene [386], see figure 30.

The human *ABL* gene encodes a ubiquitously expressed 145 kD nonreceptor tyrosine kinase [387] and is the homologue of the *v-abl* oncogene carried by the abelson murine leukemia virus (A-MuLV) [388]. The normal ABL protein is involved in the regulation of the cell cycle and apoptosis [389], in the cellular response to genotoxic stress [390] and in integrin signaling [391]. The 160 kD BCR protein is a ubiquitously expressed serine threonine kinase [387]. Several *in vitro* experiments argue for a role of BCR in signal transduction [392,393] but the biological relevance is still not clear as the bcr knock-out mice are viable and have no severe defects that would confirm a critical role of BCR for the signal transduction [394].

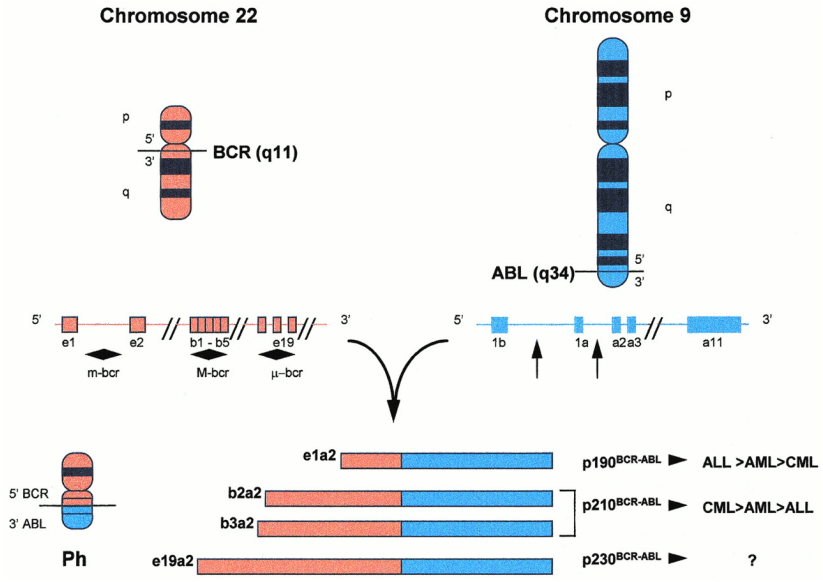

Figure 30: The translocation of t(9,22)(q34;q11) and the fusion mRNA molecules in CML

The shortened chromosome 22 (known as Ph chromosome) is generated by the translocation of the 3' segments of the *ABL* gene on chromosome 9 to the 5' parts of the *BCR* gene on chromosome 22. Different breads at several *BCR*s on chromosome 22 results in different sizes of the *BCR* gene that is fused to the 3' segments of the *ABL* gene leading to four different mRNAs of various length (e1a2, b2a2, b3a2, e19a2) encoding for three different BCR-ABL fusion proteins with different molecular weights and probably functions (p190, p210, p230) (adapted from Faderl et al., 1998).

The breakpoints within the *ABL* gene at 9q34 can occur at different positions over a more than 300 kb area at the 5' end either upstream of the first alternative exon Ib, downstream of the second alternative exon Ia or more frequently between the two [395]. However, splicing of the primary hybrid transcript leads to an mRNA in which the different *BCR* sequences are always fused to the *ABL* exon a2. The breakpoints within the *BCR* gene localize to 1 of 3 breakpoint cluster regions (bcr). In most CML and AML as well as in 1/3 of Ph-positive ALL patients the break occurs in the major breakpoint cluster region (M-bcr) spanning exons b1-b5. Alternative splicing leads to fusion transcripts with either b2a2 or b3a2 junctions. From these mRNAs is the 210 kD chimeric protein ($P210^{BCR-ABL}$) derived. In other patients with ALL, AML and rarely with CML, the breakpoints are further upstream in the minor breakpoint cluster region (m-bcr) between the alternative exons e1 and e2. The spliced e1a2 mRNA is translated into the 190 kD protein ($P190^{BCR-ABL}$). In patients with neutrophilic CML [396] as well as in some rare cases of CML [397], breakpoints downstream of exon 19 within the micro breakpoint cluster region (μ-bcr) give rise to the fusion transcript e19a2, which is translated into a 230 kD protein ($P230^{BCR-ABL}$), see figure 30.

During the reciprocal translocation not only the *BCR-ABL* fusion gene is formed but also a second fusion gene, the *ABL-BCR* gene, on the 9q+ chromosome. It is only expressed in 2/3 of all the CML patients [398] and the contribution to the pathogenesis of CML is still unclear.

While under non-transforming condition the ABL proto-oncoprotein is restricted to the nucleus where it is bound to chromatin or in the cytoplasm colocalized to F-actin [387], the chimeric oncoprotein BCR-ABL is exclusively located to the cytoplasm. The abnormal cytoplasmic localization and the constitutively activated tyrosine kinase activity, which is 5-10 fold increased compared to ABL, are crucial to the transforming activity of BCR-ABL by recruiting and activating several pathways such as the Ras, PI3K, and Jak/STAT pathways transducing intracellular signals, which ultimately lead to abnormal cellular adhesion, survival and differentiation as well as enhanced proliferation and inhibition of apoptosis [398], see figure 31.

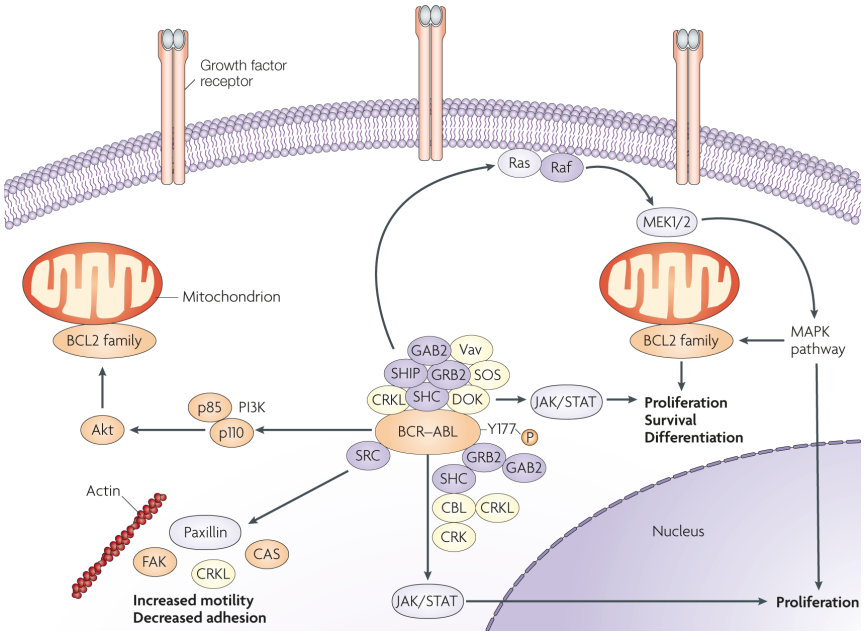

Figure 31: Signaling pathways influenced by BCR-ABL in CML

Together with several mediators BCR-ABL leads to the activation of Ras, which together with Raf activates MEK1/2 resulting in the activation of the MAPK pathway, thereby increasing growth factor independent proliferation. BCR-ABL also increases cell survival by suppressing apoptosis through activation of the PI3K pathway. The interfering of BCR-ABL with components of the focal adhesion complex, such as FAK, actin or paxillin leads to the activation of the CRKL/FAK/PYK2 complex resulting in reduced cell adhesion. BCR-ABL also associates with the JAK/STAT pathway further influencing cell growth, differentiation and death. BCR-ABL further influences survival proteins from the Bcl-2 family of anti- and proapoptotic regulators. Finally, BCR-ABL also interferes with pathways mediating responses to chemotactic factors, thereby increasing cell migration (adapted from Weisberg et al., 2007) [399].

$P210^{BCR-ABL}$ has several domains that are able to bind adapter proteins such as Grb2, Shc, CRK-like protein (Crkl) and casitas B-lineage lymphoma pro-oncogene protein (Cbl), leading to the activation of the Ras signaling pathway [400-402], which plays a key role in the pathogenesis of CML [403]. Downstream signaling from Ras is mediated by the MAPK such as the Jun kinase pathway [404]. $P210^{BCR-ABL}$ also constitutively activates the PI3K pathway by binding to insulin receptor substrate 1 (IRS1) [405] and Crkl or Cbl [406,407] leading to the suppression of the programmed cell death and increasing cell survival.

STAT1 and STAT5 of the JAK/STAT5 pathway are constitutively phosphorylated directly by $P210^{BCR-ABL}$ and independent of the RAS signaling pathway [408], which leads to the up-regulation of the anti-apoptotic protein BCL-X_L [409]. Raf, Akt, c-Myc and Bad have also been identified to be involved in the BCR-ABL signaling pathways as they can be activated by $P210^{BCR-ABL}$ [410-413].

BCR-ABL is also associated with proteins of the focal adhesion complex like actin, paxillin, vinculin, talin and FAK, as it constitutively phosphorylates tyrosine residues of Crkl. The fact that Crkl was still phosphorylated in cell lines with a mutant form of BCR-ABL unable to bind Crkl and still associated with $P210^{BCR-ABL}$ argues not only for a direct but also indirect influence of BCR-ABL on Crkl [414]. This activation of CRKL/FAK/PYK2 leads to a decrease in cell adhesion. However, the reduced adhesion of BCR-ABL transformed cell lines is controversial as there are also several reports postulating an increased integrin mediated adhesion potential of $P210^{BCR-ABL}$ expressing cells [415]. Although all the different signaling pathways affected by the BCR-ABL have been extensively investigated, none of them alone can explain all the phenotypic features described in CML, arguing for a complex interplay between the signaling pathways being necessary for the transforming effect of BCR-ABL.

6.11.1.1. CML Treatment Strategies

The most curative treatment strategy for CML is the allogeneic BM transplantation. But as mentioned before, this treatment is not possible for most of the CML patients because critical risk factors such as high age and the phase of the disease in which the patients are, stem cell transplantation are usually only performed by CP patients, make a transplantation feasible, because of the high risk of mortality during the treatment. Another limitation is the availability of BM donors.

Alternatives for the patients who are not eligible for a transplant are cytoreductive chemotherapies with agents like hydroxyurea and busulfan to control the leukocyte counts and reduce the tumor weight. In the 1980s a new therapy with the antiproliferative agent interferon-α (IFN-α) became the treatment of choice for CP CML patients, as it was superior to preceding regimes leading to complete cytogenetic remissions in up to 30% of CML patients [416]. However, duration of remission was unpredictable and many patients only poorly tolerated the IFN-α therapy, therefore limiting the drug dosage due to the severe side effects or breaking up the treatment. From 2001 on, imatinib mesylate (STI571, Gleevec, Glivec, Novartis, Basel, Switzerland) came on the marked for the treatment of CML. The remarkable therapeutic efficacy of imatinib displaced the IFN-α and all the other previous therapies and became the gold standard for CML treatment. Imatinib is a small molecule inhibitor of the tyrosine kinase activity of BCR-ABL, c-ABL, PDGF and c-kit [417-419], which acts by blocking the tyrosine kinase ATP-binding site. The effect on other tyrosine kinases than BCR-ABL is the reason for several off-target effects of imatinib, such as changes of serum phosphate levels [420], a reversible and dose-dependent hypogammaglobulinemia and lymphocytopenia [421], apoptosis induction of cardiomyocytes [422],

immunosuppression [423] and impaired function of several hematopoietic cell types such as monocytes [424], DCs [425] and T cell [426]. Nevertheless, imatinib treatment leads to a significantly greater percentage of cytogenetic remissions with less treatment-related morbidity [427]. The remarkable success of the imatinib treatment was given by a 85% estimated overall survival rate, a 81% event-free survival rate and a 83% cumulative complete cytogenetic response (CCyR) rate for first-line imatinib-treated patients after 8 years of follow-up [428]. But the remaining heterogeneity in the response to imatinib treatment shows that this therapy is not a pharmacological cure and further development of new drugs such as second-generation small molecule inhibitors (i.e. Dasatinib, Ponatinib or Deciphera [429]), as well as new therapies targeting other biological targets in the CML cells in conjunction with imatinib are necessary to help patients which e.g. developed a resistance to imatinib due to mutations in the BCR-ABL kinase domain [430]. A further problem with imatinib is that in the majority of patients, expected to achieve CCgR, a minimal residual disease persists. Even patients where BCR-ABL transcripts are not detectable anymore, harbor around 10^7 leukemic cells in their bodies [431]. For these patients, there is a high likelihood for relapse of CML if the administration of imatinib is stopped [432]. Furthermore, it was shown that the remaining Ph chromosome positive BM cells had HSC character [433] and that these CML leukemic stem cells (LSC) are highly resistant to the imatinib treatment compared to the bigger mass of differentiated CML cells. The LSCs retain the ability to reproduce multilineage hematopoietic cells [434], leading to a fast and vast expansion of malignant myeloid cells displacing normal hematopoiesis and finally leading to CML relapse upon discontinuation of treatment. Currently, for most patients an indefinite medication is the only possibility to prevent disease relapse [435], which is associated with a risk of incompatibility or even toxicity and, not to underrate, considerable expense [436].

6.12. The leukemia (Cancer) Stem Cell Hypothesis

More than 50 years ago it was first shown that leukemias and other types of cancer are heterogeneous in their growth potential, as only a small fraction of leukemic cells isolated from patients were able to grow or form colonies *in vitro,* or were able to build Spl colonies in *in vivo* mouse transplantation experiments [437,438]. This observation could be explained by two possibilities. First, it could be that all the leukemic cells have the same low growth potential. Second, the clonogenic and leukemogenic activity could be restricted to a small, more primitive fraction of the whole leukemic cell pool. Bonnet and Dick as well as Lapidot and colleagues demonstrated in the 1990s that in human AML only leukemic blasts, purified

as Thy1$^-$, CD34$^+$, CD38$^-$ cells, were able to induce AML after transplantation into SCID mice [439,440]. This was in contrast to more committed progenitors, which are CD34$^+$, CD38$^+$ positive and lacked such a potential. Thereafter, it became clear that only a small, defined subset of cells was consistently clonogenic. These results argue for the LSC hypothesis, which postulates that leukemias and many other cancer types arise from rather small populations of stem cell like cancer cells that have the ability for indefinite self-renewal [438]. The concept of LSC is nowadays well established and similar tumorigenic cells could have been identified in other solid tumors such as e.g. pancreatic, colorectal and breast cancers [441-443].

In most leukemia as well as cancers the origin of LSCs or cancer stem cells (CSCs), respectively, has not been identified with certainty. In general, there are two possibilities how LSCs or CSCs can develop. Since LSCs and CSCs have several properties with HSCs in common such as the ability to self-renew or certain developmental pathways, it is most likely that LSCs or CSCs are derived from neoplastic transformed normal HSCs. HSCs also have a greater opportunity to accumulate mutations as they are retained throughout the entire lifespan of an organism compared to more mature cells, which persist only for a short period. But also more committed progenitors or differentiated mature cells that have reacquired self-renewal properties by mutations, could be the origin for LSCs or CSCs, see figure 32.

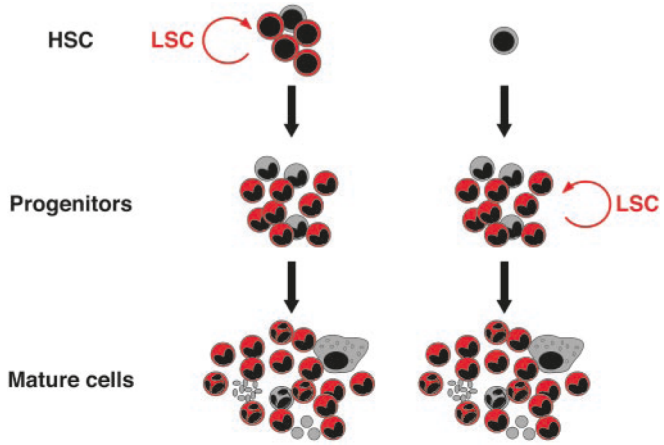

Figure 32: Two different origins of LSCs

As LSCs share several properties with normal HSCs, it is possible that mutations in these stem cells lead already very early during cell development to neoplastic transformations (right). But also more restricted progenitors can become LSCs when they reacquire stem cell properties such as self-renewal through mutations (left). In both cases the LSCs will produce leukemic cells leading to comparable end-stage leukemias (adapted from Passegue et al., 2003) [43].

In subtypes of human AML and CML there is increasing evidence that leukemias arise from mutations that accumulate in HSCs. For example, in the case of CML the Ph chromosome can

be detected in several different hematopoietic lineages like nearly all myeloid, erythroid and some B and T cells [444], indicating that the original translocation takes place in a HSC with multilineage differentiation capacity. BCR-ABL positive cells, isolated from CML BM, are $CD34^+$ $CD38^-$ $CD90^+$, a cell population with a high HSC activity in normal BM [445,446].

In CML and AML a small pool of the LSCs are in a quiescent, G0 phase of the cell cycle [447-449], which might be one explanation why these cells are relatively resistant to chemotherapy. The regulation of LSC self-renewal and quiescence is, as for normal HSCs, dependent on the BM microenvironment [450]. It is postulated, that the machinery for migration, homing and lodgment in BM niches usually used by HSCs is "hijacked" by LSCs and that LSCs occupy and even displace HSCs from their niches [451]. The important regulatory signals from the environment to the LSCs are postulated to be critical for the resistance of LCSs to conventional therapies. Therefore, a new strategy could be to alter the microenvironment or to interfere with the supportive bidirectional interactions between the LSCs and their niches to overcome the primary disease resistance. This could be e.g. the inhibition or alteration of homing mechanisms, cell adhesion molecules, cytokine signaling or self-renewal pathways (e.g. Notch or Wnt).

The integrins $\alpha4\beta1$, important for homing to and interaction with the BM niche (described above) is also expressed on AML blasts and it was shown that patients with reduced levels of $\alpha4\beta1$ had a better response to chemotherapy [452] probably due to the altered interaction of the leukemic cells with their environment. Furthermore *in vitro* experiments showed that AML blasts bound to fibronectin via $\alpha4\beta1$ trigger PI3K-Akt signaling, which protects these blasts from chemotherapy. In contrast, neutralizing $\alpha4\beta1$ antibody in combination with the chemotherapeutic agent cytarabine can eradicate residual AML in a SCID xenograft transplantation model [452]. In addition, antibodies against the adhesion molecule CD44, expressed on normal HSC but also LSCs, had an eliminating effect on AML stem cells in patients, which might be explained by the disruption of the LSC from its microenvironment [453]. These results argue for the use of antibodies, targeting adhesion molecules, as an alternative treatment strategy to eliminate LSCs.

An example for therapies targeting cytokine signaling networks are chemical compounds such as the CXCR4 antagonists AMD3465 or AMD3100 effecting the interaction between CXCL12 and its specific receptor CXCR4 on leukemic cells, leading to the disruption of the chemoprotective effects of stromal cell-leukemia cell interactions or the mobilization of leukemic cells increases chemosensitivity [454,455]. Signaling pathways involved in stem-cell self-renewal such as the Wnt and Notch pathways are partly regulated by

components of the niche [167,219]. Data that support a regulatory role of the Notch pathway in AML LSCs or Wnt signaling in CML BC [446,456] argue for the use of inhibitors of these pathways as a further promising approach to eliminate LSCs protected by the niche.

Primarily quiescent LSCs are also discussed as a reason for CML relapse in patients, who had sustained, complete cytogenetic remission in response to continuous imatinib treatment after the stop of therapy [457,458]. These observations and findings from transplantation experiments with BCR-ABL positive BM cells of imatinib pretreated mice that were still able to generate CML in the recipient mice suggests that the quiescent LSCs are resistant to the antiproliferative effects of imatinib in comparison to the proliferative active progenitors [459-461]. Therefore, an other possible strategy to sensitize quiescent LSCs in 'minimal residual disease' such as in CML to antiproliferative agents could be the activation of LSCs and to promote their cell-cycle entry by cytokines and other agents known to activate normal stem cells, such as G-CSF and IFN-α, as well as arsenic trioxide in combination with the imatinib treatment [462].

LSCs but also HSCs express a high number of multidrug transporters of the ABC family, such as multidrug resistance-1 (MDR1) responsible for the active efflux of different cancer drugs and thereby also contributing to the chemoresistance of LSCs [463,464]. Niche targeting therapies might also contribute to weaken these cell intrinsic resistance mechanisms.

Finally, as LSCs and normal HSCs behave in the above-mentioned processes very similar, e.g. they share self-renewal pathways, treatments to target LSCs might also have a unacceptable toxicity to normal HSCs. The challenge is therefore to discover differences between normal HSCs and LSCs that enable the development of drugs, which selectively impair the proliferation, survival or self-renewal of LSCs, while sparing normal HSCs.

7. Aim of the Thesis

Kindlin-3 together with talin is required for the activation of integrins on hematopoietic cells. The kindlin-3 deficient mouse shows a lethal phenotype shortly after birth. The mice suffer from sever hemorrhages, neutrophilia, osteopetrosis and anemia. These multiple phenotypes can result from a defective integrin activity in several differentiated hematopoietic cell types and/or hematopoietic stem and progenitor cells (HSPCs), which are the origin of all hematopoietic cell types.

Adhesion molecules, especially integrins, are essential for the regulation of HSPCs in the BM to ensure a proper production of hematopoietic effector cells for the entire life of an organism. Defects in HSPC regulation can lead to a similar phenotype as observed in the kindlin-3 deficient mice, including pancytopenia, anemia and a reduced survival after BMT. The main aim of this thesis was, therefore, to investigate whether a dysfunction of kindlin-3 in early HSPCs of the adult hematopoietic system contributes to the observed blood defects. In order to investigate effects of kindlin-3 loss in BM HSPCs of adult mice we had to overcome the lethal phenotype of kindlin-3 deficient mice shortly after birth. Therefore, we generated fetal liver chimeras and investigated the functionality of kindlin-3 deficient HSPCs in a comparable approach with HSPCs from wt control chimeras in *in vivo* experiments under homeostasis and hematopoietic stress as well as in *ex vivo* experiments (**paper 1**).

A further aim of this thesis was to study the role of kindlin-3 in mature hematopoietic cell types and specific disease models. To investigate the neutrophelia in the kindlin-3 deficient mice we used *in vitro* and *in vivo* approaches to address the question, if a defective activation of not only β1 and β3 integrins, as previous shown on platelets, but also of β1, β2 and β3 on neutrophils due to the absence of kindlin-3 can be the reason for the severe neutrophila (**paper 2**). As the kindlin-3 mice also suffer from osteopetrosis, which could be induced by a dysfunction of bone resorbing OCLs, we asked if kindlin-3 is involved in activation of integrins on OCLs and hence regulate OCL-mediated bone resorption. We therefore, compared the function of kindlin-3 deficient OCLs with OCLs lacking different types of integrins (**paper 3**). We also observed that kindlin-3 null mice develop progressive thymus atrophy and kindlin-3 deficient chimeras were not able to produce T cells pointing to an important role of kindlin-3 in T cell development in the thymus. Thymic T cell development depends on the constant repopulation of the organ by T cell progenitors, being first generated in the fetal liver and later in the BM. Based on the fact that kindlin-3 deficient HSPCs have a severe BM homing defect and kindlin-3 deficient neutrophils show a leukocyte adhesion defect, we investigated extravasation and homing efficiency of kindlin-3 deficient T cell

progenitors into the pre- and post-vascular thymus with a combination of *in vitro* and *in vivo* experiments. In addition, we studied intrathymic differentiation of kindlin-3 deficient T cell progenitors and their interactions with different cell types within the thymus parenchyma (**paper 4**). In a previous study we showed that entry of autoreactive T cells into brain to induce EAE resembling MS in humans requires the activity of α4β1 integrin. We therefore investigated if a potential defect in the extravasation of kindlin-3 deficient T cells could also have an influence in the development of EAE. To address this question we studied kindlin-3 deficient mice in different *in vivo* EAE mouse models as well as *in vitro* adhesion assays (**paper 5**).

In another study we asked how much kindlin-3 is required to maintain blood cell functions. To address this question we generated hypomorphic kindlin-3 mice expressing different amounts of kindlin-3 and analyzed their phenotype as well as the functionality of different hematopoietic cells in *in vivo* and *in vitro* experiments (**paper 6**). To investigate the interaction between kindlin-3 and β1 integrins in more detail, we used platelets as a model system and addressed the following questions. Fist, do β1 integrins play an important role in the functionality of platelets? Second, is there also a dose-dependence for the function of β1 integrins on platelets? And finally, is the interaction of kindlin-3 with β1 necessary for normal platelet functions? To address these questions we compared the functions of platelets from β1 integrin deficient mice, β1 integrin hypomorphic mice (expressing only 3% of β1 integrins) and kindlin-3 binding-deficient β1 integrin mutant mice in *in vitro* and *in vivo* experiments (**paper 7**). Finally, we tested why kindlin-1 expressed in skin leads to increased tumor susceptibility. In a series of *in vivo* and *in vitro* experiments we could show that kindlin-1 influences the activity of cutaneous epithelial stem cells (**paper 8**).

8. Brief Summaries of Publications

Paper 1:

Kindlin-3 controls quiescence of hematopoietic stem cells in mice.

Ruppert R, Moser M, Sperandio M, Rognoni E, Orban M, Oostendorp RAJ, Steffen Massberg S, and Fässler R

Adhesion molecules, especially integrins, are responsible for a precise positioning of HSCs in the specific BM microenvironment, termed niche, thereby influencing the exposure of HSCs to regulatory factors essential to ensure a life-long hematopoietic cell production. HSCs express multiple classes of integrins, which are critically important for their homing to and function in the BM as well as mobilization from the BM into the blood circulation. The functional activity of integrins is controlled by an activation step, which requires binding of talin and kindlin-3 to the cytoplasmic domains of β integrin subunits, followed by the assembly of a signaling hub at the integrin tails.

To investigate the role of kindlin-3 in the regulation of HSCs homeostasis, we had to overcome the lethal phenotype of the kindlin-3 deficient mice shortly after birth. Therefore, we generated chimeric mice by transplanting fetal liver cells into lethally irradiated recipients. Loss of kindlin-3 expression in HSCs severely impairs their BM homing potential due to defects in adhesion to the microvascular endothelium. Kindlin-3 deficient HSCs ($K3^{-/-}$ HSCs) in the BM intersitium are constantly proliferating and spontaneously mobilized into the peripheral blood, resulting in a rapid HSC exhaustion and a reduced survival potential of the recipient mice. Loss of quiescence is likely caused by defective lodgment into the BM niche, leading to the loss of "stemness" in $K3^{-/-}$ HSCs, causing a strongly reduced engraftment potential in serial BM transplantation. In mice transplanted with $K3^{-/-}$ and wt BM cells, $K3^{-/-}$ HSCs can enter quiescence, but activated $K3^{-/-}$ HSPCs were still reduced and replaced by wt HSPCs under homeostatic conditions. However, induction of hematopoietic stress in these mix-chimeras leads to the complete displacement of the $K3^{-/-}$ HSCs, demonstrating that integrin-mediated HSC adhesion in the BM is essential for active but dispensable for quiescent HSCs. The defective engraftment further precluded the development of a chronic myeloid leukemia (CML) by BCR-ABL transduced $K3^{-/-}$ BM cells transplanted into sublethally irradiated mice.

In conclusion, the global impairment of integrins shows that they are important for basic HSC functions such as homing, mobilization, proper localization in the niche, proliferation,

differentiation or the maintenance of stem cell identity during homeostasis and essential in situations of hematopoietic stress and malignancies.

Paper 2:

Kindlin-3 is required for β2 integrin-mediated leukocyte adhesion to endothelial cells.

Moser M, Bauer M, Schmid S, **Ruppert R**, Schmidt S, Sixt M, Wang HV, Sperandio M, and Fässler R

Proper activation of integrins is crucial for the function of all hematopoietic cells. Kindlin-3 is a FERM domain-containing protein expressed specifically in hematopoietic cells and necessary for activation of β1 and β3 integrins on platelets. Impaired β1 and β3 but also β2 integrin activation occurs on platelets and leukocytes in patients suffering from a rare autosomal recessive disease called leukocyte adhesion deficiency (LAD-III). The LAD-III patients display severe hemorrhages and impaired leukocyte adhesion to inflamed endothelia. With this work we were able to demonstrate that kindlin-3 is essential for the activation of β2 integrins and that depletion of kindlin-3 leads to a LAD-III like phenotype in mice. The activation of β2 integrins is mediated by a direct binding of kindlin-3 to the membrane distal NxxF motif of the cytoplasmic tail of the β subunit. This interaction was proven to be fundamental for neutrophil spreading on β2 integrin ligands such as ICAM-1 and binding to iC3b, which is the product of complement C3 activation and fibrinogen. In addition, the chemokine-triggered adhesion of neutrophils is impaired. Furthermore, *in vivo* experiments on $K3^{-/-}$ BM chimeras revealed that $K3^{-/-}$ neutrophils fail to extravasate into inflamed tissues and intravital microscopy on cremaster muscle venules showed that loss of kindlin-3 expression leads to loss of firm neutrophil adhesion and arrest on activated endothelial cells, which was further confirmed in *in vitro* adhesion assays. However, we did not observe any defects in selectin-mediated rolling. In conclusion, kindlin-3 is a fundamental activator of β1, β3 as well as β2 integrins and its deletion leads to a LAD-III-like phenotype in mice.

Paper 3:

Kindlin-3-mediated signaling from multiple integrin classes is required for osteoclast-mediated bone resorption.

Schmidt S, Nakchbandi I, **Ruppert R**, Kawelke N, Hess MW, Pfaller K, Jurdic P, Fässler R, and Moser M

Mutation of the kindlin-3 gene in humans leads to a leukocyte adhesion deficiency type III (LAD-III) disorder. Some of the LAD-III patients also suffer from osteopetrosis. The exact mechanism of this defective bone turnover is still unclear. In general, bone homeostasis is dependant on the balance between bone formation performed by OBs, and bone resorption performed by OCLs. With our experiments we could show that loss of kindlin-3 in mice leads to severe osteopetrosis due to defects in adhesion and spreading of bone-resorbing OCLs. Although long bones of kindlin-3 deficient mice have a severe, early onset osteopetrosis, the number of OCLs is even increased. *In vitro* analysis of the kindlin-3 deficient OCLs revealed normal marker gene expression, normal protease activity and only a mild defect in their differentiation, which can be overcome by high concentrations of M-CSF. The bone resobing function of OCLs is dependant on formation of podosoms, actin rich structures connected to the bone matrix trough, mainly, αVβ3 integrins. Mature OCLs organize podosomes into sealing zones, which tightly circumvent the active sites of bone resorption and contain high concentrations of secreted protons and bone resorbing enzymes. A proper podosome function is necessary for formation of sealing zones and bone resorption. We were able to demonstrate that the deletion of kindlin-3 leads to impaired activation of integrin β1, β2, and β3 on osteoclasts, thereby abrogating the assembly of functional podosomes. In the absence of kindlin-3 podosomal actin core formation did occur, however, mature kindlin-3 deficient osteoclasts were unable to organize their podosoms in belts (on glass) or sealing zones (on bone matrices). In line with these results, we were able to further demonstrate that deletion of β1, β2, and β3 integrin classes impairs the development of podosomes, similarly to kindlin-3 deletion, while the deletion of single integrins classes did not impair the podosom formation but rather only their resorptive function. Taken together we were able to show that OCLs depend on the kindlin-3 mediated activation of all their specific integrins for maintaining bone homeostasis. Until now αvβ3 was considered the most important integrin on osteoclasts.

Paper 4:

Role of kindlin-3 in T cell progenitor homing and thymocyte development.

Moretti FA, **Ruppert R,** Fässler R and Moser M

T cell progenitors are generated in the BM but T cell differentiation takes place in the thymus. Therefore, a continuous repopulation of the thymus by progenitor cells is essential for an appropriate production of T cells. Thymic T cell development depends on interactions with various cell types critical for T cell progenitor homing to the thymus anlage and the stepwise progression during thymocyte maturation. Hereby the role of integrins is not defined, which might be due to functional compensations by different integrin members. To elucidate the role of integrins during T cell progenitor homing and subsequent differentiation, we studied T cell development in mice lacking the blood cell specific general integrin regulator kindlin-3. We observed that kindlin-3 null mice develop a progressive thymus atrophy and could further show that this is mainly caused by an impaired homing of T cell progenitors to the vascularized thymus in an *in vivo* homing assay carried out with fetal liver cells from wild-type and kindlin-3-null embryos transplanted into RAG-2-null mice lacking mature T cells. T cell progenitors, which entered the thymus anlage during development, were able to differentiate into single $CD4^+$ and $CD8^+$ T cells and emigrate into the circulation. Experiments showed that kindlin-3 deficient fetal liver-derived T cell progenitors colonize the avascular thymus primordium, albeit less efficient than wild-type T cell progenitors. Flow cytometic analysis of the fetal liver HSPC revealed that kindlin-3 deficient T cell progenitors are normally produced but accumulate in the circulation. *In vitro* assays revealed that the kindlin-3 deficient T cell progenitors are functional as they efficiently migrate towards a chemokine gradient, produced by the thymus epithelial cells and differentiate into the different T cell subsets once they have passed the vasculature. Furthermore, kindlin-3 deficient thymocytes migrate correctly through distinct thymic regions and show normal maturation, *in vivo* BrdU label assays revealed that they exhibit a reduced proliferation capacity due to a weakened crosstalk with a reduced number of thymic antigen-presenting cells. Taken together we were able to show that the colonization of the vascularized thymus by BM-derived T cell progenitors during late embryogenesis and after birth is kindlin-3 and integrin-dependent, while the fetal population of the embryonic thymus anlage by T cell progenitors can occur in a kindlin-3 and integrin-independent manner.

Paper 5:

Kindlin-3 regulates integrin activation and adhesion reinforcement of effector T cells.

Moretti FA, Moser M, Lyck R, Abadier M, **Ruppert R**, Engelhardt B, and Fässler R

The integrin α4β1 heterodimer expressed on activated T cells is necessary for their capture, rolling on, and firm adhesion to endothelial cells. Furthermore, activated T cells use the αLβ2 integrin heterodimer for subsequent crawling and extravasation. Inhibition of α4β1 can block extravasation of activated T cells and is, therefore, used as treatment of autoimmune diseases such as MS. In this study we investigated if the integrin activator kindlin-3 in T cells is required to induce autoimmune diseases in mice.

By immunization of mice lacking kindlin-3 in T cells with autoantigen we demonstrated that deletion of kindlin-3 in effector T cells does not impair their extravasation and consequent induction of EAE. Opposite to this, the deletion of kindlin-3 in autoreactive T cells impaired their extravasation into the naïve CNS upon adoptive transfer into mice and thereby prevented the induction of a passive EAE compared to wt autoreactive T cells. However, kindlin-3 deficient autoreactive T cells are able to extravasate into inflamed CNS due to a high expression of integrin ligands on the brain microvasculature. We were further able to show that kindlin-3 null effector T cells can adhere to high concentrations of α4β1 integrins and ICAM-1 under conditions of physiological sheer stress in *in vitro* flow chamber assays, although with a reduced efficiency compared to wild type T cells. However, despite the ability of few of this arrested T cells to polarize and start crawling, only small number of them remained firmly adherent for longer period of time. Therefore, we could conclude that in the conditions of low integrin ligand expression, kindlin-3 is essential for activation of α4β1 and αLβ2 integrin and subsequent ligand binding as well as stabilization of integrin-ligand bonds, while under conditions of high ligand levels kindlin-3 is less crucial.

Paper 6:

Platelets and neutrophils require different Kindlin-3 copy numbers to control integrin-mediated functions *in vivo*.

Schmidt S, Moretti F, Zeiler M, **Ruppert R**, Mann M, Sperandio M, Fässler R, and Moser M

Integrins are cell adhesion receptors, which anchor cell to the ECM and regulate numerous cellular processes such as cell migration, proliferation, differentiation and survival. Integrin activation is regulated by two protein families: talins (talin-1 and -2) and kindlins (kindlin-1, -2, and -3). Kindlin-3 and talin-1 are expressed on hematopoietic cells and both control integrin activation thought their tightly controlled binding to the β integrin tail, subsequently influencing numerous hematopoietic cell functions. Little is known about the signaling processes regulating the interaction between both proteins and integrins or if both proteins, bind at the same time or sequentially to the β integrin tail. Furthermore it is also unclear if a specific stoichiometry of both proteins is critical for the activation of integrins.

To test how much kindlin-3 is required for a normal function of platelets and neutrophils we generated hypomorphic kindlin-3 mouse mutants expressing 50%, 10% and 5% of kindlin-3. Despite limited activation of integrins, mice expressing 5% and 10% of kindlin-3 were viable. However, these mice had reduced platelet adhesion and aggregation and therefore showed severe bleeding during tail-bleeding assay. Interestingly, kindlin-3 hypomorph mice showed only mild leukocyte adhesion deficiency in the ear and in the cremaster muscle upon inflammation induction, although neutophils isolated from these mice had a sever adhesion defect compared to wt cells in a static adhesion assay. Platelets and neutrophils show equal levels of both kindlin-3 and talin-1 per cell as shown by absolute quantification. In addition, quantification of β2, and β3 integrins revealed that platelets have a 2:1 ratio of kindlin-3 and talin-1 in relation to β3 integrin molecules. Neutrophils, however, have a 1:2 ratio of kindlin-3 and talin-1 in relation to β2 integrin molecules. In conclusion we showed that 5% of kindlin-3 in mice is sufficient for a normal development and maintenance of hematopoietic homeostasis, albeit with increased leukocyte counts. Furthermore, this shows that the normal expression of kindlin-3 is necessary for platelet-mediated hemostasis. Contrary to this, leukocytes require much lower levels of kindlin-3 as the hypomorphic kindlin-3 neutrophils showed efficient adhesion and extravasation.

Paper 7:

β1 integrin-mediated signals are required for platelet granule secretion and hemostasis in mouse.

Petzold T, **Ruppert R**, Pandey D, Barocke V, Meyer H, Lorenz M, Zhang L, Siess W, Massberg S, and Moser M

Platelets depend crucially on integrins for adhesion and aggregation in the process of arterial thrombosis as well as during hemostasis. Circulating platelets express integrins in an inactive conformation, which are rapidly activated by extracellular stimuli at sites of vascular injury. An essential role for the platelet-specific αIIbβ3 integrin is already well understood, while the role of β1 integrins expressed on platelets is still controversial.

Therefore, we used β1-null mice, hypomorph mice expressing 3% of wild-type β1 integrin levels, and activation-deficient β1 integrin mutants to analyzed the function of β1 integrins during arterial thrombosis. Platelets isolated from all three types of mutants showed a deficient adhesion to and spreading on collagen *in vitro*. The adhesion defects of the three mutant platelet types were further confirmed in an *in vivo* carotid ligation model. Adding of Mn^{2+} and thereby bypassing integrin inside-out signaling, rescued the spreading defect only in the activation-deficient β1 integrin mutant platelets. The fact that kindlin-3 is not able to bind the cytoplasmic tail of these mutants indicates that a direct interaction between kindlin-3 and β1 integrin is not required for integrin outside-in signaling. In a tail-bleeding assay we investigated the role of β1 for occlusive thrombus formation and observed that 3% of β1 integrin is sufficient to enable a normal hemostasis. We next investigated activation of Rac-1, actin dynamics and granule secretion in the different mutant platelets, which were only affected in the hypomorphic platelets indicating that 3% of β1 expression is sufficient for a rapid Rac-1 activation required to remodel the platelet actin cytoskeleton and granule secretion in response to fibrous collagen. In summary, we found that β1 integrins on platelets function as a signaling receptor rather than as adhesion receptor, and thereby have an essential role for platelet granule secretion and hemostasis in mice. This new *in vivo* role of β1 intergins makes them a promising antithrombotic target that should be further explored.

Paper 8:

Kindlin-1 controls cutaneous epithelial stem cell proliferation by modulating Wnt ligand and TGFβ availability.

Rognoni E, Widmaier M, Jakobson M, **Ruppert R**, Ussar S, Katsougkri D, Böttcher RT, Lai-Cheong JE, Rifkin DB, McGrath J, and Fässler R

Epidermal and hair follicle (HF) keratinocytes express the integrin activating proteins kindlin-1 and kindlin-2, which are highly similar in their sequence but cannot compensate for each other. In humans, mutations in the kindlin-1 gene leads to an autosomal recessive genodermatosis called Kindlier Syndrome (KS), which is characterized by trauma-induced skin blisters, premature skin ageing, pigmentation defects, photosensitivity, and increased risk for malignancies such as skin cancer. Since compromised integrins protect from skin tumors we wanted to investigate how the integrin activator kindlin-1 induces tumor formation.

To this end we generated a knock-out mouse where the deletion of kindlin-1 is restricted to keratinocytes (Kind1-K5 mice) and observed that the phenotype of the mice resembles the phenotype of KS patients. In addition, Kind1-K5 mice show a misregulation of the epithelial stem cell homeostasis resulting in enlarged and hyperactive stem cell compartments leading to hyperthickened epidermis, ectopic hair follicle development and increased skin tumor susceptibility. The aberrant hair coat was caused by a kindlin-1 specific and β1 integrin-independent mechanism, while aberrant keratinocyte adhesion was due to a dysfunction of β1-class integrins.

Under normal conditions the HF bulge harbors dormant stem cells, which have to become sequentially active to maintain the hair cycle. The regulation of stem cell activity is mediated by a tight interplay between signaling pathways keeping stem cells quiescent such as BMP and TGFβ signaling and activating signaling pathways such as canonical Wnt/β-catenin signaling. The integrin αvβ6 is important for the release of TGFβ from the latency associated protein and thereby suppresses the proliferation of bulge SCs. *In vivo* and *in vitro* experiments show that kindlin-1 deficient keratinocytes express a higher amount of the αvβ6 integrin but that these integrins are functionally inactive resulting in reduced TGFβ release. This finding indicates that kindlin-1 is required for activation of αvβ6 and subsequent TGFβ release. We also found that loss of kindlin-1 in keratinocytes results in increased nuclear translocation of β-catenin/Lef1 and Wnt/β-catenin signaling by *in vitro* experiments and *in vivo* by intercrossing the Kind1-K5 mouse with the TOPgal reporter mouse. Furthermore, we could show that loss of kindlin-3 results in a dysregulated expression of Wnt ligands, which was cell

autonomous and integrin-independent. To test whether the decreased TGFβ and augmented Wnt signaling in the Kind1-K5 mice increases the skin tumor susceptibility, we treated the Kind1-K5 mouse with DMBA and TPA. A single DMBA treatment was sufficient to induced tumor development with more and slightly larger tumors in Kind1-K5 animals compared to controls, indicating that the hyperproliferative state of Kind1-K5 keratinocytes promotes tumor development. In summary, our findings promote a novel and essential function of kindlin-1 in control of cutaneous epithelial stem cell homeostasis by balancing TGF-β mediated growth inhibitory and Wnt/β-catenin mediated growth-promoting signals.

Paper 9:

CD98hc facilitates B cell proliferation and adaptive humoral immunity.

Cantor J, Browne CD, **Ruppert R**, Féral CC, Fässler R, Rickert RC, and Ginsberg MH

Maintenance of the adaptive immunity is highly dependent on the selective proliferation of antigen-specific lymphocytes and consequent clonal expansion. It has been shown that the vertebrate membrane protein CD98 heavy chain (hc) is higher expressed on proliferating lymphocytes. Initially CD98hc has been described as a lymphocyte-activation antigen but its function in the immune system is still not clear jet. This protein has two different functions: first it functions as an amino acid transport and second it mediates integrin signaling.

To address the question if CD98hc is involved in the rapid lymphocyte proliferation required for effective adaptive immunity, we generated mice with a B cell specific deletion of the Slc3a2 gene ($Slc3a2^{f/f}CD19\text{-}Cre^{+}$ mice), encoding for CD98hc and thereby overcame the embryonic lethal phenotype of the CD98hc deficient mice. We observed that resulting $Slc3a2^{f/f}CD19\text{-}Cre^{+}$ mice had normal maturation and distribution of peripheral B cells and normal morphology of secondary lymphoid organs and concluded that the early B cell activation was not affected by the deletion of CD98hc. However, the $Slc3a2^{f/f}CD19\text{-}Cre^{+}$ mice had a lower antibody response after immunization compared to control mice, due to a complete suppression of B cell proliferation and plasma cell formation by CD98hc-null B cells. Viral transfection of CD98hc-deficient BM cells with CD98hc mutants, enabling the separation of the transporter function from the integrin dependent signaling functions of CD98hc and transplantation into lethally irradiated recipient mice revealed that the a mutant form of CD98hc mediating integrin signaling but not amino acid transport supported the proliferation of CD98hc-deficient B cells indicating that interaction between CD98hc and integrins is important for B cell proliferation. Loss of CD98hc further led to defects in

integrin-dependent events such as failure to sustain Erk1/2 activation and impaired down regulation of the cyclin-dependent kinase inhibitor p27, which is in common with the observed reduced B cell proliferation. Furthermore, mitogenic stimulation of a mixture of CD98hc-deficient and CD98hc-sufficient B cells resulted in an increased number of CD98hc-sufficient cells, indicating that CD98hc mediates a selective advantage in proliferating B cells. In conclusion, CD98hc is necessary for integrin-dependent clonal expansion of B cells, which is necessary for adaptive immunity, thereby becoming prevalent in vertebrates.

Paper 10:

The Mechanism of Kindlin-Mediated Activation of Integrin αIIbβ3.

Ye F, Petrich BG, Anekal P, Lefort CT, Kasirer-Friede A, Shattil SJ, **Ruppert R**, Moser M, Fässler R, and Ginsberg MH

The integrin activation and increased ligand binding has the crucial role in numerous processes from development, cell migration, ECM assembly, tumor metastasis, hemostasis, to thrombosis. Integrin activation is dependent on talin interaction with integrin β tail and is followed by both increased integrin monomer affinity and increased receptor clustering. In addition, loss of kindlin also leads to impaired integrin activation. How kindlin and talin cooperate in the process of integrin activation is still unclear. It is possible that kindlin promotes talin binding to integrin β tail. However, kindlins do not cause an increased association of talin with integrins. The kindlins have a high structure similarity to talin head domain (THD).

To test the effect of purified kindlin-3 on individual integrins we compared the effect of kindlin-3 and THD on the affinity of purified monomeric αIIbβ3 integrin, inserted in phospholipid bilayers (nanodiscs). We observed that kindlin-3, unlike THD, had little effect on integrin affinity under this *in vitro* conditions. In addition, kindlin-3 did not increase the activation by THD. We next addressed the question if kindlins differently promote the binding affinity of αIIbβ3 integrin to monovalent or multivalent ligands. We observed that kindlins enhanced the binding of αIIbβ3 to multivalent but not monovalent ligands and that for this effect neither an intact actin cytoskeleton nor myosin II-driven contractility was necessary. This was further confirmed by silencing kindlin-2 in Chinese hamster ovary cells expressing an active αIIbβ3 mutant, showing that binding of the oligomeric 3FN10 ligand was inhibited but not binding of monovalent 3FN10. To investigate the effect of kindlin-3 on

mouse platelets in an *in vivo* experiment, we generated mix-chimera by mixing in a 1:1 ratio either kindlin-3 or talin deficient hematopoietic cells with wt DdRed hematopoietic cells and injected them into lethally irradiated recipient mice. We observed that kindlin-3 deletion in platelets and nucleated cells leads to drastically reduced αIIbβ3 binding to multivalent but not monovalent ligands, whereas deletion of talin had major effects on both ligand types. In addition, we were able to demonstrate by total internal reflection fluorescence (TIRF) and electron microscopy that silencing of kindlins leads to reduced clustering of ligand-bound αIIbβ3. In conclusion, unlike talin, kindlins exert little influence on affinity of integrins for monovalent ligands but do increase clustering of talin-activated integrins, thereby enhancing multivalent ligand binding. Despite our input this finding is highly debated in our laboratory.

Paper 11:

Knock-down and knockout of β1-integrin in hepatocytes impairs liver regeneration through inhibition of growth factor signaling.

Speicher T, Siegenthaler B, Bogorad RL, **Ruppert R**, Petzold T, Padrissa-Altes S, Bachofner M, Anderson DG, Kotelianski V, Fässler R, and Sabine Werner

Extensive remodeling of cell-cell and cell-matrix contacts is essential for liver regenerative capability. Despite this, the roles of integrins, a major class of adhesion molecules, in liver regeneration have been poorly studied and still remain unclear.

In this study, we aspired to determine the functions of β1 integrins in liver regeneration by using $\beta1^{fl/fl}$-Mx1Cre mice, in which the deletion of β1 integrins is inducible by administration of polyinosinic-polycytidylic acid (polyI:C), or mice in which the deletion of β1 integrins is mediated by intravenous delivery of siRNAs formulated into nanoparticles, efficiently ablating β1-integrin expression in hepatocytes. We were able to demonstrate that in non-challenged livers, loss of β1 integrins was not harmfull. However, after partial hepatectomy a severe liver necrosis and reduced heptocyte proliferation was observed. The deletion of β1 integrins in hepatocytes led to impaired ligand-induced phosphorylation of the EGF and HGF receptors and subsequently to defects in down-stream signaling such as phosphorylation of Erk, Akt or c-Met both *in vitro* and *in vivo*. In summary, we could conclude that β1 integrins play a crucial role in liver regeneration. In addition, we were able to demonstrate that liver specific gene targeting by nanoparticle-based delivery of siRNAs can be a useful tool to study gene functions in the regenerating liver.

9. Acknowledgements

I would like to thank all the people who contributed with their help, knowledge and support to this thesis.

First, I most sincerely thank Prof. Dr. Reinhard Fässler for giving me the opportunity to work in his department, for his trust in me and my work, his continuous support, discussions and excellent supervision.

PD Dr. Markus Moser I thank for his supervision, discussion and technical support. I learned a lot from his excellent technical expertise.

Further, I want to thank Prof. Dr. Markus Sperandio for being the second referee of my thesis and Prof. Dr. Christian Wahl-Schott, PD Dr. Robert Oostendorp, Prof. Dr. Martin Biel, and PD Dr. Dietmar E. Martin for agreeing to be members of my thesis committee and for taking the time to review my work.

Very special thanks to all the collaboration partners, namely Prof. Dr. Steffen Massberg, Prof. Dr. Markus Sperandio, PD Dr. Robert Oostendorp, Dr. Martin Orban, Susanne Bierschenk and Sarah Longhi, for the fruitful collaborations, contributing a lot to this work.

I want to thank Dr. Marc Schmidt-Supprian, Christoph, Klaus and David for the helpful discussions, support and great time in as well as outside the lab.

I also want to thank all current and former members of the Fässler lab, for their help and discussion and for creating a good working atmosphere as well as the funny time outside the lab. I specially want to mention here Michi, Tom, Mandoo, Julien, Ralph, Tim, When-Shin, Emanuel, Moritz, Tobi, Alex, Karin, Michal, Misha, Sarah, and Moik.

I am also grateful to the members of the animal facility, especially Dr. Heinz Brandstetter and Dr. Corinna Mörth who were extremely cooperative. Special thanks to all the animal caretakers, who have been of extreme help to me, especially Bianca, Mia, Jens, and Flo.

Most importantly, I must express my gratitude to my parents, my brother and my sweet Korana. I could not have done this work without their constant support. Thank you!

10. Curriculum Vitae

Raphael Ruppert

Date of birth:	31st of July 1980
Place of birth:	Erlangen
Nationality:	German

EDUCATION

Sep. 2007 - present	**Max Planck Institute of Biochemistry**, Martinsried, Germany PhD student in the Department of Molecular Medicine, Prof. Dr. Reinhard Fässler PhD Thesis: "Role of integrins in regulation and maintenance of hematopoietic and leukemic stem cells in mouse models"
Jan. 2006 – Sep. 2006	**Max Planck Institute for Brain Research**, Frankfurt am Main, Germany Department of Neuroanatomy, Prof. Dr. Heinz Wässle Diploma thesis with Dr. Dieter Engelkamp Title: "The Role of Robo3 and N4wbp5 during midline crossing of neurons"
Oct. 2001 – Apr. 2007	**Technical University**, Darmstadt, Germany Diploma studies in biology Major field of study: Biochemistry, Cell- and Developmental Biology, Genetics Final grade: 1.0 with Honors
Jul. 1997 - Jun. 2000	**Schuldorf Bergstraße,** Seeheim-Jugenheim, Germany Secondary school University entrance qualification (Allgemeine Hochschulreife) Final grade: good (1.9)
Aug. 1991 – Jul. 1997	**Melibokusschule,** Alsbach, Germany Secondary school
Aug. 1987 – Jun. 1991	**Hans-Quick Schule,** Bickenbach, Germany Primary school

11. References

1. Tan SY, Brown J (2006) Rudolph Virchow (1821-1902): "pope of pathology". Singapore Med J 47: 567–568.

2. Takahashi K, Yamanaka S (2006) Induction of pluripotent stem cells from mouse embryonic and adult fibroblast cultures by defined factors. Cell 126: 663–676. doi:10.1016/j.cell.2006.07.024.

3. Takahashi K, Tanabe K, Ohnuki M, Narita M, Ichisaka T, et al. (2007) Induction of pluripotent stem cells from adult human fibroblasts by defined factors. Cell 131: 861–872. doi:10.1016/j.cell.2007.11.019.

4. Yu J, Vodyanik MA, Smuga-Otto K, Antosiewicz-Bourget J, Frane JL, et al. (2007) Induced pluripotent stem cell lines derived from human somatic cells. Science 318: 1917–1920. doi:10.1126/science.1151526.

5. Obokata H, Wakayama T, Sasai Y, Kojima K, Vacanti MP, et al. (2014) Stimulus-triggered fate conversion of somatic cells into pluripotency. Nature 505: 641–647. doi:10.1038/nature12968.

6. Sell S (2010) Stem Cells Handbook. Humana Press. 1 pp.

7. Lee M, Vasioukhin V (2008) Cell polarity and cancer--cell and tissue polarity as a non-canonical tumor suppressor. Journal of Cell Science 121: 1141–1150. doi:10.1242/jcs.016634.

8. Morrison SJ, Kimble J (n.d.) Asymmetric and symmetric stem-cell divisions in development and cancer. Nature 441: 1068–1074. doi:10.1038/nature04956.

9. Lemischka I (2002) A few thoughts about the plasticity of stem cells. Experimental Hematology 30: 848–852.

10. Manohar R, Lagasse E (2009) Transdetermination: a new trend in cellular reprogramming. Mol Ther 17: 936–938. doi:10.1038/mt.2009.93.

11. Alison MR, Poulsom R, Jeffery R, Dhillon AP, Quaglia A, et al. (2000) Hepatocytes from non-hepatic adult stem cells. Nature 406: 257. doi:10.1038/35018642.

12. Lagasse E, Connors H, Al-Dhalimy M, Reitsma M, Dohse M, et al. (2000) Purified hematopoietic stem cells can differentiate into hepatocytes in vivo. Nat Med 6: 1229–1234. doi:10.1038/81326.

13. Theise ND, Nimmakayalu M, Gardner R, Illei PB, Morgan G, et al. (2000) Liver from bone marrow in humans. Hepatology 32: 11–16. doi:10.1053/jhep.2000.9124.

14. Kocher AA, Schuster MD, Szabolcs MJ, Takuma S, Burkhoff D, et al. (2001) Neovascularization of ischemic myocardium by human bone-marrow-derived angioblasts prevents cardiomyocyte apoptosis, reduces remodeling and improves cardiac function. Nat Med 7: 430–436. doi:10.1038/86498.

15. Orlic D, Kajstura J, Chimenti S, Jakoniuk I, Anderson SM, et al. (2001) Bone marrow cells regenerate infarcted myocardium. Nature 410: 701–705. doi:10.1038/35070587.

16. Ferrari G, Cusella-De Angelis G, Coletta M, Paolucci E, Stornaiuolo A, et al. (1998) Muscle regeneration by bone marrow-derived myogenic progenitors. Science 279: 1528–1530.

17. Gussoni E, Soneoka Y, Strickland CD, Buzney EA, Khan MK, et al. (1999) Dystrophin expression in the mdx mouse restored by stem cell transplantation. Nature 401: 390–394. doi:10.1038/43919.

18. Brazelton TR, Rossi FM, Keshet GI, Blau HM (2000) From marrow to brain: expression of neuronal phenotypes in adult mice. Science 290: 1775–1779.

19. Mezey E, Chandross KJ, Harta G, Maki RA, McKercher SR (2000) Turning blood into brain: cells bearing neuronal antigens generated in vivo from bone marrow. Science 290: 1779–1782.

20. Wagers AJ, Weissman IL (2004) Plasticity of adult stem cells. Cell 116: 639–648.

21. Kumar R, Sharma A, Pattnaik A, Varadwaj P (2010) Stem cells: An overview with respect to cardiovascular and renal disease. J Nat Sc Biol Med 1: 43. doi:10.4103/0976-9668.71674.

22. Ogawa M (1993) Differentiation and proliferation of hematopoietic stem cells. Blood 81: 2844–2853.

23. Osawa M, Hanada K, Hamada H, Nakauchi H (1996) Long-term lymphohematopoietic reconstitution by a single CD34-low/negative hematopoietic stem cell. Science 273: 242–245.

24. Weissman IL (2000) Stem cells: units of development, units of regeneration, and units in evolution. Cell 100: 157–168.

25. Wilson A, Laurenti E, Oser G, van der Wath RC, Blanco-Bose W, et al. (2008) Hematopoietic Stem Cells Reversibly Switch from Dormancy to Self-Renewal during Homeostasis and Repair. Cell 135: 1118–1129. doi:10.1016/j.cell.2008.10.048.

26. Cheshier SH, Morrison SJ, Liao X, Weissman IL (1999) In vivo proliferation and cell cycle kinetics of long-term self-renewing hematopoietic stem cells. Proceedings of the National Academy of Sciences 96: 3120–3125. doi:10.1073/pnas.96.6.3120.

27. Bradford GB, Williams B, Rossi R, Bertoncello I (1997) Quiescence, cycling, and turnover in the primitive hematopoietic stem cell compartment. Experimental Hematology 25: 445–453.

28. Jacobson LO, Marks EK, Robson M, Zirkle RE (1949) The effect of spleen protection on mortality following x-irradiation. J Lab Clin Med: 1538–1543.

29. Lorenz E, Congdon C, Uphoff D (1951) Modification of Acute Irradiation Injury in Mice and Guinea-Pigs by Bone Marrow Injection. Radiology: 863–877.

30. Jacobson LO, Simmons EL, Marks EK, Eldredge JH (1951) Recovery from radiation injury. Science.

31. Till JE, McCulloch EA (1961) A direct measurement of the radiation sensitivity of

normal mouse bone marrow cells. Radiat Res 14: 213–222.

32. Becker AJ, McCulloch EA, Till JE (1963) Cytological demonstration of the clonal nature of spleen colonies derived from transplanted mouse marrow cells. Nature 197: 452–454.

33. Wu AM, Till JE, Siminovitch L, McCulloch EA (1967) A cytological study of the capacity for differentiation of normal hemopoietic colony-forming cells. J Cell Physiol 69: 177–184. doi:10.1002/jcp.1040690208.

34. Na Nakorn T (2002) Myeloerythroid-restricted progenitors are sufficient to confer radioprotection and provide the majority of day 8 CFU-S. Journal of Clinical Investigation 109: 1579–1585. doi:10.1172/JCI200215272.

35. Morrison SJ, Weissman IL (1994) The long-term repopulating subset of hematopoietic stem cells is deterministic and isolatable by phenotype. Immunity 1: 661–673.

36. Sigvardsson M (2009) New light on the biology and developmental potential of haematopoietic stem cells and progenitor cells. J Intern Med 266: 311–324. doi:10.1111/j.1365-2796.2009.02154.x.

37. Seita J, Weissman IL (2010) Hematopoietic stem cell: self-renewal versus differentiation. WIREs Syst Biol Med 2: 640–653. doi:10.1002/wsbm.86.

38. Traver D, Akashi K, Manz M, Merad M, Miyamoto T, et al. (2000) Development of CD8alpha-positive dendritic cells from a common myeloid progenitor. Science 290: 2152–2154.

39. Manz MG, Traver D, Miyamoto T, Weissman IL, Akashi K (2001) Dendritic cell potentials of early lymphoid and myeloid progenitors. Blood 97: 3333–3341.

40. Akashi K, Traver D, Miyamoto T, Weissman IL (2000) A clonogenic common myeloid progenitor that gives rise to all myeloid lineages. Nature 404: 193–197. doi:10.1038/35004599.

41. Orkin SH (2000) Diversification of haematopoietic stem cells to specific lineages. Nat Rev Genet 1: 57–64. doi:10.1038/35049577.

42. Zhu J, Emerson SG (2002) Hematopoietic cytokines, transcription factors and lineage commitment. Oncogene 21: 3295–3313. doi:10.1038/sj.onc.1205318.

43. Passegue E, Jamieson CHM, Ailles LE, Weissman IL (2003) Normal and leukemic hematopoiesis: Are leukemias a stem cell disorder or a reacquisition of stem cell characteristics? Proceedings of the National Academy of Sciences 100: 11842–11849. doi:10.1073/pnas.2034201100.

44. Matsuzaki Y, Kinjo K, Mulligan RC, Okano H (2004) Unexpectedly efficient homing capacity of purified murine hematopoietic stem cells. Immunity 20: 87–93.

45. Yilmaz ÖH, Kiel MJ, Morrison SJ (2006) SLAM family markers are conserved among hematopoietic stem cells from old and reconstituted mice and markedly increase their purity. Blood 107: 924–930. doi:10.1182/blood-2005-05-2140.

46. Doulatov S, Notta F, Laurenti E, Dick JE (2012) Hematopoiesis: a human perspective. Cell Stem Cell 10: 120–136. doi:10.1016/j.stem.2012.01.006.

47. Purton LE, Scadden DT (2007) Limiting Factors in Murine Hematopoietic Stem Cell Assays. Cell Stem Cell 1: 263–270. doi:10.1016/j.stem.2007.08.016.

48. Goodell MA, Brose K, Paradis G, Conner AS, Mulligan RC (1996) Isolation and functional properties of murine hematopoietic stem cells that are replicating in vivo. Journal of Experimental Medicine 183: 1797–1806.

49. Li CL, Johnson GR (1992) Rhodamine123 reveals heterogeneity within murine Lin-, Sca-1+ hemopoietic stem cells. Journal of Experimental Medicine 175: 1443–1447.

50. McAlister I, Wolf NS, Pietrzyk ME, Rabinovitch PS, Priestley G, et al. (1990) Transplantation of hematopoietic stem cells obtained by a combined dye method fractionation of murine bone marrow. Blood 75: 1240–1246.

51. Phillips RL, Reinhart AJ, Van Zant G (1992) Genetic control of murine hematopoietic stem cell pool sizes and cycling kinetics. Proc Natl Acad Sci USA 89: 11607–11611.

52. Wolf NS, Koné A, Priestley GV, Bartelmez SH (1993) In vivo and in vitro characterization of long-term repopulating primitive hematopoietic cells isolated by sequential Hoechst 33342-rhodamine 123 FACS selection. Experimental Hematology 21: 614–622.

53. Spangrude GJ, Brooks DM (1992) Phenotypic analysis of mouse hematopoietic stem cells shows a Thy-1-negative subset. Blood 80: 1957–1964.

54. Spangrude GJ, Brooks DM (1993) Mouse strain variability in the expression of the hematopoietic stem cell antigen Ly-6A/E by bone marrow cells. Blood 82: 3327–3332.

55. Morrison SJ, Hemmati HD, Wandycz AM, Weissman IL (1995) The purification and characterization of fetal liver hematopoietic stem cells. Proc Natl Acad Sci USA 92: 10302–10306.

56. Randall TD, Weissman IL (1997) Phenotypic and functional changes induced at the clonal level in hematopoietic stem cells after 5-fluorouracil treatment. Blood 89: 3596–3606.

57. Sato T, Laver JH, Ogawa M (1999) Reversible expression of CD34 by murine hematopoietic stem cells. Blood 94: 2548–2554.

58. Bradley TR, Metcalf D (1966) The growth of mouse bone marrow cells in vitro. Aust J Exp Biol Med Sci 44: 287–299.

59. van Os R, Kamminga LM, de Haan G (2004) Stem cell assays: something old, something new, something borrowed. Stem Cells 22: 1181–1190. doi:10.1634/stemcells.2004-0095.

60. Domen J, Weissman IL (1999) Self-renewal, differentiation or death: regulation and manipulation of hematopoietic stem cell fate. Molecular Medicine Today 5: 201–208.

61. Morrison SJ, Uchida N, Weissman IL (1995) The biology of hematopoietic stem cells. Annu Rev Cell Dev Biol 11: 35–71. doi:10.1146/annurev.cb.11.110195.000343.

62. Jordan CT, Lemischka IR (1990) Clonal and systemic analysis of long-term hematopoiesis in the mouse. Genes & Development 4: 220–232.

63. Coulombel L (2004) Identification of hematopoietic stem/progenitor cells: strength and drawbacks of functional assays. Oncogene 23: 7210–7222. doi:10.1038/sj.onc.1207941.

64. McCune JM, Namikawa R, Kaneshima H, Shultz LD, Lieberman M, et al. (1988) The SCID-hu mouse: murine model for the analysis of human hematolymphoid differentiation and function. Science 241: 1632–1639.

65. Kamel-Reid S, Dick JE (1988) Engraftment of immune-deficient mice with human hematopoietic stem cells. Science 242: 1706–1709.

66. Péault B, Weissman IL, Baum C, McCune JM, Tsukamoto A (1991) Lymphoid reconstitution of the human fetal thymus in SCID mice with CD34+ precursor cells. Journal of Experimental Medicine 174: 1283–1286.

67. Larochelle A, Vormoor J, Hanenberg H, Wang JC, Bhatia M, et al. (1996) Identification of primitive human hematopoietic cells capable of repopulating NOD/SCID mouse bone marrow: implications for gene therapy. Nat Med 2: 1329–1337.

68. Traggiai E, Chicha L, Mazzucchelli L, Bronz L, Piffaretti J-C, et al. (2004) Development of a human adaptive immune system in cord blood cell-transplanted mice. Science 304: 104–107. doi:10.1126/science.1093933.

69. Cumano A, Dieterlen-Lievre F, Godin I (1996) Lymphoid potential, probed before circulation in mouse, is restricted to caudal intraembryonic splanchnopleura. Cell 86: 907–916.

70. Godin I, Cumano A (2002) The hare and the tortoise: an embryonic haematopoietic race. Nature Reviews Immunology 2: 593–604. doi:10.1038/nri857.

71. Medvinsky A, Dzierzak E (1996) Definitive hematopoiesis is autonomously initiated by the AGM region. Cell 86: 897–906.

72. Müller AM, Medvinsky A, Strouboulis J, Grosveld F, Dzierzak E (1994) Development of hematopoietic stem cell activity in the mouse embryo. Immunity 1: 291–301.

73. Pietilä I, Vainio S (2005) The embryonic aorta-gonad-mesonephros region as a generator of haematopoietic stem cells. APMIS 113: 804–812. doi:10.1111/j.1600-0463.2005.apm_368.x.

74. de Bruijn MF, Speck NA, Peeters MC, Dzierzak E (2000) Definitive hematopoietic stem cells first develop within the major arterial regions of the mouse embryo. EMBO J 19: 2465–2474. doi:10.1093/emboj/19.11.2465.

75. Taoudi S, Medvinsky A (2007) Functional identification of the hematopoietic stem cell niche in the ventral domain of the embryonic dorsal aorta. Proc Natl Acad Sci USA 104: 9399–9403. doi:10.1073/pnas.0700984104.

76. Dzierzak E, Speck NA (2008) Of lineage and legacy: the development of mammalian hematopoietic stem cells. Nat Immunol 9: 129–136. doi:10.1038/ni1560.

77. Sabin FR (1917) Origin and development of the primitive vessels of the chick and of the pig. ContribEmbryol: 61–124.

78. Huber TL, Kouskoff V, Fehling HJ, Palis J, Keller G (2004) Haemangioblast commitment is initiated in the primitive streak of the mouse embryo. Nature 432: 625–630. doi:10.1038/nature03122.

79. Sabin FR (1920) Studies on the origin of blood vessels and of red corpuscles as seen in the living blastoderm of the chick during the second day of incubation. Contributions to Embryology 9: 213–262.

80. Sugiyama D, Ogawa M, Hirose I, Jaffredo T, Arai K-I, et al. (2003) Erythropoiesis from acetyl LDL incorporating endothelial cells at the preliver stage. Blood 101: 4733–4738. doi:10.1182/blood-2002-09-2799.

81. Jaffredo T, Bollerot K, Sugiyama D, Gautier R, Drevon C (2005) Tracing the hemangioblast during embryogenesis: developmental relationships between endothelial and hematopoietic cells. Int J Dev Biol 49: 269–277. doi:10.1387/ijdb.041948tj.

82. North TE, de Bruijn MFTR, Stacy T, Talebian L, Lind E, et al. (2002) Runx1 expression marks long-term repopulating hematopoietic stem cells in the midgestation mouse embryo. Immunity 16: 661–672.

83. Bertrand JY, Giroux S, Golub R, Klaine M, Jalil A, et al. (2005) Characterization of purified intraembryonic hematopoietic stem cells as a tool to define their site of origin. Proc Natl Acad Sci USA 102: 134–139. doi:10.1073/pnas.0402270102.

84. Inman KE, Downs KM (2007) The murine allantois: emerging paradigms in development of the mammalian umbilical cord and its relation to the fetus. Genesis 45: 237–258. doi:10.1002/dvg.20281.

85. Gekas C, Dieterlen-Lièvre F, Orkin SH, Mikkola HKA (2005) The placenta is a niche for hematopoietic stem cells. Developmental Cell 8: 365–375. doi:10.1016/j.devcel.2004.12.016.

86. Ottersbach K, Dzierzak E (2005) The murine placenta contains hematopoietic stem cells within the vascular labyrinth region. Developmental Cell 8: 377–387. doi:10.1016/j.devcel.2005.02.001.

87. Downs KM (1998) The murine allantois. Curr Top Dev Biol 39: 1–33.

88. Kumaravelu P, Hook L, Morrison AM, Ure J, Zhao S, et al. (2002) Quantitative developmental anatomy of definitive haematopoietic stem cells/long-term repopulating units (HSC/RUs): role of the aorta-gonad-mesonephros (AGM) region and the yolk sac in colonisation of the mouse embryonic liver. Development. 2002

Nov;129(21):4891-9.

89. Takeuchi M, Sekiguchi T, Hara T, Kinoshita T, Miyajima A (2002) Cultivation of aorta-gonad-mesonephros-derived hematopoietic stem cells in the fetal liver microenvironment amplifies long-term repopulating activity and enhances engraftment to the bone marrow. Blood 99: 1190–1196.

90. Ema H, Nakauchi H (2000) Expansion of hematopoietic stem cells in the developing liver of a mouse embryo. Blood 95: 2284–2288.

91. Jenkinson EJ, Jenkinson WE, Rossi SW, Anderson G (2006) The thymus and T-cell commitment: the right niche for Notch? Nature Reviews Immunology 6: 551–555. doi:10.1038/nri1883.

92. Djaldetti M, Bessler H, Rifkind RA (1972) Hematopoiesis in the embryonic mouse spleen: an electron microscopic study. Blood 39: 826–841.

93. Houssaint E (1981) Differentiation of the mouse hepatic primordium. II. Extrinsic origin of the haemopoietic cell line. Cell Differ 10: 243–252.

94. Johnson GR, Moore MA (1975) Role of stem cell migration in initiation of mouse foetal liver haemopoiesis. Nature 258: 726–728.

95. Orkin SH, Zon LI (2008) Hematopoiesis: an evolving paradigm for stem cell biology. Cell 132: 631–644. doi:10.1016/j.cell.2008.01.025.

96. Olsen BR, Reginato AM, Wang W (2000) Bone Development - Annual Review of Cell and Developmental Biology, 16(1):191.

97. Suárez-Álvarez B, López-Vázquez A, López-Larrea C (2012) Mobilization and homing of hematopoietic stem cells. Adv Exp Med Biol 741: 152–170. doi:10.1007/978-1-4614-2098-9_11.

98. Massberg S, Schaerli P, Knezevic-Maramica I, Köllnberger M, Tubo N, et al. (2007) Immunosurveillance by Hematopoietic Progenitor Cells Trafficking through Blood, Lymph, and Peripheral Tissues. Cell 131: 994–1008. doi:10.1016/j.cell.2007.09.047.

99. Shizuru JA, Negrin RS, Weissman IL (2005) Hematopoietic stem and progenitor cells: clinical and preclinical regeneration of the hematolymphoid system. Annu Rev Med 56: 509–538. doi:10.1146/annurev.med.54.101601.152334.

100. Papayannopoulou T (2003) Bone marrow homing: the players, the playfield, and their evolving roles. Curr Opin Hematol 10: 214–219.

101. Springer TA (1994) Traffic signals for lymphocyte recirculation and leukocyte emigration: the multistep paradigm. Cell 76: 301–314.

102. Bonig H (2006) Hierarchy of molecular-pathway usage in bone marrow homing and its shift by cytokines. Blood 107: 79–86. doi:10.1182/blood-2005-05-2023.

103. Lapidot T (2005) How do stem cells find their way home? Blood 106: 1901–1910. doi:10.1182/blood-2005-04-1417.

104. Bonig H (2004) PTX-sensitive signals in bone marrow homing of fetal and adult hematopoietic progenitor cells. Blood 104: 2299–2306. doi:10.1182/blood-2004-04-1605.

105. Quesenberry PJ, Becker PS (1998) Stem cell homing: rolling, crawling, and nesting. Proc Natl Acad Sci USA 95: 15155–15157.

106. Ley K, Laudanna C, Cybulsky MI, Nourshargh S (2007) Getting to the site of inflammation: the leukocyte adhesion cascade updated. Nature Reviews Immunology 7: 678–689. doi:10.1038/nri2156.

107. Mazo IB, Quackenbush EJ, Lowe JB, Andrian von UH (2002) Total body irradiation causes profound changes in endothelial traffic molecules for hematopoietic progenitor cell recruitment to bone marrow. Blood 99: 4182–4191.

108. Mazo IB, Andrian von UH (1999) Adhesion and homing of blood-borne cells in bone marrow microvessels. J Leukoc Biol 66: 25–32.

109. Mazo IB, Gutierrez-Ramos JC, Frenette PS, Hynes RO, Wagner DD, et al. (1998) Hematopoietic progenitor cell rolling in bone marrow microvessels: parallel contributions by endothelial selectins and vascular cell adhesion molecule 1. Journal of Experimental Medicine 188: 465–474.

110. Papayannopoulou T, Priestley GV, Nakamoto B, Zafiropoulos V, Scott LM (2001) Molecular pathways in bone marrow homing: dominant role of alpha(4)beta(1) over beta(2)-integrins and selectins. Blood 98: 2403–2411.

111. Peled A, Petit I, Kollet O, Magid M, Ponomaryov T, et al. (1999) Dependence of human stem cell engraftment and repopulation of NOD/SCID mice on CXCR4. Science 283: 845–848.

112. Adams GB, Alley IR, Chung U-I, Chabner KT, Jeanson NT, et al. (2009) Haematopoietic stem cells depend on Gαs-mediated signalling to engraft bone marrow. Nature 459: 103–107. doi:10.1038/nature07859.

113. Katayama Y, Hidalgo A, Peired A, Frenette PS (2004) Integrin alpha4beta7 and its counterreceptor MAdCAM-1 contribute to hematopoietic progenitor recruitment into bone marrow following transplantation. Blood 104: 2020–2026. doi:10.1182/blood-2003-12-4157.

114. Feuerer M, Beckhove P, Mahnke Y, Hommel M, Kyewski B, et al. (2004) Bone marrow microenvironment facilitating dendritic cell: CD4 T cell interactions and maintenance of CD4 memory. Int J Oncol 25: 867–876.

115. Dimitroff CJ, Lee JY, Rafii S, Fuhlbrigge RC, Sackstein R (2001) CD44 is a major E-selectin ligand on human hematopoietic progenitor cells. J Cell Biol 153: 1277–1286.

116. Vermeulen M, Le Pesteur F, Gagnerault MC, Mary JY, Sainteny F, et al. (1998) Role of adhesion molecules in the homing and mobilization of murine hematopoietic stem and progenitor cells. Blood 92: 894–900.

117. Avigdor A, Goichberg P, Shivtiel S, Dar A, Peled A, et al. (2004) CD44 and

hyaluronic acid cooperate with SDF-1 in the trafficking of human CD34+ stem/progenitor cells to bone marrow. Blood 103: 2981–2989. doi:10.1182/blood-2003-10-3611.

118. Petit I, Goichberg P, Spiegel A, Peled A, Brodie C, et al. (2005) Atypical PKC-zeta regulates SDF-1-mediated migration and development of human CD34+ progenitor cells. Journal of Clinical Investigation 115: 168–176. doi:10.1172/JCI21773.

119. Yong KL, Watts M, Shaun Thomas N, Sullivan A, Ings S, et al. (1998) Transmigration of CD34+ cells across specialized and nonspecialized endothelium requires prior activation by growth factors and is mediated by PECAM-1 (CD31). Blood 91: 1196–1205.

120. Imbert A-M, Belaaloui G, Bardin F, Tonnelle C, Lopez M, et al. (2006) CD99 expressed on human mobilized peripheral blood CD34+ cells is involved in transendothelial migration. Blood 108: 2578–2586. doi:10.1182/blood-2005-12-010827.

121. Katayama Y (2003) PSGL-1 participates in E-selectin-mediated progenitor homing to bone marrow: evidence for cooperation between E-selectin ligands and 4 integrin. Blood 102: 2060–2067. doi:10.1182/blood-2003-04-1212.

122. Bowie MB, McKnight KD, Kent DG, McCaffrey L, Hoodless PA, et al. (2006) Hematopoietic stem cells proliferate until after birth and show a reversible phase-specific engraftment defect. Journal of Clinical Investigation 116: 2808–2816. doi:10.1172/JCI28310.

123. Passegue E, Wagers A, Giuriato S, Anderson W, Weissman I (2005) Global analysis of proliferation and cell cycle gene expression in the regulation of hematopoietic stem and progenitor cell fates. Journal of Experimental Medicine 202: 1599–1611. doi:10.1084/jem.20050967.

124. Anasetti C, Amos D, Beatty PG, Appelbaum FR, Bensinger W, et al. (1989) Effect of HLA compatibility on engraftment of bone marrow transplants in patients with leukemia or lymphoma. N Engl J Med 320: 197–204. doi:10.1056/NEJM198901263200401.

125. Broxmeyer HE, Douglas GW, Hangoc G, Cooper S, Bard J, et al. (1989) Human umbilical cord blood as a potential source of transplantable hematopoietic stem/progenitor cells. Proc Natl Acad Sci USA 86: 3828–3832.

126. Broxmeyer HE, Hangoc G, Cooper S, Ribeiro RC, Graves V, et al. (1992) Growth characteristics and expansion of human umbilical cord blood and estimation of its potential for transplantation in adults. Proc Natl Acad Sci USA 89: 4109–4113.

127. Zheng Y, Watanabe N, Nagamura-Inoue T, Igura K, Nagayama H, et al. (2003) Ex vivo manipulation of umbilical cord blood-derived hematopoietic stem/progenitor cells with recombinant human stem cell factor can up-regulate levels of homing-essential molecules to increase their transmigratory potential. Experimental Hematology 31: 1237–1246.

128. Voermans C, Kooi ML, Rodenhuis S, van der Lelie H, van der Schoot CE, et al. (2001) In vitro migratory capacity of CD34+ cells is related to hematopoietic

recovery after autologous stem cell transplantation. Blood 97: 799–804.

129. Ramírez M, Segovia JC, Benet I, Arbona C, Güenechea G, et al. (2001) Ex vivo expansion of umbilical cord blood (UCB) CD34(+) cells alters the expression and function of alpha 4 beta 1 and alpha 5 beta 1 integrins. Br J Haematol 115: 213–221.

130. Trumpp A, Essers M, Wilson A (2010) Awakening dormant haematopoietic stem cells. Nature Reviews Immunology 10: 201–209. doi:10.1038/nri2726.

131. Wright DE, Wagers AJ, Gulati AP, Johnson FL, Weissman IL (2001) Physiological migration of hematopoietic stem and progenitor cells. Science 294: 1933–1936. doi:10.1126/science.1064081.

132. Welner RS, Kincade PW (2007) Stem cells on patrol. Cell 131: 842–844. doi:10.1016/j.cell.2007.11.010.

133. Pitchford SC, Furze RC, Jones CP, Wengner AM, Rankin SM (2009) Differential mobilization of subsets of progenitor cells from the bone marrow. Cell Stem Cell 4: 62–72. doi:10.1016/j.stem.2008.10.017.

134. Levesque JP (2001) Vascular cell adhesion molecule-1 (CD106) is cleaved by neutrophil proteases in the bone marrow following hematopoietic progenitor cell mobilization by granulocyte colony-stimulating factor. Blood 98: 1289–1297. doi:10.1182/blood.V98.5.1289.

135. Heissig B, Hattori K, Dias S, Friedrich M, Ferris B, et al. (2002) Recruitment of stem and progenitor cells from the bone marrow niche requires MMP-9 mediated release of kit-ligand. Cell 109: 625–637.

136. Kollet O, Dar A, Shivtiel S, Kalinkovich A, Lapid K, et al. (2006) Osteoclasts degrade endosteal components and promote mobilization of hematopoietic progenitor cells. Nat Med 12: 657–664. doi:10.1038/nm1417.

137. Lévesque J-P, Hendy J, Takamatsu Y, Simmons PJ, Bendall LJ (2003) Disruption of the CXCR4/CXCL12 chemotactic interaction during hematopoietic stem cell mobilization induced by GCSF or cyclophosphamide. Journal of Clinical Investigation 111: 187–196. doi:10.1172/JCI15994.

138. Christopherson KW, Cooper S, Broxmeyer HE (2003) Cell surface peptidase CD26/DPPIV mediates G-CSF mobilization of mouse progenitor cells. Blood 101: 4680–4686. doi:10.1182/blood-2002-12-3893.

139. Mendez-Ferrer S, Chow A, Merad M, Frenette PS (2009) Circadian rhythms influence hematopoietic stem cells. Curr Opin Hematol 16: 235–242. doi:10.1097/MOH.0b013e32832bd0f5.

140. Mendez-Ferrer S, Frenette PS (2007) Hematopoietic stem cell trafficking: regulated adhesion and attraction to bone marrow microenvironment. Annals of the New York Academy of Sciences 1116: 392–413. doi:10.1196/annals.1402.086.

141. Katayama Y, Battista M, Kao W-M, Hidalgo A, Peired AJ, et al. (2006) Signals from the Sympathetic Nervous System Regulate Hematopoietic Stem Cell Egress from Bone Marrow. Cell 124: 407–421. doi:10.1016/j.cell.2005.10.041.

142. Mendez-Ferrer S, Lucas D, Battista M, Frenette PS (2008) Haematopoietic stem cell release is regulated by circadian oscillations. Nature 452: 442–447. doi:10.1038/nature06685.

143. Cottler-Fox MH, Lapidot T, Petit I, Kollet O, DiPersio JF, et al. (2003) Stem Cell Mobilization. ASH 2003: 419–437.

144. Broxmeyer HE, Orschell CM, Clapp DW, Hangoc G, Cooper S, et al. (2005) Rapid mobilization of murine and human hematopoietic stem and progenitor cells with AMD3100, a CXCR4 antagonist. Journal of Experimental Medicine 201: 1307–1318. doi:10.1084/jem.20041385.

145. Bonig H, Wundes A, Chang K-H, Lucas S, Papayannopoulou T (2008) Increased numbers of circulating hematopoietic stem/progenitor cells are chronically maintained in patients treated with the CD49d blocking antibody natalizumab. Blood 111: 3439–3441. doi:10.1182/blood-2007-09-112052.

146. Papayannopoulou T (2001) Molecular pathways in bone marrow homing: dominant role of alpha4beta1 over beta2-integrins and selectins. Blood 98: 2403–2411. doi:10.1182/blood.V98.8.2403.

147. Jansen J, Hanks S, Thompson JM, Dugan MJ, Akard LP (2005) Transplantation of hematopoietic stem cells from the peripheral blood. J Cell Mol Med 9: 37–50.

148. Cyster JG (2005) Chemokines, sphingosine-1-phosphate, and cell migration in secondary lymphoid organs. Annu Rev Immunol 23: 127–159. doi:10.1146/annurev.immunol.23.021704.115628.

149. Rosen H, Goetzl EJ (2005) Sphingosine 1-phosphate and its receptors: an autocrine and paracrine network. Nature Reviews Immunology 5: 560–570. doi:10.1038/nri1650.

150. Massberg S, Andrian von UH (2006) Fingolimod and sphingosine-1-phosphate--modifiers of lymphocyte migration. N Engl J Med 355: 1088–1091. doi:10.1056/NEJMp068159.

151. Yatomi Y, Igarashi Y, Yang L, Hisano N, Qi R, et al. (1997) Sphingosine 1-phosphate, a bioactive sphingolipid abundantly stored in platelets, is a normal constituent of human plasma and serum. J Biochem 121: 969–973.

152. Hla T, Venkataraman K, Michaud J (2008) The vascular S1P gradient-cellular sources and biological significance. Biochim Biophys Acta 1781: 477–482. doi:10.1016/j.bbalip.2008.07.003.

153. Schwab SR, Pereira JP, Matloubian M, Xu Y, Huang Y, et al. (2005) Lymphocyte sequestration through S1P lyase inhibition and disruption of S1P gradients. Science 309: 1735–1739. doi:10.1126/science.1113640.

154. Nagai Y, Garrett KP, Ohta S, Bahrun U, Kouro T, et al. (2006) Toll-like receptors on hematopoietic progenitor cells stimulate innate immune system replenishment. Immunity 24: 801–812. doi:10.1016/j.immuni.2006.04.008.

155. Hoshino K, Takeuchi O, Kawai T, Sanjo H, Ogawa T, et al. (1999) Cutting edge:

Toll-like receptor 4 (TLR4)-deficient mice are hyporesponsive to lipopolysaccharide: evidence for TLR4 as the Lps gene product. J Immunol 162: 3749–3752.

156. Auffray C, Sieweke MH, Geissmann F (2009) Blood Monocytes: Development, Heterogeneity, and Relationship with Dendritic Cells. Annu Rev Immunol 27: 669–692. doi:10.1146/annurev.immunol.021908.132557.

157. Schofield R (1978) The relationship between the spleen colony-forming cell and the haemopoietic stem cell. Blood Cells 4: 7–25.

158. Eliasson P, Jönsson J-I (2010) The hematopoietic stem cell niche: low in oxygen but a nice place to be. J Cell Physiol 222: 17–22. doi:10.1002/jcp.21908.

159. Eliasson P, Rehn M, Hammar P, Larsson P, Sirenko O, et al. (2010) Hypoxia mediates low cell-cycle activity and increases the proportion of long-term-reconstituting hematopoietic stem cells during in vitro culture. Experimental Hematology 38: 301–310.e302. doi:10.1016/j.exphem.2010.01.005.

160. Kulkeaw K, Ishitani T, Kanemaru T, Fucharoen S, Sugiyama D (2010) Cold exposure down-regulates zebrafish hematopoiesis. Biochemical and Biophysical Research Communications 394: 859–864. doi:10.1016/j.bbrc.2010.01.047.

161. Adamo L, Naveiras O, Wenzel PL, McKinney-Freeman S, Mack PJ, et al. (2009) Biomechanical forces promote embryonic haematopoiesis. Nature 459: 1131–1135. doi:10.1038/nature08073.

162. Guzmán A, García C, Marín A-P, Tortajada A, Ruiz MT, et al. (2008) Formation of micronucleated erythrocytes in mouse bone-marrow under conditions of hypothermia is not associated with stimulation of erythropoiesis. Mutation Research/Genetic Toxicology and Environmental Mutagenesis 656: 8–13. doi:10.1016/j.mrgentox.2008.06.016.

163. Proulx C, Dupuis N, St-Amour I, Boyer L, Lemieux RA (2004) Increased megakaryopoiesis in cultures of CD34-enriched cord blood cells maintained at 39°C. Biotechnol Bioeng 88: 675–680. doi:10.1002/bit.20288.

164. Ehninger AA, Trumpp AA (2011) The bone marrow stem cell niche grows up: mesenchymal stem cells and macrophages move in. Journal of Experimental Medicine 208: 421–428. doi:10.1084/jem.20110132.

165. Kiel MJ, Morrison SJ (2008) Uncertainty in the niches that maintain haematopoietic stem cells. Nature Reviews Immunology 8: 290–301.

166. Wilson A, Oser GM, Jaworski M, Blanco-Bose WE, Laurenti E, et al. (2007) Dormant and self-renewing hematopoietic stem cells and their niches. Annals of the New York Academy of Sciences 1106: 64–75. doi:10.1196/annals.1392.021.

167. Calvi LM, Adams GB, Weibrecht KW, Weber JM, Olson DP, et al. (2003) Osteoblastic cells regulate the haematopoietic stem cell niche. Nat Cell Biol 425: 841–846. doi:10.1038/nature02040.

168. Zhang J, Niu C, Ye L, Huang H, He X, et al. (2003) Identification of the haematopoietic stem cell niche and control of the niche size. Nature 425: 836–841.

doi:10.1038/nature02041.

169. Visnjic D, Kalajzic I, Gronowicz G, Aguila HL, Clark SH, et al. (2001) Conditional ablation of the osteoblast lineage in Col2.3deltatk transgenic mice. J Bone Miner Res 16: 2222–2231. doi:10.1359/jbmr.2001.16.12.2222.

170. Kiel MJ, Radice GL, Morrison SJ (2007) Lack of evidence that hematopoietic stem cells depend on N-cadherin-mediated adhesion to osteoblasts for their maintenance. Cell Stem Cell 1: 204–217. doi:10.1016/j.stem.2007.06.001.

171. Lymperi S, Horwood N, Marley S, Gordon MY, Cope AP, et al. (2008) Strontium can increase some osteoblasts without increasing hematopoietic stem cells. Blood 111: 1173–1181. doi:10.1182/blood-2007-03-082800.

172. Haug JS, He XC, Grindley JC, Wunderlich JP, Gaudenz K, et al. (2008) N-cadherin expression level distinguishes reserved versus primed states of hematopoietic stem cells. Cell Stem Cell 2: 367–379. doi:10.1016/j.stem.2008.01.017.

173. Puch S, Armeanu S, Kibler C, Johnson KR, Muller CA, et al. (2001) N-cadherin is developmentally regulated and functionally involved in early hematopoietic cell differentiation. Journal of Cell Science 114: 1567–1577.

174. Hosokawa K, Arai F, Yoshihara H, Iwasaki H, Nakamura Y, et al. (2010) Knockdown of N-cadherin suppresses the long-term engraftment of hematopoietic stem cells. Blood 116: 554–563. doi:10.1182/blood-2009-05-224857.

175. Kiel MJ, Acar M, Radice GL, Morrison SJ (2009) Hematopoietic stem cells do not depend on N-cadherin to regulate their maintenance. Cell Stem Cell 4: 170–179.

176. Driessen RL, Johnston HM, Nilsson SK (2003) Membrane-bound stem cell factor is a key regulator in the initial lodgment of stem cells within the endosteal marrow region. Experimental Hematology 31: 1284–1291.

177. Arai F, Hirao A, Ohmura M, Sato H, Matsuoka S, et al. (2004) Tie2/angiopoietin-1 signaling regulates hematopoietic stem cell quiescence in the bone marrow niche. Cell 118: 149–161.

178. Yoshihara H, Arai F, Hosokawa K, Hagiwara T, Takubo K, et al. (2007) Thrombopoietin/MPL signaling regulates hematopoietic stem cell quiescence and interaction with the osteoblastic niche. Cell Stem Cell 1: 685–697.

179. de Haan G, Weersing E, Dontje B, van Os R, Bystrykh LV, et al. (2003) In vitro generation of long-term repopulating hematopoietic stem cells by fibroblast growth factor-1. Developmental Cell 4: 241–251.

180. L'Hôte CGM, Knowles MA (2005) Cell responses to FGFR3 signalling: growth, differentiation and apoptosis. Exp Cell Res 304: 417–431. doi:10.1016/j.yexcr.2004.11.012.

181. Nilsson SK, Johnston HM, Whitty GA, Williams B, Webb RJ, et al. (2005) Osteopontin, a key component of the hematopoietic stem cell niche and regulator of primitive hematopoietic progenitor cells. Blood 106: 1232–1239. doi:10.1182/blood-2004-11-4422.

182. Adams GB, Chabner KT, Alley IR, Olson DP, Szczepiorkowski ZM, et al. (2006) Stem cell engraftment at the endosteal niche is specified by the calcium-sensing receptor. Nature 439: 599–603. doi:10.1038/nature04247.

183. Rahn JJ, Shen Q, Mah BK, Hugh JC (2004) MUC1 initiates a calcium signal after ligation by intercellular adhesion molecule-1. J Biol Chem 279: 29386–29390. doi:10.1074/jbc.C400010200.

184. Miyamoto K, Yoshida S, Kawasumi M, Hashimoto K, Kimura T, et al. (2011) Osteoclasts are dispensable for hematopoietic stem cell maintenance and mobilization. J Exp Med 208: 2175–2181. doi:10.1084/jem.20101890.

185. Winkler IG, Sims NA, Pettit AR, Barbier V, Nowlan B, et al. (2010) Bone marrow macrophages maintain hematopoietic stem cell (HSC) niches and their depletion mobilizes HSCs. Blood 116: 4815–4828. doi:10.1182/blood-2009-11-253534.

186. Kacena MA, Gundberg CM, Horowitz MC (2006) A reciprocal regulatory interaction between megakaryocytes, bone cells, and hematopoietic stem cells. Bone 39: 978–984. doi:10.1016/j.bone.2006.05.019.

187. Naveiras O, Nardi V, Wenzel PL, Hauschka PV, Fahey F, et al. (2009) Bone-marrow adipocytes as negative regulators of the haematopoietic microenvironment. Nature 460: 259–263. doi:10.1038/nature08099.

188. Kiel MJ, Yilmaz ÖH, Iwashita T, Yilmaz OH, Terhorst C, et al. (2005) SLAM Family Receptors Distinguish Hematopoietic Stem and Progenitor Cells and Reveal Endothelial Niches for Stem Cells. Cell 121: 1109–1121. doi:10.1016/j.cell.2005.05.026.

189. Mendez-Ferrer S, Michurina TV, Ferraro F, Mazloom AR, MacArthur BD, et al. (2010) Mesenchymal and haematopoietic stem cells form a unique bone marrow niche. Nature 466: 829–U859. doi:10.1038/nature09262.

190. Yamazaki S, Ema H, Karlsson G, Yamaguchi T, Miyoshi H, et al. (2011) Nonmyelinating Schwann Cells Maintain Hematopoietic Stem Cell Hibernation in the Bone Marrow Niche. Cell 147: 1146–1158. doi:10.1016/j.cell.2011.09.053.

191. Omatsu Y, Sugiyama T, Kohara H, Kondoh G, Fujii N, et al. (2010) The essential functions of adipo-osteogenic progenitors as the hematopoietic stem and progenitor cell niche. Immunity 33: 387–399. doi:10.1016/j.immuni.2010.08.017.

192. Sugiyama T, Kohara H, Noda M, Nagasawa T (2006) Maintenance of the hematopoietic stem cell pool by CXCL12-CXCR4 chemokine signaling in bone marrow stromal cell niches. Immunity 25: 977–988. doi:10.1016/j.immuni.2006.10.016.

193. Yin T (2006) The stem cell niches in bone. Journal of Clinical Investigation 116: 1195–1201. doi:10.1172/JCI28568.

194. Kopp H-G, Avecilla ST, Hooper AT, Rafii S (2005) The bone marrow vascular niche: home of HSC differentiation and mobilization. Physiology (Bethesda) 20: 349–356. doi:10.1152/physiol.00025.2005.

195. Chow A, Lucas D, Hidalgo A, Mendez-Ferrer S, Hashimoto D, et al. (2011) Bone marrow CD169+ macrophages promote the retention of hematopoietic stem and progenitor cells in the mesenchymal stem cell niche. J Exp Med 208: 261–271. doi:10.1084/jem.20101688.

196. Celso Lo C, Fleming HE, Wu JW, Zhao CX, Miake-Lye S, et al. (2008) Live-animal tracking of individual haematopoietic stem/progenitor cells in their niche. Nature 457: 92–97. doi:10.1038/nature07434.

197. Xie Y, Yin T, Wiegraebe W, He XC, Miller D, et al. (2008) Detection of functional haematopoietic stem cell niche using real-time imaging. Nature 457: 97–101. doi:10.1038/nature07639.

198. Nilsson SK, Simmons PJ, Bertoncello I (2006) Hemopoietic stem cell engraftment. Experimental Hematology 34: 123–129. doi:10.1016/j.exphem.2005.08.006.

199. Coulombel L, Vuillet MH, Leroy C, Tchernia G (1988) Lineage- and stage-specific adhesion of human hematopoietic progenitor cells to extracellular matrices from marrow fibroblasts. Blood 71: 329–334.

200. van der Loo JC, Xiao X, McMillin D, Hashino K, Kato I, et al. (1998) VLA-5 is expressed by mouse and human long-term repopulating hematopoietic cells and mediates adhesion to extracellular matrix protein fibronectin. Journal of Clinical Investigation 102: 1051–1061. doi:10.1172/JCI3687.

201. Nilsson SK, Haylock DN, Johnston HM, Occhiodoro T, Brown TJ, et al. (2003) Hyaluronan is synthesized by primitive hemopoietic cells, participates in their lodgment at the endosteum following transplantation, and is involved in the regulation of their proliferation and differentiation in vitro. Blood 101: 856–862. doi:10.1182/blood-2002-05-1344.

202. Hosokawa K, Arai F, Yoshihara H, Nakamura Y, Gomei Y, et al. (2007) Function of oxidative stress in the regulation of hematopoietic stem cell-niche interaction. Biochemical and Biophysical Research Communications 363: 578–583. doi:10.1016/j.bbrc.2007.09.014.

203. Tothova Z, Kollipara R, Huntly BJ, Lee BH, Castrillon DH, et al. (2007) FoxOs are critical mediators of hematopoietic stem cell resistance to physiologic oxidative stress. Cell 128: 325–339. doi:10.1016/j.cell.2007.01.003.

204. Ceradini DJ, Kulkarni AR, Callaghan MJ, Tepper OM, Bastidas N, et al. (2004) Progenitor cell trafficking is regulated by hypoxic gradients through HIF-1 induction of SDF-1. Nat Med 10: 858–864. doi:10.1038/nm1075.

205. Parmar K, Mauch P, Vergilio J-A, Sackstein R, Down JD (2007) Distribution of hematopoietic stem cells in the bone marrow according to regional hypoxia. Proc Natl Acad Sci USA 104: 5431–5436. doi:10.1073/pnas.0701152104.

206. Lévesque J-P, Winkler IG, Hendy J, Williams B, Helwani F, et al. (2007) Hematopoietic progenitor cell mobilization results in hypoxia with increased hypoxia-inducible transcription factor-1 alpha and vascular endothelial growth factor A in bone marrow. Stem Cells 25: 1954–1965. doi:10.1634/stemcells.2006-0688.

207. Kubota Y, Takubo K, Suda T (2008) Bone marrow long label-retaining cells reside in the sinusoidal hypoxic niche. Biochemical and Biophysical Research Communications 366: 335–339. doi:10.1016/j.bbrc.2007.11.086.

208. Warr MR, Pietras EM, Passegué E (2011) Mechanisms controlling hematopoietic stem cell functions during normal hematopoiesis and hematological malignancies. WIREs Syst Biol Med 3: 681–701. doi:10.1002/wsbm.145.

209. Goey H, Keller JR, Back T, Longo DL, Ruscetti FW, et al. (1989) Inhibition of early murine hemopoietic progenitor cell proliferation after in vivo locoregional administration of transforming growth factor-beta 1. J Immunol 143: 877–880.

210. Larsson J, Blank U, Helgadottir H, Björnsson JM, Ehinger M, et al. (2003) TGF-beta signaling-deficient hematopoietic stem cells have normal self-renewal and regenerative ability in vivo despite increased proliferative capacity in vitro. Blood 102: 3129–3135. doi:10.1182/blood-2003-04-1300.

211. Larsson J, Blank U, Klintman J, Magnusson M, Karlsson S (2005) Quiescence of hematopoietic stem cells and maintenance of the stem cell pool is not dependent on TGF-beta signaling in vivo. Experimental Hematology 33: 592–596. doi:10.1016/j.exphem.2005.02.003.

212. Larsson J, Goumans MJ, Sjöstrand LJ, van Rooijen MA, Ward D, et al. (2001) Abnormal angiogenesis but intact hematopoietic potential in TGF-beta type I receptor-deficient mice. EMBO J 20: 1663–1673. doi:10.1093/emboj/20.7.1663.

213. Utsugisawa T, Moody JL, Aspling M, Nilsson E, Carlsson L, et al. (2006) A road map toward defining the role of Smad signaling in hematopoietic stem cells. Stem Cells 24: 1128–1136. doi:10.1634/stemcells.2005-0263.

214. Karlsson G, Blank U, Moody JL, Ehinger M, Singbrant S, et al. (2007) Smad4 is critical for self-renewal of hematopoietic stem cells. Journal of Experimental Medicine 204: 467–474. doi:10.1084/jem.20060465.

215. Reya T, Duncan AW, Ailles L, Domen J, Scherer DC, et al. (2003) A role for Wnt signalling in self-renewal of haematopoietic stem cells. Nature 423: 409–414. doi:10.1038/nature01593.

216. Kirstetter P, Anderson K, Porse BT, Jacobsen SEW, Nerlov C (2006) Activation of the canonical Wnt pathway leads to loss of hematopoietic stem cell repopulation and multilineage differentiation block. Nat Immunol 7: 1048–1056. doi:10.1038/ni1381.

217. Scheller M, Huelsken J, Rosenbauer F, Taketo MM, Birchmeier W, et al. (2006) Hematopoietic stem cell and multilineage defects generated by constitutive β-catenin activation. Nat Immunol 7: 1037–1047. doi:10.1038/ni1387.

218. Sugimura R, He XC, Venkatraman A, Arai F, Box A, et al. (2012) Noncanonical wnt signaling maintains hematopoietic stem cells in the niche. Cell 150: 351–365. doi:10.1016/j.cell.2012.05.041.

219. Fleming HE, Janzen V, Celso Lo C, Guo J, Leahy KM, et al. (2008) Wnt Signaling in the Niche Enforces Hematopoietic Stem Cell Quiescence and Is Necessary to Preserve Self-Renewal In Vivo. Cell Stem Cell 2: 274–283.

220. Suda T, Arai F (2008) Wnt Signaling in the Niche. Cell 132: 729–730. doi:10.1016/j.cell.2008.02.017.

221. Jeannet G, Scheller M, Scarpellino L, Duboux S, Gardiol N, et al. (2008) Long-term, multilineage hematopoiesis occurs in the combined absence of beta-catenin and gamma-catenin. Blood 111: 142–149. doi:10.1182/blood-2007-07-102558.

222. Cobas M, Wilson A, Ernst B, Mancini SJC, MacDonald HR, et al. (2004) Beta-catenin is dispensable for hematopoiesis and lymphopoiesis. Journal of Experimental Medicine 199: 221–229. doi:10.1084/jem.20031615.

223. Kumano K, Chiba S, Kunisato A, Sata M, Saito T, et al. (2003) Notch1 but not Notch2 is essential for generating hematopoietic stem cells from endothelial cells. Immunity 18: 699–711.

224. Robert-Moreno A, Guiu J, Ruiz-Herguido C, López ME, Inglés-Esteve J, et al. (2008) Impaired embryonic haematopoiesis yet normal arterial development in the absence of the Notch ligand Jagged1. EMBO J 27: 1886–1895. doi:10.1038/emboj.2008.113.

225. Robert-Moreno A (2005) RBPj -dependent Notch function regulates Gata2 and is essential for the formation of intra-embryonic hematopoietic cells. Development 132: 1117–1126. doi:10.1242/dev.01660.

226. Karanu FN, Murdoch B, Gallacher L, Wu DM, Koremoto M, et al. (2000) The notch ligand jagged-1 represents a novel growth factor of human hematopoietic stem cells. Journal of Experimental Medicine 192: 1365–1372.

227. Varnum-Finney B, Xu L, Brashem-Stein C, Nourigat C, Flowers D, et al. (2000) Pluripotent, cytokine-dependent, hematopoietic stem cells are immortalized by constitutive Notch1 signaling. Nat Med 6: 1278–1281. doi:10.1038/81390.

228. Varnum-Finney B, Purton LE, Yu M, Brashem-Stein C, Flowers D, et al. (1998) The Notch ligand, Jagged-1, influences the development of primitive hematopoietic precursor cells. Blood 91: 4084–4091.

229. Duncan AW, Rattis FM, DiMascio LN, Congdon KL, Pazianos G, et al. (2005) Integration of Notch and Wnt signaling in hematopoietic stem cell maintenance. Nat Immunol 6: 314–322. doi:10.1038/ni1164.

230. Stier S, Cheng T, Dombkowski D, Carlesso N, Scadden DT (2002) Notch1 activation increases hematopoietic stem cell self-renewal in vivo and favors lymphoid over myeloid lineage outcome. Blood 99: 2369–2378.

231. Mancini SJC, Mantei N, Dumortier A, Suter U, MacDonald HR, et al. (2005) Jagged1-dependent Notch signaling is dispensable for hematopoietic stem cell self-renewal and differentiation. Blood 105: 2340–2342. doi:10.1182/blood-2004-08-3207.

232. Maillard I, Koch U, Dumortier A, Shestova O, Xu L, et al. (2008) Canonical notch signaling is dispensable for the maintenance of adult hematopoietic stem cells. Cell Stem Cell 2: 356–366. doi:10.1016/j.stem.2008.02.011.

233. Bhardwaj G, Murdoch B, Wu D, Baker DP, Williams KP, et al. (2001) Sonic

hedgehog induces the proliferation of primitive human hematopoietic cells via BMP regulation. Nat Immunol 2: 172–180. doi:10.1038/84282.

234. Dierks C, Beigi R, Guo G-R, Zirlik K, Stegert MR, et al. (2008) Expansion of Bcr-Abl-positive leukemic stem cells is dependent on Hedgehog pathway activation. Cancer Cell 14: 238–249. doi:10.1016/j.ccr.2008.08.003.

235. Zhao C, Chen A, Jamieson CH, Fereshteh M, Abrahamsson A, et al. (2009) Hedgehog signalling is essential for maintenance of cancer stem cells in myeloid leukaemia. Nature 458: 776–779. doi:10.1038/nature07737.

236. Merchant A, Joseph G, Wang Q, Brennan S, Matsui W (2010) Gli1 regulates the proliferation and differentiation of HSCs and myeloid progenitors. Blood 115: 2391–2396. doi:10.1182/blood-2009-09-241703.

237. Trowbridge JJ, Scott MP, Bhatia M (2006) Hedgehog modulates cell cycle regulators in stem cells to control hematopoietic regeneration. Proc Natl Acad Sci USA 103: 14134–14139. doi:10.1073/pnas.0604568103.

238. Gao J, Graves S, Koch U, Liu S, Jankovic V, et al. (2009) Hedgehog signaling is dispensable for adult hematopoietic stem cell function. Cell Stem Cell 4: 548–558. doi:10.1016/j.stem.2009.03.015.

239. Hofmann I, Stover EH, Cullen DE, Mao J, Morgan KJ, et al. (2009) Hedgehog signaling is dispensable for adult murine hematopoietic stem cell function and hematopoiesis. Cell Stem Cell 4: 559–567. doi:10.1016/j.stem.2009.03.016.

240. Wilson A, Trumpp A (2006) Bone-marrow haematopoietic-stem-cell niches. Nature Reviews Immunology 6: 93–106. doi:10.1038/nri1779.

241. Verfaillie CM, Catanzaro P (1996) Direct contact with stroma inhibits proliferation of human long-term culture initiating cells. Leukemia 10: 498–504.

242. Hurley RW, McCarthy JB, Verfaillie CM (1995) Direct adhesion to bone marrow stroma via fibronectin receptors inhibits hematopoietic progenitor proliferation. Journal of Clinical Investigation 96: 511–519. doi:10.1172/JCI118063.

243. Jiang Y, Prosper F, Verfaillie CM (2000) Opposing effects of engagement of integrins and stimulation of cytokine receptors on cell cycle progression of normal human hematopoietic progenitors. Blood 95: 846–854.

244. Levesque JP, Leavesley DI, Niutta S, Vadas M, Simmons PJ (1995) Cytokines increase human hemopoietic cell adhesiveness by activation of very late antigen (VLA)-4 and VLA-5 integrins. Journal of Experimental Medicine 181: 1805–1815.

245. Eaves CJ, Cashman JD, Kay RJ, Dougherty GJ, Otsuka T, et al. (1991) Mechanisms that regulate the cell cycle status of very primitive hematopoietic cells in long-term human marrow cultures. II. Analysis of positive and negative regulators produced by stromal cells within the adherent layer. Blood 78: 110–117.

246. Prosper F, Verfaillie CM (2001) Regulation of hematopoiesis through adhesion receptors. J Leukoc Biol 69: 307–316.

247. LAM BS, Adams GB (2010) Hematopoietic stem cell lodgment in the adult bone marrow stem cell niche. International Journal of Laboratory Hematology 32: 551–558. doi:10.1111/j.1751-553X.2010.01250.x.

248. Ghaffari S, Dougherty GJ, Lansdorp PM, Eaves AC, Eaves CJ (1995) Differentiation-associated changes in CD44 isoform expression during normal hematopoiesis and their alteration in chronic myeloid leukemia. Blood 86: 2976–2985.

249. Verfaillie CM, Benis A, Iida J, McGlave PB, McCarthy JB (1994) Adhesion of committed human hematopoietic progenitors to synthetic peptides from the C-terminal heparin-binding domain of fibronectin: cooperation between the integrin alpha 4 beta 1 and the CD44 adhesion receptor. Blood 84: 1802–1811.

250. Vestweber D, Blanks JE (1999) Mechanisms that regulate the function of the selectins and their ligands. Physiol Rev 79: 181–213.

251. Möhle R, Murea S, Kirsch M, Haas R (1995) Differential expression of L-selectin, VLA-4, and LFA-1 on CD34+ progenitor cells from bone marrow and peripheral blood during G-CSF-enhanced recovery. Experimental Hematology 23: 1535–1542.

252. Jung U, Ramos CL, Bullard DC, Ley K (1998) Gene-targeted mice reveal importance of L-selectin-dependent rolling for neutrophil adhesion. Am J Physiol 274: H1785–H1791.

253. Robinson SD, Frenette PS, Rayburn H, Cummiskey M, Ullman-Culleré M, et al. (1999) Multiple, targeted deficiencies in selectins reveal a predominant role for P-selectin in leukocyte recruitment. Proc Natl Acad Sci USA 96: 11452–11457.

254. Labow MA, Norton CR, Rumberger JM, Lombard-Gillooly KM, Shuster DJ, et al. (1994) Characterization of E-selectin-deficient mice: demonstration of overlapping function of the endothelial selectins. Immunity 1: 709–720.

255. Spertini O, Cordey AS, Monai N, Giuffrè L, Schapira M (1996) P-selectin glycoprotein ligand 1 is a ligand for L-selectin on neutrophils, monocytes, and CD34+ hematopoietic progenitor cells. J Cell Biol 135: 523–531.

256. Bazil V, Brandt JE, Hoffman R (1997) Resistance of human hematopoietic stem cells to a monoclonal antibody recognizing CD43. Stem Cells 15 Suppl 1: 13–8–discussion18–9. doi:10.1002/stem.5530150804.

257. Watt SM, Bühring HJ, Rappold I, Chan JY, Lee-Prudhoe J, et al. (1998) CD164, a novel sialomucin on CD34(+) and erythroid subsets, is located on human chromosome 6q21. Blood 92: 849–866.

258. Craig W, Poppema S, Little MT, Dragowska W, Lansdorp PM (1994) CD45 isoform expression on human haemopoietic cells at different stages of development. Br J Haematol 88: 24–30.

259. Young PE, Baumhueter S, Lasky LA (1995) The sialomucin CD34 is expressed on hematopoietic cells and blood vessels during murine development. Blood 85: 96–105.

260. Healy L, May G, Gale K, Grosveld F, Greaves M, et al. (1995) The stem cell antigen

CD34 functions as a regulator of hemopoietic cell adhesion. Proc Natl Acad Sci USA 92: 12240–12244.

261. Cheng J, Baumhueter S, Cacalano G, Carver-Moore K, Thibodeaux H, et al. (1996) Hematopoietic defects in mice lacking the sialomucin CD34. Blood 87: 479–490.

262. Levesque JP, Zannettino AC, Pudney M, Niutta S, Haylock DN, et al. (1999) PSGL-1-mediated adhesion of human hematopoietic progenitors to P-selectin results in suppression of hematopoiesis. Immunity 11: 369–378.

263. Watt SM, Butler LH, Tavian M, Bühring HJ, Rappold I, et al. (2000) Functionally defined CD164 epitopes are expressed on CD34(+) cells throughout ontogeny but display distinct distribution patterns in adult hematopoietic and nonhematopoietic tissues. Blood 95: 3113–3124.

264. Zannettino AC, Bühring HJ, Niutta S, Watt SM, Benton MA, et al. (1998) The sialomucin CD164 (MGC-24v) is an adhesive glycoprotein expressed by human hematopoietic progenitors and bone marrow stromal cells that serves as a potent negative regulator of hematopoiesis. Blood 92: 2613–2628.

265. Simmons PJ, Levesque JP, Haylock DN (2001) Mucin-like molecules as modulators of the survival and proliferation of primitive hematopoietic cells. Annals of the New York Academy of Sciences 938: 196–206–discussion206–7.

266. Grassinger J, Haylock DN, Storan MJ, Haines GO, Williams B, et al. (2009) Thrombin-cleaved osteopontin regulates hemopoietic stem and progenitor cell functions through interactions with alpha9beta1 and alpha4beta1 integrins. Blood 114: 49–59. doi:10.1182/blood-2009-01-197988.

267. Papayannopoulou T, Craddock C, Nakamoto B, Priestley GV, Wolf NS (1995) The VLA4/VCAM-1 adhesion pathway defines contrasting mechanisms of lodgement of transplanted murine hemopoietic progenitors between bone marrow and spleen. Proc Natl Acad Sci USA 92: 9647–9651.

268. Hirsch E, Iglesias A, Potocnik AJ, Hartmann U, Fässler R (1996) Impaired migration but not differentiation of haematopoietic stem cells in the absence of β1 integrins. Nature 380: 171–175. doi:10.1038/380171a0.

269. Potocnik AJ, Brakebusch C, Fassler R (2000) Fetal and adult hematopoietic stem cells require beta1 integrin function for colonizing fetal liver, spleen, and bone marrow. Immunity 12: 653–663.

270. Williams DA, Rios M, Stephens C, Patel VP (1991) Fibronectin and VLA-4 in haematopoietic stem cell–microenvironment interactions. Nature 352: 438–441. doi:10.1038/352438a0.

271. Bungartz G (2006) Adult murine hematopoiesis can proceed without beta1 and beta7 integrins. Blood 108: 1857–1864. doi:10.1182/blood-2005-10-007658.

272. Elices MJ, Osborn L, Takada Y, Crouse C, Luhowskyj S, et al. (1990) VCAM-1 on activated endothelium interacts with the leukocyte integrin VLA-4 at a site distinct from the VLA-4/fibronectin binding site. Cell 60: 577–584.

273. Mould AP, Humphries MJ (1991) Identification of a novel recognition sequence for the integrin alpha 4 beta 1 in the COOH-terminal heparin-binding domain of fibronectin. EMBO J 10: 4089–4095.

274. Hemler ME (1990) VLA Proteins in the Integrin Family: Structures, Functions, and Their Role on Leukocytes. Annu Rev Immunol 8: 365–400. doi:10.1146/annurev.iy.08.040190.002053.

275. Scott LM, Priestley GV, Papayannopoulou T (2003) Deletion of α4 integrins from adult hematopoietic cells reveals roles in homeostasis, regeneration, and homing. Mol Cell Biol 23: 9349–9360. doi:10.1128/MCB.23.24.9349–9360.2003.

276. Priestley GV, Scott LM, Ulyanova T, Papayannopoulou T (2006) Lack of alpha4 integrin expression in stem cells restricts competitive function and self-renewal activity. Blood 107: 2959–2967. doi:10.1182/blood-2005-07-2670.

277. Arroyo AG, Yang JT, Rayburn H, Hynes RO (1999) Alpha4 integrins regulate the proliferation/differentiation balance of multilineage hematopoietic progenitors in vivo. Immunity 11: 555–566.

278. Jiang Y, Bonig H, Ulyanova T, Chang K, Papayannopoulou T (2009) On the adaptation of endosteal stem cell niche function in response to stress. Blood 114: 3773–3782.

279. Craddock CF, Nakamoto B, Andrews RG, Priestley GV, Papayannopoulou T (1997) Antibodies to VLA4 integrin mobilize long-term repopulating cells and augment cytokine-induced mobilization in primates and mice. Blood 90: 4779–4788.

280. Papayannopoulou T, Priestley GV, Nakamoto B (1998) Anti-VLA4/VCAM-1Induced Mobilization Requires Cooperative Signaling Through the kit/mkit Ligand Pathway. Blood 91: 2231–2239.

281. Papayannopoulou T (2000) Mechanisms of stem-/progenitor-cell mobilization: The anti-VLA-4 paradigm. Seminars in Hematology 37: 11–18. doi:10.1016/S0037-1963(00)90084-2.

282. Levesque JP, Simmons PJ (1999) Cytoskeleton and integrin-mediated adhesion signaling in human CD34+ hemopoietic progenitor cells. Experimental Hematology 27: 579–586.

283. RW H, JB M, EA W, CM V (1997) Monoclonal antibody crosslinking of the alpha 4 or beta 1 integrin inhibits committed clonogenic hematopoietic progenitor proliferation. Experimental Hematology 25: 321–328.

284. Wilson A, Murphy MJ, Oskarsson T (2004) c-Myc controls the balance between hematopoietic stem cell self-renewal and differentiation. Genes & Development 18: 2747–2763. doi:10.1101/gad.313104.

285. Stier S (2005) Osteopontin is a hematopoietic stem cell niche component that negatively regulates stem cell pool size. J Exp Med 201: 1781–1791. doi:10.1084/jem.20041992.

286. Teixidó J, Hemler ME, Greenberger JS, Anklesaria P (1992) Role of beta 1 and beta

2 integrins in the adhesion of human CD34hi stem cells to bone marrow stroma. Journal of Clinical Investigation 90: 358–367. doi:10.1172/JCI115870.

287. Pruijt JF, van Kooyk Y, Figdor CG, Lindley IJ, Willemze R, et al. (1998) Anti-LFA-1 blocking antibodies prevent mobilization of hematopoietic progenitor cells induced by interleukin-8. Blood 91: 4099–4105.

288. Fibbe WE, Pruijt JF, van Kooyk Y, Figdor CG, Opdenakker G, et al. (2000) The role of metalloproteinases and adhesion molecules in interleukin-8-induced stem-cell mobilization. Seminars in Hematology 37: 19–24.

289. Umemoto T, Yamato M, Shiratsuchi Y, Terasawa M, Yang J, et al. (2006) Expression of Integrin beta3 is correlated to the properties of quiescent hemopoietic stem cells possessing the side population phenotype. J Immunol 177: 7733–7739.

290. LaFlamme SE, Homan SM, Bodeau AL, Mastrangelo AM (1997) Integrin cytoplasmic domains as connectors to the cell's signal transduction apparatus. Matrix Biol 16: 153–163.

291. Zheng C, Xing Z, Bian ZC, Guo C, Akbay A, et al. (1998) Differential regulation of Pyk2 and focal adhesion kinase (FAK). The C-terminal domain of FAK confers response to cell adhesion. J Biol Chem 273: 2384–2389.

292. Shimizu Y, Hunt SW (1996) Regulating integrin-mediated adhesion: one more function for PI 3-kinase? Immunol Today 17: 565–573.

293. Hynes RO (2002) Integrins: bidirectional, allosteric signaling machines. Cell 110: 673–687.

294. Hynes RO, Zhao Q (2000) The evolution of cell adhesion. J Cell Biol 150: F89–F96.

295. Humphries JD, Byron A, Humphries MJ (2006) Integrin ligands at a glance. Journal of Cell Science 119: 3901–3903. doi:10.1242/jcs.03098.

296. Bökel C, Brown NH (2002) Integrins in DevelopmentMoving on, Responding to, and Sticking to the Extracellular Matrix. Developmental Cell 3: 311–321. doi:10.1016/S1534-5807(02)00265-4.

297. van der Flier A, Sonnenberg A (2001) Function and interactions of integrins. Cell and Tissue Research 305: 285–298.

298. Hynes RO (2004) The emergence of integrins: a personal and historical perspective. Matrix Biol 23: 333–340. doi:10.1016/j.matbio.2004.08.001.

299. Tamkun JW, DeSimone DW, Fonda D, Patel RS, Buck C, et al. (1986) Structure of integrin, a glycoprotein involved in the transmembrane linkage between fibronectin and actin. Cell 46: 271–282.

300. Takada Y, Ye X, Simon S (2007) The integrins. Genome Biol 8.

301. Arnaout MA, Mahalingam B, Xiong J-P (2005) Integrin structure, allostery, and bidirectional signaling. Annu Rev Cell Dev Biol 21: 381–410. doi:10.1146/annurev.cellbio.21.090704.151217.

302. Humphries MJ, Symonds EJH, Mould AP (2003) Mapping functional residues onto integrin crystal structures. Curr Opin Struct Biol 13: 236–243.

303. Hughes PE, Diaz-Gonzalez F, Leong L, Wu C, McDonald JA, et al. (1996) Breaking the integrin hinge. A defined structural constraint regulates integrin signaling. J Biol Chem 271: 6571–6574.

304. Vinogradova O, Haas T, Plow EF, Qin J (2000) A structural basis for integrin activation by the cytoplasmic tail of the alpha IIb-subunit. Proc Natl Acad Sci USA 97: 1450–1455. doi:10.1073/pnas.040548197.

305. Vinogradova O, Velyvis A, Velyviene A, Hu B, Haas T, et al. (2002) A structural mechanism of integrin alpha(IIb)beta(3) “inside-out” activation as regulated by its cytoplasmic face. Cell 110: 587–597.

306. Calderwood DA, Fujioka Y, de Pereda JM, García-Alvarez B, Nakamoto T, et al. (2003) Integrin beta cytoplasmic domain interactions with phosphotyrosine-binding domains: a structural prototype for diversity in integrin signaling. Proc Natl Acad Sci USA 100: 2272–2277. doi:10.1073/pnas.262791999.

307. Xiong J-P, Stehle T, Diefenbach B, Zhang R, Dunker R, et al. (2001) Crystal structure of the extracellular segment of integrin alpha Vbeta3. Science 294: 339–345. doi:10.1126/science.1064535.

308. Lau T-L, Dua V, Ulmer TS (2008) Structure of the integrin alphaIIb transmembrane segment. J Biol Chem 283: 16162–16168. doi:10.1074/jbc.M801748200.

309. Ma Y-Q, Qin J, Plow EF (2007) Platelet integrin alpha(IIb)beta(3): activation mechanisms. J Thromb Haemost 5: 1345–1352. doi:10.1111/j.1538-7836.2007.02537.x.

310. Depraetere H, Wille C, Gansemans Y, Stanssens P, Lauwereys M, et al. (1997) The integrin alpha 2 beta 1 (GPIa/IIa)-I-domain inhibits platelet-collagen interaction. Thromb Haemost 77: 981–985.

311. Zhu J, Luo B-H, Xiao T, Zhang C, Nishida N, et al. (2008) Structure of a complete integrin ectodomain in a physiologic resting state and activation and deactivation by applied forces. Mol Cell 32: 849–861. doi:10.1016/j.molcel.2008.11.018.

312. Askari JA, Buckley PA, Mould AP, Humphries MJ (2009) Linking integrin conformation to function. Journal of Cell Science 122: 165–170. doi:10.1242/jcs.018556.

313. Ruggeri ZM (2002) Platelets in atherothrombosis. Nat Med 8: 1227–1234. doi:10.1038/nm1102-1227.

314. Li Z, Delaney MK, O'Brien KA, Du X (2010) Signaling during platelet adhesion and activation. Arterioscler Thromb Vasc Biol 30: 2341–2349. doi:10.1161/ATVBAHA.110.207522.

315. Han J, Lim CJ, Watanabe N, Soriani A, Ratnikov B, et al. (2006) Reconstructing and deconstructing agonist-induced activation of integrin alphaIIbbeta3. Curr Biol 16: 1796–1806. doi:10.1016/j.cub.2006.08.035.

316. Moser M, Nieswandt B, Ussar S, Pozgajova M, Fässler R (2008) Kindlin-3 is essential for integrin activation and platelet aggregation. Nat Med 14: 325–330. doi:10.1038/nm1722.

317. Moser M, Bauer M, Schmid S, Ruppert R, Schmidt S, et al. (2009) Kindlin-3 is required for beta2 integrin-mediated leukocyte adhesion to endothelial cells. Nat Med 15: 300–305.

318. Shattil SJ, Kim C, Ginsberg MH (2010) The final steps of integrin activation: the end game. Nat Rev Mol Cell Biol 11: 288–300. doi:10.1038/nrm2871.

319. Alon R, Ley K (2008) Cells on the run: shear-regulated integrin activation in leukocyte rolling and arrest on endothelial cells. Current Opinion in Cell Biology 20: 525–532. doi:10.1016/j.ceb.2008.04.003.

320. Bertagnolli ME, Locke SJ, Hensler ME, Bray PF, Beckerle MC (1993) Talin distribution and phosphorylation in thrombin-activated platelets. Journal of Cell Science 106 (Pt 4): 1189–1199.

321. Goksoy E, Ma Y-Q, Wang X, Kong X, Perera D, et al. (2008) Structural basis for the autoinhibition of talin in regulating integrin activation. Mol Cell 31: 124–133. doi:10.1016/j.molcel.2008.06.011.

322. Calderwood DA (2004) Integrin activation. Journal of Cell Science 117: 657–666. doi:10.1242/jcs.01014.

323. Wegener KL, Partridge AW, Han J, Pickford AR, Liddington RC, et al. (2007) Structural basis of integrin activation by talin. Cell 128: 171–182. doi:10.1016/j.cell.2006.10.048.

324. Critchley DR, Gingras AR (2008) Talin at a glance. Journal of Cell Science 121: 1345–1347. doi:10.1242/jcs.018085.

325. Franco SJ, Rodgers MA, Perrin BJ, Han J, Bennin DA, et al. (2004) Calpain-mediated proteolysis of talin regulates adhesion dynamics. Nat Cell Biol 6: 977–983. doi:10.1038/ncb1175.

326. Legate KR, Wickström SA, Fässler R (2009) Genetic and cell biological analysis of integrin outside-in signaling. Genes & Development 23: 397–418. doi:10.1101/gad.1758709.

327. Ma Y-Q, Yang J, Pesho MM, Vinogradova O, Qin J, et al. (2006) Regulation of integrin alphaIIbbeta3 activation by distinct regions of its cytoplasmic tails. Biochemistry 45: 6656–6662. doi:10.1021/bi060279h.

328. Montanez E, Ussar S, Schifferer M, Bösl M, Zent R, et al. (2008) Kindlin-2 controls bidirectional signaling of integrins. Genes & Development 22: 1325–1330. doi:10.1101/gad.469408.

329. Ussar S, Moser M, Widmaier M, Rognoni E, Harrer C, et al. (2008) Loss of Kindlin-1 causes skin atrophy and lethal neonatal intestinal epithelial dysfunction. PLoS Genet 4: e1000289. doi:10.1371/journal.pgen.1000289.

330. Shi X, Ma Y-Q, Tu Y, Chen K, Wu S, et al. (2007) The MIG-2/Integrin Interaction Strengthens Cell-Matrix Adhesion and Modulates Cell Motility. J Biol Chem 282: 20455–20466. doi:10.1074/jbc.M611680200.

331. Harburger DS, Bouaouina M, Calderwood DA (2009) Kindlin-1 and -2 directly bind the C-terminal region of beta integrin cytoplasmic tails and exert integrin-specific activation effects. J Biol Chem 284: 11485–11497. doi:10.1074/jbc.M809233200.

332. Ma Y-Q, Qin J, Wu C, Plow EF (2008) Kindlin-2 (Mig-2): a co-activator of beta3 integrins. J Cell Biol 181: 439–446. doi:10.1083/jcb.200710196.

333. Ye F, Hu G, Taylor D, Ratnikov B, Bobkov AA, et al. (2010) Recreation of the terminal events in physiological integrin activation. J Cell Biol 188: 157–173. doi:10.1083/jcb.200908045.

334. Kahner BN, Kato H, Banno A, Ginsberg MH, Shattil SJ, et al. (2012) Kindlins, integrin activation and the regulation of talin recruitment to αIIbβ3. PLoS ONE 7: e34056. doi:10.1371/journal.pone.0034056.

335. Lefort CT, Rossaint J, Moser M, Petrich BG, Zarbock A, et al. (2012) Distinct roles for talin-1 and kindlin-3 in LFA-1 extension and affinity regulation. Blood 119: 4275–4282. doi:10.1182/blood-2011-08-373118.

336. Calderwood DA, Yan B, de Pereda JM, Alvarez BG, Fujioka Y, et al. (2002) The phosphotyrosine binding-like domain of talin activates integrins. J Biol Chem 277: 21749–21758. doi:10.1074/jbc.M111996200.

337. Bledzka K, Liu J, Xu Z, Perera HD, Yadav SP, et al. (2012) Spatial coordination of kindlin-2 with talin head domain in interaction with integrin β cytoplasmic tails. J Biol Chem 287: 24585–24594. doi:10.1074/jbc.M111.336743.

338. Moser M, Legate KR, Zent R, Fassler R (2009) The Tail of Integrins, Talin, and Kindlins. Science 324: 895–899. doi:10.1126/science.1163865.

339. Meves A, Stremmel C, Böttcher RT, Fässler R (2013) β1 integrins with individually disrupted cytoplasmic NPxY motifs are embryonic lethal but partially active in the epidermis. J Invest Dermatol 133: 2722–2731. doi:10.1038/jid.2013.232.

340. Xiong J-P, Stehle T, Goodman SL, Arnaout MA (2003) New insights into the structural basis of integrin activation. Blood 102: 1155–1159. doi:10.1182/blood-2003-01-0334.

341. Ingber DE (2006) Mechanical control of tissue morphogenesis during embryological development. Int J Dev Biol 50: 255–266. doi:10.1387/ijdb.052044di.

342. Schiller HB, Friedel CC, Boulegue C, Fässler R (2011) Quantitative proteomics of the integrin adhesome show a myosin II-dependent recruitment of LIM domain proteins. EMBO Rep 12: 259–266. doi:10.1038/embor.2011.5.

343. Schiller HB, Fässler R (2013) Mechanosensitivity and compositional dynamics of cell-matrix adhesions. EMBO Rep 14: 509–519. doi:10.1038/embor.2013.49.

344. Zaidel-Bar R, Geiger B (2010) The switchable integrin adhesome. Journal of Cell

Science 123: 1385–1388. doi:10.1242/jcs.066183.

345. Hamann A, Andrew DP, Jablonski-Westrich D, Holzmann B, Butcher EC (1994) Role of alpha 4-integrins in lymphocyte homing to mucosal tissues in vivo. J Immunol 152: 3282–3293.

346. Prieto J, Takei F, Gendelman R, Christenson B, Biberfeld P, et al. (1989) MALA-2, mouse homologue of human adhesion molecule ICAM-1 (CD54). Eur J Immunol 19: 1551–1557. doi:10.1002/eji.1830190906.

347. Schwartz MA, Ginsberg MH (2002) Networks and crosstalk: integrin signalling spreads. Nat Cell Biol 4: E65–E68. doi:10.1038/ncb0402-e65.

348. Cabodi S, Moro L, Bergatto E, Boeri Erba E, Di Stefano P, et al. (2004) Integrin regulation of epidermal growth factor (EGF) receptor and of EGF-dependent responses. Biochem Soc Trans 32: 438–442. doi:10.1042/BST0320438.

349. Beattie J, McIntosh L, van der Walle CF (2010) Cross-talk between the insulin-like growth factor (IGF) axis and membrane integrins to regulate cell physiology. J Cell Physiol 224: 605–611. doi:10.1002/jcp.22183.

350. Margadant C, Sonnenberg A (2010) Integrin-TGF-beta crosstalk in fibrosis, cancer and wound healing. EMBO Rep 11: 97–105. doi:10.1038/embor.2009.276.

351. Weinstein EJ, Bourner M, Head R, Zakeri H, Bauer C, et al. (2003) URP1: a member of a novel family of PH and FERM domain-containing membrane-associated proteins is significantly over-expressed in lung and colon carcinomas. Biochim Biophys Acta 1637: 207–216.

352. Ussar S, Wang H-V, Linder S, Fässler R, Moser M (2006) The Kindlins: subcellular localization and expression during murine development. Exp Cell Res 312: 3142–3151. doi:10.1016/j.yexcr.2006.06.030.

353. Kloeker S, Major MB, Calderwood DA, Ginsberg MH, Jones DA, et al. (2004) The Kindler syndrome protein is regulated by transforming growth factor-beta and involved in integrin-mediated adhesion. J Biol Chem 279: 6824–6833. doi:10.1074/jbc.M307978200.

354. Hamada K, Shimizu T, Matsui T, Tsukita S, Hakoshima T (2000) Structural basis of the membrane-targeting and unmasking mechanisms of the radixin FERM domain. EMBO J 19: 4449–4462. doi:10.1093/emboj/19.17.4449.

355. Hamada K, Shimizu T, Yonemura S, Tsukita S, Tsukita S, et al. (2003) Structural basis of adhesion-molecule recognition by ERM proteins revealed by the crystal structure of the radixin-ICAM-2 complex. EMBO J 22: 502–514. doi:10.1093/emboj/cdg039.

356. Schlessinger J, Lemmon MA (2003) SH2 and PTB Domains in Tyrosine Kinase Signaling. Science Signaling 2003: re12. doi:10.1126/scisignal.1912003re12.

357. Chishti AH, Kim AC, Marfatia SM, Lutchman M, Hanspal M, et al. (1998) The FERM domain: a unique module involved in the linkage of cytoplasmic proteins to the membrane. Trends Biochem Sci 23: 281–282.

358. Balla T (2005) Inositol-lipid binding motifs: signal integrators through protein-lipid and protein-protein interactions. Journal of Cell Science 118: 2093–2104. doi:10.1242/jcs.02387.

359. DiNitto JP, Lambright DG (2006) Membrane and juxtamembrane targeting by PH and PTB domains. Biochim Biophys Acta 1761: 850–867. doi:10.1016/j.bbalip.2006.04.008.

360. Blaikie P, Immanuel D, Wu J, Li N, Yajnik V, et al. (1994) A region in Shc distinct from the SH2 domain can bind tyrosine-phosphorylated growth factor receptors. J Biol Chem 269: 32031–32034.

361. García-Alvarez B, de Pereda JM, Calderwood DA, Ulmer TS, Critchley D, et al. (2003) Structural determinants of integrin recognition by talin. Mol Cell 11: 49–58.

362. Ma L (2004) Pleckstrin homology domains: not just for phosphoinositides. Biochem Soc Trans 32: 707–711.

363. Lemmon MA, Ferguson KM (2000) Signal-dependent membrane targeting by pleckstrin homology (PH) domains. Biochem J 350 Pt 1: 1–18.

364. Lemmon MA, Ferguson KM (2001) Molecular determinants in pleckstrin homology domains that allow specific recognition of phosphoinositides. Biochem Soc Trans 29: 377–384.

365. Kern JS, Herz C, Haan E, Moore D, Nottelmann S, et al. (2007) Chronic colitis due to an epithelial barrier defect: the role of kindlin-1 isoforms. J Pathol 213: 462–470. doi:10.1002/path.2253.

366. Lai-Cheong JE, Liu L, Sethuraman G, Kumar R, Sharma VK, et al. (2007) Five new homozygous mutations in the KIND1 gene in Kindler syndrome. J Invest Dermatol 127: 2268–2270. doi:10.1038/sj.jid.5700830.

367. Lotem M, Raben M, Zeltser R, Landau M, Sela M, et al. (2001) Kindler syndrome complicated by squamous cell carcinoma of the hard palate: successful treatment with high-dose radiation therapy and granulocyte-macrophage colony-stimulating factor. Br J Dermatol 144: 1284–1286. doi:10.1046/j.1365-2133.2001.04262.x.

368. Siegel D, Ashton G, Penagos H, Lee J, Feiler H, et al. (2003) Loss of Kindlin-1, a Human Homolog of the Caenorhabditis elegans Actin–Extracellular-Matrix Linker Protein UNC-112, Causes Kindler Syndrome. The American Journal of Human Genetics 73: 174–187. doi:10.1086/376609.

369. Ashton GHS, McLean WHI, South AP, Oyama N, Smith FJD, et al. (2004) Recurrent mutations in kindlin-1, a novel keratinocyte focal contact protein, in the autosomal recessive skin fragility and photosensitivity disorder, Kindler syndrome. J Invest Dermatol 122: 78–83. doi:10.1046/j.0022-202X.2003.22136.x.

370. Kato K, Shiozawa T, Mitsushita J, Toda A, Horiuchi A, et al. (2004) Expression of the mitogen-inducible gene-2 (mig-2) is elevated in human uterine leiomyomas but not in leiomyosarcomas. Hum Pathol 35: 55–60.

371. Tu Y, Wu S, Shi X, Chen K, Wu C (2003) Migfilin and Mig-2 link focal adhesions to

filamin and the actin cytoskeleton and function in cell shape modulation. Cell 113: 37–47.

372. Linder S (2005) Podosomes at a glance. Journal of Cell Science 118: 2079–2082. doi:10.1242/jcs.02390.

373. Linder S, Aepfelbacher M (2003) Podosomes: adhesion hot-spots of invasive cells. Trends Cell Biol 13: 376–385.

374. Schmidt S, Moser M, Sperandio M (2013) The molecular basis of leukocyte recruitment and its deficiencies. Mol Immunol 55: 49–58. doi:10.1016/j.molimm.2012.11.006.

375. Crowley CA, Curnutte JT, Rosin RE, André-Schwartz J, Gallin JI, et al. (1980) An inherited abnormality of neutrophil adhesion. Its genetic transmission and its association with a missing protein. N Engl J Med 302: 1163–1168. doi:10.1056/NEJM198005223022102.

376. Etzioni A, Frydman M, Pollack S, Avidor I, Phillips ML, et al. (1992) Brief report: recurrent severe infections caused by a novel leukocyte adhesion deficiency. N Engl J Med 327: 1789–1792. doi:10.1056/NEJM199212173272505.

377. van de Vijver E, Maddalena A, Sanal O, Holland SM, Uzel G, et al. (2012) Hematologically important mutations: leukocyte adhesion deficiency (first update). Blood Cells Mol Dis 48: 53–61. doi:10.1016/j.bcmd.2011.10.004.

378. Feng C, Li Y-F, Yau Y-H, Lee H-S, Tang X-Y, et al. (2012) Kindlin-3 mediates integrin αLβ2 outside-in signaling, and it interacts with scaffold protein receptor for activated-C kinase 1 (RACK1). J Biol Chem 287: 10714–10726. doi:10.1074/jbc.M111.299594.

379. Sabnis H, Kirpalani A, Horan J, McDowall A, Svensson L, et al. (2010) Leukocyte adhesion deficiency-III in an African-American patient. Pediatr Blood Cancer 55: 180–182. doi:10.1002/pbc.22386.

380. Schmidt S, Nakchbandi I, Ruppert R, Kawelke N, Hess MW, et al. (2011) Kindlin-3-mediated signaling from multiple integrin classes is required for osteoclast-mediated bone resorption. J Cell Biol 192: 883–897. doi:10.1083/jcb.201007141.

381. Moore G, Knight G, Blann A (2010) Fundamentals of Biomedical Science - Haematology. Oxford University Press.

382. Nowell PC, Hungerford DA (1960) Chromosome studies on normal and leukemic human leukocytes. J Natl Cancer Inst 25: 85–109.

383. Marley SB, Gordon MY (2005) Chronic myeloid leukaemia: stem cell derived but progenitor cell driven. Clin Sci 109: 13–25. doi:10.1042/CS20040336.

384. Jaffe ES, Harris NL, Stein H, Vardiman JW (2002) World Health Organization Classification of Tumours: Pathology and Genetics of Tumours of Haematopoietic and Lymphoid Tissues. Ann Oncol 13: 490–491.

385. Goldman JM, Szydlo R, Horowitz MM, Gale RP, Ash RC, et al. (1993) Choice of

pretransplant treatment and timing of transplants for chronic myelogenous leukemia in chronic phase. Blood 82: 2235–2238.

386. Faderl S, Kantarjian HM, Talpaz M, Estrov Z (1998) Clinical significance of cytogenetic abnormalities in adult acute lymphoblastic leukemia. Blood 91: 3995–4019.

387. Laneuville P (1995) Abl tyrosine protein kinase. Seminars in Immunology 7: 255–266. doi:10.1006/smim.1995.0030.

388. Abelson HT, Rabstein LS (1970) Lymphosarcoma: virus-induced thymic-independent disease in mice. Cancer Research 30: 2213–2222.

389. Sawyers CL, McLaughlin J, Goga A, Havlik M, Witte O (1994) The nuclear tyrosine kinase c-Abl negatively regulates cell growth. Cell 77: 121–131.

390. Yuan ZM, Shioya H, Ishiko T, Sun X, Gu J, et al. (1999) p73 is regulated by tyrosine kinase c-Abl in the apoptotic response to DNA damage. Nature 399: 814–817. doi:10.1038/21704.

391. Lewis JM, Schwartz MA (1998) Integrins regulate the association and phosphorylation of paxillin by c-Abl. J Biol Chem 273: 14225–14230.

392. Reuther GW, Fu H, Cripe LD, Collier RJ, Pendergast AM (1994) Association of the protein kinases c-Bcr and Bcr-Abl with proteins of the 14-3-3 family. Science 266: 129–133.

393. Ma G, Lu D, Wu Y, Liu J, Arlinghaus RB (1997) Bcr phosphorylated on tyrosine 177 binds Grb2. Oncogene 14: 2367–2372. doi:10.1038/sj.onc.1201053.

394. Voncken JW, van Schaick H, Kaartinen V, Deemer K, Coates T, et al. (1995) Increased neutrophil respiratory burst in bcr-null mutants. Cell 80: 719–728.

395. Melo JV (1996) The diversity of BCR-ABL fusion proteins and their relationship to leukemia phenotype. Blood 88: 2375–2384.

396. Pane F, Frigeri F, Sindona M, Luciano L, Ferrara F, et al. (1996) Neutrophilic-chronic myeloid leukemia: a distinct disease with a specific molecular marker (BCR/ABL with C3/A2 junction). Blood 88: 2410–2414.

397. Wilson G, Frost L, Goodeve A, Vandenberghe E, Peake I, et al. (1997) BCR-ABL transcript with an e19a2 (c3a2) junction in classical chronic myeloid leukemia. Blood 89: 3064.

398. Deininger MW, Goldman JM, Melo JV (2000) The molecular biology of chronic myeloid leukemia. Blood 96: 3343–3356.

399. Weisberg E, Manley PW, Cowan-Jacob SW, Hochhaus A, Griffin JD (2007) Second generation inhibitors of BCR-ABL for the treatment of imatinib-resistant chronic myeloid leukaemia. Nat Rev Cancer 7: 345–356. doi:10.1038/nrc2126.

400. Pendergast AM, Quilliam LA, Cripe LD, Bassing CH, Dai Z, et al. (1993) BCR-ABL-induced oncogenesis is mediated by direct interaction with the SH2 domain of

the GRB-2 adaptor protein. Cell 75: 175–185.

401. Skorski T (1994) Negative regulation of p120GAP GTPase promoting activity by p210bcr/abl: implication for RAS-dependent Philadelphia chromosome positive cell growth. J Exp Med 179: 1855–1865. doi:10.1084/jem.179.6.1855.

402. Puil L, Liu J, Gish G, Mbamalu G, Bowtell D, et al. (1994) Bcr-Abl oncoproteins bind directly to activators of the Ras signalling pathway. EMBO J 13: 764–773.

403. Sawyers CL, McLaughlin J, Witte ON (1995) Genetic requirement for Ras in the transformation of fibroblasts and hematopoietic cells by the Bcr-Abl oncogene. Journal of Experimental Medicine 181: 307–313.

404. Raitano AB, Halpern JR, Hambuch TM, Sawyers CL (1995) The Bcr-Abl leukemia oncogene activates Jun kinase and requires Jun for transformation. Proc Natl Acad Sci USA 92: 11746–11750.

405. Traina F, Carvalheira JBC, Saad MJA, Costa FF, Saad STO (2003) BCR-ABL binds to IRS-1 and IRS-1 phosphorylation is inhibited by imatinib in K562 cells. FEBS Lett 535: 17–22.

406. M S, R S, K O, N U, MA D, et al. (1996) The proto-oncogene product p120CBL and the adaptor proteins CRKL and c-CRK link c-ABL, p190BCR/ABL and p210BCR/ABL to the phosphatidylinositol-3' kinase pathway. Oncogene 12: 839–846.

407. Gesbert F, Sellers WR, Signoretti S, Loda M, Griffin JD (2000) BCR/ABL regulates expression of the cyclin-dependent kinase inhibitor p27Kip1 through the phosphatidylinositol 3-Kinase/AKT pathway. J Biol Chem 275: 39223–39230. doi:10.1074/jbc.M007291200.

408. Ilaria RL, Van Etten RA (1996) P210 and P190(BCR/ABL) induce the tyrosine phosphorylation and DNA binding activity of multiple specific STAT family members. J Biol Chem 271: 31704–31710.

409. Gesbert F, Griffin JD (2000) Bcr/Abl activates transcription of the Bcl-X gene through STAT5. Blood 96: 2269–2276.

410. Skorski T, Nieborowska-Skorska M, Szczylik C, Kanakaraj P, Perrotti D, et al. (1995) C-RAF-1 serine/threonine kinase is required in BCR/ABL-dependent and normal hematopoiesis. Cancer Research 55: 2275–2278.

411. Sawyers CL (1993) The role of myc in transformation by BCR-ABL. Leuk Lymphoma 11 Suppl 1: 45–46. doi:10.3109/10428199309047862.

412. Skorski T (1997) Transformation of hematopoietic cells by BCR/ABL requires activation of a PI-3k/Akt-dependent pathway. EMBO J 16: 6151–6161. doi:10.1093/emboj/16.20.6151.

413. Neshat MS, Raitano AB, Wang HG, Reed JC, Sawyers CL (2000) The survival function of the Bcr-Abl oncogene is mediated by Bad-dependent and -independent pathways: roles for phosphatidylinositol 3-kinase and Raf. Mol Cell Biol 20: 1179–1186.

414. Kolibaba KS, Bhat A, Heaney C, Oda T, Druker BJ (1999) CRKL binding to BCR-ABL and BCR-ABL transformation. Leuk Lymphoma 33: 119–126. doi:10.3109/10428199909093732.

415. Fierro FA, Taubenberger A, Puech P-H, Ehninger G, Bornhauser M, et al. (2008) BCR/ABL Expression of Myeloid Progenitors Increases β1-Integrin Mediated Adhesion to Stromal Cells. Journal of Molecular Biology 377: 1082–1093. doi:10.1016/j.jmb.2008.01.085.

416. Talpaz M, Kantarjian HM, McCredie K, Trujillo JM, Keating MJ, et al. (1986) Hematologic Remission and Cytogenetic Improvement Induced by Recombinant Human Interferon Alpha Ain Chronic Myelogenous Leukemia. N Engl J Med 314: 1065–1069. doi:10.1056/NEJM198604243141701.

417. Manley PW, Cowan-Jacob SW, Buchdunger E, Fabbro D, Fendrich G, et al. (2002) Imatinib: a selective tyrosine kinase inhibitor. Eur J Cancer 38 Suppl 5: S19–S27.

418. Buchdunger E, Cioffi CL, Law N, Stover D, Ohno-Jones S, et al. (2000) Abl protein-tyrosine kinase inhibitor STI571 inhibits in vitro signal transduction mediated by c-kit and platelet-derived growth factor receptors. J Pharmacol Exp Ther 295: 139–145.

419. Okuda K, Weisberg E, Gilliland DG, Griffin JD (2001) ARG tyrosine kinase activity is inhibited by STI571. Blood 97: 2440–2448.

420. Berman E, Nicolaides M, Maki RG, Fleisher M, Chanel S, et al. (2006) Altered bone and mineral metabolism in patients receiving imatinib mesylate. N Engl J Med 354: 2006–2013. doi:10.1056/NEJMoa051140.

421. Steegmann JL, Moreno G, Alaez C, Osorio S, Granda A, et al. (2003) Chronic myeloid leukemia patients resistant to or intolerant of interferon alpha and subsequently treated with imatinib show reduced immunoglobulin levels and hypogammaglobulinemia. Haematologica 88: 762–768.

422. Kerkelä R, Grazette L, Yacobi R, Iliescu C, Patten R, et al. (2006) Cardiotoxicity of the cancer therapeutic agent imatinib mesylate. Nat Med 12: 908–916. doi:10.1038/nm1446.

423. Mattiuzzi GN, Cortes JE, Talpaz M, Reuben J, Rios MB, et al. (2003) Development of Varicella-Zoster virus infection in patients with chronic myelogenous leukemia treated with imatinib mesylate. Clin Cancer Res 9: 976–980.

424. Dewar AL, Domaschenz RM, Doherty KV, Hughes TP, Lyons AB (2003) Imatinib inhibits the in vitro development of the monocyte/macrophage lineage from normal human bone marrow progenitors. Leukemia 17: 1713–1721. doi:10.1038/sj.leu.2403071.

425. Appel S, Rupf A, Weck MM, Schoor O, Brümmendorf TH, et al. (2005) Effects of imatinib on monocyte-derived dendritic cells are mediated by inhibition of nuclear factor-kappaB and Akt signaling pathways. Clin Cancer Res 11: 1928–1940. doi:10.1158/1078-0432.CCR-04-1713.

426. Cwynarski K, Laylor R, Macchiarulo E, Goldman J, Lombardi G, et al. (2004) Imatinib inhibits the activation and proliferation of normal T lymphocytes in vitro.

Leukemia 18: 1332–1339. doi:10.1038/sj.leu.2403401.

427. O'Brien SG, Guilhot F, Larson RA, Gathmann I, Baccarani M, et al. (2003) Imatinib compared with interferon and low-dose cytarabine for newly diagnosed chronic-phase chronic myeloid leukemia. N Engl J Med 348: 994–1004. doi:10.1056/NEJMoa022457.

428. Cilloni D, Saglio G (2012) Molecular pathways: BCR-ABL. Clin Cancer Res 18: 930–937. doi:10.1158/1078-0432.CCR-10-1613.

429. Van Etten RA, Chan WW, Zaleskas VM (2008) Switch pocket inhibitors of the ABL tyrosine kinase: distinct kinome inhibition profiles and in vivo efficacy in mouse models of CML and B-lymphoblastic leukemia induced by BCR-ABL T315I. …ASH Annual Meeting Abstracts 112: 576.

430. Branford S, Rudzki Z, Walsh S, Grigg A, Arthur C, et al. (2002) High frequency of point mutations clustered within the adenosine triphosphate–binding region of BCR/ABL in patients with chronic myeloid leukemia or Ph-positive acute lymphoblastic leukemia who develop imatinib (STI571) resistance. Blood 99: 3472–3475.

431. Kaeda J, Chase A, Goldman JM (2002) Cytogenetic and Molecular Monitoring of Residual Disease in Chronic Myeloid Leukaemia. Acta Haematol 107: 64–75. doi:10.1159/000046635.

432. Rousselot P, Huguet F, Rea D, Legros L, Cayuela JM, et al. (2007) Imatinib mesylate discontinuation in patients with chronic myelogenous leukemia in complete molecular remission for more than 2 years. Blood 109: 58–60. doi:10.1182/blood-2006-03-011239.

433. Chu S, Xu H, Shah NP, Snyder DS, Forman SJ, et al. (2005) Detection of BCR-ABL kinase mutations in CD34+ cells from chronic myelogenous leukemia patients in complete cytogenetic remission on imatinib mesylate treatment. Blood 105: 2093–2098. doi:10.1182/blood-2004-03-1114.

434. Fialkow PJ, Jacobson RJ, Papayannopoulou T (1977) Chronic myelocytic leukemia: clonal origin in a stem cell common to the granulocyte, erythrocyte, platelet and monocyte/macrophage. Am J Med 63: 125–130.

435. Michor F, Hughes TP, Iwasa Y, Branford S, Shah NP, et al. (2005) Dynamics of chronic myeloid leukaemia. Nature 435: 1267–1270. doi:10.1038/nature03669.

436. Cortes J, Hochhaus A, Hughes T, Kantarjian H (2011) Front-line and salvage therapies with tyrosine kinase inhibitors and other treatments in chronic myeloid leukemia. J Clin Oncol 29: 524–531. doi:10.1200/JCO.2010.31.3619.

437. Park CH, Bergsagel DE, McCulloch EA (1971) Mouse myeloma tumor stem cells: a primary cell culture assay. J Natl Cancer Inst 46: 411–422.

438. Reya T, Morrison SJ, Clarke MF, Weissman IL (2001) Stem cells, cancer, and cancer stem cells. Nature 414: 105–111. doi:10.1038/35102167.

439. Lapidot T, Sirard C, Vormoor J, Murdoch B, Hoang T, et al. (1994) A cell initiating

human acute myeloid leukaemia after transplantation into SCID mice. Nature 367: 645–648. doi:10.1038/367645a0.

440. Bonnet D, Dick JE (1997) Human acute myeloid leukemia is organized as a hierarchy that originates from a primitive hematopoietic cell. Nat Med 3: 730–737.

441. Al-Hajj M, Wicha MS, Benito-Hernandez A, Morrison SJ, Clarke MF (2003) Prospective identification of tumorigenic breast cancer cells. Proc Natl Acad Sci USA 100: 3983–3988. doi:10.1073/pnas.0530291100.

442. O'Brien CA, Pollett A, Gallinger S, Dick JE (2007) A human colon cancer cell capable of initiating tumour growth in immunodeficient mice. Nature 445: 106–110. doi:10.1038/nature05372.

443. Li C, Heidt DG, Dalerba P, Burant CF, Zhang L, et al. (2007) Identification of Pancreatic Cancer Stem Cells. Cancer Research 67: 1030–1037.

444. Haferlach T, Winkemann M, Nickenig C, Meeder M, Ramm-Petersen L, et al. (1997) Which compartments are involved in Philadelphia-chromosome positive chronic myeloid leukaemia? An answer at the single cell level by combining May-Grünwald-Giemsa staining and fluorescence in situ hybridization techniques. Br J Haematol 97: 99–106.

445. Baum CM, Weissman IL, Tsukamoto AS, Buckle AM, Péault B (1992) Isolation of a candidate human hematopoietic stem-cell population. Proc Natl Acad Sci USA 89: 2804–2808.

446. Jamieson CHM, Ailles LE, Dylla SJ, Muijtjens M, Jones C, et al. (2004) Granulocyte-macrophage progenitors as candidate leukemic stem cells in blast-crisis CML. N Engl J Med 351: 657–667. doi:10.1056/NEJMoa040258.

447. Hope KJ, Jin L, Dick JE (2004) Acute myeloid leukemia originates from a hierarchy of leukemic stem cell classes that differ in self-renewal capacity. Nat Immunol 5: 738–743. doi:10.1038/ni1080.

448. Guan Y, Gerhard B, Hogge DE (2003) Detection, isolation, and stimulation of quiescent primitive leukemic progenitor cells from patients with acute myeloid leukemia (AML). Blood 101: 3142–3149. doi:10.1182/blood-2002-10-3062.

449. Holyoake T, Jiang X, Eaves C, Eaves A (1999) Isolation of a highly quiescent subpopulation of primitive leukemic cells in chronic myeloid leukemia. Blood 94: 2056–2064.

450. Li L, Neaves WB (2006) Normal stem cells and cancer stem cells: the niche matters. Cancer Research 66: 4553–4557. doi:10.1158/0008-5472.CAN-05-3986.

451. Lane SW, Scadden DT, Gilliland DG (2009) The leukemic stem cell niche: current concepts and therapeutic opportunities. Blood 114: 1150–1157. doi:10.1182/blood-2009-01-202606.

452. Matsunaga T, Takemoto N, Sato T, Takimoto R, Tanaka I, et al. (2003) Interaction between leukemic-cell VLA-4 and stromal fibronectin is a decisive factor for minimal residual disease of acute myelogenous leukemia. Nat Med 9: 1158–1165.

453. Jin L, Hope KJ, Zhai Q, Smadja-Joffe F, Dick JE (2006) Targeting of CD44 eradicates human acute myeloid leukemic stem cells. Nat Med 12: 1167–1174. doi:10.1038/nm1483.

454. Zeng Z, Shi YX, Samudio IJ, Wang R-Y, Ling X, et al. (2009) Targeting the leukemia microenvironment by CXCR4 inhibition overcomes resistance to kinase inhibitors and chemotherapy in AML. Blood 113: 6215–6224. doi:10.1182/blood-2008-05-158311.

455. Nervi B, Ramirez P, Rettig MP, Uy GL, Holt MS, et al. (2009) Chemosensitization of acute myeloid leukemia (AML) following mobilization by the CXCR4 antagonist AMD3100. Blood 113: 6206–6214. doi:10.1182/blood-2008-06-162123.

456. Wu M, Kwon HY, Rattis F, Blum J, Zhao C, et al. (2007) Imaging hematopoietic precursor division in real time. Cell Stem Cell 1: 541–554. doi:10.1016/j.stem.2007.08.009.

457. Bhatia R, Holtz M, Niu N, Gray R, Snyder DS, et al. (2003) Persistence of malignant hematopoietic progenitors in chronic myelogenous leukemia patients in complete cytogenetic remission following imatinib mesylate treatment. Blood 101: 4701–4707. doi:10.1182/blood-2002-09-2780.

458. Cortes J, O'Brien S, Kantarjian H (2004) Discontinuation of imatinib therapy after achieving a molecular response. Blood 104: 2204–2205. doi:10.1182/blood-2004-04-1335.

459. Graham SM, Jørgensen HG, Allan E, Pearson C, Alcorn MJ, et al. (2002) Primitive, quiescent, Philadelphia-positive stem cells from patients with chronic myeloid leukemia are insensitive to STI571 in vitro. Blood 99: 319–325.

460. Copland M, Hamilton A, Elrick LJ, Baird JW, Allan EK, et al. (2006) Dasatinib (BMS-354825) targets an earlier progenitor population than imatinib in primary CML but does not eliminate the quiescent fraction. Blood 107: 4532–4539.

461. Jørgensen HG, Allan EK, Jordanides NE, Mountford JC, Holyoake TL (2007) Nilotinib exerts equipotent antiproliferative effects to imatinib and does not induce apoptosis in CD34+ CML cells. Blood 109: 4016–4019. doi:10.1182/blood-2006-11-057521.

462. Essers MAG, Trumpp A (2010) Targeting leukemic stem cells by breaking their dormancy. Mol Oncol 4: 443–450. doi:10.1016/j.molonc.2010.06.001.

463. Dean M, Fojo T, Bates S (2005) Tumour stem cells and drug resistance. Nat Rev Cancer 5: 275–284. doi:10.1038/nrc1590.

464. Mahadevan D, List AF (2004) Targeting the multidrug resistance-1 transporter in AML: molecular regulation and therapeutic strategies. Blood 104: 1940–1951. doi:10.1182/blood-2003-07-2490.

12. Appendix

The appendix includes reprints of the paper 1 to 11. The supplementary information as well as supplementary movies for each paper can be found on the enclosed CD.

12.1 Paper 1: Kindlin-3 controls quiescence of hematopoietic stem cells in mice.

12.2 Paper 2: Kindlin-3 is required for β2 integrin-mediated leukocyte adhesion to endothelial cells.

12.3 Paper 3: Kindlin-3-mediated signaling from multiple integrin classes is required for osteoclast-mediated bone resorption.

12.4 Paper 4: Role of kindlin-3 in T cell progenitor homing and thymocyte development.

12.5 Paper 5: Kindlin-3 regulates integrin activation and adhesion reinforcement of effector T cells.

12.6 Paper 6: Platelets and neutrophils require different Kindlin-3 copy numbers to control integrin-mediated functions.

12.7 Paper 7: β1 integrin-mediated signals are required for platelet granule secretion and hemostasis in mouse.

12.8 Paper 8: Kindlin-1 controls cutaneous epithelial stem cell proliferation by modulating Wnt ligand and TGFβ availability.

12.9 Paper 9: CD98hc facilitates B cell proliferation and adaptive humoral immunity.

12.10 Paper 10: The Mechanism of Kindlin-Mediated Activation of Integrin αIIbβ3.

12.11 Paper 11: Knock-down and knockout of β1-integrin in hepatocytes impairs liver regeneration through inhibition of growth factor signaling.

12.1 Paper 1:

Kindlin-3 controls quiescence of hematopoietic stem cells in mice.

Kindlin-3 controls quiescence of hematopoietic stem cells in mice

Raphael Ruppert[1], Markus Moser[1], Markus Sperandio[2], Emanuel Rognoni[1], Martin Orban[3], Robert A. J. Oostendorp[4], Steffen Massberg[3], and Reinhard Fässler[1]*

[1]Department of Molecular Medicine, Max Planck Institute of Biochemistry, Martinsried, Germany; [2]Walter Brendel Center for Experimental Medicine, Ludwig Maximilian University, Munich, Germany; [3]Med. Clinic and Policlinic I, Klinikum der Universität, Munich, Germany; [4]3rd Department of Internal Medicine, Klinikum rechts der Isar der Technischen Universität München, Munich, Germany.

*Correspondence should be addressed to R. F. (faessler@biochem.mpg.de)

SUMMARY

Hematopoietic stem cells (HSCs) express several integrins, whose function(s) are tightly controlled by integrin activating proteins. One of these proteins is Kindlin-3, which was shown to activate several integrin classes in differentiated blood cells. Here we tested Kindlin-3 function in HSCs and report that Kindlin-3 loss impaired HSC homing, engraftment and entry into quiescence resulting in HCS exhaustion and reduced survival of transplanted recipient mice. While the reduced homing efficiency was due to impaired adhesion of HSCs to the microvascular endothelium, loss of quiescence was likely caused by defective lodgment into the BM niche resulting in the hyperproliferation, spontaneous mobilization and finally exhaustion of HSCs. Importantly, the defective engraftment precluded the development of a chronic myeloid leukemia (CML) by BCR-ABL transduced BM cells in sublethally irradiated mice. Thus our findings assign Kindlin-3 a central role in HSC homeostasis and malignancies.

INTRODUCTION

Mature blood cells are derived from a small number of hematopoietic stem cells (HSCs), which reside in the bone marrow (BM). HSCs are characterized by their low cycling rate and their ability to self-renew throughout the lifespan of an organism. After hematopoietic injury (e.g. bleeding) quiescent HSCs become activated, divide asymmetrically, replenish the pool of hematopoietic effector cells and then return to the quiescent state (Trumpp et al., 2010).

To maintain HSCs throughout the lifespan of an animal, the oscillation of HSCs between quiescence, self-renewal and differentiation is precisely regulated in a specific microenvironment referred to as the stem cell niche (Morrison and Spradling, 2008).

The regulation of these HSC properties is achieved by cytokines, chemokines and growth factors released by niche cells (Rizo, 2006), interactions of HSCs with niche cells (Kiel and Morrison, 2008), and extracellular matrix (ECM) proteins (van der Loo et al., 1998), and calcium gradients established by osteoclasts during bone remodeling (Adams et al., 2006). An impairment of the HSC-niche interplay can be disastrous and result in loss of quiescence, uncontrolled activation and finally exhaustion of HSCs, or even the development of blood malignancies.

The interactions of HSCs with niche cells and ECM are mediated by several adhesion molecules including the hyaluronan receptor CD44, N-cadherin and integrins (Wilson and Trumpp, 2006). Integrins are α/β heterodimers that mediate binding to ECM and counter receptors (Hynes, 2002). HSCs express several classes of integrins; multiple members of the β1 class (α2β1, α4β1, α5β1, α6β1, α9β1), αLβ2 from the β2 class and αvβ3 from the αv-class (Grassinger et al., 2009). *In vivo* and *in vitro* studies using genetics or inhibitory antibodies revealed that loss of integrins perturb HSC homing to the BM (Potocnik et al., 2000), their mobilization into the circulation (Magnon and Frenette, 2008), proliferation and differentiation (Arroyo et al., 1999). Whether integrins also play a role in maintaining HSC quiescence and stemness is less clear. Moreover, it is also not clear whether and how integrins influence leukemic stem cells (LSC) and thus hematopoietic malignancies.

Integrin ligand binding and signaling requires an activation step, which is induced following Talin and Kindlin binding to the cytoplasmic domains of integrin β subunits and associated with allosteric changes in the integrin ectodomain and transmembrane domains (Moser et al., 2009a; Shattil et al., 2010). Kindlins are evolutionary conserved

and consist of three members. Hematopoietic cells express Kindlin-3 (Ussar et al., 2006) whose deletion in mice abrogates integrin activation resulting in hemorrhages, leukocyte adhesion defects and osteopetrosis (Moser et al., 2009b; 2008; Schmidt et al., 2011). A human disease with similar abnormalities called leukocyte adhesion deficiency type III is also caused by null mutations of the *Kindlin-3* gene (Kuijpers et al., 2009; Malinin et al., 2009; Svensson et al., 2009).

Despite the prominent role of Kindlin-3 in several hematopoietic lineages, it has not been studied in HSCs. Therefore, we investigated the HSC properties in mice carrying a disrupted Kindlin-3 gene (*Fermt3*). We report that $K3^{-/-}$ HSCs fail to reconstitute recipient mice in serial transplantations due to reduced homing to the BM, diminished retention in the BM and an inability of LT-HSCs to become quiescent leading to an exhaustion of HSCs. Furthermore, BCR-ABL transformed $K3^{-/-}$ HSCs are unable to induce a CML-like disease in sublethally irradiated mice due to their poor engraftment in the presence of wild type (wt) HSCs. These findings assign Kindlin-3 an essential role in HSPC homeostasis and in preventing hematopoietic malignancies.

RESULTS

Kindlin-3 is required for HSC engraftment

Kindlin-3 is highly expressed in wt ($K3^{+/+}$) and absent in Kindlin-3-null ($K3^{-/-}$) FACS-purified hematopoietic stem and precursor cells (HSPCs) (Figure S1A). Since FACS-based isolation of cells only enrich for HSCs, we will refer to the populations used in this study as HSPCs to account for potential progenitor cell contamination. To test whether Kindlin-3 is required for HSPC function we generated fetal liver (FL) chimeras by transplanting $5x10^6$ unfractionated FL cells (C57BL/6; $CD45.2^+$) from $K3^{+/+}$ or $K3^{-/-}$ E14.5 littermate embryos into lethally irradiated wt congenic B6.SJL ($CD45.1^+$) recipient mice (Figure S1B). Lifetime analysis revealed that the median survival of $K3^{+/+}$ FL cell recipients (termed $K3^{+/+}$ chimeras) and $K3^{-/-}$ FL cell recipients (termed $K3^{-/-}$ chimeras) was 48.7 and 24.6 weeks, respectively (Figure 1A).

To exclude that the diminished survival of $K3^{-/-}$ chimeras was due to transplantation of a reduced total number of HSPCs in $K3^{-/-}$ FLs we harvested mononuclear cells (MNCs) from FLs and determined the relative frequency of $lin^-Mac\text{-}1^{med}AA4.1^+Sca\text{-}1^+c\text{-}kit^+$ (FL-LSK) cells (Figure S1C) (Jordan et al., 1990; Okada et al., 1992). The results showed that, despite a 2.75-fold decrease in the total number of MNCs in E14.5 FLs of $K3^{-/-}$ mice (Figure S1D), the relative FL-LSK cell number was significantly elevated compared to control FLs (Figure S1C, E) indicating that the absolute number of LSK cells per FL was similar in $K3^{+/+}$ and $K3^{-/-}$ mice (Figure S1F). Further assessment of committed hematopoietic precursor cells with the colony-forming unit-culture (CFU-C) assay and more immature, long-term culture initiating cells (LTC-ICs) revealed that the frequencies of CFU-Cs and LTC-ICs in FLs of $K3^{-/-}$ mice were increased (Figure S1G, S1I). However, the increase was not compensatory, since their absolute numbers per FL were decreased (Figure S1H, S1J). Since identical numbers of $K3^{+/+}$ and $K3^{-/-}$ FL MNCs were transplanted, the higher frequency of HSPCs among $K3^{-/-}$ FL MNCs implies that $K3^{-/-}$ chimeras received more donor HSPCs than $K3^{+/+}$chimeras, which excluded a lack of HSPCs in $K3^{-/-}$ FLs as a cause for their reduced survival.

Next we tested whether defects in lineage differentiation caused the diminished survival of $K3^{-/-}$ chimeras by quantifying different hematopoietic lineages in BM, spleen (Spl) and peripheral blood (PB) of moribund and healthy chimeras 3 to 4 months after transplantation. Moribund $K3^{-/-}$ chimeras were characterized by a pronounced pancytopenia in the BM affecting B-, T-, erythroid cells, neutrophils and

monocytes/macrophages, and in PB and Spl affecting B-, T- and erythroid cells (Figure 1B, 1C, S1K, L, Table S1). This was never observed in $K3^{+/+}$ chimeras. Healthy $K3^{-/-}$ chimeras had reduced T cells and erythroid cells and increased myeloid and B cells in the PB (Figure S1K, Table S1). The increase in myeloid cells is consistent with their previously reported inability to leave the vasculature (Moser et al 2008). In BM and Spl the numbers of $K3^{-/-}$ MNCs were normal, while cell counts of lymphoid, erythroid and myeloid lineages were differentially affected (Figure 1B, 1C, S1L). However, they were still sufficiently high to exclude a severe differentiation defect as a cause for the increased lethality of $K3^{-/-}$ chimeras. To exclude secondary defects due to imminent death, all further experiments were done with healthy $K3^{-/-}$ chimeras.

Kindlin-3 is required for BM homing of HSPCs

Homing of HSPCs to the BM requires β1 integrins (Magnon and Frenette, 2008) whose affinity is controlled by Kindlin-3 (Moser et al., 2009a). To assess the role of Kindlin-3 in homing, we analysed short-term homing of FACS-isolated $lin^{-}Sca\text{-}1^{+}c\text{-}kit^{+}$ (LSK) cells from the BM of $K3^{+/+}$ and $K3^{-/-}$ chimeras. Injection of fluorescently labeled LSK cells into lethally irradiated wt recipient mice revealed that $K3^{-/-}$ LSK cells homed about 5 times less efficient to the BM than $K3^{+/+}$ LSK cells 18 h after transplantation as quantified by FACS (Figure 2A). These findings were further confirmed by intravital 2-photon microscopy imaging of the central sinus and the surrounding BM cavity of the mouse calvaria, which also showed around 5 times less $K3^{-/-}$ LSK cells within the BM interstitium 18 h after transplantation (Figure 2B, C). Closer analysis revealed a significant reduction of $K3^{-/-}$ LSK cells firmly adhering to the vessel surface (defined as adhesion to the same spot for at least 60 s) (Figure 2D). While most $K3^{-/-}$ LSK cells remained on the same spot for a few seconds, the $K3^{+/+}$ LSK cells remained on the same spot up to 30 min (Figure 2E and Movie S1- S3).

The similar integrin expression profile of $K3^{+/+}$ and $K3^{-/-}$ LSK cells (Figure S2A, B) suggested that integrin function(s) rather than integrin levels were affected by the loss of Kindlin-3 expression. To test this hypothesis under flow conditions, we analyzed integrin-dependent adhesion of LSK cells in an *ex vivo* microflow chamber assay (Frommhold et al., 2008). Consistent with previous findings (Mazo et al., 2011), the numbers of adherent $K3^{+/+}$ LSK cells from the BM of chimeric mice (Figure 2F) or FL (Figure S2C) were highest on surfaces coated with recombinant murine (rm) VCAM-1, rmE-selectin and rmCXCL12. Adhesion of $K3^{+/+}$ LSK cell was efficiently blocked with

antibodies against α4 integrin. In sharp contrast, $K3^{-/-}$ LSK cells from BM (Figure 2F) or FL (Figure S2C) adhered poorly to flow chambers coated with rmVCAM-1, rmE-selectin and rmCXCL12 or with rmVCAM-1 and rmE-selectin, suggesting that loss of Kindlin-3 dramatically impairs β1 integrin-dependent LSK cell adhesion. Importantly though, the low level adhesion of $K3^{-/-}$ LSK cells was still sufficient to enable residual homing to the BM compartment (Figure 2A-C). Interestingly, $K3^{+/+}$ as well as $K3^{-/-}$ LSK cell from FL or BM did not adhere to immobilized ICAM-1 under flow (Fig. S2D, E). These results suggest that α4β1 integrin is the predominant adhesion receptor that requires Kindlin-3 to firmly arrest LSK cells under flow conditions.

LT-HSCs are present in the BM of $K3^{-/-}$ chimeras

The reduced homing of $K3^{-/-}$ LSK cells indicates that $K3^{-/-}$ HSPCs enter the BM but fail to accomplish a long-term reconstitution of the hematopoietic system. To test whether HSPCs were indeed present in the BM of $K3^{-/-}$ chimeras we performed CFU-C and LTC-IC assays with donor derived BM cells 4 months after transplantation. Normal numbers of CFU-Cs and a similar frequency of LTC-ICs were present in the $K3^{+/+}$ and $K3^{-/-}$ BM (Figure 3A, B). These functional assays support the existence of HSPCs in the BM of $K3^{-/-}$chimeras. To further corroborate their presence in the BM we phenotypically identified and quantified them with FACS using specific antibodies against CD34 and the signal lymphocyte activating molecule (SLAM) receptors (CD150 and CD48) (Kiel et al., 2005; Morita et al., 2010). At 1-13 months after transplantation the total number of $K3^{-/-}$ LSK cells in the BM was normal, while the LSK subpopulations were markedly altered (Figure 3C, D). The $CD150^{+}CD48^{-}$ LSK population, together with its subpopulations $CD150^{+}CD48^{-}CD34^{-}$ (enriched with quiescent LT-HSCs) and $CD150^{+}CD48^{-}CD34^{+}$ (enriched with more actively cycling cells) (Wilson et al., 2008) were significantly reduced in the BM of $K3^{-/-}$ chimeras. Instead, the $CD150^{+}CD48^{+}$ and $CD150^{-}CD48^{+}$ LSK populations were increased (Figure 3C, D) suggesting a shift from the quiescent to the proliferating pool of HSPCs in $K3^{-/-}$ chimeras.

To determine whether populations enriched in LT-HSCs in the BM change over time we analyzed the chimeras 1, 2, 4 and 9-13 months after transplantation. While the percentages of the $K3^{+/+}$ and $K3^{-/-}$ LSK subpopulations to total LSK cells differed one month after BM transplantation, the total numbers of the $CD150^{+}CD48^{-}$ and $CD150^{+}CD48^{-}CD34^{-}$ LSK subpopulations were comparable between $K3^{+/+}$ and $K3^{-/-}$ chimeras (Figure 3E-G). While the numbers of $CD150^{+}CD48^{-}$ and $CD150^{+}CD48^{-}CD34^{-}$

LSK cells steadily increased in the $K3^{+/+}$ BM, they remained low in the $K3^{-/-}$ BM (Figure 3F, G). These results indicate that populations enriched in LT-HSCs are present in the BM of $K3^{-/-}$ chimeras but fail to expand with age.

Kindlin-3 maintains HSC quiescence and BM retention

The reduction of populations enriched in LT-HSCs in the BM of $K3^{-/-}$ chimeras could be due to an uncontrolled proliferation, differentiation to multipotent progenitors and/or impaired BM retention leading to their premature exhaustion. To test whether LT-HSCs are hyperactive we first determined the sensitivity of $K3^{+/+}$ and $K3^{-/-}$ chimeras to the cytostatic drug, 5-Fluorouracil (5-FU), which eliminates cycling but not quiescent HSCs (Essers et al., 2009). In response to 5-FU treatment 2 out of 22 $K3^{+/+}$ chimeras and all $K3^{-/-}$ chimeras died suggesting that HSCs are actively cycling, and quiescent LT-HSCs are absent or extremely low in $K3^{-/-}$ chimeras. Pre-treatment with polyI:C, which induces interferon-α expression (Pichlmair and Reis e Sousa, 2007) and drives HSCs to the cell cycle (Essers et al., 2009), also sensitized $K3^{+/+}$ chimeras to 5-FU (Figure 4A, B).

The increased proliferative activity of $K3^{-/-}$ HSCs was confirmed with the BrdU uptake assay, which revealed that 3-4 months after BM transplantation the percentages of $BrdU^+$ LSK, $CD150^+CD48^-$ and $CD150^+CD34^-$ LSK cells were increased in the $K3^{-/-}$ BM, while the percentage of $BrdU^+$ $lin^-Sca\text{-}1^-c\text{-}kit^+$ (LK) progenitor cells, which are highly proliferative, was similar in the BM of $K3^{+/+}$ and $K3^{-/-}$ chimeras (Figure 4C). Furthermore, DNA and Ki67 measurements in LSK cells also identified an increase in cycling LSK cells in the BM of $K3^{-/-}$ chimeras (Figure 4D, E). Similarly, the mRNA expression profile of the cyclin-dependent kinase inhibitors (CKIs) p21, p27, and p57 in $CD150^+$ LSK cells demonstrated that p57, which is required to maintain quiescence and stemness of HSCs (Tesio and Trumpp, 2011) was significantly decreased in $K3^{-/-}$ $CD150^+$ LSK cells (Figure 4F).

Finally, label-retaining cell (LRC) assays (Wilson et al., 2008) also corroborated that the numbers of slowly dividing HSCs were reduced in the $K3^{-/-}$ BM. Administration of BrdU for 16 days labeled all HSPC populations in $K3^{+/+}$ and $K3^{-/-}$ BM (Figure 4G). After a BrdU-free chase of 45 days the percentage of BrdU label-retaining cells (LRCsBrdU) in the LSK, $CD150^-CD48^+$, $CD150^+CD48^+$, $CD150^+CD48^-$ and $CD150^+CD34^-$ LSK populations were significantly diminished in the $K3^{-/-}$ BM (Figure 4H).

Despite the high proliferative activity of $K3^{-/-}$ HSPCs, the numbers of MNCs (Figure 1B) or LSK cells (Figure 3D) were not increased in the BM of healthy $K3^{-/-}$ chimeras

suggesting that in addition to their proliferation defect, $K3^{-/-}$ HSPCs are not properly retained in the BM. In line with this hypothesis, we observed increased frequencies and total numbers of LK in PB and LSK cells in Spl and PB (Figure 4I, J) and increased frequencies of CFU-Cs in Spl and PB of $K3^{-/-}$ chimeras (Figure S3A). Furthermore, transplantation of PB MNCs together with rescue Spl cells into lethally irradiated recipients demonstrated the presence of HSPCs in the PB of $K3^{-/-}$ chimeras (Figure 4K-N). While the $K3^{+/+}$ PB MNCs hardly contributed to total leukocytes, myeloid and lymphoid (i.e. B and T cells) lineages, PB MNCs from $K3^{-/-}$ chimeras readily contributed to a multi-lineage hematopoietic chimerism in recipient mice up to 16 weeks after transplantation indicating that the PB of the $K3^{-/-}$ chimeras contains an increased number of circulating HSPCs. The absence of T cells in $K3^{-/-}$ chimeras (Figure 4N) is due to an extravasation defect of preT cells into the thymus (manuscript in preparation).

To further corroborate the BM retention defect we induced mobilization of HSPCs with granulocyte colony-stimulating factor (G-CSF) (Figure 4O, S3B). G-CSF treatment of $K3^{+/+}$ chimeras increased LSK cells in the PB to the same extent as in PBS-treated $K3^{-/-}$ chimeras. G-CSF treatment of $K3^{-/-}$ chimeras induced a further increase of LSK numbers in the PB (Figure 4O). In the Spl, the LSK cell population was higher in $K3^{+/+}$ than in $K3^{-/-}$ chimeras (Figure S3B), which was probably due to the reduced extravasation potential of $K3^{-/-}$ HSPCs. These data demonstrate that the HSCs in the $K3^{-/-}$ chimeras are constitutively cycling and that $K3^{-/-}$ HSPCs are less efficiently retained in the BM.

Loss of Kindlin-3 leads to a premature exhaustion of HSCs

Quiescent HSCs mediate long-term multi-lineage reconstitution (Trumpp et al., 2010; Wilson et al., 2008). Since most HSCs in the $K3^{-/-}$ chimeras were activated, we hypothesized that long-term multi-lineage reconstitution and thus survival of recipient mice exposed to an extreme hematopoietic stress such as serial BM transplantations will be severely abrogated without Kindlin-3. Although the 1^{st} generation $K3^{-/-}$ chimeras suffered from increased lethality (Figure 1A), approximately 50% of them maintained a multi-lineage long-term reconstitution for more than 5 months. We isolated $5x10^6$ whole BM (WBM) cells from these mice and transferred them intravenously (i.v.) into lethally irradiated secondary wt congenic B6.SJL recipients. While all 42 recipients transplanted with $K3^{+/+}$ WBM cells were radio-protected for more than 10 weeks, only 4 out of the 55 recipients of $K3^{-/-}$ WBM cells were sufficiently protected to survive for 10 weeks. We

next transferred WBM cells from 9 $K3^{+/+}$ and the 4 surviving $K3^{-/-}$ 2nd generation donors to 5 tertiary recipients for each secondary donor and observed that within 10 weeks after transplantation 41 out of the 45 recipients of $K3^{+/+}$ WBM cells were protected against lethal irradiation, while all of the 20 recipients of $K3^{-/-}$ WBM cells succumbed. As expected, $K3^{+/+}$ WBM cells enabled long-term engraftment in quaternary (Figure 5A) and quinary recipients (data not shown).

To ensure that the severe reconstitution defect of $K3^{-/-}$ WBM cells did not result from a reduced number of HSPCs in transplanted WBM cells but rather from HSPC dysfunctions described above, we also performed transplantation experiments with $1x10^3$ $CD150^+$ LSK cells sorted by FACS from BM of $K3^{+/+}$ and $K3^{-/-}$ primary donor chimeras (Figure S4A) and supplemented the secondary recipients with $5x10^6$ congenic BL6.SJL unfractionated Spl cells. The experiments revealed that $K3^{+/+}$ $CD150^+$ LSK donor cells induced a very high percentage of donor-derived myeloid, B and T cells in the PB 5 weeks after transplantation, which further increased at 11 weeks. In contrast, recipients of $K3^{-/-}$ $CD150^+$ LSK donor cells showed a significantly lower cell lineage reconstitution in the PB 5 weeks after transplantation that was further diminished after 11 weeks (Figure 5B). The contribution to differentiated cell lineages was similar in BM (Figure S4B) and Spl (Figure S4C) where almost all cells in recipients of $K3^{+/+}$ $CD150^+$ LSK cells were donor-derived, while recipients of $K3^{-/-}$ $CD150^+$ LSK cells contained less than 5% donor-derived cells. Moreover, almost all cells in the different HSPC populations were donor-derived in $K3^{+/+}$ $CD150^+$ LSK cell recipients, while in most of the $K3^{-/-}$ $CD150^+$ LSK cell recipients the percentage of donor-derived HSPCs was around 10% (Figure 5C). These findings demonstrate that proliferative stress severely impairs the stemness of $K3^{-/-}$ HSCs and drastically compromises long-term BM reconstitution.

$K3^{-/-}$ HSC defects are cell autonomous

Hematopoietic injury (e.g. blood loss) activates quiescent HSCs until all hematopoietic cells are replenished (Trumpp et al., 2010). $K3^{-/-}$ chimeras suffer from anemia, which could induce HSC activation. Therefore, we designed a range of experiments to define whether $K3^{-/-}$ HSC quiescence is lost in an autonomous or non-autonomous manner.

First, we restored the anemia of $K3^{-/-}$ chimeras (Table S1) by generating mixed chimeric mice (mix-chimeras) with FL cells from E14.5 $K3^{+/+}$ or $K3^{-/-}$ embryos (C57BL/6; $CD45.2^+$) mixed with competitor FL cells from E14.5 wt congenic B6.SJL ($CD45.1^+$) embryos and transplanted both together into lethally irradiated F1 recipients

($CD45.2^+CD45.1^+$) (Figure S5A) in a 1:1 ratio for $K3^{+/+}$ and 20:1 for $K3^{-/-}$ mix-chimeras. Despite the efficient reversal of the anemia (Table S2), $K3^{-/-}$ ($CD45.2^+$) LK and LSK cell numbers remained significantly increased in the PB compared to wt LK and LSK competitor cells ($CD45.1^+$) (Figure 6A), indicating that the elevation of $K3^{-/-}$ HSPCs in the PB occurs in a cell autonomous manner. Second, we showed with LRC assays that a BrdU pulse of 18 days labeled almost all HSPCs in $K3^{+/+}$ or $K3^{-/-}$ mix-chimeras (Figure 6B) and that a chase of 45 to 50 days decreased the percentages of LRCsBrdU in the LSK, $CD150^-CD48^+$ and $CD150^+CD48^-$ LSK populations in the $K3^{-/-}$ mix-chimeras indicating that the increased proliferation rate is cell autonomous. The LRCsBrdU cells in the $CD150^+CD48^+$ and $CD150^+CD34^-$ LSK populations were also diminished in $K3^{-/-}$ mix-chimeras, although the difference was not statistically significant (Figure 6C). Third, we demonstrate that hematopoietic stress induced by 5-FU treatment of $K3^{+/+}$ or $K3^{-/-}$ mix-chimeras diminished the ratio between $K3^{-/-}$ to congenic competitor LSK cells by approximately 7-fold (Figure 6D), while the ratio between $K3^{+/+}$ and congenic competitor LSK cells remained unaffected indicating that 5-FU sensitivity is of a cell autonomous nature. Fourth, we compared G-CSF induced mobilization of LSK cells to the PB between $K3^{+/+}$ and $K3^{-/-}$ mix-chimeras (Figure 6E) and found that the high basal levels of $K3^{-/-}$ LSK cells in PBS-treated $K3^{-/-}$ mix-chimeras further increased after G-CSF treatment, while, the $K3^{+/+}$ and the congenic competitor derived LSK cells in $K3^{+/+}$ and $K3^{-/-}$ mix-chimeras increased after application of G-CSF to the basal $K3^{-/-}$ LSK cell level, demonstrating that the mobilization defect of $K3^{-/-}$ HSCs is also cell autonomous. Fifth, we investigated the long-term reconstitution potential of $K3^{+/+}$ and $K3^{-/-}$ HSPCs isolated from the mix-chimeras in a competitive repopulation assay. Around 450 FACS-purified $K3^{+/+}$ or $K3^{-/-}$ $CD150^+CD45.2^+$ LSK cells (Figure S5B) were mixed with $5x10^6$ whole Spl cells from congenic B6.SJL mice and transplanted into lethally irradiated congenic B6.SJL recipients. Four weeks after transplantation the percentages of $K3^{+/+}$ and $K3^{-/-}$ donor-derived whole leukocytes, myeloid cells and B cells were similar in the respective recipient mice. The $K3^{+/+}$ donor-derived cells increased over a period of 8 and 12 weeks after transplantation, while the $K3^{-/-}$ donor-derived cells decreased in the vast majority of recipients (Figure 6F-I). Interestingly, the $CD45.1^+$ to $CD45.2^+$ ratio remained constant between HSPCs and mature effector cells in $K3^{+/+}$ mix-chimeras and diminished in $K3^{-/-}$ mix-chimeras (Figure S5C, D) pointing to an additional differentiation defect of $K3^{-/-}$ HSPCs and/or a premature release of $K3^{-/-}$ HSPC from the BM resulting in a decreased production of effector cells. This suggests that the percentage of $K3^{-/-}$ derived mature

effector cells in the PB may not correctly reflect the ratio of the HSPC in the BM. Therefore, we assessed the percentage of donor-derived cells in the different HSPC populations in the BM. Twelve months after transplantation, $K3^{+/+}$ $CD150^{+}CD45.2^{+}$ LSK donor cells produced nearly 100% of all HSPC populations analyzed, while in recipients of $K3^{-/-}$ $CD150^{+}CD45.2^{+}$ LSK cells the average engraftment capacity was significantly reduced to approximately 50% (Figure 6J), indicating that the $K3^{-/-}$ HSCs reconstitution defect is cell autonomous. Sixth, we investigated whether impaired integration to the BM niche influences the quiescence and stemness of $K3^{-/-}$ HSCs. To disrupt the *Kindlin-3* allele after successful HSC lodgment in the BM niche we generated chimeras using BM cells with floxed *Kindlin-3* alleles and a $Rosa26^{Cre\text{-}ERT2}$ transgene and transplanted them to congenic B6.SJL recipients ($K3^{fl/fl}Rosa26^{Cre\text{-}ERT2}$ chimera), thus restricting Cre expression to hematopoietic cells. Weekly 5–FU treatment of tamoxifen-induced $K3^{fl/fl}Rosa26^{Cre\text{-}ERT2}$ chimeras revealed that 90% died within 20 days, whereas the majority of control chimeras survived (Figure 6K) confirming that $K3^{-/-}$ HSCs display an impaired stress response independent of their initial niche lodgment.

These findings demonstrate that the abnormal mobilization, increased proliferation, enhanced 5-FU sensitivity and diminished engraftment of $K3^{-/-}$ HSPCs are all autonomous defects.

BCR-ABL expression in $K3^{-/-}$ BM cells cannot induce CML

Different hematological malignancies including CML are maintained by a small population of LSCs (Wang and Dick, 2005), which share several properties of normal HSCs including quiescence, long-term repopulating potential defined by disease transfer to recipient mice (Wang et al., 1998), and the interaction with the HSC niche. Since $K3^{-/-}$ HSCs lost their quiescence and long-term repopulation potential, we hypothesized that malignantly transformed $K3^{-/-}$ HSPCs should fail to induce disease. To test this hypothesis in a BCR-ABL induced mouse model for CML, BM donor cells were harvested from $K3^{+/+}$ or $K3^{-/-}$ chimeras and infected *in vitro* with a retrovirus carrying the $P210^{BCR\text{-}ABL}$ cDNA linked via an internal ribosomal entry site (IRES) to GFP. Infected cells were FACS-sorted for GFP expression and transplanted into sublethally irradiated recipients. Almost all recipients of $P210^{BCR\text{-}ABL}$ positive $K3^{+/+}$ cells died within 100 days post-transplantation while only 1 out of 14 recipients of $P210^{BCR\text{-}ABL}$ positive $K3^{-/-}$ cells died (Figure 7A). The animals died from a fatal myeloproliferative disease (MPD) (Wertheim et al., 2002), which shares several features with CML including

predominance of Gr-1^{+}/Mac-1^{+} cells in the BM, Spl and PB (Figure 7B), splenomegaly and pulmonary hemorrhage (not shown). Disease progression monitoring demonstrated that recipients of P210$^{BCR\text{-}ABL}$ positive K3$^{+/+}$ cells suffered from a dramatic expansion of GFP^{+} cells in the PB 8 days after transplantation, which further increased until they died. In contrast, the amount of P210$^{BCR\text{-}ABL}$ positive K3$^{-/-}$ cells in the PB was less pronounced 8 days after transplantation, decreased below 20% by 15 days (Figure 7C) and were virtually undetectable at around 100 days after transplantation (data not shown), indicating that the P210$^{BCR\text{-}ABL}$ positive K3$^{-/-}$ BM cells were unable to engraft due to host cell competitions. Importantly, BM analysis for the presence of GFP^{+} whole leukocytes and myeloid cells 19 days after transplantation revealed that 65% leukocytes and 71% myeloid cells were GFP^{+} in a recipient of P210$^{BCR\text{-}ABL}$ positive K3$^{+/+}$ cells and 52% leukocytes and 22% myeloid cells in a recipient of P210$^{BCR\text{-}ABL}$ positive K3$^{-/-}$ cells indicating that P210$^{BCR\text{-}ABL}$ positive K3$^{-/-}$ BM cells reached the BM interstitium. The recipient of P210$^{BCR\text{-}ABL}$ positive K3$^{-/-}$ BM cells that died 44 days after transplantation developed a fatal MPD with GFP^{+} cells which were almost exclusively of myeloid origin in BM, Spl and PB similar to the recipient of P210$^{BCR\text{-}ABL}$ positive K3$^{+/+}$ BM cells that died 43 days after transplantation (Figure 7B). This finding suggests that the reduced efficiency in disease induction is due to decreased homing efficiency and engraftment rather than due to a general inability to induce MPD by P210$^{BCR\text{-}ABL}$ positive K3$^{-/-}$ BM cells.

DISCUSSION

Kindlin-3 is expressed in all hematopoietic cells including HSPCs and is required for bidirectional integrin signaling (Moser et al., 2009a). HSPCs express several integrins and therefore, one would predict that Kindlin-3 serves important roles for HSC homeostasis and the development of malignant diseases such as leukemia. To test this hypothesis, we designed a range of experiments, which assigned several important function(s) to Kindlin-3 in normal, and BCR-ABL transformed HSPCs. The results of our study demonstrate that Kindlin-3 is dispensable for the generation of HSCs, however it plays key roles for several important HSPC properties; first, Kindlin-3 supports the homing of HSPCs to the BM by facilitating integrin-mediated adhesion to the vessel wall. Second, it facilitates the retention of HSPCs in the BM microenvironment. Third, Kindlin-3 is essential to maintain HSCs in a quiescent state and prevents their premature exhaustion under hematopoietic stress. Fourth, Kindlin-3 is required for the engraftment of BCR-ABL expressing BM cells and to induce a CML-like disease in sublethally irradiated mice.

The homing of HSPC to the BM is a multistep process that commences with their adhesion to the BM vessel wall and continues with their transendothelial migration finally leading to colonization of the stem cell niches (Magnon and Frenette, 2008). Our analysis showed that disruption of the Kindlin-3 gene in HSPCs diminished BM homing, which is clearly caused by an integrin-binding defect. Loss of Kindlin-3 enabled a few HSPCs to assume long lasting adhesions to endothelial cells and to cross the vessel wall, which gave rise to significant numbers of $K3^{-/-}$ HSCs within 1 month of transplantation. It is clear from previous reports that β1 class integrins (mainly through α4β1 and most likely also through α9β1 binding to VCAM-1) are essential for BM homing of HSPCs (Magnon and Frenette, 2008; Potocnik et al., 2000; Taooka et al., 1999). Our findings demonstrate that the impaired activation of β1 and most likely all other integrin classes on HSPCs still permits $K3^{-/-}$ HSPCs to home to the BM compartment, although at a much reduced efficiency. These data indicate that the ability of Kindlin-3 to shift the equilibrium of a large fraction of integrins toward high activity is not absolutely required although it significantly improves the process.

Our data also show that the number of HSPCs in the circulation and Spl is significantly elevated, which could be caused by a combination of defects including diminished re-homing of circulating HSPCs to the BM (Massberg et al., 2007; Wright et al., 2001),

and spontaneous mobilization of HSPCs. Since the number of normally circulating HSCs is rather small (Wright et al., 2001), a significant contribution of a re-homing defect of $K3^{-/-}$ cells to the increased amount of circulating HSPCs is rather unlikely. It is much more probable that Kindlin-3 helps to retain HSPCs in the BM microenvironment by enabling their adhesion to various integrin ligands, which is lost in the absence of Kindlin-3. Indeed, treatment of control chimeras with G-CSF increased the number of circulating LSK cells to a level found in untreated $K3^{-/-}$ chimeras. However, G-CSF treatment of $K3^{-/-}$ chimeras further increased the already significantly elevated peripheral $K3^{-/-}$ HSPCs. Therefore, a defective retention in the BM as well as the hyperproliferation of $K3^{-/-}$ HSPCs is most likely contributing to their peripheral accumulation.

Although the impairment of integrins is usually associated with reduced cellular proliferation rates (Arroyo et al., 1999), $K3^{-/-}$ HSCs were hyperproliferative, which eventually resulted in HSC exhaustion with reduced number of LT-HSCs in old chimeras and pancytopenia leading to moribund $K3^{-/-}$ chimeras. The exhaustion of HSCs indicates that Kindlin-3 is an important player for maintaining quiescence and self-renewal potential of HSCs. This cell autonomous function is also lost in non-anemic $K3^{-/-}$ mix-chimeras, in which anemia-induced feedback loops known to activate HSCs are silent. In 100% $K3^{-/-}$ chimeras, however, the proliferative rates of $K3^{-/-}$ HSCs became even more pronounced indicating that anemia can indeed accelerate the exhaustion of $K3^{-/-}$ HSCs. This notion was further confirmed by exposing HSCs to other stress factors such as serial transplantations, or 5-FU treatments, which disclosed the enormous vulnerability of hyperproliferating $K3^{-/-}$ HSCs.

Why is the proliferation rate of $K3^{-/-}$ HSCs elevated? We propose that there is insufficient incorporation of $K3^{-/-}$ HSCs into the BM niche, which may compromise the complex bidirectional interactions between HSCs and the niche resulting in an inadequate activation of 'quiescence' signals. The activation of quiescence and self-renewal mediating signaling pathways by secreted, soluble factors or cellular counter receptors (e.g. Wnt, TGF-β or Notch) depends on a tight interaction of HSCs with niche components (e.g. niche cells or ECM). A potential role for the interaction of HSCs and niche components has been assigned to different integrins such as $\alpha4\beta1$, $\alpha5\beta1$ and $\alpha L\beta2$ (Wilson and Trumpp, 2006). In $K3^{-/-}$ HSCs these and likely other integrins are collectively impaired, which severely affects the engagement of HSCs with several integrin ligands probably leading to the dislodgment from niche components. Finally,

one also needs to consider that Kindlin-3 may have additional, yet unknown functions inside or outside of integrin adhesion sites that inhibit 'proliferation' signals in HSCs. The loss of such function(s) in $K3^{-/-}$ HSPCs could potentially also lead to uncontrolled proliferation.

The impaired HSPC extravasation and niche homing has also profound consequences for malignancy. Transduction of HSPCs with the BCR-ABL oncogene leads to the development of a CML-like MPD in sublethally irradiated recipient mice. In the absence of Kindlin-3, transduced $K3^{-/-}$ WBM cells arrive in the BM but failed to induce CML, which is most likely due to their extrusion from the niches by the resident host wt HSCs. There are *in vitro* studies on the role of integrin-mediated adhesion for CML cells and BCR-ABL transformed hematopoietic cell lines, which reached opposing conclusions regarding their function (Fierro et al., 2008; Peled et al., 2002). In our *in vivo* study the function of a large number, if not all integrins on BCR-ABL positive BM cells was impaired, which prevents CML. Since the disease inhibition was more pronounced than when other adhesion molecules such as CD44 was deleted (Krause et al., 2006), Kindlin-3 emerges as a potential target for leukemia treatment. Inhibiting Kindlin-3 could have a dual effect; the reduced integrin-mediated adhesion would diminish drug resistance and drive LSCs to the cell cycle, which makes them even more sensitive to cytotoxic treatments.

EXPERIMENTAL PROCEDURES

Mice

$K3^{-/-}$ chimeras have been described (Moser et al., 2008). Mice were kept under specific pathogen-free conditions in the animal facility of the Max Planck Institute of Biochemistry. All mouse experiments were performed with approval by the District Government of Upper Bavaria.

Flow cytometry

For FACS analysis MNCs from BM (2x femur, 2x tibia, 2x pelvis, 2x humerus), PB or Spl were isolated, immunostained according to standard procedures and analyzed with a FACSCalibur or FACSCantoII or sorted for subpopulations with a FACSAriaII (BD Biosciences). HSPC subpopulations were gated as shown in Figure 3C. Antibodies are described in the extended experimental procedures.

Short-term homing assay

FACS-sorted LSK cells were stained with cell tracker CMTMR. Short-term homing was assessed directly after injection to the right external carotid artery or 18 h after tail vein injection using 2-photon intravital microscopy (LaVision BioTec) or flow cytometry.

In vitro flow chamber assay

Microflow chambers were prepared as previously described (Frommhold et al., 2008), see Extended Experimental Procedures. Cells were perfused through coated capillaries for 12 min under shear (shear stress 1 dyne/cm^2). After washing and fixation of adherent cells with Türks solution for 80 s, adherent cells were quantified using a ZEISS Axioskop40 microscope (Zeiss).

BM and PB transplantation

For noncompetitive serial transplantation, WBM cells were isolated from 1 mouse of the previous generation and $5x10^6$ cells were i.v. injected each in 5 lethally irradiated congenic B6.SJL wt recipients. After 10-12 weeks transplantation to the next generation recipients was performed using the same conditions. For competitive BM HSC transplantation 1000 FACS-sorted BM $CD150^+$ LSK cells from $K3^{+/+}$ or $K3^{-/-}$ chimeras or 450 FACS-sorted BM $CD150^+$ LSK cells from $K3^{+/+}$ or $K3^{-/-}$ mix-chimeras together with $5x10^6$ whole Spl competitor cells were injected to the tail vein of lethally irradiated F1 wt recipients. The percentage of donor-derived cells in the PB of recipient mice was

analyzed 5 and 11 weeks and in BM and Spl 11 weeks after transplantation by FACS. For competitive PB transplantation, $3x10^6$ PB MNCs were mixed with $4x10^6$ host-type whole Spl cells and injected to the tail vein of lethally irradiated congenic B6.SJL wt recipients. Percentage of donor-derived lymphoid and myeloid cells in the PB of recipient mice was analyzed 5, 8, 12 and 16 weeks after transplantation. In all transplantation experiments recipient mice received a total body irradiation of 13.5 Gy (7.5 Gy and 6 Gy 4 h apart).

Administration of 5-FU

For the polyI:C (GE Healthcare) and 5-Fluorouracil (5-FU; Sigma-Aldrich) double treatment, polyI:C (10 mg/kg) and 5-FU (150 mg/kg) were injected intraperitoneally in BM chimeras (3-4 months after transplantation). For weekly 5-FU treatment, 5-FU was injected intraperitoneally at dose of 150 mg/kg for first two injections and 100 mg/kg for the following injections. In both experiments survival was monitored daily.

***In vivo* CML mouse model**

The CML mouse model developed by Wertheim et al. (Wertheim et al., 2002) was used as described in extended experimental procedures.

Statistical analysis

Unless otherwise noted, all values are reported as mean ±SD. Statistical tests used for each experiment are described in the figure legends. Statistical significance was assumed at $p < 0.05$. All statistical analyses were performed using Prism software (GraphPad Software).

ACKNOWLEDGEMENTS

We thank Karin Hirsch, Susanne Bierschenk and Sarah Longhi for expert technical assistance, Dr. Ernesto Bockamp for the R26creERT2 mouse, Dr. Justus Duyster for providing the BCR-ABL constructs and initial help with the BCR-ABL transduction experiments, and Dr. Roy Zent for critically reading the manuscript. The work was supported by the DFG (SFB 914) and the Max Planck Society.

REFERENCES

Adams, G.B., Chabner, K.T., Alley, I.R., Olson, D.P., Szczepiorkowski, Z.M., Poznansky, M.C., Kos, C.H., Pollak, M.R., Brown, E.M., and Scadden, D.T. (2006). Stem cell engraftment at the endosteal niche is specified by the calcium-sensing receptor. Nature *439*, 599–603.

Arroyo, A.G., Yang, J.T., Rayburn, H., and Hynes, R.O. (1999). Alpha4 integrins regulate the proliferation/differentiation balance of multilineage hematopoietic progenitors in vivo. Immunity *11*, 555–566.

Essers, M.A.G., Offner, S., Blanco-Bose, W.E., Waibler, Z., Kalinke, U., Duchosal, M.A., and Trumpp, A. (2009). IFNα activates dormant haematopoietic stem cells in vivo. Nature *458*, 904–908.

Fierro, F.A., Taubenberger, A., Puech, P.-H., Ehninger, G., Bornhauser, M., Muller, D.J., and Illmer, T. (2008). BCR/ABL Expression of Myeloid Progenitors Increases β1-Integrin Mediated Adhesion to Stromal Cells. Journal of Molecular Biology *377*, 1082–1093.

Frommhold, D., Ludwig, A., Bixel, M.G., Zarbock, A., Babushkina, I., Weissinger, M., Cauwenberghs, S., Ellies, L.G., Marth, J.D., Beck-Sickinger, A.G., et al. (2008). Sialyltransferase ST3Gal-IV controls CXCR2-mediated firm leukocyte arrest during inflammation. J Exp Med *205*, 1435–1446.

Grassinger, J., Haylock, D.N., Storan, M.J., Haines, G.O., Williams, B., Whitty, G.A., Vinson, A.R., Be, C.L., Li, S., Sørensen, E.S., et al. (2009). Thrombin-cleaved osteopontin regulates hemopoietic stem and progenitor cell functions through interactions with alpha9beta1 and alpha4beta1 integrins. Blood *114*, 49–59.

Hynes, R.O. (2002). Integrins: bidirectional, allosteric signaling machines. Cell *110*, 673–687.

Jordan, C.T., McKearn, J.P., and Lemischka, I.R. (1990). Cellular and developmental properties of fetal hematopoietic stem cells. Cell *61*, 953–963.

Kiel, M.J., and Morrison, S.J. (2008). Uncertainty in the niches that maintain haematopoietic stem cells. Nature Reviews Immunology *8*, 290–301.

Kiel, M.J., Yilmaz, Ö.H., Iwashita, T., Yilmaz, O.H., Terhorst, C., and Morrison, S.J. (2005). SLAM Family Receptors Distinguish Hematopoietic Stem and Progenitor Cells and Reveal Endothelial Niches for Stem Cells. Cell *121*, 1109–1121.

Krause, D.S., Lazarides, K., Andrian, von, U.H., and Van Etten, R.A. (2006). Requirement for CD44 in homing and engraftment of BCR-ABL–expressing leukemic stem cells. Nat. Med. *12*, 1175–1180.

Kuijpers, T.W., van de Vijver, E., Weterman, M.A.J., de Boer, M., Tool, A.T.J., van den Berg, T.K., Moser, M., Jakobs, M.E., Seeger, K., Sanal, O., et al. (2009). LAD-1/variant syndrome is caused by mutations in FERMT3. Blood *113*, 4740–4746.

Magnon, C., and Frenette, P.S. (2008). Hematopoietic stem cell trafficking (Cambridge (MA): Harvard Stem Cell Institute).

Malinin, N.L., Zhang, L., Choi, J., Ciocea, A., Razorenova, O., Ma, Y.-Q., Podrez, E.A., Tosi, M., Lennon, D.P., Caplan, A.I., et al. (2009). A point mutation in KINDLIN3 ablates activation of three integrin subfamilies in humans. Nat. Med. *15*, 313–318.

Massberg, S., Schaerli, P., Knezevic-Maramica, I., Köllnberger, M., Tubo, N., Moseman, E.A., Huff, I.V., Junt, T., Wagers, A.J., Mazo, I.B., et al. (2007). Immunosurveillance by Hematopoietic Progenitor Cells Trafficking through Blood, Lymph, and Peripheral Tissues. Cell *131*, 994–1008.

Mazo, I.B., Massberg, S., and Andrian, von, U.H. (2011). Hematopoietic stem and progenitor cell trafficking. Trends in Immunology *32*, 493–503.

Morita, Y., Ema, H., and Nakauchi, H. (2010). Heterogeneity and hierarchy within the most primitive hematopoietic stem cell compartment. J Exp Med *207*, 1173–1182.

Morrison, S.J., and Spradling, A.C. (2008). Stem cells and niches: mechanisms that promote stem cell maintenance throughout life. Cell *132*, 598–611.

Moser, M., Legate, K.R., Zent, R., and Fassler, R. (2009a). The Tail of Integrins, Talin, and Kindlins. Science *324*, 895–899.

Moser, M., Bauer, M., Schmid, S., Ruppert, R., Schmidt, S., Sixt, M., Wang, H.-V., Sperandio, M., and Fässler, R. (2009b). Kindlin-3 is required for beta2 integrin-mediated leukocyte adhesion to endothelial cells. Nat. Med. *15*, 300–305.

Moser, M., Nieswandt, B., Ussar, S., Pozgajova, M., and Fässler, R. (2008). Kindlin-3 is essential for integrin activation and platelet aggregation. Nat. Med. *14*, 325–330.

Okada, S., Nakauchi, H., Nagayoshi, K., Nishikawa, S., Miura, Y., and Suda, T. (1992). In vivo and in vitro stem cell function of c-kit- and Sca-1-positive murine hematopoietic cells. Blood *80*, 3044–3050.

Peled, A., Hardan, I., Trakhtenbrot, L., Gur, E., Magid, M., Darash-Yahana, M., Cohen, N., Grabovsky, V., Franitza, S., Kollet, O., et al. (2002). Immature Leukemic CD34 +CXCR4 +Cells from CML Patients Have Lower Integrin-Dependent Migration and Adhesion in Response to the Chemokine SDF-1. Stem Cell *20*, 259–266.

Pichlmair, A., and Reis e Sousa, C. (2007). Innate recognition of viruses. Immunity *27*, 370–383.

Potocnik, A., Brakebusch, C., and Fassler, R. (2000). Fetal and Adult Hematopoietic Stem Cells Require β1 Integrin Function for Colonizing Fetal Liver, Spleen, and Bone Marrow. Immunity 1–11.

Rizo, A. (2006). Signaling pathways in self-renewing hematopoietic and leukemic stem cells: do all stem cells need a niche? Human Molecular Genetics *15*, R210–R219.

Schmidt, S., Nakchbandi, I., Ruppert, R., Kawelke, N., Hess, M.W., Pfaller, K., Jurdic, P., Fassler, R., and Moser, M. (2011). Kindlin-3-mediated signaling from multiple integrin classes is required for osteoclast-mediated bone resorption. J. Cell Biol. *192*, 883–897.

Shattil, S.J., Kim, C., and Ginsberg, M.H. (2010). The final steps of integrin activation: the

end game. Nat Rev Mol Cell Biol *11*, 288–300.

Svensson, L., Howarth, K., McDowall, A., Patzak, I., Evans, R., Ussar, S., Moser, M., Metin, A., Fried, M., Tomlinson, I., et al. (2009). Leukocyte adhesion deficiency-III is caused by mutations in KINDLIN3 affecting integrin activation. Nat. Med. *15*, 306–312.

Taooka, Y., Chen, J., Yednock, T., and Sheppard, D. (1999). The integrin alpha9beta1 mediates adhesion to activated endothelial cells and transendothelial neutrophil migration through interaction with vascular cell adhesion molecule-1. J. Cell Biol. *145*, 413–420.

Tesio, M., and Trumpp, A. (2011). Breaking the Cell Cycle of HSCs by p57 and Friends. Cell Stem Cell *9*, 187–192.

Trumpp, A., Essers, M., and Wilson, A. (2010). Awakening dormant haematopoietic stem cells. Nature Reviews Immunology *10*, 201–209.

Ussar, S., Wang, H.-V., Linder, S., Fässler, R., and Moser, M. (2006). The Kindlins: subcellular localization and expression during murine development. Exp. Cell Res. *312*, 3142–3151.

van der Loo, J.C., Xiao, X., McMillin, D., Hashino, K., Kato, I., and Williams, D.A. (1998). VLA-5 is expressed by mouse and human long-term repopulating hematopoietic cells and mediates adhesion to extracellular matrix protein fibronectin. Journal of Clinical Investigation *102*, 1051–1061.

Wang, J.C., Lapidot, T., Cashman, J.D., Doedens, M., Addy, L., Sutherland, D.R., Nayar, R., Laraya, P., Minden, M., Keating, A., et al. (1998). High level engraftment of NOD/SCID mice by primitive normal and leukemic hematopoietic cells from patients with chronic myeloid leukemia in chronic phase. Blood *91*, 2406–2414.

Wang, J.C.Y., and Dick, J.E. (2005). Cancer stem cells: lessons from leukemia. Trends Cell Biol. *15*, 494–501.

Wertheim, J.A., Miller, J.P., Xu, L., He, Y., and Pear, W.S. (2002). The biology of chronic myelogenous leukemia:mouse models and cell adhesion. Oncogene *21*, 8612–8628.

Wilson, A., and Trumpp, A. (2006). Bone-marrow haematopoietic-stem-cell niches. Nature Reviews Immunology *6*, 93–106.

Wilson, A., Laurenti, E., Oser, G., van der Wath, R.C., Blanco-Bose, W., Jaworski, M., Offner, S., Dunant, C.F., Eshkind, L., Bockamp, E., et al. (2008). Hematopoietic Stem Cells Reversibly Switch from Dormancy to Self-Renewal during Homeostasis and Repair. Cell *135*, 1118–1129.

Wright, D.E., Wagers, A.J., Gulati, A.P., Johnson, F.L., and Weissman, I.L. (2001). Physiological migration of hematopoietic stem and progenitor cells. Science *294*, 1933–1936.

FIGURE LEGENDS

Figure 1: Survival of K3$^{-/-}$ chimeras and distribution of K3$^{-/-}$ HSPCs

(A) Kaplan-Meier survival curve of 1st generation K3$^{+/+}$ and K3$^{-/-}$ FL chimeras (***p<0.0001 by log-rank test), n=41-47 per genotype.

(B) Total number of MNCs from BM (2x femur, 2x tibia, 2x pelvis, 2x humerus) and whole Spl. K3$^{+/+}$ chimeras are compared with healthy and moribund K3$^{-/-}$ chimeras (***p< 0.0001 by Kruskal-Wallis test and Dunn's multiple comparison post-test), n=10-15 per group. Data are mean cell counts ±SD.

(C) Total number of B cells (B220^{+}), T cells (CD3e^{+}), erythroid cells (Erythro; Ter119^{+}), neutrophils (Neutro; Gr-1^{hi}Mac-1^{+}) and monocyets/macrophages (Mono/Macro; Gr-1^{int}Mac-1^{+}) in the BM of K3$^{+/+}$, healthy and moribund K3$^{-/-}$ chimeras. Data are presented as box-and-whisker plots. The horizontal lines inside the boxes represent the median, the box edges show the lower and upper quartiles, and the whiskers indicate the minimum and maximum (*p<0.05, **p<0.01, ***p<0001 by Kruskal–Wallis test and Dunn's multiple comparison post-test). n=10-15 per genotype.

Figure 2: BM homing of K3$^{-/-}$ LSK cells

(A) Short-term homing assay with labeled BM LSK cells from K3$^{+/+}$ and K3$^{-/-}$ chimeras quantified by FACS. Shown are mean percentage of injected cells in BM after 18 h ±SD (**p=0.0046 by unpaired t-test), n=5-6 per genotype.

(B) Quantification of extravasated K3$^{+/+}$ and K3$^{-/-}$ LSK cells in BM by intravital 2-photon microscopy 18 h after transplantation, given as mean value ±SD of the absolute number of transmigrated cells per 1x10^{5} injected LSK cells (*p=0.0159 by Mann-Whitney test), n=4-5 per genotype.

(C) Representative images illustrating transmigration of K3$^{+/+}$ (upper panels) and K3$^{-/-}$ LSK cells (lower panels) up to 6 h after injection in Col2.3-GFP recipients. LSK cells, white (CMTMR); bone, blue (second harmonic signal); blood, red (Q-Tracker 695 nm). Arrowheads indicate LSK cells transmigrating across endothelium (white dashed lines), left colum before and right colum after transmigration. Scale bars are 100 μm.

(D) LSK cells of either genotype were visualized in BM microvessels for up to 6 h after injection. The numbers of adherent LSK cells are shown as percentage (mean ±SD) of all LSK cells visualized. (***p=0.0006 by unpaired t-test), n=5 per genotype.

(E) Representative images of adherent K3$^{+/+}$ (upper panels) and K3$^{-/-}$ (lower panels) LSK cells at indicated time points after transfer (upper right corner). LSK cells, red

(CMTMR); bone, blue (second harmonic signal); blood, green (FITC-dextran). Arrows, arrowheads and asterisk indicate different single LSK cells; white dashed line outlines endothelium; Scale bars indicate 100 μm.

(F) Adhesion of sorted $K3^{+/+}$, $K3^{-/-}$ and $K3^{+/+}$ preincubated with a α4 integrin blocking mAb BM LSK cells on VCAM-1 under shear, analyzed in microflow chambers. Microflow chambers were precoated with: rmE-selectin 'E' alone; rmE-selectin and VCAM-1 or rmE-selectin, CXCL12 and VCAM-1. Scale bars represent mean percentage of adherent cells to total LSK cells ±SEM (*p<0.05, **p<0.01 by Kruskal–Wallis test and Dunn's multiple comparison post-test), n≥4 per group.

Figure 3: Kindlin-3 deficient HSCs home to the BM

(A) Frequency of CFU-Cs in sorted $CD45.2^{+}$ BM cells isolated from chimeras 4 months after transplantation (p=0.8857 by Mann-Whitney test). n=4 per genotype. Scale bars show average cell counts ±SD.

(B) LTC-IC assay performed by limiting dilutions of donor derived BM MNCs from $K3^{+/+}$ and $K3^{-/-}$ FL chimeras 4 months after transplantation. The percentage of wells in each experimental group that failed to generate colony-forming units is plotted against the number of test MNCs cells. The frequency of LTC-ICs is shown at the bottom. (p=0.965 by Person chi-squared test), n= 4 per genotype.

(C) Representative FACS plots of BM cells derived from chimeras 1-13 months after transplantation gated for HSPCs using SLAM markers. The left column shows c-kit and Sca-1 expression on lin^{-} cells. Gating from left to right on LSK cells, $CD150^{+}CD48^{-}$ subsets within the LSK population and the $CD34^{-}$ or $CD34^{+}$ subsets of this population, respectively. Numbers above each boxed gate refer to the frequencies in BM (percentages of live leukocytes ±SD), n=24-27 per genotype.

(D) Quantification of (C). $CD150^{-}CD48^{+}$ (*p=0.0121 by unpaired t-test); $CD150^{+}CD48^{+}$ (***p<0.0001 by unpaired t-test); $CD150^{+}CD48^{-}$ (***p<0.0001 by Mann-Whitney test); $CD150^{+}CD48^{-}CD34^{+}$ (***p=0.0003 by unpaired t-test) and $CD150^{+}CD48^{-}CD34^{-}$ (***p<0.0001 by Mann-Whitney test) LSK cells. Mean cell numbers ±SD are given. n=24-27 per genotype.

(E) Representative FACS plots of BM LSK cells from $K3^{+/+}$ and $K3^{-/-}$ chimeras, gated for CD150 against CD48. FACS plots show the distribution of 3 populations, $CD150^{+}CD48^{-}$ cells (upper left gate); $CD150^{-}CD48^{+}$ cells (upper right gate); $CD150^{+}CD48^{-}$ cells (lower gate) 1, 2, 4 and 9-13 months after transplantation. Numbers next to each gate represent

mean percentage ±SD of events within the LSK population, n=3-11 per genotype and time point.

(F) Quantification of the $CD150^{+}CD48^{-}$ LSK population of BM cells from $K3^{+/+}$ and $K3^{-/-}$ chimeras. Compared are the $K3^{+/+}$ and $K3^{-/-}$ mean cell counts ±SD 1, 4 and 9-13 months after transplantation (1 month: p=0.4 by Mann-Whitney test; 4 months: ***p<0.0001; by unpaired t-test; 9-13 months: ***p=0.0001 by unpaired t-test). n=3-8 per genotype.

(G) Quantification of the $CD150^{+}CD48^{-}CD34^{-}$ LSK population of BM cells from $K3^{+/+}$ and $K3^{-/-}$ FL chimeras. Compared are the $K3^{+/+}$ and $K3^{-/-}$ mean cell counts ±SD 1, 4 and 9-13 months after transplantation (1 month: p=0.2 by Mann-Whitney test; 4 months: ***p=0.0005 by unpaired t-test; 9-13 months: **p=0.002 by unpaired t-test). n=3-9 per genotype.

Figure 4: $K3^{-/-}$ HSC remain hyperactive and accumulate in the PB

(A-B) Poly(I:C) and 5-FU double treatment of $K3^{+/+}$ and $K3^{-/-}$ chimeras. (A) Diagram of tested drug combinations and timing. (B) Kaplan-Meier survival curves of experimental groups indicated in (A) (***p<0.0001 by log-rank test), n=16-22 per treatment group. Data are combined from 5 independent experiments.

(C) *In vivo* BrdU uptake assay. Mean percentage ±SD of $BrdU^{+}$ cells determined by FACS in LK cells (p=0.4078 by unpaired t-test), LSK cells (***p=0.0009 by unpaired t-test), $CD150^{+}CD48^{-}$ (**p=0.0014 by Mann-Whitney test) and $CD150^{+}CD34^{-}$ (***p=0.0004 by Mann-Whitney test) LSK cells.

(D) Representative FACS plots of a cell cycle analysis of BM LSK cells. Cells were stained with DAPI and intracellular (ic) Ki67 and analyzed by FACS. The different cell cycle phases are indicated in the scheme above.

(E) Quantification of (D). Percentage of $icKi67^{+}$ BM LSK cells (G1 + S + G2/M phase cells), obtained by FACS. Horizontal bars indicate mean values ±SD (**p=0.0022 by paired t-test). n=18 per genotype.

(F) Relative expression of p21, p27 and p57 mRNA in sorted $CD150^{+}$ LSK cells, analyzed by qPCR. Data are normalized for GAPDH expression and presented as mean ±SD from individual mice. n=6-7 per genotype (***p=0.0007 by unpaired t-test).

(G-H) LRC-assay. (G) Percentage of $BrdU^{+}$ cells (LRCsBrdU) present in subsets of LSK populations after 16 days of labeling, obtained by FACS. (H) Mean percentage ±SD of LRCsBrdU in each of the LSK subset population after 45 days of chase phase. Total LSK cells (***p<0.0001); $CD150^{-}CD48^{+}$ (***p<0.0001); $CD150^{+}CD48^{+}$ (***p=0.0006);

$CD150^+CD48^-$ (**p=0.0014); $CD150^+CD34^-$ (*p=0.0350) LSK cells were analyzed by unpaired t-test, n=7-8 per genotype.

(I) Representative FACS plots showing the expression of c-kit and Sca-1 on lin^- cells from Spl and PB. The frequencies of LK (orange box) and LSK cells (green box) are marked above plots (percentages of live leukocytes ±SD). n=24-26 per genotype.

(J) Quantification of LK and LSK cells in Spl (upper row) and in PB (lower row) analyzed by FACS. Scale bars show mean cell counts ±SD (***p<0.0001; **p=0.0031 by Mann-Whitney test). n=25-26 per genotype.

(K-N) Multilineage engraftment potential of PB cells isolated from $K3^{+/+}$ and $K3^{-/-}$ chimeras. Percentage donor-derived whole leukocytes ($CD45^+$) (K), myeloid cells ($Gr\text{-}1^+$, $Mac\text{-}1^+$, and $Gr\text{-}1^+Mac\text{-}1^+$) (L), B cells ($B220^+$) (M), or T cells ($CD3e^+$) (N) are shown from PB 5, 8, 12 and 16 weeks after transplantation. Data are plotted for individual recipients n=5 for $K3^{+/+}$ (blue lines) and n=19 for $K3^{-/-}$ (red lines) from 3 independent transplantation experiments. Significant differences in average lineage engraftment 16 weeks post transplantation are indicated (leukocytes: *p=0.0157, myeloid cells: **p=0.0085, B cells: **p=0.0028, T cells: **p=0.0008 by Mann-Whitney test).

(O) Mobilization of LSK cells from $K3^{+/+}$ and $K3^{-/-}$ chimeras to the PB, shown as LSK cells per ml blood after G-CSF or PBS treatment. Significance at day 6 is indicated ($K3^{+/+}$ vs. $K3^{-/-}$ with G-CSF: ***p<0.0001, $K3^{+/+}$ vs. $K3^{-/-}$ with PBS: **p=0.0049 by unpaired t-test). n=3-5 per genotype.

Figure 5: Premature exhaustion of $K3^{-/-}$ HSCs in serial BM transplantation

(A) Analysis of radioprotection by donor $K3^{+/+}$ und $K3^{-/-}$ WBM cells in 3 rounds of serial BM transplantations. Kaplan-Meier survival curve of the 2nd generation, 3rd generation and 4th generation recipients are shown. Results are combined from 9 independent transplantation experiments. n=42-55 recipients per genotype (***p<0.0001 by log-rank test).

(B) Blood cell counts of the 2nd generation recipients transplanted with 1000 BM $CD150^+$ LSK cells sorted from $K3^{+/+}$ or $K3^{-/-}$ chimeras with $5x10^6$ host-type whole Spl cells. Percentages of donor-derived whole leukocytes ($CD45^+$), myeloid cells ($Gr\text{-}1^+$, $Mac\text{-}1^+$, and $Gr\text{-}1^+Mac\text{-}1^+$), B cells ($B220^+$), or T cells ($CD3e^+$) in PB 5 and 11 weeks post transplantation are shown. Scale bars show the mean percent ±SD (***p<0.0001 by Mann-Whitney test).

(C) Percentage of donor-derived HSPCs in BM of 2nd generation recipients after 11 weeks, obtained by FACS. Horizontal bars indicate mean values ±SD (***p<0.0001 by Mann-Whitney test). n=28-29 from 5 independent experiments.

Figure 6: The defects in K3$^{-/-}$ HSCs are cell autonomous

(A) Representative FACS plots of PB from K3$^{+/+}$ and K3$^{-/-}$ mix-chimeras 4 months after transplantation. Upper row shows whole leukocytes gated for CD45.2 against CD45.1. In lower row lin^{-} cells (pregate not shown) of CD45.2^{+} and CD45.1^{+} populations are gated for c-kit against Sca-1. Gates for LK (right) and LSK cells (left) are shown. Numbers next to the gates represent the overall frequencies (percent of live PB leukocytes) ±SD from events in each gate, n=6-8 per genotype.

(B-C) LRC assay in K3$^{+/+}$ and K3$^{-/-}$ mix-chimeras. (B) Percentage of LRCsBrdU in different subsets of LSK populations after 18 days of labeling, obtained by FACS. (C) Percentage of LRCsBrdU in each of the LSK sub-populations after 45-50 days of chase phase. Total LSK cells (**p=0.0073); CD150^{-}CD48^{+} (*p=0.0309); CD150^{+}CD48^{+} (ns: p=0.0894); CD150^{+}CD48^{-} (**p=0.0017); CD150^{+}CD34^{-} (ns: p=0.0583) LSK cells by paired t-test. Scale bars show mean percentage ±SD, n= 4 per genotype.

(D) 5-FU treatment (day 0 and 7) of K3$^{+/+}$ and K3$^{-/-}$ mix-chimeras. LSK cells from BM analyzed by FACS for percentage of CD45.1^{+} and CD45.2^{+} cells before and 45 days after first 5-FU injection. Histogram shows the mean percentage ±SD (***p<0.0001 by unpaired t-test). n=9 per genotype in 2 independent experiments.

(E) G-CSF induced mobilization of BM LSK cells from K3$^{+/+}$ and K3$^{-/-}$ mix-chimeras. MNCs from PB were analyzed by FACS for LSK cells. Histogram shows the mean number of LSK cells per ml PB ±SD. (**p<0.01 and ***p<0.001 by one-way ANOVA followed by Tukey's multiple comparison test).

(F-I) Results of a competitive repopulation assay with BM CD150^{+}CD45.2^{+} LSK cells FACS-sorted from K3$^{+/+}$ and K3$^{-/-}$ mix-chimeras. Each recipient received 450 CD150^{+}CD45.2^{+} LSK cells together with 5x10^{6} host-type whole Spl cells. Percent donor-derived whole leukocytes (CD45^{+}) (F), myeloid cells (Gr-1^{+}, Mac-1^{+}, and Gr-1^{+}Mac-1^{+}) (G), B cells (B220^{+}) (H), or T cells (CD3e^{+}) (I) from PB 4, 8 and 12 weeks post transplantation are shown. Data are plotted for individual recipients K3$^{+/+}$ (blue solid lines) and K3$^{-/-}$ (red lines). Significant differences in average lineage engraftment 12 weeks post transplantation are indicated (leukocytes: ***p<0.0001 by unpaired t-test; myeloid, B cells and T cells: ***p<0.0001 by Mann-Whitney test). n=14-17 from 4

independent experiments.

(J) Percentage of donor-derived HSPCs in BM of 2nd generation recipients after 12 weeks obtained by FACS. Horizontal bars indicate mean values ±SD (***p<0.0001 by Mann-Whitney test). n=14-17 from 4 independent experiments.

(K) Kaplan-Meier survival curve showing response of $K3^{fl/fl}Rosa26^{Cre\text{-}ERT2}$ (n=10) and control mice to a sequential 5-FU treatment. Mice were treated with 5-FU weekly, and survival was monitored daily. Kindlin-3 gene deletion was induced by administration of tamoxifen (TAM) 5 weeks before 5-FU treatment. The control group contained $K3^{fl/fl}Rosa26^{Cre\text{-}ERT2}$ (w/o TAM n=7), $wtRosa26^{Cre\text{-}ERT2}$ (with TAM n=6 or w/o TAM n=5) and $K3^{fl/fl}$ (with TAM n=2 or w/o TAM n=2) mice, (***p<0.0001 by log-rank test).

Figure 7: BCR-ABL expressing $K3^{-/-}$ BM cells fail to induce CML

(A) Kaplan-Maier survival curve of sublethally irradiated recipient mice, transplanted with $8x10^4$ $K3^{+/+}$ or $K3^{-/-}$ WBM cells, isolated from chimeras, stably expressing $P210^{BCR\text{-}ABL}$ (***p<0.0001 by log-rank test), n=14-24 from 3 independent experiments.

(B) Analysis of a representative recipient transplanted with $P210^{BCR\text{-}ABL}$ positive $K3^{+/+}$ and the single recipient of $P210^{BCR\text{-}ABL}$ positive $K3^{-/-}$ WBM cells developing a CML, at the time of death (43-44 days after transplantation). Percentage of myeloid cells ($Gr\text{-}1^+$ or $Mac\text{-}1^+$ or $Gr\text{-}1^+Mac\text{-}1^+$) within the GFP ($P210^{BCR\text{-}ABL}$) positive population is indicated by striped areas.

(C) Percent of GFP ($P210^{BCR\text{-}ABL}$) expressing leukocytes in PB of recipients 8, 12 or 15 days after transplantation. Scale bars show mean percentage ±SD (8 days: **p=0.0043, 12 days: ***p<0.0001, 15 days: ***p<0.0001 by unpaired t-test). n=8 per genotype.

Figure

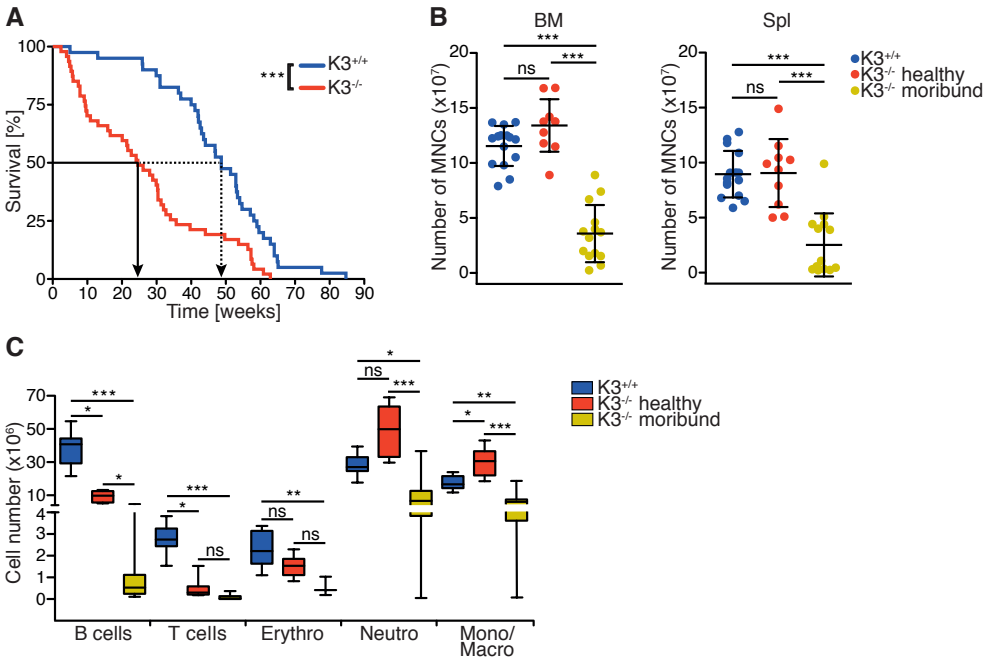

Figure 1
Ruppert et al.

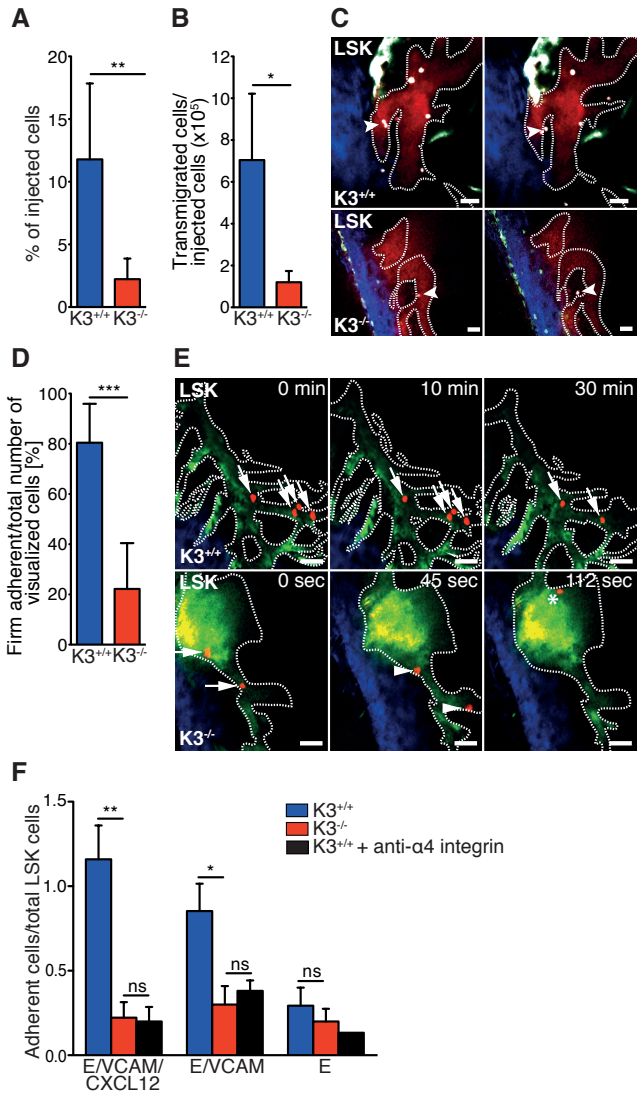

Figure 2
Ruppert et al.

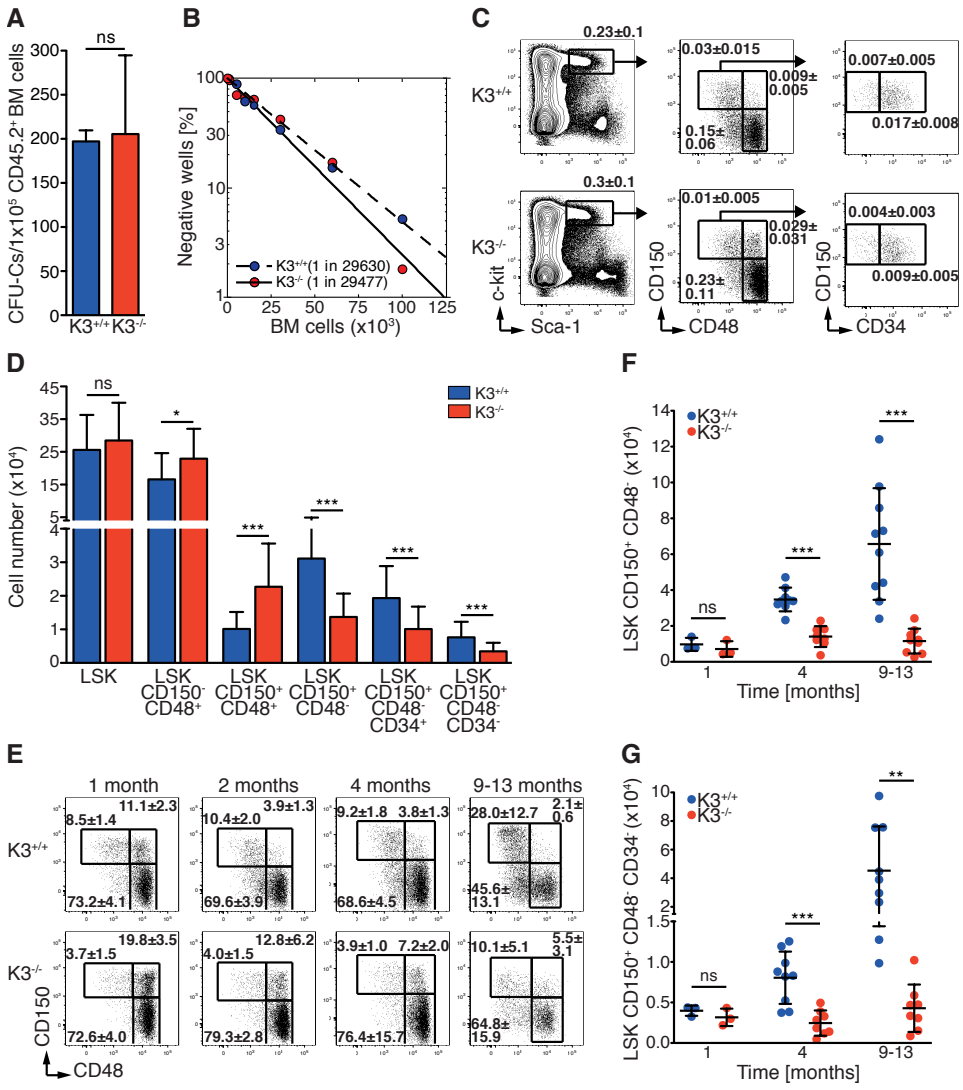

Figure 3
Ruppert et al.

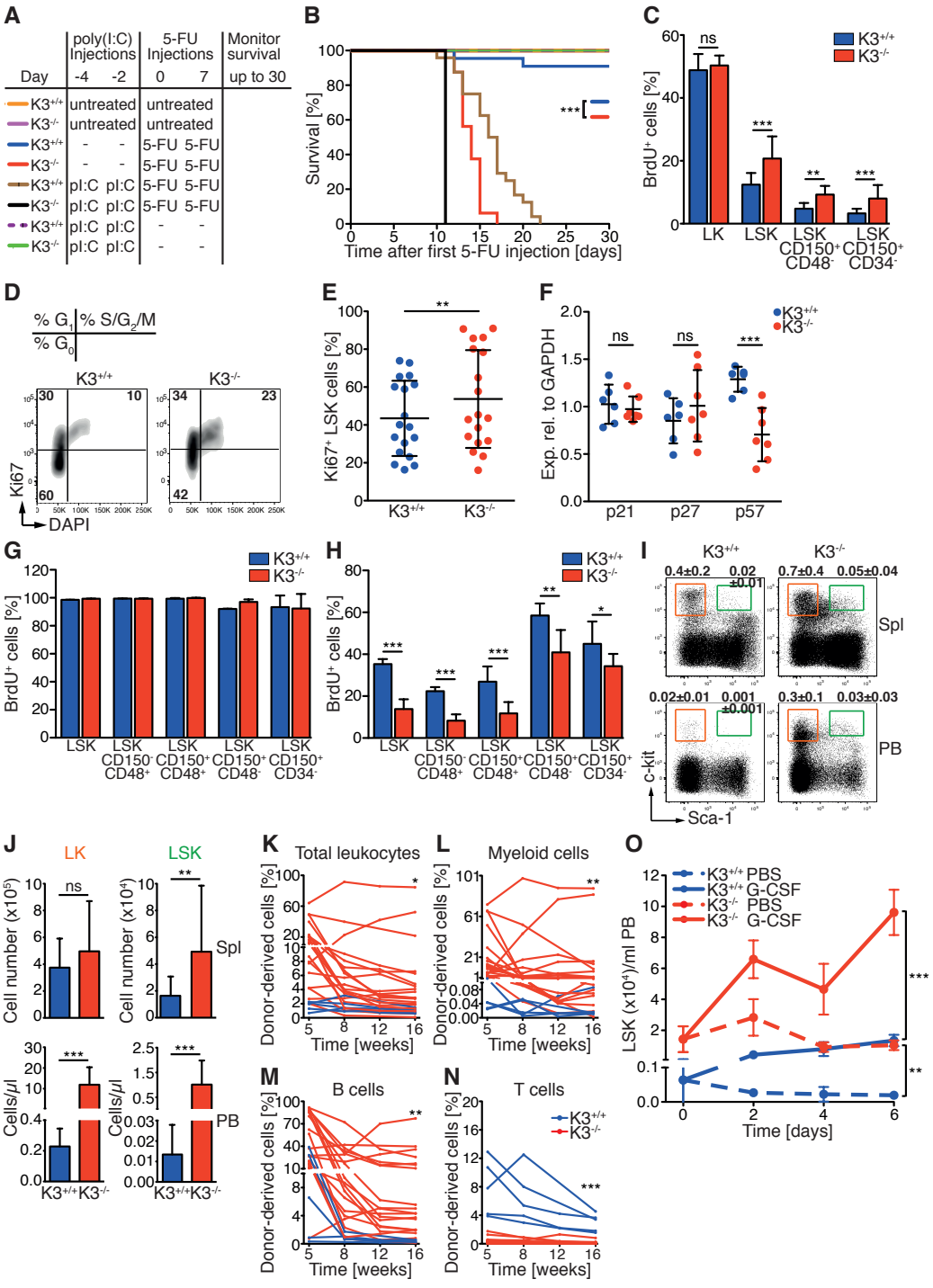

Figure 4
Ruppert et al.

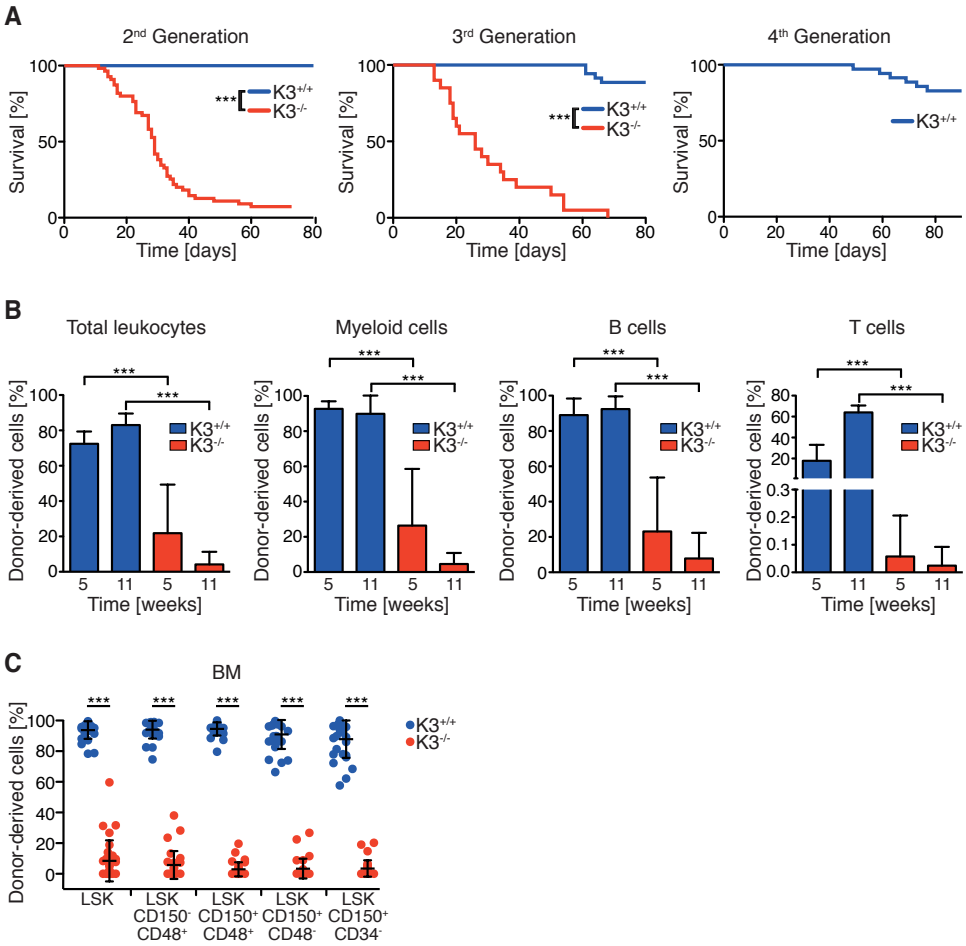

Figure 5
Ruppert et al.

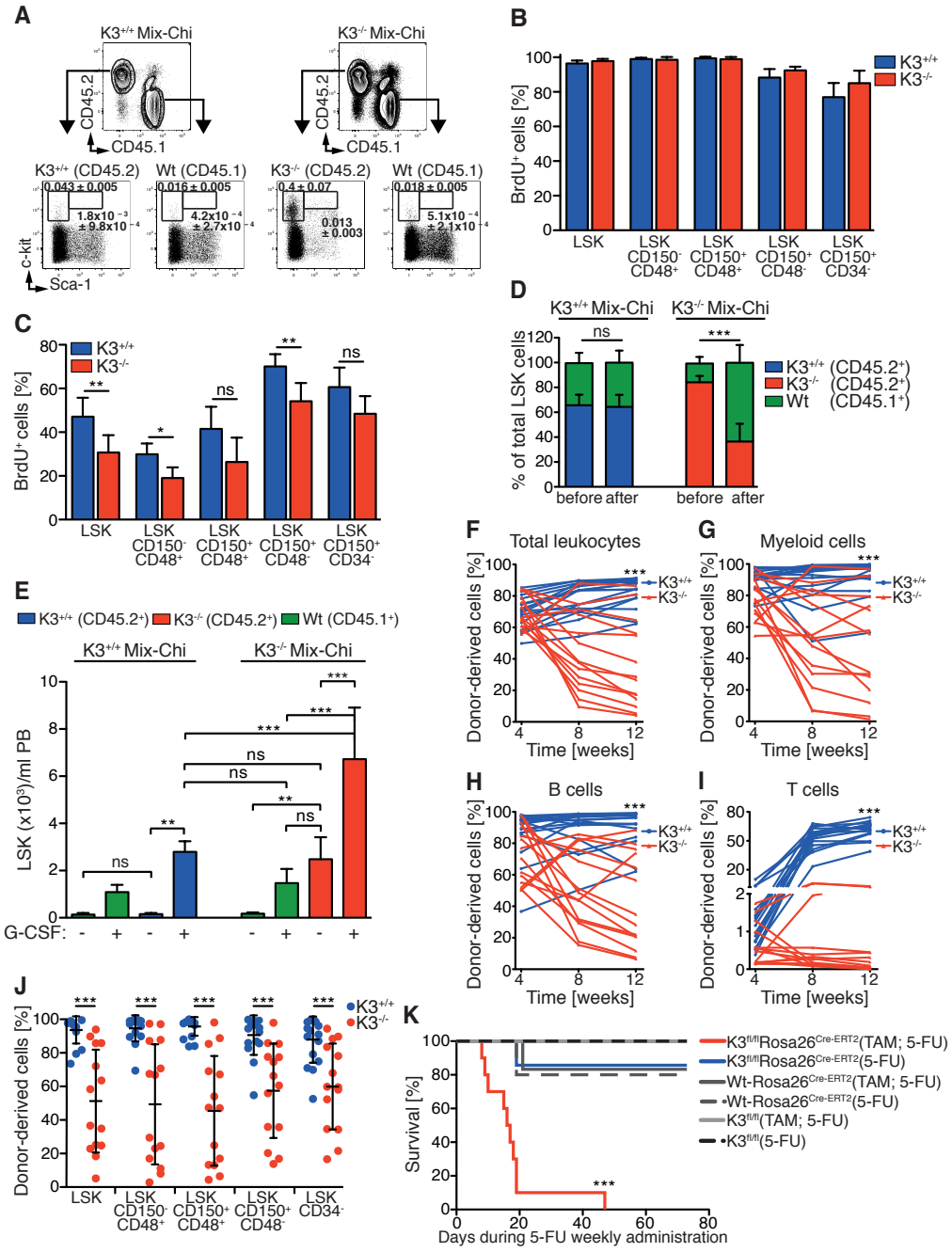

Figure 6
Ruppert et al.

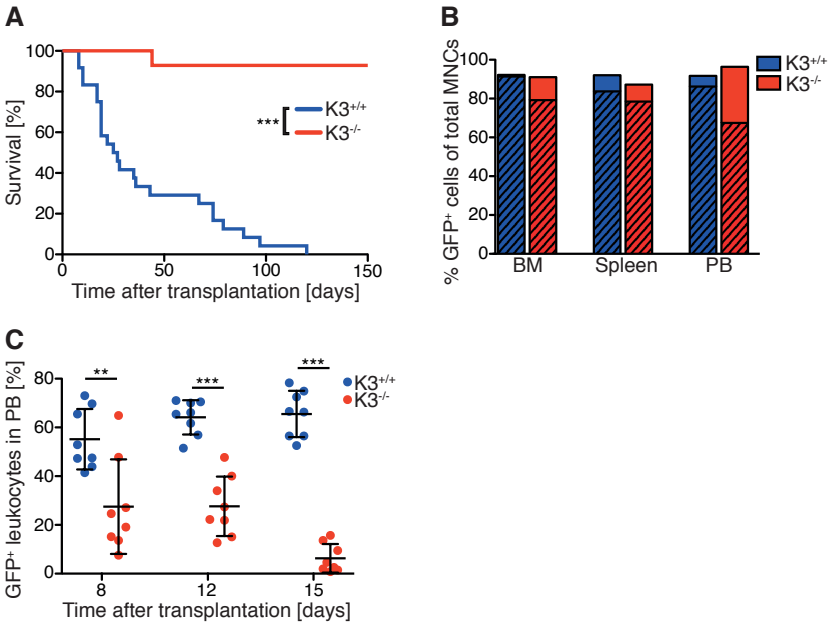

Figure 7
Ruppert et al.

12.2 Paper 2:

Kindlin-3 is required for β2 integrin-mediated leukocyte adhesion to endothelial cells.

LETTERS

nature medicine

Kindlin-3 is required for β_2 integrin–mediated leukocyte adhesion to endothelial cells

Markus Moser[1], Martina Bauer[1], Stephan Schmid[2], Raphael Ruppert[1], Sarah Schmidt[1], Michael Sixt[1], Hao-Ven Wang[1], Markus Sperandio[2] & Reinhard Fässler[1]

Integrin activation is essential for the function of all blood cells, including platelets and leukocytes[1]. The blood cell–specific FERM domain protein Kindlin-3 is required for the activation of the β_1 and β_3 integrins on platelets[2]. Impaired activation of β_1, β_2 and β_3 integrins on platelets and leukocytes is the hallmark of a rare autosomal recessive leukocyte adhesion deficiency syndrome in humans called LAD-III, characterized by severe bleeding and impaired adhesion of leukocytes to inflamed endothelia[3]. Here we show that Kindlin-3 also binds the β_2 integrin cytoplasmic domain and is essential for neutrophil binding and spreading on β_2 integrin-dependent ligands such as intercellular adhesion molecule-1 and the complement C3 activation product iC3b. Moreover, loss of Kindlin-3 expression abolished firm adhesion and arrest of neutrophils on activated endothelial cells *in vitro* and *in vivo*, whereas selectin-mediated rolling was unaffected. Thus, Kindlin-3 is essential to activate the β_1, β_2 and β_3 integrin classes, and loss of Kindlin-3 function is sufficient to cause a LAD-III–like phenotype in mice.

Leukocyte adhesion to vessel walls and subsequent transmigration into tissues is mediated through a sequential adhesion cascade, which allows blood cells to overcome the high shear forces within blood vessels. The cascade is initiated by transient selectin-carbohydrate interactions, which trigger leukocyte rolling on the surface of activated endothelial cells. Rolling leukocytes sense immobilized chemokines, and chemokine receptor signaling induces activation of β_2 integrins. Activated β_2 integrins mediate firm binding to counter-receptors on the endothelial cell followed by transmigration of leukocytes through the endothelial layer[4]. The central role of integrins and selectins in this multistep process is impressively highlighted by leukocyte adhesion deficiency (LAD) syndromes in man, which can be caused either by mutations in the gene encoding β_2 integrin (LAD-I)[5] or by impaired glycosylation of selectin ligands (LAD-II)[6–8].

In recent years, several groups have identified individuals suffering from a novel form of LAD syndrome that has been termed LAD-III or LAD-I variant. LAD-III is inherited in an autosomal recessive manner and is characterized by a complete inability to induce activation of β_1, β_2 and β_3 integrins in hematopoietic cells, resulting in severe bleeding due to impaired platelet aggregation and recurrent infections due to abrogated leukocyte adhesion to activated endothelial cells[3]. Activation of leukocyte integrins can be triggered by various receptor signaling pathways, including chemokine receptors. These signals have been proposed to induce the binding of talin to integrin β_1, β_2 and β_3 cytoplasmic domains, resulting in a shift of integrins from a low-affinity to a high-affinity state for ligands (integrin activation)[9]. As talin is ubiquitously expressed, and talin ablation leads to early embryonic lethality in mice[10], it is highly unlikely that mutations in the gene encoding talin cause LAD-III. One group of researchers found a mutation in a splice acceptor site of the *CALDAGGEF1* (official symbol *RASGRP2*) gene and loss of *CALDAGGEF1* messenger RNA in two subjects with LAD-III (ref. 11). Notably, mice lacking CALDAG-GEF1 also suffer from defects in platelet and leukocyte integrin function[12]. Moreover, CALDAG-GEF1 functions as a guanine exchange factor for the small GTPase Rap1, which, in turn, activates leukocyte and platelet integrins downstream of multiple receptors including receptors for chemokines[11]. However, other individuals with LAD-III lack mutations in the *CALDAGGEF1* gene (see Svensson *et al.*[13] and Malinin *et al.*[14] in this issue) and show normal Rap1 activity in platelets and leukocytes[15,16], suggesting that mutations in another gene cause this disease.

We recently showed that the FERM domain–containing, integrin β tail–binding protein Kindlin-3 (encoded by the *Fermt3* gene, called *Kindlin3* here) is required to activate β_1 and β_3 integrins in platelets[2]. Kindlin-3 belongs to a unique family (Kindlin-1, Kindlin-2 and Kindlin-3) of focal adhesion proteins. Kindlin-1 is expressed in epithelial cells, and mutations in the gene encoding Kindlin-1 cause a skin-blistering disease in man called Kindler syndrome[17]. Kindlin-2 is widely expressed, and gene ablation in mice results in peri-implantion lethality due to severely compromised function of β_1 and β_3 integrins[18]. Kindlin-3 is exclusively expressed in hematopoietic cells[19], and mice lacking *Kindlin3* (*Kindlin3*$^{-/-}$ mice) suffer from fatal anemia, which is caused by severe bleeding and erythrocytopenia[2,20]. *Kindlin3*$^{-/-}$ mice also show markedly reduced size and cellularity of spleen and thymus and lack detectable mesenteric lymph nodes (**Supplementary Fig. 1** online).

[1]Department of Molecular Medicine, Max Planck Institute of Biochemistry, Am Klopferspitz 18, 82152 Martinsried, Germany. [2]Walter Brendel Center for Experimental Medicine, Ludwig-Maximilians-Universität, Marchioninistrasse 15, 81377 Munich, Germany. Correspondence should be addressed to R.F. (faessler@biochem.mpg.de).

Received 23 September 2008; accepted 5 January 2009; Published online 22 February 2009; doi:10.1038/nm.1921

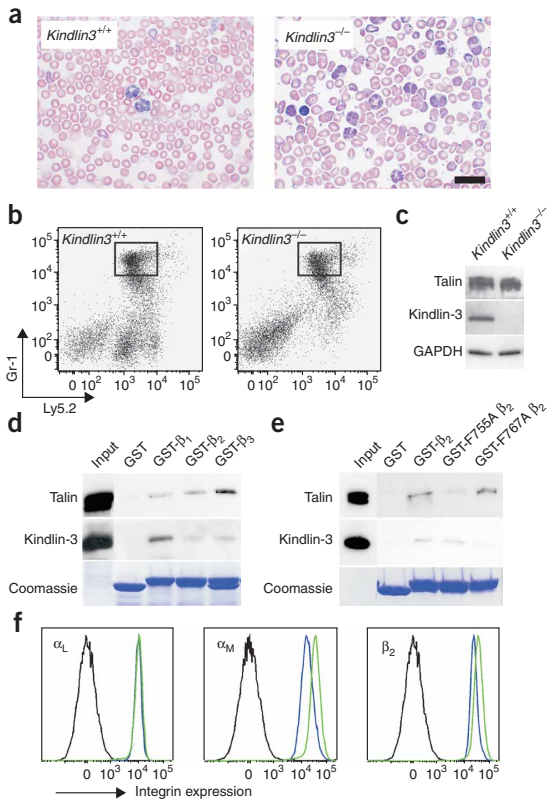

Figure 1 Characterization of PMNs in *Kindlin3*$^{-/-}$ chimeric mice. (**a**) Peripheral blood smears from control and *Kindlin3*$^{-/-}$ chimeras. Scale bar, 20 μm. (**b**) FACS profile of bone marrow–derived cells from control and *Kindlin3*$^{-/-}$ chimeras stained for Gr-1–FITC and CD45.2 (Ly5.2)–allophycocyanin. PMNs from the boxed area were sorted and used for all *in vitro* experiments. (**c**) Western blot analysis of sorted PMNs from *Kindlin3*$^{+/+}$ and *Kindlin3*$^{-/-}$ chimeras showing talin and Kindlin-3 expression. Glyceraldehyde 3-phosphate dehydrogenase (GAPDH) was used as a loading control. (**d**,**e**) GST fusions to β_1, β_2 and β_3 (**d**) and β_2, F755A β_2 and F767A β_2 (**e**) integrin cytoplasmic domains were incubated with platelet cell lysates and used in pulldown assays to assess the binding of these integrin domains to talin and Kindlin-3. (**f**) Surface expression of α_L, α_M and β_2 integrins on PMNs from control and *Kindlin3*$^{-/-}$ chimeras (black lines show isotype controls; blue lines show *Kindlin3*$^{+/+}$; green lines show *Kindlin3*$^{-/-}$).

To test whether Kindlin-3 deficiency leads to defective leukocyte adhesion and function, we generated fetal liver cell chimeras from wild-type (*Kindlin3*$^{+/+}$) and *Kindlin3*$^{-/-}$ embryos to circumvent postnatal lethality of *Kindlin3*$^{-/-}$ mice[2] and analyzed their polymorphonuclear granulocytes (PMNs) *in vitro* and *in vivo*. Peripheral blood smears 5 weeks after the fetal liver cell transfer indicated that the number of PMNs was markedly increased in *Kindlin3*$^{-/-}$ chimeras (**Fig. 1a**). This was confirmed by determining the absolute counts of PMNs in peripheral blood, which reached 3,500 ± 1,000 cells per μl (mean ± s.d.; $n = 9$) in *Kindlin3*$^{+/+}$ and 31,200 ± 27,000 cells per μl ($n = 9$) in *Kindlin3*$^{-/-}$ fetal liver cell chimeras (counts of other blood cell types are shown in **Supplementary Table 1** online). Despite the severe granulocytosis, the size and nuclear morphology of PMNs from peripheral blood or bone marrow as well as the expression of surface markers such as Gr-1 were similar in *Kindlin3*$^{+/+}$ and *Kindlin3*$^{-/-}$ chimeras (**Fig. 1a**,**b**). Western blot analysis confirmed loss of Kindlin-3 expression in bone marrow–derived *Kindlin3*$^{-/-}$ PMNs, whereas talin amounts were normal (**Fig. 1c**). Pull-down experiments with recombinant β_1, β_2 and β_3 integrin cytoplasmic tails incubated with platelet lysates showed a clear Kindlin-3 interaction with the β_2 integrin cytoplasmic tail, although this binding was weaker compared with binding of Kindlin-3 to β_1 or β_3 integrin cytoplasmic domains (**Fig. 1d**). The cytoplasmic domain of β_1 and β_3 integrins contains two NXXY (where X is any amino acid) motifs, whereas the β_2 integrin tail contains two NXXF motifs (**Supplementary Fig. 2** online). To test whether Kindlin-3 shares a similar spatial binding property on the integrin β_2 tail as on β_1 and β_3 integrin tails, we substituted each phenylalanine residue in these motifs individually with an alanine (F755A or F767A) and performed pull-down experiments. Kindlin-3 still bound to the F755A β_2 integrin tail mutant but was unable to interact with the F767A β_2 integrin tail mutant (**Fig. 1e**), indicating that the binding occurs at the distal NXXF motif and is spatially conserved among all integrin tails tested so far. FACS analysis revealed normal amounts of α_L and slightly increased amounts of α_M and β_2 integrin subunits on *Kindlin3*$^{-/-}$ PMNs (**Fig. 1f**). Furthermore, the expression of other surface receptors such as CD43, CD44 and P-selectin glycoprotein ligand-1 was also not altered in the absence of Kindlin-3 expression (**Supplementary Fig. 3** online). Together these data indicate that the absence of Kindlin-3 expression permits the formation and maturation of PMNs. Similar to the granulocytosis observed in individuals with LAD-I, LAD-II and LAD-III as well as in β_2 integrin–deficient mice[21], there is granulocytosis in *Kindlin3*$^{-/-}$ chimeric mice, presumably due to a compensatory response to impaired granulocyte number or function in tissues or both.

Next we tested whether β_2 integrins can be activated in the absence of Kindlin-3 by seeding *Kindlin3*$^{-/-}$ PMNs on glass surfaces coated with intercellular adhesion molecule-1 (ICAM-1), the endothelial counter-receptor for the leukocyte integrins $\alpha_L\beta_2$ and $\alpha_M\beta_2$ that are crucial for tight adhesion and arrest of rolling PMNs on activated endothelium. Untreated PMNs did not show substantial adhesion and spreading (**Fig. 2a**), indicating that they were not activated during their isolation. In the presence of phorbol-12-myristate-13-acetate (PMA), a diacylglycerol analog triggering intracellular signaling events leading to activation of integrins ('inside-out' signaling), PMNs from *Kindlin3*$^{+/+}$ chimeras rapidly adhered and spread on ICAM-1. In contrast, adhesion and spreading of *Kindlin3*$^{-/-}$ PMNs on ICAM-1 was completely absent (**Fig. 2a**). To test whether the defect in β_2 integrin activation in *Kindlin3*$^{-/-}$ PMNs is due specifically to a defect in 'inside-out' signaling, we used $MnCl_2$ to induce β_2 integrin activation. We incubated PMNs in suspension with fluorescently labeled fibrinogen, a ligand for the $\alpha_M\beta_2$ and $\alpha_v\beta_3$ integrins, and measured the extent of fibrinogen binding by FACS. Notably, *Kindlin3*$^{+/+}$ and *Kindlin3*$^{-/-}$ PMNs bound comparable amounts of fibrinogen (**Fig. 2b**). Together, these findings indicate that Kindlin-3 is a key player in the intracellular signaling cascade leading to β2 integrin activation.

To corroborate the dependence of β_2 integrin activation on Kindlin-3, we measured PMN adhesion and spreading on immobilized immune complexes, which is triggered by Fcγ receptor–mediated inside-out activation of $\alpha_M\beta_2$ integrin and binding to the activated complement component iC3b[22]. Whereas control PMNs adhered strongly to immune complexes and approximately half of the adherent PMNs spread, Kindlin-3–deficient PMNs adhered weakly to immune complexes and did not spread (**Fig. 2c**,**d**). The adhesion of mutant PMNs to immune complexes occurred in an Fcγ receptor–dependent

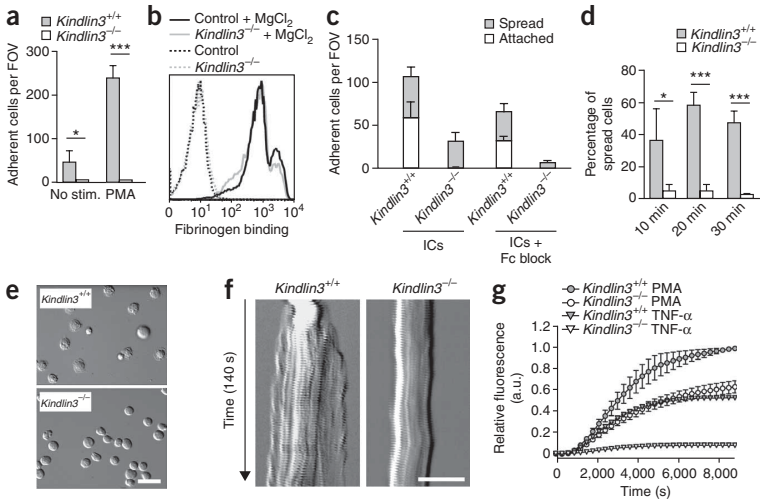

Figure 2 Functional properties of *Kindlin3*$^{-/-}$ PMNs. (**a**) Adhesion of neutrophils to coated ICAM-1. Control and *Kindlin3*$^{-/-}$ PMNs were treated with or without PMA ($n = 4$, each assay was performed in triplicate). FOV, field of view. (**b**) Fibrinogen binding of control and *Kindlin3*$^{-/-}$ PMNs, as analyzed by flow cytometry. Cells were incubated with either EDTA as a negative control or with $MnCl_2$. (**c**) Adhesion of PMNs on immune complexes. *Kindlin3*$^{+/+}$ and *Kindlin3*$^{-/-}$ PMNs were plated on immune complexes (IC) in the absence or presence of antibody to Fcγ receptor (Fc block) ($n = 3$, each assay was performed in triplicate). (**d**) Spreading of PMNs on immune complexes. *Kindlin3*$^{+/+}$ and *Kindlin3*$^{-/-}$ PMNs were stimulated with TNF-α before plating. Spreading was analyzed 10, 20 and 30 min after plating ($n = 4$). In **a** and **d**, graphs show means ± s.d.; Student's *t* test was used for comparing different datasets. (*, $P < 0.05$; **, $P < 0.01$; ***, $P < 0.001$). (**e**) Differential interference contrast microscopy of *Kindlin3*$^{+/+}$ and *Kindlin3*$^{-/-}$ PMNs 20 min after plating on immune complexes. Scale bar, 25 μm. (**f**) Kymographs of a *Kindlin3*$^{+/+}$ or a *Kindlin3*$^{-/-}$ PMN plated on immune complexes and imaged with differential interference contrast microscopy. Scale bar, 10 μm. (**g**) Oxidative burst after β_2 integrin–mediated activation of PMNs. Sorted PMNs from *Kindlin3*$^{+/+}$ and *Kindlin3*$^{-/-}$ chimeras were stimulated with either TNF-α or PMA and then the production of free ROIs was measured. Data are means ± s.d. of three independent experiments, each conducted in triplicate. a.u., arbitrary units.

manner, as Fcγ receptor blockage abolished *Kindlin3*$^{-/-}$ PMN cell adhesion (**Fig. 2c**). Quantification of cell morphology after plating revealed that around 60% of *Kindlin3*$^{+/+}$ PMNs became flattened on immobilized immune complexes, whereas no significant spreading was observed with *Kindlin3*$^{-/-}$ PMNs (**Fig. 2d**). For closer inspection, we followed PMNs contacting the immune complex–coated surfaces with time-lapse video microscopy using differential interference contrast optics. Upon surface contact, *Kindlin3*$^{+/+}$ PMNs spread within a time frame of less than 1 min and subsequently remained flattened and stationary with a ruffling periphery (**Fig. 2e** and **Supplementary Video 1** online). In sharp contrast, *Kindlin3*$^{-/-}$ PMNs showed severely impaired spreading, despite active surface dynamics with peripheral ruffling and occasional small lamellae that extended onto the surface (**Fig. 2e** and **Supplementary Video 1**). To characterize spreading behavior, we quantified the plasma membrane extension rates of spreading PMNs by kymography. Spreading control PMNs rapidly increased their diameters within 60 s after contacting the surface, whereas the diameter of *Kindlin3*$^{-/-}$ PMNs remained unchanged (**Fig. 2f**).

The spreading of preactivated PMNs on adhesive surfaces triggers a β_2 integrin–dependent degranulation and a respiratory burst that can be measured as free reactive oxygen intermediates (ROIs). Therefore, we seeded PMNs pretreated with tumor necrosis factor-α (TNF-α) on immune complexes and quantified the kinetics of ROI release. In line with findings from PMNs derived from β_2 integrin–deficient mice[23] and subjects with LAD-I (ref. 24), *Kindlin3*$^{-/-}$ PMNs were completely unresponsive, whereas *Kindlin3*$^{+/+}$ cells showed a burst of ROI (**Fig. 2g**). PMA treatment partially bypasses the adhesion dependency of the reaction[24]. Accordingly, under PMA stimulation *Kindlin3*$^{-/-}$ PMNs showed a considerable rescue of ROI production, indicating a constitutive capability to undergo respiratory burst and confirming the normal differentiation state of these cells (**Fig. 2g**).

To explore the consequences of abolished β_2 integrin activation in *Kindlin3*$^{-/-}$ chimeras, we studied leukocyte extravasation into the perivascular tissue *in vivo*. Initially, we applied phorbol esters (croton oil) to the ears of the mice and examined infiltration of PMNs into perivascular tissue 4 h later by determining PMN distribution in relation to the vascular basement membrane. In *Kindlin3*$^{+/+}$ chimeric mice, many Gr-1–positive cells transmigrated into the interstitium, where they became evenly distributed (**Fig. 3a**). In contrast, in *Kindlin3*$^{-/-}$ chimeric mice, Gr-1–positive cells were abolished completely absent from the perivascular tissue, but were visible within the vasculature (**Fig. 3a**). We next investigated rolling, adhesion and extravasation of PMNs from nonchimeric *Kindlin3*$^{+/-}$ mice (as a control) and from *Kindlin3*$^{+/+}$ and *Kindlin3*$^{-/-}$ chimeric mice in TNF-α–stimulated cremaster muscle venules. In line with the croton oil experiment, Giemsa staining of treated cremaster tissues revealed a strong and widespread influx of *Kindlin3*$^{+/-}$ or *Kindlin3*$^{+/+}$ PMNs into the interstitium 3 hours after TNF-α application, whereas extravasation of *Kindlin3*$^{-/-}$ PMNs was markedly reduced (**Fig. 3b**). Together these findings indicate that *Kindlin3*$^{-/-}$ chimeric mice suffer from a considerable PMN extravasation deficiency as in individuals with LAD-I, LAD-II or LAD-III.

To determine which step in the extravasation cascade is affected by the absence of Kindlin-3, we analyzed leukocyte rolling and adhesion in TNF-α–stimulated cremaster muscle venules of nonchimeric *Kindlin3*$^{+/-}$ mice and *Kindlin3*$^{+/+}$ and *Kindlin3*$^{-/-}$ chimeric mice by intravital microscopy. Microvascular parameters such as vessel diameter, blood flow velocity and wall shear rate were similar among all three types of mice (**Supplementary Table 2** online), despite a significant elevation of PMN counts in the peripheral blood of *Kindlin3*$^{-/-}$ chimeric mice ($P < 0.05$). In line with previous observations[25] and as shown here, TNF-α treatment markedly lowered systemic leukocyte counts in *Kindlin3*$^{+/-}$ mice and in *Kindlin3*$^{+/+}$ chimeric mice (**Supplementary Table 2**). TNF-α–treatment in *Kindlin3*$^{-/-}$ chimeric mice also decreased systemic leukocyte counts, but these counts were significantly higher than in *Kindlin3*$^{+/-}$ mice or *Kindlin3*$^{+/+}$ chimeric mice (**Supplementary Table 2**, $P < 0.05$).

In TNF-α–stimulated cremaster muscle venules of *Kindlin3*$^{-/-}$ chimeric mice, the number of adherent leukocytes was significantly reduced (220 ± 100 cells per mm^2) when compared to *Kindlin3*$^{+/-}$ mice or *Kindlin3*$^{+/+}$ chimeric mice (980 ± 90 cells per mm^2 and

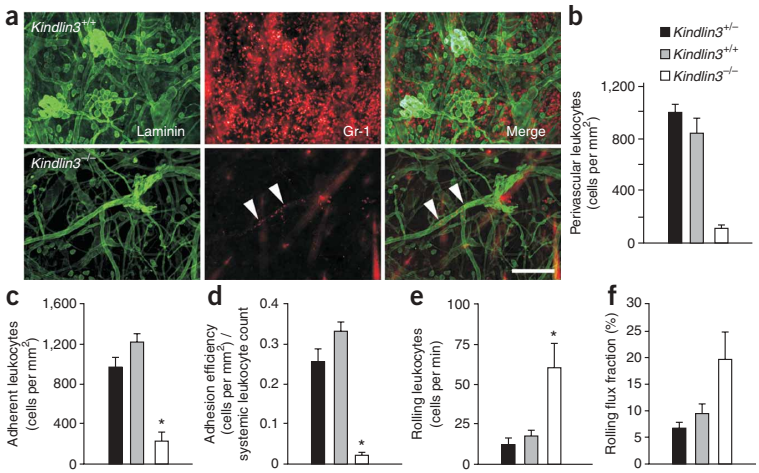

Figure 3 Abrogated leukocyte adhesion and extravasation in *Kindlin3*$^{-/-}$ chimeras. (**a**) Sections of phorbol ester–treated ears from *Kindlin3*$^{+/+}$ and *Kindlin3*$^{-/-}$ chimeric mice, stained with a pan-laminin antibody (green) to visualize endothelial basement membranes and Gr-1 (red) to visualize neutrophils. Arrowheads indicate Gr-1–positive cells within blood vessels of *Kindlin3*$^{-/-}$ chimeras. Scale bar, 200 μm. (**b**) Quantification of perivascular leukocytes in whole-mount Giemsa staining of TNF-α–stimulated cremaster muscles from non-chimeric *Kindlin3*$^{+/-}$ mice (15 venules in four mice), *Kindlin3*$^{+/+}$ (15 venules in four mice) and *Kindlin3*$^{-/-}$ (21 venules in four mice) chimeras 3 h after cytokine application. Data are means ± s.e.m. (**c**) Leukocyte adhesion in TNF-α–stimulated cremaster muscle venules assessed in 13 cremaster muscle venules of four *Kindlin3*$^{+/-}$ mice, 19 venules of six *Kindlin3*$^{+/+}$ chimeric mice and 13 cremaster muscle venules of four *Kindlin3*$^{-/-}$ chimeric mice. (**d**) Leukocyte adhesion efficiency, given as the number of adherent leukocytes per mm^2 vascular surface area divided by the systemic leukocyte count. (**e**) Quantification of rolling leukocytes passing an imaginary perpendicular line over the vessel in 1 min. (**f**) Leukocyte rolling flux fractions, calculated to account for differences in systemic leukocyte counts between *Kindlin3*$^{+/+}$ mice and *Kindlin3*$^{-/-}$ mice. All values are given as means ± s.e.m. Significant differences ($P < 0.05$) between groups are indicated by an asterisk.

1,220 ± 80 cells per mm^2, respectively, $P < 0.05$ versus *Kindlin3*$^{-/-}$ chimeric mice), indicating that Kindlin-3 is crucial for leukocyte adhesion *in vivo* (**Fig. 3c**). Because leukocyte adhesion is greatly influenced by the number of available circulating leukocytes, we also calculated leukocyte adhesion efficiency, which is defined by the ratio of adherent leukocytes to circulating leukocytes. Owing to the high systemic leukocyte count in *Kindlin3*$^{-/-}$ chimeras, the adhesion efficiency was dramatically reduced in *Kindlin3*$^{-/-}$ chimeric mice (0.02 ± 0.01) when compared to *Kindlin3*$^{+/-}$ mice or *Kindlin3*$^{+/+}$ chimeric mice (0.25 ± 0.033 and 0.35 ± 0.03, respectively, $P < 0.05$ versus *Kindlin3*$^{-/-}$ chimeric mice; **Fig. 3d**).

Next, we analyzed leukocyte rolling in TNF-α–stimulated cremaster muscle venules, which depends on P-selectin and E-selectin in this model[25]. We observed a significant increase in the number of rolling leukocytes in *Kindlin3*$^{-/-}$ chimeric mice (60 ± 16 cells per min) as compared to *Kindlin3*$^{+/-}$ mice or *Kindlin3*$^{+/+}$ chimeric mice (12 ± 4 cells per min and 18 ± 3 cells per min, respectively, $P < 0.05$ versus *Kindlin3*$^{-/-}$ mice; **Fig. 3e** and **Supplementary Videos 2** and **3** online). However, after correcting leukocyte rolling for differences in the total number of systemic leukocytes (rolling flux fraction), we did not observe any significant difference in rolling between *Kindlin3*$^{+/+}$ and *Kindlin3*$^{-/-}$ chimeric mice (**Fig. 3f**). We also analyzed mean leukocyte

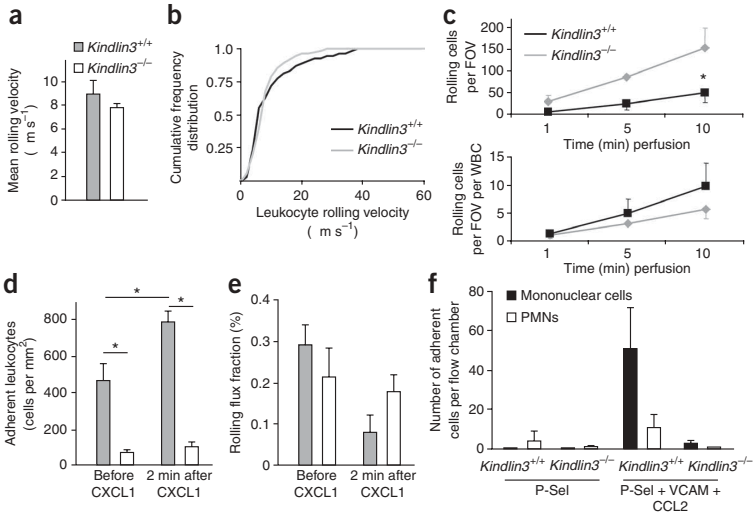

Figure 4 Leukocyte rolling and adhesion under *in vivo* and *in vitro* conditions. (**a**,**b**) Mean leukocyte rolling velocity (**a**) and the cumulative frequency distribution (**b**) of leukocyte rolling velocities from analysis of TNF-α–stimulated postcapillary venules of cremaster muscles from *Kindlin3*$^{+/+}$ ($n = 54$ venules from four mice) and *Kindlin3*$^{-/-}$ ($n = 111$ venules from four mice) chimeric mice. (**c**) Top, quantification of leukocyte rolling in an *ex vivo* flow chamber system (P-selectin–coated microglass capillaries) perfused with whole blood from *Kindlin3*$^{+/+}$ ($n = 5$ chambers from four mice) and *Kindlin3*$^{-/-}$ ($n = 3$ chambers from four mice) chimeric mice. Bottom, the number of rolling leukocytes was corrected for differences in systemic leukocyte counts between *Kindlin3*$^{+/+}$ and *Kindlin3*$^{-/-}$ chimeric mice. WBC, white blood cell. (**d**,**e**) Assessment of leukocyte adhesion (**d**) and leukocyte rolling (**e**) in unstimulated cremaster muscle venules of *Kindlin3*$^{+/+}$ ($n = 4$) and *Kindlin3*$^{-/-}$ ($n = 3$) chimeric mice before and 2 min after injection of the arrest chemokine CXCL1. (**f**) β1 integrin–dependent adhesion of leukocytes from *Kindlin3*$^{+/+}$ ($n = 3$) and *Kindlin3*$^{-/-}$ chimeric mice ($n = 3$) *ex vivo*. Flow chambers were coated with P-selectin only or a mixture of P-selectin, VCAM-1 and CCL2, connected to the carotid artery, perfused with whole blood for 10 min, and the number of adhered PMNs and mononuclear cells was counted. For each condition, chambers in at least three mice were used. All data are shown as means ± s.e.m.; significant differences ($P < 0.05$) are indicated by asterisk.

rolling velocities and cumulative frequency distribution of leukocyte rolling velocities and found that they were similar in *Kindlin3*$^{+/+}$ and *Kindlin3*$^{-/-}$ chimeric mice, suggesting that selectin-mediated rolling is not disturbed in the absence of Kindlin-3 (**Fig. 4a**,**b**). This was further confirmed in an *ex vivo* flow chamber assay[26], where leukocyte rolling on immobilized recombinant mouse (rm) P-selectin was indistinguishable between leukocytes from *Kindlin3*$^{+/+}$ and *Kindlin3*$^{-/-}$ chimeric mice after correction for differences in systemic leukocyte counts (**Fig. 4c**). To further confirm the *in vivo* leukocyte adhesion defect of *Kindlin3*$^{-/-}$ chimeric mice, we blocked leukocyte rolling in TNF-α–stimulated cremaster muscle venules by systemic injection of blocking antibodies against P- and E-selectin during intravital microscopic observation. The blocking antibodies abruptly abolished leukocyte rolling in *Kindlin3*$^{+/-}$ mice and in *Kindlin3*$^{+/+}$ and *Kindlin3*$^{-/-}$ chimeric mice as previously described for wild-type mice[27]. Five minutes after antibody injection, a substantial number of adherent leukocytes were still present in *Kindlin3*$^{+/-}$ mice and in *Kindlin3*$^{+/+}$ chimeric mice (940 ± 80 cells per mm^2 and 1,070 ± 90 cells per mm^2, respectively, data not shown), whereas only a few adherent leukocytes were observed in *Kindlin3*$^{-/-}$ chimeric mice (230 ± 50 cells per mm^2, data not shown; **Supplementary Videos 4** and **5** online). Taken together, these data indicate that Kindlin-3 is not required for leukocyte rolling on inflamed endothelium but is essential for their firm adhesion.

To investigate whether Kindlin-3 is also required for chemokine-induced leukocyte arrest *in vivo*, we systemically injected the neutrophil arrest–inducing chemokine CXCL1 (also known as keratinocyte-derived chemokine, KC)[25] into *Kindlin3*$^{+/+}$ and *Kindlin3*$^{-/-}$ chimeric mice and observed leukocyte adhesion and rolling. CXCL1 injection into *Kindlin3*$^{+/+}$ mice triggered a significant increase in the number of adherent leukocytes in postcapillary venules of the exteriorized cremaster muscle, which was accompanied by a marked drop in the number of rolling leukocytes (**Fig. 4d**,**e** and **Supplementary Video 6** online). In contrast, injection of CXCL1 into *Kindlin3*$^{-/-}$ chimeric mice did not change leukocyte adhesion and rolling (**Fig. 4d**,**e** and **Supplementary Video 7** online), showing that chemokine-triggered leukocyte arrest is also almost completely absent in *Kindlin3*$^{-/-}$ mice.

Finally, we addressed the role of Kindlin-3 in β_1 integrin–mediated leukocyte adhesion with an autoperfused flow chamber assay[26]. Chambers were coated with a mixture of rmP-selectin, rm vascular cell adhesion molecule-1 (VCAM-1) and rmCCL2 or with rmP-selectin only and connected to the carotid artery of *Kindlin3*$^{+/+}$ or *Kindlin3*$^{-/-}$ chimeric mice. Leukocyte adhesion was assessed 10 min after the start of perfusion with whole blood. In *Kindlin3*$^{+/+}$ chimeric mice, mononuclear cells adhered preferably to the surface coated with all three proteins compared to the surface coated with rmP-selectin only, for which adhered cells were almost completely absent (**Fig. 4f**). In contrast, in *Kindlin3*$^{-/-}$ chimeric mice, leukocytes failed to adhere to the surface coated with all three proteins (**Fig. 4f**), suggesting that Kindlin-3 is crucial for β_1 integrin– and β2 integrin–dependent adhesion.

Our study demonstrates that Kindlin-3 is essential for the activation of β_2 integrins in PMNs. Consequently, lack of Kindlin-3 expression prevents adhesion and spreading of PMNs on β_2 integrin ligands such as ICAM-1 and iC3b and results in a severe leukocyte adhesion deficiency *in vivo*. The mechanism underlying Kindlin-3–mediated activation β2 integrin is similar to that underlying its activation of the β1 and β3 integrins, as Kindlin-3 is capable of binding the distal NXXF motif of the β_2 integrin cytoplasmic domain, albeit with a lower efficiency than its binding to this motif in the β_1 and β_3 integrins.

The defects seen in *Kindlin3*$^{-/-}$ mice—a severe leukocyte adhesion deficiency and fatal bleeding—bear a striking similarity to the symptoms observed in individuals with LAD-III. Furthermore, the gene defect causing LAD-III has been mapped to chromosome 11 in humans, where the *Kindlin3* gene is located. *Kindlin3* is thus a prime candidate to be mutated in LAD-III. However, a recent study identified a mutation in the *CALDAGGEF1* gene, which encodes a RAP-1 guanine exchange factor, to cause LAD-III (ref. 11). Notably, Svensson *et al.*[13] report in this issue that subjects with LAD-III who have mutations in *CALDAGGEF1* also carry nonsense mutations in their *Kindlin3* gene. Furthermore, reexpression of a *Kindlin3* cDNA fully rescued the adhesion and spreading defect in leukocytes from these subjects. In contrast, reexpression of *CALDAGGEF1* did not rescue these defects. It will be useful now to clarify whether mutations in different genes such as *CALDAGGEF1* and *Kindlin3* can indeed give rise to the same LAD-III syndrome and how and where they function in the signaling pathway that leads to β_2 integrin activation. Studies with mouse mutants suggest that deficiencies of either protein can lead to a LAD-like phenotype[2,12], although CALDAG-GEF1-deficient mice seem to have slightly milder defects than those lacking Kindlin-3. The reason for this difference could be that Kindlin-3 controls both inside-out and 'outside-in' signaling of integrins[2], whereas CALDAG-GEF1 has a role only in Rap-mediated inside-out integrin activation[11].

METHODS

Generation of fetal liver cell chimeras. We recently generated *Kindlin3*-deficient mice[2]. We obtained fetal liver cells from embryonic day 15 *Kindlin3*$^{+/+}$ or *Kindlin3*$^{-/-}$ embryos by pushing liver tissue through a cell strainer (Falcon). We injected 4 × 10^6 cells into the tail vein of lethally irradiated (10 Gy) recipient C57BL/6 mice (Charles River Laboratories). Four to five weeks after transfer, we either isolated PMNs from the bone marrow or used the mice for intravital microscopy. All mouse experiments were performed with approval by the District Government of Upper Bavaria.

Intravital microscopy. We injected rmTNF-α (R&D Systems) intrascrotally at a dose of 500 ng per mouse in a volume of 0.3 ml sterile saline. Two hours later, we anesthetized the mice as previously described[25] and placed them onto a heating pad to maintain body temperature at 37 °C. After intubation and carotid artery cannulation for blood sampling and application of antibodies and chemokines, we surgically prepared the cremaster muscle for intravital microscopy as previously described[28]. Briefly, after opening the scrotum, we exteriorized the cremaster muscle and spread it over a cover glass. We gently moved the epididymis and testis aside to get microscopic access to the cremaster muscle microcirculation and its postcapillary venules. We performed intravital microscopy on an upright microscope (Olympus BX51) with a saline immersion objective (40× and 0.8 numerical aperture). We recorded experiments via CCD camera (model CF8/1, Kappa) on a Panasonic S-VHS recorder. We also made recordings with a digital camera (LaVision Biotech) and stored them on a computer with Imspector software package (LaVision Biotech). We then used the digital recordings offline to generate movie clips with ImageJ software (US National Institutes of Health). During the experiment, we obtained systemic blood samples (10 μl into 90 μl Türck's solution, Merck) to assess systemic white blood cell counts. In some experiments, we stimulated the postcapillary venules of the exteriorized cremaster muscle by systemic injection of keratinocyte-derived chemokine (CXCL1, 600 ng per mouse, Natutec) and assessed leukocyte rolling and adhesion before and 2 min after injection of CXCL1 as previously described[25].

Data analysis of intravital experiments. We measured vessel diameter and vessel segment length of postcapillary venules with a digital image processing system[29]. We obtained centerline red blood cell velocities in microvessels of the cremaster muscle by a dual photodiode and a digital on-line cross-correlation program (Circusoft Instrumentation), and we converted them offline to mean blood flow velocities as previously described[28]. We assessed wall shear rates as previously reported[30]. We defined rolling flux as the number of rolling cells per min. We defined rolling PMN flux fraction as the percentage of rolling PMNs in all PMNs passing the same vessel in 1 min[28]. We considered PMNs that did not

move for more than 30 s to be adherent. We assessed the number of adherent leukocytes as the number of adherent cells per mm^2 vessel surface area[25].

Whole-mount histology. To assess extravasated leukocytes in TNF-α–stimulated cremaster muscles, we prepared whole mounts of cremaster muscles as previously described[25]. Briefly, while the cremaster muscle was still mounted on the stage for intravital microscopy, we fixed the tissue with 4% paraformaldehyde in 0.1 M phosphate buffer (pH 7.4). We removed the cremaster muscle and mounted it flat on a superfrost glass slide (Menzel), air-dried it for 5–10 min and fixed it in 4% paraformaldehyde in 0.1 M phosphate buffer (pH 7.4) for 24 h at 4 °C. After fixation, we washed the tissue three times in 0.1 M phosphate buffer with 5% ethanol, stained it with Giemsa (Sigma) at 20 °C for 5 min and developed it in 0.01% acetic acid for contrast. We washed the developed slides in water, 75% ethanol, 95% ethanol, 100% ethanol and fresh xylene and then mounted them in mounting medium (AGAR Scientific). We assessed the number of extravasated leukocytes in Giemsa-stained cremaster muscles with a Zeiss upright microscope and a 100× and 1.3 numerical aperture oil immersion objective (Zeiss).

***Ex vivo* flow chamber assay.** We used an autoperfused flow chamber assay as previously described[26]. Briefly, we used rectangular microglass capillaries (VitroCom) as flow chambers. We coated the flow chambers with rmP-selectin (20 μg ml^{-1}, R&D Systems), rmCCL2 (3 μg ml^{-1}, Natutec) and rmVCAM-1 (15 μg ml^{-1}, R&D Systems). We blocked nonspecific binding by incubating the flow chambers with 10% casein (Sigma) for 2 h at 20 °C. After blocking, we rinsed the flow chambers with normal saline and connected them to the mouse carotid artery via polyethylene tubing. We fixed the flow chamber itself under an upright fluorescence microscope (BX51 WI, Olympus) with a saline immersion objective (20× and 0.95 numerical aperture, Olympus). We observed rolling of leukocytes within the flow chamber for 10 min and recorded their rolling via a charge-coupled device camera system (CF8HS; Kappa) on a Panasonic S-VHS recorder. We assessed leukocyte adhesion after a 10-min perfusion by counting adherent mononuclear cells and neutrophils in a 10-mm flow chamber segment; the adherent cells were stained by gentle flushing of the chamber with Türck's stain (Merck).

Statistical analyses. We performed statistical analyses was with the GraphPad Prism software (version 5.00, GraphPad). Data are presented as means ± s.d. or means ± s.e.m. We used unpaired Student's *t* tests or one-way analysis of variance followed by a multiple pairwise comparison test (Dunn's test) as appropriate to compare datasets. Asterisks indicate significant differences (*, $P < 0.05$, **, $P < 0.01$ and ***, $P < 0.005$).

Additional methods. Detailed methodology is described in the **Supplementary Methods** online.

Note: Supplementary information is available on the Nature Medicine website.

ACKNOWLEDGMENTS

We thank the members of the Fässler lab for discussions, R. Zent for careful reading of the manuscript, K. Kessenbrock for help with the oxidative burst experiment, T. Lämmermann for help with the skin inflammation assay and S. Dietzel for help with generating the movie clips. The work was funded by the Deutsche Forschungsgemeinschaft and the Max Planck Society.

AUTHOR CONTRIBUTIONS

M.M., M.S. and R.F. designed and supervised research, analyzed data and wrote the paper. M.M., M.B., S. Schmid, R.R., S. Schmidt, M. Sixt, H.-V.W. and M. Sperandio performed experiments. All authors discussed the results and commented on the manuscript.

Published online at http://www.nature.com/naturemedicine/
Reprints and permissions information is available online at http://npg.nature.com/reprintsandpermissions/

1. Hynes, R.O. Integrins: bidirectional, allosteric signaling machines. *Cell* **110**, 673–687 (2002).
2. Moser, M., Nieswandt, B., Ussar, S., Pozgajova, M. & Fassler, R. Kindlin-3 is essential for integrin activation and platelet aggregation. *Nat. Med.* **14**, 325–330 (2008).
3. Alon, R. & Etzioni, A. LAD-III, a novel group of leukocyte integrin activation deficiencies. *Trends Immunol.* **24**, 561–566 (2003).
4. Ley, K., Laudanna, C., Cybulsky, M.I. & Nourshargh, S. Getting to the site of inflammation: the leukocyte adhesion cascade updated. *Nat. Rev. Immunol.* **7**, 678–689 (2007).
5. Anderson, D.C. & Springer, T.A. Leukocyte adhesion deficiency: an inherited defect in the Mac-1, LFA-1, and p150,95 glycoproteins. *Annu. Rev. Med.* **38**, 175–194 (1987).
6. Karsan, A. *et al.* Leukocyte adhesion deficiency type II is a generalized defect of *de novo* GDP-fucose biosynthesis. Endothelial cell fucosylation is not required for neutrophil rolling on human nonlymphoid endothelium. *J. Clin. Invest.* **101**, 2438–2445 (1998).
7. Lubke, T. *et al.* Complementation cloning identifies CDG-IIc, a new type of congenital disorders of glycosylation, as a GDP-fucose transporter deficiency. *Nat. Genet.* **28**, 73–76 (2001).
8. Luhn, K., Wild, M.K., Eckhardt, M., Gerardy-Schahn, R. & Vestweber, D. The gene defective in leukocyte adhesion deficiency II encodes a putative GDP-fucose transporter. *Nat. Genet.* **28**, 69–72 (2001).
9. Sampath, R., Gallagher, P.J. & Pavalko, F.M. Cytoskeletal interactions with the leukocyte integrin beta2 cytoplasmic tail. Activation-dependent regulation of associations with talin and alpha-actinin. *J. Biol. Chem.* **273**, 33588–33594 (1998).
10. Monkley, S.J. *et al.* Disruption of the talin gene arrests mouse development at the gastrulation stage. *Dev. Dyn.* **219**, 560–574 (2000).
11. Pasvolsky, R. *et al.* A LAD-III syndrome is associated with defective expression of the Rap-1 activator CalDAG-GEFI in lymphocytes, neutrophils, and platelets. *J. Exp. Med.* **204**, 1571–1582 (2007).
12. Bergmeier, W. *et al.* Mice lacking the signaling molecule CalDAG-GEFI represent a model for leukocyte adhesion deficiency type III. *J. Clin. Invest.* **117**, 1699–1707 (2007).
13. Svensson, L. *et al.* Leukocyte adhesion deficiency-III is caused by mutations in *KINDLIN3* affecting integrin activation. *Nat. Med.* advance online publication doi:10.1038/nm.1931 (22 February 2009).
14. Malinin, N.L. *et al.* A point mutation in *KINDLIN3* ablates activation of three integrin subfamilies in humans. *Nat. Med.* advance online publication doi:10.1038/nm.1917 (22 February 2009).
15. Kuijpers, T.W. *et al.* Natural history and early diagnosis of LAD-1/variant syndrome. *Blood* **109**, 3529–3537 (2007).
16. Kuijpers, T.W. *et al.* Leukocyte adhesion deficiency type 1 (LAD-1)/variant. A novel immunodeficiency syndrome characterized by dysfunctional β_2 integrins. *J. Clin. Invest.* **100**, 1725–1733 (1997).
17. Jobard, F. *et al.* Identification of mutations in a new gene encoding a FERM family protein with a pleckstrin homology domain in Kindler syndrome. *Hum. Mol. Genet.* **12**, 925–935 (2003).
18. Montanez, E. *et al.* Analysis of integrin functions in peri-implantation embryos, hematopoietic system, and skin. *Methods Enzymol.* **426**, 239–289 (2007).
19. Ussar, S., Wang, H.V., Linder, S., Fassler, R. & Moser, M. The Kindlins: subcellular localization and expression during murine development. *Exp. Cell Res.* **312**, 3142–3151 (2006).
20. Kruger, M. *et al.* SILAC mouse for quantitative proteomics uncovers kindlin-3 as an essential factor for red blood cell function. *Cell* **134**, 353–364 (2008).
21. Scharffetter-Kochanek, K. *et al.* Spontaneous skin ulceration and defective T cell function in CD18 null mice. *J. Exp. Med.* **188**, 119–131 (1998).
22. Jones, S.L., Knaus, U.G., Bokoch, G.M. & Brown, E.J. Two signaling mechanisms for activation of α_M β_2 avidity in polymorphonuclear neutrophils. *J. Biol. Chem.* **273**, 10556–10566 (1998).
23. Mocsai, A., Zhou, M., Meng, F., Tybulewicz, V.L. & Lowell, C.A. Syk is required for integrin signaling in neutrophils. *Immunity* **16**, 547–558 (2002).
24. Nathan, C. *et al.* Cytokine-induced respiratory burst of human neutrophils: dependence on extracellular matrix proteins and CD11/CD18 integrins. *J. Cell Biol.* **109**, 1341–1349 (1989).
25. Frommhold, D. *et al.* Sialyltransferase ST3Gal-IV controls CXCR2-mediated firm leukocyte arrest during inflammation. *J. Exp. Med.* **205**, 1435–1446 (2008).
26. Smith, M.L., Sperandio, M., Galkina, E.V. & Ley, K. Autoperfused mouse flow chamber reveals synergistic neutrophil accumulation through P-selectin and E-selectin. *J. Leukoc. Biol.* **76**, 985–993 (2004).
27. Sperandio, M. *et al.* Severe impairment of leukocyte rolling in venules of core 2 glucosaminyltransferase-deficient mice. *Blood* **97**, 3812–3819 (2001).
28. Sperandio, M., Pickard, J., Unnikrishnan, S., Acton, S.T. & Ley, K. Analysis of leukocyte rolling *in vivo* and *in vitro*. *Methods Enzymol.* **416**, 346–371 (2006).
29. Pries, A.R. A versatile video image analysis system for microcirculatory research. *Int. J. Microcirc. Clin. Exp.* **7**, 327–345 (1988).
30. Long, D.S., Smith, M.L., Pries, A.R., Ley, K. & Damiano, E.R. Microviscometry reveals reduced blood viscosity and altered shear rate and shear stress profiles in microvessels after hemodilution. *Proc. Natl. Acad. Sci. USA* **101**, 10060–10065 (2004).

12.3 Paper 3:

Kindlin-3-mediated signaling from multiple integrin classes is required for osteoclast-mediated bone resorption.

Published February 28, 2011

JCB: Article

Kindlin-3–mediated signaling from multiple integrin classes is required for osteoclast-mediated bone resorption

Sarah Schmidt,[1] Inaam Nakchbandi,[1,2] Raphael Ruppert,[1] Nina Kawelke,[1,2] Michael W. Hess,[3] Kristian Pfaller,[3] Pierre Jurdic,[4] Reinhard Fässler,[1] and Markus Moser[1]

[1]Max Planck Institute of Biochemistry, D-82152 Martinsried, Germany
[2]University of Heidelberg, D-69120 Heidelberg, Germany
[3]Innsbruck Medical University, Division of Histology and Embryology, A-6020 Innsbruck, Austria
[4]University of Lyon, Ecole Normale Supérieure de Lyon, 69364 Lyon, France

The blood cell–specific kindlin-3 protein is required to activate leukocyte and platelet integrins. In line with this function, mutations in the *KINDLIN-3* gene in man cause immunodeficiency and severe bleeding. Some patients also suffer from osteopetrosis, but the underlying mechanism leading to abnormal bone turnover is unknown. Here we show that kindlin-3–deficient mice develop severe osteopetrosis because of profound adhesion and spreading defects in bone-resorbing osteoclasts. Mechanistically, loss of kindlin-3 impairs the activation of β1, β2, and β3 integrin classes expressed on osteoclasts, which in turn abrogates the formation of podosomes and sealing zones required for bone resorption. In agreement with these findings, genetic ablation of all integrin classes abolishes the development of podosomes, mimicking kindlin-3 deficiency. Although loss of single integrin classes gives rise to podosomes, their resorptive activity is impaired. These findings show that osteoclasts require their entire integrin repertoire to be regulated by kindlin-3 to orchestrate bone homeostasis.

Introduction

Integrins are α/β heterodimeric cell surface receptors that bind extracellular matrix proteins and cell counter receptors. A hallmark of integrins is their ability to reversibly shift between different affinity states for their ligands. The shift from an inactive to an active conformation is triggered by the direct binding of talin and kindlin to the cytoplasmic domains of β1, β2, and β3 integrins, and is called integrin inside-out signaling (Moser et al., 2009b). Active integrins recruit and assemble large multimolecular complexes at their short cytoplasmic domains controlling several cellular processes such as organization of the cytoskeleton, migration, proliferation, differentiation, and apoptosis (integrin outside-in signaling; Legate et al., 2009).

Kindlins are a family of evolutionary conserved, intracellular FERM (4.1, ezrin, radixin, moesin) domain–containing proteins that are recruited to integrin adhesion sites (Moser et al., 2009b). Mammals have three members, called kindlin-1, -2, and -3. In contrast to the widely expressed kindlin-1 and -2, kindlin-3 expression is restricted to hematopoietic cells (Weinstein et al., 2003; Ussar et al., 2006). The importance of kindlin-3 for integrin activation in vivo was first described in kindlin-3–deficient mice, which suffer from bleeding and leukocyte adhesion defects (Moser et al., 2008, 2009a). Further cellular and molecular analyses of mouse and human blood cells revealed that kindlin-3 is required for activation of αIIbβ3 on platelets and β2 integrins on leukocytes (Moser et al., 2009b). Based on these findings, several groups identified mutations in the human kindlin-3 gene in patients with leukocyte adhesion deficiency (LAD) type III syndrome, which

Correspondence to Markus Moser: moser@biochem.mpg.de

Abbreviations used in this paper: AP, alkaline phosphatase; FAK, focal adhesion kinase; GAPDH, glyceraldehyde 3-phosphate dehydrogenase; LAD, leukocyte adhesion deficiency; M-CSF, macrophage-colony stimulating factor; MMP, matrix metalloproteinase; ON, overnight; OPG, osteoprotegerin; pQCT, peripheral quantitative computer tomography; PTH, parathyroid hormone; RANKL, receptor activator of nuclear factor κB ligand; TRAP, tartrate-resistant acid phosphatase; WASp, Wiskott-Aldrich syndrome protein.

Supplemental Material can be found at:
http://jcb.rupress.org/content/suppl/2011/02/28/jcb.201007141.DC1.html

The Rockefeller University Press $30.00
J. Cell Biol. Vol. 192 No. 5 883–897
www.jcb.org/cgi/doi/10.1083/jcb.201007141

Published February 28, 2011

is characterized by recurrent bacterial and fungal infections and severe bleeding (Kuijpers et al., 2009; Malinin et al., 2009; Moser et al., 2009a; Svensson et al., 2009). In addition to the severe platelet and leukocyte dysfunction, increased bone mass was observed in several LAD-III patients (Kilic and Etzioni, 2009; McDowall et al., 2010; Sabnis et al., 2010). It was recently proposed that the osteopetrosis is caused by increased osteogenic potential of mesenchymal stem cells (Malinin et al., 2009).

Bone remodeling depends on a tight interplay of osteoblasts that form bone and osteoclasts that resorb bone. Osteoblasts are derived from mesenchymal stem cells and cluster their integrins in adhesion sites termed focal adhesions (FAs). Osteoclasts are large, multinucleated cells that derive from the monocyte lineage and arrange their integrins in adhesion structures called podosomes. Podosomes contain a dotlike core of actin filaments, which is perpendicularly oriented to the plasma membrane and surrounded by a ringlike arrangement of adhesion, adaptor, and signaling molecules such as integrins, paxillin, vinculin, talin, protein kinases, and actin-associated molecules (Linder and Kopp, 2005). Podosomes are found in all cells of the monocytic cell lineage (macrophages, dendritic cells, etc.), smooth muscle cells, endothelial cells, src-transformed fibroblasts, and certain epithelial cells (Linder and Aepfelbacher, 2003). Bone-resorbing osteoclasts arrange their podosomes by interconnecting the actin cytoskeleton into densely packed rings called sealing zones. They delineate the active sites of bone resorption and form a pocket, into which protons and bone-resorbing proteases are secreted (Luxenburg et al., 2007). Sealing zones are attached to the bone matrix via αvβ3 integrin. Although mature osteoclasts express integrins of the β1, β2, and αv families, it is believed that αvβ3 integrins are the major adhesion proteins in osteoclast biology. This observation is largely based on the matrix degradation defects observed in Glanzmann patients or mice carrying null mutations in the β3 integrin gene. The reduced resorptive activity was thought to be caused by loss of αvβ3-mediated signaling that regulates cell polarity and cytoskeletal reorganization (McHugh et al., 2000; Faccio et al., 2003a). It cannot be excluded, however, that β1 and/or β2 integrins also play a role in osteoclast-mediated bone resorption in vivo (Helfrich et al., 1996; Rao et al., 2006).

Increased bone mineralization has been proposed to be the cause for the osteopetrosis in LAD-III patients (Malinin et al., 2009). It remains unclear, however, whether loss of kindlin-3 is indeed responsible for the increased bone mass and whether this bone abnormality is caused by an osteoblast and/or osteoclast dysfunction. In this paper, we find that kindlin-3–deficient mice develop a severe osteopetrotic phenotype caused by osteoclast dysfunctions. We show that kindlin-3–deficient osteoclasts fail to activate all their integrin classes, which in turn leads to their inability to spread and reorganize the actin cytoskeleton, as well as a failure to form podosomes and sealing zones and to degrade bone matrix. Our results indicate that all integrin classes are required for osteoclast-mediated bone resorption.

Results

Kindlin-3–deficient mice develop severe osteopetrosis

Kindlin-3–deficient (kindlin-3$^{-/-}$) mice die a few days after birth because of a severe anemia caused by massive bleeding and erythrocyte defects (Krüger et al., 2008; Moser et al., 2008). To analyze whether kindlin-3 affects bone development, we performed histology and peripheral quantitative computer tomography (pQCT) on long bones from kindlin-3$^{-/-}$ mice. At postnatal day 4 (P4), kindlin-3$^{-/-}$ bones showed a significant increase in trabecular bone accompanied by a marked decrease in bone marrow (Fig. 1 A). Van Kossa staining showed increased calcified bone (Fig. 1 B). pQCT analysis confirmed a significant increase in bone mineral density (BMD; Fig. 1 C). Bone surface as determined by static histomorphometry was markedly increased in the absence of kindlin-3 (Fig. 1 D).

To define the onset of the osteopetrosis, we compared the histology of control and mutant long bones from different developmental stages. At embryonic day 14 (E14), long bones from kindlin-3$^{-/-}$ embryos showed normal primary ossification centers surrounded by a normal coat of membranous bone (Fig. S1 A). At E16, kindlin-3$^{-/-}$ bones displayed increased ossification, and at birth, the bone mass further increased at the expense of the bone marrow cavity (Fig. S1 A). Alkaline phosphatase (AP) staining of osteoblasts and tartrate-resistant acid phosphatase (TRAP)-positive osteoclasts did not significantly differ between control and mutant bones at E14, E16, and P1 (Fig. S1, A and B).

Loss of kindlin-3 leads to severe osteoclast dysfunction

It has been proposed that a dysfunction of osteoblasts is responsible for increased bone density in LAD-III patients (Malinin et al., 2009). To test whether this is also the case in kindlin-3$^{-/-}$ mice, we performed histomorphometric analysis, which showed normal osteoblast numbers per unit of bone surface in kindlin-3$^{-/-}$ bones (Fig. S2 A). Calvaria-derived osteoblasts isolated from wild-type and kindlin-3$^{-/-}$ pups revealed comparable levels of gene expression for osteoblastic markers such as AP, osteocalcin, and collagen I as well as normal AP activity (Fig. S2, B, D, and E). Furthermore, the generation of mineralized bone nodules in vitro was similar in osteoblasts from both genotypes. (Fig. S2, F–H). Finally, and in line with the normal biological activity of kindlin-3$^{-/-}$ osteoblasts, wild-type osteoblasts expressed kindlin-2 but neither kindlin-3 nor kindlin-1 (Fig. S2 C).

To determine whether osteoclasts are defective, we performed TRAP staining and histomorphometric measurements of P4 kindlin-3$^{-/-}$ bones, which revealed that the number of TRAP-positive osteoclasts per bone surface was significantly increased by more than threefold (Fig. 1, E and F). Despite the elevated number of osteoclasts, the surface covered by osteoclasts was significantly decreased in kindlin-3$^{-/-}$ bones (Fig. 1 G). Consistent with the failure to erode bone, Ca^{2+} levels in the serum of kindlin-3$^{-/-}$ mice were significantly decreased (Fig. 1 H), and parathyroid hormone (PTH) levels were increased (Fig. 1 I). Indeed, cultured osteoclasts differentiated from wild-type blood

Published February 28, 2011

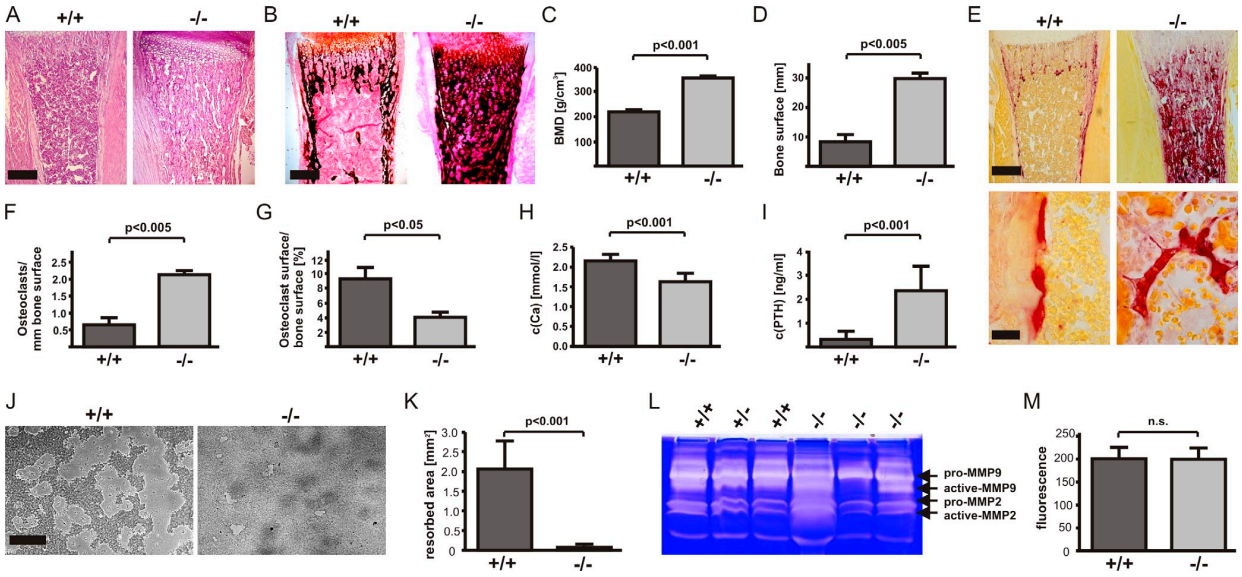

Figure 1. **Kindlin-3$^{-/-}$ mice develop severe osteopetrosis.** (A and B) Histology of tibiae of P4 wild-type and kindlin-3$^{-/-}$ mice stained with hematoxylin and eosin (A) and van Kossa (B). (C and D) Quantitative peripheral computer tomography measurements determining bone mineral density (C) and histomorphometric analysis to determine bone surface from bones of P4 wild-type and kindlin-3$^{-/-}$ mice (D); *n* = 3. (E) Histology of tibiae of P4 wild-type and kindlin-3$^{-/-}$ mice stained for TRAP activity. (F and G) Histomorphometric analyses determining the number of osteoclasts (F) and surface covered by osteoclasts (G) of wild-type and kindlin-3$^{-/-}$ mice; *n* = 3. (H) Ca^{2+} levels in serum of P4 wild-type and kindlin-3$^{-/-}$ mice; *n* = 8. (I) PTH levels in plasma of P3 wild-type and kindlin-3$^{-/-}$ mice; *n* = 10. (J and K) Resorption pits (J) and their quantification (K) of wild-type and kindlin-3$^{-/-}$ osteoclasts cultured on calcium apatite coated slides; *n* = 7. (L) Zymography of cell culture supernatants from primary wild-type and kindlin-3$^{-/-}$ osteoclasts. (M) Cathepsin K activity from lysates of primary wild-type and kindlin-3$^{-/-}$ osteoclasts; *n* = 11. Data are presented as mean ± SD (error bars). P-values indicate significant differences from wild-type (Student's *t* test). n.s., not significant. Bars: (A and B) 250 µm; (E, top) 250 µm; (E, bottom) 25 µm; (J) 100 µm.

precursors expressed high levels of kindlin-3 but neither kindlin-1 nor -2 (Fig. 2 B and Fig. S2 C).

These data suggest that kindlin-3$^{-/-}$ osteoclasts are functionally impaired. To address this finding, we tested the resorptive activity of kindlin-3$^{-/-}$ osteoclasts by seeding them on an artificial calcified matrix (osteologic slides) as well as dentin discs. Although wild-type osteoclasts resorbed large areas of mineralized matrix, kindlin3$^{-/-}$ osteoclasts were incapable of doing so (Fig. 1 J and not depicted). Morphometric image analysis of the resorbed areas revealed that resorption by kindlin-3$^{-/-}$ osteoclasts was >20-fold lower than wild-type cells (Fig. 1 K). The profound resorption defects were not accompanied by diminished secretion of proteolytic enzymes, as secretion of matrix metalloproteinase 2 (MMP2) and -9 and cathepsin K activities were indistinguishable between control and kindlin-3$^{-/-}$ osteoclasts (Fig. 1, L and M).

Altogether, these findings indicate that osteopetrosis in kindlin-3$^{-/-}$ mice is caused by a dysfunction of osteoclasts rather than osteoblasts.

Kindlin-3 is not required for osteoclast differentiation

Osteoclasts originate from monocytic precursors in response to the actions of macrophage-colony stimulating factor (M-CSF) and receptor activator of nuclear factor κB ligand (RANKL; Teitelbaum and Ross, 2003). Although the serum levels of M-CSF were similar (unpublished data), circulating levels of RANKL were increased eightfold in kindlin-3$^{-/-}$ mice (Fig. 2 A). Serum concentrations of osteoprotegerin (OPG), an inhibitor of RANKL, were similar between wild-type and kindlin-3$^{-/-}$ mice. Treatment of kindlin-3$^{-/-}$ osteoclasts with RANKL in vitro induced a strong and sustained p38 and JNK phosphorylation that was comparable to wild-type osteoclasts (Fig. S3). The high levels of RANKL in the serum and the normal response to RANKL by kindlin-3$^{-/-}$ osteoclasts provides a plausible explanation for the increased osteoclastogenesis in kindlin-3$^{-/-}$ bones.

M-CSF and RANKL treatment induced the expression of osteoclastogenic markers such as cathepsin K, MMP9, and calcitonin receptor in wild-type and kindlin-3$^{-/-}$ fetal liver cells (Fig. 2 B). Even though induction of marker gene expression was slightly delayed in kindlin-3$^{-/-}$ cells, they nevertheless reached wild-type levels 6 d after cytokine treatment (Fig. 2 B). It should be noted that the expression of kindlin-3 remained stable throughout the differentiation period, and that kindlin-1 and -2 were expressed in neither wild-type nor kindlin-3$^{-/-}$ cells upon cytokine treatment (Fig. 2 C).

Finally, we determined the number of nuclei in the osteoclasts as a marker for pre-osteoclast fusion and differentiation. Notably, in vitro generated kindlin-3$^{-/-}$ osteoclasts showed a lower tendency to form larger (>20 nuclei) polykaryons (Fig. 2 D), presumably because of decreased adhesion and cell spreading; however, a significant shift toward more multinucleated osteoclasts was detected in bone sections from kindlin-3$^{-/-}$ mice (Fig. 2 E). This discrepancy can be explained by the increased number of osteoclast precursors triggered by the elevated RANKL levels in kindlin-3$^{-/-}$ mice.

Published February 28, 2011

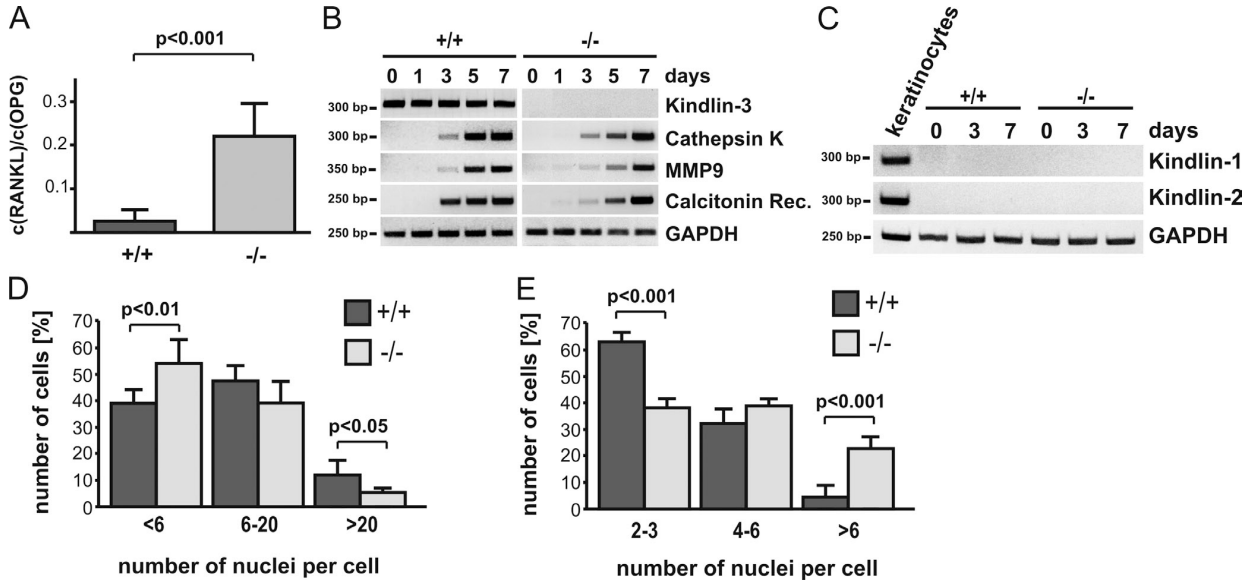

Figure 2. **Differentiation of kindlin-3$^{-/-}$ osteoclasts.** (A) RANKL/OPG ratio in plasma of P3 wild-type and kindlin-3$^{-/-}$ mice; $n = 11$. (B) RT-PCR of osteoclastogenic markers upon M-CSF and RANKL treatment of wild-type and kindlin-3$^{-/-}$ fetal liver cells. (C) RT-PCR of kindlin-1 and -2 expression during in vitro osteoclast differentiation. RNA from keratinocytes served as positive control. (D) Number of nuclei per osteoclast 5 d after induction of differentiation; 1,004 cells of each genotype obtained from five independent experiments were analyzed. (E) Osteoclast nuclear numbers determined from histological sections of P4 tibiae. 63 and 252 osteoclasts from wild-type and kindlin-3$^{-/-}$ bone sections were analyzed, respectively. Data are presented as mean ± SD (error bars). P-values indicate significant differences from wild-type (Student's *t* test).

Altogether, these data suggest that although osteoclast differentiation is slightly delayed in the absence of kindlin-3 in vitro, it occurs efficiently in kindlin-3$^{-/-}$ mice.

Kindlin-3 promotes osteoclast adhesion by regulating integrin activation

Kindlin-3 is required for the activation of integrins and integrin-mediated adhesion (Moser et al., 2008, 2009a). To evaluate osteoclast adhesion, we seeded wild-type and kindlin-3$^{-/-}$ osteoclasts on osteopontin, a natural ligand for osteoclasts. Although wild-type osteoclasts adhered readily to osteopontin, kindlin-3$^{-/-}$ osteoclasts showed significantly reduced adhesion (Fig. 3 A). Interestingly, kindlin-3$^{-/-}$ osteoclasts adhered to both glass and cell culture plastic, particularly when cultured over several days. Because the transmembrane proteoglycan CD44 has also been shown to support osteoclast adhesion to osteopontin, fibronectin, collagen, and laminin (Goodison et al., 1999; Ponta et al., 2003), we hypothesized that CD44 might mediate the remaining osteoclast adhesion in the absence of kindlin-3. To test this hypothesis, we incubated pre-osteoclasts with a blocking anti-CD44 antibody and observed that the adhesion of kindlin-3$^{-/-}$ cells to fibronectin was further reduced, which indeed indicates that CD44 contributes to osteoclast adhesion (Fig. S4, A and B).

To determine integrin expression, we measured their levels on macrophages, as the large size and strong adhesive properties of mature osteoclasts prevented their analysis by flow cytometry. Indeed, kindlin-3$^{-/-}$ macrophages express ∼76% and 63% of β1 and β3 integrins, respectively, when compared with wild-type macrophages. The expression of αvβ5, which decreases during osteoclast maturation, and α4β1, α5β1, and αLβ2 were similar in wild-type and kindlin-3$^{-/-}$ cells; however, αMβ2 was reduced to ∼80% in kindlin-3$^{-/-}$ cells. (Fig. 3 B and Fig. S4 C). Next, we addressed the affinity states of integrins by determining the binding of the 9EG7 antibody, which recognizes activated mouse β1 integrins, and the binding of a fluorescently labeled FN fragment (FNIII7-10), which is bound by active αv (αvβ3 and αvβ5) and α5β1 integrins. Resting kindlin-3$^{-/-}$ macrophages failed to bind 9EG7 and showed considerably reduced FNIII7-10 binding, whereas $MnCl_2$ treatment, which can bypass inside-out–mediated integrin activation, markedly increased 9EG7 and FNIII7-10 binding (Fig. 3, C and D). Furthermore, adhesion to ICAM-1, a ligand for β2 integrins, was strongly diminished in kindlin-3$^{-/-}$ macrophages compared with control cells (Fig. 3 E). Manganese treatment only partially rescued the adhesion defect of kindlin-3$^{-/-}$ cells, which suggests that kindlin-3 also operates in integrin outside-in signaling.

Collectively, these data indicate that loss of kindlin-3 results in a severe adhesion defect caused by impaired activation and outside-in signaling of β1, β2, and αv integrins.

Osteoclasts require kindlin-3 for integrin and growth factor signaling

Biochemical signaling events triggered by integrins and growth factor receptors control osteoclast adhesion, spreading, fusion, and differentiation (Ross and Teitelbaum, 2005). Wild-type osteoclasts generated from fetal liver cells differentiated into well-spread, multinucleated osteoclasts within 4–6 d of culture (Fig. 4 A). In contrast, kindlin-3$^{-/-}$ fetal liver cells, which also

Published February 28, 2011

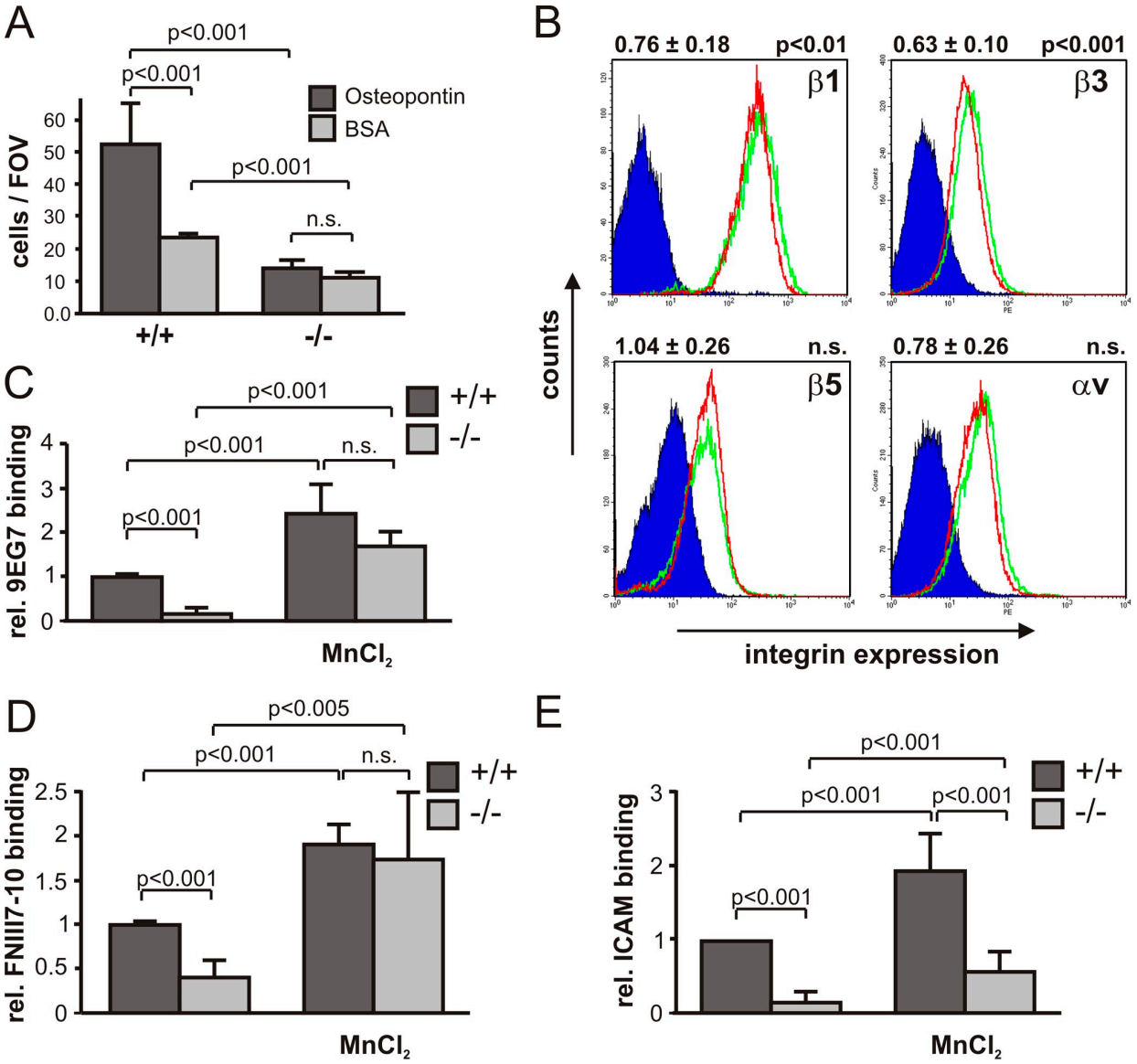

Figure 3. **Integrin defects in kindlin-3$^{-/-}$ osteoclasts.** (A) Adhesion of primary wild-type and kindlin-3$^{-/-}$ osteoclasts to osteopontin. Number of adherent cells per field of view (FOV) is shown. (B) Surface expression of β1, β3, β5, and αV integrins on wild-type (green) and kindlin-3$^{-/-}$ (red) macrophages. Isotype control staining is shown in dark blue. Numbers above graphs indicate integrin expression on kindlin-3$^{-/-}$ cells (mean ± SD) relative to wild-type cells (n = 6). (C) 9EG7 binding on wild-type and kindlin-3$^{-/-}$ macrophages in the presence or absence of 2 mM $MnCl_2$. (D) Binding of Alexa Fluor 647–labeled FNIII7-10 by wild-type and kindlin-3$^{-/-}$ macrophages in the presence or absence of 3 mM $MnCl_2$. Data show mean ± SD of four independent experiments and were subtracted by background binding of the isotype and EDTA control, respectively. (E) Wild-type and kindlin-3$^{-/-}$ macrophages plated on ICAM-1 in the presence or absence of 1 mM $MnCl_2$. P-values indicate significant differences from wild-type (Student's t test).

produced multinucleated TRAP-positive cells, failed to spread (Fig. 4 A). Phalloidin staining showed an actin belt beneath the plasma membrane of control osteoclasts, whereas kindlin-3$^{-/-}$ osteoclasts displayed randomly distributed actin patches in their cytoplasm (Fig. 4 B). Mn^{2+}-mediated activation of integrins was unable to improve the spreading defect, suggesting that kindlin-3 is also required for integrin outside-in signaling, which is central in organizing the osteoclast cytoskeleton (unpublished data). Retroviral expression of EGFP–kindlin-3 into kindlin-3$^{-/-}$ fetal liver cells rescued the formation of well-spread osteoclasts. Notably, expression of integrin-binding mutant EGFP–kindlin-3 (EGFP–kindlin-3–QA; Moser et al., 2008) did not rescue osteoclast spreading, whereas fusion significantly improved compared with cells infected with a control virus (Fig. S5, A and B).

Next, we analyzed whether integrin-mediated adhesion signaling can still occur in the absence of kindlin-3. Adhesion on vitronectin triggered phosphorylation of c-Src and focal adhesion kinase (FAK) in wild-type pre-osteoclasts, but induced only a weak phosphorylation in kindlin-3$^{-/-}$ pre-osteoclasts

Published February 28, 2011

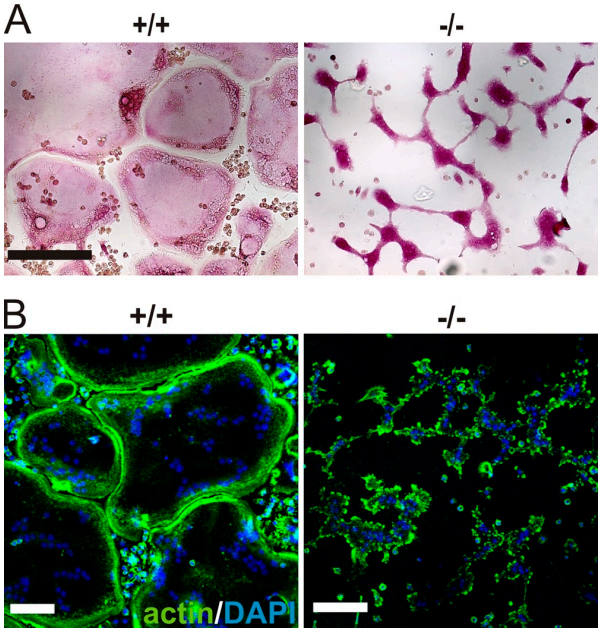

Figure 4. **Defective spreading of kindlin-3$^{-/-}$ osteoclasts.** (A) Wild-type and kindlin-3$^{-/-}$ osteoclasts grown on glass coverslips and stained for TRAP. (B) F-actin (stained with phalloidin, green) and nuclei (DAPI, blue) in wild-type and kindlin-3$^{-/-}$ osteoclasts. Bars, 100 µm.

(Fig. 5 A), further corroborating the finding that integrin-mediated signaling is severely compromised in the absence of kindlin-3. This weak activation is either triggered by integrin-independent signaling processes or by some residual integrin activity that exists even in the absence of kindlin-3.

A previous study demonstrated that loss of αvβ3 integrin function in osteoclasts can be compensated by high concentrations of M-CSF (Faccio et al., 2003b). To test whether kindlin-3 loss can also be overcome by high levels of cytokines, we treated wild-type and mutant fetal liver cells with RANKL and different concentrations of M-CSF. Wild-type fetal liver cells differentiated within 4 d into large, multinucleated osteoclasts when cultured at low M-CSF levels (20 ng/ml), whereas kindlin-3$^{-/-}$ fetal liver cells rarely fused into polykaryons. High levels of M-CSF (100 ng/ml) rescued polykaryon formation but not the spreading defect of kindlin-3$^{-/-}$ cells (Fig. 5 B). Moreover, although low levels of M-CSF failed to induce normal phosphorylation of Erk, Akt, and Syk in kindlin-3$^{-/-}$ osteoclasts, high levels were able to induce normal phosphorylation of these signaling proteins (Fig. 5 C), which suggests normal differentiation of kindlin-3$^{-/-}$ osteoclasts in the presence of high M-CSF levels.

Altogether, these findings show that kindlin-3 recruitment to integrins is required for their activation, actin reorganization, and cell spreading, as well as amplification of growth factor signaling in osteoclasts.

Kindlin-3 is required for the formation and arrangement of podosomes

Osteoclast adhesion is mediated by the formation of specialized adhesion structures called podosomes when they are cultured on glass or bone matrix. Wild-type pre-osteoclasts were able to form typical podosomes consisting of a central actin core surrounded by a ring of adhesion molecules including αv(β3) and β1 integrins, vinculin, paxillin, and talin (Fig. 6, A, C, and D; and not depicted). Kindlin-3$^{-/-}$ cells formed small, actin core–like structures surrounded by a diffuse actin cloud. Vinculin, talin, and paxillin colocalized with the actin cloud, whereas αv and β1 integrins were diffusely distributed throughout the plasma membrane (Fig. 6, A, C, and D; and not depicted). Fluorescence intensity profiling through actin-core units revealed that actin cores alternate with vinculin rings in wild-type podosomes, whereas this alternating pattern of actin and vinculin staining was lost in kindlin-3$^{-/-}$ cells (Fig. 6 B). Approximately half (59.9% ± 11.1%) of the actin dots from kindlin-3$^{-/-}$ cells were depleted of vinculin and considered to be podosome structures even though a discrete vinculin ring was rarely observed. Re-expression of GFP–kindlin-3 into kindlin-3$^{-/-}$ pre-osteoclasts restored the size of the F-actin dots and the ringlike distribution of vinculin around the F-actin cores (Fig. S5 C). On the contrary, the integrin-binding mutant EGFP–kindlin-3–QA did not rescue podosome formation in kindlin-3$^{-/-}$ pre-osteoclasts and showed a diffuse distribution throughout the cell membrane when expressed in control pre-osteoclasts (Fig. S5 C). The percentage of cells that form normal podosomes was similar in EGFP–kindlin-3–expressing control and kindlin-3$^{-/-}$ cells, whereas re-expression of the EGFP–kindlin-3–QA resulted in significantly fewer podosome-forming cells (Fig. S5 D). Re-expression of the integrin-binding mutant kindlin-3 did just partially improve the diffuse vinculin and F-actin localization in kindlin-3$^{-/-}$ cells (Fig. S5 C). In line with the normal podosome formation in EGFP–kindlin-3–expressing kindlin-3$^{-/-}$ cells, αv integrins colocalized with vinculin to podosome rings, whereas αv integrins were diffusively distributed in the membrane of kindlin-3$^{-/-}$ cells expressing an EGFP–kindlin-3–QA construct (Fig. S5 E). Finally, the resorptive activity of kindlin-3$^{-/-}$ osteoclasts expressing an EGFP–kindlin-3–QA was five times less compared with kindlin-3–deficient osteoclasts expressing wild-type EGFP–kindlin-3 (Fig. S5 F).

High-resolution scanning electron microscopy confirmed that kindlin-3$^{-/-}$ osteoclasts were able to form small actin patches, which were surrounded by a loose network of radial actin fibers (Fig. 7 A). In sharp contrast, control osteoclasts formed large actin cores within podosome clusters, which were extensively interconnected by thick actin bundles (Fig. 7 A). Despite their smaller size, the actin cores of kindlin-3$^{-/-}$ cells colocalized with cortactin, Arp2/3, and Wiskott-Aldrich syndrome protein (WASp), which are known core components of podosomes (Linder and Aepfelbacher, 2003), indicating that podosomal actin core formation occurs in the absence of kindlin-3 and activated integrins (Fig. 7, B–D).

Mature osteoclasts arrange their podosomes into different higher ordered structures. On glass, they form a ring at the periphery of the cell called the podosomal belt (Fig. 8 A); whereas on mineralized matrices, they form several smaller ringlike adhesion structures called sealing zones (Fig. 8 B; Jurdic et al., 2006). Kindlin-3$^{-/-}$ osteoclasts were not able to form podosomal rings on glass surfaces or on sealing zones

Published February 28, 2011

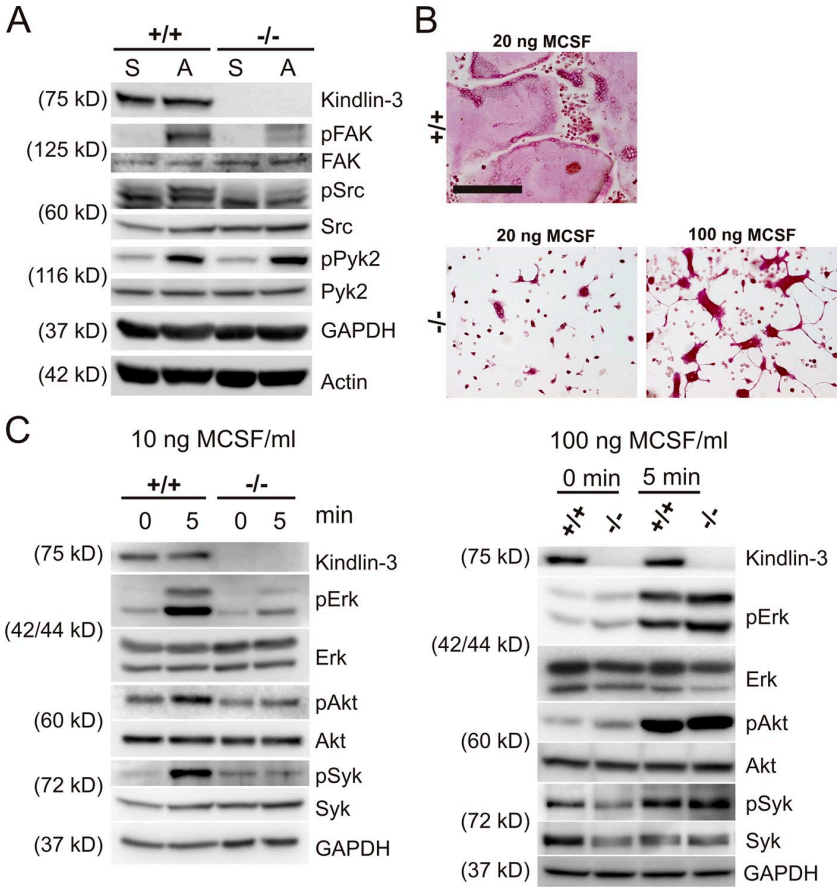

Figure 5. **Impaired adhesion and M-CSF signaling in kindlin-3$^{-/-}$ pre-osteoclasts.** (A) Wild-type and kindlin-3$^{-/-}$ pre-osteoclasts either maintained in suspension (S) or replated on vitronectin (A). Western blotting for kindlin-3, p-FAK, FAK, p-src, Src, p-Pyk2, and Pyk2. GAPDH and actin served as loading controls. (B) TRAP staining of wild-type and kindlin-3$^{-/-}$ osteoclasts treated with 40 ng/ml RANKL together with either 20 ng/ml or 100 ng/ml M-CSF. Bar, 250 µm. (C) Starved wild-type and kindlin-3$^{-/-}$ osteoclasts treated with either 10 ng/ml or 100 ng/ml M-CSF. Western blotting for activated Erk and Akt. Activated Syk was determined by immunoprecipitation followed by immunoblotting with anti-phosphotyrosine (4G10) antibody.

on bone matrices. F-actin and vinculin often colocalized in patches and were usually localized to the cell periphery (Fig. 8, A and B). The formation of podosomal belts and sealing zones requires an intact microtubule network (Destaing et al., 2003, 2005). We therefore analyzed microtubule organization and acetylation by immunofluorescence microscopy and Western blot analysis. Both the total and acetylated microtubule pools were similar between kindlin-3$^{-/-}$ and wild-type osteoclasts (Fig. 8, C and D). Furthermore, phosphorylation and the total amount of Pyk2, which is required for microtubule stability and acetylation in osteoclasts (Gil-Henn et al., 2007), were not altered in kindlin-3$^{-/-}$ cells (Fig. 5 A), an observation that was also made in β3 integrin–deficient osteoclasts (Faccio et al., 2003a).

These data indicate that kindlin-3 is not required for initial actin core formation. However, actin core maturation and interconnection, podosome formation, and their subsequent assembly into belts and sealing zones depend on kindlin-3.

β1, β2, and αv integrin classes are required for normal osteoclast function

αvβ3 integrin is considered the major functional integrin on osteoclasts. In contrast to the severe osteopetrotic phenotype of kindlin-3–deficient mice, however, loss of αvβ3 leads to a mild and protracted osteopetrosis in mice and humans. This discrepancy led us to hypothesize that additional integrins contribute to the kindlin-3$^{-/-}$ osteoclast defect. To test this, we established osteoclast cultures from mice lacking the β1, β2, or αv integrin genes, respectively, and from mice lacking a combination of two or all three integrin genes. In addition, we generated osteoclasts from β3 integrin–deficient mice to test whether other αv integrins in addition to αvβ3 play a significant role in osteoclast biology. Bone marrow cells with a single or αv/β1 or β1/β2 double integrin-null mutation differentiated into multinucleated, spread, and TRAP-positive osteoclasts. Osteoclasts lacking both αv and β2 integrins formed polykaryons but were less efficient in spreading and localizing their nuclei to the cell periphery (Fig. 9 A). Bone marrow cells lacking β1/β2/αv integrins were only able to form a few mono- and binucleated cells with TRAP activity, which suggests that loss of all integrin classes severely impairs osteoclastogenesis in vitro (Fig. 9 A). Notably, although these cells did not spread, they weakly adhered on glass.

Individual podosomes, podosome clusters, and podosome belts of β1, β2, and β1/β2 double integrin-null cells were indistinguishable from wild-type cells. αv- and β3-deficient cells showed smaller podosome clusters with irregular distributed podosome units (Fig. 9 B). Deletion of αv together with β1 or β2 integrins abolished cluster formation completely, and typical podosomes with a discrete vinculin ring were rarely

Published February 28, 2011

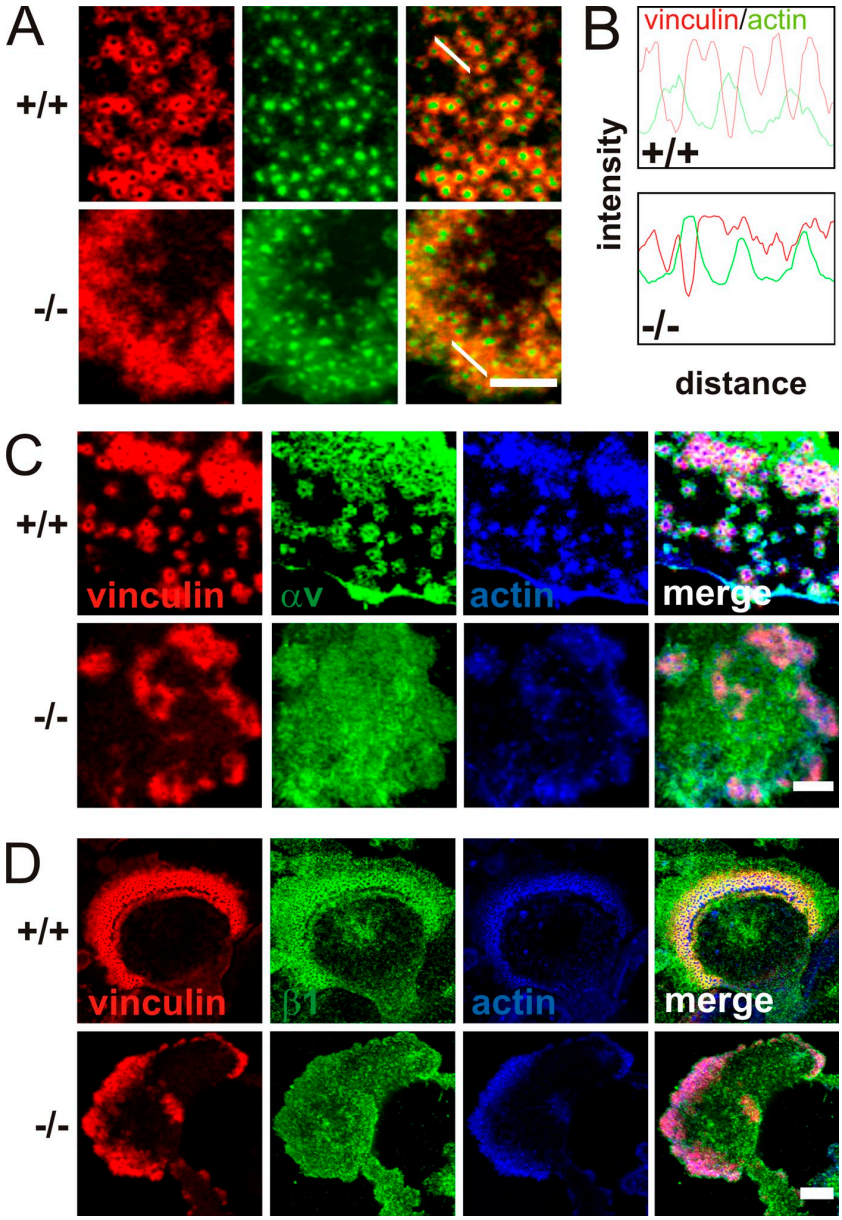

Figure 6. **Impaired podosome formation in kindlin-3$^{-/-}$ osteoclasts.** (A) Vinculin (red) and F-actin staining (phalloidin, green) of pre-osteoclasts plated on glass coverslips and observed by confocal microscopy. (B) Fluorescence intensity profile through three actin-core units (indicated by the white lines in A) of wild-type and kindlin-3$^{-/-}$ pre-osteoclasts. (C and D) vinculin (red) and F-actin staining (phalloidin, blue) together with αv integrin (green; C) or β1 integrin (green; D). Bars (A and C) 5 µm; (D) 10 µm.

observed (Fig. 9 B). Similar to loss of kindlin-3, cells lacking β1/β2/αv integrins formed small actin dots lacking an adhesion ring (Figs. 9 B and 6 A). In agreement with these observations, we found that the diameter of the actin core was significantly smaller (~650 nm) in podosomes from kindlin-3$^{-/-}$, β1/β2/αv triple-null, and αv/β1 and αv/β2 double-null pre-osteoclasts when compared with wild-type cells (~800 nm) or cells with a single integrin or a double β1/β2 integrin gene ablation (Fig. 9 C). Podosome belts of αv-deficient cells often failed to surround the entire cell and were significantly thinner than belts from β3-deficient cells, which showed a belt size that was intermediate between control and αv-deficient osteoclasts (Fig. 9, D and E). αv/β1 as well as αv/β2 integrin–deficient osteoclasts showed even thinner actin belts, which contained fewer and irregularly localized actin dots (Fig. 9, D and E).

Finally, we differentiated bone marrow–derived cells on a calcified matrix and evaluated their sealing zones and their capability to resorb matrix. The absence of a single integrin or the simultaneous loss of β1 and β2 still allowed sealing zone formation (Fig. 10 A), whereas the absence of αv together with either β1 or β2 integrins abolished the formation of a distinct ring (Fig. 10 A). The resorptive activity of αv/β1- and αv/β2-deficient osteoclasts was reduced to 30% of the wild-type level. Despite the presence of sealing zones in single integrin-null osteoclasts, their resorptive activity was diminished by 50%, indicating that each individual integrin family member contributes to functional sealing zone formation and bone degradation (Fig. 10 B).

Published February 28, 2011

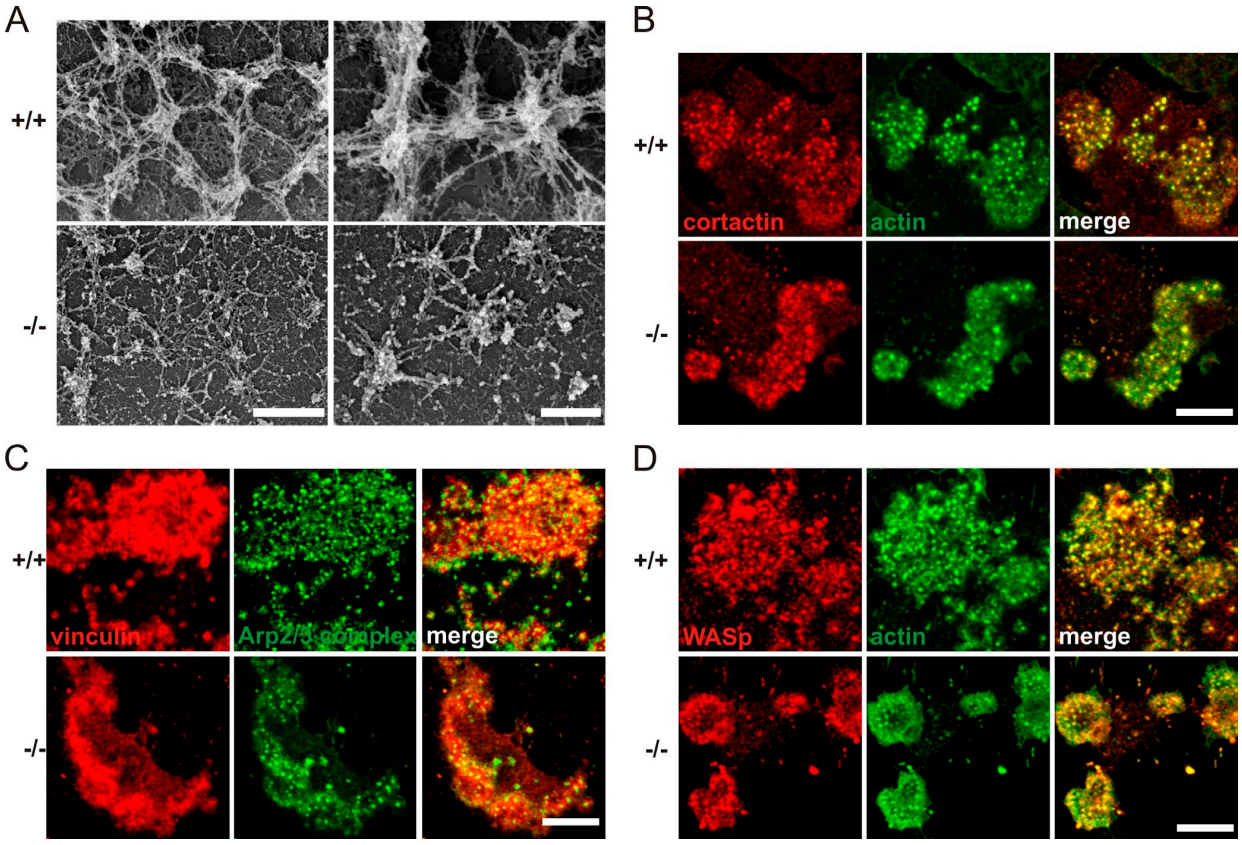

Figure 7. **Podosomal actin core formation is not abolished in kindlin-3$^{-/-}$ cells.** (A) Scanning electron microscopy of basal membrane preparations of wild-type and kindlin-3$^{-/-}$ osteoclasts. (B–D) Colocalization of cortactin (red) and F-actin (phalloidin, green; B), F-actin (red) and Arp2/3 (green; C), and WASp (red) and F-actin (green; D) in podosome clusters of wild-type and kindlin-3$^{-/-}$ pre-osteoclasts analyzed by confocal microscopy. Bars: (A, left) 1 µm; (A, right) 500 nm; (B–D) 10 µm.

Discussion

Several LAD-III patients have displayed increased bone mineral density (Kilic and Etzioni, 2009; Malinin et al., 2009; McDowall et al., 2010; Sabnis et al., 2010), which points to the possibility that kindlin-3 plays a role in bone homeostasis. In search for an explanation of this observation, Malinin et al. (2009) reported that mesenchymal stem cells isolated from LAD-III patients produced significantly higher amounts of cartilage and bone in transplantation experiments, and concluded that the increased bone mass was caused by increased matrix deposition by hyperactive osteoblasts. Although kindlin-3 is highly and exclusively expressed in hematopoietic cells, osteoblasts express kindlin-2 but lack kindlin-3 expression, which suggests that the increased bone mass in LAD-III patients either developed independently of kindlin-3 or was caused by a dysfunction of a cell type other than osteoblasts. In this paper, we tested this hypothesis by analyzing bone formation in mice lacking kindlin-3.

Kindlin-3$^{-/-}$ mice develop a severe osteopetrosis that is already apparent at birth. When we first analyzed the osteoblasts of kindlin-3–deficient mice in vivo and in vitro, we found that they appeared normal in terms of their numbers, morphological appearance, localization to the bone, expression of marker genes, and matrix production. The only abnormality we could detect was a significantly elevated RANKL/OPG ratio in the serum of kindlin-3$^{-/-}$ mice. RANKL secretion by osteoblasts is triggered in response to PTH, which is released by the parathyroid gland when serum Ca^{2+} levels decrease because of diminished bone resorption (Grant et al., 1990; Suda et al., 1999). An immediate consequence of high RANKL levels is enhanced differentiation of osteoclasts, which derive from the monocytic lineage and express high levels of kindlin-3. Indeed, we found reduced levels of Ca^{2+} and markedly increased levels of PTH in the blood of kindlin-3$^{-/-}$ mice. Consistent with the high circulating RANKL levels, we found a dramatic increase in the number of multinucleated osteoclasts in bones of kindlin-3$^{-/-}$ mice. These osteoclasts, however, completely failed to degrade bone matrix in vitro. In search for a mechanistic explanation for the dysfunction of kindlin-3$^{-/-}$ osteoclasts, we identified several cellular defects that could be ascribed to kindlin-3's principal task to activate several classes of integrins and subsequently mediate their outside-in signaling properties.

Our findings show that differentiation of kindlin-3$^{-/-}$ osteoclasts is slightly delayed and that fusion into multinucleated polykaryons is less efficient under in vitro conditions. However, the number of large polykaryons is significantly higher in kindlin-3$^{-/-}$ bones. This is most likely caused by increased RANKL-induced osteoclastogenesis that compensates

Published February 28, 2011

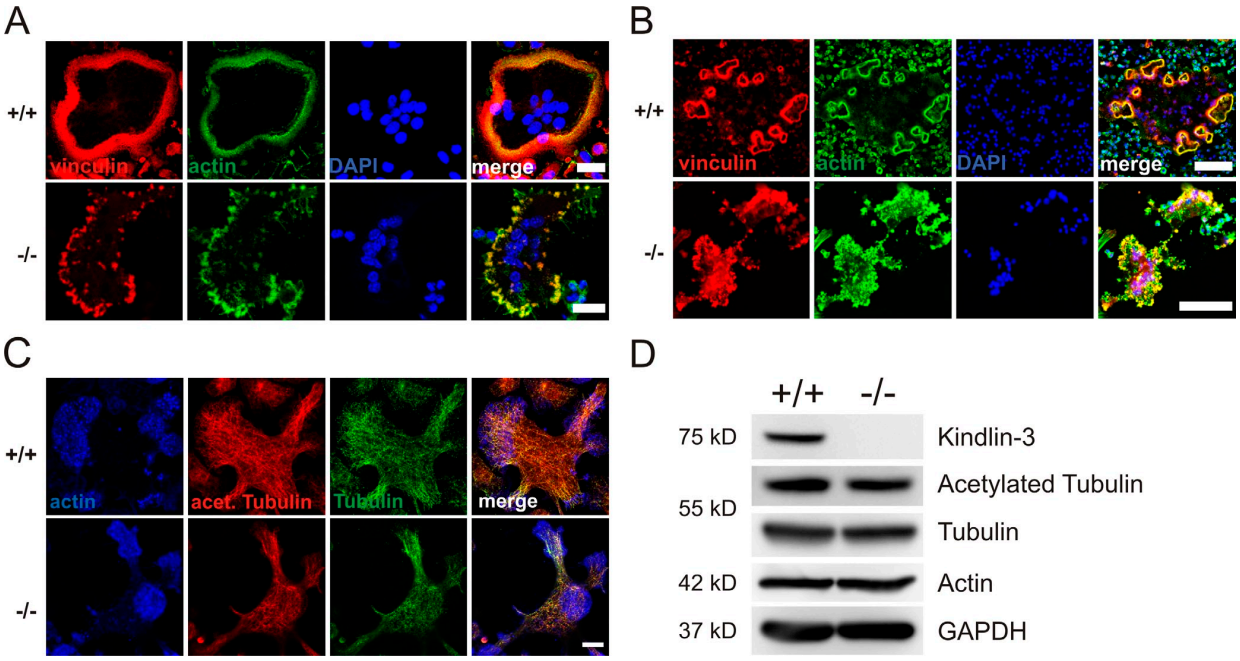

Figure 8. **Abnormal F-actin distribution but normal microtubule organization and acetylation in kindlin-3$^{-/-}$ osteoclasts.** (A) Vinculin (red) and F-actin staining (phalloidin, green) of wild-type and kindlin-3$^{-/-}$ osteoclasts plated on glass coverslips. (B) Vinculin (red) and F-actin staining (phalloidin, green) of wild-type and kindlin-3$^{-/-}$ osteoclasts plated on mineral surface of osteologic slides. DAPI (blue) shows nuclei (A and B). (C) Wild-type and kindlin-3$^{-/-}$ osteoclasts were labeled with phalloidin (blue), anti-acetylated tubulin (green), and anti-tubulin antibodies. (D) Cell lysates from wild-type and kindlin-3$^{-/-}$ osteoclasts were immunoblotted with antibodies against kindlin-3, acetylated tubulin, and tubulin. Antibodies against actin and GAPDH were used as loading controls. Bars: (A) 25 µm; (B) 100 µm; (C) 10 µm.

the fusion defects in vivo. Although TRAP-positive, multinucleated kindlin-3$^{-/-}$ osteoclasts are present at very high numbers in kindlin-3$^{-/-}$ mice, their shape and ability to adhere to bone surfaces is severely impaired. Similarly, adhesion to and binding of several extracellular matrix proteins and to ICAM-1 is also almost completely abrogated. We have previously shown that kindlin-3 interaction with β1 and β3 tails is required to activate platelet integrins and that binding to β2 tails is required to activate leukocyte integrins (Moser et al., 2008, 2009a). Our findings here demonstrate that this essential function of kindlin-3 is also conserved in osteoclasts. Osteoclasts require kindlin-3 to mediate β1 and αv integrin binding to fibronectin and osteopontin and β2 integrin binding to ICAM-1. This suggests that αvβ3 integrins, considered the most important integrin class

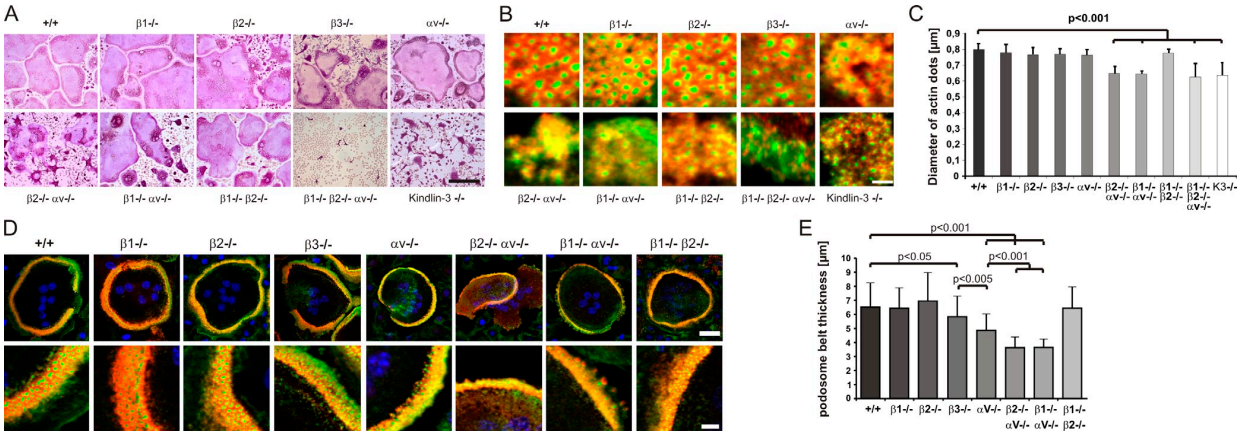

Figure 9. **Podosomes and actin belts in integrin-deficient osteoclasts.** (A) Wild-type and single, double, and triple integrin-deficient osteoclasts stained for TRAP. (B) Vinculin (red) and F-actin staining (phalloidin, green) of wild-type and integrin-deficient pre-osteoclasts plated on glass. (C) Diameters of actin dots in pre-osteoclasts with indicated genotypes measured using MetaMorph software; *n* = 6/5/5/8/9/6/6/6/8/9 different cells from each genotype taken to measure the actin core size. (D) Vinculin (red) and F-actin staining (phalloidin, green) of wild-type and integrin-deficient osteoclasts plated on glass. DAPI (blue) shows nuclei. (E) Diameter of podosomal belts of wild-type and integrin-deficient osteoclasts plated on glass. Data are presented as mean ± SD (error bars). P-values indicate significant differences from wild-type (Student's *t* test). Bars: (A) 100 µm; (B) 2 µm; (D, top) 25 µm; (D, bottom) 5 µm.

Published February 28, 2011

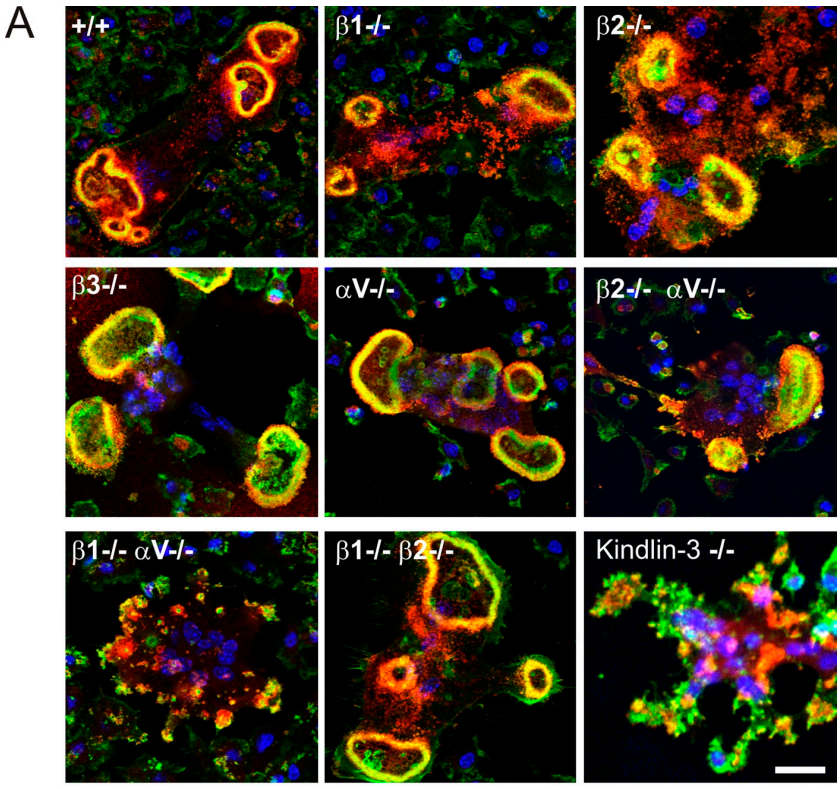

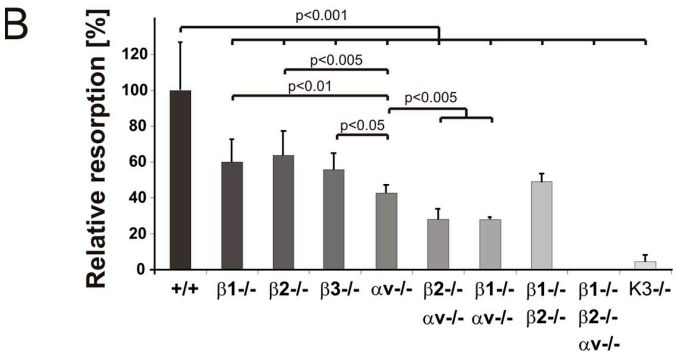

Figure 10. **Sealing zones of integrin-deficient osteoclasts.** (A) Vinculin (red) and F-actin staining (phalloidin, green) of wild-type and integrin-deficient osteoclasts plated on a mineral surface. DAPI staining (blue) shows nuclei. Bar, 25 µm. (B) Resorption activity of wild-type and integrin-deficient osteoclasts plated on calcium apatite-coated slides quantified with MetaMorph. Number of analyzed slides per genotype: n = 26/6/6/6/6/3/3/3/8. Data are presented as mean ± SD (error bars). P-values indicate significant differences from wild-type (Student's t test).

of osteoclasts, are just one of several integrin players during osteoclast-mediated bone resorption. This finding was corroborated by a series of genetic experiments in which we ablated several integrin genes either individually or in combination in osteoclasts. The experiments revealed an already strongly reduced resorptive activity of osteoclasts when the β1, β2, or αv integrin genes were individually ablated, and a further functional decline when two integrin classes were absent from osteoclasts. The finding that αv-deficient osteoclasts show a significantly more pronounced defect in matrix degradation compared with β3-deficient osteoclasts corroborates our hypothesis that other integrins beside αvβ3 also play an important role in osteoclast function. The ablation of all three integrin classes does not permit osteoclast development in vitro. This made it impossible to test their resorptive activity. In light of the severe defects in osteoclasts lacking two classes of integrins, it is fair to assume that loss of all three integrin classes leads to a further impairment. These findings provide an explanation for the much more severe osteopetrotic phenotype of kindlin-3$^{-/-}$ mice compared with β3 integrin mutants. Interestingly, in contrast to the failure of osteoclast differentiation in the absence of β1, β2, and αv integrins, kindlin-3 deficiency does not impair osteoclast differentiation both in vivo and in vitro. The reason for this observation is not clear. Because kindlins and talins shift the equilibrium of integrins toward their activation state, it is possible that certain processes such as cell fusion can proceed with just a few activated integrins and thus do not require the kindlin-3–mediated equilibrium shift, whereas other processes such as adhesion and podosome formation require a larger number of activated integrins. These questions can be addressed with osteoclasts of engineered mice carrying hypomorphic alleles for β1, β2, and αv integrins. If true, very low levels of integrins

Published February 28, 2011

should allow cell fusion but not bone resorption to proceed. An alternative scenario could be that cells that are plated for several days in the presence of serum and integrin ligands can activate integrins from outside and trigger integrin signaling even without efficient inside-out signaling. This is obviously not possible in the absence of all integrin classes.

Loss of kindlin-3 expression or a triple knockout of the β1, β2, and αv integrin genes is also accompanied by impaired podosome formation. Podosomes consist of an integrin ring and a central actin core. Interestingly, small actin cores containing core proteins such as cortactin, Arp2/3, and WASp form in kindlin-3–deficient osteoclasts. Similarly, β1/β2/αv-integrin deficient macrophages also form actin cores with a reduced diameter, indicating that the induction of actin polymerization occurs independently of integrin action, whereas their maturation requires an integrin signaling program. This observation is in agreement with previous studies showing that actin core formation and osteoclast adhesion to the substratum can also be mediated by the transmembrane proteoglycan CD44 in an integrin-independent manner (Chabadel et al., 2007). Actin cores lacking an adhesion ring are also found in c-src–deficient osteoclasts, which suggests that c-src activity is central for their maturation and acts as an upstream signaling molecule required for the assembly of integrins and cytoplasmic adhesion proteins (Destaing et al., 2008; Saltel et al., 2008).

Treatment of kindlin-3$^{-/-}$ osteoclasts with Mn^{2+} significantly improved integrin-mediated adhesion but restored neither the defective F-actin reorganization nor podosome organization and assembly. This finding is in agreement with several reports demonstrating that kindlins mediate both inside-out as well as outside-in integrin signaling (Larjava et al., 2008; Moser et al., 2009b; Plow et al., 2009). Moreover, this interesting observation also indicates that integrin arrangement around F-actin cores cannot be accomplished solely by an active integrin; kindlin-3 and/or kindlin-3–associated proteins are required in addition. Another consequence of the abrogated integrin outside-in signaling in kindlin-3$^{-/-}$ osteoclasts includes diminished FAK and Syk activation upon adhesion to extracellular matrix and impaired Erk and Akt phosphorylation that is seen only upon treatment with low concentrations of M-CSF, whereas high M-CSF levels are associated with normal Erk and Akt phosphorylation, indicating that integrin outside-in signals represent an amplifier of M-CSF–induced c-Fms signaling.

This study shows for the first time that osteoclast-mediated bone resorption depends on multiple integrin classes, which are under control of kindlin-3. Further work will be required to elucidate the individual contributions of each integrin subclass during podosome maturation and assembly, and whether certain signaling pathways that control the organization of the cytoskeleton and the formation of sealing zones are directed by specific integrins in osteoclasts.

Materials and methods

Reagents

Recombinant murine M-CSF and receptor activator of NF-κB ligand (RANKL) were obtained from R&D Systems and PeproTech, respectively. Osteopontin was purified from bovine plasma (provided by D. Heinegard, University of Lund, Lund, Sweden; Franzén and Heinegård, 1985).

Mice

Kindlin-3$^{-/-}$ and integrin β3$^{-/-}$ mice have been described previously (Hodivala-Dilke et al., 1999; Moser et al., 2008). Multiple integrins were deleted by intercrossing mice carrying conditional null mutations in the αv ($\alpha v^{flox/flox}$) and β1 ($\beta 1^{flox/flox}$) genes (Potocnik et al., 2000), a constitutive null mutation in the β2 (β2$^{-/-}$) gene (Scharffetter-Kochanek et al., 1998), and the Mx1Cre transgene (Kühn et al., 1995). All mice were from a mixed 129/SvJxC57BL/6 background. Cre expression in the hematopoietic system was induced by a single intraperitoneal injection of 250 mg polyI/C (GE Healthcare). 7 d after polyI/C treatment, bone marrow cells were isolated and checked for integrin surface expression via FACS. All animals were kept under specific pathogen-free conditions at the animal facility of the Max Planck Institute of Biochemistry.

Antibodies

The following antibodies were used for immunostaining of cells: mouse anti-vinculin antibody, mouse anti-talin, mouse anti-cortactin, rabbit anti-actin, and mouse anti-acetylated tubulin (all from Sigma-Aldrich); rat anti-tubulin, rat anti-integrin β1, and rat anti-integrin αv (all from Millipore); mouse anti–p-Tyrosine (clone pY99) and mouse anti-WASp (both from Santa Cruz Biotechnology, Inc.); rabbit anti-p16 subunit of Arp2/3 complex (Abcam); and FITC and Cy3-labeled secondary antibodies (Jackson ImmunoResearch Laboratories, Inc.). Phalloidin dyes were obtained from Invitrogen.

The following antibodies were used for flow cytometry: hamster IgG anti-integrin β1, isotype control hamster IgG, and isotype control mouse IgG1 (all from Biolegend); rat IgG2a anti-integrin β2, rat IgG2a anti-integrin β7, rat IgG2a anti-integrin α4, rat IgG2a anti-integrin α5, rat IgG2a anti-integrin αL, rat IgG1 anti-integrin αv, isotype control rat IgG1, isotype control rat IgG2a, and rat anti-integrin β1 clone 9EG7 (all from BD); and hamster IgG anti-integrin β3, mouse IgG1 anti-integrin β5, and rat IgG2b anti-integrin αM, isotype control rat IgG2b (all from eBioscience).

The following antibodies were used for Western blotting: mouse anti–glyceraldehyde 3-phosphate dehydrogenase (anti-GAPDH; Merck); rabbit anti-actin and mouse anti-talin (both from Sigma-Aldrich); rabbit anti-JNK, rabbit anti-pJNK Thr183/Tyr185, rabbit anti-p38, rabbit anti-pp38 Thr180/Tyr182, rabbit anti-pSrc Tyr418, rabbit anti-Pyk2, rabbit anti-pPyk2 Tyr402, rabbit anti-P42/44 MAPK, rabbit anti-pP42/44 MAPK Thr202/Tyr204, rabbit anti-Akt, and rabbit anti-pAkt Ser473 (all from Cell Signaling Technology); rabbit anti-FAK and rat anti-tubulin (both from Millipore); rabbit anti-pFAK Tyr397 and rabbit anti-src (both from Invitrogen); and mouse anti-Syk (Abcam).

Histology

Long bones were dissected, freed from soft tissue, and either embedded in plastic (Osteo-Bed Bone Embedding kit, Polysciences Inc.) or decalcified in 10% EDTA/PBS and embedded in paraffin. Paraffin sections were stained with hematoxylin and eosin and for TRAP activity using a commercial kit (Sigma-Aldrich). AP and van Kossa staining were performed according to standard protocols. The number of nuclei in osteoclasts was determined in plastic embedded bone sections from three different 4-d-old animals.

Pictures were taken by bright field microscopy with a microscope (Axioskop; Carl Zeiss, Inc.) equipped with a camera (DC500; Leica), 10× NA 0.3, 20× NA 0.50, and 40× NQ 0.75 objectives, and IM50 software. Pictures were edited with Photoshop (Adobe).

Measurement of RANKL, OPG, and PTH concentrations

Blood was collected from P2–P5 mice after decapitation using a microvette (CB 300 LH; Sarstedt); samples were then centrifuged for 3 min at 7,000 *g* and the plasma was harvested. The concentrations of RANKL and OPG were determined with ELISA kits from R&D Systems, and the intact PTH concentration was determined with an ELISA kit from Immutopics International.

Osteoclast culture

Osteoclasts were differentiated in vitro either from fetal liver cells or from bone marrow. E14.5 wild-type and kindlin-3$^{-/-}$ fetal liver cells were obtained by pushing the fetal liver through a 70-µm cell strainer (BD). The cells were kept in α-MEM supplemented with 20 ng/ml M-CSF overnight (ON). Nonadherent cells were collected after 24 h. Leukocytes were isolated from the interface after centrifugation at 1,000 *g* for 20 min in leukocyte separation medium (Laboratoires Eurobio), then washed with α-MEM medium and seeded at a concentration of 2,000 cells/mm^2 in osteoclast differentiation medium (α-MEM containing 10% heat inactivated FCS, 100 U/ml penicillin, and 100 µg/ml streptomycin with 50 ng/ml M-CSF and 40 ng/ml RANKL). Cells were cultured at 37°C in 5% CO_2 for 5–8 d, and medium was changed every second day. Staining for TRAP

Published February 28, 2011

activity was performed after 5 d in culture. Pictures were taken with a microscope (Axioskop) using a 20× NA 0.50 objective (see Histology).

For pre-osteoclast generation, 5×10^6 interface cells were plated on a 10-cm dish and cultured in osteoclast differentiation medium for 2 d. Cells were washed with PBS and lifted with 10 mM EDTA in PBS. Adherent cells that were treated with osteoclast differentiation medium for at least 2 d but had yet not fused into polykaryons were defined as pre-osteoclasts.

Isolation and functional assays with primary osteoblasts

Mouse calvarial osteoblasts were isolated from newborn mice as described previously (Wu et al., 1992). 8×10^4 primary osteoblasts were cultured in α-MEM in a 12-well plate until confluence. Osteoblastogenic medium (α-MEM, 10% FCS, 5 mM β-glycerophosphate, and 10 mg/ml ascorbic acid) was added to induce osteoblast differentiation. Osteoblast identity was confirmed at day 4 of differentiation by RT-PCR for AP, osteocalcin, and collagen I expression.

AP staining was performed on osteoblasts fixed in 4% PFA for 15 min and stained with DIG III solution (0.4% nitro-blue tetrazolium chloride [NBT]/5-bromo-4-chloro-3′-indolyphosphate p-toluidine salt [BCIP], 0.4 M Tris-HCl, pH 9.5, 0.4 M NaCl, and 0.2 M $MgCl_2$). To determine AP activity, osteoblasts from 12-well plates were collected in 500 µl lysis buffer (10 mM Tris-HCl, pH 7.5, 0.5 mM $MgCl_2$, 0.1% Triton X-100, and 1× protease inhibitors) and homogenized by sonication for 20 s followed by centrifugation. 50 µl of the supernatant was mixed with 50 µl of 10 mM p-nitrophenylphosphate (Sigma-Aldrich) in 0.1 M glycine, 1 mM $MgCl_2$, and 1 mM $ZnCl_2$, pH 10.4, and incubated for 30 min at 37°C. 50 µl 1 M NaOH was added to stop the reaction, and absorption at 405 nm was measured. Assays were performed in triplicate and the AP activity was normalized to the initial protein content.

Alizarin red S (ARS) staining and quantification of in vitro mineralization of osteoblasts was performed at day 21 after induction of osteoblast differentiation as described previously (Gregory et al., 2004). In brief, cells were fixed in 4% PFA for 15 min at RT, washed twice with ddH_2O, and incubated with 2% ARS, pH 4.2 (adjusted with NH_4OH) for 20 min while shaking. Cells were washed five times with ddH_2O for 5 min each and pictured. Bound ARS was dissolved in 10% acetic acid for 30 min at RT. The cell layer was scraped from the plate, transferred to a reaction tube, and vigorously shaken for 30 s. The suspension was overlayed with mineral oil, heated to exactly 85°C for 10 min, and kept on ice for 5 min. After centrifugation at 20,000 *g* for 15 min, two equivalents of 10% NH_4OH were added to five equivalents of ARS solution to get a pH of 4.1–4.5. This solution was measured at 405 nm in triplicate.

Pictures were obtained using a stereomicroscope (MZ FLIII; Leica) equipped with a Plan-Apochromat 1.0× objective, a ProgRes C14 camera, and Photoshop (Adobe) software.

RT-PCR

RT-PCR was used to examine the expression levels of osteoclast and osteoblast marker genes. Osteoclasts were obtained as described; cells at time point day 0 were taken immediately after performing the gradient centrifugation, cells at time point day 1 were cultured for 24 h in differentiation medium containing RANKL and M-CSF, and so on.

Total RNA was isolated using an RNeasy kit (QIAGEN). cDNA was obtained using the SuperScriptTM III Reverse transcription kit (Invitrogen). The following primers were used: calcitonin receptor 1b forward, 5′-TTTACCGACGAGCAACGCCTACGC-3′, and reverse, 5′-CATGTAGGACTCGGCCTCGTGGG-3′; cathepsin K forward, 5′-GCTATATGACCACTGCTTTCCAATACG-3′, and reverse, 5′-ACTGCATGGTTCACATTATCACGGTC-3′; GAPDH forward, 5′-TCGTGGATCTGACGTGCCGCCTG-3′, and reverse, 5′-CACCACCCTGTTGCTGTAGCCGT-3′; collagenI forward, 5′-AAGAGGCGAGAGAGGTTTCC-3′, and reverse, 5′-ATCACCAGGTTCACCTTTCG-3′; kindlin-3 forward, 5′-AGCTGTCTCTGCTGCGTGCTC-3′, and reverse, 5′-ATACCTTGCTGCATGAGGCAC-3′; MMP9 forward, 5′-CGAGTGGACGCGACCGTAGTTGG-3′, and reverse, 5′-CAGGCTTAGAGCCACGACCATACAG-3′; kindlin-1 forward, 5′-CTACACCTTCTTTGACTTG-3′, and reverse, 5′-AGGGATGTCAGTTATGTC-3′; kindlin-2 forward, 5′-GTACCGAAGTAGACTGCAAGG-3′, and reverse, 5′-CATACGGCATATCAAGTAGGC-3′; AP forward, 5′-CCTTTGTGGCTCTCTCCAAG-3′, and reverse, 5′-CTGGCCTTCTCATCCAGTTC-3′; and osteocalcin forward, 5′-AAGCAGGAGGGCAATAAGGT-3′, and reverse, 5′-AGCTGCTGTGACATCCATAC-3′.

Adhesion assays

12-mm glass slides were coated for 6 h at RT with 5 µg/ml bovine osteopontin in PBS or with 3% BSA. The adhesion assay was performed with osteoclasts, which were directly isolated from long bones as described previously (Flores et al., 1992; Ek-Rylander et al., 1994). In brief, all four legs of newborn wild-type and kindlin-$3^{-/-}$ mice were minced and rotated for 1 h at 37°C in α-MEM containing 10% FCS. Afterward, the freed cells were seeded onto the coated-glass slides for 1 h and the slides were carefully washed with medium to remove nonadherent cells. The adherent cells were allowed to spread ON and were then TRAP-stained.

Macrophage adhesion on ICAM-1 was performed as described previously (Chavakis et al., 2008). In brief, 96-well plates were coated with 4 µg/ml recombinant human ICAM-1 (R&D Systems) in coating buffer (150 mM NaCl, 20 mM Tris-HCl, and 2 mM $MgCl_2$, pH 9) ON at 4°C, blocked with 3% BSA in PBS for 1 h at RT, then incubated with 50,000 macrophages for 30 min in a tissue culture incubator in the presence or absence of 1 mM $MnCl_2$. Each condition was assayed in quadruplet. After washing with PBS containing 1% BSA, adherent cells were fixed in 4% PFA for 10 min and stained with 5 mg/ml crystal violet in 2% ethanol for 30 min. After washing, the remaining dye was dissolved in 2% SDS. Staining intensity was measured in an ELISA plate reader at 550 nm.

Resorption assay

Osteoclasts isolated from bones of P2–P4 wild-type and kindlin-$3^{-/-}$ mice or in vitro differentiated from fetal liver cells or bone marrow were plated in osteoclast differentiation medium on osteologic slides (BD) for 1 wk. To quantify matrix resorption, cells were removed from the slides by treating them with 1% Triton X-100 and mechanical agitation, pictures were obtained with a microscope (Axioskop; 20× NA 0.50 objective, see Histology), and the resorbed area was measured using MetaMorph software. Alternatively, cells were cultured on dentin discs (Immunodiagnostic Systems) and resorption pits were visualized by staining with 1% toluidine blue in 0.5% sodium tetraborate for 3 min.

Immunofluorescence

Cells were plated on 12-mm coverslips coated with FCS for 1 h at 37°C, fixed with 4% PFA in PBS for 10 min or with 4% PFA for 1 min followed by a methanol fixation for 10 min at −20°C, and permeabilized with 0.25% Triton X-100 in PBS for 20 min. Blocking was performed for 1 h with 3% BSA in PBS. Cells were then incubated with the primary antibody in blocking solution for 3 h at RT or at 4°C ON. F-actin was visualized with Alexa Fluor 488–Phalloidin or Alexa Fluor 647–Phalloidin. Cells were imaged at RT with a SP2 confocal microscope (DMIRE2; Leica) using Leica Confocal Software (version 2.5 Build 1227) with 40× NA 1.25 and 100× NA 1.40 oil objective lenses. Single channels were imaged sequentially. All pictures were processed with Photoshop (Adobe).

Actin core size was measured in the actin channel by using MetaMorph software from at least six cells of each genotype. 50 actin dots were measured from each individual cell. The podosome belt size was obtained by measuring the thickness of the vinculin ring of at least 20 belts from osteoclasts that were differentiated in three or more independent preparations. Actin cores from at least 10 different pre-osteoclasts were analyzed. From each cell, 25 actin cores were analyzed.

Retroviral infections

EGFP–kindlin-3 and EGFP–kindlin-3–QA constructs (Moser et al., 2008) were amplified and directionally cloned using the EcoRI and BamHI sites of the pCLMFG retroviral vector (Naviaux et al., 1996). Vesicular stomatitis virus G–pseudotyped retroviral vectors were produced by transient transfection of 293T (human embryonic kidney) cells. Viral particles were concentrated from cell culture supernatant as described previously (Pfeifer et al., 2000) and used for infection of fetal liver cells. Fetal liver cells were prepared for differentiation into osteoclasts as described. Cells were cultured in medium containing 10 ng/ml M-CSF and 40 ng/ml RANKL for 5 d, and were used for TRAP and immunofluorescence staining and matrix degradation assays, or were lysed for Western blotting.

Gelatin zymography

Osteoclasts were isolated from bones of P2–P4 wild-type and kindlin-$3^{-/-}$ mice, plated in osteoclast differentiation medium in a single 24 well for about 1 wk, and washed and incubated with serum-free α-MEM for 24 h. The conditioned medium was harvested, concentrated in Centricon filter units (10 kD cut-off; Millipore), mixed with nonreducing SDS sample buffer, and run on an SDS gel with a 4% stacking gel and a 12% running gel containing 0.2% gelatin. Gels were incubated twice for 15 min at RT in 0.2% Triton X-100 in ddH_2O and then for several days at 37°C in MMP reaction buffer (50 mM Tris-HCl, pH 7.5, 0.2 M NaCl, 5 mM $CaCl_2$, and 0.02% NaN_3). The bands of gelatinolytic activity were revealed after staining with Coomassie blue.

Published February 28, 2011

Cathepsin K activity measurement
Functional cathepsin K concentration was measured in protein lysates of cultured osteoclasts using a Cathepsin K Activity Assay kit (BioVision, Inc.). The assay was performed according to the manufacturer's instructions using 50 µg protein lysate per measurement.

Bone mineral density and histomorphometric measurements
pQCT of the distal femur was performed with XCT Research SA+ (StraTec Medizintechnik). Bone density was measured exactly in the middle of the bone length using peel mode 2 with the threshold set at 100. Calcein labeling was performed as follows: 50 µl of 5 mg/ml calcein (Sigma-Aldrich) in 0.9% NaCl and 50 mM $NaHCO_3$ was injected at P0 and exactly 24 h later intraperitoneally. Mice were sacrificed 15 h after the second injection and long bones were dissected, fixed in 70% ethanol, and embedded in polymethylmethacrylate. 3-µm sections of the distal femur were deplasticized and stained for Masson-Goldner with hematoxylin (Gill II; Carl Roth), acid fuchsin-ponceau xylidine, and phosphomolybdic acid-orange G for visualizing cells, and osteoid and light green for visualizing mineralized matrix. Cancellous bone was examined in the 1-mm band below the growth plate, whereas primary cancellous bone was examined in the first 200 µm and secondary cancellous bone in the remaining 800 µm. Data presented were combined for both types. Histomorphometric analysis was performed according to the standards set forth by the American Society for Bone and Mineral Research (Parfitt et al., 1987). The following parameters were examined: osteoid surface (OS), bone surface (BS), osteoblast number (Ob.N), osteoclast number (Oc.N), and osteoclast surface (Oc.S). Measurements were performed by a person blinded to the genotype of the mice.

Flow cytometry
Fetal liver cell–derived macrophages and pre-osteoclasts were incubated with Fc receptor–blocking antibody (Millipore) and then with the appropriate fluorophore-conjugated monoclonal antibodies for 30 min on ice. Analysis was performed with a FACSCalibur (BD). β1 integrin activation was induced with 2 mM Mn^{2+} and analyzed with the 9EG7 antibody and a fluorophore-conjugated anti–rat antibody. 9EG7 binding was normalized to β1 integrin surface levels.

FNIII7-10 binding assay
Human FNIII7-10 fragment was subcloned into pET15b plasmid (Invitrogen), expressed in bacteria, and subsequently labeled with Alexa Fluor 647 carboxylic acid via a succinimidyl ester (Invitrogen) as described previously (Czuchra et al., 2006). To assess ligand-binding properties, fetal liver–derived macrophages were harvested and incubated with Alexa Fluor 647–coupled FNIII7-10 fragment in TBS in the presence or absence of 10 mM EDTA or 2 mM $MnCl_2$, respectively, and then subjected to flow cytometry analysis. Mean fluorescence of EDTA-treated cells was considered unspecific signal and was subtracted from all values.

Blocking of CD44-mediated adhesion
Osteoclast precursors were lifted using 10 mM EDTA in PBS and were first incubated for 15 min with an Fc receptor–blocking antibody followed by a 15 min incubation with either an anti-CD44–blocking antibody (BD) or rat IgG2b (eBioscience) before seeding on a fibronectin-coated surface. After adhesion for 30 min, cells were carefully rinsed with PBS and fixed with 4% PFA. Pictures were obtained using a microscope (Axiovert 40C; Carl Zeiss, Inc.) with a camera (Prosilica), a 10× objective lens, and FireWire Recorder software.

RANKL- and M-CSF-signaling
Mature osteoclasts were serum starved in α-MEM for 3–4 h and treated with either recombinant M-CSF (100 ng/ml or 10 ng/ml) or recombinant RANKL (100 ng/ml) for the times indicated. Cells were washed in cold PBS, lysed on ice with modified RIPA lysis buffer (50 mM Tris-HCl, pH7.3, 150 mM NaCl, 2 mM EDTA, 1% Triton X-100, 0.5% sodium deoxycholate, 1× protease inhibitor mixture [Roche], and 1× phosphatase inhibitor cocktail 1+2 [Sigma-Aldrich]) and incubated on ice for 10 min. Cell lysates were cleared by centrifugation at 14,000 rpm for 10 min at 4°C, and 40 µg of total lysates was subjected to 10% SDS-PAGE, transferred onto polyvinylidene fluoride membranes, blocked for 1 h in 5% BSA in TBS-T for detecting phosphorylated proteins or in 5% skim milk in TBS-T for detecting other proteins, then incubated with primary antibodies at 4°C ON followed by probing with HRP-labeled secondary antibodies (Jackson ImmunoResearch Laboratories).

For detection of Syk phosphorylation, 500 µg of lysate was used for immunoprecipitation. Lysate was incubated with 3 µg of primary antibody ON at 4°C on a rotator, then protein G–Sepharose beads (Sigma-Aldrich) were added to the lysates, incubated for 3 h at 4°C on a rotator, washed three times in lysis buffer, and boiled in 3× SDS sample buffer for 5 min. After centrifugation, proteins were separated by 10% SDS-PAGE, Western blotted, and probed using an HRP-labelled 4G10 antibody (Millipore).

Electron microscopy
Primary osteoclasts were cultured on glass coverslips and then "unroofed" as described previously (Heuser, 2000; Luxenburg et al., 2007). In brief, cells were exposed to hypotonic buffer (20% PHEM, 6 mM Pipes, 5 mM Hepes, 0.4 mM Mg_2SO_4, and 2 mM EGTA) and broken by brief sonication for 2 s. The resulting ventral membrane preparations were fixed with 2.5% (vol/vol) glutaraldehyde in 0.1 M phosphate buffer (pH 7.4, 1 h at RT), postfixed with 1% (wt/vol) aqueous OsO_4, dehydrated, critical-point dried, and sputter-coated with 10 nm Au-Pd. Samples were viewed at 5 kV with a scanning electron microscope (DSM 982-Gemini; Carl Zeiss, Inc.).

Statistical analysis
A Student's *t* test was used to analyze histomorphometric data, osteoblast data, ELISA assays, β1 integrin activation, osteoclast fusion, belt thickness, resorption, and adhesion. $P < 0.05$ was considered to be statistically significant. All graphs include standard deviation error bars.

Online supplemental material
Fig. S1 shows histological sections of control and kindlin-3$^{-/-}$ long bones from different developmental stages indicating progressive ossification in kindlin-3$^{-/-}$ mice. Fig. S2 shows normal biological activity of kindlin-3$^{-/-}$ osteoblasts. Fig. S3 shows normal p38 and JNK phosphorylation of kindlin-3$^{-/-}$ osteoclasts upon RANKL treatment in vitro. Fig. S4 shows that CD44 contributes to the residual adhesion of kindlin-3$^{-/-}$ pre-osteoclasts and integrin surface expression levels on control and kindlin-3$^{-/-}$ macrophages. Fig. S5 shows that retroviral-expressed EGFP–kindlin-3 rescues cell spreading, podosome formation, and matrix degradation in kindlin-3$^{-/-}$ osteoclasts, whereas expression of an integrin-binding mutant EGFP–kindlin-3 construct fails to do so.

We thank the Fässler laboratory members for discussion and Kyle Legate for critically reading the manuscript, Hildegard Reiter for performing the retroviral infections, Dick Heinegard for osteopontin, Angelika Flörl (Innsbruck Medical University, Austria) for excellent technical assistance with the electron microscopy work, and Chantal Domenget (University of Lyon, France) for support with osteoclast culture. We also thank Shahin Begum and Richard Hynes (Massachusetts Institute of Technology, Cambridge, MA) for isolating and providing bones from β3 integrin-deficient mice.

The work was supported by seventh framework program of the European Union and the Max Planck Society. The authors declare that they have no competing financial interests.

Submitted: 26 July 2010
Accepted: 2 February 2011

References

Chabadel, A., I. Bañon-Rodríguez, D. Cluet, B.B. Rudkin, B. Wehrle-Haller, E. Genot, P. Jurdic, I.M. Anton, and F. Saltel. 2007. CD44 and beta3 integrin organize two functionally distinct actin-based domains in osteoclasts. *Mol. Biol. Cell.* 18:4899–4910. doi:10.1091/mbc.E07-04-0378

Chavakis, E., G. Carmona, C. Urbich, S. Göttig, R. Henschler, J.M. Penninger, A.M. Zeiher, T. Chavakis, and S. Dimmeler. 2008. Phosphatidylinositol-3-kinase-gamma is integral to homing functions of progenitor cells. *Circ. Res.* 102:942–949. doi:10.1161/CIRCRESAHA.107.164376

Czuchra, A., H. Meyer, K.R. Legate, C. Brakebusch, and R. Fässler. 2006. Genetic analysis of beta1 integrin "activation motifs" in mice. *J. Cell Biol.* 174:889–899. doi:10.1083/jcb.200604060

Destaing, O., F. Saltel, J.C. Géminard, P. Jurdic, and F. Bard. 2003. Podosomes display actin turnover and dynamic self-organization in osteoclasts expressing actin-green fluorescent protein. *Mol. Biol. Cell.* 14:407–416. doi:10.1091/mbc.E02-07-0389

Destaing, O., F. Saltel, B. Gilquin, A. Chabadel, S. Khochbin, S. Ory, and P. Jurdic. 2005. A novel Rho-mDia2-HDAC6 pathway controls podosome patterning through microtubule acetylation in osteoclasts. *J. Cell Sci.* 118:2901–2911. doi:10.1242/jcs.02425

Destaing, O., A. Sanjay, C. Itzstein, W.C. Horne, D. Toomre, P. De Camilli, and R. Baron. 2008. The tyrosine kinase activity of c-Src regulates actin dynamics and organization of podosomes in osteoclasts. *Mol. Biol. Cell.* 19:394–404. doi:10.1091/mbc.E07-03-0227

Published February 28, 2011

Ek-Rylander, B., M. Flores, M. Wendel, D. Heinegård, and G. Andersson. 1994. Dephosphorylation of osteopontin and bone sialoprotein by osteoclastic tartrate-resistant acid phosphatase. Modulation of osteoclast adhesion in vitro. *J. Biol. Chem.* 269:14853–14856.

Faccio, R., D.V. Novack, A. Zallone, F.P. Ross, and S.L. Teitelbaum. 2003a. Dynamic changes in the osteoclast cytoskeleton in response to growth factors and cell attachment are controlled by beta3 integrin. *J. Cell Biol.* 162:499–509. doi:10.1083/jcb.200212082

Faccio, R., S. Takeshita, A. Zallone, F.P. Ross, and S.L. Teitelbaum. 2003b. c-Fms and the alphavbeta3 integrin collaborate during osteoclast differentiation. *J. Clin. Invest.* 111:749–758.

Flores, M.E., M. Norgård, D. Heinegård, F.P. Reinholt, and G. Andersson. 1992. RGD-directed attachment of isolated rat osteoclasts to osteopontin, bone sialoprotein, and fibronectin. *Exp. Cell Res.* 201:526–530. doi:10.1016/0014-4827(92)90305-R

Franzén, A., and D. Heinegård. 1985. Isolation and characterization of two sialoproteins present only in bone calcified matrix. *Biochem. J.* 232:715–724.

Gil-Henn, H., O. Destaing, N.A. Sims, K. Aoki, N. Alles, L. Neff, A. Sanjay, A. Bruzzaniti, P. De Camilli, R. Baron, and J. Schlessinger. 2007. Defective microtubule-dependent podosome organization in osteoclasts leads to increased bone density in Pyk2(-/-) mice. *J. Cell Biol.* 178:1053–1064. doi:10.1083/jcb.200701148

Goodison, S., V. Urquidi, and D. Tarin. 1999. CD44 cell adhesion molecules. *MP, Mol. Pathol.* 52:189–196. doi:10.1136/mp.52.4.189

Grant, F.D., P.R. Conlin, and E.M. Brown. 1990. Rate and concentration dependence of parathyroid hormone dynamics during stepwise changes in serum ionized calcium in normal humans. *J. Clin. Endocrinol. Metab.* 71:370–378. doi:10.1210/jcem-71-2-370

Gregory, C.A., W.G. Gunn, A. Peister, and D.J. Prockop. 2004. An Alizarin red-based assay of mineralization by adherent cells in culture: comparison with cetylpyridinium chloride extraction. *Anal. Biochem.* 329:77–84. doi:10.1016/j.ab.2004.02.002

Helfrich, M.H., S.A. Nesbitt, P.T. Lakkakorpi, M.J. Barnes, S.C. Bodary, G. Shankar, W.T. Mason, D.L. Mendrick, H.K. Väänänen, and M.A. Horton. 1996. Beta 1 integrins and osteoclast function: involvement in collagen recognition and bone resorption. *Bone.* 19:317–328. doi:10.1016/S8756-3282(96)00223-2

Heuser, J. 2000. The production of 'cell cortices' for light and electron microscopy. *Traffic*. 1:545–552. doi:10.1034/j.1600-0854.2000.010704.x

Hodivala-Dilke, K.M., K.P. McHugh, D.A. Tsakiris, H. Rayburn, D. Crowley, M. Ullman-Culleré, F.P. Ross, B.S. Coller, S. Teitelbaum, and R.O. Hynes. 1999. Beta3-integrin-deficient mice are a model for Glanzmann thrombasthenia showing placental defects and reduced survival. *J. Clin. Invest.* 103:229–238. doi:10.1172/JCI5487

Jurdic, P., F. Saltel, A. Chabadel, and O. Destaing. 2006. Podosome and sealing zone: specificity of the osteoclast model. *Eur. J. Cell Biol.* 85:195–202. doi:10.1016/j.ejcb.2005.09.008

Kilic, S.S., and A. Etzioni. 2009. The clinical spectrum of leukocyte adhesion deficiency (LAD) III due to defective CalDAG-GEF1. *J. Clin. Immunol.* 29:117–122. doi:10.1007/s10875-008-9226-z

Krüger, M., M. Moser, S. Ussar, I. Thievessen, C.A. Luber, F. Forner, S. Schmidt, S. Zanivan, R. Fässler, and M. Mann. 2008. SILAC mouse for quantitative proteomics uncovers kindlin-3 as an essential factor for red blood cell function. *Cell*. 134:353–364. doi:10.1016/j.cell.2008.05.033

Kühn, R., F. Schwenk, M. Aguet, and K. Rajewsky. 1995. Inducible gene targeting in mice. *Science*. 269:1427–1429. doi:10.1126/science.7660125

Kuijpers, T.W., E. van de Vijver, M.A. Weterman, M. de Boer, A.T. Tool, T.K. van den Berg, M. Moser, M.E. Jakobs, K. Seeger, O. Sanal, et al. 2009. LAD-1/variant syndrome is caused by mutations in FERMT3. *Blood*. 113:4740–4746. doi:10.1182/blood-2008-10-182154

Larjava, H., E.F. Plow, and C. Wu. 2008. Kindlins: essential regulators of integrin signalling and cell-matrix adhesion. *EMBO Rep.* 9:1203–1208. doi:10.1038/embor.2008.202

Legate, K.R., S.A. Wickström, and R. Fässler. 2009. Genetic and cell biological analysis of integrin outside-in signaling. *Genes Dev.* 23:397–418. doi:10.1101/gad.1758709

Linder, S., and M. Aepfelbacher. 2003. Podosomes: adhesion hot-spots of invasive cells. *Trends Cell Biol.* 13:376–385. doi:10.1016/S0962-8924(03)00128-4

Linder, S., and P. Kopp. 2005. Podosomes at a glance. *J. Cell Sci.* 118:2079–2082. doi:10.1242/jcs.02390

Luxenburg, C., D. Geblinger, E. Klein, K. Anderson, D. Hanein, B. Geiger, and L. Addadi. 2007. The architecture of the adhesive apparatus of cultured osteoclasts: from podosome formation to sealing zone assembly. *PLoS ONE*. 2:e179. doi:10.1371/journal.pone.0000179

Malinin, N.L., L. Zhang, J. Choi, A. Ciocea, O. Razorenova, Y.Q. Ma, E.A. Podrez, M. Tosi, D.P. Lennon, A.I. Caplan, et al. 2009. A point mutation in KINDLIN3 ablates activation of three integrin subfamilies in humans. *Nat. Med.* 15:313–318. doi:10.1038/nm.1917

McDowall, A., L. Svensson, P. Stanley, I. Patzak, P. Chakravarty, K. Howarth, H. Sabnis, M. Briones, and N. Hogg. 2010. Two mutations in the KINDLIN3 gene of a new leukocyte adhesion deficiency III patient reveal distinct effects on leukocyte function in vitro. *Blood*. 115:4834–4842. doi:10.1182/blood-2009-08-238709

McHugh, K.P., K. Hodivala-Dilke, M.H. Zheng, N. Namba, J. Lam, D. Novack, X. Feng, F.P. Ross, R.O. Hynes, and S.L. Teitelbaum. 2000. Mice lacking beta3 integrins are osteosclerotic because of dysfunctional osteoclasts. *J. Clin. Invest.* 105:433–440. doi:10.1172/JCI8905

Moser, M., B. Nieswandt, S. Ussar, M. Pozgajova, and R. Fässler. 2008. Kindlin-3 is essential for integrin activation and platelet aggregation. *Nat. Med.* 14:325–330. doi:10.1038/nm1722

Moser, M., M. Bauer, S. Schmid, R. Ruppert, S. Schmidt, M. Sixt, H.V. Wang, M. Sperandio, and R. Fässler. 2009a. Kindlin-3 is required for beta2 integrin-mediated leukocyte adhesion to endothelial cells. *Nat. Med.* 15:300–305. doi:10.1038/nm.1921

Moser, M., K.R. Legate, R. Zent, and R. Fässler. 2009b. The tail of integrins, talin, and kindlins. *Science*. 324:895–899. doi:10.1126/science.1163865

Naviaux, R.K., E. Costanzi, M. Haas, and I.M. Verma. 1996. The pCL vector system: rapid production of helper-free, high-titer, recombinant retroviruses. *J. Virol.* 70:5701–5705.

Parfitt, A.M., M.K. Drezner, F.H. Glorieux, J.A. Kanis, H. Malluche, P.J. Meunier, S.M. Ott, and R.R. Recker. 1987. Bone histomorphometry: standardization of nomenclature, symbols, and units. *J. Bone Miner. Res.* 2:595–610. doi:10.1002/jbmr.5650020617

Pfeifer, A., T. Kessler, S. Silletti, D.A. Cheresh, and I.M. Verma. 2000. Suppression of angiogenesis by lentiviral delivery of PEX, a noncatalytic fragment of matrix metalloproteinase 2. *Proc. Natl. Acad. Sci. USA*. 97:12227–12232. doi:10.1073/pnas.220399597

Plow, E.F., J. Qin, and T. Byzova. 2009. Kindling the flame of integrin activation and function with kindlins. *Curr. Opin. Hematol.* 16:323–328. doi:10.1097/MOH.0b013e32832ea389

Ponta, H., L. Sherman, and P.A. Herrlich. 2003. CD44: from adhesion molecules to signalling regulators. *Nat. Rev. Mol. Cell Biol.* 4:33–45. doi:10.1038/nrm1004

Potocnik, A.J., C. Brakebusch, and R. Fässler. 2000. Fetal and adult hematopoietic stem cells require beta1 integrin function for colonizing fetal liver, spleen, and bone marrow. *Immunity*. 12:653–663. doi:10.1016/S1074-7613(00)80216-2

Rao, H., G. Lu, H. Kajiya, V. Garcia-Palacios, N. Kurihara, J. Anderson, K. Patrene, D. Sheppard, H.C. Blair, J.J. Windle, et al. 2006. Alpha9beta1: a novel osteoclast integrin that regulates osteoclast formation and function. *J. Bone Miner. Res.* 21:1657–1665. doi:10.1359/jbmr.060718

Ross, F.P., and S.L. Teitelbaum. 2005. alphavbeta3 and macrophage colony-stimulating factor: partners in osteoclast biology. *Immunol. Rev.* 208:88–105. doi:10.1111/j.0105-2896.2005.00331.x

Sabnis, H., A. Kirpalani, J. Horan, A. McDowall, L. Svensson, A. Cooley, T. Merck, S. Jobe, N. Hogg, and M. Briones. 2010. Leukocyte adhesion deficiency-III in an African-American patient. *Pediatr. Blood Cancer*. 55:180–182.

Saltel, F., A. Chabadel, E. Bonnelye, and P. Jurdic. 2008. Actin cytoskeletal organisation in osteoclasts: a model to decipher transmigration and matrix degradation. *Eur. J. Cell Biol.* 87:459–468. doi:10.1016/j.ejcb.2008.01.001

Scharffetter-Kochanek, K., H. Lu, K. Norman, N. van Nood, F. Munoz, S. Grabbe, M. McArthur, I. Lorenzo, S. Kaplan, K. Ley, et al. 1998. Spontaneous skin ulceration and defective T cell function in CD18 null mice. *J. Exp. Med.* 188:119–131. doi:10.1084/jem.188.1.119

Suda, T., N. Takahashi, N. Udagawa, E. Jimi, M.T. Gillespie, and T.J. Martin. 1999. Modulation of osteoclast differentiation and function by the new members of the tumor necrosis factor receptor and ligand families. *Endocr. Rev.* 20:345–357. doi:10.1210/er.20.3.345

Svensson, L., K. Howarth, A. McDowall, I. Patzak, R. Evans, S. Ussar, M. Moser, A. Metin, M. Fried, I. Tomlinson, and N. Hogg. 2009. Leukocyte adhesion deficiency-III is caused by mutations in KINDLIN3 affecting integrin activation. *Nat. Med.* 15:306–312. doi:10.1038/nm.1931

Teitelbaum, S.L., and F.P. Ross. 2003. Genetic regulation of osteoclast development and function. *Nat. Rev. Genet.* 4:638–649. doi:10.1038/nrg1122

Ussar, S., H.V. Wang, S. Linder, R. Fässler, and M. Moser. 2006. The Kindlins: subcellular localization and expression during murine development. *Exp. Cell Res.* 312:3142–3151. doi:10.1016/j.yexcr.2006.06.030

Weinstein, E.J., M. Bourner, R. Head, H. Zakeri, C. Bauer, and R. Mazzarella. 2003. URP1: a member of a novel family of PH and FERM domain-containing membrane-associated proteins is significantly over-expressed in lung and colon carcinomas. *Biochim. Biophys. Acta*. 1637:207–216.

Wu, H., R. Fässler, A. Schnieke, D. Barker, K.H. Lee, V. Chapman, U. Francke, and R. Jaenisch. 1992. An X-linked human collagen transgene escapes X inactivation in a subset of cells. *Development*. 116:687–695.

12.4 Paper 4:

Role of kindlin-3 in T cell progenitor homing and thymocyte development.

Role of kindlin-3 in T cell progenitor homing and thymocyte development

Federico A. Moretti[1], Raphael Ruppert[1], Reinhard Fässler[1], Markus Moser[1#]

[1]Max-Planck-Institute of Biochemistry, Department Molecular Medicine, Am Klopferspitz 18, D-82152 Martinsried

Keywords: Kindlin-3, integrin, thymus development, T cells homing

Corresponding author:
Markus Moser (moser@biochem.mpg.de)

ABSTRACT

T cell development depends on interactions with various cell types, which are critical for T cell progenitor homing to the thymus anlage and the stepwise progression during thymocyte maturation. During these processes the role of integrins is not defined, which might be due to functional compensations by different integrin members. To elucidate the role of integrins during T cell progenitor homing and subsequent differentiation, we studied T cell development in mice lacking the blood cell specific general integrin regulator kindlin-3. Kindlin-3 null mice develop a progressive thymus atrophy, which is mainly caused by an impaired homing of T cell progenitors to the vascularized thymus. Interestingly, during early thymus development kindlin-3 deficient fetal liver-derived T cell progenitors can home to the avascular thymus primordium, albeit less efficiently than wild-type T cell progenitors. We further show that those T cell progenitors, which managed to enter the thymus anlage, further develop into single positive CD4+ and CD8+ T cells and emigrate into the circulation. Although kindlin-3 deficient thymocytes migrate correctly through distinct thymic regions and show normal maturation, they exhibit a reduced proliferation capacity, which is due to a weakened crosstalk with a reduced number of thymic APCs.

INTRODUCTION

In contrast to most hematopoietic lineages, which develop within the bone marrow (BM), T cells complete their development within the specialized environment of the thymus. Since the hematopoietic stem cells and T cell progenitors are generated in the BM, T cell development depends on the continuous repopulation of the thymus by blood-born T cell progenitors (Jotereau 1987; Foss 2001; Cai 2007). T cell progenitor homing starts before the thymus is vascularized, which occurs at embryonic day (E) 15. Initial colonization of the thymic anlage can be already observed at E11.5 by fetal liver (FL)-derived progenitors, which leave the adjacent pharyngeal vessels and migrate towards and enter the thymic primordium. Upon thymus vascularization, T cell progenitors can directly enter the thymus anlage, where direct interactions with thymic epithelial cells (TECs), macrophages and dendritic cells (DCs) coordinate their proliferation, differentiation and selection before they are released into the periphery.

T cell progenitor homing to the thymus requires their adhesion and transmigration through the pharyngeal vessels at the pre-vascular stage and the post-capillary venules at the cortico-medullary junction (CMJ) of the vascularised thymus. Although the molecular mechanisms controlling T cell progenitor extravasation have not been investigated in detail, it is assumed that they follow the classical multistep leukocyte adhesion cascade consisting of initial selectin-mediated rolling, activation by chemokines, and integrin-dependent adhesion, adhesion strengthening and crawling before the leukocyte transmigrates through the endothelium (Ley 2007). In line with this assumption, mouse mutants lacking P-selectin glycoprotein ligand-1 (PSGL-1) and studies with function-blocking antibodies against α4 and/or β2 integrin revealed fewer thymic progenitors in the adult thymus indicating that both selectin-mediated rolling and integrin-mediated adhesion are important for T cell progenitor homing to the adult thymus (Rossi 2005; Scimone 2006). However, genetic ablation of various integrins, such as α4 (Arroyo 1996), αL (Schmits 1996), α6 (Georges-Labouesse 1996), β2 (Scharffetter-Kochanek 1998), β7 (Wagner 1996; Bungartz 2006) as well as the integrin ligand ICAM-1 (Sligh 1993; Xu 1994) had no effect on thymic colonization. In addition, the molecular events forming the basis of T cell progenitor homing to the pre-vascular thymus has not yet been addressed.

Once within the thymus, progenitors then follow a defined route through distinct regions within the thymus, where specific interactions with different thymic antigen presenting cell (APC) subsets trigger proliferation and differentiation and the formation of self-tolerant T cells (Wood 1985; Lorenz 1989a; Lorenz 1989b; Jayaraman 1992; Sebzda 1999; Wu 2005;

Mackay 2001; Li 2009). Whether T cell progenitor extravasation and homing to the pre- and post-vascular thymus as well as intrathymic differentiation are integrin dependent or whether a functional compensation by different receptors occurs in vivo is not known yet.

In this study, we investigated the role of integrins during T cell progenitor homing and subsequent differentiation by analysing kindlin-3 deficient mice. Kindlins, like talins, are intracellular proteins that directly bind to the cytoplasmic domain of integins and thereby control the ligand-binding affinity state of the integrin. Kindlin-3 is one member of the kindlin gene family, which is exclusively expressed in the hematopoietic system (Weinstein 2003; Ussar 2006). The paramount importance of kindlin-3 in controlling the three major integrin classes, β1, β2 and β3 integrins, in different hematopoietic cells is demonstrated by the severe phenotype of kindlin-3-deficient mice. These mice die postnatally with severe haemorrhages, structural defects of the erythrocyte membrane skeleton, a leukocyte adhesion defect and a severe osteopetrosis (Moser 2008, Krüger 2008, Schmidt 2011, Moser 2009). Importantly, mutations in the human kindlin-3 gene cause a rare leukocyte adhesion deficiency type-III (LAD-III) syndrome, which is characterized by the same disease pattern as observed in the kindlin-3 knockout mice (Mory 2008; Kuijpers 2009; Malinin 2009; Svensson 2009). Surprisingly, LAD-III patients show a lymphocytosis suggesting that T cell development does not require kindlin-3-mediated integrin regulation (Alon 2003; Pasvolsky 2007). Based on this finding, we investigated T-lymphopoiesis in kindlin-3-deficient mice.

Here we show that kindlin-3-deficient mice develop a progressive thymus atrophy, which is caused by impaired colonization of the vascularised thymus by the bone marrow (BM)-derived T cell progenitors during late embryogenesis and after birth. In strong contrast, colonization of the non-vascularized thymic primordium by kindlin-3-deficient FL-derived progenitors does occur indicating that T cell progenitor homing to the early thymus does not critically depend on integrins. Progenitors that managed to enter the thymus differentiate into mature single positive CD4 and CD8 T cells. Nevertheless, their proliferation is markedly decreased, which might be due to the reduced presence and a weakened interaction with macrophages and dendritic cells within the thymus parenchyma and a disturbed crosstalk with TECs.

RESULT

Mice lacking kindlin-3 develop progressive thymus atrophy

We have previously reported that kindlin-3-deficient (kindlin-3$^{-/-}$) mice show a reduced cellularity of the postnatal thymus (Moser, 2009). To study this in more detail, we first analyzed thymopoiesis during embryonic and postnatal development. As shown in Fig. 1A and B, thymi from both wild-type and kindlin-3$^{-/-}$ mice grow in size until postnatal day 3 (P3). Thereafter, kindlin-3$^{-/-}$ thymi became atrophic. In line with this macroscopic observation, an increase in thymus cellularity of both genotypes was measured until P3, even though the kindlin-3$^{-/-}$ thymus cellularity remained significantly reduced compared to controls at all time points. While the cell number of wild-type thymi subsequently increased, the thymus cellularity of kindlin-3$^{-/-}$ mice decreased (Fig 1C). Kindlin-3$^{-/-}$ mice usually die within the first week after birth (Moser 2008) excluding an analysis later then P8.

Next, we evaluated the thymic cyto-architecture on thymus sections by standard hematoxylin & eosin stainings (Fig. 1D). Despite the difference in size, both wild-type and mutant thymi were organized into a cortex and a medulla. P0 thymi showed numerous medullary islets interspersed within the cortex, which subsequently enlarged and fused to give a mature central medulla at P3. A regular formation of a cortico-medullary junction (CMJ), with separation of CD4/CD8-double positive (DP) T cells in the cortex from CD4- and CD8-single positive (SP) T cells in the medulla, can also be observed in kindlin-3$^{-/-}$ thymi by immunofluorescence stainings at P3. Furthermore, a normally organized thymic epithelial meshwork and vascular system is present in kindlin-3 mutant thymi (Supplementary Fig. 1A). However, the atrophic thymi of kindlin-3$^{-/-}$ mice at P6 and P8 showed a progressive enlargement of the medulla in relation to a strong reduction of the cortex, suggesting a biased development towards CD4- and CD8-SP T cells (Fig. 1D). This trend was indeed confirmed by flow cytometry (Fig. 1E, F and G). Importantly, at both P3 and P6 the CD4/CD8-double negative (DN) cell populations, which contain the most immature intrathymic T cells, were significantly reduced in their frequencies in kindlin-3$^{-/-}$ thymi (Fig. 1F and G). Despite the shift towards SP T cell populations in kindlin-3$^{-/-}$ thymi, all T cell subsets were significantly reduced in cell number compared to controls (Supplementary Fig. 1B and C); however, T cell maturation, which depends on a functional T cell receptor (TCR)/CD3 complex and a regulated expression of certain co-stimulatory glycoproteins, such as CD5 and CD24 (Fehling 1997; Michie 2002; Punt 1994; Azzam 1998; McKean 2001), was not affected by the absence of kindlin-3 (Supplementary Fig. 1D).

Importantly, expression of kindlin-3 in different T cell subsets and complete absence of kindlin-3 without a compensatory up-regulation of kindlin-1 and -2 expression in the thymus of kindlin-3-deficient mice was confirmed by Western-blot analysis (Supplementary Fig. 1E and F).

Taken together, these findings clearly indicate that kindlin-3 is dispensable for intrathymic T cell migration, differentiation and maturation, but T cell numbers and distribution critically depend on kindlin-3.

Kindlin-3$^{-/-}$ BM-derived T cell progenitors do not extravasate to the postnatal thymus

Next we wanted to investigate why kindlin-3$^{-/-}$ thymi contain significantly less immature T cells (Fig. 1F and G). Therefore, we depleted P3 and P6 thymi from all mature cells resulting in a population enriched in DN_{1-4} cells (referred to as lineage negative, Lin^{neg}), which was significantly reduced in kindlin-3$^{-/-}$ thymi (Fig. 2A and B). Further gating for cKIT and CD44 separated DN_{1-2} from DN_{3-4} cell populations and revealed the complete absence of DN1 and DN2 cells in kindlin-3$^{-/-}$ thymi (Fig. 2A and C). As DN1 and DN2 cells are the immediate intrathymic descendants of circulating T cell progenitors, we investigated whether these T cell progenitors are present in the circulation of kindlin-3$^{-/-}$ mice. Interestingly, a strong accumulation of myeloid (Lin^{neg}, $cKIT^{+}$, SCA-1^{-}) and lymphoid (Lin^{neg}, $cKIT^{+}$, SCA-1^{+}) hematopoietic progenitor cells (HPCs) was detectable in the peripheral blood of kindlin-3$^{-/-}$ mice suggesting an impaired extravasation from the blood into the thymus (Fig. 2D and E).

In order to study T cell progenitor homing to the adult thymus in a different system, we transferred fetal liver cells from E14.5 wild-type and kindlin-3$^{-/-}$ embryos into RAG-2 knock-out (RAG-2$^{-/-}$) mice, in which T cell development is blocked at the DN3 stage due to loss of V(D)J rearrangement (Shinkai 1992). Thymus size, weight, cellularity (Fig. 3A-C) and peripheral blood (Supplementary Fig. 2) of these chimeras were then analyzed 8 to 10 weeks later. Injection of control FL cells resulted in the complete reconstitution of the thymus and the repopulation of all DN populations in RAG2$^{-/-}$ mice, whereas kindlin-3$^{-/-}$ FL cells failed to do so (Fig. 3A-F). Nevertheless, like in kindlin-3 null mice, an accumulation of kindlin-3$^{-/-}$ HPCs was detected in the chimeras (data not shown). Notably a few kindlin-3$^{-/-}$ progenitors managed to enter the thymus and differentiated into DN4 cells (Fig. 3D and F). These cells further differentiated into a moderate number of CD4-and CD8-SP T cells, which were then released into the circulation (Supplementary Fig. 2A and B).

Altogether, these results indicate a crucial role of kindlin-3 for T cell progenitor homing to the adult thymus, but once within the thymus, the progenitor's differentiation into mature T-cells proceeds in a kindlin-3 independent fashion.

Diminished fetal thymus colonization in embryos lacking kindlin-3$^{-/-}$

Since thymi of newborn kindlin-3$^{-/-}$ mice lack DN1 and DN2 cells but contained DN3 and DN4 cells we assumed that these cells must have been entered the thymus during fetal development. To address this issue, we studied the presence and immigration of CD45^{+} hematopoietic progenitor cells into the thymic primordium by immunofluorescence stainings on embryonic sections (Fig. 4A). In line with previous reports (Douagi 2000; Itoi 2001) the first wave of hematopoietic progenitors can be observed in the perithymic mesenchyme at E11.5 and subsequently enter the primordium (E12) and proliferate (E12.5). At these time points, the number of progenitors in the proximity and within the thymus primordium was markedly reduced in kindlin-3$^{-/-}$ mice (Fig. 4B). However, despite the reduced efficiency in T cell progenitor homing to the kindlin-3$^{-/-}$ thymus primordium, the thymus was fully packed by thymocytes at E13.5 (Fig. 4A), of which a significant number was identified as DN1 and DN2 cells (Fig. 4C). Strikingly, a dramatic drop in the DN_{1-2} population of kindlin-3$^{-/-}$ thymi was observed at E16.5 (Fig. 4D and E), exactly at a developmental stage when thymus vascularisation takes place (Liu 2006). Taken together, T cell progenitor homing to the pre-vascularized thymic primordium can occur in a less efficient manner in the absence of kindlin-3.

Kindlin-3$^{-/-}$ FL-derived T cell progenitors do not efficiently cross the vasculature

Since the reduced number of kindlin-3$^{-/-}$ progenitors, which migrate and enter the embryonic thymus primordium, might be due to a reduced number of progenitors in the embryonic circulation we investigated their production and release from the fetal liver by flow cytometry. The cellularity of kindlin-3$^{-/-}$ FL cells is reduced (data not shown) causing an increased frequency of kindlin-3 null progenitors compared to control FL. Nevertheless, the absolute numbers of T cell progenitors (Lin^{neg}, cKIT^{hi}, CD45^{+} and PIR^{+}) (Kawamoto 2000; Masuda 2005) in kindlin-3$^{-/-}$ FL were similar to that in kindlin-3$^{+/+}$ FL (Fig. 5A, B and C). In addition, a gradual abnormal accumulation of FL-derived myeloid/erythroid (Lin^{neg}, cKIT^{hi}, PIR^{-}) and T-lymphoid (Lin^{neg}, cKIT^{hi}, PIR^{+}) HPCs (Katsura 2002) was detected in the circulation of kindlin-3$^{-/-}$ fetuses suggesting that progenitor extravasation out of the pharyngeal vessels is affected in the absence of kindlin-3 (Fig. 5D and E).

In order to exclude the possibility that kindlin-3$^{-/-}$ progenitors are lost either in the circulation or in the perithymic interstitium because of an inability to sense the chemokine gradient generated by the thymic primordium, we monitored progenitor migration and thymus colonization in vitro by time-lapse video microscopy. In this assay, alymphoid deoxyguanosine (dGuo)-treated thymic lobes from wild-type E15.5 SJL embryos (CD45.1^{+}) were positioned in close proximity to FL-derived hematopoietic precursor cells (Lin^{neg} cells) from either kindlin-3$^{+/+}$ or kindlin-3$^{-/-}$ E14.5 C57BL/6 (CD45.2^{+}) embryos and progenitor migration towards the thymic lobes was then monitored for 36 to 48 hours. As shown in Fig. 5F and in the Movies S3A and S3B (Supplementary Fig. 3), both kindlin-3$^{-/-}$ and kindlin-3$^{+/+}$ FL cells moved directionally towards the thymic lobe, while no progenitor cells showed a directed migration in the absence of a chemokine-producing thymic lobe (Movie S3C).

To confirm that FL cells, which have successfully entered the thymic lobes, have the potential to develop into mature T cells, the lobes were recovered from the collagen matrix and cultured for additional 18 days under conventional fetal thymus organ culture (FTOC) conditions. Importantly, both CD45.2^{+} kindlin-3$^{-/-}$ and kindlin-3$^{+/+}$ donor cells developed into DP, CD4- and CD8-SP cells (Fig. 5G).

Taken together, these data indicate that kindlin-3$^{-/-}$ T cell progenitors are normally produced in the fetal liver and accumulate in the circulation. Importantly, once kindlin-3$^{-/-}$ progenitors have passed the vasculature, they efficiently migrate towards the chemokine gradient produced by the thymus epithelial cells and differentiate into different T cell subsets.

Intrathymic vessels strongly express VCAM-1 and ICAM-1

In order to find an explanation for the difference in T cell precursor homing to the pre- and post-vascular thymus, we analysed the expression of adhesion molecules known to be involved in leukocyte extravasation (Ley 2007). No difference in the expression of α4, αL, β1, β2, β3 and β7 integrins on FL-derived HPCs (Lin^{neg}, cKIT^{+}) and T cell-specific progenitor cells (Lin^{neg}, cKIT^{+}, PIR^{+}) was detected on control and kindlin-3$^{-/-}$ cells using flow cytometry (Fig. 6A). Moreover, immunofluorescence staining for VCAM-1 and ICAM-1, which are the vascular ligands for α4β1 (VLA-1) and αLβ2 (LFA-1) integrins, respectively, showed strong expression on intrathymic blood vessels and stromal cells of an E18.5 fetal thymus (Fig. 6B). In contrast, a rather weak expression of VCAM-1 and ICAM-1 was detected in the lumen of pharyngeal vessels of E12.5 embryos (Fig. 6C). These observations further support the hypothesis that integrin-mediated adhesion plays a crucial role for the extravasation process via the intrathymic microvasculature (Lepique 2003).

Reduced proliferation of Kindlin-3 thymocytes

In addition to impaired T cell progenitor homing, a reduced proliferation or an increased cell death of thymocytes might contribute to the decreased thymus cellularity and progressive thymus atrophy of kindlin-3-deficient mice.

Therefore, we determined the number of apoptotic cells within the P3 thymus by immunohistochemistry against cleaved caspase-3 (Fig. 7A) and by annexin V staining using flow cytometry (Fig. 7B). Both number (Fig. 7C) and frequency (Fig. 7D) of thymic apoptotic cells were not altered in kindlin-$3^{-/-}$ compared to control mice. A more detailed analysis, which allowed discrimination between different T cell subsets, revealed that none of these populations showed increased annexin V staining in kindlin-$3^{-/-}$ cells compared to wild-type cells (Fig.7E). In contrast, thymocyte proliferation, which was determined by in vivo bromodeoxyuridine (BrdU) labeling was significantly reduced in P3 kindlin-$3^{-/-}$ thymi as shown by both immunohistochemistry (Fig. 7F and H) and flow cytometry (Fig. 7G and I). Reduced proliferation was detected in both DP and SP T cell populations (Fig 7L).

Reduced T cell proliferation might be a consequence of a disrupted thymic microenvironment. Therefore, we first analysed the presence and organisation of cortical (cTECs) and medullary (mTECs) thymic epithelial cells (Van Vliet 1984). Despite the absence of the DN_{1-2} population in kindlin-$3^{-/-}$mice, both cortical and medullary TECs were present and properly organized in a three-dimensional-meshwork at P0 and P3 (Fig. 8A and B). However, at later time points, particularly mTECs showed a tendency to cluster leading to the formation of cysts at P6 (Fig 8B). Even more expanded thymic cysts are visible in thymus sections at P8 (Fig 1D) suggesting an impaired thymic crosstalk between thymocytes and TECs in the absence of kindlin-3. Next we investigated the presence of macrophages and dendritic cells in kindlin-3-deficient thymi. Strikingly, significant reductions in the amount of both kindlin-$3^{-/-}$ MΦs ($CD11b^{hi}$, $CD11c^{low}$) and DCs ($CD11c^{hi}$, $CD11b^{low}$) were detected in the thymus of kindlin-$3^{-/-}$ mice, including the kindlin-$3^{-/-}$ FL cell chimeras, by flow cytometry (Fig. 8C, D and E). This observation indicates that blood-borne myeloid progenitors show a similar homing defect like the T cell progenitors.

Finally, we tested T cell proliferation upon contact with antigen presenting cells (APC). To this end we used T cells from mice with a T cell specific deletion of the kindlin-3 gene (kindlin-3fl/fl / CD4-Cre), which express T cell receptors specific for the MOG35-55 peptide (2D2 mice) (Moretti, 2013). Naïve CD4+ T splenocytes were isolated from these kindlin-3fl/fl/2D2+/CD4-Cre mice and control kindlin-3fl/fl/2D2+ animals, labelled with

carboxyfluorescein diacetate succinidyl ester (CSFE) and co-cultured with MOG35-55-loaded dendritic cells. After 3 days T cells were harvested and their proliferative response was tracked by CSFE dye dilution. Interestingly, kindlin-3 deficient T cells, which were in contact with DCs loaded with high concentration of MOG35-55 peptide (10ug/ml), showed a similar proliferative response compared to control cells, whereas kindlin-3-deficient T cells showed a significant reduction in proliferation at lower MOG35-55 concentrations (0.1 and 1.0ug/ml) (Fig). Altogether, these results suggest that thymus atrophy of kindlin-3-deficient mice is also caused by a reduced proliferation of thymocytes due to a defective crosstalk with APCs.

DISCUSSION

During thymopoiesis T cells and their progenitors undergo a series of defined and coordinated developmental stages beginning with the initial homing of lymphoid progenitor cells originated from the fetal liver or bone marrow followed by proliferation, differentiation and selection steps at certain environments within the thymus, which finally lead to self tolerant mature T cells. In recent years significant progress has been made in the understanding which chemokine cues guide thymic progenitors from the bloodstream to the thymus and position developing T cells within the thymus (Takahama 2006). In addition, much is known about the transcriptional networks, which control T cell fate specification (Koch and Radtke 2011). In contrast, the molecular details of thymus homing have not been elucidated fully. It is assumed that similar to the extravasation process of leukocytes, T cell progenitors follow a defined cascade of chemoattraction, selectin-mediated rolling and integrin-dependent adhesion and transmigration (Ley 2007). In line with this assumption, mouse mutants of the selectin ligand PSGL-1 show reduced progenitor homing to the thymus (Rossi 2005); however, mice with defects in individual integrins, such as α4 or β2 integrins, revealed no defect in T cell development, which might be caused by a functional compensation by different integrins.

In the present study, we investigated the role of integrins during T cell homing and subsequent T cell maturation within the thymus in mice lacking the general integrin regulator kindlin-3. In contrast to LAD-III patients, which develop a lymphocytosis suggesting a minor role of kindlin-3 for T cell development, Kindlin-3 null mice exhibit progressive thymus atrophy. The reason for the difference between mice and humans are unclear, since both species suffer from the same severe bleeding and leukocyte adhesion defects confirming the essential role of this protein for integrin regulation in various hematopoietic cell types. On the contrary, while kindlin-3 null mice developed a profound osteopetrosis, an increased bone mass have not been detected in all LAD-III patients indicating clear differences in the phenotypes of mice and man. We have excluded that other kindlin members compensate for the loss of kindlin-3 in murine T cells, as those are neither expressed in wild-type cells nor is their expression induced in kindlin-3 null cells. Studies on kindlin-1 or 2 expressions in human T cells from LAD-III patients have not been conducted.

During development two different pathways mediate the seeding of the thymus with T cell progenitors. Before thymus vascularization, T cell progenitors leave the pharyngeal vessels and migrate through mesenchymal tissue before they reach the epithelial thymic anlage. Once the thymus has become vascularized during late gestation, fetal liver and bone marrow (BM)-derived lymphoid progenitors directly enter the thymus at large post-capillary venules at the

thymus cortico-medullary junctions. Our study clearly shows that T cell progenitor homing to the vascularized thymus critically depend on kindlin-3. Kindlin-3 is required for stable adhesion mediated by at least the three major integrin classes (β1, β2 and β3 integrins) (Schmidt 2011). Since loss of individual integrins or studies with function-blocking antibodies showed no or only a partial reduction in T lymphocyte homing (Scimone 2006), our study demonstrate that kindlin-3-dependent regulation of integrins are essential for T lymphoid progenitor homing to the vascularized thymus and loss of one integrin member can be functionally compensated by other integrins.

To our surprise we observed a rather efficient homing of T cell progenitors to the non-vascularized thymus anlage, which occurs as early as E11.5. Our data indicate that integrins are also involved in this process, since homing is slightly delayed and fewer progenitors find their way to the thymus primordium of kindlin-3 null embryos. In support of this assumption, we found an accumulation of progenitors in the circulation of mutant embryos. However, the reduced number of progenitors around or within the thymus at these early developmental stages is neither caused by an impaired production of progenitors in the fetal liver nor by differences in the integrin expression on the progenitors of kindlin-3 null mice. Furthermore, in vitro homing assays of FL-derived hematopoietic precursor cells to alymphoid thymic lobes confirmed the histological observations that T cell progenitors from kindlin-3 null mice can sense the chemokine gradient produced by the thymic epithelial cells and can efficiently migrate towards the thymic lobules.

Why can T cell progenitors extravasate the pharyngeal vessel at early developmental stages but fail to leave the post-capillary venules at the cortico-medullary junctions of the vascularized thymus? Several reasons are conceivable. Differences in the adhesive properties of T cell progenitors derived from the fetal liver versus the bone marrow are possible. However, since a sharp decline in the DN1 and DN2 populations of kindlin-3 deficient thymi occurs before a functional bone marrow has been formed, it is rather unlikely that the progenitors differ in their adhesive properties. Two other reasons are more plausible. An immunohistological analysis revealed that intrathymic vessels at the cortico-medullary junction express high levels of the integrin ligands VCAM-1 and ICAM-1 confirming that integrin-mediated adhesion plays a central role. On the contrary, since pharyngeal vessels show only weak VCAM-1 and ICAM-1 expression, it is fair to speculate that other adhesion receptors, such as CD44, might play a role in early T cell progenitor adhesion as well. The hypothesis that the different vessels have different adhesive features is also promoted by the drop of DN1 and DN2 populations of the thymus at E16.5, when T cell progenitor homing is

shifted towards the intrathymic vessel pathway. A further important parameter, which may influence the homing capabilities of T cell progenitors, is the difference in the hydrodynamic forces that these cells are exposed to during development. It can be assumed that the blood pressure rises during maturation of the cardio-vascular system and that less adhesive forces are required for the adhesion of blood cells to capillaries during early developmental stages compared to later stages. Integrin-mediated adhesion of cells depends on conformational changes of the integrin heterodimer leading to a high ligand-binding affinity state, which is triggered by the direct binding of talin and kindlin proteins to the β integrin cytoplasmic tail (Moser 2009). More recently, progress in the understanding of the molecular mechanisms of talin and kindlin-mediated integrin regulation has been made. In vivo studies on talin-1 and kindlin-3-deficient neutrophils suggested the model that initial activation of integrins towards an intermediate, ligand-binding competent state requires only talin-1, while the shift towards the high affinity state requires additional kindlin-3 binding (Lefort, 2012). Similarly, studies on effector T cells and on the platelet αIIbβ3 integrin indicated that kindlin-3 is required for stabilizing the integrin-ligand interaction by promoting integrin clustering (Moretti 2013; Ye 2013). Taken this into account, it is possible that a weak adhesion of kindlin-3 deficient T cell progenitors to pharyngeal vessels is sufficient for their extravasation, whereas firm kindlin-3 dependent adhesion to intrathymic capillaries is required for progenitor extravasation when vascular flow rates are higher. In addition, an interesting phenomenon is the specific effect, which kindlin-3 exerts on αLβ2 versus α4β1 integrins. While αLβ2 integrin mediated adhesion to ICAM-1 is very sensitive to kindlin-3 deficiency, α4β1 mediated adhesiveness is less affected even under shear flow conditions (Manevich-Mendelson 2009). Thus, a primarily α4β1 integrin-driven adhesion might be responsible for the initial seeding of the non-vascularized thymus with lymphoid progenitor cells.

Despite the severe defect in kindlin-3-deficient T cell progenitor homing to the vascularized thymus, those T cell progenitors, which were able to enter the thymus either during early developmental stages or to the adult thymus of RAG2-null mice, undergo well-characterized sequential developmental maturation steps to produce mature T cells within defined thymic areas. Histological and immunohistological analyses revealed a normal thymus architecture of kindlin-3 deficient mice consisting of the four major compartments, the subcapsular zone, the cortex, the medulla and the cortico-medullary junction. Importantly, both cortical and medullary TECs were present and organized in a three dimensional meshwork, which was not distinguishable from wild-type thymi. The presence of DP thymocytes in the cortex and SP CD4 and CD8 T cells in the medulla of kindlin-3 deficient postnatal thymi, indicates that the

positioning of developing T cells within the thymus, which is guided by chemokines produced by thymic stromal cells is not impaired. Nevertheless, already at P6 medullary TECs show a tendency to form cysts indicating a defective communication between thymocytes and thymic stroma cells in the absence of kindlin-3.

We also detected a reduction in the number of macrophages and dendritic cells in kindlin-3 deficient thymi. Since the earliest T cell progenitors still retain the potential to give rise to DCs, natural killer cells and macrophages, it is not surprising that due to the homing defect the number of macrophages and DCs is reduced in the thymus of kindlin-3 null mice. In addition, we observed a reduced proliferative response of kindlin-3 deficient naïve T cells upon priming with low concentration of antigens presented by a DC. Altogether, our data suggest that the reduced number of APCs and the weakened crosstalk with thymic epithelial cells and APCs also contribute to the thymus atrophy of kindlin-3 deficient mice.

MATERIALS AND METHODS

Mice and chimeras

Kindlin-3$^{-/-}$ mice have been described previously (Moser 2008). All mice were from a mixed 129/SvJ x C57BL/6 background.

The day on which a vaginal plug was first observed was designated as embryonic day 0.5 (E0.5).

Fetal liver (FL) cell chimeras were generated as previously described (Tulunay 1975; Prümmer 1986). Briefly, 5-6 x10^6 of whole kindlin-3$^{-/-}$ or kindlin-3$^{+/+}$ E14.5 FL cells were injected per mouse through the tail vain of sub-lethally irradiated (1x 6 Gy) RAG2$^{-/-}$ mice (Shinkai 1992). Chimeras were analyzed 8 to 10 weeks after repopulation.

Pictures of dissected thymi were taken with a ProgRes C14 camera (JenOptic) connected to the Leica MZ FLIII stereomicroscope.

Thymic single cell suspensions were counted using a counting chamber and the total viable cell numbers identified by the trypan blue dye exclusion method.

Relative frequencies of diverse cell populations were obtained by flow-cytometry analysis.

All animals were mated and maintained under specific pathogen-free conditions at the animal facility of the Max Planck Institute of Biochemistry.

Western blot analysis

Identical protein amounts (~20 μg) were run on a 10% SDS-PAGE and analyzed by Western blot with rabbit anti-mouse polyclonal antibodies kindlin-1 and kindlin-3 (home made), kindlin-2 (Sigma) or with mouse anti-GAPDH monoclonal antibody (Calbiochem). Serial ECL expositions of the membranes were performed to determine the optimal linear range with a LAS-4000 imager (Fujifilm).

Multi-color flow cytometry analysis and cell sorting

Multi-color flow-cytometric analysis and cell sorting were performed using FACS-Calibur and FACS-Aria flow cytometers, respectively. Data for viable cells, which were determined by forward light scatter and propidium iodide exclusion, were obtained with Cell Quest software. All antibodies we used were purchased from eBioscience or DB Pharmingen.

Removal of mature cells from organ single-cell suspensions to obtain cells of the lineage negative (Lin^{neg}) was performed using the following cocktails of biotinylated antibodies:

Anti-B220, anti-CD19, anti-TER119, anti-NK1.1, anti-CD11b (Mac-1), anti-Gr-1, anti-CD8α, anti-CD3e, anti-TCRβ, anti-TCRγδ and anti-CD11c for fetal and adult thymi. Anti-TER119,

anti-B220, anti-CD11b, anti-Gr-1, anti-CD11c, anti-NK1.1, anti-CD4 and-CD8α for postnatal peripheral blood. Anti-B220, anti-CD19, anti-TER119, anti-NK1.1, anti-Gr-1 and anti-Thy1.2 for fetal liver and fetal blood.

Biotinylated cells were then stained either with PerCP-Cy5.5-coniugated or FITC-coniugated Streptavidin and excluded by FL3 or FL1 FACS channels. The resulting Lin^{neg} cell population was further gated with anti-CD25-FITC, anti-CD44-PE and anti-cKIT-APC for thymocytes; with anti-SCA1-PE and anti-cKIT-APC for postnatal peripheral blood cells; with anti-CD45-FITC, anti-PIR-PE and anti-cKIT-APC or anti-cKIT-PerCP, anti-PIR-APC and anti-Integrin-PE for fetal liver cells; with anti-PIR-PE and anti-cKIT-APC for fetal blood cells.

Mature T cells were analyzed for surface receptor expression with anti-CD4-FITC, anti CD8-APC, anti-CD3-PE, anti-CD5-PE, anti-CD24-PE and TCRβ-PE.

Lin^{neg} FL-cells used for generating chimeras and for the time-lapse visualization of thymus attraction were obtained by negative selection through MACS separation columns after staining biotinylated cells with anti-Biotin-coupled magnetic beads according to the manufacturer's instructions (MACS Miltenyi Biotec).

Immunofluorescience analysis of embryos and thymi

4% PFA prefixed, frozen embryos and thymi embedded in Shandon Cryomatrix compound (Thermo Scientific) were first sliced into 8-10 μm thick sections and stained with the following antibodies:

For the embryos: rabbit anti-Fibronectin polyclonal antibody (Chemicon), mouse anti-panCytokeratin monoclonal antibody (Sigma), rat anti-CD45-FITC (eBioscience), goat anti-CD106 (VCAM-1, R&D Systems), hamster anti-CD54 (ICAM-1, Pharmingen) and rat anti CD31 (PECAM-1, Pharmingen) followed by Alexa-Fluor-647-conjugated anti-rabbit IgG, Alexa-Fluor-546-conjugated anti-mouse IgG, Alexa-Fluor-488-conjugated anti-rat IgG, Alexa-Fluor-647-conjugated anti-mouse IgG, Fluor-546-conjugated anti-goat IgG, and Fluor-546-conjugated anti-hamster IgG antibodies (Invitrogen).

For the thymus: rabbit anti-panLaminin polyclonal antibody (gift from Rupert Timpl), mouse anti-pan-FITC-Cytokeratin monoclonal antibody (Sigma), rat anti-CD31 (PECAM-1, Pharmingen), rat anti-CD4-FITC (eBioscience), rat anti CD8-Biotin (eBioscience), anti-CD106 (VCAM-1, R&D Systems), hamster anti-CD54 (ICAM-1, Pharmingen), rat anti-ER-TR4 and anti-ER-TR5 polyclonal antibodies (gift from Eric Vroegindeweij) followed by Alexa-Fluor-647-conjugated anti-rabbit IgG, Alexa-Fluor-647-conjugated anti-rat IgG, Alexa-Fluor-488-conjugated anti-Fluorescein/Oregon green IgG, Cy3-coniugated Streptavidin

(Jackson), Alexa-Fluor-488-conjugated anti-rat IgG, Fluor-546-conjugated anti-goat IgG, and Fluor-546-conjugated anti-hamster IgG antibodies (Invitrogen). Thymic sections were fixed with acetone instead of PFA only for the anti-ER-TR4 and anti-ER-TR5 staining.
The stained sections were mounted with a fluorescence mounting medium (Elvanol). The images were acquired with a fluorescence microscope (Imager.Z1, Zeiss) and analyzed by the Axio Vision 40 (version 4.8.2.0) software (Zeiss), utilizing 10x, 20x and 40x magnification.

Immunohistologic analysis of the thymus

4% PFA fixed and paraffin-embedded thymi were sliced into 8 µm tick sections and stained with antibodies. The sections were then counterstained with Mayer's haematoxylin (Merck), mounted in Entellan (Merck), and coverslipped. Haematoxylin and Eosin (H/E) staining was performed according to a standard protocol. Images were acquired with the light microscope Axioskop (Zeiss) and analyzed with the adobe ImageReady/TWAIN software.

Apoptosis assays

Thymocytes from P3 mice were stained with PE-labeled Annexin V and 7-AAD according to the manufacturer's instructions (BD Pharmingen Apoptosis Detection Kit). T cells were additionally stained for anti-CD4-FITC and anti-CD8-APC and FACS analyzed.
Paraffin-embedded thymus sections were stained with rabbit anti-mouse cleaved caspase-3 antibody (Cell Signalling). Apoptotic cells were detected by DAB staining after treatment with the immunoperoxidase Vectastain ABC system (Vector Laboratories).

Proliferation assays

P3 mouse newborns were given intraperitoneal injections of 50 µg of bromodeoxyuridine (BrdU) per each gram of body weight. At 1 hour after injection, thymocytes were isolated and stained with FITC-labeled anti-BrdU monoclonal antibody (BD Pharmingen BrdU Flow Kit), anti-CD4-PerCP and anti-CD8-PE antibodies, and analyzed by flow cytometry.
Alternatively, paraffin-embedded thymus sections were DAB stained after incubation with a POD-coupled anti-BrdU antibody (Roche).

Time-lapse visualization of thymus attraction

Time-lapse imaging of horizontal cell migration to fetal thymus lobes was recorded as described previously (Ueno 2005; Liu 2005). Briefly, 10 µL freshly neutralized collagen solution (1.72 mg/mL PureCol, Advanced BioMatrix, in RPMI 1640-based culture medium)

containing 1-2 x10^5 fetal liver cells (Lin^{neg}) from either kindlin-$3^{+/+}$ or kindlin-$3^{-/-}$ C57BL/6 ($CD45.2^+$) animals was placed in a 35 mm plastic dish and solidified at 37°C for 10 minutes. An E15.5 fetal thymus lobe from wild-type SJL ($CD45.1^+$) mouse, pre-treated for 6 days with 1.35 mM 2-deoxyguanosine (dGuo; Sigma) was positioned approximately 0.5 mm away from the cell spot. The culture was submerged in 1.72 mg/mL collagen medium and solidified at 37°C for 30 minutes. The dish was placed in 5% CO_2 under an Axiovert 40 CFL microscope (Zeiss) equipped with a digital CCD camera. The culture was time-lapse monitored for 36 to 48 hours using a home-written software. After colonization, fetal thymus lobes were removed from the collagen gel, rinsed, and further cultured for 18 days under conventional organ culture conditions. Thymi were than pooled and squeezed and the resulting single cell suspensions were stained with anti-CD45.2 to isolate the donor-derived thymocytes and further gated for anti-CD4-FITC and anti-CD8-APC.

Fetal Thymus Organ Culture

Seeded thymus lobes were cultured on 0.8 μm isopore membrane filters (Millipore) supported by a Gelfoam sponge (Pfizer) at an interface between 5% CO_2-humidified air and RPMI 1640-based culture medium containing 10% FCS, 100 U/ml penicillin and 100 μg/ml streptomycin (PAA), 2 mM L-glutamine (PAA), 1X non-essential amino acids (Gibco), 1 mM sodium pyruvate (Gibco), 10 mM HEPES, 50 μM 2-mercaptoethanol (Sigma). Details have been described (Ueno 2005).

Reaggregate thymus organ culture (RTOC)

Wild-type E15.5 SJL ($CD45.1^+$) thymi were digested in RPMI 1640 culture medium containing 2% FCS, 25 mM HEPES, 1 mg/ml collagenase Type II (Worthington Biochemical Corporation) and 25 μg/ml DNase I (Boehringer Mannheim) for 30 min at 37°C. Cell-cell complexes were disrupted by addition of 0.5 M EDTA (1:100) for 5 min at 37°C. Leukocytes were MACS depleted using anti-Biotin-coupled magnetic beads according to the manufacturer's instructions (MACS Miltenyi Biotec), after prestaining with a biotinylated anti-CD45.1 antibody. The negatively sorted TECs (~5 x10^5) were then mixed 1.1, 1:3 and 1:5 with kindlin-$3^{-/-}$ or kindlin-$3^{+/+}$ DP cells to reform a thymus lobe-like structure as previously described (Ueno 2005). Reaggreates were cultured for 7 days in a 5% CO_2, 37°C incubator and FACS analyzed for CD3, CD4 and CD8. DP cells were positively MACS sorted from E17.5 fetuses with anti-CD4 and anti-CD8 antibodies.

Isolation and FACS analysis of thymic dendritic cells (DCs) and macrophages (MΦs) during mouse ontogeny

Isolation of myeloid cells from the thymus was carried out as previously described with modifications (Vremec 1992; Vremec 2000; Shortman 1989). Briefly, 3 to 5 thymi from E14.5, E19.5 and P3 animals were pooled, cut into small fragments and digested with frequent mixing for 30 min at room temperature (~25°C) in modified RPMI 1640-FCS medium containing collagenase (1 mg/ml; type II; Worthington Biochemical Corporation) and DNase I (0,1 mg/ml; Boehringer Mannheim). To disrupt DC/T cell and MΦ/T cell complexes, EDTA pH 7.2 (0.01 M final conc.) was added, and mixing continued for 5 min. Undigested fibrous material was then removed by filtration through a cell-strainer (BD Falcon). All subsequent steps were at 4°C using a divalent balanced salt solution containing EDTA pH 7.2 and FCS (EDTA-BSS-FCS). Cells were recovered from the digest by centrifugation, the pellet was washed with cold EDTA-BSS-FCS and then incubated (not for E14.5 thymi) for 30 min at 4°C with the following biotinylated mAbs (eBioscience): anti-CD19, anti-erythrocyte (TER-119), anti-TCRβ and anti-TCRγδ (BD Pharmingen). All mAb were titrated and used at near-saturating concentrations. The cells coated with biotinylated mAbs were then removed using anti-Biotin-coupled magnetic beads according to the manufacturer's instructions (MACS Miltenyi Biotec). The DC/MΦ enriched population was stained with anti-CD11c-FITC (BD Pharmingen) and anti-CD11b-PE (eBioscience) and analyzed by flow cytometry.

Statistic analysis

Means, standard deviations and statistical comparisons with Student's t-test (*P<0.05, **P<0.01, ***P<0.001) were made using Microsoft Excel software.

LITERATURE

Alon, R., M. Aker, S. Feigelson, M. Sokolovsky-Eisenberg, D.E. Staunton, G. Cinamon, V. Grabovsky, R. Shamri, and A. Etzioni. 2003. A novel genetic leukocyte adhesion deficiency in subsecond triggering of integrin avidity by endothelial chemokines results in impaired leukocyte arrest on vascular endothelium under shear flow. *Blood* 101:4437-4445.

Arroyo, M.P., K.M. Downey, A.G. So, and T.S. Wang. 1996. Schizosaccharomyces pombe proliferating cell nuclear antigen mutations affect DNA polymerase delta processivity. *The Journal of biological chemistry* 271:15971-15980.

Azzam, H.S., A. Grinberg, K. Lui, H. Shen, E.W. Shores, and P.E. Love. 1998. CD5 expression is developmentally regulated by T cell receptor (TCR) signals and TCR avidity. *The Journal of experimental medicine* 188:2301-2311.

Bungartz, G., S. Stiller, M. Bauer, W. Muller, A. Schippers, N. Wagner, R. Fassler, and C. Brakebusch. 2006. Adult murine hematopoiesis can proceed without beta1 and beta7 integrins. *Blood* 108:1857-1864.

Cai, A.Q., K.A. Landman, B.D. Hughes, and C.M. Witt. 2007. T cell development in the thymus: from periodic seeding to constant output. *Journal of theoretical biology* 249:384-394.

Douagi, I., I. Andre, J.C. Ferraz, and A. Cumano. 2000. Characterization of T cell precursor activity in the murine fetal thymus: evidence for an input of T cell precursors between days 12 and 14 of gestation. *European journal of immunology* 30:2201-2210.

Fehling, H.J., and H. von Boehmer. 1997. Early alpha beta T cell development in the thymus of normal and genetically altered mice. *Current opinion in immunology* 9:263-275.

Foss, D.L., E. Donskoy, and I. Goldschneider. 2001. The importation of hematogenous precursors by the thymus is a gated phenomenon in normal adult mice. *The Journal of experimental medicine* 193:365-374.

Georges-Labouesse, E., N. Messaddeq, G. Yehia, L. Cadalbert, A. Dierich, and M. Le Meur. 1996. Absence of integrin alpha 6 leads to epidermolysis bullosa and neonatal death in mice. *Nature genetics* 13:370-373.

Itoi, M., H. Kawamoto, Y. Katsura, and T. Amagai. 2001. Two distinct steps of immigration of hematopoietic progenitors into the early thymus anlage. *International immunology* 13:1203-1211.

Jayaraman, S., Y. Luo, and M.E. Dorf. 1992. Tolerance induction in T helper (Th1) cells by thymic macrophages. *Journal of immunology* 148:2672-2681.

Jotereau, F., F. Heuze, V. Salomon-Vie, and H. Gascan. 1987. Cell kinetics in the fetal mouse thymus: precursor cell input, proliferation, and emigration. *Journal of immunology* 138:1026-1030.

Katsura, Y. 2002. Redefinition of lymphoid progenitors. *Nature reviews. Immunology* 2:127-132.

Kawamoto, H., T. Ikawa, K. Ohmura, S. Fujimoto, and Y. Katsura. 2000. T cell progenitors emerge earlier than B cell progenitors in the murine fetal liver. *Immunity* 12:441-450.

Koch, U., F. Radtke. 2011. Mechanisms of T cell development and transformation. *Annual Reviews Cell Developmental Biology*. 27:539-562.

Kruger, M., M. Moser, S. Ussar, I. Thievessen, C.A. Luber, F. Forner, S. Schmidt, S. Zanivan, R. Fassler, and M. Mann. 2008. SILAC mouse for quantitative proteomics uncovers kindlin-3 as an essential factor for red blood cell function. *Cell* 134:353-364.

Kuijpers, T.W., E. van de Vijver, M.A. Weterman, M. de Boer, A.T. Tool, T.K. van den Berg, M. Moser, M.E. Jakobs, K. Seeger, O. Sanal, S. Unal, M. Cetin, D. Roos, A.J. Verhoeven, and F. Baas. 2009. LAD-1/variant syndrome is caused by mutations in FERMT3. *Blood* 113:4740-4746.

Lepique, A.P., S. Palencia, H. Irjala, and H.T. Petrie. 2003. Characterization of vascular adhesion molecules that may facilitate progenitor homing in the post-natal mouse thymus. *Clinical & developmental immunology* 10:27-33.

Ley, K., C. Laudanna, M.I. Cybulsky, and S. Nourshargh. 2007. Getting to the site of inflammation: the leukocyte adhesion cascade updated. *Nature reviews. Immunology* 7:678-689.

Li, J., J. Park, D. Foss, and I. Goldschneider. 2009. Thymus-homing peripheral dendritic cells constitute two of the three major subsets of dendritic cells in the steady-state thymus. *The Journal of experimental medicine* 206:607-622.

Liu, C., F. Saito, Z. Liu, Y. Lei, S. Uehara, P. Love, M. Lipp, S. Kondo, N. Manley, and Y. Takahama. 2006. Coordination between CCR7- and CCR9-mediated chemokine signals in prevascular fetal thymus colonization. *Blood* 108:2531-2539.

Liu, C., T. Ueno, S. Kuse, F. Saito, T. Nitta, L. Piali, H. Nakano, T. Kakiuchi, M. Lipp, G.A. Hollander, and Y. Takahama. 2005. The role of CCL21 in recruitment of T-precursor cells to fetal thymi. *Blood* 105:31-39.

Lefort, C.T, J. Rossaint, M. Moser, B.G. Petrich, A. Zarbock, S.J. Monkley, D.R. Critchley, M.H. Ginsberg, R. Fässler, K. Ley. 2012. Distinct roles for talin-1 and kindlin-3 in LFA-1 extension and affinity regulation. *Blood* 119:4275-4282.

Lorenz, R.G., and P.M. Allen. 1989a. Thymic cortical epithelial cells can present self-antigens in vivo. *Nature* 337:560-562.

Lorenz, R.G., and P.M. Allen. 1989b. Thymic cortical epithelial cells lack full capacity for antigen presentation. *Nature* 340:557-559.

Mackay, C.R., and U.H. von Andrian. 2001. Immunology. Memory T cells--local heroes in the struggle for immunity. *Science* 291:2323-2324.

Malinin, N.L., L. Zhang, J. Choi, A. Ciocea, O. Razorenova, Y.Q. Ma, E.A. Podrez, M. Tosi, D.P. Lennon, A.I. Caplan, S.B. Shurin, E.F. Plow, and T.V. Byzova. 2009. A point mutation in KINDLIN3 ablates activation of three integrin subfamilies in humans. *Nature medicine* 15:313-318.

Manevich-Mendelson, E., S.W Feigelson, R. Pasvolsky, M. Aker, V. Grabovsky, Z. Shulman, S.S. Kilic, M.A. Rosenthal-Allieri, S. Ben-Dor, A. Mory, A. Bernard, M. Moser, A. Etzioni, R. Alon. 2009. Loss of Kindlin-3 in LAD-III eliminates LFA-1 but not VLA-4 adhesiveness developed under shear flow conditions. *Blood* 114:2344-2353.

Masuda, K., M. Itoi, T. Amagai, N. Minato, Y. Katsura, and H. Kawamoto. 2005. Thymic anlage is colonized by progenitors restricted to T, NK, and dendritic cell lineages. *Journal of immunology* 174:2525-2532.

McKean, D.J., C.J. Huntoon, M.P. Bell, X. Tai, S. Sharrow, K.E. Hedin, A. Conley, and A. Singer. 2001. Maturation versus death of developing double-positive thymocytes reflects competing effects on Bcl-2 expression and can be regulated by the intensity of CD28 costimulation. *Journal of immunology* 166:3468-3475.

Michie, A.M., and J.C. Zuniga-Pflucker. 2002. Regulation of thymocyte differentiation: pre-TCR signals and beta-selection. *Seminars in immunology* 14:311-323.

Moretti, F.A., M. Moser, R. Lyck, M. Abadier, R. Ruppert, B. Engelhardt, and R. Fassler. 2013. Kindlin-3 regulates integrin activation and adhesion reinforcement of effector T cells. *Proceedings of the National Academy of Sciences of the United States of America* 110:17005-17010.

Mory, A., S.W. Feigelson, N. Yarali, S.S. Kilic, G.I. Bayhan, R. Gershoni-Baruch, A. Etzioni, and R. Alon. 2008. Kindlin-3: a new gene involved in the pathogenesis of LAD-III. *Blood* 112:2591.

Moser, M., M. Bauer, S. Schmid, R. Ruppert, S. Schmidt, M. Sixt, H.V. Wang, M. Sperandio, and R. Fassler. 2009. Kindlin-3 is required for beta2 integrin-mediated leukocyte adhesion to endothelial cells. *Nature medicine* 15:300-305.

Moser, M., B. Nieswandt, S. Ussar, M. Pozgajova, and R. Fassler. 2008. Kindlin-3 is essential for integrin activation and platelet aggregation. *Nature medicine* 14:325-330.

Pasvolsky, R., S.W. Feigelson, S.S. Kilic, A.J. Simon, G. Tal-Lapidot, V. Grabovsky, J.R. Crittenden, N. Amariglio, M. Safran, A.M. Graybiel, G. Rechavi, S. Ben-Dor, A. Etzioni, and R. Alon. 2007. A LAD-III syndrome is associated with defective expression of the Rap-1 activator CalDAG-GEFI in lymphocytes, neutrophils, and platelets. *The Journal of experimental medicine* 204:1571-1582.

Prummer, O., and T.M. Fliedner. 1986. The fetal liver as an alternative stem cell source for hemolymphopoietic reconstitution. *International journal of cell cloning* 4:237-249.

Punt, J.A., J.L. Roberts, K.P. Kearse, and A. Singer. 1994. Stoichiometry of the T cell antigen receptor (TCR) complex: each TCR/CD3 complex contains one TCR alpha, one TCR beta, and two CD3 epsilon chains. *The Journal of experimental medicine* 180:587-593.

Rossi, F.M., S.Y. Corbel, J.S. Merzaban, D.A. Carlow, K. Gossens, J. Duenas, L. So, L. Yi, and H.J. Ziltener. 2005. Recruitment of adult thymic progenitors is regulated by P-selectin and its ligand PSGL-1. *Nature immunology* 6:626-634.

Scharffetter-Kochanek, K., H. Lu, K. Norman, N. van Nood, F. Munoz, S. Grabbe, M. McArthur, I. Lorenzo, S. Kaplan, K. Ley, C.W. Smith, C.A. Montgomery, S. Rich, and A.L. Beaudet. 1998. Spontaneous skin ulceration and defective T cell function in CD18 null mice. *The Journal of experimental medicine* 188:119-131.

Schmidt, S., I. Nakchbandi, R. Ruppert, N. Kawelke, M.W. Hess, K. Pfaller, P. Jurdic, R. Fassler, and M. Moser. 2011. Kindlin-3-mediated signaling from multiple integrin classes is required for osteoclast-mediated bone resorption. *The Journal of cell biology* 192:883-897.

Schmits, R., T.M. Kundig, D.M. Baker, G. Shumaker, J.J. Simard, G. Duncan, A. Wakeham, A. Shahinian, A. van der Heiden, M.F. Bachmann, P.S. Ohashi, T.W. Mak, and D.D. Hickstein. 1996. LFA-1-deficient mice show normal CTL responses to virus but fail to reject immunogenic tumor. *The Journal of experimental medicine* 183:1415-1426.

Scimone, M.L., I. Aifantis, I. Apostolou, H. von Boehmer, and U.H. von Andrian. 2006. A multistep adhesion cascade for lymphoid progenitor cell homing to the thymus. *Proceedings of the National Academy of Sciences of the United States of America* 103:7006-7011.

Sebzda, E., S. Mariathasan, T. Ohteki, R. Jones, M.F. Bachmann, and P.S. Ohashi. 1999. Selection of the T cell repertoire. *Annual review of immunology* 17:829-874.

Shinkai, Y., G. Rathbun, K.P. Lam, E.M. Oltz, V. Stewart, M. Mendelsohn, J. Charron, M. Datta, F. Young, A.M. Stall, and et al. 1992. RAG-2-deficient mice lack mature lymphocytes owing to inability to initiate V(D)J rearrangement. *Cell* 68:855-867.

Shortman, K., D. Vremec, A. D'Amico, F. Battye, and R. Boyd. 1989. Nature of the thymocytes associated with dendritic cells and macrophages in thymic rosettes. *Cellular immunology* 119:85-100.

Sligh, J.E., Jr., C.M. Ballantyne, S.S. Rich, H.K. Hawkins, C.W. Smith, A. Bradley, and A.L. Beaudet. 1993. Inflammatory and immune responses are impaired in mice deficient in intercellular adhesion molecule 1. *Proceedings of the National Academy of Sciences of the United States of America* 90:8529-8533.

Svensson, L., K. Howarth, A. McDowall, I. Patzak, R. Evans, S. Ussar, M. Moser, A. Metin, M. Fried, I. Tomlinson, and N. Hogg. 2009. Leukocyte adhesion deficiency-III is caused by mutations in KINDLIN3 affecting integrin activation. *Nature medicine* 15:306-312.

Takahama, Y.2006. Journey through the thymus: stromal guides for T-cell development and selection. *Nature Reviews* 6:127-135.

Tulunay, O., R.A. Good, and E.J. Yunis. 1975. Protection of lethally irradiated mice with allogeneic fetal liver cells: influence of irradiation dose on immunologic

reconstitution. *Proceedings of the National Academy of Sciences of the United States of America* 72:4100-4104.

Ueno, T., C. Liu, T. Nitta, and Y. Takahama. 2005. Development of T-lymphocytes in mouse fetal thymus organ culture. *Methods in molecular biology* 290:117-133.

Ussar, S., H.V. Wang, S. Linder, R. Fassler, and M. Moser. 2006. The Kindlins: subcellular localization and expression during murine development. *Experimental cell research* 312:3142-3151.

van Vliet, E., M. Melis, and W. van Ewijk. 1984. Immunohistology of thymic nurse cells. *Cellular immunology* 87:101-109.

Vremec, D., J. Pooley, H. Hochrein, L. Wu, and K. Shortman. 2000. CD4 and CD8 expression by dendritic cell subtypes in mouse thymus and spleen. *Journal of immunology* 164:2978-2986.

Vremec, D., M. Zorbas, R. Scollay, D.J. Saunders, C.F. Ardavin, L. Wu, and K. Shortman. 1992. The surface phenotype of dendritic cells purified from mouse thymus and spleen: investigation of the CD8 expression by a subpopulation of dendritic cells. *The Journal of experimental medicine* 176:47-58.

Wagner, N., J. Lohler, E.J. Kunkel, K. Ley, E. Leung, G. Krissansen, K. Rajewsky, and W. Muller. 1996. Critical role for beta7 integrins in formation of the gut-associated lymphoid tissue. *Nature* 382:366-370.

Weinstein, E.J., M. Bourner, R. Head, H. Zakeri, C. Bauer, and R. Mazzarella. 2003. URP1: a member of a novel family of PH and FERM domain-containing membrane-associated proteins is significantly over-expressed in lung and colon carcinomas. *Biochimica et biophysica acta* 1637:207-216.

Wood, G.W. 1985. Macrophages in the thymus. *Survey of immunologic research* 4:179-191.

Wu, L., and K. Shortman. 2005. Heterogeneity of thymic dendritic cells. *Seminars in immunology* 17:304-312.

Xu, H., J.A. Gonzalo, Y. St Pierre, I.R. Williams, T.S. Kupper, R.S. Cotran, T.A. Springer, and J.C. Gutierrez-Ramos. 1994. Leukocytosis and resistance to septic shock in intercellular adhesion molecule 1-deficient mice. *The Journal of experimental medicine* 180:95-109.

Ye, F., B.G. Petrich, P. Anekal, C.T. Lefort, A. Kasirer-Friede, S.J. Shattil, R. Ruppert, M. Moser,R. Fässler, H.H. Ginsberg. 2013. The mechanism of kindlin-mediated activation of integrin IIb 3. *Current Biology* 23:2288-2295.

FIGURE LEGEND

Figure 1. Cellular characterization of the kindlin-3$^{-/-}$ thymus. (A and B) Pictures of kindlin-3$^{+/+}$ (upper panel) and kindlin-3$^{-/-}$ (lower panel) E14.5 to E18.5 fetal thymi, and P0 to P8 postnatal thymi. (C) Single-cell suspensions isolated from individual thymi of indicated time points (E14.5 to P6) were counted and values expressed in a logarithmic scale. (D) Haematoxylin and Eosin (H/E) staining of paraffin-embedded thymus sections. (E) Representative FACS profiles for CD4 and CD8 of thymocytes isolated from P3 and P6 thymi. Numbers within the FACS plots represent percentages of CD4/CD8 double negative (DN), CD4/CD8 double positive (DP), CD4 and CD8 single positive populations. (F and G) The frequency of each thymocyte population was measured by flow cytometry as shown in panel E. Bars indicate means ± standard errors. n = numbers of animals. *$P < 0.05$; **$P < 0.01$; ***$P < 0.001$; NS, not significant.

Figure 2. Cellular characterization of the kindlin-3$^{-/-}$ thymus and blood lineage negative populations. (A) Thymocytes from kindlin-3$^{-/-}$ and kindlin-3$^{+/+}$ thymi of indicated time points were three-color stained for Lin (B220, CD19, TER119, NK1.1, Mac-1, Gr-1, CD11c, CD8α, CD3e, TCRβ, and TCRγδ), cKIT and CD44 to identify the DN_{1-2} (Lin^{neg}, cKIT^{hi}, CD44^{hi}) and the DN_{3-4} (Lin^{neg}, cKIT^{low}, CD44^{low}) populations. (B and C) Frequencies and absolute cell numbers of P3 Lin^{neg} and DN_{1-2} thymocytes were calculated from the flow cytometric analysis as shown in panel A. (D) Peripheral blood cells from P3 animals was first ACK-lysed and then three-color stained for Lin (TER119, B220, CD11b, Gr-1, CD11c, NK1.1, CD4 and CD8α), cKIT and SCA-1. (E) Frequencies of the hematopoietic progenitor cell (HPC) populations: whole HPCs (Lin^{neg}, cKIT^{+}), potential myeloid (Lin^{neg}, cKIT^{+}, SCA1^{-}) and lymphoid (Lin^{neg}, cKIT^{+}, SCA1^{+}) progenitor subsets. Numbers within the representative FACS plots indicate cell percentages. Bars indicate means ± standard errors. n = numbers of animals. *$P < 0.05$; **$P < 0.01$; ***$P < 0.001$.

Figure 3. Analysis of the fetal liver cell chimeras. (A) Images, (B) weights and (C) cell numbers of thymi from the indicated adult mice (WT and RAG2$^{-/-}$) and 10-week-old chimeras. (D) Thymocytes from controls and chimeric thymi were four-color stained for Lin (B220, CD19, TER119, NK1.1, Mac-1, Gr-1, CD11c, CD8α, CD3e, TCRβ, and TCRγδ), cKIT, CD44 and CD25 to identify the DN_{1-2} (Lin^{neg}, cKIT^{hi}, CD44^{hi}) and the DN_{3-4} (Lin^{neg}, cKIT^{low}, CD44^{low}) populations (upper panel), and DN1 (Lin^{neg}, CD44^{hi}, CD25^{-}), DN2 (Lin^{neg}, CD44^{hi}, CD25^{+}), DN3 (Lin^{neg}, CD44^{low}, CD25^{+}) and DN4 (Lin^{neg}, CD44^{low}, CD25^{-}) single

subsets (lower panel). (E and F) Frequencies of DN_{1-2} and DN4 thymocytes were calculated from the flow cytometric analysis as shown in panel D. Numbers within the representative FACS plots indicate cell percentages. Bars indicate means ± standard errors. n = numbers of animals. *$P < 0.05$; **$P < 0.01$; ***$P < 0.001$.

Figure 4. Fetal thymus colonization in kindlin-3$^{-/-}$ mice during development. (A and B) Sagittal sections of frozen embryos at the indicated ages were stained for fibronectin to visualize the perithymic mesenchyme (blue), for cytokeratin to identify the thymic primordium (green) and for CD45 to label potential T cell progenitor cells. Plotted in panel B are the means ± standard errors of the numbers of $CD45^+$ cells in and surrounding the thymic primordium. Representative images are shown in panel C, and the numbers of sections analyzed (N) are indicated in panel B. (C) Fetal thymocytes from kindlin-$3^{-/-}$ and control thymi at the indicated time points were three-color stained for Lin (B220, CD19, TER119, NK1.1, Mac-1, Gr-1, CD11c, CD8α, CD3e, TCRβ, and TCRγδ), cKIT and CD44 to identify the DN_{1-2} (Lin^{neg}, $cKIT^{hi}$, $CD44^{hi}$) and the DN_{3-4} (Lin^{neg}, $cKIT^{low}$, $CD44^{low}$) populations. Representative FACS plots are shown. (D and E) Frequencies and total numbers of DN_{1-2} were extrapolated from the flow cytometric analysis as shown in panel C. Bars indicate means ± standard errors. n = numbers of animals. *$P < 0.05$; **$P < 0.01$; ***$P < 0.001$.

Figure 5. Cellular characterization of fetal liver-derived T cell progenitors. (A) Single cell suspensions from kindlin-$3^{-/-}$ and control fetal livers at the indicated time points were four-color stained for Lin (B220, CD19, TER119, NK1.1, Gr-1 and Thy1.2), cKIT, CD45 and PIR. Representative FACS plots are shown. (B and C) Frequencies and total numbers of PIR^+ T cell progenitors per fetal liver were extrapolated from the flow cytometric analysis as shown in panel A. (D) Blood from indicated embryos were collected and three-color stained for Lin (B220, CD19, TER119, NK1.1, Gr-1 and Thy1.2), cKIT and PIR. Representative FACS plots are shown. (E) Frequencies of circulating PIR^+ T cell progenitors were extrapolated from the flow cytometric analysis as shown in panel D. (F) Representative images (10x magnification) of TLVA at indicated time points. The edge of a drop of $2x\ 10^5$ Lin^{neg} fetal liver cells (from kindlin-$3^{-/-}$ or control C57BL/6 $CD45.2^+$ embryos) is shown at the right side of the panels, in the absence (top panels) or presence of a dGuo-treated fetal thymus lobe (from wild-type SJL $CD45.1^+$ embryos), shown at the left side of the panels. (G) dGuo-treated fetal thymus lobes seeded with FL cells as in panel G were further cultured for 18 days under conventional organ culture conditions as shown in panel F. Cells were 4-color stained

for CD45.1, CD45.2, CD4, and CD8. Shown are representative FACS profiles. Bars indicate means ± standard errors. n = numbers of animals. *$P < 0.05$; **$P < 0.01$; ***$P < 0.001$; NS, not significant.

Figure 6. Fetal liver (FL)-derived T cell progenitor adhesion assays. (A) Expression of integrins on HPCs (Lin^{neg}, $cKIT^{+}$) and T cell progenitors (Lin^{neg}, $cKIT^{+}$, PIR^{+}). FL cells from E13.5 kindlin-$3^{-/-}$ and control embryos were four-color stained for Lin (B220, CD19, TER119, NK1.1, Gr-1 and Thy1.2), cKIT, PIR and one of the indicated integrins. (B) Cryostat sections of the vascularized fetal thymus from wild-type E18.5 fetuses were stained for the endothelial adhesion receptors VCAM-1 and ICAM-1 (red), and PECAM-1 (green) to identify the intrathymic microvasculature. (C) Cryostat sections of E12 embryos were stained for VCAM-1, ICAM-1 (red), PECAM-1 (green) and pan-Cytokeratin (blue) to identify the thymic primordium. A, atrium; T, thymus; PV, pharyngeal vessel.

Figure 7. Apoptosis and proliferation assays. (A and C) Paraffin-embedded sections of kindlin-$3^{-/-}$ and kindlin-$3^{+/+}$ P3 thymi were stained for the apoptotic cell marker cleaved caspase-3 and counterstained with Mayer´s haematoxylin (blue). Representative images are shown in panel A, and the numbers of apoptotic cells and sections (N) analyzed are indicated in panel C. (B, D and E) Single cell suspensions of thymocytes from kindlin-$3^{-/-}$ and control P3 thymi were in-vitro stained for Annexin V, 7-AAD, the apoptotic and dead cell markers respectively, CD4 and CD8, and FACS analyzed. Representative FACS plots showing the total amount of thymic apoptotic cells (Annexin V^{+}, 7-AAD^{-}) are shown in panel B and plotted in panel D. Frequencies of apoptotic cells in each T cell subpopulation are shown in panel E. (F and H) Paraffin-embedded sections of thymi from kindlin-$3^{-/-}$ and kindlin-$3^{+/+}$ P3 mice that received intraperitoneally a dose of the cell proliferation marker BrdU were stained with an antibody anti-BrdU and counterstained with Mayer´s haematoxylin (blue). Representative images are shown in panel F, and the numbers of BrdU+ cells and sections (N) analyzed are indicated in panel H. (G, I and L) Single cell suspensions of thymocytes from $BrdU^{+}$ thymi were in-vitro stained for BrdU, CD4 and CD8, and FACS analyzed. Representative FACS plots showing the total amount of thymic proliferating cells ($BrdU^{+}$) are shown in panel G and plotted in panel I. Frequencies of $BrdU^{+}$ cells in each T cell subpopulation are shown in panel E. Bars indicate means ± standard errors. n = numbers of animals. *$P < 0.05$; **$P < 0.01$; ***$P < 0.001$; NS, not significant.

Figure 8. Analysis of the thymic stromal cells in kindlin-3$^{-/-}$ mice during development. (A and B) Cryostat sections (20x magnification) of thymi from kindlin-3$^{-/-}$ and kindlin-3$^{+/+}$ P0, P3 and P6 animals were stained for anti-CD4 (green), anti-CD8 (blue) and anti-ER-TR4 (red, panel A) or ER-TR5 (red, panel B), markers for the cortical (cTECs) and medullary (mTECs) thymic epithelial cells, respectively. Cells in cyan indicate the co-expression of CD4 and CD8, therefore being CD4/CD8 double positive cells. mTEC-lined cysts are visible in the medulla of kindlin-3$^{-/-}$ P6 thymus. C, cortex; M, medulla. (C, D and E) Single cell suspensions from a pool of four E14.5, three E19.5 fetal thymi and one P3 thymus, enriched for macrophages (CD11b^{hi}, CD11c^{low}) and dendritic cells (CD11c^{hi}, CD11b^{low}), were two-color stained for anti-CD11b and anti-CD11c. Representative FACS plots at the indicated time points are shown in panel C and cell percentages are plotted in panel D and E. Bars indicate means ± standard errors. N = numbers of experiments. *$P < 0.05$; **$P < 0.01$; ***$P < 0.001$; NS, not significant.

Supplementary Figure 1. (A) Cryostat sections of P3 kindlin-3$^{+/+}$ and kindlin-3$^{-/-}$ thymi were stained with anti-pan-Laminin (red), anti-CD4 (green) and anti-CD8 (blue) (left panel), and with anti-pan-Cytokeratin (green), anti-PECAM-1 (red) and DAPI (blue) (right panel). Cells in cyan indicate the co-expression of CD4 and CD8, therefore being CD4/CD8 double positive cells. M, medulla; C, cortex; Ca, capsule; V, vessel; CMJ, cortico-medullary junction. (B and C) Quantification of the absolute numbers of thymocytes present in each T cell subpopulation (DN, DP, CD4-SP, CD8-SP) of P3 and P6 thymi. Bars indicate means ± standard errors. n = numbers of animals. *$P < 0.05$; **$P < 0.01$; ***$P < 0.001$. (D) FACS analysis of surface receptor expression on thymocytes isolated from P3 kindlin-3$^{-/-}$ and kindlin-3$^{+/+}$ thymi. Isotype matched controls (blue histograms); kindlin-3$^{+/+}$ cells (green histograms); kindlin-3$^{+/+}$ cells (red histograms). (E) Cell lysates from the whole P3 kindlin-3$^{-/-}$ and kindlin-3$^{+/+}$ thymi was analyzed by Western blot for expression of kindlin-1, -2 and -3. Keratinocyte and embryonic stem cell (HSC) lysate were used as positive controls for kindlin-1 and -2, respectively. The protein load was controlled by detecting GAPDH in the same extracts. (F) Western blot of protein lysates from sorted DN, DP, CD4^{+} and CD8^{+}-SP cells.

Supplementary Figure 2. (A) Representative FACS plots showing peripheral blood T-lymphocytes (PBL) in adult mice (WT and RAG2$^{-/-}$) and chimeras. (B) Frequencies of circulating CD4^{+} and CD8^{+} T cells were calculated from the flow cytometric analysis as

shown in panel D. Numbers within the FACS plots indicate cell percentages. Bars indicate means ± standard errors. n = numbers of animals. **P* < 0.05; ***P* < 0.01; ****P* < 0.001.

Supplementary Figure 3. (A) *In vitro* proliferation of kindlin-$3^{fl/fl}$/$2D2^{+}$/$CD4Cre^{+}$ ($K3/Cre^{2D2}$) or control kindlin-$3^{fl/fl}$/$2D2^{+}$ (WT^{2D2}) T cells was analyzed by flow cytometry after priming with MOG_{35-55} peptide-loaded DCs (left panel) or antibodies (right panel). CFSE staining from one representative kindlin-3-null and control sample are shown. Red-lined histograms represent control samples that received DCs without MOG_{35-55} peptide or no stimulating antibodies. The percentage of dividing cells (B), the division (C) and proliferation (D) index and the cell counts (E) were calculated from the generation sizes (n = 5).

FIGURE 1

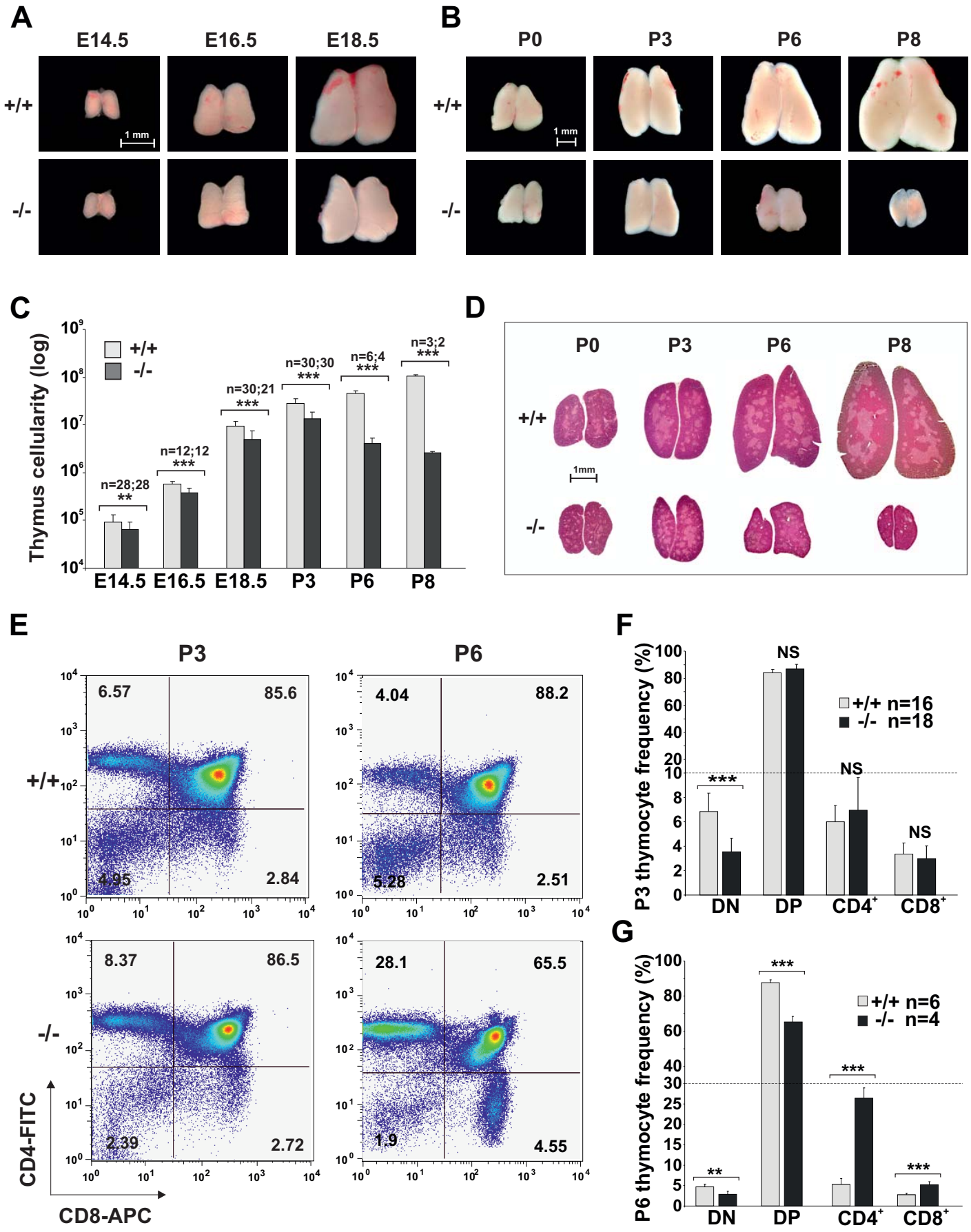
A
E14.5
E16.5
E18.5
+/+
-/-
1 mm
B
P0
P3
P6
P8
C
Thymus cellularity (log)
+/+
-/-
n=28;28
**
n=12;12
***
n=30;21
***
n=30;30
***
n=6;4
***
n=3;2
***
E14.5 E16.5 E18.5 P3 P6 P8
D
P0 P3 P6 P8
1mm
E
P3
P6
6.57
85.6
4.95
2.84
4.04
88.2
5.28
2.51
8.37
86.5
2.39
2.72
28.1
65.5
1.9
4.55
CD4-FITC
CD8-APC
F
P3 thymocyte frequency (%)
+/+ n=16
-/- n=18
NS
***
DN DP CD4+ CD8+
G
P6 thymocyte frequency (%)
+/+ n=6
-/- n=4
**
***
DN DP CD4+ CD8+

FIGURE 2

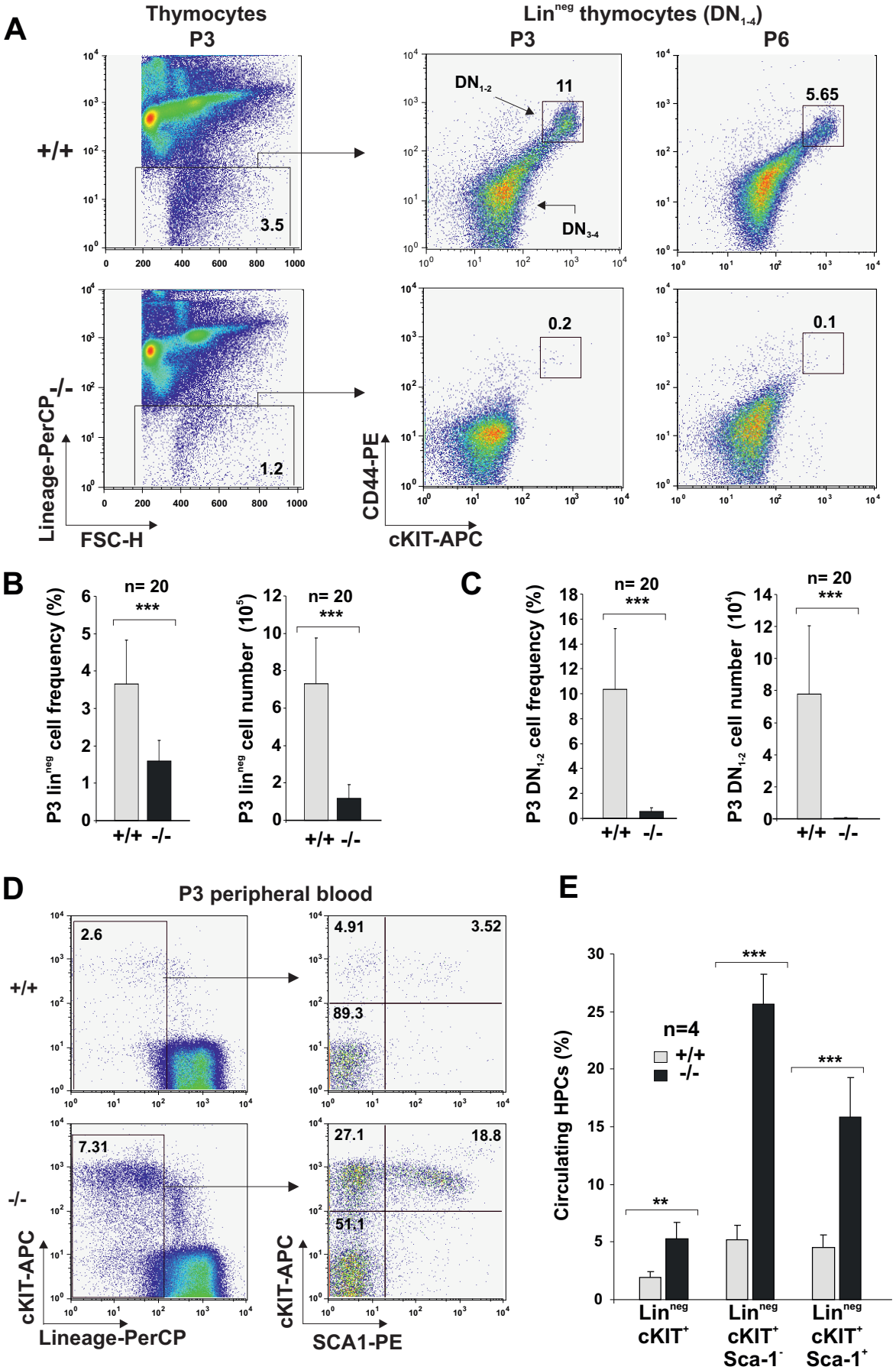
A
Thymocytes
P3
Lin^neg thymocytes (DN1-4)
P3
P6
+/+
-/-
3.5
1.2
DN1-2
DN3-4
11
5.65
0.2
0.1
Lineage-PerCP
FSC-H
CD44-PE
cKIT-APC
B
n= 20
***
P3 lin^neg cell frequency (%)
P3 lin^neg cell number (10^5)
+/+ -/-
C
P3 DN1-2 cell frequency (%)
P3 DN1-2 cell number (10^4)
D
P3 peripheral blood
2.6
4.91
3.52
89.3
7.31
27.1
18.8
51.1
cKIT-APC
Lineage-PerCP
SCA1-PE
E
Circulating HPCs (%)
n=4
+/+
-/-
**
Lin^neg cKIT+
Lin^neg cKIT+ Sca-1-
Lin^neg cKIT+ Sca-1+

FIGURE 3

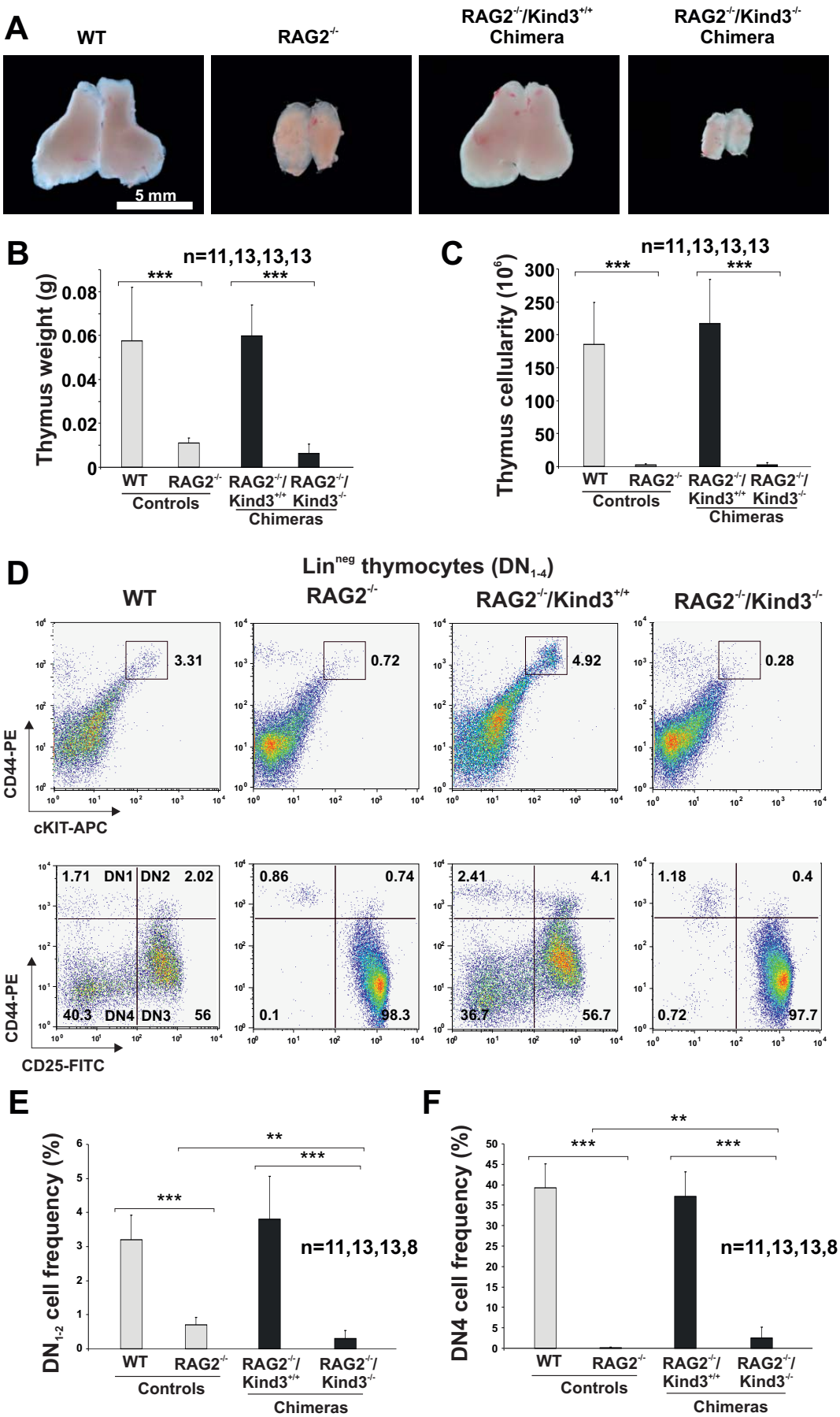
A
WT
RAG2-/-
RAG2-/-/Kind3+/+ Chimera
RAG2-/-/Kind3-/- Chimera
5 mm
B
n=11,13,13,13
Thymus weight (g)
0.08
0.06
0.04
0.02
0
***
***
WT
RAG2-/-
RAG2-/-/ Kind3+/+
RAG2-/-/ Kind3-/-
Controls
Chimeras
C
n=11,13,13,13
Thymus cellularity (10^6)
300
250
200
150
100
50
0
***
***
WT
RAG2-/-
RAG2-/-/ Kind3+/+
RAG2-/-/ Kind3-/-
Controls
Chimeras
D
Lin^neg thymocytes (DN1-4)
WT
RAG2-/-
RAG2-/-/Kind3+/+
RAG2-/-/Kind3-/-
CD44-PE
cKIT-APC
3.31
0.72
4.92
0.28
CD44-PE
CD25-FITC
1.71 DN1 DN2 2.02
40.3 DN4 DN3 56
0.86 0.74
0.1 98.3
2.41 4.1
36.7 56.7
1.18 0.4
0.72 97.7
E
DN1-2 cell frequency (%)
6
5
4
3
2
1
0
**
***
***
n=11,13,13,8
WT
RAG2-/-
RAG2-/-/ Kind3+/+
RAG2-/-/ Kind3-/-
Controls
Chimeras
F
DN4 cell frequency (%)
50
45
40
35
30
25
20
15
10
5
0
**
***
***
n=11,13,13,8
WT
RAG2-/-
RAG2-/-/ Kind3+/+
RAG2-/-/ Kind3-/-
Controls
Chimeras

FIGURE 4

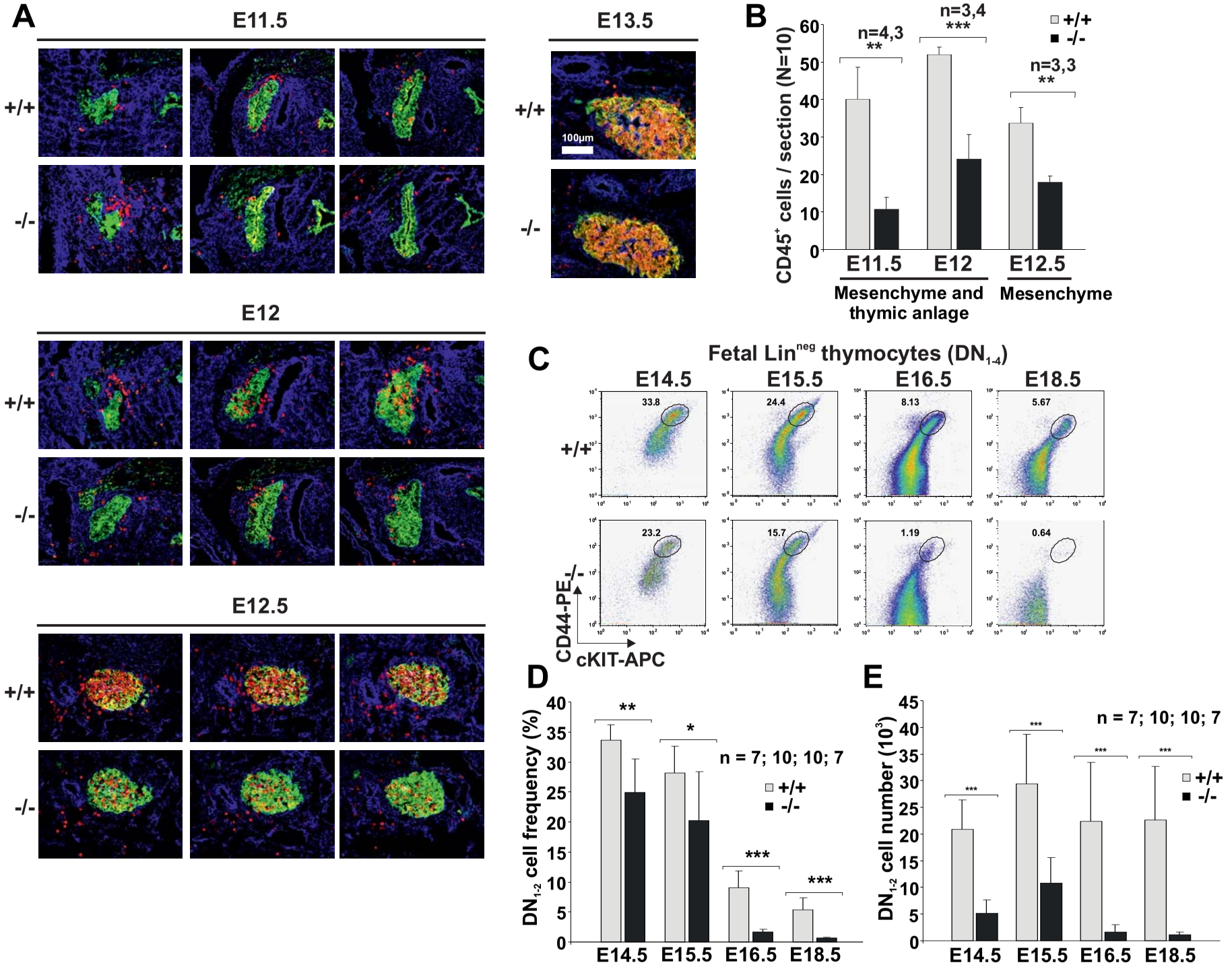
A
E11.5
E13.5
E12
E12.5
+/+
-/-
100µm
B
CD45+ cells / section (N=10)
n=4,3
**
n=3,4
***
n=3,3
**
+/+
-/-
E11.5
E12
E12.5
Mesenchyme and thymic anlage
Mesenchyme
C
Fetal Lin^neg thymocytes (DN1-4)
E14.5
E15.5
E16.5
E18.5
33.8
24.4
8.13
5.67
23.2
15.7
1.19
0.64
CD44-PE
cKIT-APC
D
DN1-2 cell frequency (%)
n = 7; 10; 10; 7
E
DN1-2 cell number (10^3)
n = 7; 10; 10; 7

FIGURE 5

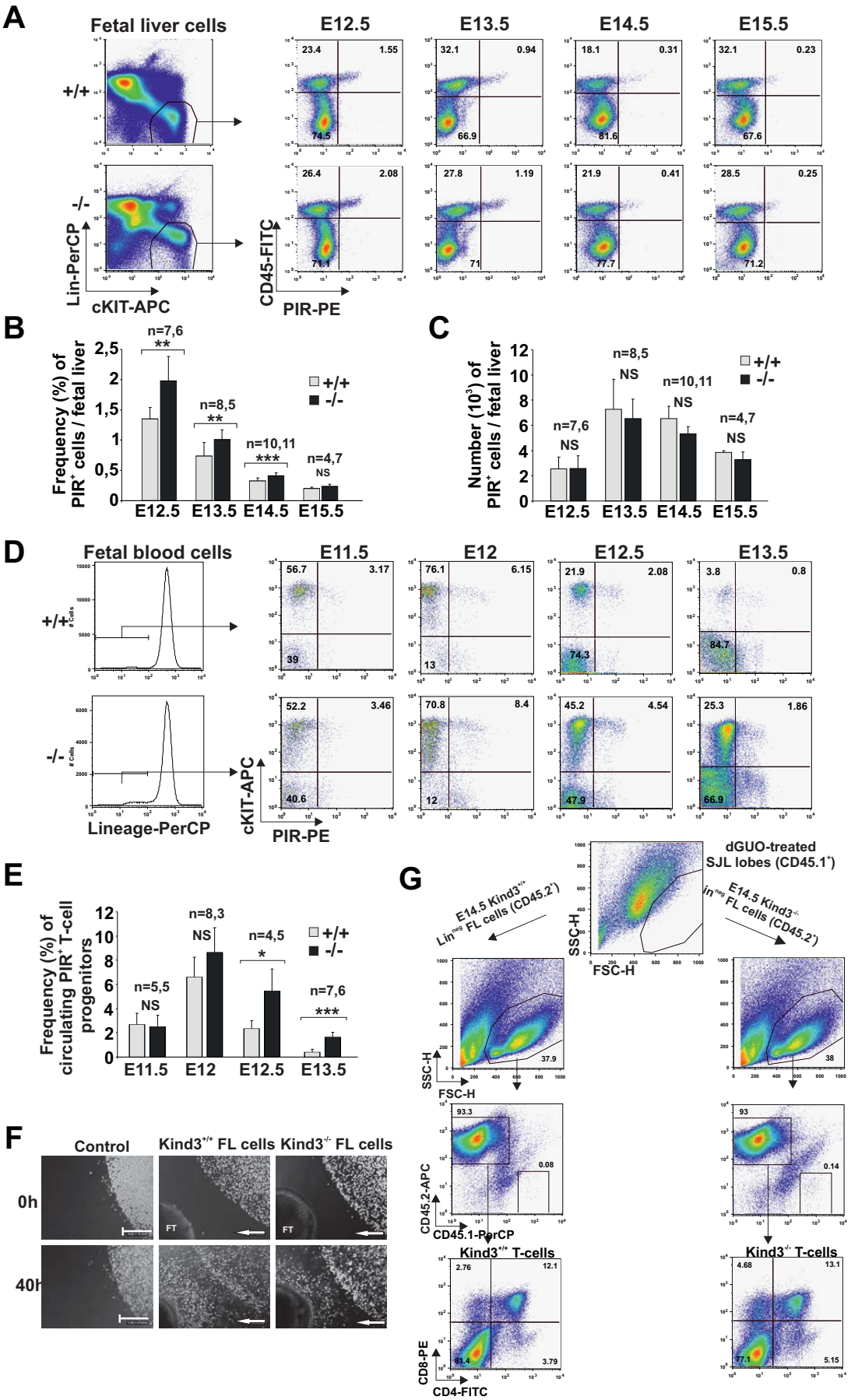
A
Fetal liver cells
E12.5
E13.5
E14.5
E15.5
+/+
-/-
Lin-PerCP
cKIT-APC
CD45-FITC
PIR-PE
B
Frequency (%) of PIR+ cells / fetal liver
n=7,6
**
n=8,5
**
n=10,11
***
n=4,7
NS
+/+
-/-
E12.5 E13.5 E14.5 E15.5
C
Number (10^3) of PIR+ cells / fetal liver
n=7,6
NS
n=8,5
NS
n=10,11
NS
n=4,7
NS
+/+
-/-
E12.5 E13.5 E14.5 E15.5
D
Fetal blood cells
E11.5
E12
E12.5
E13.5
+/+
-/-
Lineage-PerCP
cKIT-APC
PIR-PE
E
Frequency (%) of circulating PIR+ T-cell progenitors
n=5,5
NS
n=8,3
NS
n=4,5
*
n=7,6
***
+/+
-/-
E11.5 E12 E12.5 E13.5
F
Control
Kind3+/+ FL cells
Kind3-/- FL cells
0h
40h
FT
G
E14.5 Kind3+/+ Lin-neg FL cells (CD45.2+)
E14.5 Kind3-/- Lin-neg FL cells (CD45.2+)
dGUO-treated SJL lobes (CD45.1+)
SSC-H
FSC-H
CD45.2-APC
CD45.1-PerCP
Kind3+/+ T-cells
Kind3-/- T-cells
CD8-PE
CD4-FITC

FIGURE 6

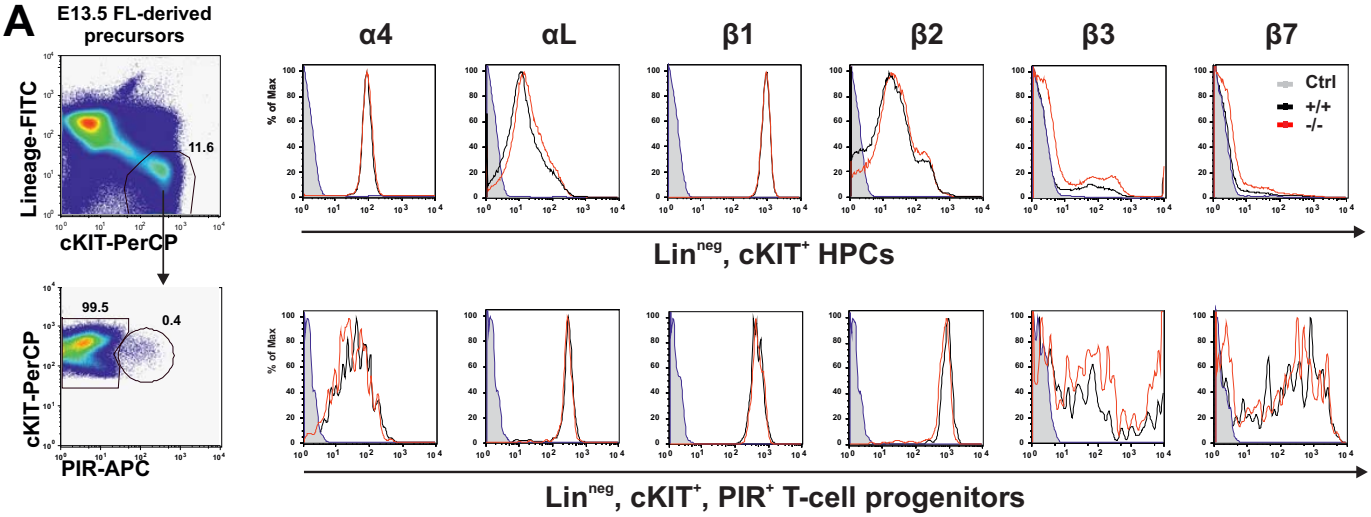
A
E13.5 FL-derived precursors
Lineage-FITC
cKIT-PerCP
11.6
99.5
0.4
PIR-APC
α4
αL
β1
β2
β3
β7
Ctrl
+/+
-/-
% of Max
Lin^neg, cKIT^+ HPCs
Lin^neg, cKIT^+, PIR^+ T-cell progenitors

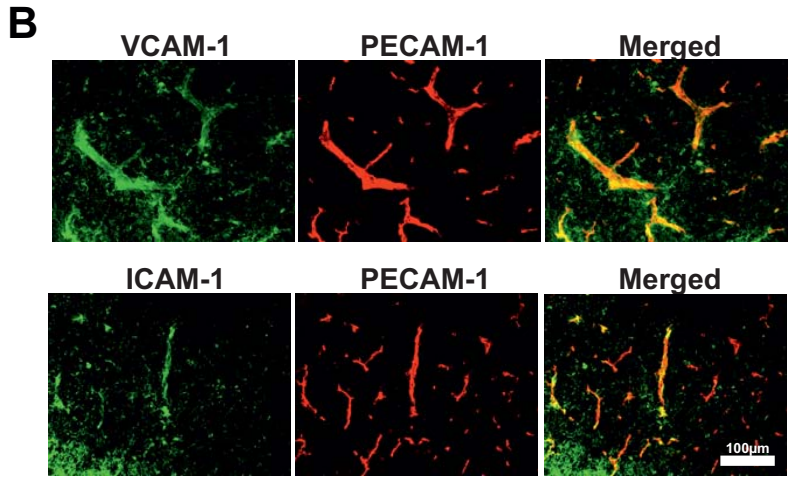
B
VCAM-1
PECAM-1
Merged
ICAM-1
PECAM-1
Merged
100μm

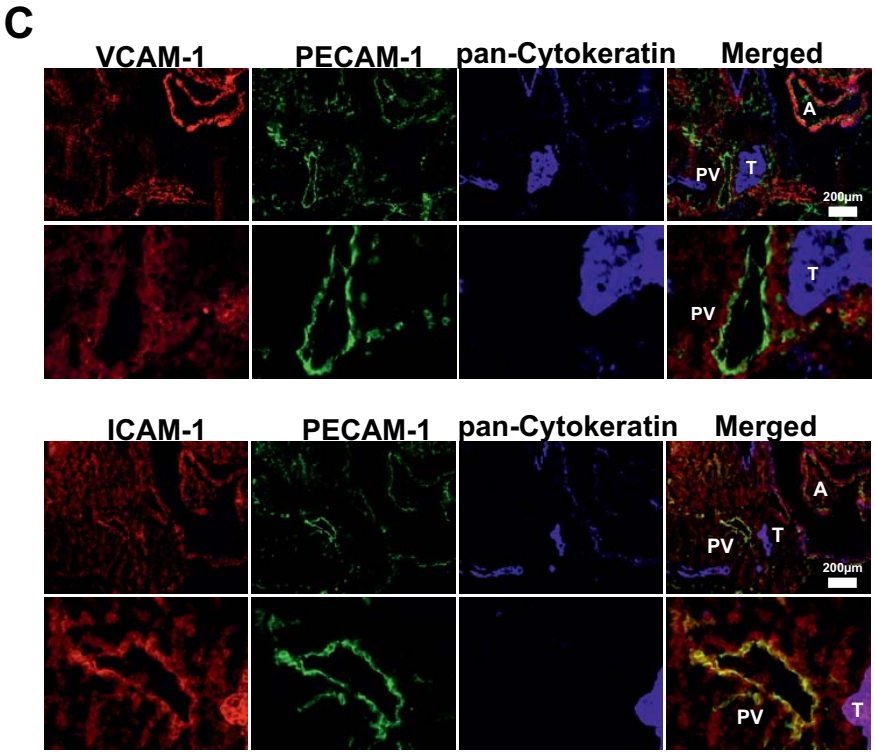
C
VCAM-1
PECAM-1
pan-Cytokeratin
Merged
A
PV
T
200μm
ICAM-1
PECAM-1
pan-Cytokeratin
Merged

FIGURE 7

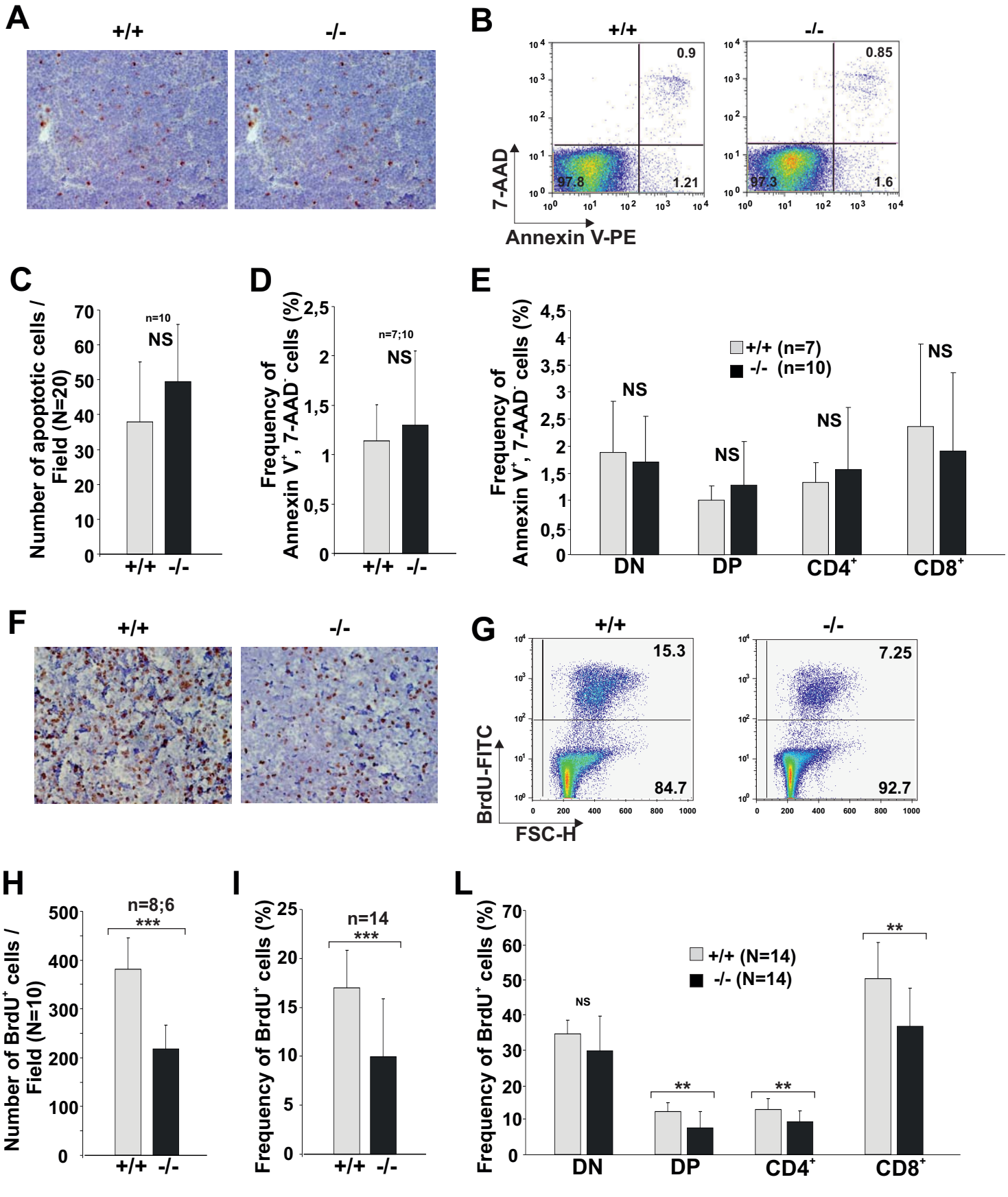
A
+/+
-/-
B
+/+
-/-
0.9
1.21
97.8
0.85
1.6
97.3
7-AAD
Annexin V-PE
C
Number of apoptotic cells / Field (N=20)
n=10
NS
+/+ -/-
D
Frequency of Annexin V+, 7-AAD- cells (%)
n=7;10
NS
+/+ -/-
E
Frequency of Annexin V+, 7-AAD- cells (%)
+/+ (n=7)
-/- (n=10)
NS
DN
DP
CD4+
CD8+
F
+/+
-/-
G
+/+
-/-
15.3
84.7
7.25
92.7
BrdU-FITC
FSC-H
H
Number of BrdU+ cells / Field (N=10)
n=8;6
***
+/+ -/-
I
Frequency of BrdU+ cells (%)
n=14
***
+/+ -/-
L
Frequency of BrdU+ cells (%)
+/+ (N=14)
-/- (N=14)
NS
**
DN
DP
CD4+
CD8+

FIGURE 8

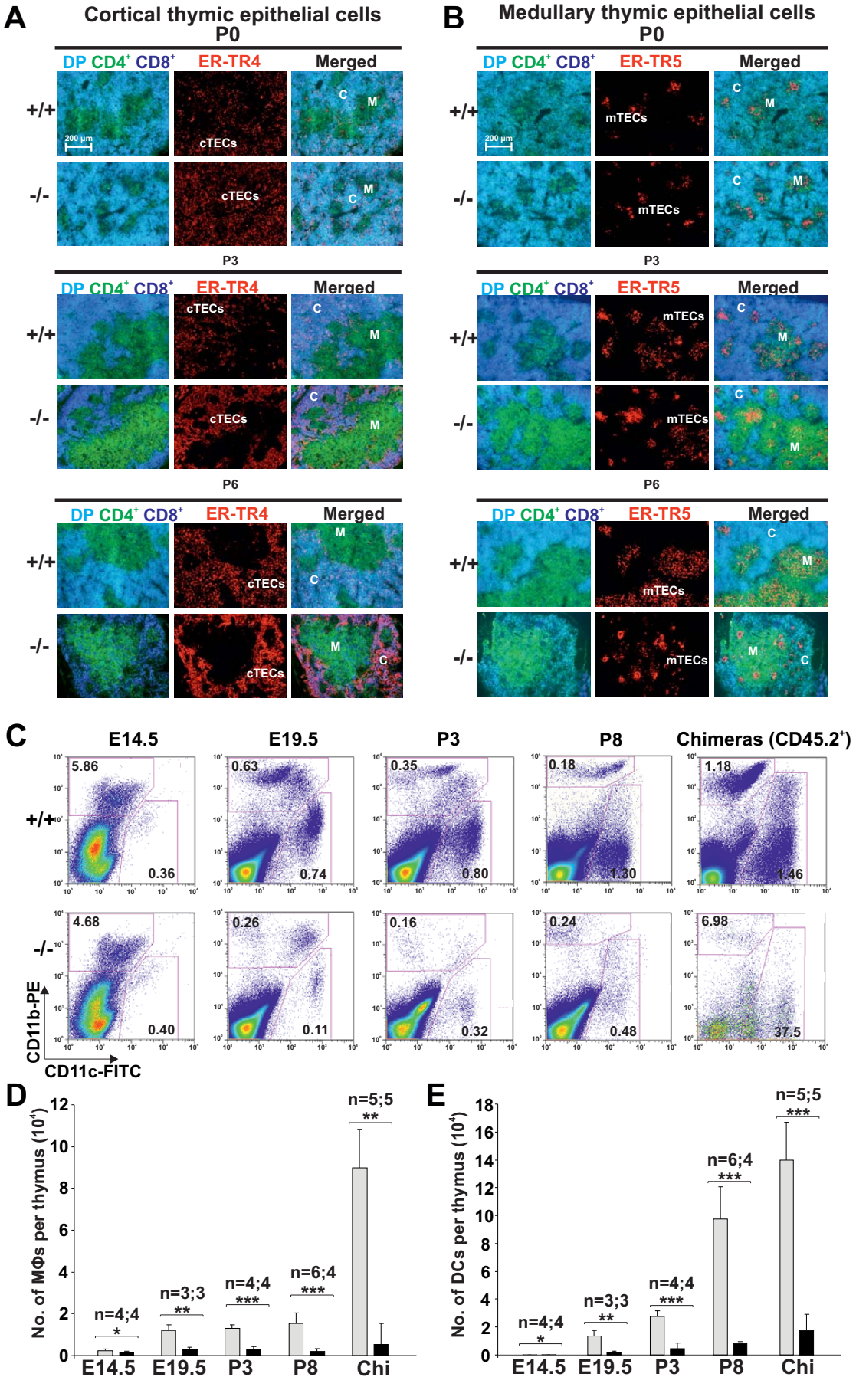
A
Cortical thymic epithelial cells
P0
DP CD4+ CD8+
ER-TR4
Merged
+/+
-/-
200 µm
cTECs
C
M
P3
P6
B
Medullary thymic epithelial cells
ER-TR5
mTECs
C
M
C
5.86
0.36
0.63
0.74
0.35
0.80
0.18
1.30
1.18
1.46
4.68
0.40
0.26
0.11
0.16
0.32
0.24
0.48
6.98
37.5
E14.5
E19.5
P3
P8
Chimeras (CD45.2+)
CD11b-PE
CD11c-FITC
D
No. of MΦs per thymus (10⁴)
n=4;4
n=3;3
n=4;4
n=6;4
n=5;5
*
**
***
E14.5
E19.5
P3
P8
Chi
E
No. of DCs per thymus (10⁴)

Suppl. Fig 1

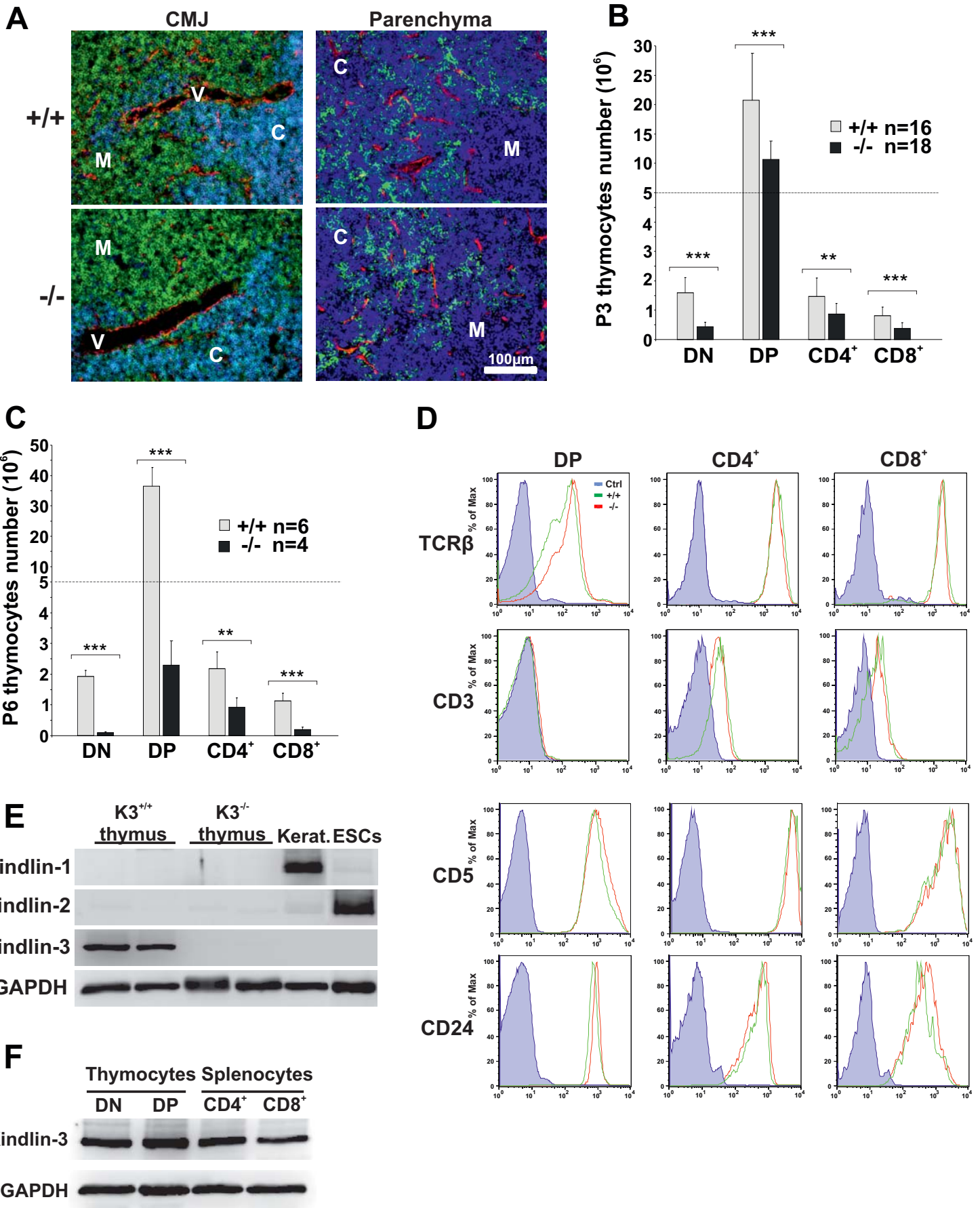
A
CMJ
Parenchyma
+/+
-/-
V
C
M
100µm
B
P3 thymocytes number (10^6)
+/+ n=16
-/- n=18
***
**
DN
DP
CD4+
CD8+
C
P6 thymocytes number (10^6)
+/+ n=6
-/- n=4
D
DP
CD4+
CD8+
TCRβ
CD3
CD5
CD24
% of Max
Ctrl
+/+
-/-
E
K3+/+ thymus
K3-/- thymus
Kerat. ESCs
Kindlin-1
Kindlin-2
Kindlin-3
GAPDH
F
Thymocytes
Splenocytes
DN
DP
CD4+
CD8+
Kindlin-3
GAPDH

Suppl. Fig 2

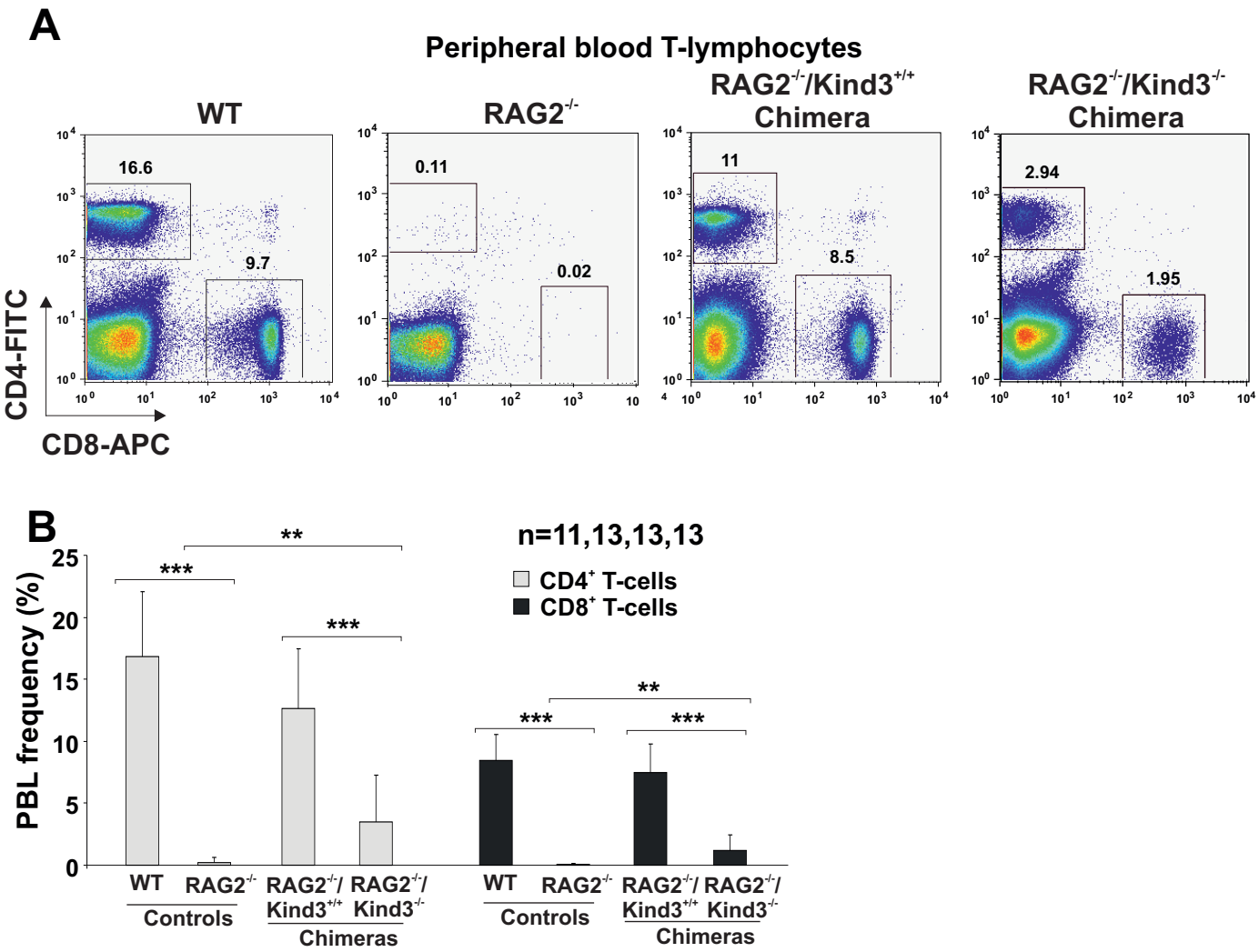
A
Peripheral blood T-lymphocytes
WT
RAG2-/-
RAG2-/-/Kind3+/+ Chimera
RAG2-/-/Kind3-/- Chimera
16.6
9.7
0.11
0.02
11
8.5
2.94
1.95
CD4-FITC
CD8-APC
B
n=11,13,13,13
CD4+ T-cells
CD8+ T-cells
PBL frequency (%)
WT
RAG2-/-
RAG2-/-/ Kind3+/+
RAG2-/-/ Kind3-/-
Controls
Chimeras

Suppl. Fig 3

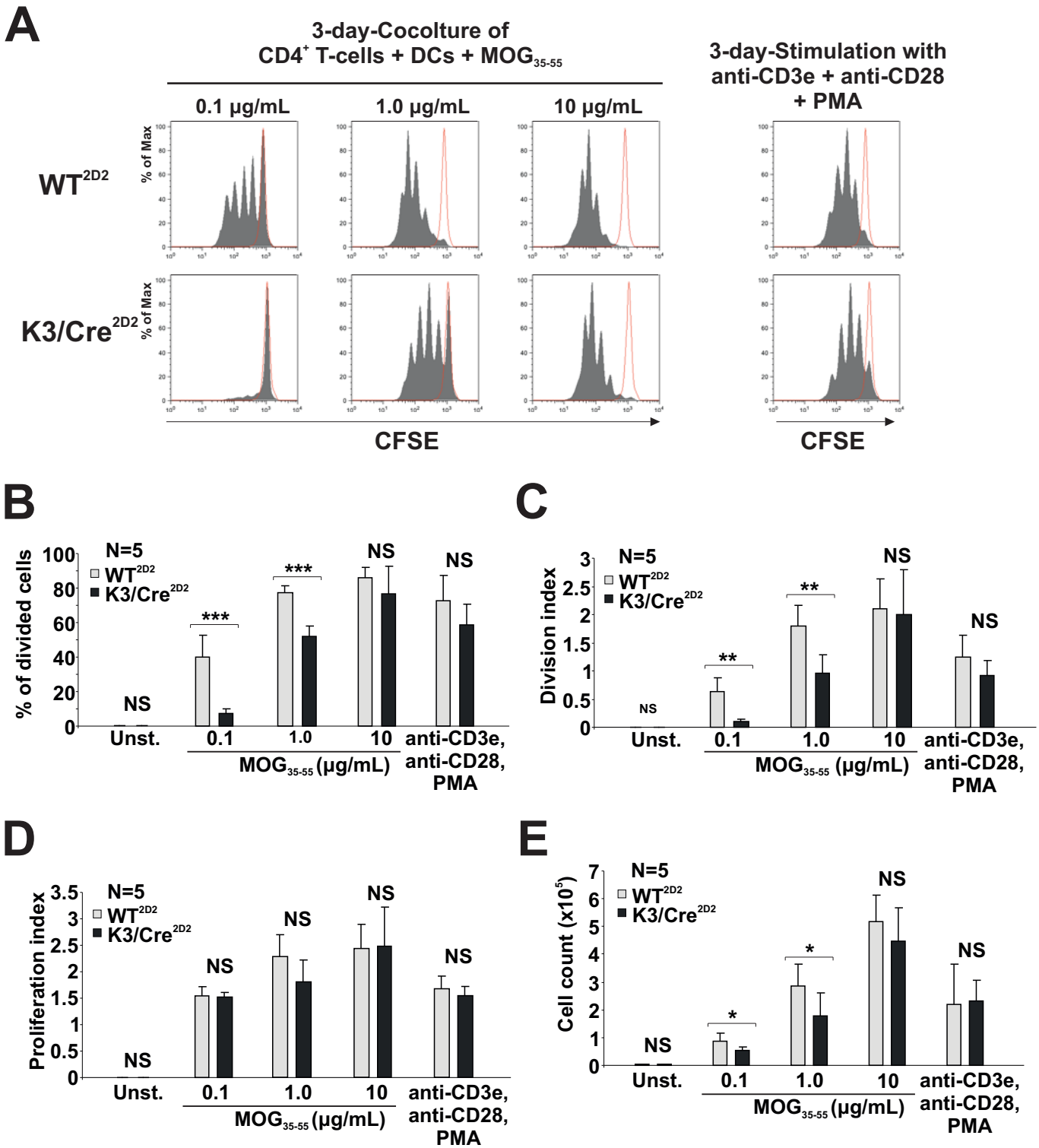
A
3-day-Cocolture of
CD4+ T-cells + DCs + MOG35-55
3-day-Stimulation with
anti-CD3e + anti-CD28
+ PMA
0.1 µg/mL
1.0 µg/mL
10 µg/mL
WT2D2
K3/Cre2D2
% of Max
CFSE
B
% of divided cells
N=5
WT2D2
K3/Cre2D2
***
NS
Unst.
0.1
1.0
10
MOG35-55 (µg/mL)
anti-CD3e,
anti-CD28,
PMA
C
Division index
**
D
Proliferation index
E
Cell count (x10^5)
*

12.5 Paper 5:

Kindlin-3 regulates integrin activation and adhesion reinforcement of effector T cells.

Kindlin-3 regulates integrin activation and adhesion reinforcement of effector T cells

Federico A. Moretti[a,1], Markus Moser[a,1], Ruth Lyck[b], Michael Abadier[b], Raphael Ruppert[a], Britta Engelhardt[b], and Reinhard Fässler[a,2]

[a]Department of Molecular Medicine, Max Planck Institute of Biochemistry, D-82152 Martinsried, Germany; and [b]Theodor Kocher Institute, University of Bern, CH-3012 Bern, Switzerland

Edited by Timothy A. Springer, Immune Disease Institute, Program in Cellular and Molecular Medicine, Children's Hospital Boston, Boston, MA, and approved September 10, 2013 (received for review August 28, 2013)

Activated T cells use very late antigen-4/α4β1 integrin for capture, rolling on, and firm adhesion to endothelial cells, and use leukocyte function-associated antigen-1/αLβ2 integrin for subsequent crawling and extravasation. Inhibition of α4β1 is sufficient to prevent extravasation of activated T cells and is successfully used to combat autoimmune diseases, such as multiple sclerosis. Here we show that effector T cells lacking the integrin activator Kindlin-3 extravasate and induce experimental autoimmune encephalomyelitis in mice immunized with autoantigen. In sharp contrast, adoptively transferred autoreactive T cells from Kindlin-3–deficient mice fail to extravasate into the naïve CNS. Mechanistically, autoreactive Kindlin-3–null T cells extravasate when the CNS is inflamed and the brain microvasculature expresses high levels of integrin ligands. Flow chamber assays under physiological shear conditions confirmed that Kindlin-3–null effector T cells adhere to high concentrations of vascular cell adhesion molecule-1 and intercellular adhesion molecule-1, albeit less efficiently than WT T cells. Although these arrested T cells polarize and start crawling, only few remain firmly adherent over time. Our data demonstrate that the requirement of Kindlin-3 for effector T cells to induce α4β1 and αLβ2 integrin ligand binding and stabilization of integrin–ligand bonds is critical when integrin ligand levels are low, but of less importance when integrin ligand levels are high.

integrin affinity | EAE

In experimental autoimmune encephalitis (EAE), autoreactive $CD4^+$ Th cells, which recognize components of the myelin sheath of nerve fibers, extravasate into the CNS and induce breakdown of the blood–brain barrier and severe inflammation, leading to the destruction of brain tissue (1). Integrins play pivotal roles during this process. P-selectin–mediated rolling and α4β1 (VLA4)-VCAM-1 (vascular cell adhesion molecule-1)–mediated capture of encephalitogenic T cells on the brain endothelium is followed by αLβ2 (LFA-1)-ICAM-1/2 (intercellular adhesion molecule-1/2)–mediated T-cell polarization, crawling, and diapedesis (2). Once the T cells have passed the circulation, they become reprimed by antigen-presenting cells, which expose self-antigens of the myelin to further stimulate T-cell proliferation (3).

A hallmark of integrins is their ability to shift from an inactive to an active state (i.e. inside-out signalling), which is associated with an allosteric change of the integrin ectodomain and transmembrane domains and results in adhesion, sensing of substrate stiffness, and signal transduction (i.e. outside-in signalling) (4, 5). The allosteric modulation of the affinity state of integrins is regulated by talin and kindlin binding to the cytoplasmic domain of the β subunit (6) and is of particular importance for circulating platelets and leukocytes, which require fast attachment to blood vessel walls to seal leaks or react to inflammation. In addition to chemical allostery, integrin affinity also can be regulated by increasing the lifetime of integrin–ligand bonds, which can be achieved by integrin clustering, also known as avidity modulation (7, 8), and/or by application of tension (by, e.g., myosin II motors) to the adhesive bonds, resulting in the formation of catch bonds (9, 10). Whether kindlins are involved in bond lifetime regulation is not known.

Kindlins are evolutionary conserved and consist of three members (11). Hematopoietic cells express Kindlin-3 (11), the deletion of which in mice abrogates integrin activation, resulting in hemorrhages, leukocyte adhesion defects, and osteopetrosis (12–14). A human disease with similar abnormalities, leukocyte adhesion deficiency type III (LADIII), is also caused by null mutations of the *Kindlin-3* (*FERMT3*) gene (15–17). The severe LADIII defects lead to perinatal lethality, hindering the analysis of Kindlin-3 in specific blood cell lineages. We used conditional gene targeting to circumvent the problem of lethality and investigated the role of Kindlin-3 in effector T cells using EAE as model for T-cell–induced inflammation (18, 19). We report that autoreactive T cells lacking Kindlin-3 cannot extravasate and induce EAE when transferred into healthy mice. Interestingly, however, a high density of integrin ligands on inflamed vascular endothelial cells is sufficient to enable autoreactive T-cell extravasation and disease induction, and also to induce α4β1- and αLβ2-mediated effector T-cell adhesion and αLβ2-mediated crawling even under physiological shear conditions. These findings indicate that increased ligand concentrations can partially substitute Kindlin-3–mediated inside-out signaling, and that Kindlin-3 regulates both the activation of β1 and β2 integrins and the stabilization of integrin–ligand bonds.

Significance

T cells use integrins for adhesion to endothelial cells and extravasation. Thus, their blocking with Abs prevents T cell extravasation and ameliorates autoimmune diseases, such as multiple sclerosis (MS). Given the side effects of these Abs, we explored the integrin activator Kindlin-3 as potential therapeutic target. Mice lacking Kindlin-3 in T cells were immunized with an autoantigen to induce experimental autoimmune encephalitis (EAE), a model of MS. Although these mice developed EAE, adoptively transferred autoreactive T cells from Kindlin-3–deficient mice to healthy recipients failed to induce EAE. We found that autoreactive Kindlin-3–null T cells extravasate only when the brain microvasculature expresses high integrin ligand levels. Thus, blockage of Kindlin-3 is not a viable alternative approach to treating MS.

Author contributions: F.A.M., M.M., R.L., B.E., and R.F. designed research; F.A.M., M.M., R.L., M.A., and R.R. performed research; F.A.M., M.M., R.L., M.A., and R.R. analyzed data; and M.M. and R.F. wrote the paper.

The authors declare no conflict of interest.

This article is a PNAS Direct Submission.

[1]F.A.M. and M.M. contributed equally to this work.

[2]To whom correspondence should be addressed. E-mail: faessler@biochem.mpg.de.

This article contains supporting information online at www.pnas.org/lookup/suppl/doi:10.1073/pnas.1316032110/-/DCSupplemental.

Results

Kindlin-3 Is Not Required to Induce Active EAE. To analyze the role of Kindlin-3 in T cells, we backcrossed mice carrying a floxed Kindlin-3 gene 11 times with C57BL/6 mice (Kindlin-3$^{fl/fl}$, referred to as controls) and subsequently deleted the Kindlin-3 gene with C57BL/6 mice carrying the CD4Cre transgene (20). Western blot analysis demonstrated that CD4$^+$ and CD8$^+$ T cells isolated from the spleen of conditional Kindlin-3$^{fl/fl}$/CD4Cre (hereinafter, K3/Cre) mice lack Kindlin-3 expression (Fig. S1*A*). Kindlin-3 loss still allows the production of normal numbers of CD4$^+$ and CD8$^+$ T cells in the thymus, peripheral blood, and spleen of K3/Cre mice, suggesting that homeostatic T-cell proliferation, differentiation, and distribution in peripheral hematopoietic organs occur independent of Kindlin-3 (Fig. S1 *B*–*D*).

We next investigated whether effector T cells require Kindlin-3 for extravasation and induction of an inflammatory disease. To this end, we immunized mice with the encephalitogenic MOG$_{35–55}$ peptide to induce active EAE (aEAE) (19). K3/Cre mice and control littermates exhibited a similar EAE onset (Fig. 1*A*) with such clinical symptoms as weight loss (Fig. 1*B*) and paralysis (Fig. 1*C*). Immunostaining of the lumbar region of spinal cords revealed that diseased K3/Cre and control animals contained similar numbers of CD45^{high} inflammatory cells and CD45^{medium} microglial cells, Mac-1–positive monocytes/macrophages, and Gr-1-expressing granulocytes and macrophages. Furthermore, the subarachnoidal space and the spinal cord parenchyma of K3/Cre and control mice contained a comparable infiltrate of autoreactive CD4$^+$ T cells (Fig. 1*D*). Importantly, isotype control Ab staining verified the specificity of the immunostaining. FACS sorting of T cells from K3/Cre CNS infiltrates revealed normal numbers of CD4$^+$ T cells (Fig. S1*E*), and Western blot analysis confirmed the loss of Kindlin-3 expression (Fig. 1*E*). Taken together, these findings suggest that Kindlin-3–deficient T cells are able to extravasate and induce EAE.

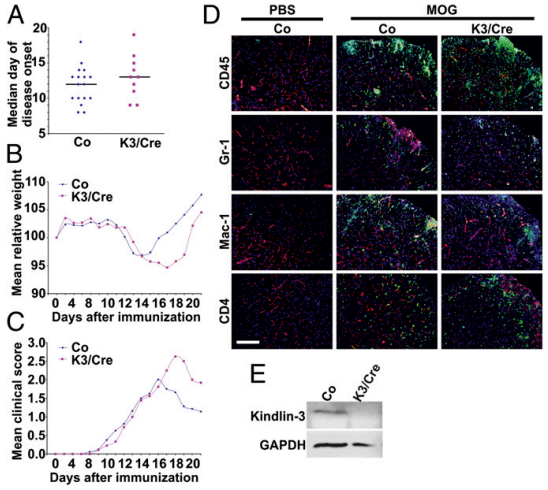

Fig. 1. aEAE in mice lacking Kindlin-3 expression in T cells. (*A*) Median day of disease onset in Kindlin-3$^{fl/fl}$/CD4Cre$^+$ (K3/Cre) and control (Co) mice with aEAE. (*B* and *C*) Relative weight normalized to day 0 (*B*) and clinical disease score (*C*) of mice with aEAE. Data points indicate means of 16 Co mice and 9 K3/Cre mice from two independent experiments. (*D*) Healthy control (PBS-treated) and diseased (MOG peptide-treated) mice with ongoing aEAE (clinical disease score 4) were killed, and spinal cord white matter was analyzed by immunostaining. Infiltrating leukocytes were stained with anti-CD45, anti-CD4, anti-Mac-1, or anti-Gr-1 Abs (green); blood vessels were stained with a pan-laminin Ab (red); and nuclei were stained with DAPI (blue). (Scale bar: 200 μm.) (*E*) Western blot analysis of protein lysates of FACS-sorted CD4$^+$ cells from the CNS of K3/Cre and Co mice with ongoing aEAE. GAPDH served as a loading control.

Kindlin-3 Is Required to Induce Passive EAE. The development of aEAE and the presence of Kindlin-3–deficient T cells in brain infiltrates of K3/Cre mice suggest that Kindlin-3 is not required for effector T-cell extravasation. To corroborate this finding, we tested whether Kindlin-3–deficient encephalitogenic T-cell blasts are able to induce passive EAE (pEAE) (18) in WT C57BL/6 mice. To this end, we crossed K3/Cre and littermate control mice with 2D2 mice, which express an MHC-II–restricted T-cell receptor (TCR) that specifically recognizes the MOG$_{35–55}$ peptide (21). We isolated naïve CD4$^+$ T splenocytes from Kindlin-3$^{fl/fl}$/2D2$^+$/CD4Cre$^+$ (hereinafter, K3/Cre^{2D2}) and control Kindlin-3$^{fl/fl}$/2D2$^+$ (hereinafter, Co^{2D2}) mice and primed them for several days in vitro with MOG$_{35–55}$-loaded dendritic cells (DCs) to induce proliferation and differentiation into memory (i.e., CD62L^{hi}/CD44^{hi}) and effector (i.e., CD62L^{low}/CD44^{hi}) T cells (Fig. 2*A*). The differentiated T-cell populations derived from K3/Cre^{2D2} mice expressed normal levels of integrins and T-cell–specific maturation and activation markers (Fig. S2*A*), and lacked Kindlin-3 protein expression (Fig. 2*B*). Importantly, encephalitogenic T cells did not express α9β1 integrins (Fig. S2*B*), which can bind VCAM-1 as well.

To test whether Kindlin-3 affects T-cell differentiation into Th1, Th2, or Th17 cells, we performed intracellular FACS staining for IL-2, IFN-γ, TNF-α, IL-4, and IL-17. In these experiments, most Co^{2D2} and K3/Cre^{2D2} cells were positive for IFN-γ and TNF-α, indicating that they are Th1-polarized rather than Th17-polarized (Fig. S2*C*). Consistent with the essential role of Kindlin-3 in integrin activation, resting and phorbol 12-myristate 13-acetate (PMA)-stimulated K3/Cre^{2D2} effector T cells showed significantly reduced levels of 9EG7 epitope, which is induced in activated β1 integrins. Bypassing cellular activation by the addition of manganese resulted in comparable 9EG7 binding of Co^{2D2} and K3/Cre^{2D2} effector T cells (Fig. S2*D*). Similarly, binding assays with soluble VCAM-1 revealed that both resting and PMA-stimulated K3/Cre^{2D2} effector T cells bound significantly less VCAM-1 than control cells, which was rescued with manganese (Fig. S2*E*).

We next transferred the encephalitogenic T-cell blasts into sublethally irradiated WT C57BL/6 mice. As expected, the transfer of Co^{2D2} T-cell blasts induced EAE pathology with T-cell infiltration into the spinal cord, weight loss, and paralysis at approximately 11 d after the adoptive cell transfer (Fig. 2 *C*–*E*). Unexpectedly, however, none of the recipient mice that received K3/Cre^{2D2} T-cell blasts developed EAE (Fig. 2 *C*–*E*), and in all recipients, Kindlin-3–deficient encephalitogenic 2D2$^+$ T cells were detectable in the circulation for more than 3 wk after K3/Cre^{2D2} T-cell transfer (Fig. S2*F*). Thus, in contrast to aEAE, the adoptive T-cell transfer experiments indicate that loss of Kindlin-3 protein in T-cell blasts prevents entry into a healthy CNS and thus induction of EAE.

Kindlin-3 Regulates Initial Arrest and Firm Adhesion to VLA-4 and LFA-1. Why can Kindlin-3–deficient encephalitogenic T cells enter the brain parenchyma to induce aEAE, but not pEAE? Induction of aEAE was achieved by immunization with antigens and the simultaneous treatment with complete Freund's adjuvant (CFA) and pertussis toxin (PT), which induces elevated expression of VCAM-1 and ICAM-1 on endothelial cells (Fig. 3 *A* and *B*) (22, 23). In contrast, in pEAE, T-cell blasts encounter naïve endothelial cells expressing low levels of ICAM-1 and VCAM-1. Thus, we hypothesized that high surface levels of endothelial cell adhesion molecules overcome compromised adhesive properties of Kindlin-3–deficient effector T cells and subsequent disease induction, whereas low integrin-ligand expression permits

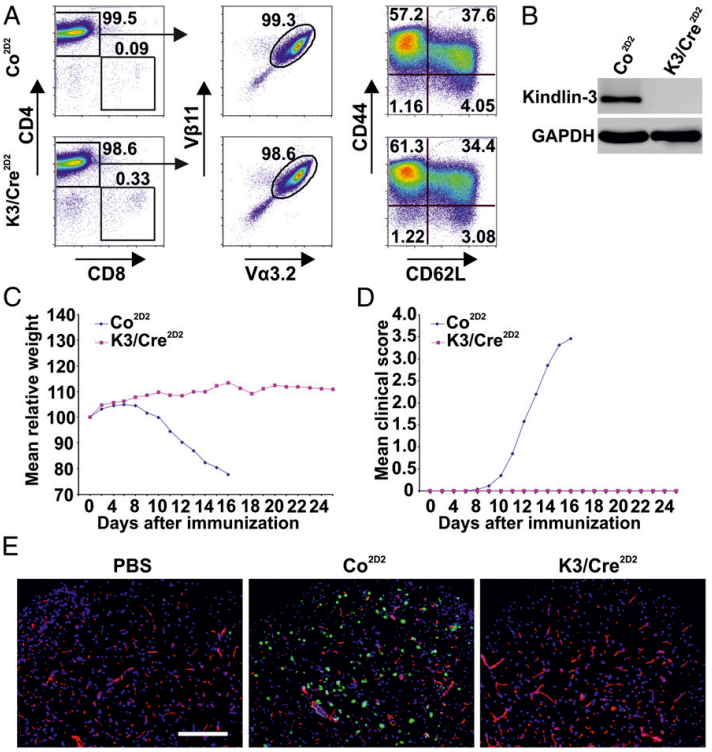

Fig. 2. Adoptively transferred autoreactive Kindlin-3–deficient T cells fail to induce EAE. (*A*) FACS analysis of in vitro-generated autoreactive T cells. Anti-CD4 and anti-CD8 Abs were used to identify $CD4^+$ T helper cells (*Left*), anti-Vα3.2 and anti-Vβ11 were used to identify $2D2^+$ cells (*Center*), and anti-CD62L and anti-CD44 were used to identify memory ($CD62L^{hi}/CD44^{hi}$) and effector ($CD62L^{low}/CD44^{hi}$) T cells (*Right*). (*B*) Western blot analysis of in vitro-primed and MACS-sorted Kindlin-$3^{fl/fl}$/$2D2^+$/$CD4Cre^+$ ($K3/Cre^{2D2}$) and control Kindlin-$3^{fl/fl}$/2D2 (Co^{2D2}) T cells. GAPDH served as a loading control. (*C* and *D*) Relative weight normalized to day 0 (*C*) and clinical disease score (*D*) of naïve WT C57BL/6 mice injected with encephalitogenic $K3/Cre^{2D2}$ and Co^{2D2} T cells. Data points represent means from three independent Co^{2D2} (n = 13) and $K3/Cre^{2D2}$ (n = 20) T-cell transfer experiments. (*E*) Immunostaining of the lumbar spinal cord white matter from C57BL/6 mice injected with either PBS or in vitro-generated encephalitogenic Co^{2D2} or $K3/Cre^{2D2}$ T cells. Infiltrating lymphocytes were stained with anti-CD4 Ab (green), blood vessels were stained with a pan-laminin Ab (red), and nuclei were stained with DAPI (blue). (Scale bar: 200 μm.)

adhesion and extravasation only after Kindlin-3–mediated integrin activation.

To test this hypothesis, we generated an inflamed, activated brain endothelium by inducing aEAE (clinical disease score 2) and injected either carboxyfluoresceine diacetate, succinimidyl ester (CFSE)-labeled Co^{2D2} or $K3/Cre^{2D2}$ T-cell blasts into the diseased mice. Immunohistology of spinal cords at 18 h after transfer revealed that Kindlin-3–null CFSE-labeled $CD4^+$ T cells, like WT cells, were indeed present in vessels, meninges, and brain parenchyma of these animals (Fig. 3 *C* and *D*). The quantification of CFSE-labeled T-cell numbers in spinal cord sections from mice injected with Co^{2D2} or $K3/Cre^{2D2}$ T-cell blasts revealed similar T-cell numbers in the spinal cord parenchyma (Fig. 3*E*).

To further validate whether the quantity of endothelial cell adhesion molecules can indeed modulate integrin-mediated adhesion of Kindlin-3–deficient effector T cells, we tested the flow-resistant binding of Co^{2D2} or $K3/Cre^{2D2}$ T-cell blasts to recombinant mouse VCAM-1 (rmVCAM-1) or recombinant mouse ICAM-1 (rmICAM-1) immobilized at different concentrations (24). In the same manner as for pEAE induction, T cells were isolated from spleen and lymph nodes and activated with MOG_{35-55}-loaded DCs. The activated T cells were allowed to accumulate on immunoglobulin cell adhesion molecules (IgCAMs) at very low shear forces (0.1 dyn/cm^2) and then exposed to an increased shear force of 1.5 dyn/cm^2 to wash away nonbound effector T cells (i.e., arrested T cells) and to assess for continuous shear-resistant firm adhesion (i.e., firmly adherent T cells). The numbers of arrested T cells per field of view (FOV) were counted when the laminar flow was reached at 15 s after shear enhancement, and the numbers of firmly adherent T cells per FOV were determined after 5, 10, and 15 min of continuous laminar flow. The experiments were controlled by coating the flow chambers with a nonintegrin ligand [100 nM Delta and Notch-like Epidermal growth factor-related Receptor precursor (DNER)-Fc] that demonstrated no T-cell adhesion. In agreement with our previous findings (25), Co^{2D2} T cells arrested and spread on immobilized rmVCAM-1 (Movie S1), but failed to crawl perpendicular and against the shear, which requires LFA-1–ICAM-1/2 interactions (25). The number of arrested Co^{2D2} T cells was approximately twofold higher than the number of $K3/Cre^{2D2}$ T cells on 100 nM rmVCAM-1 (Fig. 3*F*). The numbers of arrested Co^{2D2} and $K3/Cre^{2D2}$ T cells relative to the arrested T cells on 100 nM rmVCAM-1 decreased with decreasing concentrations (40 nM and 10 nM) of rmVCAM-1 (Fig. 3*G*). However, in relation to control cells, significantly fewer $K3/Cre^{2D2}$ T cells were arrested on 40 nM and 10 nM rmVCAM-1 (Fig. 3*G*). Notably, after exposure to physiological shear force on 100 nM rmVCAM-1 for 15 min, approximately 80% of the Co^{2D2} T cells remained firmly attached, whereas the proportion of firmly attached $K3/Cre^{2D2}$ T cells decreased to 60% after 5 min of continuous shear force and to 40% after 15 min of shear force (Fig. 3*H*). Thus, during continuous laminar flow, a significant number of $K3/Cre^{2D2}$ T cells maintained adhesive contact with rmVCAM-1, although at significantly lower numbers compared with Co^{2D2} T cells (Movie S2). Importantly, preincubation of T cells with an anti-α4β1 Ab blocked T-cell adhesion to VCAM-1, verifying the specificity of the T-cell interaction with rmVCAM-1.

We also analyzed LFA-1–mediated T-cell adhesion, polarity, and crawling on 10 nM, 40 nM, and 100 nM rmICAM-1 in flow experiments. The number of arrested Co^{2D2} T cells on 100 nM rmICAM-1 at 15 s after shear enhancement was fourfold higher than the numbers of $K3/Cre^{2D2}$ effector T cells (Fig. 3*I*).

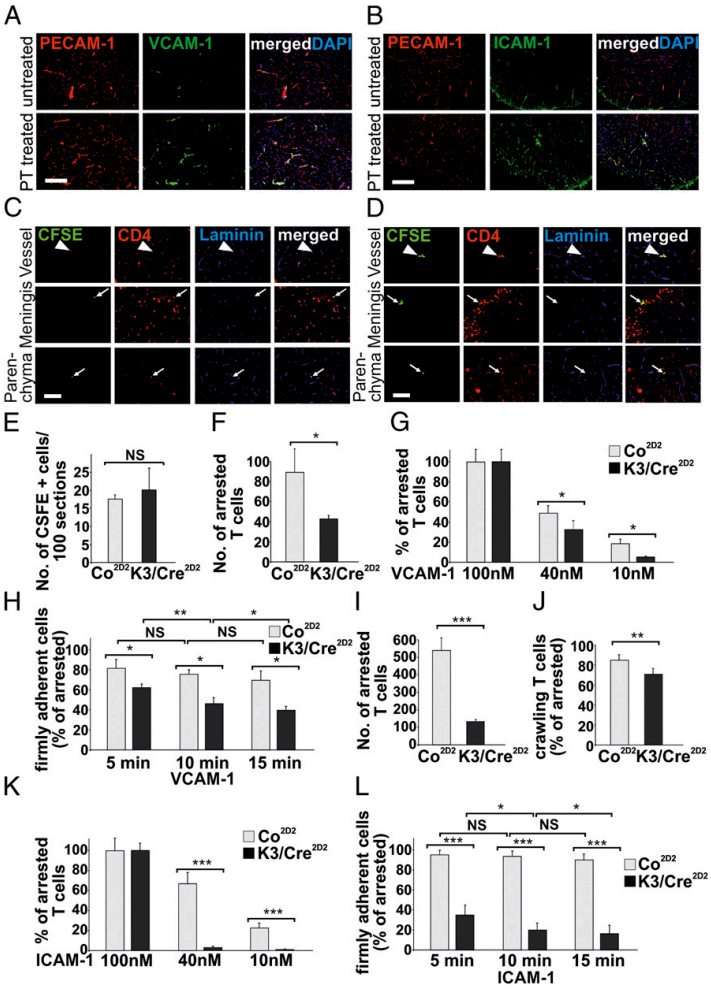

Fig. 3. Kindlin-3 controls firm adhesion of T cells to VCAM-1 and ICAM-1. (*A* and *B*) Spinal cords from untreated and pertussis toxin (PT)-treated animals were stained with anti–VCAM-1 (*A*) and anti–ICAM-1 (*B*) Abs (green). Blood vessels were stained with PECAM-1 Ab (red), and nuclei were stained with DAPI (blue). (Scale bar: 200 μm.) (*C* and *D*) Autoreactive $CFSE^+$-labeled (green) Co^{2D2} T cells (*C*) and $K3/Cre^{2D2}$ T cells (*D*) injected into recipient C57BL/6 animals with ongoing aEAE (clinical disease score 2). Sections from lumbar spinal cords were stained with an anti-CD4 Ab (red) to identify infiltrating T lymphocytes. Blood vessels were stained with a pan-laminin Ab (blue). Arrowheads indicate $CSFE^+$ $CD4^+$ T cells within or in close proximity to blood vessels, and arrows indicate peripheral T cells in the parenchyma or meninges. (Scale bar: 100 μm.) (*E*) Numbers of $CFSE^+$-labeled Co^{2D2} and $K3/Cre^{2D2}$ T cells in the lumbar region of the spinal cord at 18 h after transfer into mice with aEAE (clinical disease score 2). (*F*) Number of T cells arrested on surfaces coated with 100 nM rmVCAM-1 (n = 4 movies for Co; 4 movies for K3/Cre) per FOV. (*G*) Number of arrested T cells determined on surfaces coated with 100 nM (n = 4; 4), 40 nM (n = 4; 4), or 10 nM (n = 4; 4) rmVCAM-1, expressed as percent of arrested T cells on 100 nM VCAM-1. (*H*) Numbers of attached T cells determined at 5, 10 and 15 min of laminar flow at 1.5 dyn/cm^2, expressed as percent of arrested T cells determined at 15 s after shear increase. (*I*) Number of T cells arrested on surfaces coated with 100 nM rmICAM-1 (n = 4; 4). (*J*) Percentage of arrested T cells with crawling activity on 100 nM rmICAM-1 (n = 3; 3). (*K*) Number of arrested T cells determined on surfaces coated with 100 nM (n = 4; 4), 40 nM (n = 4; 4), and 10 nM (n = 4; 4) rmICAM-1 and expressed as percent of arrested T cells on 100 nM ICAM-1. (*L*) Percentage of firmly attached T cells on 100 nM (n = 3; 3) rmICAM-1. Numbers of attached T cells were determined at 5, 10, and 15 min of laminar flow at 1.5 dyn/cm^2 and expressed as percent of arrested T cells determined at 15 s after shear increase. $*P < 0.05$; $**P < 0.01$; $***P < 0.001$; NS, not significant. Data are mean ± SD.

Interestingly, 85% of arrested Co^{2D2} effector T cells and 71% of arrested $K3/Cre^{2D2}$ effector T cells rapidly polarized and began crawling on 100 nM rmICAM-1 (Fig. 3*J* and Movies S3 and S4). Although the proportions of arrested Co^{2D2} effector T cells were decreased on 40 nM and 10 nM rmICAM-1 (to 68% and 23%, respectively) almost no $K3/Cre^{2D2}$ effector T cells were arrested on 40 nM and 10 nM ICAM-1 (4% and 2%, respectively) (Fig. 3*K*). After exposure to physiological shear force, 90% of Co^{2D2} T cells remained firmly attached during the entire 15-min shear force exposure, compared with only 18% of $K3/Cre^{2D2}$ T cells (Fig. 3*L*). Treatment with an anti–LFA-1 Ab prevented adhesion of effector T cells to ICAM-1–coated flow chambers, underscoring the specificity of our assay.

Taken together, these findings indicate that high levels of VCAM-1 allow the arrest and adhesion of a significant number of Kindlin-3–deficient effector T cells under flow, whereas high levels of ICAM-1 enabled adhesion of a few Kindlin-3–deficient effector T cells, which polarized and crawled before they also finally detached.

T Cell Spreading and Adhesion on Brain Microvascular Endothelium Requires Kindlin-3. To investigate how Kindlin-3 affects effector T-cell adhesion and crawling in an ex vivo system, we performed live cell imaging with primary mouse brain microvascular endothelial cells (pMBMECs) (25, 26) stimulated with TNF-α to induce a proinflammatory phenotype with up-regulated expression of VCAM-1 and ICAM-1. After a flow chamber was mounted on the pMBMECs, the chamber was perfused with Co^{2D2} or $K3/Cre^{2D2}$ T cells at low shear force (0.1 dyn/cm^2), to allow accumulation of T cells within a 4-min period. Subsequently, effector T cells were exposed to shear force (0.7 dyn/cm^2) for 10 min, and the interactions of dynamic effector T cells with the brain endothelium were imaged and quantified. The experiments revealed that after 15 s of shear force exposure, both Co^{2D2} T cells and $K3/Cre^{2D2}$ T cells were able to arrest on activated endothelial cells and were immediately polarized (Movies S5 and S6); however, the number of arrested $K3/Cre^{2D2}$ T cells was reduced to 48% of Co^{2D2} T cells (Fig. 4*A*). After 5 min and 10 min of laminar flow, the number of adherent $K3/Cre^{2D2}$ T cells further decreased to 29% and 21%, respectively, whereas the number of

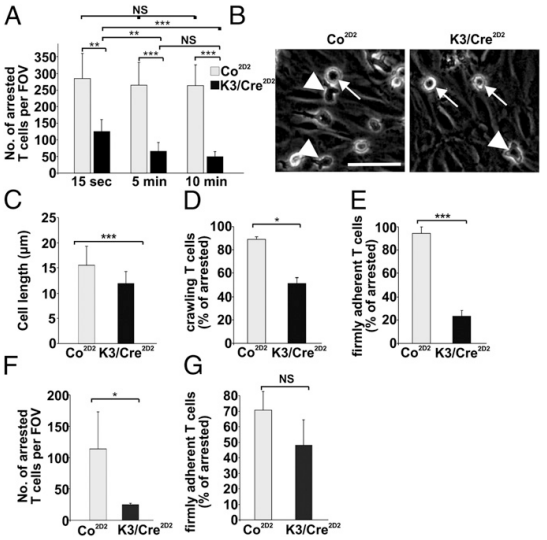

Fig. 4. Kindlin-3 promotes firm adhesion of T cells to primary brain microvascular endothelial cells. T-cell crawling and firm arrest on WT pMBMECs was analyzed by live cell imaging in a flow chamber experimental setup. (*A*) Numbers of arrested and firmly adherent T cells per FOV on WT pMBMECs determined 15 s, 5 min, and 10 min after onset of a 0.7-dyn/cm^2 shear ($n = 7$; 8). (*B*) Arrested K3/Cre^{2D2} T cells are more roundish and less polarized compared with Co^{2D2} T cells on WT pMBMECs. Arrows indicate stationary and more roundish cells, and arrowheads indicate polarized and migratory cells. (*C*) Mean cell lengths of Co^{2D2} and K3/Cre^{2D2} T cells ($n = 105$; 110). (*D*) Percentage of arrested (determined at 15 s after shear enhancement) Co^{2D2} and K3/Cre^{2D2} T cells with crawling activity on WT pMBMECs ($n = 3$ movies for Co; 3 movies for K3/Cre). (*E*) Percentage of arrested T cells able to resist 10 min of shear of 0.7 dyn/cm^2 on pMBMECs ($n = 3$; 3). (*F*) Number of arrested T cells per FOV on ICAM-1/-2 double KO pMBMECs at 15 s after onset of a 0.7-dyn/cm^2 shear ($n = 4$; 4). (*G*) Percentage of arrested T cells from ICAM-1/-2 double KO pMBMECs after 10 min of laminar flow at 0.7 dyn/cm^2 ($n = 4$; 4). *$P < 0.05$; **$P < 0.01$; ***$P < 0.001$. NS, not significant. Data are mean ± SD.

Co^{2D2} T cells remained unchanged (Fig. 4*A*). Although the adherent K3/Cre^{2D2} T cells polarized on the endothelial cell layer, this polarization was less efficient. Co^{2D2} T cells polarized and adopted a mean cell length of 15.50 ± 3.8 µm, whereas K3/Cre^{2D2} T cells polarized with a mean cell length of 11.9 ± 2.3 µm (Fig. 4 *B* and *C*). Importantly, approximately 50% of the adherent and polarized K3/Cre^{2D2} T cells initiated crawling on the brain endothelium before finally detaching within the 10 min of shear exposure (Fig. 4 *D* and *E*). Interestingly, flow chamber assays on TNF-α–treated pMBMECs isolated from ICAM-1^{null}/ICAM-2$^{-/-}$ mice (25) confirmed the important role of VCAM-1 (Fig. 3*E*) in the arrest and firm adhesion of K3/Cre^{2D2} T cells at 15 s after shear enhancement (Fig. 4*F*) and after 10 min of laminar flow (Fig. 4*G*).

Discussion

Inhibition of α4β1 with blocking Abs ameliorates the course of MS and thus has become a powerful therapy for MS (3). Likewise, genetic ablation of β1 in mice inhibits EAE (27), a widely used model for MS in rodents. Because EAE is triggered by autoreactive CD4$^+$ T cells, we used this model to examine the role of the integrin-activating adaptor protein Kindlin-3 for effector T-cell adhesion and crawling on brain endothelial cells, and to test whether Kindlin-3 is required to induce this inflammatory disease.

Stable integrin–ligand interactions require the conversion of the integrin conformation toward a high-affinity state and the subsequent stabilization of integrin–ligand bonds (4, 6). Consequently, it can be assumed that a loss of integrin activation in autoreactive T cells should abrogate α4β1 function and thus also prevent EAE. In line with this expectation, transfer of autoreactive T cells lacking the essential integrin activator Kindlin-3 prevented the development of EAE in recipient mice. In sharp contrast to these findings, however, Kindlin-3–deficient T cells efficiently induced active EAE, despite efficient and complete Kindlin-3 gene deletion. A likely explanation for the different outcomes is the different integrin ligand levels expressed on endothelial cells at the time of EAE induction. This hypothesis is supported by the efficient extravasation of adoptively transferred Kindlin-3–deficient effector T-cell blasts into an inflamed brain that expresses high levels of VCAM-1 and ICAM-1 on endothelial cells.

Why are Kindlin-3–deficient T-cell blasts able to adhere, arrest, and extravasate at sites of high integrin–ligand expression, despite their reduced VCAM-1 and 9EG7 binding? Our flow chamber experiments revealed that Kindlin-3–deficient effector T cells can adopt an affinity state for α4β1 integrin that allows remarkably efficient T-cell capture and transient arrest on recombinant VCAM-1. In contrast, transient effector T-cell adhesion to recombinant ICAM-1 was much more strongly impaired, indicating that αLβ2 integrins critically depend on Kindlin-3 for adoption of a high-affinity state. Interestingly, however, increasing levels of VCAM-1 as well as ICAM-1 increased the arrest of Kindlin-3–deficient effector T cells under shear force. Despite this efficient arrest of Kindlin-3–deficient effector T cells at high VCAM-1 levels, firm adhesion on recombinant VCAM-1 and endothelial cells was reduced. These findings are in line with a previous report showing that chemokine-stimulated Kindlin-3–deficient LAD-III effector T cells show transient adhesion, but not stable adhesion, to VCAM-1 under flow conditions (28). Furthermore, these findings suggest that α4β1 on Kindlin-3–deficient effector T cells can adopt an affinity state sufficient for the production of weak α4β1–VCAM-1 interactions. The number of weak α4β1–VCAM-1 interactions on activated brain endothelial cells may increase to a level that enables sufficient numbers of T-cell blasts to firmly adhere, extravasate, and induce disease.

A similar mechanism also operates with αLβ2 on Kindlin-3–deficient effector T cells and has been suggested for Kindlin-3–deficient neutrophils, on which αLβ2 can adopt an intermediate conformation allowing slow leukocyte rolling on endothelial cells (29). This intermediate conformation of αLβ2 requires Talin-1, suggesting that the initial contact with ICAM-1 is Kindlin-3–independent, whereas further conformational changes associated with the high-affinity state are Kindlin-3–dependent (29). A similar finding also has been reported for αIIbβ3 integrin binding to fibrinogen, which occurs in the presence of Talin-1 alone (30).

A further striking finding of the present study is that a small but significant number of Kindlin-3–deficient T cells adhered to recombinant ICAM-1– or TNF-α–treated endothelial cells and began to polarize and crawl, albeit less efficiently than WT T cells. This clearly indicates that β2 integrins induce outside-in signals even in the absence of Kindlin-3 and before reaching a fully active conformation. In contrast, the majority of Kindlin-3–deficient T cells attached to VCAM-1, ICAM-1, or TNF-α–treated endothelial cells are unable to resist higher shear forces, indicating that strengthening of integrin interactions with these ligands requires further changes in α4β1 and αLβ2 that are mediated by Kindlin-3 (31, 32). It is possible that these changes represent conformational changes of the integrin ectodomain induced by tension and resulting in the formation of catch bonds that increase bond lifetimes. It is also possible that Kindlin-3 increases bond lifetimes by clustering integrins, thereby enabling avidity that combines the strength of multiple integrin–ligand bonds (33). The mechanism regulated by Kindlin-3, and whether

this pathway can be exploited to combat inflammation, remain to be identified and tested.

Materials and Methods

Animals. Kindlin-3 floxed (Kindlin-3$^{fl/fl}$) mice, in which exons 3–6 of the Kindlin-3 gene is flanked with loxP sites, were backcrossed more than 11 times with C57BL/6 mice, then intercrossed with C57BL/6 mice carrying a CD4 promoter-driven Cre recombinase transgene (20). To obtain $MOG_{35–55}$-specific TCR transgenic mice deficient for the Kindlin-3 gene, Kindlin-3$^{fl/fl}$/CD4Cre^{+} mice were intercrossed with 2D2 transgenic mice (21). All mice were bred in the animal facilities at the Max Planck Institute of Biochemistry. All EAE experiments were performed in accordance with the license of the government of Oberbayern.

Induction of aEAE and pEAE. aEAE was induced by s.c. administration of $MOG_{35–55}$ peptide as described previously (34). pEAE was induced by an i.v. transfer of 2×10^6 encephalitogenic T cells into WT sex-matched C57BL/6 mice sublethally irradiated with 3.5 Gy. To obtain encephalitogenic T cells, spleen and axillary, brachial, inguinal, and paraaortal lymph nodes were isolated from Kindlin-3$^{fl/fl}$/2D2^{+}/CD4Cre^{+} and control Kindlin-3$^{fl/fl}$/2D2^{+} mice. Single-cell suspensions were obtained, and after ammonium-chloride-potassium lysis of RBCs, cells from two mice were cocultured with 4×10^6 DCs loaded for 2 h with 20 μg/mL $MOG_{35–55}$ peptide. After 4 d of coculture, the cell suspensions were split 1:2 into medium containing 5 ng/mL IL-2 (R&D Systems). After another 6 d of culture, dead cells were removed by density gradient centrifugation (Nycoprep 1.077; Axis-Shield). A total of 2×10^6 cells per well were incubated overnight in 24-well plates coated with 1 μg/mL anti-mouse CD3e and CD28 Abs (both from eBioscience) and in the presence of recombinant murine IL-18 (20 ng/mL; MBL) and IL-12 (25 ng/mL) and IL-23 (10 ng/mL; both from R&D Systems). The cells were then washed three times with PBS and transferred i.v. into recipient mice. Clinical disease score and weight of the mice with aEAE and transfer EAE were checked daily. Scoring of the mice was as follows: 0, healthy; 1, limp tail; 2, hind leg weakness; 3, one paralyzed hind leg; 4, two paralyzed hind legs; 5, moribund.

Live Cell Imaging Under Flow Conditions. Live cell imaging on TNF-α–stimulated pMBMECs isolated from WT or ICAM-1^{null}/ICAM-2$^{-/-}$ C57BL/6 mice, or on immobilized recombinant mouse ICAM-1 (rmICAM-1), VCAM-1 (rmVCAM-1), or DNER (rmDNER; all from R&D Systems) was performed as described previously (25, 26). CD3e- and CD28-activated T cell blasts (2×10^6/mL) were allowed to accumulate for 3–4 min at low shear force (0.1 dyn/cm^2). Then, dynamic T cell interactions with pMBMECs or immobilized rmICAM-1 and rmVCAM-1 were recorded under physiological shear force (1.5 dyn/cm^2) for 15 s (defined as arrested T cells) and for 5, 10, and 15 min (defined as firmly adherent T cells). Specific integrin-mediated adhesion to ICAM-1 and VCAM-1 was tested by pretreating T cells with rat mAbs specific for mouse α4 integrin (PS/2) and mouse LFA-1 (FD448.1). An anti-human CD44 (9B5) Ab was used as negative control. All Abs were incubated with the T cells for 20 min at a concentration of 10 μg/mL

Flow Cytometry. Single-cell suspensions of hematopoietic organs were prepared and staining for FACS analysis was done as described previously (34) and detailed in *SI Materials and Methods*. For intracellular cytokine stainings, T-cell blasts were stimulated for 4 h with 50 ng/mL PMA, 500 ng/mL ionomycin, and 10 μg/mL brefeldin A (Sigma-Aldrich), and cytokine expression was analyzed as described previously (27).

For analysis of soluble VCAM-1–Fc binding, 0.5×10^6 effector T cells were incubated with 100 μg/mL VCAM-Fc (R&D Systems) for 15 min at 37 °C in HBSS binding media supplemented with 0.2% BSA, Ca^{2+} and Mg^{2+} (1 mM each), Mn^{2+} (2 mM), or PMA (100 ng/mL). Cells were then washed once, incubated with PE-donkey anti-human IgG (Jackson ImmunoResearch) for an additional 20 min on ice, washed twice, and analyzed by FACS.

Statistical Analysis. Means, SDs, and statistical comparisons with the Student *t* test (*$P < 0.05$; **$P < 0.01$; ***$P < 0.001$) were performed using Microsoft Excel software.

ACKNOWLEDGMENTS. We thank Michal Grzejszczyk, Claudia Blatti, and Mark Liebi for expert technical assistance; Kevin Flynn for a careful read of the manuscript; and the Microscopy Imaging Center of the University of Bern for support. The work was supported by the Swiss National Science Foundation (Grant 31003A_149420, to B.E. and R.L.), the Deutsche Forschugsgemeinschaft (Grant SFB914, to M.M. and R.F.), and the Max Planck Society (R.F.).

1. McFarland HF, Martin R (2007) Multiple sclerosis: A complicated picture of autoimmunity. *Nat Immunol* 8(9):913–919.
2. Engelhardt B (2010) T cell migration into the central nervous system during health and disease: Different molecular keys allow access to different central nervous system compartments. *Clin Exp Neuroimmunol* 1:79–93.
3. Steinman L (2005) Blocking adhesion molecules as therapy for multiple sclerosis: Natalizumab. *Nat Rev Drug Discov* 4(6):510–518.
4. Hynes RO (2002) Integrins: Bidirectional, allosteric signaling machines. *Cell* 110(6):673–687.
5. Kim C, Ye F, Ginsberg MH (2011) Regulation of integrin activation. *Annu Rev Cell Dev Biol* 27:321–345.
6. Moser M, Legate KR, Zent R, Fässler R (2009) The tail of integrins, talin, and kindlins. *Science* 324(5929):895–899.
7. Kinashi T (2005) Intracellular signalling controlling integrin activation in lymphocytes. *Nat Rev Immunol* 5(7):546–559.
8. Paszek MJ, Boettiger D, Weaver VM, Hammer DA (2009) Integrin clustering is driven by mechanical resistance from the glycocalyx and the substrate. *PLOS Comput Biol* 5(12):e1000604.
9. Kong F, García AJ, Mould AP, Humphries MJ, Zhu C (2009) Demonstration of catch bonds between an integrin and its ligand. *J Cell Biol* 185(7):1275–1284.
10. Marshall BT, et al. (2003) Direct observation of catch bonds involving cell-adhesion molecules. *Nature* 423(6936):190–193.
11. Ussar S, Wang HV, Linder S, Fässler R, Moser M (2006) The Kindlins: Subcellular localization and expression during murine development. *Exp Cell Res* 312(16):3142–3151.
12. Moser M, et al. (2009) Kindlin-3 is required for beta2 integrin-mediated leukocyte adhesion to endothelial cells. *Nat Med* 15(3):300–305.
13. Moser M, Nieswandt B, Ussar S, Pozgajova M, Fässler R (2008) Kindlin-3 is essential for integrin activation and platelet aggregation. *Nat Med* 14(3):325–330.
14. Schmidt S, et al. (2011) Kindlin-3–mediated signaling from multiple integrin classes is required for osteoclast-mediated bone resorption. *J Cell Biol* 192(5):883–897.
15. Kuijpers TW, et al. (2009) LAD-1/variant syndrome is caused by mutations in *FERMT3*. *Blood* 113(19):4740–4746.
16. Malinin NL, et al. (2009) A point mutation in *KINDLIN3* ablates activation of three integrin subfamilies in humans. *Nat Med* 15(3):313–318.
17. Svensson L, et al. (2009) Leukocyte adhesion deficiency-III is caused by mutations in *KINDLIN3* affecting integrin activation. *Nat Med* 15(3):306–312.
18. Stromnes IM, Goverman JM (2006) Passive induction of experimental allergic encephalomyelitis. *Nat Protoc* 1(4):1952–1960.
19. Stromnes IM, Goverman JM (2006) Active induction of experimental allergic encephalomyelitis. *Nat Protoc* 1(4):1810–1819.
20. Lee PP, et al. (2001) A critical role for Dnmt1 and DNA methylation in T cell development, function, and survival. *Immunity* 15(5):763–774.
21. Bettelli E, et al. (2003) Myelin oligodendrocyte glycoprotein-specific T cell receptor transgenic mice develop spontaneous autoimmune optic neuritis. *J Exp Med* 197(9):1073–1081.
22. Bergman RK, Munoz JJ, Portis JL (1978) Vascular permeability changes in the central nervous system of rats with hyperacute experimental allergic encephalomyelitis induced with the aid of a substance from *Bordetella* pertussis. *Infect Immun* 21(2):627–637.
23. Steffen BJ, Butcher EC, Engelhardt B (1994) Evidence for involvement of ICAM-1 and VCAM-1 in lymphocyte interaction with endothelium in experimental autoimmune encephalomyelitis in the central nervous system in the SJL/J mouse. *Am J Pathol* 145(1):189–201.
24. Constantin G, et al. (2000) Chemokines trigger immediate beta2 integrin affinity and mobility changes: Differential regulation and roles in lymphocyte arrest under flow. *Immunity* 13(6):759–769.
25. Steiner O, et al. (2010) Differential roles for endothelial ICAM-1, ICAM-2, and VCAM-1 in shear-resistant T cell arrest, polarization, and directed crawling on blood-brain barrier endothelium. *J Immunol* 185(8):4846–4855.
26. Coisne C, Lyck R, Engelhardt B (2013) Live cell imaging techniques to study T cell trafficking across the blood–brain barrier in vitro and in vivo. *Fluids Barriers CNS* 10(1):7.
27. Bauer M, et al. (2009) Beta1 integrins differentially control extravasation of inflammatory cell subsets into the CNS during autoimmunity. *Proc Natl Acad Sci USA* 106(6):1920–1925.
28. Manevich-Mendelson E, et al. (2009) Loss of Kindlin-3 in LAD-III eliminates LFA-1 but not VLA-4 adhesiveness developed under shear flow conditions. *Blood* 114(11):2344–2353.
29. Lefort CT, et al. (2012) Distinct roles for talin-1 and kindlin-3 in LFA-1 extension and affinity regulation. *Blood* 119(18):4275–4282.
30. Ye F, et al. (2010) Recreation of the terminal events in physiological integrin activation. *J Cell Biol* 188(1):157–173.
31. Hao JJ, et al. (2008) Enrichment of distinct microfilament-associated and GTP-binding proteins in membrane/microvilli fractions from lymphoid cells. *J Proteome Res* 7(7):2911–2927.
32. Hyduk SJ, et al. (2011) Talin-1 and kindlin-3 regulate alpha4beta1 integrin-mediated adhesion stabilization, but not G protein-coupled receptor-induced affinity up-regulation. *J Immunol* 187(8):4360–4368.
33. Feng C, et al. (2012) Kindlin-3 mediates integrin αLβ2 outside-in signaling, and it interacts with scaffold protein receptor for activated-C kinase 1 (RACK1). *J Biol Chem* 287(14):10714–10726.
34. Montanez E, et al. (2007) Analysis of integrin functions in peri-implantation embryos, hematopoietic system, and skin. *Methods Enzymol* 426:239–289.

12.6 Paper 6:

Platelets and neutrophils require different Kindlin-3 copy numbers to control integrin-mediated functions *in vivo*.

Platelets and neutrophils require different Kindlin-3 copy numbers to control integrin-mediated functions *in vivo*

Sarah Klapproth[1,2], Federico Moretti[1], Marlis Zeiler[3], Raphael Ruppert[1], Matthias Mann[3], Markus Sperandio[2], Reinhard Fässler[1], Markus Moser[1#]

[1]Max-Planck-Institute of Biochemistry, Department of Molecular Medicine, Am Klopferspitz 18, D-82152 Martinsried, Germany; [2]Walter Brendel Center for Experimental Medicine, Ludwig-Maximilians-University Munich, D-81377 Munich, Germany; [3]Max-Planck-Institute of Biochemistry, Department of Proteomics and Signaltransduction, Am Klopferspitz 18, D-82152 Martinsried, Germany

Keywords: Kindlin-3, talin-1, integrin, integrin activation, LAD-III

Corresponding author:
Markus Moser (moser@biochem.mpg.de)

ABSTRACT

Many of the diverse functions of blood cells depend on integrins and the cytoplasmic proteins kindlin-3 and talin-1. To relate specific functions of platelets and polymorphonuclear neutrophils (PMNs) to specific kindlin-3 levels we generated mouse strains expressing 50%, 10% and 5% of kindlin-3. We report that in contrast to Kindlin-3 null mice, which die of severe bleeding and leucocyte adhesion deficiency, mice expressing as little as 5-10% of kindlin-3 were viable, although only a limited number of integrins could be activated on platelets and neutrophils. Interestingly, tail wounding led to a severely prolonged bleeding tendency due to reduced platelet adhesion and aggregation but leukocyte adhesion to endothelial cells in the inflamed ear and the cremaster muscle was rather mildly impaired. Absolute quantification of protein copy numbers revealed similar kindlin-3 and talin-1 copy numbers in platelets and neutrophils. Interestingly, the ratio of the copy number of kindlin-3 and talin-1 relative to β3 integrin in platelets was 2:1, whereas in neutrophils the ratio relative to β2 integrins was 1:2. These data indicate that platelet-mediated hemostasis requires high kindlin-3 levels to ensure full-fledged integrin activation, whereas leukocyte adhesion and extravasation require lower levels of active integrins.

INTRODUCTION

Integrins are cell adhesion receptors that consist of α and β subunits. They anchor cells to the extracellular matrix and assemble large signaling hubs, with which they regulate essential cellular processes including cell adhesion, migration, proliferation, survival and differentiation. A hallmark of integrins is their ability to reversibly switch between an active and an inactive conformation. In their inactive conformation they have low affinity for ligands, while upon activation (inside-out signaling) the affinity increases, which leads to ligand binding, integrin clustering and finally signaling (outside-in signaling). Two principal protein families are known to regulate integrin affinity, the talins (talin-1 and -2) and kindlins (kindlin-1, -2, -3). They both bind directly β integrin tails and thereby induce the allosteric change in the integrin ectodomain (Moser et al., 2009b).

A fast allosteric change and rapid integrin-ligand interaction is particularly important for blood cells such as platelets and leukocytes, whose surface integrins continuously encounter ligands in plasma or on the vascular endothelium, respectively. Therefore, it is of fundamental importance for these cells to maintain integrins in an inactive state and rapidly activate them on demand, for example during bleeding when platelet aggregation is needed to seal vascular injuries, or during infection when leukocytes need to extravasate and kill microbial invaders. Blood cells express talin-1 and kindlin-3 whose binding to β integrin tails is tightly controlled by mechanism(s) that are largely unknown. Furthermore, it is also unclear whether a specific stoichiometry is critical for the integrin activation process.

In the present study, we engineered several mouse strains expressing different kindlin-3 protein levels. This allowed testing how different talin-1/kindlin-3 ratios influence integrin-mediated functions. We found that 5% of kindlin-3 in blood cells is sufficient for embryonic and postnatal development. However, upon exposure to stress the low levels of kindlin-3 impair adhesive functions of platelets and polymorphonuclear neutrophil (PMNs). Furthermore, platelets possess more kindlin-3 and talin-1 relative to their integrin levels than PMNs suggesting that rapid and full-fledged integrin activation is required for platelet functions, while only a limited number of integrins are activated during leukocyte extravasation.

RESULTS AND DISCUSSION

Generation of conditional and hypomorphic kindlin-3 mouse mutants

Kindlin-3 deficient mice die shortly after birth of anemia caused by bleeding and erythrocyte defects (Kruger et al., 2008; Moser et al., 2009b). To enable the disruption of the kindlin-3 gene at later stages or in specific blood cells, we generated a conditional kindlin-3 mouse by flanking exon 3-6 with *loxP* sites (suppl. Fig. 1). An intercross of these kindlin-3 floxed (K3fl/fl) mice with a deleter Cre strain produced offspring lacking exon 3-6 and the *frt*-flanked neomycin cassette, and as expected, with the same defects observed in constitutive kindlin-3 null mice (Moser et al., 2009a; Moser et al., 2009b) (suppl. Fig. 1D,E). We noticed that the presence of the neomycin cassette in intron 6 of the floxed kindlin-3 gene (suppl. Fig. 1A; K3+/n mice) significantly reduced kindlin-3 protein levels (Figure 1A,B). Intercrossing these mice to homozygosity (K3n/n) or with mice carrying a kindlin-3 null allele (K3n/-) further reduced kindlin-3 protein levels in spleen and thymus to around 10% and 5%, respectively (Figure 1A,B). Sequence analysis of kindlin-3 mRNA revealed aberrant splicing into the neomycin cassette as the major cause for reduced protein levels (data not shown). Thus, the introduction of a neomycin cassette into intron 6 of the kindlin-3 gene produced a hypomorphic kindlin-3 allele and by intercrossing these mice with wild type or kindlin-3 null mice we could differently reduce kindlin-3 protein levels.

Surprisingly, the different hypomorphic mouse strains including the K3n/- mice developed and aged normally, were fertile and showed normal cellularity in spleen and thymus (suppl. Fig. 2A-C). Furthermore, their erythroid counts in blood were normal indicating that they did not suffer from microbleedings or erythrocyte defects. However, the total number of white blood cells (WBC), in particular PMNs and lymphocytes, was significantly increased in K3n/n and K3n/- mice suggesting that low kindlin-3 levels compromise leukocyte extravasation and tissue patrolling (supplementary table 1).

Kindlin-3 hypomorphic mice show a bleeding tendency

Kindlin-3 deficiency causes fatal bleedings in mice and man (Kuijpers et al., 2009; Malinin et al., 2009; Moser et al., 2008; Svensson et al., 2009). Although platelets from K3n/n and K3n/- mice expressed around 10% and 5% of kindlin-3 levels, respectively, compared to wild type controls (Fig. 2A), they did not suffer from spontaneous hemorrhages during development or postnatal life (Fig. 2B, and data not shown). However, bleeding assays revealed that wild type and K3+/n mice stopped bleeding within 5 min, while K3n/n mice

suffered from a similar bleeding tendency as kindlin-3 null mice (Fig. 2C). Interestingly, thrombin treatment of wild type and K3+/n platelets robustly induced binding of fibrinogen by platelet αIIbβ3, while fibrinogen binding was reduced to less than 20% in K3n/n and K3n/- platelets and almost entirely lost in K3-/- platelets (Fig. 2D). Consistently, thrombin-induced activation of αIIbβ3 integrins measured by flow cytometry using the JON/A-PE antibody decreased concomitantly with lowering levels of kindlin-3 in platelets (Fig. 2E). Adhesion and spreading of platelets from K3n/n and K3n/- mice on a fibrinogen-coated surface was severely impaired (Fig. 2F). Since treatment of platelets with manganese, which can bypass integrin activation (Mould et al., 2002) rescued fibrinogen binding (not shown) and platelet adhesion but not platelet spreading (Fig. 2F), we conclude that the diminished kindlin-3 levels in K3n/n and K3n/- platelets impaired both integrin activation and outside-in signaling leading to actin reorganization. These findings were corroborated with *in vitro* aggregation assays, in which platelets from K3n/n and K3n/- mice produced much smaller aggregates (Fig. 2G) and displayed a biphasic aggregation response (Fig. 2H); the platelet shape change was followed by a rapid initial aggregation, while the second phase of aggregation, which depends on secreted auto- and paracrine factors, was significantly reduced in K3n/n and K3n/- platelets. Addition of fibrinogen normalized the second aggregation phase suggesting that indeed integrin-triggered platelet degranulation and release of secondary agonists is impaired and/or delayed in kindlin-3 hypomorphic platelets (Fig. 2G). Furthermore, thrombin-induced platelet clot retraction was delayed with platelets from K3n/n and K3n/- mice in platelet-rich plasma; however, addition of manganese normalized the clot retraction times indicating that acto-myosin induced pulling forces are induced by active integrins independent of kindlin-3 (Fig. 2I), while actin reorganization and platelet spreading require active integrins and depend on kindlin-3 (Fig. 2F).

Altogether, these data indicate that lowering kindlin-3 in platelets to 5-10% of wild type levels allows them to activate a limited number of integrins, which is sufficient to fulfill basal functions but insufficient to scope with stress conditions.

K3n/n and K3n/- mice suffer from leukocyte adhesion defects

Absence of Kindlin-3 also impairs β2 integrin functions on leukocytes resulting in leukocyte adhesion deficiency in mouse and man (Moser et al., 2009a). PMNs from the bone marrow of wild type, K3n/+, K3n/n and K3n/- mice displayed reduced kindlin-3 levels ranging from 50% in K3n/+, to 10% in K3n/n and 5% in K3n/- mice (Fig. 3A). With these different mouse

strains we investigated in several experiments to which extent leukocyte adhesion, extravasation and phagocytosis become compromised when kindlin-3 drops below a certain threshold. First, stimulation of K3n/n and K3n/- PMNs with phorbol-12-myristate-13-acetate (PMA) showed diminished adhesion to ICAM-1, although adhesion levels were still significantly higher than for K3-/- PMNs (Fig. 3B). Next, we treated earflaps with phorbol ester (crotoin oil) for 1 h and observed a delay in the extravasation of K3n/n and K3n/- PMNs compared to wild type and K3+/n PMNs. Notably, 4 h after treatment K3n/n and K3n/- PMNs have crossed the vascular wall and distributed in the interstitium like wild type PMNs, while K3-/- PMNs failed to extravasate (Fig. 3C). In order to study leukocyte adhesion and extravasation more quantitatively we analysed TNFα-stimulated cremaster muscle venules *in vivo* using intravital microscopy. The experiments revealed that leukocyte adhesion was normal in wild type and K3n/+ mice, decreased by about 20% in K3n/n mice and by about 50% in K3n/- mice (Fig. 3D). Concomitantly with the reduced *in vivo* adhesion of leukocytes, the numbers of rolling leukocytes were increased in K3n/- mice (Fig 3E). Similarly, β2 integrin-mediated phagocytosis of serum-opsonized bacteria was reduced in K3n/n and K3n/- PMNs and abolished in K3-/- PMNs (Fig. 3F). Altogether, these findings indicate that the low kindlin-3 levels in K3n/n and K3n/- PMNs impairs phagocytosis and adhesion. However, the compromised adhesion still allows a rather efficient leukocyte extravasation in inflammatory models.

Kindlin-3, talin-1 and integrin copy numbers in platelets and PMNs

The basal functions of platelets and PMNs from K3n/n and K3n/- mice are efficiently executed *in vivo*. However, upon stress exposure the functions of platelets and PMNs become compromised. Interestingly, stress situations affect K3n/n and K3n/- derived platelets more severely than leukocytes. To test whether this difference could be due to different copy number ratios of kindlin-3 and talin-1 proteins in platelets versus leukocytes we performed Western blot analysis with purified blood cell populations. In comparison with various white blood cells platelets contain high levels of kindlin-3 and talin-1 (Fig. 4A). Analysis of the platelet proteome by high resolution mass spectrometry (MS) (Cox and Mann, 2011) confirmed that kindlin-3, talin-1 and β3 integrins are among the most abundant platelet proteins (Fig. 4B).

To determine the stoichiometry of kindlin-3, talin-1, β2 and β3 integrins in platelets and PMNs, we used a recently developed MS method to quantify absolute protein numbers by expressing parts of the target protein sequence in a heavy labeled form (Zeiler et al.).

Specifically, short protein fragments of approximately 150 amino acids from murine kindlin-3, talin-1, β3 and β2 integrins were fused to the albumin-binding protein (ABP) and expressed in the presence of $^{13}C_6{}^{15}N_2$-lysine (Lys^8) and $^{13}C_6{}^{15}N_4$-arginine (Arg^{10}) in an auxotrophic *Escheria coli* strain, which labeled them with heavy isotopes. A precisely quantified cocktail of different stable isotope labeled protein standards from kindlin-3, talin-1, β2 and β3 integrins was then mixed with platelet and PMN lysates and their absolute copy numbers per cell were calculated after determining the heavy to light ratio by MS (Fig 4C; for details see material and methods and Zeiler et al., 2012). Kindlin-3 expression in platelet lysates from wild type, K3+/n, K3n/n and K3n/- mice revealed a stepwise decrease, while talin-1 and β3 integrin levels were similar in the different platelet populations (Fig. 4D). The measurements also revealed that a wild type platelet contained between 260,000 and 290,000 copies of talin-1 and kindlin-3, respectively, and about 130,000 copies of β3 integrin molecules (Fig. 4D). The PMNs also contained a stoichiometric number of kindlin-3 and talin-1 molecules of about 420,000 molecules per cell each. Furthermore, the total numbers of β2 integrins were approximately 800,000 molecules per cell, and hence was twice the number of talin-1 and kindlin-3 (Fig. 4E). These data indicate that platelets have an excess of talin-1 and kindlin-3 over integrins, whereas PMNs have an excess of integrins over talin-1 and kindlin-3.

Integrin-dependent functions of blood cells are strictly controlled by kindlin-3. In this study kindlin-3 hypomorphic mice were generated to address which levels of kindlin-3 are required for basal and stress induced platelet and PMNs functions. The results allow drawing interesting conclusions; first, expression of 5 to 10% of kindlin-3 in blood cells is sufficient for survival. Second, the steady state functions of platelets and PMNs with 5-10% of normal kindlin-3 levels are maintained, although the elevated WBC counts indicate reduced tissue patrolling. Third, low kindlin-3 expression allows activation of only a reduced number of integrins leading to decreased ligand binding and adhesion. This shows that kindlin-3 does not act in a catalytic manner. Fourth, under stress conditions such as bleeding or inflammation the low levels of kindlin-3 limit platelet functions more than PMN functions indicating that platelets require a higher threshold of kindlin-3 to cope with their demands. Fifth, although kindlin-3 is required for integrin-dependent intracellular signalling controlling platelet spreading and degranulation, it is not required for acto-myosin pulling and platelet contraction, which is in contrast to talin-1 (Haling et al., 2011).

Why are decreased kindlin-3 levels affecting platelets more than PMNs? The integrin-mediated adhesion machinery is highly expressed in platelets indicating that it is of paramount importance for the organism. The binding of plasma fibrinogen might require more functional integrins than the binding of PMNs to insoluble ICAM-1, which is upregulated and clustered on inflamed endothelial cells allowing a fast rebinding of broken integrin-ligand bonds. We determined the absolute numbers of kindlin-3, talin-1, β2 and β3 integrins in platelets and PMNs and found stoichiometric expression of both integrin activators, which further corroborates their cooperativeness during integrin regulation. In addition, surface density of β3 integrins on platelets (approximately 20,000 copies per μm^2 platelet surface area based on a total surface area of 8 μm^2) and the corresponding concentration of talin-1 and kindlin-3 in platelets (40,000 copies each per fL platelet volume; total platelet volume appr. 7fL (von Hundelshausen et al., 2007)) are much higher than the corresponding values in PMNs (3,000 copies of β2 integrins per μm^2 neutrophil surface area and 1,500 copies of talin-1 and kindlin-3 per fL PMN volume; based on 250 μm^2 surface area and 300fL volume for PMNs (Ting-Beall et al., 1993)). These values may very well reflect differences in mechanical stress, platelets and neutrophils are exerted to (platelet adhesion in arteries versus neutrophil adhesion in venules). Furthermore, the twofold excess of talin-1 and kindlin-3 over β3 integrins in platelets ensuring rapid and full-fledged integrin activation critical for primary hemostasis. On the contrary, PMNs express only half as much integrin activators than β2 integrins suggesting that only a limited number of β2 integrins is activated. Remarkably, even neutrophils from kindlin-3 hypomporphic mice can efficiently adhere and leave the inflamed vasculature. Probably because a highly dynamic and strongly restricted number of active β2 integrins on leukocytes is sufficient to control the dynamic interaction with the inflamed endothelium and subendothelial tissue. In this regard, studies on leukocyte adhesion deficiency type I patients also showed that the severity of clinical infectious complications is directly related to the degree of β2 integrin deficiency. Severely immune deficient patients have essentially undetectable β2 integrin expression on leukocytes, whereas moderate phenotypes are found in patients expressing 2.5 to 6% of β2 integrins on PMNs (Anderson et al., 1985; Anderson and Springer, 1987). The clinical data mentioned above, together with our results, indicate that integrin activation and function is regulated in a large part by the precise control of the stoichiometry of integrin activators relative to integrin levels, thus enabling different blood cells to achieve their diverse biological functions.

MATERIAL AND METHODS

Animals:

Kindlin-3$^{-/-}$ mice have been described previously (Moser et al., 2008). To generate conditional kindlin-3 mouse mutants (kindlin-3 fl/fl) a targeting vector was cloned, in which exons three to six of the kindlin-3 gene were flanked by loxP sites. This vector was electroporated into 129 ES cells. A Neo-cassette flanked by frt sites allowed G418 selection. Several homologous recombinant clones were injected into C57BL/6 blastocysts and resulted in germ line chimeras. The presence of the Neo-cassette within the kindlin-3 genomic locus resulted in strongly reduced kindlin-3 expression giving rise to a hypomorphic kindlin-3 allele. Mating with mice carrying a wild type, hypomorphic or kindlin-3 null (K3-/-) allele resulted in offspring with different levels of kindlin-3. In parallel, the Neo-cassette was removed from the kindlin-3 genomic locus by mating kindlin-3 hypomorphic mice with a strain expressing a deleter flipase resulting in conditional kindlin-3 mice. Finally, conditional kindlin-3 mice were crossed with a deleter Cre mouse strain (Betz et al., 1996) to obtain K3-/- mice.

All mouse experiments were performed with the approval of the District Government of Bavaria.

Generation of fetal liver cell chimeras:

Fetal liver cells were obtained from embryonic day 15 K3+/+ or K3-/- embryos by pushing liver tissue through a cell strainer (Falcon). 4 x 10^6 cells were then injected into the tail vein of lethally irradiated (twice 6.5 Gy) recipient C57BL/6 mice. Mice were used not before 6 weeks after transfer.

Antibodies:

The following antibodies were used for immunostaining of cells: mouse anti-vinculin antibody, (from Sigma-Aldrich); Cy3-labeled secondary antibody (Jackson ImmunoResearch Laboratories, Inc.). Phalloidin-488 dye was obtained from Invitrogen.

The following antibodies were used for flow cytometry: hamster IgG anti-integrin β1, isotype control hamster IgG, and isotype control mouse IgG1 (all from Biolegend); rat IgG2a anti-integrin β2, rat IgG2a anti-integrin β7, rat IgG2a anti-integrin α4, rat IgG2a anti-integrin α5, rat IgG2a anti-integrin αL, rat IgG1 anti-integrin αv, isotype control rat IgG1, and isotype control rat IgG2a (all from BD); hamster IgG anti-integrin β3, mouse IgG1 anti-integrin β5, rat IgG2b anti-integrin αM and isotype control rat IgG2b (all from eBioscience).

The following antibodies were used for Western blotting: mouse anti-glyceraldehyde 3-phosphate dehydrogenase (anti-GAPDH; Merck); rabbit anti-actin and mouse anti-talin (both from Sigma-Aldrich); rabbit anti-P42/44 MAPK, rabbit anti-pP42/44 MAPK Thr202/Tyr204, rabbit anti-Akt, and rabbit anti-pAkt Ser473 (all from Cell Signaling Technology); rabbit anti-kindlin-3 antibody is home made (Ussar et al., 2006).

Peripheral blood cell counts:

Mice were bled from the retro-orbital sinus into EDTA-coated tubes. Blood cell counts were determined using a Hemavet 950 analyzer (Drew Scientific Inc., Oxford, CT).

Cell preparation:

CD4-positive T-cells were isolated from spleen using the CD4+ T cell Isolation Kit II from Miltenyi Biotech (Bergisch Gladbach, Germany). PMNs (polymorphonuclear neutrophils) were FACS sorted from whole bone marrow for high expression of Gr1 using a FITC-labeled antibody (eBioscience). B220-positive B-cells were FACS-sorted from whole spleen. Macrophages and dendritic cells (DCs) were derived from whole bone marrow by culturing in medium containing M-CSF and GM-CSF.

Platelet analyses:

Integrin activation studies were performed with blood samples washed twice with modified Tyrode´s HEPES buffer (134 mM NaCl, 0.34 mM Na_2HPO_4, 2.9 mM KCl, 12 mM $NaHCO_3$, 20 mM HEPES, pH 7.0) containing 5 mM glucose, 0.35% bovine serum albumin (BSA) and 1 mM $CaCl_2$, which then were activated with 0.1 U/ml thrombin (Sigma Aldrich) and either stained with fluorophore-labeled anti-activated αIIbβ3 (JON/A, Emfret Analytics) or fibrinogen (Molecular Probes).

Platelet adhesion and spreading was analysed on fibrinogen-coated (1mg/ml; Sigma Aldrich) glass bottom dishes blocked with 3% BSA. Washed platelets were re-suspended at a concentration of 0.5x 10^6 platelets/ml and then further diluted 1:10 in Tyrode's-HEPES buffer. Shortly before plating, platelets were activated with 0.01 U/ml thrombin. Platelets were allowed to spread for 10 min and imaged by differential interference contrast (DIC) microscopy. Additionally, washed platelets were allowed to adhere to fibrinogen in the presence of 3 mM Mn^{2+} without thrombin stimulation.

Platelet aggregation was measured with 2 x 10^8/ml washed platelets stimulated with 0.1 U/ml Thrombin in the absence or presence of 100 ug/ml human fibrinogen. Light

transmission was recorded on a ChronoLog aggregometer over 15 min and was expressed as arbitrary units with the transmission through buffer defined as 100% transmission.

Platelet clot retraction was measured in platelet-rich plasma (PRP) obtained from blood drawn into 1/10 volume of 3.8% sodium citrate. Platelets were diluted to 1x 10^8/ml with platelet-poor plasma obtained from wild type mice. PRP was added to siliconized glass cuvettes containing a paperclip, and clot retraction was initiated after addition of 2 mM $CaCl_2$ and 1 U/ml thrombin (Sigma Aldrich). In parallel, samples were also treated with 0.5 mM $MnCl_2$. Samples were incubated at 25°C for 2 hrs and clot retraction was analysed by weighing the residual serum to calculate the percentage of serum extruded from the clot at the indicated time points.

Skin inflammation model:

Croton oil (Sigma-Aldrich) was diluted to 1% in acetone and topically applied to the ventral and the dorsal sides (20µl each) of ears from K3+/+, K3n/n, K3n/- and K3-/- chimeric mice. After 1 and 4 h, mice were sacrificed and the earflaps were split into two halves by carefully separating the dorsal and ventral skin. For histological analysis, dorsal and ventral ear halves were subjected to whole-mount immunostaining. After fixation in paraformaldehyde (PFA), ear halves were blocked with 1% BSA (PAA Laboratories) in PBS for 1h at room temperature, probed with biotin-labeled anti-Gr-1 (RB6-8C5; BD Biosciences-Pharmingen) to identify PMNs and anti-pan-laminin (L9393; Sigma-Aldrich) to visualize vessels, diluted in 1% BSA in PBS overnight at 4°C (wile shaking), and finally washed with 1% BSA in PBS. Antibodies were detected with a repeated cycle of staining with anti-rabbit Alexa Fluor 488 (Invitrogen) and anti-rat Cy3 (Dianova) before tissue was embedded in elvanol and representative images taken with a Zeiss Axio Imager equipped with an ApoTome (Zeiss).

Intravital microscopy:

rmTNF-α (R&D Systems) was injected intrascrotally at a dose of 500 ng per mouse in a volume of 0.15 ml sterile physiological NaCl solution. Two hours later, the mice were anesthesized (Frommhold et al., 2008) and placed onto a heating pad to maintain body temperature at 37 °C. After intubation and carotid artery cannulation for blood sampling and application of antibodies and chemokines, the cremaster muscle was surgically prepared for intravital microscopy as previously described (Sperandio et al., 2006).

Intravital microscopy was performed on an upright microscope (Olympus BX51) with a saline immersion objective (40x and 0.8 numerical aperture). Experiments were recorded via CCD camera (model CF8/1, Kappa) on a Panasonic S-VHS recorder and with a digital camera (LaVision Biotech), and stored on a computer with Imspector software package (LaVision Biotech). The digital recordings were used offline to generate movie clips with ImageJ software (US National Institutes of Health). During the experiment, systemic blood samples were obtained (10 µl into 90 µl Türck's solution, Merck) to assess systemic white blood cell counts. Rolling flux was defined as the number of rolling cells per min and rolling PMN flux fraction as the percentage of rolling PMNs in all PMNs passing the same vessel in 1 min (Sperandio et al., 2006). PMNs that did not move for more than 30 s were considered to be adherent. The number of adherent leukocytes was assessed as the number of adherent cells per mm^2 vessel surface area (Frommhold et al., 2008).

Adhesion assays:

For PMN adhesion to ICAM-1, 96-well plates were coated with 4 µg/ml recombinant human ICAM-1 (R&D Systems) in coating buffer (150 mM NaCl, 20 mM Tris-HCl, and 2 mM $MgCl_2$, pH 9) ON at 4°C and blocked with 3% BSA in PBS for 1 h at RT. PMNs sorted from bone marrow were either left untreated, or treated either with 33 ng/ml PMA (Phorbol-12-Myristate-13-Acetate; Calbiochem) or 1 mM $MnCl_2$. The adhesion assay was performed with 50.000 cells per well for 30 min. Adherent cells were fixed with 4% PFA after washing. The number of adherent cells was determined by acquisition of 3 phase contrast pictures from each well.

Phagocytosis assay:

Phagocytosis was measured using the pHrodoTM Red *E.coli* BioParticle Phagocytosis Kit for Flow cytometry (invitrogen) according to the manufacturer´s instructions. Blood was collected from the retro-orbital sinus and each blood sample was measured in triplicates. Granulocytes were identified by their position in a forward vs. side scatter plot.

Absolut quantification of proteins in platelets and neutrophils:

We produced two protein standards spanning over different regions of talin-1, b3 and b2 integrins, and 3 standards for kindlin-3. The protein standards were designed with an approximate length of 150 amino acids and with as many unique tryptic cleavage sites as possible. They covered in kindlin-3 the aminoacids 114-276, 304-477 and 522-605; in

talin-1 1752-1948 and 2021-2188; in β3 integrin 34-162 and 589-714; and in β2 integrin 176-325 and 334-480. Subsequently they were fused to the albumin binding protein (ABP), whose cDNA was was inserted into the expression vector pET28a(+) then fused with the gene sequences of interest using HindIII and XhoI. In a next step the proteins fused to ABP were expressed in an auxotrophic E. coli strain and labeled with 'heavy' isotopes ($^{13}C_6{}^{15}N_2$-lysine and $^{13}C_6{}^{15}N_4$-arginine). The labeled proteins were purified via His_6-Tag using spin columns from Qiagen (Hilden, Germany).

The proteins of interest were quantified as previously described (Zeiler et al.). In brief, unlabeled ABP was quantified beforehand with amino acid analysis. These measurements were used to quantify the 'heavy' protein standards via SILAC ratios. The different protein standards with known concentration were then mixed. The platelets or neutrophils were lysed and the 'protein standard mix' was spiked in at approximately endogenous level. The mixture was further processed using the filter-aided sample preparation (FASP) method (Wisniewski et al., 2009), in which proteins were captured on a 30 kDa filter and SDS was removed with an urea-containing buffer. Proteins were alkylated with iodoacetamide and typsinized. The peptides were measured by MS, and peptide ratios between endogenous and labeled peptides were extracted.

For the platelet proteome FASP peptides were further fractionated with strong anion exchange chromatography. Six fractions of pH 11, 8, 6, 5, 4 and 3 were obtained.

All samples were measured using the LTQ-Orbitrap Elite or Q Exactive proteomic pipeline (Michalski et al., 2012). Raw mass spectrometric data were analyzed using the MaxQuant software (Cox and Mann, 2008). Detailed description of the MS analysis as well as the data analysis can be found in the supplementary material.

For calculation of the absolute copy number per cell we used the peptide ratios and converted the ratios to pmol. We took the median of all peptides amounts (derived from different protein standards) to calculate the copy number. We required at least 3 peptides for the quantification of each protein.

Statistical analysis

All data are shown as mean ± SD or mean ± SEM as indicated in the figure legends. To test significance level an unpaired student t-Test was performed.

Supplementary Material

Liquid chromatography and mass spectrometry analysis. The peptides were separated on a 20 cm column packed with Reprosil-Pur 1.9 µm resin (Dr. Maisch GmbH, Ammerbuch-Entringen, Germany) using an UPLC system (Thermo Fisher Scientific). A linear gradient 180 min 5–25% buffer B (80% acetonitrile, 0,5 % acetic acid) at a constant flow rate of 300nl/min was applied. The UPLC was coupled via nanoelectrospray ion source (Proxeon Biosystems) to an LTQ-Orbitrap Elite mass spectrometer (Michalski et al., 2012). The data was acquired with a data-dependent top10 method, automatically selecting the most abundant precursor ions for fragmentation. Full scans, 300-1750m/z, were measured with a target value 1e6 at a resolution of 60,000 followed by 10 fragmentation spectra using higher energy collisional dissociation also measured in the Orbitrap using 5e4 ions at a resolution of 15,000. The injection time for MS spectra was restricted to 100 ms and for MS/MS spectra to 150 ms.

The platelet proteome was measured on a QExactive instrument (Michalski et al., 2011)Thermo Scientific) using the same liquid chromatography setup as described above. A linear gradient 180 min 5–35% buffer B at a constant flow rate of 300 nl/min was applied. Full scans, 300-1650m/z, were measured with a target value 3e6 at a resolution of 70,000 followed by 20 fragmentation spectra using higher energy collisional dissociation and measured in the Orbitrap using 1e6 ions at a resolution of 17,500. The injection time for MS spectra was restricted to 20 ms and for MS/MS spectra to 60 ms.

Data analysis. The raw files were analyzed using MaxQuant (version 1.3.7.4; (Cox and Mann, 2008). For peptide identification Andromeda search engine incorporated into MaxQuant (Cox et al., 2011) was used to search fragmentation spectra against the UniProtKB mouse database (downloaded on 16 June 2012), which contains 54,232 entries. 247 common contaminants were added to this database. A time-dependent mass recalibration algorithm was used for recalibration to improve the mass accuracy of precursor ions. Peptide identification was based on a search with an initial mass deviation of the precursor ion of up to 6 ppm and the allowed fragment mass deviation was set to 20 ppm. The search included cysteine carbamidomethylation as a fixed modification and N-terminal acetylation and methionine oxidation as variable modifications. Enzyme specificity was set to trypsin allowing N-terminal cleavage to proline. Two mis-cleavages were allowed and a minimum of seven amino acids per identified peptide was required. The second peptide identification option in Andromeda was enabled. For statistical evaluation of the data obtained, the posterior error probability and false discovery rate (FDR) were

used. The false discovery rate was determined by searching a reverse database and was set to 0.01 for peptide and protein identification. Additional peptides were identified by the “match between run” option in MaxQuant, which matches precursor masses in a 2 min retention time window (after realignment of the runs) based on the accurate mass.

Cox, J., and M. Mann. 2008. MaxQuant enables high peptide identification rates, individualized p.p.b.-range mass accuracies and proteome-wide protein quantification. *Nat Biotechnol* 26:1367-1372.

Cox, J., N. Neuhauser, A. Michalski, R.A. Scheltema, J.V. Olsen, and M. Mann. 2011. Andromeda: a peptide search engine integrated into the MaxQuant environment. *J Proteome Res* 10:1794-1805.

Michalski, A., E. Damoc, J.P. Hauschild, O. Lange, A. Wieghaus, A. Makarov, N. Nagaraj, J. Cox, M. Mann, and S. Horning. 2011. Mass spectrometry-based proteomics using Q Exactive, a high-performance benchtop quadrupole Orbitrap mass spectrometer. *Mol Cell Proteomics* 10:M111 011015.

Michalski, A., E. Damoc, O. Lange, E. Denisov, D. Nolting, M. Muller, R. Viner, J. Schwartz, P. Remes, M. Belford, J.J. Dunyach, J. Cox, S. Horning, M. Mann, and A. Makarov. 2012. Ultra high resolution linear ion trap Orbitrap mass spectrometer (Orbitrap Elite) facilitates top down LC MS/MS and versatile peptide fragmentation modes. *Mol Cell Proteomics* 11:O111 013698.

ACKNOWLEDGEMENTS

We thank Michal Grzejszczyk for excellent technical assistance, Kevin Flynn, Karim Dib, Roy Zent and Ambra Pozzi for critically reading the manuscript. This work was supported by the Deutsche Forschungsgemeinschaft (SFB 914 TPs A1, A5 and B1) and the Max Planck Society.

The authors declare that they have no competing financial interests.

REFERENCES

Anderson, D.C., F.C. Schmalsteig, M.J. Finegold, B.J. Hughes, R. Rothlein, L.J. Miller, S. Kohl, M.F. Tosi, R.L. Jacobs, T.C. Waldrop, and et al. 1985. The severe and moderate phenotypes of heritable Mac-1, LFA-1 deficiency: their quantitative definition and relation to leukocyte dysfunction and clinical features. *The Journal of infectious diseases* 152:668-689.

Anderson, D.C., and T.A. Springer. 1987. Leukocyte adhesion deficiency: an inherited defect in the Mac-1, LFA-1, and p150,95 glycoproteins. *Annual review of medicine* 38:175-194.

Betz, U.A., C.A. Vosshenrich, K. Rajewsky, and W. Muller. 1996. Bypass of lethality with mosaic mice generated by Cre-loxP-mediated recombination. *Current biology : CB* 6:1307-1316.

Cox, J., and M. Mann. 2008. MaxQuant enables high peptide identification rates, individualized p.p.b.-range mass accuracies and proteome-wide protein quantification. *Nature biotechnology* 26:1367-1372.

Cox, J., and M. Mann. 2011. Quantitative, high-resolution proteomics for data-driven systems biology. *Annu Rev Biochem* 80:273-299.

Cox, J., N. Neuhauser, A. Michalski, R.A. Scheltema, J.V. Olsen, and M. Mann. 2011. Andromeda: a peptide search engine integrated into the MaxQuant environment. *J Proteome Res* 10:1794-1805.

Frommhold, D., A. Ludwig, M.G. Bixel, A. Zarbock, I. Babushkina, M. Weissinger, S. Cauwenberghs, L.G. Ellies, J.D. Marth, A.G. Beck-Sickinger, M. Sixt, B. Lange-Sperandio, A. Zernecke, E. Brandt, C. Weber, D. Vestweber, K. Ley, and M. Sperandio. 2008. Sialyltransferase ST3Gal-IV controls CXCR2-mediated firm leukocyte arrest during inflammation. *The Journal of experimental medicine* 205:1435-1446.

Kruger, M., M. Moser, S. Ussar, I. Thievessen, C.A. Luber, F. Forner, S. Schmidt, S. Zanivan, R. Fassler, and M. Mann. 2008. SILAC mouse for quantitative proteomics uncovers kindlin-3 as an essential factor for red blood cell function. *Cell* 134:353-364.

Kuijpers, T.W., E. van de Vijver, M.A. Weterman, M. de Boer, A.T. Tool, T.K. van den Berg, M. Moser, M.E. Jakobs, K. Seeger, O. Sanal, S. Unal, M. Cetin, D. Roos, A.J. Verhoeven, and F. Baas. 2009. LAD-1/variant syndrome is caused by mutations in FERMT3. *Blood* 113:4740-4746.

Malinin, N.L., L. Zhang, J. Choi, A. Ciocea, O. Razorenova, Y.Q. Ma, E.A. Podrez, M. Tosi, D.P. Lennon, A.I. Caplan, S.B. Shurin, E.F. Plow, and T.V. Byzova. 2009. A point mutation in KINDLIN3 ablates activation of three integrin subfamilies in humans. *Nature medicine* 15:313-318.

Michalski, A., E. Damoc, J.P. Hauschild, O. Lange, A. Wieghaus, A. Makarov, N. Nagaraj, J. Cox, M. Mann, and S. Horning. 2011. Mass spectrometry-based proteomics using Q Exactive, a high-performance benchtop quadrupole Orbitrap mass spectrometer. *Molecular & cellular proteomics : MCP* 10:M111 011015.

Michalski, A., E. Damoc, O. Lange, E. Denisov, D. Nolting, M. Muller, R. Viner, J. Schwartz, P. Remes, M. Belford, J.J. Dunyach, J. Cox, S. Horning, M. Mann, and A. Makarov. 2012. Ultra high resolution linear ion trap Orbitrap mass spectrometer (Orbitrap Elite) facilitates top down LC MS/MS and versatile peptide fragmentation modes. *Mol Cell Proteomics* 11:O111 013698.

Moser, M., M. Bauer, S. Schmid, R. Ruppert, S. Schmidt, M. Sixt, H.V. Wang, M. Sperandio, and R. Fassler. 2009a. Kindlin-3 is required for beta2 integrin-mediated leukocyte adhesion to endothelial cells. *Nature medicine* 15:300-305.

Moser, M., K.R. Legate, R. Zent, and R. Fassler. 2009b. The tail of integrins, talin, and kindlins. *Science* 324:895-899.

Moser, M., B. Nieswandt, S. Ussar, M. Pozgajova, and R. Fassler. 2008. Kindlin-3 is essential for integrin activation and platelet aggregation. *Nature medicine* 14:325-330.

Mould, A.P., J.A. Askari, S. Barton, A.D. Kline, P.A. McEwan, S.E. Craig, and M.J. Humphries. 2002. Integrin activation involves a conformational change in the alpha 1 helix of the beta subunit A-domain. *The Journal of biological chemistry* 277:19800-19805.

Sperandio, M., J. Pickard, S. Unnikrishnan, S.T. Acton, and K. Ley. 2006. Analysis of leukocyte rolling in vivo and in vitro. *Methods in enzymology* 416:346-371.

Svensson, L., K. Howarth, A. McDowall, I. Patzak, R. Evans, S. Ussar, M. Moser, A. Metin, M. Fried, I. Tomlinson, and N. Hogg. 2009. Leukocyte adhesion deficiency-III is caused by mutations in KINDLIN3 affecting integrin activation. *Nature medicine* 15:306-312.

Ting-Beall, H.P., D. Needham, and R.M. Hochmuth. 1993. Volume and osmotic properties of human neutrophils. *Blood* 81:2774-2780.

Ussar, S., H.V. Wang, S. Linder, R. Fassler, and M. Moser. 2006. The Kindlins: subcellular localization and expression during murine development. *Experimental cell research* 312:3142-3151.

von Hundelshausen, P., and C. Weber. 2007. Platelets as immune cells: bridging inflammation and cardiovascular disease. *Circulation research* 100:27-40.

Wisniewski, J.R., A. Zougman, N. Nagaraj, and M. Mann. 2009. Universal sample preparation method for proteome analysis. *Nat Methods* 6:359-362.

Zeiler, M., W.L. Straube, E. Lundberg, M. Uhlen, and M. Mann. A Protein Epitope Signature Tag (PrEST) library allows SILAC-based absolute quantification and multiplexed determination of protein copy numbers in cell lines. *Mol Cell Proteomics* 11:O111 009613.

FIGURE LEGENDS

Figure 1: Kindlin-3 protein levels in spleen and thymus. (A) Western blot analyses of kindlin-3 in spleen and thymus lysates from K3+/+, K3n/n, K3n/- mice. GAPDH served as loading control. (B) Densitometric quantification of (A).

Figure 2: Function of platelet integrins is kindlin-3 dose dependent. (A) Densitometric quantification of kindlin-3 levels in K3+/+, K3n/n, K3n/- and K3-/- platelets (N=5;5;4;4). GAPDH served as loading control. (B) Kindlin-3 K3+/+, K3n/n, K3n/- E14.5 embryos are free bleedings. (C) Tail bleeding times of K3+/+, K3n/n, K3n/- and K3-/- chimeric mice. (D) Binding of fibrinogen to platelets after treatment with 0.1 U/ml thrombin. Resting platelets were used as control. N=5;5;5;5;3. (E) Activation of αIIbβ3 integrin on platelets upon stimulation with 0.1 U/ml thrombin. N=5;5;5;5;3. (F) Washed platelets were stimulated with 0.01 U/ml thrombin and allowed to adhere to coated fibrinogen for 10 min in the presence or absence of 3 mM Mn^{2+}. (G) Aggregates of K3+/+, K3n/n and K3n/- platelets in response to 0.1 U/ml thrombin. (H) Platelet aggregation assays with K3+/+, K3n/n, K3n/- platelets in response to thrombin in the absence and presence of 100 µg/ml fibrinogen. (I) Clot retraction of platelets from K3+/+, K3n/n, K3n/- and K3-/- mice in the absence or presence of 0.5 mM Mn^{2+}. N=7;4;6;6;7. Values are given as mean ± SD. Significant differences are indicated by asterisk (*: $p<0.05$; **: $p<0.01$; ***$p<0.001$).

Figure 3: Leukocyte adhesion is Kindlin-3 modulated. (A) Densitometric quantification of kindlin-3 levels in K3+/+, K3n/n, K3n/- and K3-/- PMNs (N=3). GAPDH served as loading control. (B) Static adhesion of PMNs to ICAM-1 upon PMA stimulation. N=4. (C) Whole mounts of ears treated with phorbol ester for 1 (left) and 4 h (right) stained with a pan-laminin antibody (LN; green) to visualize endothelial basement membranes and a Gr-1 antibody (red) to visualize PMNs. Scale bar: 200 µm. (D-E) Leukocyte adhesion and rolling in TNFα-stimulated cremaster muscle venules assessed in 12 venules of 4 K3+/+ mice, in 19 venules of 4 K3n/n mice and in 17 venules of 3 K3n/- mice. (D) Leukocyte adhesion efficiency determined as number of adherent leukocytes per mm^2 vascular surface area divided by the systemic leukocyte count. (E) Leukocyte rolling flux fraction determined as rolling leukocytes passing an imaginary perpendicular line over the vessel corrected by the total number of passing leukocytes. Values are mean ± SEM. (F) Phagocytosis of fluorescently labeled E.coli particles by K3+/+, K3n/n, K3n/- and K3-/-

PMNs. N=3;5;4;4;3. Significant differences are indicated by asterisk (*: p<0.05; **: p<0.01; ***p<0.001).

Figure 4: Quantification of kindlin-3, talin-1 and integrin protein levels in platelets and PMNs. (A) Western blot of kindlin-3 and talin-1 from different blood cell lysates. GAPDH and actin served as loading controls. (B) Copy number counts of platelet proteins were estimated with intensity based absolute quantification. (C) Schematic representation of the workflow for quantification of protein copy numbers in platelet lysates. Heavy labeled protein standards with known concentration were spiked into platelet lysates and peptide ratios were determined by mass spectrometry. (D) Mass spectrometry-based absolute quantification of the copy numbers of kindlin-3, talin-1, β3 integrin and β2 integrin in K3+/+, K3n/n and K3n/- platelets. (wt N=3; +/n, n/n and n/- N=2) . Values are given as median ± range. (E) Mass spectrometry-based absolute quantification of the copy numbers of kindlin-3, talin-1 and β2 integrin in wild type PMNs. N=3. Values are given as median ± range.

Supplementary Figure 1: Generation of mutant Kindlin-3 mice. (A) Targeting strategy of kindlin-3. Partial map of the kindlin-3 gene and the targeting vector carrying a loxP sites flanking exons 3 to 6 of the kindlin-3 gene. A frt flanked neomycin resistance cassette was inserted into intron 6. Exons are indicated as rectangles and restriction enzymes by name. Probe used for Southern blotting is shown as red rectangle. (B) Southern blot on DNA samples from R1 ES cells electroporated with the targeting construct. The genomic DNA was digested with HindIII and hybridized with the probe indicated in A. (C) Genomic PCR performed with primers indicated as red arrows in A to identify mice carrying the K3+/+, K3n/n, K3n/- and K3-/- alleles. (D) Deletion of the kindlin-3 gene by crossing conditional kindlin-3 mice with deletor Cre mice. (E) Western blots of thymus lysates from K3+/+ and K3-/- mice.

Supplementary Figure 2: Normal development of K3+/n, K3n/n, K3n/- **mice.** (A) Weight gains. (B) Cellularity of the thymus and spleen. (C) Differentiation of precursor cells into CD4- and CD8-positive T-cells.

Supplementary Table 1:

Blood counts of K3+/+, K3+/n, K3n/n, K3n/- and K3-/- chimeras. Values are shown as mean ± SD. WBC, white blood cell; NE, neutrophil; LY, lymphocyte; RBC, red blood cell; Hb, hemoglobin; PLT, platelet.

		+/+ [n=9]		+/n [n=8]		n/n [n=9]		-/n [n=9]		-/- chimera [n=4]	
		mean	SD	mean	SD	mean	SD	mean	SD	mean	SD
[10^3/µl]	**WBC**	5,70	(± 2,45)	6,38	2,05	13,30	2,58	9,76	4,01	18,23	2,97
[10^3/µl]	**NE**	1,01	(± 0,49)	1,21	0,46	4,15	1,48	2,53	2,38	13,97	2,99
[10^3/µl]	**LY**	4,32	(± 2,09)	4,72	1,49	8,37	2,27	6,62	3,68	3,33	0,55
[10^6/µl]	**RBC**	9,44	(± 1,27)	9,19	0,82	8,35	1,21	8,35	0,95	2,44	0,47
[g/dL]	**Hb**	13,93	(± 2,29)	13,56	1,19	12,56	2,12	12,71	1,53	5,78	0,77
[10^6/µl]	**PLT**	603,44	(± 138,5)	452,0	61,8	593,2	112,5	695,3	216,4	648,0	167,1

Figure 1

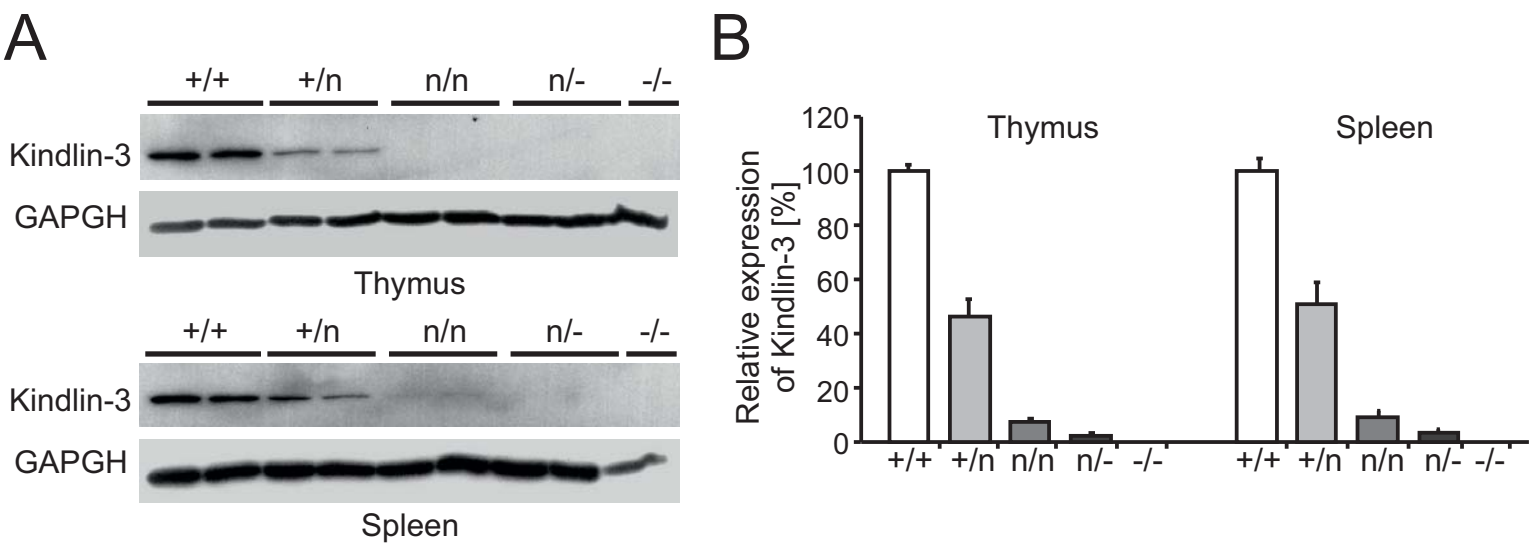
A
+/+
+/n
n/n
n/-
-/-
Kindlin-3
GAPGH
Thymus
+/+
+/n
n/n
n/-
-/-
Kindlin-3
GAPGH
Spleen
B
Relative expression of Kindlin-3 [%]
120
100
80
60
40
20
0
Thymus
Spleen
+/+
+/n
n/n
n/-
-/-
+/+
+/n
n/n
n/-
-/-

Figure 2

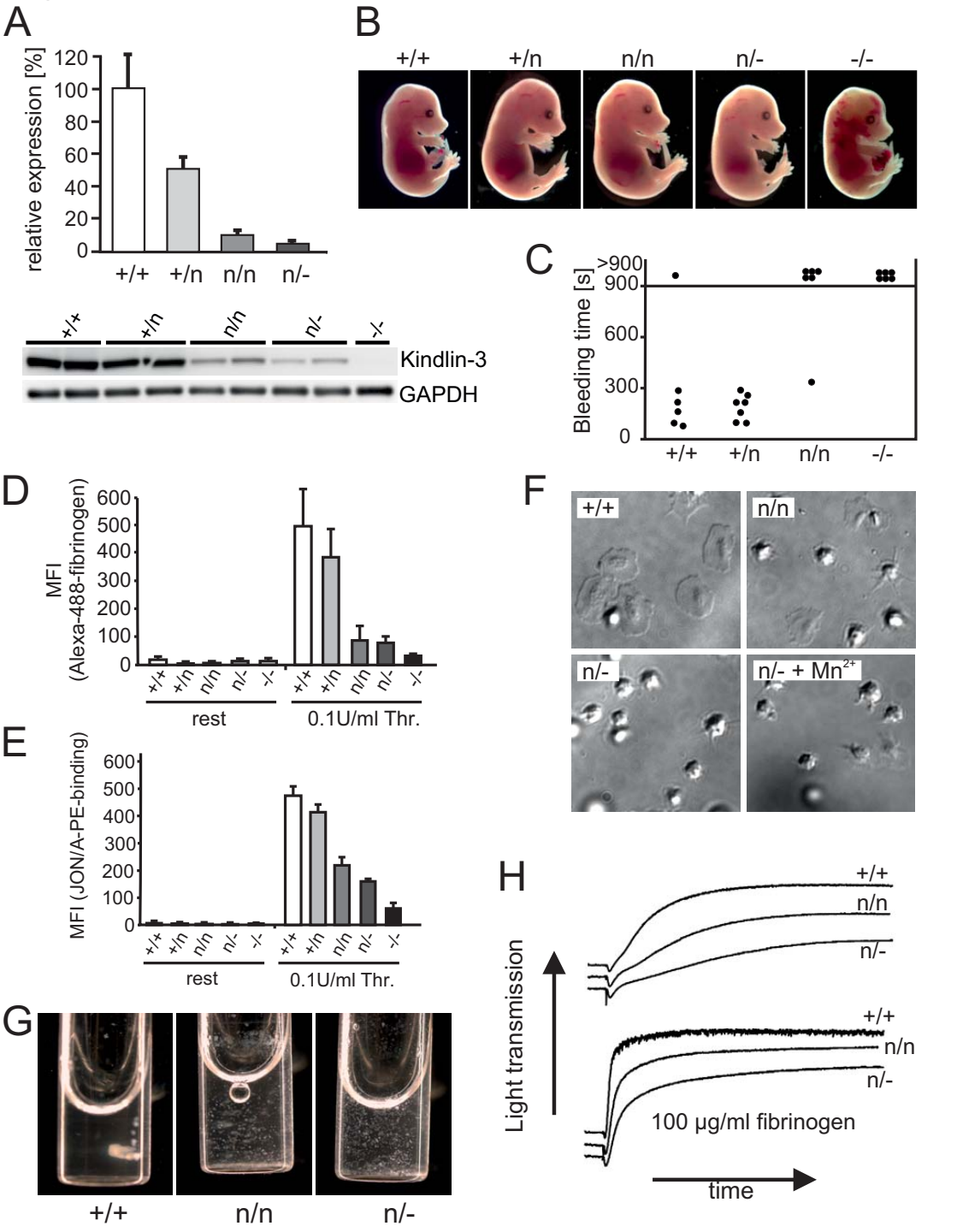
A
relative expression [%]
120
100
80
60
40
20
0
+/+ +/n n/n n/-
+/+ +/n n/n n/- -/-
Kindlin-3
GAPDH
B
+/+ +/n n/n n/- -/-
C
Bleeding time [s]
>900
900
600
300
0
+/+ +/n n/n -/-
D
MFI (Alexa-488-fibrinogen)
600
500
400
300
200
100
0
+/+ +/n n/n n/- -/-
rest
0.1U/ml Thr.
E
MFI (JON/A-PE-binding)
rest
0.1U/ml Thr.
F
+/+
n/n
n/-
n/- + Mn2+
G
+/+ n/n n/-
H
Light transmission
+/+
n/n
n/-
100 µg/ml fibrinogen
time
I
clot retraction [%]
time [min]
15 30 45 60 120
+0.5mM MnCl2
+/+
+/n
n/n
n/-
-/-

Figure 3

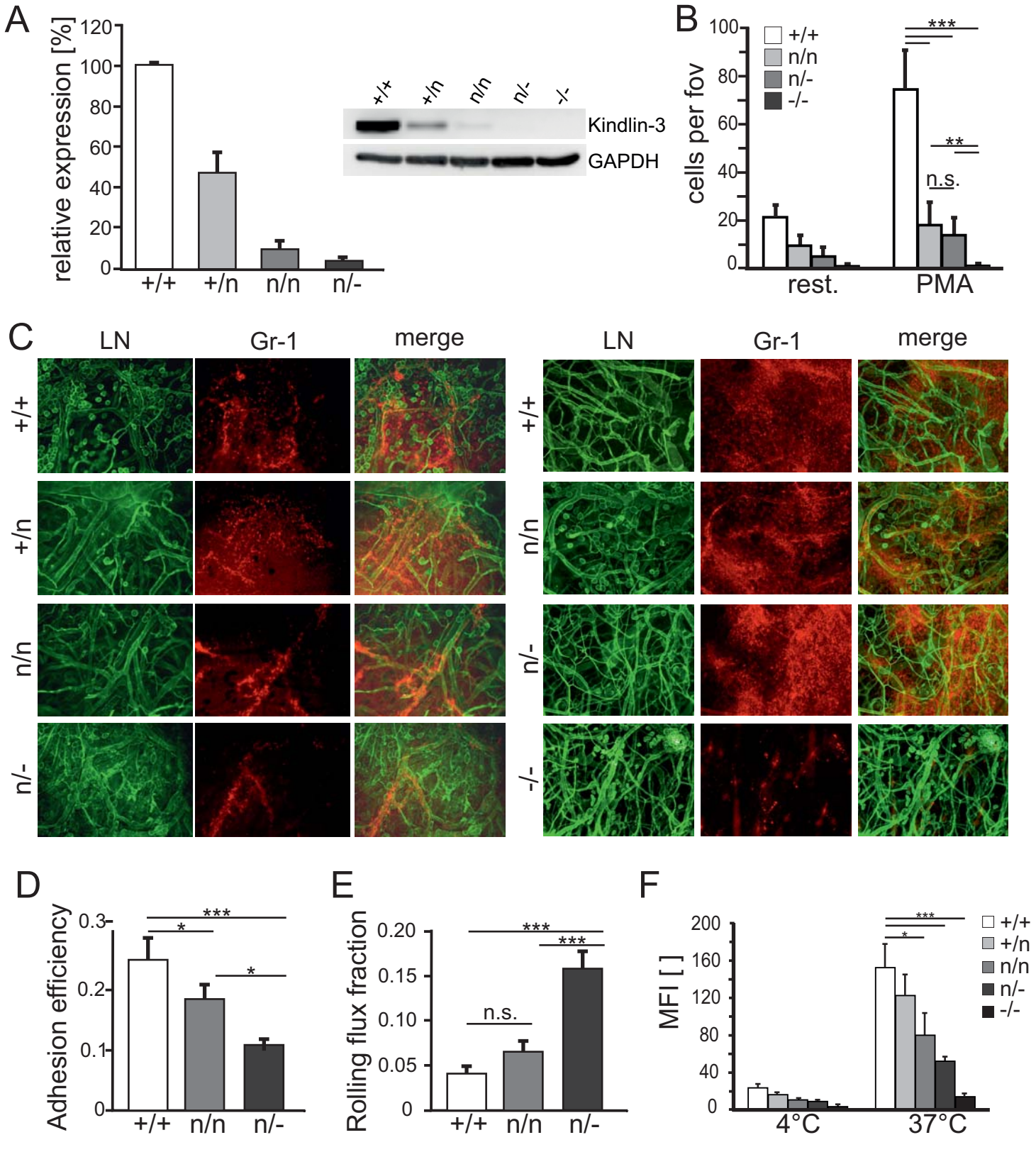
A
relative expression [%]
120
100
80
60
40
20
0
+/+
+/n
n/n
n/-
+/+
+/n
n/n
n/-
-/-
Kindlin-3
GAPDH
B
cells per fov
100
80
60
40
20
0
+/+
n/n
n/-
-/-
***
**
n.s.
rest.
PMA
C
LN
Gr-1
merge
+/+
+/n
n/n
n/-
-/-
D
Adhesion efficiency
0.3
0.2
0.1
0
***
*
*
+/+
n/n
n/-
E
Rolling flux fraction
0.20
0.15
0.10
0.05
0
***
***
n.s.
+/+
n/n
n/-
F
MFI [ ]
200
160
120
80
40
0
***
*
+/+
+/n
n/n
n/-
-/-
4°C
37°C

Figure 4

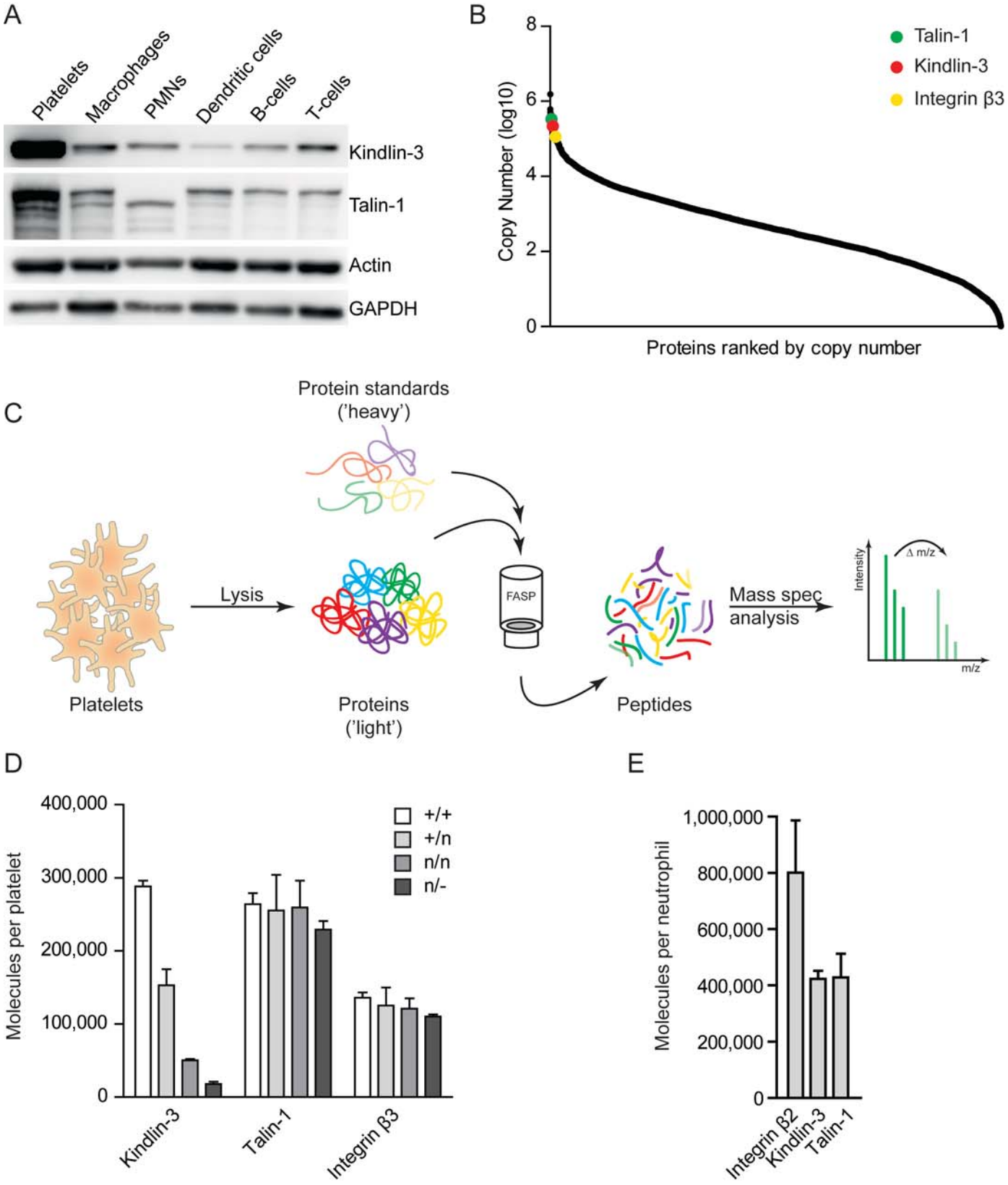
A
Platelets
Macrophages
PMNs
Dendritic cells
B-cells
T-cells
Kindlin-3
Talin-1
Actin
GAPDH
B
Copy Number (log10)
Proteins ranked by copy number
Talin-1
Kindlin-3
Integrin β3
C
Protein standards
('heavy')
Lysis
FASP
Mass spec
analysis
Intensity
Δ m/z
m/z
Platelets
Proteins
('light')
Peptides
D
Molecules per platelet
+/+
+/n
n/n
n/-
Kindlin-3
Talin-1
Integrin β3
E
Molecules per neutrophil
Integrin β2
Kindlin-3
Talin-1

Supplementary Figure 1

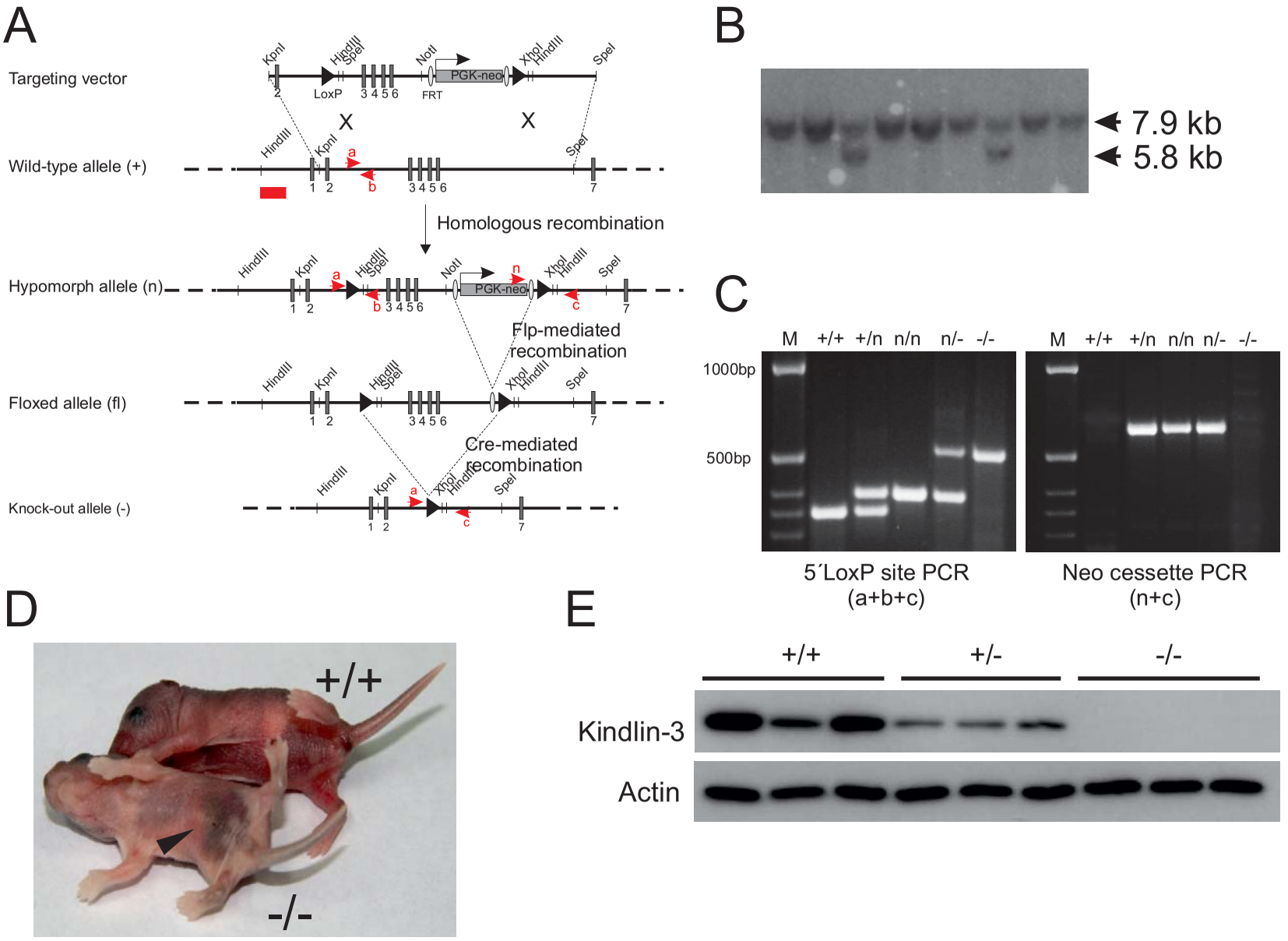

Supplementary Figure 2

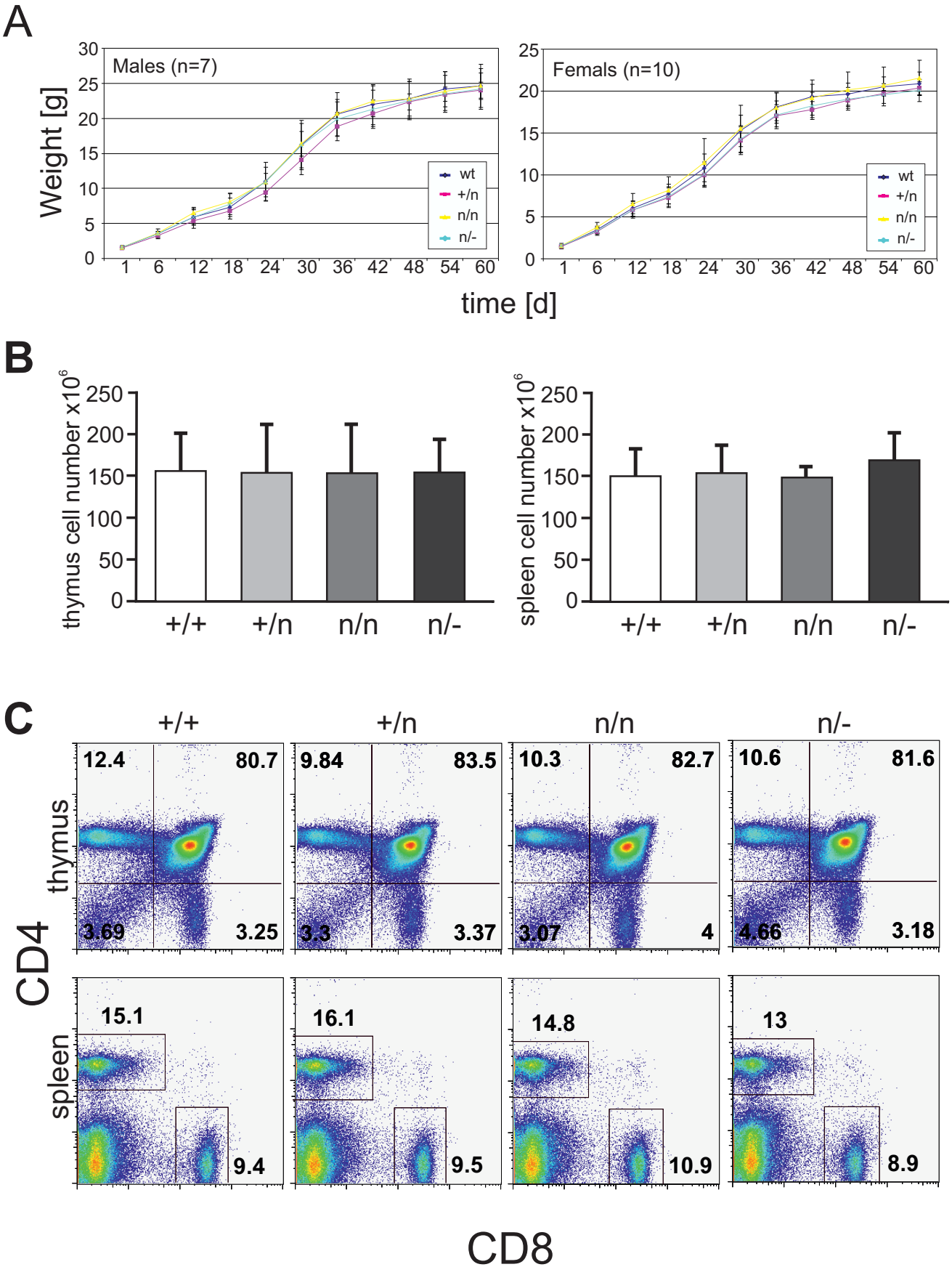

12.7 Paper 7:

β1 integrin-mediated signals are required for platelet granule secretion and hemostasis in mouse.

blood

2013 122: 2723-2731
Prepublished online September 4, 2013;
doi:10.1182/blood-2013-06-508721

β1 integrin–mediated signals are required for platelet granule secretion and hemostasis in mouse

Tobias Petzold, Raphael Ruppert, Dharmendra Pandey, Verena Barocke, Hannelore Meyer, Michael Lorenz, Lin Zhang, Wolfgang Siess, Steffen Massberg and Markus Moser

Blood (print ISSN 0006-4971, online ISSN 1528-0020), is published weekly by the American Society of Hematology, 2021 L St, NW, Suite 900, Washington DC 20036.

Regular Article

PLATELETS AND THROMBOPOIESIS

β1 integrin–mediated signals are required for platelet granule secretion and hemostasis in mouse

Tobias Petzold,[1-3] Raphael Ruppert,[1] Dharmendra Pandey,[1] Verena Barocke,[2] Hannelore Meyer,[1] Michael Lorenz,[2,3] Lin Zhang,[2,3] Wolfgang Siess,[3,4] Steffen Massberg,[2,3] and Markus Moser[1]

[1]Department of Molecular Medicine, Max Planck Institute of Biochemistry, Martinsried, Germany; [2]Medizinische Klinik und Poliklinik I, Klinikum der Universität München, Munich, Germany; [3]Munich Heart Alliance, Munich, Germany; and [4]Institute for Prevention of Cardiovascular Diseases, Universität München, Munich, Germany

Key Points

- Platelet β1 integrin–mediated signals control granule secretion and hemostasis
- β1 integrin–mediated outside-in signaling is independent of direct kindlin-integrin interaction

Integrins are critical for platelet adhesion and aggregation during arterial thrombosis and hemostasis. Although the platelet-specific αIIbβ3 integrin is known to be crucial for these processes, the in vivo role of β1 integrins is a matter of debate. Here we demonstrate that mice expressing reduced levels of β1 integrins or an activation-deficient β1 integrin show strongly reduced platelet adhesion to collagen in vitro and in a carotis ligation model in vivo. Interestingly, hypomorphic mice expressing only 3% of β1 integrins on platelets show normal bleeding times despite reduced platelet adhesion. The residual 3% of β1 integrins are able to trigger intracellular signals driving Rac-1–dependent granule release required for platelet aggregation and hemostasis. Our findings support a model, in which platelet β1 integrins serve as an important signaling receptor rather than an adhesion receptor in vivo and therefore promote β1 integrins as a promising and so far clinically unemployed antithrombotic target. (*Blood*. 2013;122(15):2723-2731)

Introduction

The rupture of atherosclerotic plaques leads to the exposure of matrix proteins, which in turn trigger arterial thrombosis, leading to stroke and cardiac infarction. Different platelet receptors sense the exposed matrix and induce platelet activation and secretion of prothrombotic molecules, leading to further platelet recruitment and finally thrombus formation. Integrins represent the major family of cell-adhesion receptors on platelets. They are heterodimeric transmembrane molecules consisting of α and β subunits. The αIIbβ3 integrin is exclusively expressed on platelets and can bind von Willebrand factor (vWF), fibrinogen, and fibronectin. In addition to αIIbβ3, platelets express three β1 integrins, α2β1, α5β1, and α6β1, albeit at lower levels, which bind to collagen, fibronectin, and laminin, respectively. Circulating platelets express integrins in a conformation with a low affinity for the ligand. At sites of vascular injury, extracellular stimuli, such as collagen binding to glycoprotein VI (GPVI), induce the formation of active integrins with high affinity for ligands. This process is termed integrin activation or integrin inside-out signaling and requires the direct interaction of talin and kindlins with the cytoplasmic domain of the β integrin subunit.[1,2]

Although the fundamental role of the αIIbβ3 integrin for platelet-mediated hemostasis is indisputable, the in vivo relevance of β1 integrins on platelets remains controversial because of either different approaches to target β1 integrin function in platelets, including the use of α2 or β1 integrin-deficient mice,[3,4] β1 integrin–blocking antibodies, synthetic collagen-derived peptides, or small-molecule inhibitors,[5-7] or to the different experimental methods used to model arterial thrombosis[8,9] and to assay bleeding tendency.[3,10] Depending on the assay, β1 integrins have been reported to be both crucial and dispensable for platelet accumulation in vivo. Several in vitro studies indicated an important role of α2β1 integrin in the activation of various signaling molecules that are known to induce integrin αIIbβ3 activation, platelet spreading, and aggregation.[11,12] In one study with two patients, investigators reported that the loss of α2β1 integrin is associated with minor bleeding[13,14] attributable to defective α2β1 integrin function, resulting in impaired platelet adhesion and aggregation to collagen or collagen-derived peptides under shear conditions.[10,15] Overall, the exact role of β1 integrins remains a matter of debate.

In the present study we therefore investigated the role of β1 integrins on platelets during arterial thrombosis by using mouse mutants that express different levels of β1 integrins or an activation-deficient β1 integrin. We report that β1-null mice or an activation-deficient β1 integrin mutant show prolonged bleeding times because of insufficient activation of Rac-1, actin dynamics, granule secretion, and platelet aggregation. Interestingly, platelets expressing 3% of wild-type β1 integrin show reduced adhesion to sites of vascular injury; however, bleeding times, Rac-1 activation, and degranulation are not affected. The relevance of these findings is discussed.

Submitted June 13, 2013; accepted August 10, 2013. Prepublished online as *Blood* First Edition paper, September 4, 2013; DOI 10.1182/blood-2013-06-508721.

R.R. and D.P. contributed equally to this study.

The online version of this article contains a data supplement.

The publication costs of this article were defrayed in part by page charge payment. Therefore, and solely to indicate this fact, this article is hereby marked "advertisement" in accordance with 18 USC section 1734.

Materials and methods

Reagents and antibodies

Thrombin and heparin were purchased from Sigma-Aldrich and convulxin (CVX), adenosine 5′-diphosphate, and U46619 were from Alexis. Horm-collagen was purchased from Nycomed. The following antibodies were used for flow cytometry: PE-integrin β1 (CD29), PE-IgG hamster isotype (Biolegend), PE-integrin β3 (CD61; eBioscience), FITC-integrin α2 (CD49b; Emfret), PE-integrin α5 (CD49e) and PE-integrin α6 (CD49f; PharMingen), FITC-9EG7 (active integrin β-1), IgG1 rat isotype control (BD Biosciences); FITC-GPIa, FITC-GPVI, FITC-GPIX, PE-CD62P, PE-JON/A (active Integrin αIIbβ3; all from Emfret), FITC-IgG2a rat isotype control, FITC-IgG2b rat isotype control (NatuTec), and PE-IgG2a rat isotype control (PharMingen).

The following antibodies were used for western blotting: antikindlin-3,[16] anti-Talin-1 (Sigma-Aldrich), antifibrinogen (γ-chain) (Abcam), antithrombospondin-1, anti-VEGF, anti-vWF (Santa Cruz Biotechnologies, Inc), anti-GAPDH (Calbiochem), anti-Rac-1 (Cell Biolabs), anti-PAK1 (phosphorylated-Thr432)/PAK2 (phosphorylated-Thr402), anti-MLC (phosphorylated-Ser19), anti-MLC (Cell Signaling), anti-FAK (phosphorylated-Y397; Biosource), anti-FAK (Upstate), and anti-β1 integrin (Millipore).

Mice

Conditional integrin β1 mice ($\beta1^{fl/fl}$), kindlin-$3^{-/-}$, integrin β1 hypomorphic ($\beta1^{Hpm/fl}$) mice, and Mx1-Cre transgenic mice have been described previously.[1,17-19] Bone marrow chimeras were generated by injecting 6×10^6 bone marrow cells into the tail vein of lethally irradiated 8-week-old C57BL/6 mice. Three weeks later, Cre expression in the hematopoietic system was induced by two intraperitoneal injections of 250 μg of polyI/C (Amersham Biosciences) with a time lag of 2 days.

Platelet preparation

Heparinized whole blood was centrifuged to isolate platelet-rich plasma. Platelets were washed in Tyrodes buffer, pH 6.5 (134 mM NaCl, 2.9 mM KCl, 12 mM $NaHCO_3$, 10 mM *N*-2-hydroxyethylpiperazine-*N*′-2-ethanesulfonic acid) containing 5 mM glucose and 0.35% bovine serum albumin (BSA) and were kept at 37°C. For experiments ex vivo, platelets were resuspended in Tyrodes buffer, pH 7.4, containing 5 mM glucose, 0.35% BSA, 1 mM $CaCl_2$, and 1 mM $MgCl_2$.

Flow cytometry

Heparinized blood was diluted 1:50 in Tyrodes buffer, pH 7.4, containing 5 mM glucose, 0.35% BSA, 1 mM $CaCl_2$, and 1 mM $MgCl_2$. To quantify surface receptor expression level, blood samples were incubated with fluorophore-conjugated antibodies for 15 minutes at room temperature and analyzed on a FACScalibur flow cytometer (Becton Dickinson, Heidelberg, Germany). For integrin activation assays, washed platelets were stimulated for 15 minutes with the indicated agonists and incubated with fluorophore-conjugated conformation sensitive antibodies.

Platelet spreading

Coverslips were coated with 1 mg/mL fibrinogen (Sigma-Aldrich) or 25 μg/mL acid soluble collagen I (Sigma-Aldrich) overnight, washed and blocked with 1% BSA. Washed platelets (1×10^6) were suspended in 150 μL of Tyrodes buffer (pH 7.4; 1 mM $CaCl_2$, 1 mM $MgCl_2$), stimulated with 0.01U/mL thrombin, and seeded on coated coverslides in the presence or absence of 0.75 mM Mn^{2+}. After 45 minutes at 37°C, differential interference contrast microscopy was performed with a Zeiss Axiovert 200M microscope with a Plan-NEOFLUAR, ×100, 1.45 oil objective (Zeiss, Jena, Germany). Pictures were acquired via the use of Metamorph software (Molecular Devices). Platelet spreading area was analyzed using ImageJ software (http://rsbweb.nih.gov/ij/).

Carotid ligation model

Experiments were performed as described by Massberg et al.[20] In brief, carotid arteries of anesthetized mice were dissected and ligated by the use of a small suture for 5 minutes. To visualize platelet adhesion, fluorescently 2′,7′-dichlorofluorescein (Molecular Probes)-labeled platelets (200×10^6/250 μL) from control and mutant mice were infused, and the number of adherent platelets at the lesion site was quantified by video-fluorescence microscopy with a high-speed, wide-field fluorescent microscope with a long distance condenser and a 20× (NA 0.95) water immersion objective and a coupled camera (ORCA-ER; Hamamatsu Photonics). Images were acquired and analyzed using a Cell^R software (Olympus). The number of adherent platelets per mm^2 is represented as percentage of adherent $\beta1^{+/+}$ platelets at the 5-minute time point.

Analysis of bleeding time

Ten- to twelve-week-old mice were anesthetized by constant isoflurane gas-narcosis and subcutaneous application of weight-adapted fentanyl (0.05 mg/kg; CuraMed Pharma GmbH) and placed on a 37°C heating pad. An 8-mm segment of the tail tip was cut off, and the bleeding tail was immediately placed into 37°C warm physiological saline solution. Time until bleeding vanished was measured. All experiments were stopped latest after 15 minutes by cauterization to prevent excessive blood loss.

Aggregation

To determine platelet aggregation, light transmission was measured over 10 minutes in a two-channel aggregometer (CHRONO-LOG) and was expressed as arbitrary units. Washed platelets (2×10^8/mL) were stimulated with different agonists in Tyrodes buffer (pH 7.4, 1 mM $CaCl_2$, 1 mM $MgCl_2$) in the presence or absence of fibrinogen (100 μg/mL) or Mn^{2+} (0.75 mM), respectively.

Evaluation of adenosine triphosphate (ATP) release

A luciferin-luciferase detection kit (CHRONO-LOG) was used to quantify the release of ATP platelets. For these experiments, platelets were stimulated in a lumino-aggregometer (CHRONO-LOG) under stirring conditions, in the presence of luciferase and luciferin. Emitted luminescence was recorded as arbitrary units, and values were expressed as signal ratio of collagen and CVX-stimulated platelets.

Serotonin and PF-4 release assays

Platelets were stimulated in an aggregometer (CHRONO-LOG) under stirring conditions for 8 minutes. Platelets were pelleted by centrifugation for 30 seconds. The serotonin and PF-4 contents within the supernatants were determined using the Serotonin ELISA (LDN, Germany) and PF-4 ELISA (Abcam) Kits following the manufacturer's instructions.

Granule protein release

Platelets were stimulated in an aggregometer in the absence of BSA as described previously. After 8 minutes, platelets were pelleted by centrifugation ($20\,000 \times g$ for 30 seconds) and immediately lysed in Laemmli buffer (60 mM Tris-Cl, pH 6.8; 2% sodium dodecyl sulfate; 10% glycerol; 5% β-mercaptoethanol; 0.01% bromophenol blue). Lysates were subjected to immunoblotting and probed with the indicated antibodies.

Rac-1 activity assay

Rac-1 activity was analyzed with a Rac-1 Activation-Assay-Kit (Cell Biolabs). Platelets were stimulated with 5 μg/mL fibrillar collagen for 60 seconds in an aggregometer as described and then lysed by addition of 2× lysis buffer (125 mM HEPES, pH 7.5; 750 mM NaCl; 5% NP-40; 50 mM $MgCl_2$; 5 mM EDTA; 10% glycerol) on ice. Cleared lysates were incubated with PAK-PBD agarose and processed according to the manufacturer's protocol. Rac-1-GTP binding was determined by western blot analysis.

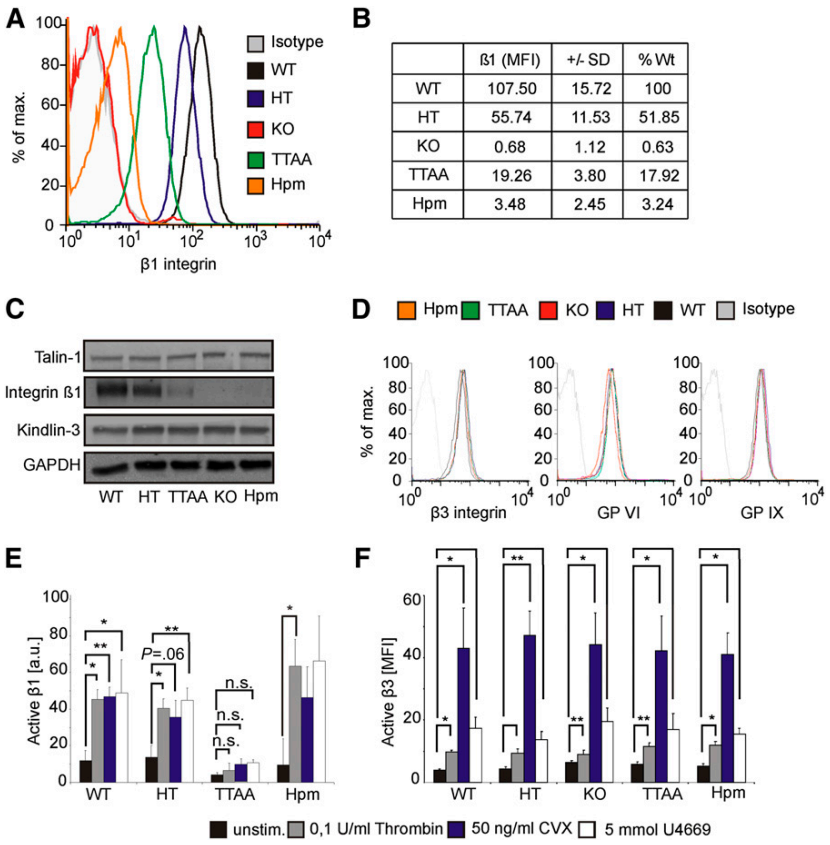

	ß1 (MFI)	+/- SD	% Wt
WT	107.50	15.72	100
HT	55.74	11.53	51.85
KO	0.68	1.12	0.63
TTAA	19.26	3.80	17.92
Hpm	3.48	2.45	3.24

Figure 1. Characterization of platelets from β1 integrin mouse mutants. Platelet β1 integrin surface expression of wild-type (WT; $\beta1^{+/+}$), HT ($\beta1^{+/-}$), KO ($\beta1^{-/-}$), TTAA ($\beta1^{TTAA}$), and Hpm ($\beta1^{Hpm}$) β1 integrin mice were analyzed by flow cytometry. (B) Geometric mean values of β1 integrin expression shown in panel A were corrected for isotype control and expressed as % of WT β1-integrin surface levels (n = 6 per group). (C) Platelet lysates were subjected to immunoblotting for β1-integrin, talin-1, kindlin-3, and glyceraldehyde-3-phosphate dehydrogenase (GAPDH). (D) Surface expression of β3 integrin, GPVI, and GPIX on platelets of indicated mouse strains. (E) Platelet β1 integrin activation was determined with the conformation-specific 9EG7 antibody via the use of flow cytometry upon stimulation with 50 ng/mL CVX, 0.1 U/mL thrombin, or 5 mM U46619. Acquired mean fluorescence intensity values were normalized to total β1 integrin expression levels and are shown as arbitrary unit (n = 3 for TTAA and Hpm, n = 4 for all other groups; bars represent mean values ± SEM; significance levels are indicated; $*P < .05$; $**P < .01$; n.s., not significant). (F) Active β3 integrins were determined with JON/A antibody after platelet stimulation with indicated stimuli. No significant difference between all tested groups was determined (n = 5 for HT and WT, n = 4 for all other groups; bars represent geometric mean values ± SEM).

Measurement of filamentous actin content

Platelets were stimulated with 5 μg/mL fibrillar collagen in an aggregometer under stirring conditions in the presence of 0.5 mM RGDS (Sigma-Aldrich). At indicated time points, platelets were fixed in 1.8% parformaldehyde, permeabilized in 0.02% Triton X-100 phosphate-buffered saline, and stained with FITC-phalloidin (Invitrogen). F-actin content was quantified using flow cytometry.

Statistical analysis

All data are shown as mean ± SEM. To test significance level, an unpaired Student *t* test was performed, and a value of $P < .05$ was considered significant. If indicated, one-way analysis of variance followed by a Tukey multiple comparison test was performed.

Ethics statement

All animal experiments were performed with approval by the District Government of Bavaria (Munich, Germany).

Results

Genetic targeting of β1 integrin

To address the role of platelet β1 integrins for platelet activation, adhesion, and aggregation, we generated mouse strains with different β1 integrin expression levels and an activation-deficient β1 integrin mutant. We derived platelets from offspring ($\beta1^{fl/fl}$ Mx1-Cre; $\beta1^{+/fl}$ Mx1-Cre) of intercrosses between floxed β1 integrin mice and the inducible Mx1-Cre strain,[18] from β1 integrin hypomorphic mice,[17] and from Kindlin binding−deficient mice carrying the TT788/789AA substitutions in the β1 integrin cytoplasmic domain.[21] Because homozygous hypomorphic β1 integrin ($\beta1^{hpm/hpm}$) mice expressing very low levels of functional β1 integrin and homozygous $\beta1^{TTAA/TTAA}$ mice die at peri-implantation, we crossed $\beta1^{+/hpm}$ and $\beta1^{+/TTAA}$ mice, respectively, with floxed β1 integrin and Mx1-Cre mice to generate $\beta1^{hpm/fl}$ Mx1-Cre and $\beta1^{TTAA/fl}$ Mx1-Cre mice. Injection of poly-IC induced the expression of the Cre-recombinase, leading to the deletion of the floxed β1 integrin gene predominantly in hematopoietic cells resulting in blood cell-restricted β1-null (KO), heterozygous (HT), hypomorphic (Hpm), and $\beta1^{TTAA}$ (TTAA) mice. To prevent off-target effects of the Mx1-Cre−mediated gene deletion described in other tissues, we restricted the deletion to the hematopoietic system by using bone marrow chimeras for in vivo experiments.[18]

Differential β1 integrin expression in mutant mice

We first quantified the surface expression of platelet β1, α2, α5, and α6 integrins by using flow cytometry. Poly-IC treatment resulted in a loss of β1 integrin surface levels on platelets from $\beta1^{fl/fl}$ Mx1-Cre mice, reduced the levels by approximately 51% in $\beta1^{+/fl}$ Mx1-Cre mice, approximately 82% in $\beta1^{TTAA/fl}$ Mx1-Cre, and approximately 97% in $\beta1^{hpm/fl}$ Mx-Cre mice (Figure 1A-B). The differences in β1 integrin expression levels were confirmed by western blot analysis (Figure 1C). A similar reduction in the surface expression of the β1 integrin−associated α2, α5, and α6 integrin subunits was measured in the different platelet populations (supplemental Table 1A; see the

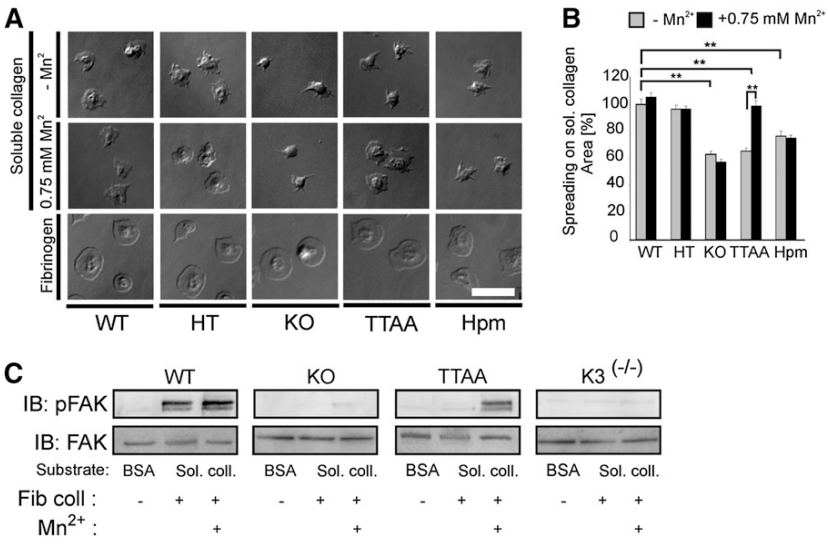

Figure 2. β1 integrin–mediated spreading and outside-in signaling is independent of kindlin-integrin interaction. (A) Spreading of thrombin-stimulated platelets on soluble collagen in the absence or presence of 0.75 mM Mn^{2+} and on fibrinogen. Representative pictures are shown 45 minutes after platelet seeding (scale bar represents 5 μm). (B) Spreading area of mutant platelets on soluble collagen is shown relative to wild-type (WT) platelets at 45 minutes (bars represent mean values ± SEM; significance level are indicated; $*P < .05$; $**P < .01$). (C) Integrin outside-in signaling was evaluated by FAK autophosphorylation at Tyr379. Washed platelets from wild-type (WT), β1 knockout (KO), and TTAA mice as well as from kindlin-3–deficient mice ($K3^{(-/-)}$) were stimulated with 5 μg/mL fibrillar collagen and seeded on soluble collagen-coated surfaces in the absence or presence of Mn^{2+}. To analyze basal FAK phosphorylation, unstimulated platelets were seeded on BSA. Cells were lysed after 30 minutes and subjected to immunoblotting for FAK Y397 phosphorylation and total FAK.

Blood Web site). Furthermore, we analyzed the distribution of β1 integrin expression on hypomorphic platelets, which showed a mean expression of 3% compared with wild-type platelets. Fluorescence-activated cell sorting analysis revealed that 80% of the platelets from hypomorphic mice express <8.5% of β1 integrins, whereas only 5% express more than 25% of β1 integrins compared with controls (supplemental Table 1B). It has been previously shown that the reduced expression of $β1^{TTAA}$ integrin was caused by increased degradation.[21] Expression of talin-1 (for quantification, see supplemental Figure 1) and kindlin-3 was similar in platelets of all genotypes (Figure 1C). Furthermore, surface levels of β3 integrin, GPVI, and GPIX also were unaffected by the different β1 levels (Figure 1D).

β1 integrin inside-out signaling depends on an intact kindlin-binding site

We then analyzed the β1 integrin activation state on platelets from the different mice. Active β1 integrins were quantified by flow cytometry by use of the conformation-specific 9EG7 antibody that recognizes the active conformation of β1 integrins and the measured values were then corrected for the different β1 integrin expression. Treatment with CVX, the thromboxane A analog U46619, and thrombin led to a similar β1 integrin activation on platelets from wild-type, heterozygous, and hypomorphic mice. In sharp contrast, all three agonists failed to activate the kindlin binding–deficient $β1^{TTAA}$ integrin (Figure 1E). Importantly, the activation of αIIbβ3 integrins was not affected by β1 integrin surface levels or the kindlin binding mutation (Figure 1F). These data show that an intact kindlin-3 binding site in β1 integrins is required for their activation in vivo and that an intact binding site for talin-1 alone is not sufficient to activate β1 integrins.

β1 integrin–mediated outside-in signaling and spreading is independent of kindlin-integrin interaction

Next, we analyzed platelet adhesion and spreading on acidic soluble collagen. Acidic soluble collagen I is bound by α2β1 integrin via a repetitive GFOGER motif. This motif is not recognized by GPVI, which binds GPOn exposed on fibrillar collagen.[5,22] In contrast to human platelets that can bind soluble collagen and generate intrinsic signaling without previous activation, mouse platelets require a weak intrinsic activation to spread on soluble collagen.[23] Taking this into account, we stimulated washed mouse platelets with 0.01 U/mL thrombin in the presence or absence of 0.75 mM Mn^{2+}. As depicted in Figure 2A, $β1^{Hpm}$ and β1-null platelets showed a severe spreading defect on soluble collagen I both in the presence or absence of Mn^{2+}. Furthermore, they formed elongated filopodia and only occasionally small lamellipodia. Activation of $β1^{TTAA}$ platelets also failed to form lamellipodia and showed a significantly reduced spreading (Figure 2A-B). Notably, spreading of $β1^{Hpm}$ platelets was not improved by increasing the coating concentration of collagen (supplemental Figure 2A). Interestingly, however, bypassing integrin inside-out signaling by Mn^{2+}-treatment rescued the spreading defect in $β1^{TTAA}$ platelets (Figure 2A-B). In light of our previous observation showing that Mn^{2+}-induced platelet spreading is abolished in kindlin-3–deficient platelets,[1] we conclude that a direct interaction between kindlin-3 and β1 integrin is not required for integrin outside-in signaling.

To further corroborate this finding we analyzed autophosphorylation of focal adhesion kinase (FAK) at position Tyr397 as an immediate effect of collagen-bound β1 integrin signaling. Indeed, $β1^{TTAA}$ platelets showed robust FAK phosphorylation in the presence of Mn^{2+}, which was neither seen in β1-null nor Kindlin-3–null platelets (Figure 2C). Of note, platelet adhesion and spreading on the α6β1 ligand laminin was similarly affected (supplemental Figure 2B). In contrast, adhesion and spreading on the αIIbβ3 ligands fibrinogen (Figure 2A) and fibronectin or on the GPVI substrate collagen-related peptide (supplemental Figure 2B) was not altered in any of the genotypes examined here. Because Mn^{2+} treatment of $β1^{TTAA}$ platelets show normal spreading, these findings indicate that a direct interaction between the integrin cytoplasmic domain and kindlin-3 is required for inside-out signaling, but this interaction is dispensable for integrin-mediated, outside-in signaling and cytoskeletal reorganization during platelet spreading.

β1 integrins are important for platelet adhesion and hemostasis

We next investigated whether the in vitro defects have consequences in vivo. The reduced β1 integrin expression in $β1^{hpm}$ mice and the expression of $β1^{TTAA}$ integrins had no impact on thrombopoiesis

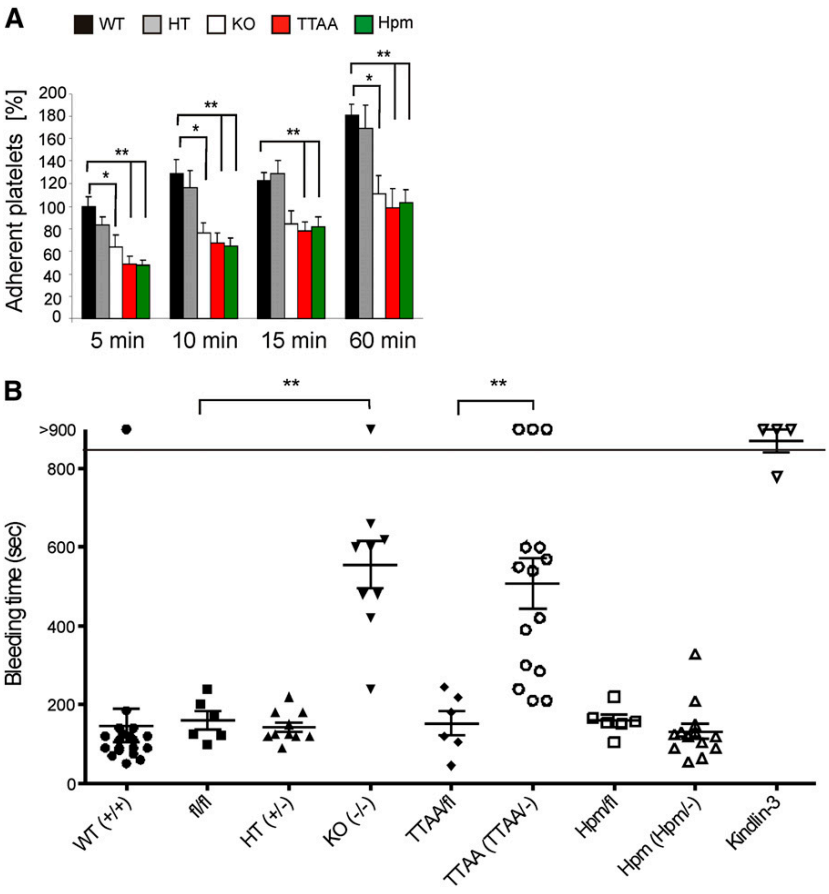

Figure 3. Reduced platelet adhesion and aggregate formation onto injured vessel walls of β1-null, $\beta1^{TTAA}$, and $\beta1^{hpm}$ mice, whereas tail bleeding times of $\beta1^{hpm}$ mice are normal. (A) Number of adherent fluorescently labeled platelets to the injured vessel wall was quantified after 5, 10, 15, and 60 minutes. Values are expressed as percentage of adherent wild-type (WT) platelets (n/mm^2) at 5 minutes (WT, n = 9; HT, n = 6; knockout [KO], n = 6; TTAA, n = 4; Hpm, n = 8; bars represent mean values ± SEM in percent, significance level are indicated; *$P < .05$; **$P < .01$ by one-way analysis of variance followed by a Tukey multiple comparison test). (B) Tail-bleeding times of chimeric mice carrying the bone marrow of the indicated genotype (WT, n = 19; fl/fl, n = 6; HT, n = 10; KO, n = 9; TTAA, n = 15; TTAA/fl, n = 6; Hpm, n = 13; Hpm/fl, n = 6; Kindlin-3$^{-/-}$, n = 4; cross line represents mean bleeding time and bars represent SEM, significance level are indicated; **$P < .01$).

because platelet counts were similar to control animals (data not shown). For studying platelet adhesion to vascular lesions in vivo, we used the in vivo carotid ligation model, in which platelets accumulate in a collagen-dependent manner[20] and which allows monitoring single-platelet adhesion to a defined subendothelial vessel wound by intravital microscopy over time. Consistent with an important role of collagen for platelet adhesion, we observed that β1 integrin−deficient platelets as well as hypomorphic and $\beta1^{TTAA}$ mutant platelets, but not platelets from heterozygous β1 integrin knockout mice, showed a strong decrease in platelet adhesion to the wounded vessel wall 5 to 60 minutes after vascular injury (Figure 3A). These findings indicate that β1 integrins significantly contribute to primary adhesion to subendothelial lesions and that 50% but not the 3% of wild-type β1 integrins (present on β1 hypomorphic platelets) are sufficient to mediate this task. The reduced adhesion of $\beta1^{TTAA}$ platelets is likely attributable to the activation defect of the β1 integrins, although we cannot fully rule out that the expression level of approximately 18% compared with wild-type platelets also contributes to the observed adhesion defect.

Next, we tested whether β1 integrins also play a role for occlusive thrombus formation and hemostasis using the tail-bleeding assay. Although wild-type, heterozygous, and animals carrying a floxed β1 integrin allele but no Mx1-Cre allele ($\beta1^{fl/fl}$, $\beta1^{TTAA/fl}$, $\beta1^{Hpm/fl}$) showed similar bleeding times of 2 to 3 minutes, β1 integrin knockout and $\beta1^{TTAA}$ mice showed significantly prolonged tail bleeding times of 8 to 9 minutes (Figure 3B), and kindlin-3− deficient mice exhibited the most severe bleeding defect as the result of impaired β1 and αIIbβ3 integrin activation.[1] Surprisingly, hypomorphic mice showed normal bleeding times. Taken together, these data indicate that β1 integrins play a crucial role for stopping bleeding and as little as 3% of them are sufficient enabling a normal hemostasis.

Defective aggregation and granule secretion in $\beta1^{TTAA}$ and β1-null mice

Occlusive thrombus formation requires a second wave of platelet recruitment, activation, and subsequent aggregation, which is triggered by the release of paracrine factors stored in platelet α and dense granules. To find an explanation for the normal tail bleeding times of β1 hypomorphic mice, we investigated platelet aggregation in more detail. In brief, washed platelets were activated with either 5 μg/mL fibrillar collagen or with 50 ng/mL CVX, which activates GPVI by inducing GPVI receptor dimerization and downstream signaling.[24] CVX induced aggregation of platelets of all genotypes (Figure 4A; supplemental Figure 3A). In contrast, β1-deficient and $\beta1^{TTAA}$ platelets failed to aggregate after stimulation with fibrillar collagen, whereas $\beta1^{hpm}$ platelets showed an intermediate response (Figure 4A). Exogenous activation of $\beta1^{TTAA}$ platelets by Mn^{2+} resulted in normal aggregation, but this did not occur in β1-deficient platelets (Figure 4B). This latter finding further supports the concept that the double threonine motif within the β1 integrin cytoplasmic domain is required for integrin inside-out but not for integrin outside-in signaling.

Unexpectedly, the addition of exogenous fibrinogen to washed platelets rescued the aggregation defect of $\beta1^{TTAA}$ and β1-null platelets (Figure 4B). Platelets contain substantial amounts of

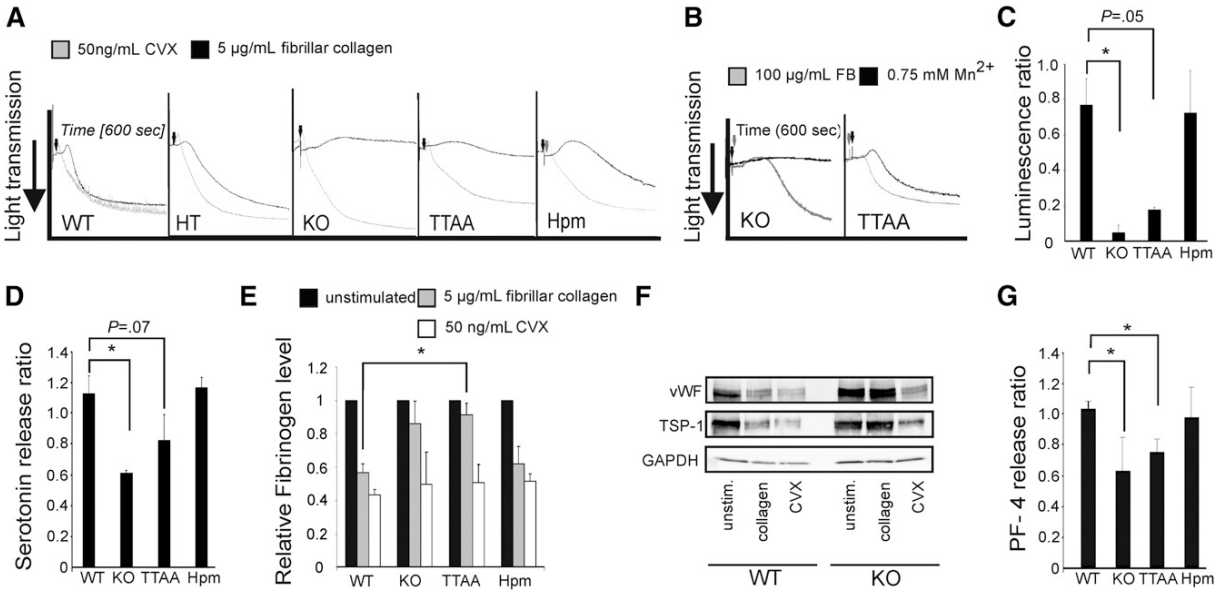

Figure 4. Collagen-induced platelet aggregation and granule secretion requires β1 integrins. (A) Washed platelets were stimulated with 5 μg/mL fibrillar collagen (black curves) or 50 ng/mL CVX (gray curves) and aggregation was recorded for 600 seconds. (B) Aggregation of β1-null (KO) and $\beta1^{TTAA}$ (TTAA) platelets in the presence of 100 μg/mL fibrinogen (gray curves) or 0.75 mM Mn^{2+} (black curves). (C) ATP release from platelet dense granules after stimulation of platelets with collagen. ATP was measured by luminescence after addition of luciferase luciferin reagent using the Lumi-aggregometer (Chronolog, Havertown, PA). Platelets were stimulated with either 5 μg/mL fibrillar collagen or 50 ng/mL CVX for 10 minutes. The relative luminescence after 8 minutes (ratio of collagen to CVX stimulated cells) is shown (bars represent mean values ± SEM of n = 3 independent experiments). (D) Serotonin release after stimulation with collagen. Platelets were stimulated with either 5 μg/mL fibrillar collagen or 50 ng/mL CVX for 8 minutes. The relative serotonin level (ratio of collagen to CVX stimulation) is shown (bars represent mean values ± SEM of n ≥ 3 independent experiments). (E) Quantification of the cellular fibrinogen content in resting platelets or 8 minutes after stimulation with either fibrillar collagen (5 μg/mL) or CVX (50 ng/mL; bars represent mean values ± SEM; significance levels are indicated; *$P < .05$; wild-type (WT), n = 3; knockout (KO), n = 3; TTAA, n = 3; hypomorphic (Hpm), n = 3; representative blots are shown in supplemental Figure 4B). (F) Platelet content of the α-granule cargo proteins vWF and thrombospondin-1 (TSP-1) in wild-type (WT) and β1-null (KO) platelets upon collagen and stimulation with CVX. (G) Ratio of PF-4 release from platelets stimulated with either 5 μg/mL fibrillar collagen or 50 ng/mL CVX for 8 minutes (bars represent mean values ± SEM of n ≥ 3 independent experiments).

fibrinogen within their granules, which they release upon stimulation (eg, by collagen). Hence, the finding that exogenous fibrinogen is able to rescue defective aggregation of $\beta1^{TTAA}$ and β1-null platelets suggests a novel role of β1 integrin in the regulation of fibrinogen release from α granules in platelets. We therefore tested whether β1 integrin-mediated signals are important for granule secretion in general. Dense granule secretion was quantified by measuring ATP release after addition of luciferin/luciferase reagent in an aggregometer. Platelets were stimulated either with 50 ng/mL CVX or 5 μg/mL fibrillar collagen, and values were calculated as a ratio between fibrillar collagen- and CVX-induced luminescence.

Although β1-null and $\beta1^{TTAA}$ platelets showed a severe defect in dense granule secretion after fibrillar collagen stimulation, $\beta1^{hpm}$ platelets showed an almost-normal exocytosis of dense granules upon collagen stimulation (Figure 4C; supplemental Figure 3B). Furthermore, the defect in dense granule secretion of β1-null and $\beta1^{TTAA}$ platelets was corroborated by reduced secretion of serotonin (Figure 4D). To analyze platelet α-granule secretion, we determined the cellular level of the α-granule cargo fibrinogen (Figure 4E; supplemental Figure 3C) before and 8 minutes after agonist treatment (5 μg/mL fibrillar collagen or 50 ng/mL CVX) by immunoblotting. Our data show that stimulation with fibrillar collagen led to a decrease in cellular fibrinogen in wild-type and hypomorphic platelets but not in β1-null and $\beta1^{TTAA}$ platelets. Importantly, the total fibrinogen content was similar in unstimulated platelets of all groups (supplemental Figure 3D), and exocytosis of other α-granule cargo proteins such as thrombospondin, vWF or PF-4 were also β1 integrin–dependent, suggesting that β1 integrin−mediated signals control platelet granule release (Figure 4F-G; supplemental Figure 3E).

β1 integrins control platelet actin polymerization and Rac-1 activation upon collagen stimulation

How does β1 integrin control platelet granule secretion? Platelet granule fusion with the outer platelet membrane requires the reorganization of the actin cytoskeleton.[25,26] Therefore, we analyzed F-actin dynamics after collagen stimulation by flow cytometry. Indeed β1-null platelets failed to increase their F-actin content after 60 seconds, whereas ~3% of β1 integrin were sufficient to rescue F-actin polymerization in hypomorphic platelets (Figure 5A).

The small GTPase Rac-1 is a central regulator of actin polymerization and granule secretion in platelets and is activated rapidly after platelet stimulation.[27] Previous studies showed that genetic and pharmacologic inhibition of Rac-1 efficiently blocks collagen-induced platelet granule secretion and reduces the stability of platelet aggregates under flow.[28] Moreover, it has also been shown that α2β1 integrins regulate actin dynamics and lamellipodia formation in platelets spread on soluble collagen in a Rac-1−dependent manner.[29] Hence, we next examined the formation of active, GTP-bound Rac-1 within 60 seconds after collagen exposure. Hypomorphic and wild-type platelets showed robust Rac-1 activation within 60 seconds, which was not observed in β1 integrin−null platelets (Figure 5B-C). In line with the reduced Rac-1 activity, phosphorylation of the Rac-1 target proteins PAK1/2 was strongly reduced in β1-null platelets 90 and 240 seconds after collagen treatment. Importantly, also hypomorphic platelets showed significant PAK phosphorylation. In contrast, phosphorylation of MLC in β1 integrin–null platelets was not different (Figure 5D). These results show that 3% of β1 integrin expression is sufficient for rapid Rac-1 activation required to

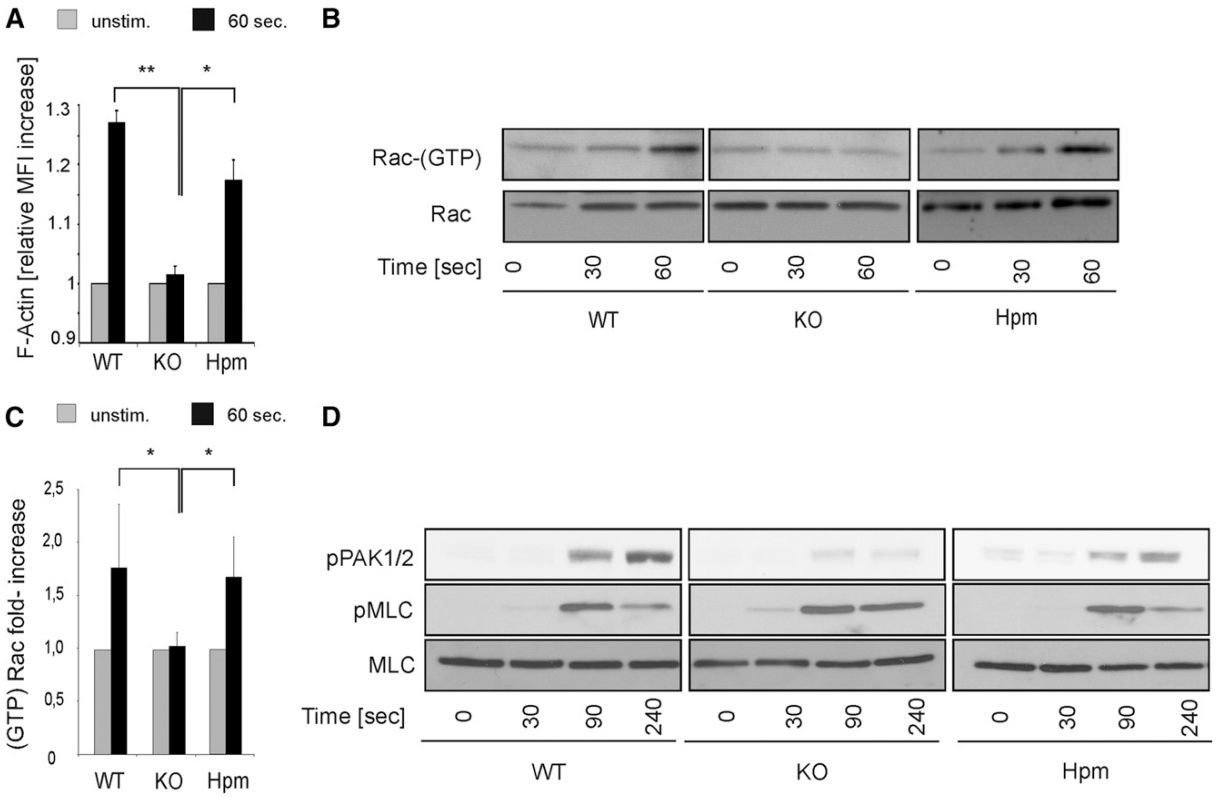

Figure 5. Normal actin polymerization, Rac activation, and PAK phosphorylation in β1 hypomorphic platelets. (A) Platelets from wild-type (WT), β1-null (KO), and hypomorphic (Hpm) mice were stimulated with 5 μg/mL fibrillar collagen for 60 seconds in the presence of 0.5 mM RGDS peptide, and the relative F-actin content was measured by flow cytometry. Curves represent mean ± SEM increase in FITC phalloidin MFI (n = 3, significance level are indicated). (B) Same platelet populations were stimulated with 5 μg/mL fibrillar collagen for 30 and 60 seconds lysed and subjected to Rac-1 GTP pulldown experiments. Total Rac-1 loading is shown below. (C) Quantification of GTP-bound active Rac-1 pulldown experiments at 60 seconds (bars represent mean values ± SEM; significance level are indicated; $*P < .05$; $**P < .01$; wild-type (WT), n = 4; β1-null (KO), n = 3; hypomorphic (Hpm), n = 4). (D) Platelets from WT, KO, and Hpm mice were stimulated with 5 μg/mL fibrillar collagen for the indicated time points, lysed and subjected to immunoblotting for *p*-Thr432/402 PAK1/2 and *p*-Ser19 myosin light chain (pMLC). Total MLC is shown as loading control.

remodel the platelet actin cytoskeleton and granule secretion in response to fibrous collagen.

Discussion

Previous authors have investigated platelet-collagen interactions by using various knockout mouse mutants, pharmacologic inhibitors, and disease models in arterial thrombosis and hemostasis. Despite conflicting results, the current model suggests that both GPVI and integrin α2β1 play significant roles as adhesion receptors; however, whether α2β1 plays an additional crucial role in platelet intracellular signaling controlling platelet aggregation and thrombus formation has not been elaborated. To address the molecular role of β1 integrins for these processes, we generated mice expressing either very low levels of functional (wild-type) β1 integrin or an activation-deficient β1 integrin, which harbors a mutation in the binding site for the essential integrin activating protein kindlin. Our studies reveal critical and distinct roles for β1 integrins in thrombosis and hemostasis dependent on their expression levels: (1) high β1 integrin levels critically contribute to platelet adhesion at sites of vascular injury; (2) β1 integrins assemble signaling platforms required to initiate full-fledged platelet activation and platelet granule secretion in response to fibrillar collagen; and (3) the level of β1 integrins can decrease to as little as 3% for sufficient activation of Rac-1 and its downstream effector molecules to finally promote F-actin formation and initiate platelet granule secretion.

Despite robust Rac-1 activation, hypomorphic platelets fail to spread on plates coated with high concentrations of soluble collagen I, suggesting that a certain number of β1 integrins (>3%) are required for platelet adhesion during spreading. Furthermore, the efficient release of dense granule cargo such as ATP or serotonin and α-granule cargo proteins such as fibrinogen is controlled by β1 integrin outside-in signaling and cannot be compensated by GPVI in the absence of β1 integrins. More potent, although rather nonphysiologic, stimuli such as CVX may mask the contribution of β1 integrin signaling and thereby underestimate its role during thrombotic processes. However, our experimental conditions might not account for complex in vivo situations, in which additional platelet-collagen interactions through vWF and β3 integrin as well as mechanical forces or soluble stimuli might contribute to platelet activation in the presence of plasma proteins such as fibrinogen.

In addition, our data on platelets expressing an activation-deficient β1 integrin are in line with the proposed model that α2β1 integrins directly participate in collagen signaling in an

activation-dependent manner.[10] Inside-out activation by α2β1 integrin is probably triggered by signals generated by GPVI. These signals can be overcome by external integrin activation by manganese, which rescues the defects in platelet adhesion, spreading, and aggregation of $\beta1^{TTAA}$ platelets. Thus, upon GPVI-mediated α2β1 activation, collagen-bound α2β1 integrin generates GPVI independent outside-in signals that are sufficient to trigger the release of secondary agonists to fully activate platelets.

Our findings also revealed that β1 integrins on platelets require an intact kindlin binding motif for their activation. This important finding further corroborates previous studies by showing that a direct interaction between kindlin-3 and the β1 integrin cytoplasmic domain is required for platelet β1 integrin activation in vivo.[21] However, we also observed that the direct interaction of kindlin-3 with the β1 tail is not required for integrin outside-in signaling and for achieving platelet spreading, FAK phosphorylation, and platelet aggregation. A similar observation has been reported recently for β2 integrins, which form a trimeric complex together with kindlin-3 and Rack-1 in T cells, and that kindlin-3 binding to β2 integrin tails can even occur to a kindlin binding-deficient β2 integrin tail.[30] Thus, kindlins need to directly bind the integrin tails for inducing inside-out signaling but a direct contact is either not required or does not occur for triggering outside-in signals. In such a scenario the dissociation of kindlin-3 from the integrin tail after activation has occurred will enable binding of other cytoplasmic proteins to the integrin tail.

Because high levels of β1 integrins are required for primary platelet adhesion to exposed matrix at sites of vascular disease but very low levels are already sufficient to trigger platelet signals required for normal hemostasis, the use of novel therapeutic agents targeting β1 integrins might be a worthwhile approach to reduce arterial thrombosis without increasing the risk for bleeding.

Acknowledgments

The authors thank Reinhard Fässler for continuous support, discussions, and help in writing the paper. They also thank Roy Zent and Ambra Pozzi for critically reading the manuscript.

This work was supported by the Deutsche Forschungsgemeinschaft (SFB 914 TP A01 and B02) and the Max Planck Society.

Authorship

Contribution: T.P. designed and performed most part of the study, analyzed data, and assisted in writing the paper; R.R. performed research and analyzed data; D.P. performed research and analyzed data; V.B. performed research and analyzed data; H.M. contributed vital reagents; M.L. performed research and analyzed data; L.Z. performed research and analyzed data; W.S. designed research and contributed to the discussion; S.M. designed research, analyzed data, and wrote the paper; and M.M. designed and performed research, analyzed data, and wrote the paper

Conflict-of-interest disclosure: The authors declare no competing financial interests.

Correspondence: Markus Moser, Max-Planck-Institute of Biochemistry, Am Klopferspitz 18, D-82152 Martinsried, Germany; e-mail: moser@biochem.mpg.de.

References

1. Moser M, Nieswandt B, Ussar S, Pozgajova M, Fässler R. Kindlin-3 is essential for integrin activation and platelet aggregation. *Nat Med.* 2008;14(3):325-330.
2. Moser M, Legate KR, Zent R, Fässler R. The tail of integrins, talin, and kindlins. *Science.* 2009; 324(5929):895-899.
3. Nieswandt B, Brakebusch C, Bergmeier W, et al. Glycoprotein VI but not alpha2beta1 integrin is essential for platelet interaction with collagen. *EMBO J.* 2001;20(9):2120-2130.
4. Holtkötter O, Nieswandt B, Smyth N, et al. Integrin alpha 2-deficient mice develop normally, are fertile, but display partially defective platelet interaction with collagen. *J Biol Chem.* 2002; 277(13):10789-10794.
5. Herr AB, Farndale RW. Structural insights into the interactions between platelet receptors and fibrillar collagen. *J Biol Chem.* 2009;284(30): 19781-19785.
6. Nissinen L, Pentikäinen OT, Jouppila A, et al. A small-molecule inhibitor of integrin alpha2 beta1 introduces a new strategy for antithrombotic therapy. *Thromb Haemost.* 2010;103(2): 387-397.
7. Miller MW, Basra S, Kulp DW, et al. Small-molecule inhibitors of integrin alpha2beta1 that prevent pathological thrombus formation via an allosteric mechanism. *Proc Natl Acad Sci USA.* 2009;106(3):719-724.
8. He L, Pappan LK, Grenache DG, et al. The contributions of the alpha 2 beta 1 integrin to vascular thrombosis in vivo. *Blood.* 2003;102(10): 3652-3657.
9. Grüner S, Prostredna M, Schulte V, et al. Multiple integrin-ligand interactions synergize in shear-resistant platelet adhesion at sites of arterial injury in vivo. *Blood.* 2003;102(12): 4021-4027.
10. Sarratt KL, Chen H, Zutter MM, Santoro SA, Hammer DA, Kahn ML. GPVI and alpha2beta1 play independent critical roles during platelet adhesion and aggregate formation to collagen under flow. *Blood.* 2005;106(4): 1268-1277.
11. Guidetti GF, Bernardi B, Consonni A, et al. Integrin alpha2beta1 induces phosphorylation-dependent and phosphorylation-independent activation of phospholipase Cgamma2 in platelets: role of Src kinase and Rac GTPase. *J Thromb Haemost.* 2009;7(7):1200-1206.
12. Bernardi B, Guidetti GF, Campus F, et al. The small GTPase Rap1b regulates the cross talk between platelet integrin alpha2beta1 and integrin alphaIIbbeta3. *Blood.* 2006;107(7): 2728-2735.
13. Kehrel B, Balleisen L, Kokott R, et al. Deficiency of intact thrombospondin and membrane glycoprotein Ia in platelets with defective collagen-induced aggregation and spontaneous loss of disorder. *Blood.* 1988;71(4): 1074-1078.
14. Nieuwenhuis HK, Akkerman JW, Houdijk WP, Sixma JJ. Human blood platelets showing no response to collagen fail to express surface glycoprotein Ia. *Nature.* 1985;318(6045):470-472.
15. Pugh N, Simpson AM, Smethurst PA, de Groot PG, Raynal N, Farndale RW. Synergism between platelet collagen receptors defined using receptor-specific collagen-mimetic peptide substrata in flowing blood. *Blood.* 2010;115(24):5069-5079.
16. Ussar S, Wang HV, Linder S, Fässler R, Moser M. The kindlins: subcellular localization and expression during murine development. *Exp Cell Res.* 2006;312(16):3142-3151.
17. Piwko-Czuchra A, Koegel H, Meyer H, et al. Beta1 integrin-mediated adhesion signalling is essential for epidermal progenitor cell expansion. *PLoS ONE.* 2009;4(5):e5488.
18. Kühn R, Schwenk F, Aguet M, Rajewsky K. Inducible gene targeting in mice. *Science.* 1995; 269(5229):1427-1429.
19. Potocnik AJ, Brakebusch C, Fässler R. Fetal and adult hematopoietic stem cells require beta1 integrin function for colonizing fetal liver, spleen, and bone marrow. *Immunity.* 2000;12(6):653-663.
20. Massberg S, Gawaz M, Grüner S, et al. A crucial role of glycoprotein VI for platelet recruitment to the injured arterial wall in vivo. *J Exp Med.* 2003; 197(1):41-49.
21. Böttcher RT, Stremmel C, Meves A, et al. Sorting nexin 17 prevents lysosomal degradation of β1 integrins by binding to the β1-integrin tail. *Nat Cell Biol.* 2012;14(6):584-592.
22. Moroi M, Jung SM. Platelet glycoprotein VI: its structure and function. *Thromb Res.* 2004;114(4): 221-233.
23. Inoue O, Suzuki-Inoue K, Dean WL, Frampton J, Watson SP. Integrin alpha2beta1 mediates outside-in regulation of platelet spreading on collagen through activation of Src kinases and PLCgamma2. *J Cell Biol.* 2003;160(5):769-780.
24. Nieswandt B, Watson SP. Platelet-collagen interaction: is GPVI the central receptor? *Blood.* 2003;102(2):449-461.
25. Woronowicz K, Dilks JR, Rozenvayn N, et al. The platelet actin cytoskeleton associates with SNAREs and participates in alpha-granule secretion. *Biochemistry.* 2010;49(21):4533-4542.

26. Flaumenhaft R, Dilks JR, Rozenvayn N, Monahan-Earley RA, Feng D, Dvorak AM. The actin cytoskeleton differentially regulates platelet alpha-granule and dense-granule secretion. *Blood.* 2005;105(10):3879-3887.
27. Pandey D, Goyal P, Dwivedi S, Siess W. Unraveling a novel Rac1-mediated signaling pathway that regulates cofilin dephosphorylation and secretion in thrombin-stimulated platelets. *Blood.* 2009;114(2):415-424.
28. McCarty OJ, Larson MK, Auger JM, et al. Rac1 is essential for platelet lamellipodia formation and aggregate stability under flow. *J Biol Chem.* 2005;280(47):39474-39484.
29. Suzuki-Inoue K, Yatomi Y, Asazuma N, et al. Rac, a small guanosine triphosphate-binding protein, and p21-activated kinase are activated during platelet spreading on collagen-coated surfaces: roles of integrin alpha(2)beta(1). *Blood.* 2001;98(13):3708-3716.
30. Feng C, Li YF, Yau YH, et al. Kindlin-3 mediates integrin αLβ2 outside-in signaling, and it interacts with scaffold protein receptor for activated-C kinase 1 (RACK1). *J Biol Chem.* 2012;287(14):10714-10726.

12.8 Paper 8:

Kindlin-1 controls cutaneous epithelial stem cell proliferation by modulating Wnt ligand and TGFβ availability.

Kindlin-1 controls cutaneous epithelial stem cell proliferation by modulating Wnt ligand and TGFβ availability

Emanuel Rognoni[1], Moritz Widmaier[1], Madis Jakobson[1], Raphael Ruppert[1], Siegfried Ussar[1], Despoina Katsougkri[1], Ralph T. Böttcher[1], Joey E. Lai-Cheong[2,4], Daniel B. Rifkin[3], John A. McGrath[4], Reinhard Fässler[1]

[1]Department of Molecular Medicine, Max Planck Institute of Biochemistry, Martinsried, Germany; [2]Department of Dermatology, King Edward VII Hospital, Windsor, UK; [3]New York University Langone, School of Medicine, New York, USA; [4]St. John's Institute of Dermatology, King's College London (Guy's Campus), London, UK.

ABSTRACT

Kindlin-1 is an integrin tail binding protein that controls integrin activation. Mutations in the Kindlin-1 gene lead to Kindler Syndrome in man, which is characterized by skin blistering, premature skin ageing and skin cancer of unknown etiology. Here we show that loss of Kindlin-1 in mouse keratinocytes recapitulates Kindler Syndrome, and in addition produces enlarged and hyperactive stem cell compartments, which lead to hyperthickened epidermis, ectopic hair follicle development and increased skin tumor susceptibility. Mechanistically, Kindlin-1 controls keratinocyte adhesion through β_1-class integrins and proliferation and differentiation of cutaneous epithelial stem cells by promoting $\alpha_v\beta_6$ integrin-mediated TGFβ activation and by inhibiting Wnt-β-catenin signaling through an integrin-independent regulation of Wnt ligand expression. Our findings assign Kindlin-1 the novel and essential task to control cutaneous epithelial stem cell homeostasis by balancing TGFβ mediated growth inhibitory and Wnt-β-catenin mediated growth-promoting signals.

INTRODUCTION

Kindler Syndrome (KS) is an autosomal-recessive disease caused by loss of function mutations in the *FERMT-1* gene, which encodes Kindlin-1. The skin is the principal affected organ of individuals with KS and displays trauma-induced blisters, photosensitivity, pigmentation defects, and increased risk for malignancies[1,2].

The Kindlins belong to a family of evolutionary conserved proteins, which are primarily found at cell-matrix adhesion sites where they bind β integrin tails and increase integrin affinity for ligand (also called integrin activation)[3–5]. In addition, they are also present at cell-cell adhesion sites, in the cytoplasm and in the nucleus where their functions are unknown[6,7]. Epidermal and hair follicle (HF) keratinocytes express Kindlin-1 and Kindlin-2. However, despite the striking sequence similarity, Kindlin-1 and -2 cannot compensate for each other indicating that they have specialized functions[3,8].

Epidermal keratinocytes express several integrins, most notably members of the β_1 integrin subfamily[9]. Keratinocytes of the HF bulge express high levels of β_1 integrins and $\alpha_v\beta_6$ integrin[10]. The HF bulge harbors dormant stem cells (SCs) that periodically become activated to sustain the hair cycle (HC)[11,12]. The alternation of bulge SC activation and dormancy is regulated by a tight interplay of antagonistic signaling pathways. SC dormancy is achieved by BMP and TGFβ signaling, while SC activation is elicited by shutting down BMP and TGFβ signaling and activating canonical Wnt-β-catenin signaling. Perturbations of these cell growth regulating signaling pathways or of integrin signaling can profoundly alter SC homeostasis and tumor incidence[13–16]. It has been shown for example, that increased integrin expression or activity is associated with an increased risk for squamous cell carcinoma[16–18]. Conversely, loss of β_1 integrin expression in skin (M. Sibilia, manuscript in preparation) or other tissues such as mammary gland markedly reduces tumor

susceptibility[19]. Moreover, it has recently been shown that Kindlin-2 can stabilize β-catenin and induce Wnt signaling in certain tumor cell lines[20]. It is therefore enigmatic why KS patients suffer from an increased tumor risk[2,21,22] despite Kindlin-1 loss and compromised integrin functions in their keratinocytes[3,23,24]. This discrepancy suggests that Kindlin-1 harbors potent tumor suppressor function(s) in keratinocytes that operate independently of the abundant and oncogenic β_1 integrins. In this paper we identified oncogenic signaling pathways that are tightly controlled by Kindlin-1.

RESULTS

Kindlin-1 loss in epidermis and HFs leads to KS-like defects

To circumvent the lethal ulcerative colitis of a constitutive[3] *Fermt-1* gene ablation, we efficiently deleted the *Fermt-1* gene in keratinocytes by breeding floxed Kindlin-1 mice with Keratin-5 (K5)-Cre transgenics[25] (Kind1-K5; **Fig. 1a–c** and **Supplementary Fig. 1a–c**). Kindlin-1 loss persisted and did not affect Kindlin-2 expression (**Supplementary Fig. 1b**). Heterozygous Kind1-K5 or homozygous floxed Kindlin-1 mice used as control strains (Control) had no apparent phenotype. Homozygous Kind1-K5 mice were born within the expected Mendelian ratio, were fertile and gained weight normally (**Supplementary Fig. 1d**).

The first histologic phenotype emerged around P21 in Kind1-K5 back skin with basement membrane (BM) splitting, small blisters at the dermal-epidermal junction and aberrant accumulation of F-actin and cell-cell adhesion proteins at the basal side of basal keratinocytes (**Fig. 1d**,**e** and **Supplementary Fig. 1e**). The same defects were also observed in mice expressing Kindlin-binding deficient β_1 integrins in keratinocytes (**Fig. 1a**) due to threonine-788/789 to alanine substitutions in the β_1 cytoplasmic domain (TTAA-K5)[26] indicating that they are caused by malfunctioning β_1 integrins (**Fig. 1f**). The blisters and BM defects triggered a regenerative response with granulocyte, monocyte and T cell infiltrates in the dermis of the back skin of Kind-K5 as well as TTAA-K5 mice (**Supplementary Fig. 1f–h**).

At postnatal age 60 (P60) Kind1-K5 mice showed progressive melanin deposits, first in the tail and then in the entire back skin (**Fig. 1g,h** and **Supplementary Fig. 1i**) resembling poikiloderma in KS. At around 3 months Kind1-K5 mice developed an irregular hair coat with small patches of densely clustered hair (**Fig. 1b**) that increased in size with age and appeared as meanders on the shaved back skin (**Fig. 1c**). At 6–8 months of age Kind1-K5 mice began to

lose hair and patches with dense hair and alopecia alternated (**Supplementary Fig. 1j**). TTAA-K5 mice developed neither pigmentation defects nor densely packed hairs (**Fig. 1b**,**c**,**e**). Kind1-K5 mice also developed areas of atrophy next to areas of hyperkeratosis in the tail and back skin, while TTAA-K5 mice displayed hyperkeratotic areas only (**Fig. 1e** and **Supplementary Fig. 2a**). While the number of Ki67-positive cells was higher in the Kind1-K5 and TTAA-K5 epidermis, especially in hyperkeratotic areas (**Supplementary Fig. 2b–d**), keratinocyte differentiation and apoptosis was unaffected in both mouse strains (**Supplementary Fig. 2e–i**).

These results show that Kindlin-1 deletion in mouse epidermis recapitulates human KS and additionally induces an aberrant hair coat, which does not develop in TTAA-K5 mice indicating that the aberrant hair coat is caused by a Kindlin-1 specific and β_1 integrin- and inflammation-independent mechanisms.

Kindlin-1 loss disturbs HC and induces ectopic HFs

Back skin histology of 6 months old Kind1-K5 mice revealed two different HF abnormalities; (i) areas with isolated and densely packed HFs (**Fig. 1g**) separated by 1–15 interfollicullar epithelium (IFE) cells compared to 37 ±10 IFE cells between control HFs, and (ii) HFs with multiple hair shafts and bulges that clustered together and contained hair strands exiting the skin through a single hair canal (**Fig. 1h**).

A detailed HC analysis revealed that HF morphogenesis and the first HC proceeded normally in Kind1-K5 mouse skin (**Supplementary Fig. 3a**). At P50, HFs from control and Kind1-K5 mice entered telogen (resting phase of the HC). While HFs from control mice remained in a long telogen until P80 before a new HC was initiated (**Supplementary Fig. 3a**), Kind1-K5 HFs immediately re-entered anagen (growth phase of the HC) (**Fig. 2a–c**) visible by the formation

of a hair germ (HG) and the expression of the transcription factor CCAAT displacement protein (CDP)[27]. We never observed premature anagen induction in TTAA-K5 mice (**Supplementary Fig. 3b**).

Whole mount staining of P80 tail epidermis showed control mouse HFs with prominent sebaceous glands (SGs), normal sized keratin-15 (Krt-15)-positive bulges and small HGs with few CDP+ cells (**Fig. 2d**). The tail skin of Kind1-K5 mice contained small ectopic HFs originating from pre-existing HFs and the IFE (**Fig. 2d**,**e**). Ectopic HF- and IFE-derived Kind1-K5 HFs were also present in the back skin and expressed the dermal papilla marker alkaline phosphatase (**Supplementary Fig. 3c**,**d**). Of note, while HF numbers increased after P50 in the murine Kind1-K5 back skin their number began declining at older age (**Supplementary Fig. 3i**).

These findings show that Kindlin-1 deficiency leads to a premature onset of anagen, the formation of ectopic HFs in the IFE and from pre-existing HFs and a decline in HF numbers at old age.

Kindlin-1 regulates cutaneous epithelial SC homeostasis

The ectopic HFs in Kind1-K5 mice pointed to a perturbed SC homeostasis. The epidermis contains different SC populations that reside in different niches[11]. While bulge SCs express CD34, Krt-15, nephronectin (Npnt)[28] and high levels of α_6 integrin (**Fig. 3a**), reliable murine IFE SC markers are still missing[11,39]. Immunostaining revealed higher numbers of CD34+ bulge cells in back skin (**Supplementary Fig. 3e**) and enlarged Krt-15+ bulges in tail whole mounts of P80 old Kind1-K5 mice compared to controls (**Fig. 3b** and **Supplementary Fig. 3f**). Krt-15+ cells were also present in the Kind1-K5 infundibulum and IFE (arrowheads in **Fig. 3b**), but never in control mice. Npnt expression expanded into the SG, the infundibulum and the

outer root sheath (**Fig. 3b**,**c**) and *Npnt* mRNA levels were higher in FACS-sorted bulge (Bu) and interfundibulum-junctional zone (IJ) cells of Kind1-K5 mice compared to controls (**Supplementary Fig. 3h**). Also the Lrig1-positive SC population of the IJ zone[30] extended towards the infundibulum and lower hair shaft of back and tail skin HFs of Kind1-K5 mice (**Fig. 3d** and **Supplementary Fig. 3g**).

Despite normal HCs and hair counts until P50 (**Supplementary Figs. 3a**,**i**), FACS quantifications of keratinocytes from P40 mouse skin revealed significantly more SCs in bulge, upper isthmus (UI) and IJ of Kind1-K5 mice compared to controls (**Fig. 3e**,**f**). A time course analysis showed that the SC compartments were already elevated at P21, peaked at P50–80 and then began declining to become significantly smaller in 12 months old Kind1-K5 mice (**Fig. 3g**). In line with a normal hair coat development SC subpopulations were unaffected in TTAA-K5 mice, at least until one year of age (**Supplementary Fig. 3j**).

To test if elevated proliferation caused the enlarged bulges, we performed 5-bromo-2'-deoxyuridine (BrdU) label-retaining cell (LRC) assays. After 10 days of chase significantly more bulge cells were $BrdU^+$ in tail whole mounts of Kind1-K5 mice compared to controls, while after 32, 70 days and 5.5 months significantly fewer bulge cells were $BrdU^+$ in Kind1-K5 mice (**Fig. 3h**,**i**).

These findings demonstrate that Kindlin-1 deficiency elevates cutaneous epithelial SC proliferation, numbers and compartments in a β_1 integrin-independent manner.

Kindlin-1 triggers $\alpha_v\beta_6$ integrin-mediated TGFβ release in skin

To determine whether Kindlin-1 loss alters integrin surface levels we analyzed integrin profiles on primary keratinocytes using FACS. Levels of β_1 and β_4 integrins were slightly lower and levels of β_5, β_8 slightly higher in Kind1-K5 cells compared to controls. β_3 integrin was not

detectable in either genotype. β_6 integrin levels were significantly elevated in Kindlin-1 deficient keratinocytes (**Fig. 4a**), as was the β_6 mRNA in FACS-sorted cutaneous SCs (**Supplementary Fig. 4a**). Immunostaining showed β_6 integrin expression extending from the bulge and outer root sheath to the infundibulum and IFE of Kind1-K5 mice (**Fig. 4b**).

Next, we investigated β_6 integrin dependent cell spreading and focal adhesion formation. While keratinocytes from Kind1-K5 mice spread normally on fibronectin (FN), they displayed severely impaired adhesion, spreading, clustering of paxillin in focal adhesion-like structures and assembly of F-actin stress fibers when plated on surfaces coated with anti-$\alpha_v\beta_6$ antibodies or α_v-specific peptidomimetic cyclic RGD (cRGD) (**Fig. 4c**,**d** and **Supplementary Fig. 4b**,**c**) indicating that $\alpha_v\beta_6$ on Kind1-K5 keratinocytes is non-functional. We confirmed $\alpha_v\beta_6$ specificity of these defects by treating keratinocytes from control mice with the β_6 blocking antibody 10D5, which phenocopied the spreading defects of Kindlin-1 deficient cells on cRGD surfaces (**Supplementary Fig. 4d**).

Active $\alpha_v\beta_6$ integrins can release TGFβ from the latency associated protein (LAP)[31], which in turn suppresses proliferation of bulge SCs[10,12,32,33]. We tested the $\alpha_v\beta_6$-dependent TGFβ release by seeding keratinocytes together with transformed mink lung epithelial cells (tMLEC) able to report TGFβ-induced luciferase on a latent TGFβ binding protein-1-LAP-TGFβ-1 rich matrix[34] (**Fig. 4e**). Keratinocytes from control mice efficiently induced the luciferase reporter, which could be inhibited with the $\alpha_v\beta_6$ blocking antibody 10D5 or the TGFβ neutralizing antibody 1D11. In sharp contrast, keratinocytes from Kind1-K5 mice were unable to release TGFβ confirming that their $\alpha_v\beta_6$ integrins are non-functional (**Fig. 4e**). In line with this *in vitro* result, TGFβ signaling was also severely impaired in bulge cells of Kind1-K5 mice *in vivo*, in which pSmad2/3 was detectable neither before nor after premature anagen induction (**Fig. 4f** and **Supplementary Fig. 4g**). Signaling by BMP via pSmad1/5/8,

which also suppresses bulge cell proliferation[35,36], was unaffected (**Supplementary Fig. 4h**). Treatment of Kindlin-1 deficient keratinocytes with soluble TGFβ-1 induced robust Smad2 phosphorylation and reduced cell proliferation (**Supplementary Fig. 4e**,**f**) indicating that TGFβ-1 signals are efficiently transduced. The severe dysfunction of $\alpha_v\beta_6$ integrins was not compensated by Kindlin-2 due to the inability of Kindlin-2 to bind β_6 tails (**Fig. 4g**). Most importantly, subjects with KS showed a similar TGFβ defect as Kind1-K5 mice with elevated expression of β_6 integrin and reduced nuclear pSmad2/3 in large areas of basal epidermal keratinocytes (**Fig. 4h**,**i**), while pSmad1/5/8 was unaffected (**Supplementary Fig. 4i**).

These findings indicate that Kindlin-1 is essential for β_6 integrin-mediated cell adhesion, cell spreading and TGFβ release required for SC quiescence.

Kindlin-1 curbs Wnt-β-catenin signaling in skin

Premature anagen induction, ectopic HF development and expansion of SC compartments also develop in mice with elevated Wnt-β-catenin signaling in keratinocytes[37–40], while reduced HF spacing and aberrant hair orientation occur in mice overexpressing the β-catenin cofactor Lef1[41] or mice with increased Notch signaling[42]. In skin of control mice β-catenin levels were high at cell-cell junctions, low in the nucleus and absent at the basal side of basal keratinocytes. In contrast, in epidermis of Kind1-K5 mice β-catenin also accumulated at basal sides of basal keratinocytes (**Fig. 5a**, arrowheads top left panel), in the nucleus of a large number of IFE cells (**Fig. 5a**, middle panel) and catagen HFs (**Fig. 5a**, lower left panel and **Supplementary Fig. 5d**, left). Furthermore, Kind1-K5 mice showed β-catenin in nuclei of developing HGs during premature anagen induction (**Supplementary Fig. 5a** upper panel, **5b**), and an extended Lef1 expression from the normal site in HGs to the bulge and IFE at all stages analyzed (**Fig. 5a** right panel and **Supplementary Figs. 5a**,**c**,**d** left panel). Notably, at

P50 shortly before bulges from Kind1-K5 mice induced premature anagen they showed high nuclear Lef1 levels indicating a premature onset of Wnt signaling. In control mice Lef1 was absent in telogen bulges and became highly expressed in nuclei of HG cells and weakly in the cytoplasm of IFE cells (**Fig. 5a** right panel and **Supplementary Fig. 5a** lower panel). Numbers of nuclear Notch effector Notch intracellular domain (NICD)-containing cells and NICD-induced *Hes1* mRNA were unaltered in HG and pericortex, but higher in the IFE of Kind1-K5 mice compared to controls at all time points analyzed (**Fig. 5b** and **Supplementary Fig. 5e**–**g**). Next we determined Wnt-β-catenin signaling by intercrossing Kind1-K5 and control mice with TOPgal reporter mice, which express β-galactosidase under a TCF-Lef controlled minimal cfos promotor[43]. In HFs from control mice TOPgal activities were high in the pericortex during anagen, low during catagen and lost in telogen with some residual activity in club hairs. In Kind1-K5 mice, the high TOPgal activity in the pericortex and bulb of anagen HFs persisted throughout catagen, decreased in telogen (**Fig. 5c** left panel and **Supplementary Fig. 5i**) and was strongly re-induced in the following anagen stage (**Supplementary Fig. 5h**). Furthermore, we observed a patch-like distribution of TOPgal in the IFE of Kind1-K5 mice, which was absent in controls (**Fig. 5c** right panel). Importantly, the IFE of humans with KS showed similar abnormalities in β-catenin-LEF1 expression with weak nuclear β-catenin in the basal cell layer and a patch-like distribution of nuclear LEF1, whereas normal human skin contained β-catenin exclusively in cell-cell contacts and LEF1 in the cytoplasm (**Fig. 5d** and **Supplementary Fig. 5j**).

These findings demonstrate that loss of Kindlin-1 induces nuclear translocation of β-catenin-Lef1 in KS and mouse skin leading to elevated Wnt-β-catenin signaling and premature anagen onset of Kind1-K5 mouse HFs.

Kindlin-1 regulates Wnt ligand expression

To find an explanation for the increased Wnt-β-catenin signaling in the absence of Kindlin-1 we compared the skin transcriptome between healthy individuals and subjects with KS using microarray. As expected, *FERMT-1* was absent in skin from subjects with KS and mRNAs encoding inflammatory proteins were high (**Fig. 5e**, for complete list see **Supplementary Table 2**). Unexpectedly, several Wnt signaling components, most notably *WNT5A* were high in individuals with KS (**Fig. 5e**). Immunostaining confirmed the aberrant expression of WNT5A in basal keratinocytes of individuals with KS (**Fig. 5f**). qPCR and *in situ* hybridization of tail whole mounts from Kind1-K5 mice corroborated high *Wnt5a* mRNAs levels in HBs, ectopic HFs and patches of IFE, which overlapped with high TOPgal activities (**Fig. 5g** and **Supplementary Fig. 6a–c**). qPCR of all known Wnt ligands and receptors revealed that several canonical (*Wnt1*, *2b*, *3a*, *9b*) and non-canonical Wnts (*Wnt6* and *2*) were also significantly higher in keratinocytes from Kind1-K5 mice compared to controls, while *Wnt4*, *7a*, *9a*, *10a* and *16* were significantly lower (**Fig. 5g** and **Supplementary Table 3**). Expression of several Frizzled (Fzd) receptors was higher, most notably *Fzd4* and *Fzd5*, and to a lesser extent the Fzd co-receptor *Lrp6*. qPCR of FACS sorted bulge cells and *in situ* hybridization of tail whole mounts from Kind1-K5 mice confirmed the high *Fzd4* mRNA levels and patch-like expression in their IFE (**Supplementary Fig. 6d**,**e**).

Transfection of Kindlin-1 deficient keratinocytes with SuperTOPFlash reporter revealed that the elevated Wnt signaling was cell autonomous (**Fig. 5h**,**i**) and that Lef1 was limiting the extent of Wnt signaling (**Supplementary Fig. 6f**). Overexpression of Wnt4, which triggers translocation of β-catenin to cell-cell junctions, thereby preventing nuclear accumulation of β-catenin and Wnt-β-catenin signaling[44], decreased SuperTOPFlash activity in Kindlin-1 deficient keratinocytes compared to GFP-transfected controls (**Fig. 5h**). Overexpression of

Wnt5a, which together with Lrp5 and Fzd4 efficiently activates the canonical Wnt-β-catenin signaling pathway[45], further increased the SuperTOPFlash reporter in Kindlin-1 deficient cells but not in control cells where Fzd4 expression was low (**Fig. 5h** and **Supplementary Fig. 6d,e**).

Re-expression of similar quantities of Kindlin-1-GFP or an integrin binding-deficient Kindlin-1-QW611/612AA-GFP, but not Kindlin-2 attenuated the increased SuperTOPFlash activities and levels of Wnt4 and Wnt5a in Kindlin-1 deficient keratinocytes (**Fig. 5i** and **Supplementary Fig. 6g–j**) indicating that inhibition of Wnt-β-catenin signaling is Kindlin-1 specific and does not require integrin binding. To exclude a role for nuclear Kindlin-1, we expressed Kindlin-1-GFP fused to two SV40 nuclear localization signals (NLS) in Kind1-null cells. Although most of the protein localized to the nucleus the elevated SuperTOPFlash activity was only partially rescued (**Fig. 5i**), likely due to Kind1-NLS-GFP spillovers into the cytoplasm (**Supplementary Fig. 6j**).

To corroborate that elevated Wnt protein secretion and high Wnt-β-catenin signaling underlies premature HF anagen induction in Kind1-K5 mice, we treated them at P49, shortly before telogen onset (**Fig. 5j** and **Supplementary Fig. 7a**) with IWP-2, which blocks Wnt protein secretion by inhibiting porcupine-mediated palmitylation of Wnts[46], or with IWR-1, which inhibits tankyrases thereby stabilizing the β-catenin destruction complex[46,47]. Both compounds efficiently blocked premature anagen induction in Kind1-K5 mice and decreased SuperTOPFlash activities *in vitro* (**Fig. 5j** and **Supplementary Fig. 7a**,**b**). In line with previous reports[42], inhibition of Wnt signaling also reduced aberrant Notch activities in Kind1-K5 keratinocytes *in vitro* and *in vivo*, which in turn normalized *Wnt4* levels[48] (**Supplementary Fig. 7c–g**).

Together these findings demonstrate that Kindlin-1 inhibits Wnt-β-catenin signaling by regulating transcription of Wnt ligands and receptors in a cell autonomous and integrin-independent manner.

Loss of Kindlin-1 increases skin tumor susceptibility

The low TGFβ and augmented Wnt signaling in humans with KS and Kind1-K5 mice represent oncogenic threats[49,50]. To test this hypothesis, we used the two-stage carcinogenesis protocol and treated mice with 7,12-dimethylbenz[a]anthracene (DMBA) and 12-O-tetradecanoylphorbol-13-acetate (TPA) for 25 weeks. Kind1-K5 mice developed tumors earlier and had more tumors than control mice (**Fig. 6a–c**). Of note, the tumor size was similar between Kind1-K5 and control mice (**Fig. 6d**), which could be due to different skin lesion subtypes. Indeed, histology of the tumor lesions revealed that hyperkeratotic and exophytic papillomas dominated in control mice, while HF-derived trichofolliculoma-like lesions, sebaceous papillomas, mixed papillomas and basal cell carcinoma (BCC)-like lesions dominated in Kind1-K5 mice (**Fig. 6e** and **Supplementary Fig. 8a**). In line with uncurbed Wnt signaling, we observed more cells with nuclear β-catenin and Lef1 in tumors from Kind1-K5 mice (**Supplementary Fig. 8b–d**).

A single DMBA treatment induced more and slightly larger tumors in Kind1-K5 mice compared to controls (**Fig. 6f–i**) indicating that the hyperproliferative state of keratinocytes in Kind1-K5 mice was sufficient to promote tumor development. Furthermore, their tumors primarily originated from HFs and SGs containing hyperactive SCs.

DISCUSSION

Loss-of-function mutations in the *FERMT-1* gene cause KS, which is characterized by skin blistering at birth, premature skin aging, pigmentation defects and increased incidence of skin cancer. The ability of Kindlin-1 to activate integrins and link them to the F-actin cytoskeleton explains the development of skin blisters and BM splitting followed by an inflammatory response. However, the notion that skin tumor development is promoted by hyperactive integrins and inhibited by compromised integrins indicates that Kindlin-1 loss activates oncogenic and/or inhibits tumor suppressor functions. The task of this study was to identify such pathway(s).

Deletion of Kindlin-1 in skin epithelial cells with the K5-Cre driver line leads to small skin blistering, BM defects, chronic skin inflammation, progressive pigmentation defects and skin atrophy and hence is alike KS. Unexpectedly, the Kind1-K5 mice also develop enlarged cutaneous epithelial SC compartments, hyperactive bulge SCs, distorted HF cycles and ectopic HF (**Supplementary Fig. 8e**). In line with the high SC proliferation, DMBA-TPA as well as DMBA only treatment induces a significantly higher tumor incidence and tumor burden in Kind1-K5 mice. Moreover, the majority of the tumors are BCC- and trichofolliculoma-like lesions suggesting that the tumors predominantly originate from HF bulge SCs.

In search for a mechanistic explanation for the dysregulated SC and tumor cell proliferation in Kind1-K5 mice, we identified two Kindlin-1 regulated signaling pathways with opposing functions on bulge SC quiescence (**Fig. 6j**). Kindlin-1 binding to the cytoplasmic tail of β_6 integrin[51] triggers $\alpha_v\beta_6$ integrin binding to the RGD motif of LAP thereby liberating TGFβ and inducing TGFβ receptor signaling and cutaneous epithelial SC quiescence. These findings are

supported by report showing that loss of β6 integrin impairs TGFβ signaling and elevates bulge SC activity *in vivo*[32].

Despite the sequence similarities of Kindlin-1 and -2[52] and their expression in control and Kind1-K5 keratinocytes, Kindlin-2 can only partially compensate for Kindlin-1 at β_1 integrin adhesion sites. Furthermore, Kindlin-2 is unable to bind β_6 tails, which prevents it to release TGFβ-1 and to suppress SC proliferation. Interestingly, other TGFβ isoforms such as TGFβ-2 activate HF stem cells by antagonizing BMP in the bulge[53]. In contrast to LAP1 however, LAP2 lacks the $\alpha v\beta_6$-binding RGD motif[54] and hence the release of TGFβ-2 and BMP signaling are not affected by Kindlin-1 loss.

It is particularly interesting that high Kindlin-1 levels have also been associated with high TGFβ-1 signaling in metastatic breast cancers[55]. Although it was not investigated how Kindlin-1 regulates TFGβ-1 signaling, this together with our findings suggest that different tumor stages may benefit from different Kindlin-1 levels; in early stage tumors low TGFβ signaling supports tumor growth, while in late stage tumors high TGFβ signaling promotes epithelial to mesenchymal transition and metastatic progression[56]. If so, subjects with KS suffering from an increased tumor risk may be protected from metastasis.

We also found elevated Wnt-β-catenin signaling in Kind1-K5 mice and KS epidermis, which is inevitably associated with a high tumor risk and severe SC and HC defects[13,50]. The defect leads to ectopic HF formation and aberrant HCs, and is due to aberrant expression of several Wnt ligands, most notably Wnt5a, which probably act in an autocrine manner. Importantly, chemical compounds that inhibit Wnt protein secretion or Wnt-β-catenin signaling the HC and Wnt signaling defects in keratinocytes from Kind1-K5 mice.

Wnt5a is best known for the ability to activate the non-canonical Wnt signaling pathway. However, Wnt5a can also elicit canonical Wnt-β-catenin signaling. The decision which

signaling pathway is induced, is dictated by the type of cell surface receptor to which Wnt5a is binding; Wnt5a binding to the Ror2 receptor tyrosine kinase inhibits the transcriptional activity of β-catenin and thus canonical signaling, whereas Wnt5a binding to Fzd4 and the Lrp5/6 co-receptors leads to β-catenin stabilization and canonical Wnt signaling[45]. Interestingly, Wnt-β-catenin signaling can activate Notch[42], which is also elevated in keratinocytes from Kind1-K5 mice and may, at least in part contribute to the Kind-K5 mouse phenotype, e.g. by suppressing *Wnt4* expression[48] and the recruitment of β-catenin to cell-cell junctions[44]. Clearly, the dysregulated expression of Wnt proteins and their receptors in Kind1-K5 mice strongly suggests that Kindlin-1 safeguards the skin and HFs against an overshooting activation of the important and at the same time potentially harmful canonical Wnt-β-catenin signals.

In summary our results show that Kindlin-1 loss results in a combination of defects caused by the dysregulation of distinct pathways; the compromised β_1 integrins impair adhesion and induce an inflammatory response; the impaired TGFβ liberation from LAP leads to HF SC hyperproliferation; and the increased Wnt signaling abrogates the resting phase of the HC, expands the SC compartments and together with the impaired TGFβ signaling and inflammation contributes to the increased tumor risk. The high epithelial SC activity eventually leads to SC exhaustion and skin atrophy later in life, which is another hallmark of KS. It is also conceivable that the ability of Kindlin-1 to shuttle between integrin sites where it mediates adhesion, migration and TGFβ release, and the cytoplasm where it curbs Wnt-β-catenin signaling may also contribute to physiologic SC homeostasis and hair development (**Fig. 6j**); mobilization of bulge SC have little or no integrin-ligand engagement and therefore, use Kindlin-1 to prevent Wnt-β-catenin signaling and their activation. Once they move to the

HG they engage integrins to ensure downward growth and therefore, have less Kindlin-1 in the cytoplasm to inhibit Wnt-β-catenin signaling.

METHODS

Mouse Strains

The conditional Kind1$^{fl/fl}$ mice carry a loxP-flanked ATG-containing exon 2 (**Supplementary Fig. 1a**) and were generated via electroporation of R1 embryonic stem (ES) cells using standard procedures[57]. Homologous recombination was verified with southern blots and positive ES clones were used to generate chimeric mice. Mice were crossed with transgenics carrying a deletor-flp recombinase to remove the neomycin cassette and with mice carrying deleter-Cre (to confirm the null phenotype) or K5-Cre transgenes, respectively[58]. For all animal studies transgenic mice were backcrossed eight times to C57BL/6. The TTAA-K5 transgenic mice were obtained through an intercross of mice carrying alanine substitutions of TT788/789 in the cytoplasmic domain of β_1 integrin[26] with β_1 floxed mice and K5-Cre transgenics. The TOPgal Wnt reporter mice[43] were intercrossed with Kind1-K5 mice. Mice were housed in a special pathogen free mouse facility and all animal experiments were carried out according to the rules of and approved by the government of Upper Bavaria.

DMBA/TPA tumor experiment

Cutaneous two stage chemical carcinogenesis was performed as previously described[59] using topical applications of 100 nmol (25 µg) DMBA (Sigma) in 100 µl of acetone and twice weekly applications of 10 nmol (6.1 µg) TPA (Sigma) in 200 µl of acetone or only acetone for 25 weeks. The tumor model was terminated after 25 weeks of TPA promotion due to critical skin health condition of Kind1-K5 mice. For tumor experiment control animals were treated with acetone or TPA only. For all animal studies seven week old mice were randomized after genotyping and sample size was estimated by non-parametric Wilcoxon Test (U-Test). Number and size of tumors were recorded once per week after the start of promotion (week

0). All mice were sacrificed at the end of the experiment. Skin lesions were analyzed by histology and graded as described previously[59–61].

Subjects with KS

Individuals with KS gave their informed written consent under protocols approved by St Thomas' Hospital Ethics Committee (COREC number 06 /Q0702 /154) and the study was conducted according to the Declaration of Helsinki Principles. For IF analysis biopsies were taken from age and site matched controls (NHS) and subjects with KS with following mutations: KS patient 1 (3-year-old Indian girl; homozygous nonsense mutation +/+ p.Glu516X) and KS patient 2 (22 year old Panamanian woman; homozygous nonsense mutation +/+ p.Arg271X).

RNA for microarray analysis was isolated from upper arm biopsies taken from three KS subjects; KS patient A, 22 year old Omani woman, homozygous nonsense mutation +/+ p.Arg271X; KS patient B, 7 year old Indian girl, homozygous nonsense mutation +/+ p.Try616X and KS patient C, 19 year old Omani woman, nonsense mutation +/+ p.Try616X. Control skin RNA was isolated from four age-, site - and sex-matched biopsies.

Gene expression micro array

Total RNA was extracted using the RNeasy Fibrous Tissue Mini kit (Qiagen) and quantity and quality were measured on a Nanodrop spectrophotometer (Nanodrop, Wilmington, DE, U.S.A.). For whole-genome Illumina expression analysis, total RNA from each skin biopsy was hybridized to an Illumina Human-Ref-6 v2 BeadChip expression array (Illumina, San Diego, CA, U.S.A.). The Illumina HumanRef-6 v2 BeadChips were scanned with an Illumina Bead Array Reader confocal scanner.

The microarray data analysis was performed using Illumina's BeadStudio Data Analysis Software (Illumina). The expression signal for all genes from each individual were grouped in KS and NHS and averaged. In order to identify statistically significant differentially regulated genes, a prefiltering set was determined for significantly higher (≥ 2-fold change) and lower expression (≤ 0.5-fold change) intensity between KS and NHS skin samples. Bonferroni's correction was applied to each *P*-value to obtain an adjusted *P*-value to identify differentially expressed mRNAs with high statistical significance (see **Supplementary Table 2**). The microarray has been submitted to NCBI under the GEO accession number GSE47642.

FACS analysis

FACS analysis and sorting was performed as previously described[62]. A suspension of primary keratinocyte in FACS-PBS (PBS with 1% BSA) were incubated for 1 h with primary antibodies on ice and then washed twice with FACS-PBS. Cell viability was assessed by 7-aminoactinomycin (7-AAD) labeling (BD Biosciences) or ethidium monoazide (EMA) staining (Invitrogen). FACS analysis was carried out using a FACSCantoTMII Cytometer (BD Biosciences) and cell sorting with an AriaFACSII high-speed sorter (BD Biosciences), both equipped with FACS DiVa software (BD Biosciences). Purity of sorted cells was determined by post sort FACS analysis and typically exceeded 95%. Integrin surface FACS analysis of primary keratinocytes was carried out as previously described[63]. Data analysis was conducted using the FlowJo program (Version 9.4.10).

Real Time PCR and Notch target gene inhibition

Total RNA from total skin or FACS sorted keratinocytes was extracted with RNeasy Mini extraction kit (Qiagen) following manufacturer's instructions. For Notch target gene inhibition analysis cells were plated on FN/collagen I coated 6-well plates (1.2×10^6 cells per

well) and the next day treated with 2.5 µM N-[N-(3,5-Difluorophenacetyl)-L-alanyl]-S-phenylglycine t-butyl ester (DAPT; Selleckchem; CatNo: S2215) in full keratinocyte growth medium (KGM) for 24 h before total RNA isolation. cDNA was prepared with a iScript cDNA Synthesis Kit (Biorad). Real Time PCR was performed with an iCycler (Biorad). Each sample was measured in triplicates and values were normalized to *Gapdh*. PCR primers are listed in **Supplementary Table 4**.

Antibodies and inhibitors

The following antibodies or molecular probes were used at indicated concentration for Western blot (W), immunofluorescence (IF), immunohistochemistry (IHC) or flow cytometry (FACS): Kindlin-1[3] (W: 1:5000, IF of tissue: 1:1000), Kindlin-2 (Sigma; CatNo: K3269; W: 1:1000), Talin (Sigma; clone 8D4; W: 1:1000), GAPDH (Calbiochem; clone 6C5; W: 1:10000), Phalloidin-Alexa488 (Invitrogen; CatNo: A12379; IF tissue: 1:500; IF of cells: 1:800), integrin α_M (Mac-1) (eBioscience; clone M1/70; IF of tissue: 1:200), GR1 (Ly6g) (eBioscience; clone RB6-8C5; IF of tissue: 1:200), CD4 (PharMing; clone H129.19; IF of tissue: 1:200), CD19 (PharMing; clone 1D3; IF of tissue: 1:200), integrin α_x (CD11c) (BD Bioscience; clone HL3; IF of tissue: 1:200), Desmoplakin (Fritzgerald Industries International; CatNo: 20R-DP002; IF tissue 1:500), α_6 integrin (Itga6) (PharMingen; clone GoH3; IF of tissue: 1:200, FACS: 1:500), Laminin-332 (a gift from Monique Aumailley, University of Cologne, Germany; IF of tissue: 1:500), Keratin10 (Krt-10) (Covance; CatNo: PRB-159P; IHC: 1:600), Keratin 15 (Krt-15) (a gift from Rudolf Grosschedl; MPI Immunobiology, Freiburg, Germany), IF: 1:500), Lef1 (a gift from Rudolf Grosschedl, MPI Immunobiology, Freiburg, Germany; IF of tissue: 1:500), Loricrin (Lor) (Covance; CatNo: PRB-145P; IF: 1:500), Ki67 (Dianova; CatNo: M7249; IHC: 1:100), cleaved caspase-3 (Asp175, cCaspase3) (Cell Signaling; CatNo: 9661; IF of tissue:

1:200), CD34 (BD Bioscience; clone RAM34; IF of tissue: 1:200, FACS: 1:100), Sca1 (BioLegend; clone D7; IF of tissue 1:200, FACS: 1:200), Lrig1 (R&D Systems, CatNo: AF3688; IF: 1:500), BrdU (Abcam; CatNo: ab6326; IF: 1:500), Keratin5 (Krt-5) (Covance; CatNo: PRB-160P; IF: 1:1000), Keratin6 (Krt-6) (Covance; CatNo: PRB-169; IF: 1:500), CDP (Santa Cruz; CatNo: sc-13024; IF: 1:500), β_1 integrin (BD Biosciences; clone Ha2/5; FACS: 1:200); β_3 integrin (BD Bioscience; clone 2C3.G2; FACS: 1:200), β_4 integrin (BD Biosciences; clone 346-11A; FACS: 1:200), β_6 integrin CH2A1 (Itgb6) (a gift from Shelia Violette, Biogen Idec; IF of mouse tissue: 1:500); β_6 integrin (Itgb6) (Chemicon; clone 10D5; IF of human tissue: 1:200, FACS: 1:200, IF of cells: 1:500), β_5 integrin (Itgb5) (a gift from Dean Sheppard, University of California, USA ; FACS: 1:200), β_8 integrin (Itgb8) (Santa Cruz; CatNo: sc-25714; FACS 1:200), paxillin (BD Bioscience; CatNo: 610051; IF: 500); pSMAD2/3 (Santa Cruz, CatNo: sc11769; IF: 1:200), pSmad2 (Millipore; W: 1:2000); total Smad2/3 (Santa Cruz; catNo: sc-8332; W: 1:1000), pSMAD1/5/8 (Millipore; CatNo: AB3848; IF of tissue: 1:200), Sox9 (a gift from Michael Wegner, University of Erlangen, Germany; IF of tissue: 1:500), Trichohyalin (AE15) (Abcam; CatNo: ab58755; IF of tissue: 1:500), activated Notch1 (NICD) (Abcam, CatNo: ab8925; IF of tissue: 1:200), and Pan Laminin (Sigma; CatNo: L9393; IF of tissue: 1:500). The following secondary antibodies were used: goat anti–rabbit Alexa488 (CatNo: A11008), goat anti–human Alexa488 (CatNo: A11013), goat anti–mouse Alexa488 (CatNo: A11029), donkey anti–goat Alexa488 (CatNo: A11055), goat anti-guinea pig Alexa 594 (CatNo: A11076), goat anti-mouse Alexa546 (CatNo: A11003), goat anti–rabbit Alexa546 (CatNo: A11010) (all from Invitrogen, FACS: 1:500, IF: 1:500), streptavidin-Cy5 (Dianova; CatNo: 016170084; FACS: 1:400), goat anti–rat HRP (Dianova; CatNo: 712035150; W: 1:10000), goat anti–mouse HRP (CatNo: 172-1011) and goat anti–rabbit HRP (CatNo: 172-1019) (all from Biorad; W: 1:10000). For mouse monoclonal primary antibodies M.O.M kit (Vector Labs) was

used according to the manufacturer's protocol. Mast cells were stained for mast cell heparin with avidin-FITC (Invitrogen; CatNo: 43-4411; IF of tissue: 1:100) as previously described[64]. Nuclei were stained with 4',6-diamidino-2-phenylindole (DAPI; Sigma).

Notch signaling inhibitor DAPT (Selleckchem; CatNo: S2215) was dissolved in ethanol at 25 $\mu g\ \mu l^{-1}$. Wnt inhibitor IWP-2 (Calbiochem; CatNo: 681671) and IWR-1 (Sigma; CatNo: I0161) were dissolved in DMSO at 2.5 $\mu g\ \mu l^{-1}$ (IWP-2) or 10 $\mu g\ \mu l^{-1}$ (IWR-1).

BrdU labeling

LRC assay was performed as previously described[27]. Briefly, 10 d old mice were injected 4 times with 50 mg kg^{-1} bodyweight BrdU every 12 h to label mitotic cells and then mice were maintained for indicated chase periods. To determine LRCs per HF bulge, tail epidermal whole mounts were prepared, z projections were acquired using a Leica SP5 confocal microscope (objective 20×) and BrdU-positive cells were counted from ≥30 HFs per animal from different whole mounts.

Cell culture

TGFβ reporter cell line tMLEC and LTBP1-TGFβ matrix producing CHO-LTBP cells were used as described previously[34]. Primary keratinocytes were isolated at P21 or at indicated time points as described previously[65]. To generate clonal keratinocyte cell lines, primary cells from Kindlin-$1^{fl/fl}$ mice were spontaneously immortalized, single clones were picked and Kindlin-1 ablation was induced by transient transfection with an adenovirus expressing Cre recombinase. Keratinocytes were cultured in KGM containing 8% chelated FCS (Invitrogen) and 45 µM Ca^{2+} in a 5% CO_2 humidified atmosphere on plastic dishes coated with a mixture of 30 $\mu g\ ml^{-1}$ collagen I (Advanced BioMatrix) and 10 $\mu g\ ml^{-1}$ FN (Invitrogen).

Inhibition of premature anagen induction and increased Notch signaling

At telogen onset (P49) back skin of control and Kind1-K5 mice was shaved and 100 µl of 200 µM IWR-1 or IWP-2 (diluted in PBS) was subcutaneously injected every 24 h into a marked skin region. 100 µl DMSO diluted in PBS was used for control experiments. At P56 the treated back skin was isolated, sectioned and stained with H/E. Ten serially sectioned HFs per animal were counted. To analyze Notch signaling back skin section were stained for NICD and NICD-positive nuclei were quantified.

Constructs and transfections

Wnt4 expression constructs (gift from Andreas Kispert, University of Hannover, Germany) and the human β-catenin expression construct (gift from Jürgen Behrens, University of Erlangen, Germany). Human WNT5A (ID18032), LEF1 (ID16709), pHes1-luc (ID43806), SuperTOPFlash (ID17165) and FOPFlash (ID12457) reporter plasmids were purchased from Addgene. pEGFP-C1 expression vector was acquired from Clontech.

GFP-tagged Kindlin-1, -2 and Kindlin-1-QWAA expression constructs were described[3] and the Kindlin1-NLS construct was generated by fusing SV40 NLS motifs to the N-terminus of Kindlin-1. The expression cassettes were driven by a CAG promotor and flanked by two ITR sites recognized by sleeping beauty transposase 100× (SB100×)[66] and transiently co-transfected with SB100× vector in a 1:1 ratio using Lipofectamine 2000 (Invitrogen) following the manufacturer's instructions. After two passages cells stably expressing the GFP-fusion protein were FACS sorted for equal expression levels, which was further confirmed by western blotting.

Histology and immunostainings

Small pieces from back skin were either PFA fixed and embedded in paraffin or frozen on dry-ice in cryo-matrix (Thermo) and sectioned. Tail skin whole-mounts were prepared and

immunostained as described[27]. Immunohistochemistry (H/E, DAPI, OilRedO, AP and Xgal) of skin sections and tail whole mounts and immunofluorescence staining of tissue sections were carried out as described[25]. To better visualize the blue β-Gal stain the epidermal whole mount was overlaid with a grayscale image. Immunostaining of human skin sections for β_6 integrin followed published protocols[67].

HF bulge sizes were quantified in epidermal tail whole mounts stained for Krt-15 and z-projections that were collected with a confocal microscope using a 20× objective. Length and diameter of Krt-15 positive bulge area was measured with the ImageJ software (Version 1.41n) and bulge volumes were calculated using the circular cylinder formula ($v=\pi\times r^2\times h$; v, volume; r, radius; h, height). The HF numbers were quantified in serial sections of comparable back skin regions from at least three mice per genotypes and indicated ages. HFs per 10× objective field of H/E stained sections were counted. HFs in anagen and early HF development were staged as described previously[68,69].

Images were collected by confocal microscopy (DMIRE2 or SP5; Leica) with a 10× , 20× NA 1.4 or 40× oil objective using the Leica Confocal Software (version 2.5 Build 1227) or by bright field microscopy (Axioskop; Carl Zeiss with a 10× NA 0.3, 20× NA 0.5 or 40× NA 0.75 objective and camera DC500 with IM50 software (Leica).

***In situ* hybridization**

Antisense riboprobes for mouse *Fzd4* (SpeI-EcoRI fragment of mouse FZD4 3'-UTR), *Wnt5a* (gift from Irma Thesleff, University of Helsinki, Finland) and Hes1 (gift from Ryoichiro. Kageyama, Kyoto University, Japan) were synthesized with T7 RNA polymerase (New England Biolabs) and DIG RNA Labeling Mix according to the manufacturer's instructions (Roche). Isolated tail skin epidermis was fixed in 4% PFA in PBS, washed in PBS for 5 min twice and

then twice for 15 min in PBS with 0.1% active diethylpyrocarbonate followed by 15 min equilibration in 5× saline-sodium citrate (SSC). Samples were first pre-hybridized for 1 h at 58 °C, in 50% formamide, 5× SSC, 40 µg/ml salmon sperm DNA, then hybridized for 16 h at 58 °C with 400 ng ml^{-1} of DIG-labeled probe in pre-hybridization mix, washed twice for 30 min in 2× SSC at RT, followed by 60 min wash at 65 °C in 2× SSC and then 60 min wash at 65 °C in 0.2× SSC. The tissues were washed in TBS for 5 min three times, blocked in 0.5% blocking reagent (Roche) in 0.1% Tween20/TBS (TBST) for 90 min at RT, then incubated in 1:5000 diluted anti-DIG AP (Roche) in 0.5% blocking reagent in TBST at 4 °C overnight. Following three 60 min washes in TBST, tissues were incubated in NTMT (100 mM NaCl, 100 mM Tris pH 9.5 50 mM $MgCl_2$, 0.1% Tween 20) for 10 min at RT. Color was developed using BM Purple AP substrate precipitating reagent (Roche) at 37 °C. The reaction was stopped for 15 min with TE buffer (Tris 10 mM, EDTA 1 mM, pH 8.0) and samples were mounted with 70% glycerol.

Peptide pull-downs

Pull-downs were performed with β_1 wt tail peptide (HDRREFAKFEKEKMNAKWDTGENPIYKSAVTTVVNPKYEGK-OH), β_1 scrambled peptide (EYEFEPDKVDTGAKGTKMAKNEKKFRNYTVHNIWESRKVAP-OH), β_6 wt tail peptide (HDRKEVAKFEAERSKAKWQTGTNPLYRGSTSTFKNVTYKHREKHKAGLSSDG-OH) and β_6 scrambled peptide (KTDHAVQGDKKLSHKKNRGTSKATFPKVRHYETEEWAALESGYGSRTFKNSR-OH). All peptides were desthiobiotinylated. Prior to use, peptides were immobilized on 35 µl Dynabeads MyOne Streptavidine C1 (10 mg ml^{-1}, Invitrogen) for 3 h at 4 °C.

Keratinocytes were lysed on ice in Mammalian Protein Extraction Reagent (Thermo Scientific) and 1 mg of cell lysate was incubated with the indicated peptides for 4 h at 4 °C.

After three washes with lysis buffer the beads were boiled in SDS-PAGE sample buffer and the supernatant loaded on 8% SDS-PAGE gels.

Preparation of $\alpha_v\beta_6$ antibody-coated cover slips

Antibody coating was carried out as described[70]. Briefly, glass slides (24×24; Menzel) were sterilized, coated with collagen I (Advanced BioMatrix) for 1 h at 37 °C, air dried, covered with nitrocellulose dissolved in methanol and air dried again. Slides were incubated with $\alpha_v\beta_6$ antibody (10D5; 10 µg ml^{-1}; Chemicon) diluted in PBS over night at 4 °C in a humidity chamber, washed once with PBS and blocked with 1% BSA for 1 h at RT.

Generation of dense gold nanoarrays functionalized with cyclic-RGD

In a typical synthesis, 7 mg ml^{-1} of polystyrene(154)-block-poly(2-vinylpyridine)(33) (PS_{154}-*b*-$P2VP_{33}$, Polymer Source) was dissolved at RT in p-xylene (Sigma) and stirred for 2 d. Hydrogen tetrachloroaurate (III) trihydrate ($HAuCl_4 \cdot 3H_2O$; Sigma) was added to the block co-polymer solution (1 $HAuCl_4$ per 2 P2VP units) and stirred for 2 d in a sealed glass vessel. Glass cover slips (Carl Roth) were cleaned in a piranha solution for at least 2 h and extensively rinsed with MilliQ water and dried under a stream of nitrogen. Micellar monolayers were prepared by dip-coating a glass cover slip into previously prepared solutions with a constant velocity equal to 24 mm min^{-1}. The dip-coated glass slides were exposed to oxygen plasma (150 W, 0.15 mbar, 45 min, PVA TEPLA 100 Plasma System). To prevent nonspecific protein adsorption or cell binding, the glass background was covalently modified with silane-terminated polyethylene glycol (PEG; molecular weight 2000)[71]. Thiol-terminated cyclic-RGD was synthesized as described before[72]. The gold nanoparticles were then functionalized with this ligand by incubating the PEG-functionalized substrates in 100 µl of a 50 µM aqueous

solution. The substrates were then thoroughly rinsed and incubated overnight with water and finally dried with nitrogen.

Spreading assay

A single cell suspension with 1.0 ×10^5 cells per well in a 6-well plate was plated in serum free KGM (1% BSA; 1% Penicillin-Streptomycin) on FN-coated glass cover slips (10 µg ml^{-1} FN in PBS for 1 h at RT) or indicated substrates for 3 h at 37 °C. Cells were imaged by bright field Axiovert 40 CFL microscope (20× objective; Carl Zeiss) and CV640 camera (Prosilica) before fixation in 4% PFA-PBS and immunostaining with indicated antibodies. Spreading area was quantified after staining with phalloidin Alexa488 (Invitrogen) with an AxioImager Z1 microscope (20× objective, Carl Zeiss) using the ImageJ software (Version 1.41n).

TGFβ stimulation assays

Keratinocytes were starved for several hours and stimulated with 5 ng/ml recombinant human TGFβ-1 (PEROTech) in serum free KGM for indicated time points, lysed and analyzed by western blotting. TGFβ modulated proliferation was determined in 70% confluent keratinocytes cultured in 6-well plates, incubated for 8 h with 10 µM 5-ethynyl-2´-deoxyuridine (EdU; Invitrogen) and indicated concentrations of TGFβ-1 and analyzed with Click-iT EdU Alexa Fluor488 Flow Cytometry Assay Kit (Invitrogen).

TGFβ release assay

TGFβ release was determined as described[34]. Briefly, CHO LTBP1 cell were seeded (5.0 × 10^4 cells per well) for 48 h in a 96 well plate in triplicates to deposit an LTBP1-TGFβ rich matrix. Cells were then detached with PBS/15 mM EDTA, the remaining LTBP1-TGFβ rich matrix washed twice with PBS and incubated with keratinocytes (2.0 × 10^4 cells per well) and tMLEC cells (1.5 × 10^4 cells per well) in a 100 µl final volume either in the absence or presence of

$\alpha_v\beta_6$ integrin blocking antibody (10D5; 20 μg ml^{-1}; Chemicon) or TGFβ neutralizing antibody (1D11; 15 μg ml^{-1}; BD Biosciences). The amount of released TGFβ was measured after 16–24 h using Bright Glo luciferase Kit (Promega).

Wnt and Notch reporter assay

Cells were plated on FN and collagen I coated 12-well plates (6.0×10^5 cells per well) before transient transfection with 0.5 μg of pHes1-luc, SuperTOPFLASH or SuperFOPFLASH reporter, indicated expression plasmid and 50 ng thymidine kinase-driven renilla (Promega) for controlling transfection efficiency. The total amount of transfected plasmid DNA was kept constant at 1.5 μg per well by using pEGFP-C1 expression vector as transfection control (Clontech). After 24 h (Wnt reporter) or 48 h (Notch reporter) luciferase activity was analyzed with a Dual Luciferase reporter assay system (Promega). To determine effect of Wnt or Notch signaling cells were treated with indicated inhibitor 18 h after transfection and luciferase activity was measured 24 h later.

Statistical Analysis

Analyses were performed with GraphPad Prism software (version 5.00, GraphPad Software). Experiments were routinely repeated at least 3 times and repeat number was increased according to effect size or sample variation. If not mentioned otherwise in the figure legend, statistical significance (*P < 0.05; **P < 0.01; ***P < 0.001; ns, not significant) was determined by the unpaired t-test (for biological effects with assumed normal distribution) or Mann-Whitney U-test. In boxplot panels the middle line represents the median, the box ends the 25^{th} and 75^{th} percentile and the whisker ends show Min/Max distribution or are at 1.5 interquartile range while outliers are shown as dots, as indicated in the figure legend. Unbiased and reproducible identification of cells with positive nuclear staining for β-catenin,

Lef1 and NICD was ensured by quantification of nuclear staining intensities with ImageJ tool (version1.41n).

References method section

57. Fässler, R. & Meyer, M. Consequences of lack of beta 1 integrin gene expression in mice. *Genes Dev.* **9(15)**, 1896-1908 (1995).

58. Ramirez, A. *et al*. A keratin K5Cre transgenic line appropriate for tissue-specific or generalized Cre-mediated recombination. *Genesis.* **39(1)**, 52-57 (2004).

59. Abel, E.L., Angel, J.M., Kiguchi, K. & DiGiovanni, J. Multi-stage chemical carcinogenesis in mouse skin: fundamentals and applications. *Nat Protoc.* **4**, 1350-1362 (2009).

60. Kasper, M. *et al.* Wounding enhances epidermal tumorigenesis by recruiting hair follicle keratinocytes. *Proc Natl Acad Sci U S A.* **108**, 4099-4104 (2011).

61. Sundberg, J.P., Sundberg, B.A. & Beamer, W.G. Comparison of chemical carcinogen skin tumor induction efficacy in inbred, mutant, and hybrid strains of mice: morphologic variations of induced tumors and absence of a papillomavirus cocarcinogen. *Mol Carcinog.* **20**, 19-32 (1997).

62. Jensen, K.B., Driskell, R.R. & Watt, F.M. Assaying proliferation and differentiation capacity of stem cells using disaggregated adult mouse epidermis. *Nat Protoc.* **5**, 898-911 (2010).

63. Lorenz, K., *et al.* Integrin-linked kinase is required for epidermal and hair follicle morphogenesis. *J Cell Biol.* **177(3)**, 501-513 (2007).

64. Kunder, C. A. *et al.* Mast cell-derived particles deliver peripheral signals to remote lymph nodes. *Exp Med*. **206(11)**, 2455-2467 (2009).

65. Montanez, E. *et al*. Analysis of integrin functions in peri-implantation embryos, hematopoietic system, and skin. *Methods Enzymol*. **426**, 239-289 (2007).

66. Mátés, L. *et al.* Molecular evolution of a novel hyperactive Sleeping Beauty transposase enables robust stable gene transfer in vertebrates. *Nat Genet.* **41(6)**, 753-761 (2009).

67. Brown, J.K. *et al.* Integrin-alphavbeta6, a putative receptor for foot-and-mouth disease virus, is constitutively expressed in ruminant airways. *J Histochem Cytochem.* **54(7)**, 807-816 (2006).

68. Müller-Röver, S. *et al.* A comprehensive guide for the accurate classification of murine hair follicles in distinct hair cycle stages. *J Invest Dermatol.* **117(1)**, 3-15 (2001).

69. Paus, R. *et al.* A comprehensive guide for the recognition and classification of distinct stages of hair follicle morphogenesis. *J Invest Dermatol.* **113(4)**, 523-532 (1999).

70. Shi, Q. & Boettiger, D. A novel mode for integrin-mediated signaling: tethering is required for phosphorylation of FAK Y397. *Mol Biol Cell.* **14(10)**, 4306-4315 (2003).

71. Blümmel, J. *et al.* Protein repellent properties of covalently attached PEG coatings on nanostructured SiO(2)-based interfaces. *Biomaterials*. **28(32)**, 4739-4747 (2007).

72. Morales-Avila, E. *et al*. Multimeric system of 99mTc-labeled gold nanoparticles conjugated to c[RGDfK(C)] for molecular imaging of tumor α(v)β(3) expression. *Bioconjug Chem*. **22(5)**, 913-922. (2011).

Acknowledgments

We thank Dr. Julien Polleux for generating gold nanoarrays, Simone Bach for expert technical assistance, Dr. Charles Mein (Barts and the London Genome Centre) for generating the human microarray data and Drs. Roy Zent and Ralf Paus for carefully reading the manuscript. This work was funded by NIH (CA034282) to D.B.R., the Wellcome Trust (PhD studentship to J.E.L-C) and the UK National Institute for Health Research (NIHR) Biomedical Research Centre based at Guy's and St Thomas' NHS Foundation Trust and King's College London to J.A.M, the Advanced ERC Grant (ERC Grant Agreement no. 322652) and the Max Planck Society to R.F.

.

Author contributions

R.F. initiated the project, R.F. and E.R. designed the experiments and wrote the paper; E.R., D.K., M.W., M.J., R.R., S.U., R.T.B. and J.E.L-C. performed experiments; E.R., M.W., M.J. and R.F. analysed data; D.B.R. and J.A.M. provided important reagents and/or analytical tools; all authors read and approved the manuscript.

References

1. Meves, A., Stremmel, C., Gottschalk, K. & Fässler, R. The Kindlin protein family: new members to the club of focal adhesion proteins. *Trends Cell Biol*. **19(10)**, 504-513 (2009).

2. Lai-Cheong, J.E. *et al.* Kindler syndrome: a focal adhesion genodermatosis. *Br J Dermatol.* **160(2)**, 233-242 (2009).

3. Ussar, S., *et al.* Loss of Kindlin-1 causes skin atrophy and lethal neonatal intestinal epithelial dysfunction. *PLoS Genet.* **4(12)**; e1000289 (2008).

4. Montanez, E., *et al.* Kindlin-2 controls bidirectional signaling of integrins. *Genes Dev.* **22(10)**, 1325-1330 (2008).

5. Moser, M., Nieswandt, B., Ussar, S., Pozgajova, M. & Fässler, R. Kindlin-3 is essential for integrin activation and platelet aggregation. *Nat Med.* **14(3)**, 325-330 (2008).

6. Dowling, J.J., Vreede, A.P., Kim, S., Golden, J. & Feldman, E.L. Kindlin-2 is required for myocyte elongation and is essential for myogenesis. *BMC Cell Biol*. **9**, 36 (2008).

7. Lai-Cheong, J.E., Ussar, S., Arita, K., Hart, I.R. & McGrath, J.A. Colocalization of kindlin-1, kindlin-2, and migfilin at keratinocyte focal adhesion and relevance to the pathophysiology of Kindler syndrome. *J Invest Dermatol.* **128**, 2156–2165 (2008).

8. He, Y., Esser, P., Heinemann, A., Bruckner-Tuderman, L. & Has, C. Kindlin-1 and -2 have overlapping functions in epithelial cells implications for phenotype modification. *Am J Pathol*. **178(3)**, 975-982 (2011).

9. Watt, F.M. Role of integrins in regulating epidermal adhesion, growth and differentiation. *EMBO J*. **21**, 3919-3926 (2002).

10. Tumbar, T. *et al.* Defining the epithelial stem cell niche in skin. *Science*. **303(5656)**, 359-363 (2004).

11. Watt, F.M. & Jensen, K.B. Epidermal stem cell diversity and quiescence. *EMBO Mol. Med*. **1**, 260–267 (2009).

12. Woo, W.M. & Oro, A.E. SnapShot: hair follicle stem cells. *Cell*. **146**, 334-334 (2011).

13. Arwert, E.N., Hoste, E. & Watt, F.M. Epithelial stem cells, wound healing and cancer. *Nat Rev Cancer*. **12**, 170-180 (2012).

14. Alonso, L. & Fuchs, E. Stem cells in the skin: waste not, Wnt not. *Genes Dev.* **17**, 1189-1200 (2003).

15. Watt, F.M. & Fujiwara, H. Cell-extracellular matrix interactions in normal and diseased skin. *Cold Spring Harb Perspect Biol*. **1**; 3(4) (2011).

16. Janes, S.M. & Watt, F.M. New roles for integrins in squamous-cell carcinoma. *Nat Rev Cancer.* **6(3)**, 175-183 (2006).

17. Evans, R.D. *et al.* A tumor-associated beta 1 integrin mutation that abrogates epithelial differentiation control. *J Cell Biol.* **160(4)**, 589-596 (2003).

18. Ferreira, M., Fujiwara, H., Morita, K. & Watt, F.M. An activating beta1 integrin mutation increases the conversion of benign to malignant skin tumors. *Cancer Res.* **69(4)**, 1334-1342 (2009).

19. White, D.E. *et al.* Targeted disruption of beta1-integrin in a transgenic mouse model of human breast cancer reveals an essential role in mammary tumor induction. *Cancer Cell*. **6(2)**, 159-170 (2004).

20. Yu, Y. *et al.* Kindlin 2 forms a transcriptional complex with β-catenin and TCF4 to enhance Wnt signalling. *EMBO Rep*. **13(8)**, 750-758 (2012).

21. Arita, K. *et al.* Unusual molecular findings in Kindler syndrome. *Br J Dermatol.* **157,** 1252-1256 (2007).

22. Emanuel, P.O., Rudikoff, D. & Phelps, R.G. Aggressive squamous cell carcinoma in Kindler syndrome. *Skinmed.* **5**, 305-307 (2006).

23. Lai-Cheong, J.E. *et al.* Loss-of-function FERMT1 mutations in kindler syndrome implicate a role for fermitin family homolog-1 in integrin activation. *Am J Pathol.* **175(4)**, 1431-1441 (2009).

24. Has, C. *et al.* Kindlin-1 Is required for RhoGTPase-mediated lamellipodia formation in keratinocytes. *Am J Pathol*. **175**, 1442-1452 (2009).

25. Brakebusch, C. *et al.* Skin and hair follicle integrity is crucially dependent on beta 1 integrin expression on keratinocytes. *EMBO J*. **19**, 3990-4003 (2000).

26. Böttcher, R.T. *et al.* Sorting nexin 17 prevents lysosomal degradation of β1 integrins by binding to the β1-integrin tail. *Nat Cell Biol*. **14**, 584-592 (2012).

27. Braun, K.M. *et al.* Manipulation of stem cell proliferation and lineage commitment: visualisation of label-retaining cells in wholemounts of mouse epidermis. *Development*. **130**, 5241-5255 (2003).

28. Fujiwara, H. *et al.* The basement membrane of hair follicle stem cells is a muscle cell niche. *Cell.* **144**, 577-589 (2011).

29. Alonso, L. & Fuchs, E. Stem cells of the skin epithelium. *Proc Natl Acad Sci U S A*. **100**, Suppl 1:11830-5. (2003).

30. Jensen, K.B. *et al.* Lrig1 expression defines a distinct multipotent stem cell population in mammalian epidermis. *Cell Stem Cell*. **4**, 427–439 (2009).

31. Munger, J.S. *et al.* The integrin alpha v beta 6 binds and activates latent TGF beta 1: a mechanism for regulating pulmonary inflammation and fibrosis. *Cell.* **96(3)**, 319-328 (1999).

32. Xie, Y., McElwee, K.J., Owen, G.R., Häkkinen, L. & Larjava, H.S. Integrin β6-deficient mice show enhanced keratinocyte proliferation and retarded hair follicle regression after depilation. *J Invest Dermatol*. **132**, 547-555 (2012).

33. Li, L. & Bhatia, R. Stem cell quiescence. *Clin Cancer Res.* **17**, 4936-4941 (2011).

34. Annes, J.P., Chen, Y., Munger, J.S. & Rifkin D.B. Integrin alphaVbeta6-mediated activation of latent TGF-beta requires the latent TGF-beta binding protein-1. *J Cell Biol.* **165(5)**, 723-734 (2004).

35. Kobielak, K., Stokes, N., de la Cruz, J., Polak, L. & Fuchs, E. Loss of a quiescent niche but not follicle stem cells in the absence of bone morphogenetic protein signaling. *Proc Natl Acad Sci U S A*. **104(24)**, 10063-10068 (2007).

36. Zhang, J. *et al.* Bone morphogenetic protein signaling inhibits hair follicle anagen induction by restricting epithelial stem/progenitor cell activation and expansion. *Stem Cells.* **24(12)**, 2826-2839 (2006).

37. Gat, U., DasGupta, R., Degenstein, L. & Fuchs, E. De Novo hair follicle morphogenesis and hair tumors in mice expressing a truncated beta-catenin in skin. *Cell*. **95(5)**, 605-614 (1998).

38. Lo Celso, C., Prowse, D.M. & Watt, F.M. Transient activation of beta-catenin signaling in adult mouse epidermis is sufficient to induce new hair follicles but continuous activation is required to maintain hair follicle tumours. *Development*. **13**, 1787-1799 (2004).

39. Lowry, W.E. *et al.* Defining the impact of beta-catenin/Tcf transactivation on epithelial stem cells. *Genes Dev.* **19**, 1596-1611 (2005).

40. Silva-Vargas, V. *et al.* Beta-catenin and Hedgehog signal strength can specify number and location of hair follicles in adult epidermis without recruitment of bulge stem cells. *Dev Cell*. **9**, 121-131 (2005).

41. Zhou, P., Byrne, C., Jacobs, J. & Fuchs, E. Lymphoid enhancer factor 1 directs hair follicle patterning and epithelial cell fate. *Genes Dev.* **9(6)**, 700-713 (1995).

42. Estrach, S. *et al.* Jagged 1 is a beta-catenin target gene required for ectopic hair follicle formation in adult epidermis. *Development*. **133(22)**, 4427-4438 (2006).

43. DasGupta, R. & Fuchs, E. Multiple roles for activated LEF/TCF transcription complexes during hair follicle development and differentiation. *Development.* **126**, 4557-4568 (1999).

44. Bernard, P., Fleming, A., Lacombe, A., Harley, V.R. & Vilain, E. Wnt4 inhibits beta-catenin/TCF signalling by redirecting beta-catenin to the cell membrane. *Biol Cell.* **100(3)**, 167-177 (2008).

45. Mikels, A.J. & Nusse, R. Purified Wnt5a protein activates or inhibits beta-catenin-TCF signaling depending on receptor context. *PLoS Biol*. **4(4)**, e115 (2006).

46. Chen, B. *et al.* Small molecule-mediated disruption of Wnt-dependent signaling in tissue regeneration and cancer. *Nat Chem Biol*. **5(2)**, 100-107 (2009).

47. Huang, S. M. *et al.* Tankyrase inhibition stabilizes axin and antagonizes Wnt signalling. *Nature*. **461(7264)**, 614-620 (2009).

48. Devgan, V., Mammucari, C., Millar, S.E., Brisken, C. & Dotto, G.P. p21WAF1/Cip1 is a negative transcriptional regulator of Wnt4 expression downstream of Notch1 activation. *Genes Dev.* **19(12)**, 1485-1495 (2005).

49. Guasch, G. *et al.* Loss of TGFbeta signaling destabilizes homeostasis and promotes squamous cell carcinomas in stratified epithelia. *Cancer Cell*. **12(4)**, 313-327 (2007).

50. Beronja, S. *et al.* RNAi screens in mice identify physiological regulators of oncogenic growth. *Nature*. **501(7466)**, 185-190 (2013).

51. Bandyopadhyay, A., Rothschild, G., Kim, S., Calderwood, D.A. & Raghavan, S. Functional differences between kindlin-1 and kindlin-2 in keratinocytes. *J Cell Sci.* **125**, 2172-2184 (2012).

52. Ussar, S., Wang, H.V., Linder, S., Fässler, R. & Moser M. The Kindlins: subcellular localization and expression during murine development. *Exp Cell Res.* **312(16)**, 3142-3151 (2006).

53. Oshimori, N. & Fuchs, E. Paracrine TGF-β signaling counterbalances BMP-mediated repression in hair follicle stem cell activation. *Cell Stem Cell*. **10(1)**, 63-75 (2012).

54. Annes, J.P. *et al.* Making sense of latent TGFbeta activation. *Cell Sci*. **116(Pt 2)**, 217-224 (2003).

55. Sin, S. *et al.* Role of the focal adhesion protein kindlin-1 in breast cancer growth and lung metastasis. J *Natl Cancer Inst.* **103(17)**, 1323-1337 (2011) .

56. Chaudhury, A. & Howe, P.H. The tale of transforming growth factor-beta (TGFbeta) signaling: a soigné enigma. *IUBMB Life*. **61(10)**, 929-939 (2009).

Figure legends

Figure 1 Kindlin-1 controls HF growth. (**a**) Model of Kindlin-1 and β_1 integrin functions in mice; Kind1-K5 mice lack Kindlin-1 in keratinocytes and TTAA-K5 mice express a Kindlin-binding deficient β_1 integrin in which threonines-788/789 are substituted with alanines. (**b**) Appearance of 7 months old control, Kind1-K5 and TTAA-K5 mice. (**c**) View of shaved back skin of 7 months old control, Kind1-K5 and TTAA-K5 mice. (**d**) Immunofluorescence staining of back skin from P21 and 7 months old mice for LN-332 (red) and α_6 integrin (green). Nuclei are stained with DAPI (blue). (**e**) H/E staining of back skin from 6 months old mice. Kind1-K5 and TTAA-K5 skin shows hyperthickened skin, hyperkeratosis and blisters (arrowhead) at the epidermal-dermal junction. (**f**) Integrin activation index on primary Kind1-K5 and TTAA-K5 keratinocytes reported as mean 9EG7 binding normalized to total β_1 integrin level ± SD (*n*=3 technical replicates). (**g**,**h**) H/E stained back skin sections of 7 months old Kind1-K5 mice. Scale bar indicates 5 mm in (**c**), 50 μm in (**d**,**e**,**g**) and 100 μm in (**h**).

Figure 2 Premature anagen induction and ectopic HF development in Kind1-K5 skin. (**a**) H/E stained back skin sections of P56 mice. (**b**) Immunostaining of HFs from P56 mice for CD34 (red) and CDP (green). Nuclei are stained with DAPI (blue). (**c**) The percentage of anagen HFs at indicated time points (mean ± SD, *n*=4 mice per genotype, ≥8 10× objective fields were counted). (**d**) Immunostaining of tail epidermal whole mounts for CDP (green), Krt-15 (red) and DAPI (blue) of P80 mice. Note ectopic HF growth in IFE of Kind1-K5 mice. (**e**) Ectopic HF outgrowth from a preexisting HF of the back skin in a 6 months old Kind1-K5 mouse stained for CDP (green) and DAPI (blue). Scale bar indicates 50 μm in (**a**,**b**) and 100 μm in (**d**,**e**). Bu, bulge; SG, sebaceous gland; HG, hair germ; HF, hair follicle; DP, dermal papilla; IFE, interfollicular epidermis; Ec, ectopic HF.

Figure 3 Kindlin-1 regulates cutaneous epithelial SC homeostasis. (**a**) Distribution and expression of marker genes in SC subpopulations of murine HFs. (**b**–**d**) Back skin immunostaining from 6 months old mice for Krt-15 (red) and Npnt (green) (**b**), (Npnt (green) and α_6 integrin (red) (**c**), and for Lrig1 (green) and α_6 integrin (red) (**d**). Arrowheads indicate Krt-15 positive cells (**b**), Npnt deposition (**c**) and Lrig1 expression (**d**) in Kind1-K5 mice. (**e**) Keratinocytes from P40 old mice were separated by FACS into α_6 integrin-high and -low and further analyzed for CD34 and Sca1 expression. (**f**) Gated populations (1–6) were quantified and represented as mean ± SD (*n*=5 Control and 3 Kind1-K5 mice). Color code in (**e–f**) corresponds to the cell population denoted in (**a**). (**g**) The relative amounts of SC subpopulations over time analyzed by FACS. Data show average fold increase (± SD) relative to control mice (*n* and *P*-values are listed in **Supplementary Table 1**). (**h**) BrdU (green) retaining cells in Krt-15 (red) stained tail whole mounts after indicated chase times. (**i**) Numbers of LRC per HF after indicated chasing periods were quantified as boxplots (10 d *n*=5 Control and 3 Kind1-K5; 32 d *n*=3 Control and 4 Kind1-K5; 80 d *n*=4 Control and 3 Kind1-K5). Boxplot whisker ends show Min/Max distribution and middle line reports the median. Nuclei are stained with DAPI (blue) (**b**–**d**,**h**). Scale bar indicates 50 µm (**b**–**d**) and 100 µm in (**h**). Bu, bulge; SG, sebaceous gland; HF, hair follicle; IFE, interfollicular epidermis; UI, upper isthmus; IJ, interfundibulum junctional zone.

Figure 4 Kindlin-1 promotes $\alpha_v\beta_6$ integrin induced TGFβ release *in vitro* and *in vivo*. (**a**) Representative histogram of integrin levels on freshly isolated keratinocytes analyzed by FACS (n=3 biological replicates). (**b**) Immunofluorescence analysis of back skin from P44 mice for β_6 integrin (cyan), CD34 (green) and Npnt (red). (**c**) Brightfield images of keratinocytes plated on FN-, $\alpha_v\beta_6$- and cRGD-coated surfaces. (**d**) Immunostaining of keratinocytes plated

on $\alpha_v\beta_6$ and cRGD surfaces for paxillin (red) and F-actin or β_6 integrin (green). (**e**) TGFβ release from extracellular matrix by keratinocytes from control or Kind1-K5 mice in the absence or presence of indicated blocking antibodies monitored with the tMLEC reporter cell line. Luciferase activity is reported as mean ± SEM (*n*=3 biological replicates). (**f**) Immunostaining of a HF from 4 months back skin for pSmad2/3 (green) and CD34 (red). (**g**) Streptavidin-bead pull-down assay with biotinylated wild type (WT) integrin tails or scrambled (Scr) peptides from keratinocyte lysates. (**h**,**i**) Immunofluorescence staining of skin sections from control and individuals with KS for β_6 integrin (**h**) and pSmad2/3 (**i**). Nuclei are stained with DAPI (blue) (**b**,**d**,**f**,**h**,**i**). Scale bar indicates 50 μm (**b**,**c**,**h**,**i**) and 25 μm (**d**,**f**). NHS, normal human skin; KS, Kindler syndrome; Bu, bulge; DP, dermal papilla; HF, hair follicle; IFE, interfollicular epidermis.

Figure 5 Kindlin-1 controls Wnt-β-catenin signaling. (**a**) Immunofluorescence staining for β-catenin (green) of HF (P44) (left panel) and IFE (P55) (middle panel) and for Lef1 and CD34 (red) of HF and IFE (4 months) (right panel) from control and Kind1-K5 mice. Arrowheads indicate aberrant β-catenin (left panel) and Lef1 (right panel) localization. (**b**) IFE immunofluorescence staining for NICD (green) from P44 control and Kind1-K5 mice. (**c**) TOPgal reporter activity in tail HFs (left panel) and IFE (right panel) from 3 months old control and Kind1-K5 mice. Arrowheads indicate HF with abnormal TOPgal activity. (**d**) Immunofluorescence staining of human skin from normal and individuals with KS for β-catenin (left panel) and LEF1 (right panel). (**e**) Skin gene expression profile of NHS (*n*=3) versus KS (*n*=3) assessed with microarray and shown as volcano plot. Genes with ≥2 fold change in KS were plotted according to the Log_2 fold change (x-axis) and Log_{10} *P*-value (y-axis). (**f**) Immunofluorescence staining for WNT5A (green) in skin of normal and individuals

with KS. (**g**) Volcano plot of qPCR gene expression profile of keratinocytes from control versus Kind1-K5 mice. Mean expression relative to *Gapdh* of Wnt ligands (circle, red) and receptors (triangle, green) were plotted according to the Log_2 fold change (x-axis) and log_{10} *P*-value (y-axis). (*n*=3 biological replicates, for mean ± SEM values see **Supplementary Table 3**). (**h**) Transient overexpression of GFP, Wnt4 and Wnt5a in floxed (WT) and Adeno-Cre treated Kindlin-1 deficient (KO) keratinocytes expressing the TOPFlash reporter. Values are corrected for the renilla control and represented as mean ± SEM fold increase relative to WT cells (*n*=5 biological replicates). (**i**) TOPFlash reporter activity in cells stably re-expressing Kindlin-1-GFP, integrin-binding deficient Kindlin-1-GFP, NLS-tagged Kindlin-1-GFP and Kindlin-2-GFP, respectively. Values are corrected for the renilla control, represented as fold increase relative to WT cells and reported as mean ± SEM (*n*=21 WT, KO; 13 Kind1-GFP; 9 Kind1-QW-GFP, 5 Kind1-NLS-GFP, Kind2-GFP; all biological replicates). (**j**) H/E staining of control and Kind1-K5 mice one day after treatment with indicated Wnt inhibitor. Nuclei are stained with DAPI (blue) (**a**,**b**,**d**,**f**). All scale bars indicate 50 µm. NHS, normal human skin; KS, Kindler syndrome, Bu, bulge; SG, sebaceous gland; HG, hair germ; HF, hair follicle; DP, dermal papilla.

Figure 6 Loss of Kindlin-1 increases skin tumor incidence. (**a–e**) Two stage carcinogenesis (*n*=26 Control and 23 Kind1-K5 mice). (**a**) Tumor incidence (*P*-value by log-rank test), (**b**) burden and (**c**) skin lesions per animal (reported as mean ± SD) after 25 weeks of treatment. (**d**) Tumor growth reported as diameter is shown in a boxplot where whisker ends are at 1.5 interquartile ranges and middle lines represent the median. (**e**) The percentage of skin lesion subtypes from control (*n*=25 lesions) and Kind1-K5 mice (*n*=47 lesions) were staged by histology and immunofluorescence analysis (see **Supplementary Fig. 8a**). (**f–i**) One stage

carcinogenesis with DMBA. (**f**) Tumor incidence, (**g**) skin lesion number, (**h**) frequency and (**i**) size of control (*n*=10) and Kind1-K5 (*n*=10) mice monitored as in (**a**–**d**). (**j**) Molecular functions of Kindlin-1; in normal cells (left panel) Kindlin-1 activates β_1-class integrins and $\alpha_v\beta_6$ integrin to facilitate adhesion and TGFβ liberation from LAP, respectively. Free TGFβ activates TGFβR leading to nuclear translocation of phosphorylated Smad2/3, which promotes SC quiescence. In Kindlin-1 deficient cells (right panel) activation of β_1-class integrins and $\alpha_v\beta_6$ is impaired leading to adhesion defects and loss of TGFβ-mediated SC quiescence. In addition, dysregulated Wnt ligand expression leading to elevation of Wnt5a leads to canonical Wnt-β-catenin signaling via the Lrp5/6-Fzd4 complex.

12.9 Paper 9:

CD98hc facilitates B cell proliferation and adaptive humoral immunity.

ARTICLES

nature immunology

CD98hc facilitates B cell proliferation and adaptive humoral immunity

Joseph Cantor[1], Cecille D Browne[2], Raphael Ruppert[3], Chloé C Féral[4], Reinhard Fässler[3], Robert C Rickert[2] & Mark H Ginsberg[1]

The proliferation of antigen-specific lymphocytes and resulting clonal expansion are essential for adaptive immunity. We report here that B cell–specific deletion of the heavy chain of CD98 (CD98hc) resulted in lower antibody responses due to total suppression of B cell proliferation and subsequent plasma cell formation. Deletion of CD98hc did not impair early B cell activation but did inhibit later activation of the mitogen-activated protein kinase Erk1/2 and downregulation of the cell cycle inhibitor p27. Reconstitution of CD98hc-deficient B cells with CD98hc mutants showed that the integrin-binding domain of CD98hc was required for B cell proliferation but that the amino acid–transport function of CD98hc was dispensable for this. Thus, CD98hc supports integrin-dependent rapid proliferation of B cells. We propose that the advantage of adaptive immunity favored the appearance of CD98hc in vertebrates.

Adaptive immunity is a vertebrate specialization that requires the selective proliferation of antigen-specific lymphocytes[1,2]. The CD98 heavy chain (CD98hc; also called 4F2hc; A000262), encoded by *Slc3a2*, is a vertebrate membrane protein whose expression is much higher in proliferating lymphocytes[3]. Originally described 25 years ago as a lymphocyte-activation antigen[3], the function of CD98hc in the immune system has remained obscure. CD98 has two distinct functions: facilitating amino acid transport[4,5] and mediating integrin signaling[6,7]. The 80-kilodalton CD98hc is covalently linked to one of several 40-kilodalton light chains, which function as amino acid transporters[4,5]. Transport of leucine and isoleucine is mediated by the CD98 heterodimer[4,5]; these amino acids are important regulators of the mTOR pathway, which governs nutrient-regulated lymphocyte function[8,9]. CD98hc also interacts with certain integrin β-subunits to mediate signaling events that control cell migration, survival and proliferation[7]. CD98hc is first found in primitive vertebrates, coincident with the appearance of adaptive immunity[2,10]. Consequently, we hypothesized that CD98hc could be involved in the rapid lymphocyte proliferation required for effective adaptive immunity.

Here we report that CD98hc facilitates humoral immunity by supporting the rapid proliferation of B cells that is necessary for clonal expansion and subsequent differentiation into plasma cells. We deleted CD98hc in B cells by crossing mice bearing a *lox*P-flanked (floxed) *Slc3a2* allele ($Slc3a2^{f/f}$) with those expressing Cre recombinase in B cells ($CD19\text{-}Cre^{+}$). The resultant $Slc3a2^{f/f}$ $CD19\text{-}Cre^{+}$ had normal maturation and distribution of peripheral B cells and normal morphology of secondary lymphoid organs. $Slc3a2^{f/f}CD19\text{-}Cre^{+}$ mice immunized with T cell–dependent or T cell–independent antigens had much lower antibody responses than did control $Slc3a2^{f/f}$ mice without CD19-Cre, because of complete suppression of B cell proliferation and plasma cell formation by CD98hc-null B cells. A mutant form of CD98hc that mediates integrin signaling but not amino acid transport supported the proliferation of CD98hc-deficient B cells; hence, the region of CD98hc that mediates integrin interaction is required for B cell proliferation and the domain that facilitates the amino acid–transport function is dispensable for this. Furthermore, mitogenic stimulation of a mixture of CD98hc-deficient and CD98hc-sufficient B cells resulted in considerable enrichment for CD98hc-sufficient cells; this finding establishes the ability of CD98hc to confer a strong selective advantage during rapid B cell proliferation. Thus, the ability of CD98hc to enable clonal expansion, which is necessary for adaptive immunity, may have favored the appearance and retention of CD98hc in vertebrates[10].

RESULTS

B cell CD98hc is needed for antibody responses

Because germline loss of CD98hc is embryonically lethal[11], we targeted CD98hc by flanking exons 1 and 2 of *Slc3a2* with *lox*P sites that specified Cre recombinase–mediated deletion of the cytoplasmic and transmembrane region of CD98hc (**Supplementary Fig. 1a** online), thus leading to complete loss of CD98hc expression[12]. We crossed $Slc3a2^{f/f}$ mice with mice bearing Cre recombinase under control of the endogenous B cell–specific *Cd19* locus[13]. The resulting $Slc3a2^{f/f}CD19\text{-}Cre^{+}$ mice had specific deletion of CD98hc in B lymphocytes

[1]Department of Medicine, University of California San Diego, La Jolla, California, USA. [2]Program of Inflammatory Disease Research, Infectious and Inflammatory Disease Center, Burnham Institute for Medical Research, La Jolla, California, USA. [3]Department of Molecular Medicine, Max Planck Institute of Biochemistry, Martinsried, Germany. [4]Institut National de la Santé et de la Recherche Médicale, Nice-Sophia Antipolis University, Nice, France. Correspondence should be addressed to M.H.G. (mhginsberg@ucsd.edu) or R.C.R. (robert@burnham.org).

Received 14 August 2008; accepted 27 January 2009; published online 8 March 2009; doi:10.1038/ni.1712

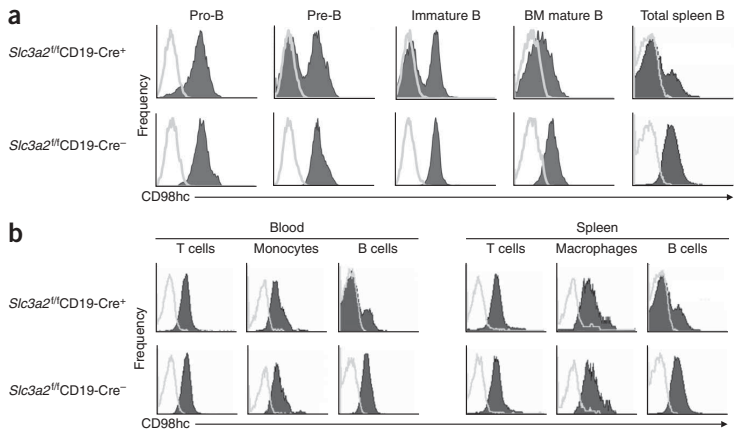

Figure 1 Deletion of CD98hc in *Slc3a2*$^{f/f}$CD19-Cre^{+} mice. (**a**) CD98hc expression (filled histograms) and staining with isotype-matched control antibody (open histograms) in bone marrow cells isolated from adult *Slc3a2*$^{f/f}$CD19-Cre^{+} and control *Slc3a2*$^{f/f}$CD19-Cre^{-} mice and measured at various stages of B cell maturation. BM, bone marrow. Data are from an experiment repeated once. (**b**) Flow cytometry of CD98hc expression (filled histograms) and staining with isotype-matched control antibody (open histograms) on T cells (CD3^{+}), monocytes or macrophages (CD11b^{+}B220^{-}) and B cells (B220^{+}) among peripheral blood and spleen cells from *Slc3a2*$^{f/f}$CD19-Cre^{+} and control *Slc3a2*$^{f/f}$CD19-Cre^{-} mice, prepared by lysis of erythrocytes. Data are from one mouse of each genotype in an experiment repeated once ($n = 4$ mice per group for each).

beginning at the transition from pro–B cell to pre–B cell, when CD19 expression is first induced[14]. In the splenic B cell compartment, 70–90% of cells lacked CD98hc (**Fig. 1a**), and we did not detect any deletion in T cells or monocytes-macrophages (**Fig. 1b**), consistent with the efficiency and specificity of CD19-Cre–mediated recombination[13]. B cells from *Slc3a2*^{flf} littermates lacking CD19-Cre (*Slc3a2*$^{f/f}$ CD19-Cre^{-} mice) were uniformly positive for CD98hc (**Fig. 1a**).

To assess whether CD98hc is important for the secretion of antibodies by B cells, we measured circulating immunoglobulin in *Slc3a2*$^{f/f}$ CD19-Cre^{+} and *Slc3a2*$^{f/f}$CD19-Cre^{-} mice. Whereas basal circulating concentrations of immunoglobulin M (IgM) were not significantly lower ($P > 0.05$) in naive *Slc3a2*$^{f/f}$CD19-Cre^{+} mice, we noted significantly less ($P < 0.025$) class-switched IgG in these mice (**Supplementary Fig. 1b**). Furthermore, after challenge with T cell–independent antigen in PBS (**Fig. 2a**) or T cell–dependent antigen in complete Freund's adjuvant (CFA; **Fig. 2b**), we noted much lower antigen-specific IgM and IgG concentrations in *Slc3a2*$^{f/f}$CD19-Cre^{+} mice than in *Slc3a2*$^{f/f}$CD19-Cre^{-} mice. This defect was not specific to Toll-like receptor signals, because we obtained similar results after immunization with T cell–dependent antigens in adjuvant lacking microbial components (incomplete Freund's adjuvant; **Fig. 2c**). In addition, this correlated with the 'gene dosage' of *Slc3a2*; *Slc3a2*$^{f/-}$ CD19-Cre^{+} mice had a more severe defect than did *Slc3a2*$^{f/+}$CD19-Cre^{+} mice (**Supplementary Fig. 2** online). Thus, B cell CD98hc is important for mounting specific antibody responses to antigenic challenge.

CD98hc is involved in integrin signaling, and integrins are involved in the localization and distribution of B cells subsets[15,16]. In addition, CD98hc is important for integrin-mediated migration of mesenchymal cells[7]. To test whether loss or misdistribution of B cell subsets could explain the impaired antibody production of *Slc3a2*$^{f/f}$CD19-Cre^{+} mice, we examined lymphoid tissue for the presence and localization of B cell subsets. Despite the involvement of CD98hc in adhesive signaling and amino acid transport[6,7,17], CD98hc-deficient follicular B cells, marginal zone B cells, transitional B cells and peritoneal B1 cells were present in normal percentages in the periphery; in addition, pro–B cells, pre–B cells, immature B cells, and mature B cells were present in normal proportions in the bone marrow (**Fig. 3a**). Similarly, we detected no significant difference in the absolute numbers of these subsets in *Slc3a2*$^{f/f}$CD19-Cre^{+} versus *Slc3a2*$^{f/f}$CD19-Cre^{-} mice ($P > 0.05$; **Supplementary Fig. 3** online). *Slc3a2*$^{f/f}$CD19-Cre^{+} mice also had normal splenic architecture, as follicular B cells segregated with intact marginal zones, and *Slc3a2*$^{f/f}$CD19-Cre^{-} and *Slc3a2*$^{f/f}$CD19-Cre^{+} mice had similar numbers of germinal centers (**Fig. 3b**). Finally, we detected no differences between naive *Slc3a2*$^{f/f}$CD19-Cre^{-} and *Slc3a2*$^{f/f}$CD19-Cre^{+} mice in terms of formed elements of the blood (**Supplementary Fig. 4** online) or the concentration of circulating natural IgM (**Fig. 3c**). Thus, CD98hc is not required for the formation of mature B cells or their ability to populate secondary lymphoid organs.

B cell CD98hc is necessary for plasma cell formation

B cells differentiate into antibody-secreting plasma cells after antigenic challenge, which suggests that a requirement for CD98hc in plasma cell formation might explain the lower humoral immune responses of *Slc3a2*$^{f/f}$CD19-Cre^{+} mice. To test that idea, we purified resting splenic B cells from *Slc3a2*$^{f/f}$CD19-Cre^{+} mice, depleted the population of

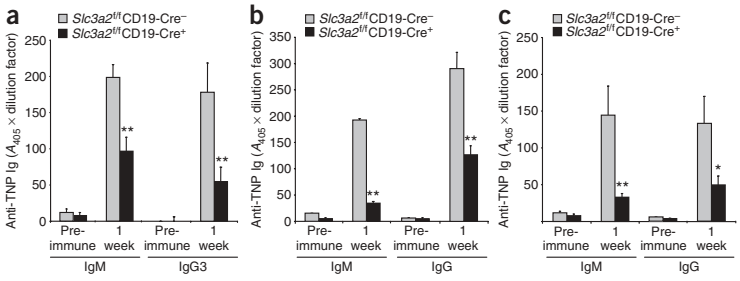

Figure 2 Impaired antibody responses in *Slc3a2*$^{f/f}$CD19-Cre^{+} mice. (**a**) Direct ELISA of anti-TNP IgM or anti-TNP IgG3 in the serum of adult *Slc3a2*$^{f/f}$CD19-Cre^{+} and control *Slc3a2*$^{f/f}$CD19-Cre^{-} mice 8–12 weeks of age, immunized with 50 μg TNP-LPS (T cell–independent antigen) in PBS; serum is from blood obtained before immunization (Pre-immune) and 1 week after immunization. (**b**,**c**) Direct ELISA of anti-TNP IgM and anti-TNP IgG in the serum of *Slc3a2*$^{f/f}$CD19-Cre^{+} and control *Slc3a2*$^{f/f}$CD19-Cre^{-} mice immunized with 100 μg TNP-KLH (T cell–dependent antigen) in CFA (**b**) or incomplete Freund's adjuvant (**c**). A_{405}, absorbance at 405 nm. *, $P = 0.057$ and **, $P < 0.025$ (two-tailed *t*-test). Data are from an experiment repeated once (error bars, s.e.m. of five mice per group).

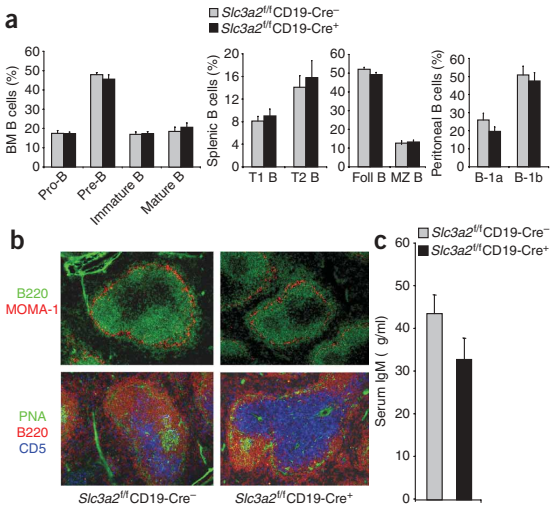

Figure 3 Normal B cell distribution and natural antibody concentrations in *Slc3a2*$^{f/f}$CD19-Cre^{+} mice. (**a**) Flow cytometry of B cell subsets from the spleen, bone marrow and peritoneum of adult *Slc3a2*$^{f/f}$CD19-Cre^{+} and control *Slc3a2*$^{f/f}$CD19-Cre^{-} mice 8–12 weeks of age. Foll, follicular; MZ, marginal zone. Data are from an experiment repeated once with similar results (error bars, s.e.m. of four mice per group). (**b**) Secondary lymphoid architecture of frozen spleen sections from *Slc3a2*$^{f/f}$CD19-Cre^{+} and littermate control *Slc3a2*$^{f/f}$CD19-Cre^{-} mice, stained to detect B220^{+} B cells, metallophilic macrophages that outline the marginal zone (MOMA-1^{+}), T cells (CD5^{+}) and germinal center B cells (positive for binding of peanut agglutinin (PNA)). Original magnification, ×10. Results are representative of three experiments. (**c**) Sandwich ELISA of total natural IgM in the serum of naive adult *Slc3a2*$^{f/f}$CD19-Cre^{+} and control *Slc3a2*$^{f/f}$CD19-Cre^{-} mice 8–12 weeks of age. $P = 0.11$ (two-tailed *t*-test). Data are from one experiment (error bars, s.e.m. of 30 mice per group).

any B cells expressing CD98hc and stimulated the remaining population with lipopolysaccharide (LPS) to induce the formation of plasma cells. B cells from *Slc3a2*$^{f/f}$CD19-Cre^{+} mice were defective both in class switching (**Fig. 4a**) and in development into CD138^{+} plasma cells (**Fig. 4b**). This phenotype bears similarities to that of β_1 integrin–deficient B cells[16]. The few plasma cells formed by *Slc3a2*$^{f/f}$CD19-Cre^{+} B cells expressed CD98hc (**Supplementary Fig. 5** online), which indicated that they were the progeny of a few remaining CD98hc-expressing cells that had escaped Cre-mediated recombination and *in vitro* depletion. Indeed, when we omitted the step of *in vitro* depletion of CD98hc-expressing cells, the 10–20% of B cells that expressed CD98hc in *Slc3a2*$^{f/f}$CD19-Cre^{+} mice generated near normal percentages of plasma cells *in vitro* (**Supplementary Figs. 6** and **7** online).

Consistent with the defective formation of antibody-secreting plasma cells, B cells from *Slc3a2*$^{f/f}$CD19-Cre^{+} mice also had impaired antibody secretion after LPS stimulation *in vitro* (**Fig. 4c**). As shown by enzyme-linked immunospot assay, *Slc3a2*$^{f/f}$CD19-Cre^{+} mice immunized with a T cell–dependent antigen also had fewer cells that secreted antigen-specific antibody immediately after isolation than did immunized *Slc3a2*$^{f/f}$CD19-Cre^{-} mice (**Fig. 4d**). These data collectively show that without CD98hc, B cells are considerably impaired in their ability to form plasma cells.

CD98hc is required for rapid B cell proliferation

Differentiation into plasma cells is preceded by many rounds of proliferation, which leads to larger numbers of antigen-specific B cells[18]; class switching is also independently regulated by cell division[19]. Published reports using blocking or crosslinking antibody suggest that CD98hc is involved in the proliferation of T cells[20,21] and keratinocytes[22]. To assess the function of CD98hc in B cell proliferation, we purified CD98hc-deficient or CD98hc-sufficient resting splenic B cells from *Slc3a2*$^{f/f}$CD19-Cre^{+} or *Slc3a2*$^{f/f}$CD19-Cre^{-} mice, respectively, labeled them with the intracellular dye CFSE, stimulated them with B cell mitogens and measured their proliferation by flow cytometry asessing dye dilution. By 5 d after stimulation, B cells from *Slc3a2*$^{f/f}$CD19-Cre^{-} mice had divided five to eight times, as shown by discrete populations of daughter cells with exponential dilution of fluorescence (**Fig. 5a**). In contrast, B cells from *Slc3a2*$^{f/f}$CD19-Cre^{+} littermates showed minimal division in response to the B cell antigen receptor–crosslinking agent antibody to IgM (anti-IgM), provided alone or together with interleukin 4 (IL-4) or anti-CD40; we obtained similar data by directly counting viable cells (**Supplementary Fig. 8** online). A few cells from *Slc3a2*$^{f/f}$CD19-Cre^{+}

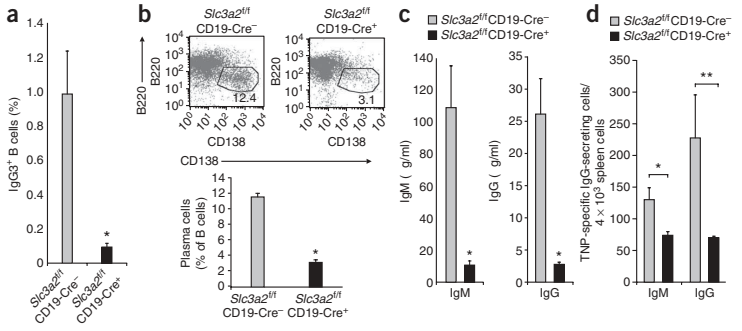

Figure 4 Defective formation of plasma cells in *Slc3a2*$^{f/f}$CD19-Cre^{+} mice. (**a**,**b**) Flow cytometry of surface IgG3 (**a**) and CD138 (syndecan-1, a plasma cell marker; **b**) on splenic B cells (CD43^{-} and CD98hc deficient) purified from *Slc3a2*$^{f/f}$ CD19-Cre^{+} and littermate control *Slc3a2*$^{f/f}$CD19-Cre^{-} mice and cultured for 5 d with LPS. Graphs present IgG3^{+} or CD138^{+} B220^{lo} cells among total B cells. Numbers adjacent to outlined areas (**b**, top) indicate percent B220^{lo}CD138^{+} cells. *, $P < 0.025$ (two-tailed *t*-test). Data are from an experiment with one mouse or an experiment repeated once with similar results (error bars, s.e.m. of three mice per group). (**c**) Sandwich ELISA of total IgM and IgG in supernatants of B cells stimulated for 4 d with LPS. *, $P < 0.05$ (two-tailed *t*-test). Data are from an experiment repeated once with similar results (error bars, s.e.m. of four mice per group). (**d**) TNP-specific IgG–secreting plasma cells among splenocytes obtained from *Slc3a2*$^{f/f}$CD19-Cre^{+} and control mice 1 week after immunization with TNP-KLH in CFA, then cultured for 2–3 h on TNP-coated polyvinylidene difluoride–membrane 96-well plates, followed by washing to remove cells and incubation with horseradish peroxidase–conjugated anti-IgG (secondary antibody); 3-amino-9-ethyl carbazole substrate was used to develop red spots. *, $P = 0.05$ and **, $P = 0.08$ (two tailed *t*-test). Data are from an experiment repeated once (error bars, s.e.m. of four mice per group).

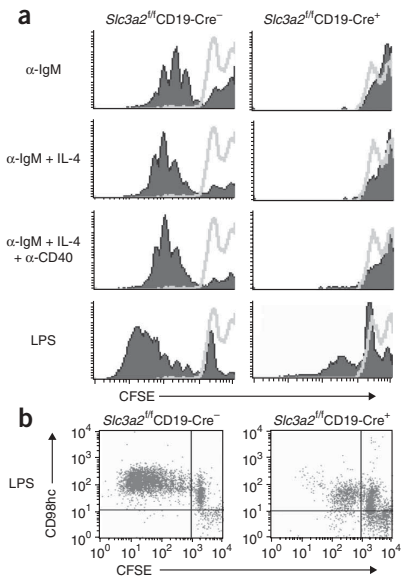

Figure 5 Proliferation of splenic B cells from *Slc3a2*$^{f/f}$CD19-Cre^{+} mice. (**a**) Flow cytometry of the proliferation of B cells (CD43 and CD98 deficient) purified from splenocytes of *Slc3a2*$^{f/f}$CD19-Cre^{+} and littermate control *Slc3a2*$^{f/f}$CD19-Cre^{-} mice 8–12 weeks of age, then labeled with CFSE and left unstimulated (resting cells; open histograms) or cultured with various stimuli (left margin) for 5 d at a density of 4×10^5 cells per well in 48-well plates (filled histograms), assessed by CFSE dilution. α-, anti-. Data are from one mouse in one experiment (representative of three mice of each genotype), repeated twice with additional mice. (**b**) Two-parameter flow cytometry of CD98hc expression on CFSE^{lo} (dividing) and CFSE^{hi} (nondividing) cells after stimulation with LPS. Data are from an experiment repeated once.

mice did undergo one to two divisions in response to stimulation with a high dose of LPS (**Fig. 5a**). However, those divided cells expressed CD98hc (**Fig. 5b**), which suggests that they had escaped Cre-mediated deletion of *Slc3a2*. Thus, CD98hc is necessary for the rapid proliferation of mature B cells in response to antigen or other mitogenic signals. In the absence of stimulation, the lack of CD98hc did not appreciably alter the viability of cultured B cells (**Supplementary Fig. 8**), which suggests that the low CD98 expression in the resting state is not required for B cell survival. Thus, CD98hc is crucial for the rapid B cell population expansion and plasma cell formation in response to external stimuli that drive adaptive humoral immunity.

CD98hc has two well documented biochemical functions. First, it interacts with certain integrin β-subunits to mediate integrin signaling[6,23] and therefore influences adhesion-induced signaling events such as activation of the kinases pp125^{FAK}, PI(3)K and Akt and the adhesion molecule p130^{CAS}, which control cell proliferation[7]. In addition, by associating with CD98 light chains such as Lat-1, CD98hc facilitates the transport of amino acids such as leucine and isoleucine[4,5]. These amino acids are important regulators of mTOR[24], a critical 'node' in a signaling pathway that controls immune responses[8,9]. Chimeric constructs in which portions of CD98hc are replaced with portions of CD69, another type II transmembrane protein, allow distinct separation of these two CD98hc functions[17] (**Fig. 6a**). We used such chimeras to identify the mechanism whereby CD98hc enables B cell proliferation.

To study the function of these chimeras in primary B cells, we infected bone marrow from *Slc3a2*$^{f/f}$CD19-Cre^{+} mice with retrovirus containing bicistronic mRNA encoding either human CD98hc or a human CD98-CD69 chimera followed by an internal ribosomal entry site and a cassette encoding green fluorescent protein (GFP). We used these transduced bone marrow cells to reconstitute lethally irradiated recipient mice to create mice in which B cells that developed and continued to express a human CD98-CD69 chimera were marked by GFP fluorescence (**Fig. 6a** and **Supplementary Figs. 9** and **10a** online). Staining with an antibody specific for mouse CD98hc enabled us to identify B cells that lacked mouse CD98hc but expressed retrovirus-encoded human CD98hc chimeras; these cells were present in the blood beginning as early as 3 weeks after bone marrow transfer. Furthermore, all B cells that expressed GFP also stained for either human CD98hc or CD69 (**Supplementary Fig. 10b**). At 6 weeks after bone marrow transfer, we purified resting CD98hc-null mouse splenic B cells, labeled them with the membrane dye DiD to monitor proliferation and stimulated them with LPS. Then, 4 d later, we analyzed proliferation by means of flow cytometry assessing dye dilution (**Fig. 6b**). We found proliferation of B cells reconstituted with full-length human CD98hc or with the integrin-interacting chimera C98T98E69 (consisting of the cytoplasmic (C) domain of CD98hc, the transmembrane (T) domain of CD98hc and the extracellular (E) domain of CD69). In contrast, the C98T69E98 chimera, which interacts with Lat-1 and mediates isoleucine transport but does not interact with integrins, failed to reconstitute proliferation. Thus, the integrin-signaling portion of CD98hc is necessary and sufficient for the proliferation of mature B cells.

Loss of CD98hc inhibits integrin-dependent events

Integrin ligation leads to signals that result in cell spreading and migration[25]. In addition, integrins act in synergy with certain tyrosine kinase receptors to prolong and sustain activation of the mitogen-activated protein kinase Erk1/2, which promotes cell proliferation[26] by

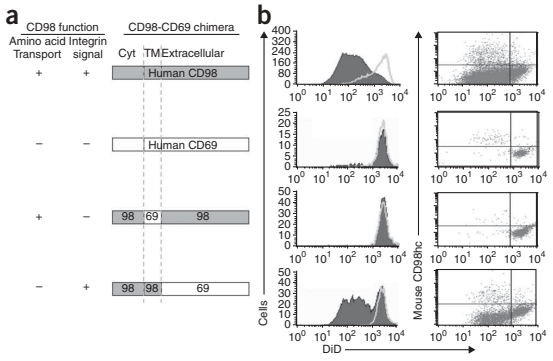

Figure 6 Mechanism by which CD98hc enables B cell proliferation. (**a**) CD98-CD69 chimeric constructs encoded by retroviruses. Cyt, cytoplasmic domain; TM, transmembrane domain; 98, CD98; 69, CD69. (**b**) Two-parameter flow cytometry to assess the proliferation of B cells (CD43^{-} and mouse CD98hc^{-}) purified from splenocytes of recipient mice 6–8 weeks after transplantation of bone marrow cells infected with the retroviruses at left (in **a**), then labeled with DiD and left unstimulated (open histograms) or cultured with LPS (at a density of 3.5×10^5 cells per well in a 48-well plate; filled histograms), measured as DiD dilution; fewer dots (right) indicate lack of proliferation. Data are from an experiment repeated twice.

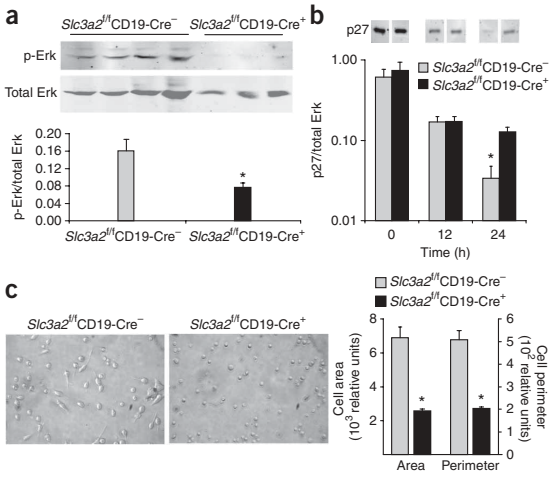

Figure 7 Integrin signaling defects in B cells lacking CD98hc. (**a**) Immunoblot analysis (top) of Erk1/2 phosphorylation (p-Erk) in B cells ($CD43^-CD98^-$) purified from splenocytes of *Slc3a2*$^{f/f}$CD19-Cre$^+$ mice ($n = 4$) and littermate control *Slc3a2*$^{f/f}$CD19-Cre$^-$ mice ($n = 3$) 8–12 weeks of age and stimulated for 17 h with anti-IgM (30 μg/ml) and IL-4 (15 ng/ml), then immediately washed with ice-cold PBS and lysed. Faint bands are present in the *Slc3a2*$^{f/f}$CD19-Cre$^+$ lanes. Each lane represents one mouse. (**b**) Immunoblot analysis (top) of p27 in B cells purified from *Slc3a2*$^{f/f}$CD19-Cre$^+$ or littermate control *Slc3a2*$^{f/f}$CD19-Cre$^-$ mice and stimulated for 0, 12 or 24 h with anti-IgM and IL-4, then washed and lysed (intervening bands are omitted for clarity). Below (**a**,**b**), staining of phosphorylated Erk1/2 (**a**) or p27 (**b**) normalized to that of total Erk. Data in **a**,**b** are from an experiment repeated once (error bars, s.e.m. of three mice per group). (**c**) Integrin-dependent spreading of B cells purified from *Slc3a2*$^{f/f}$CD19-Cre$^+$ mice (right) or littermate control *Slc3a2*$^{f/f}$CD19-Cre$^-$ mice (left), then stimulated for 24 h with anti-CD40 and IL-4 and plated for 16 h on anti-LFA-1. Original magnification, ×40. Data are from an experiment repeated once (error bars, s.e.m. of 30 cells per group). *, $P < 0.015$ (two-tailed *t*-test).

downregulating cyclin-dependent kinase inhibitors[27] and facilitating progression through the G1 phase of the cell cycle[28,29]. B cells from *Slc3a2*$^{f/f}$CD19-Cre$^+$ mice had less phosphorylation of Erk1/2 at 17 h after BCR ligation (**Fig. 7a**). In contrast, early activation (<1 h) of the kinases Erk1/2, Akt and Syk was intact in B cells lacking CD98hc (**Supplementary Fig. 11a–c** online), as was the expression of activation markers (**Supplementary Fig. 11d**). However, coincident with a failure to sustain Erk1/2 activation, *Slc3a2*$^{f/f}$CD19-Cre$^+$ B cells showed impaired downregulation of the cyclin-dependent kinase inhibitor p27 (**Fig. 7b**), consistent with the observed lack of proliferation. Thus, the absence of CD98hc selectively impairs sustained activation of Erk1/2 after BCR ligation, an event known to depend on integrins in other cell types.

To directly assess the effect of CD98hc deficiency in B cells on another integrin-dependent function, we used a B cell adhesion and spreading assay[30,31]. Activated B cells from *Slc3a2*$^{f/f}$CD19-Cre$^+$ mice failed to spread after direct antibody-mediated ligation of the integrin $\alpha_L\beta_2$ (LFA-1; **Fig. 7c**). In contrast, CD98hc-bearing B cells from their *Slc3a2*$^{f/f}$CD19-Cre$^-$ littermates spread extensively, as shown by their twofold larger cell area and perimeter relative to that of the CD98hc-deficient B cells. In sum, these data point to the potential importance of integrin signaling in B cell proliferation.

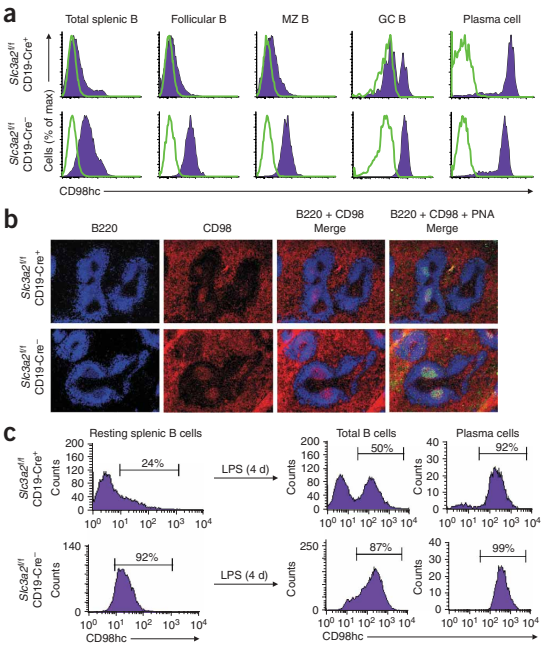

Figure 8 Selection for CD98hc$^+$ B cells during activation. (**a**) Flow cytometry of *in vivo* CD98hc expression (filled histograms) on B cells isolated from spleens of *Slc3a2*$^{f/f}$CD19-Cre$^+$ and control *Slc3a2*$^{f/f}$CD19-Cre$^-$ mice immunized with the T cell–dependent antigen TNP-KLH in CFA (one half of each spleen is used here). Open histograms, isotype-matched control antibody. max, maximum. (**b**) Microscopy of frozen sections of the remaining halves of the spleens in **a**, stained for B220 and CD98hc to assess selection of CD98hc$^+$ B cells *in vivo*; germinal centers were verified by staining with peanut agglutinin. Original magnification, ×10. Data in **a**,**b** are from one representative mouse of each genotype in an experiment repeated once ($n = 3$ mice per group). (**c**) Flow cytometry of CD98hc expression on splenic B cells purified from *Slc3a2*$^{f/f}$CD19-Cre$^+$ mice without depletion of CD98hc$^+$ cells or from control *Slc3a2*$^{f/f}$CD19-Cre$^-$ mice, assessed before (resting; left) and after (right) culture for 4 d with LPS, and stained for B220, CD98hc and CD138 (plasma cell marker) to assess selection of CD98hc$^+$ B cells *in vitro*. Numbers above bracketed lines indicate percent CD98hc$^+$ cells. Data are from one mouse in an experiment repeated twice ($n = 3$ mice per group).

As an initial test of that idea, we analyzed responses to crosslinking of the B cell antigen receptor on B cells from mice engineered to lack all leukocyte integrins[32]. Even though some of these B cells expressed a small quantity of integrin β_1, they showed less proliferation in response to BCR ligation (**Supplementary Fig. 12** online), which provides direct evidence of the involvement of integrins in B cell proliferation. The occurrence of some proliferation of these B cells raises the possibility that the loss of amino acid transport resulting from CD98hc deficiency may also contribute to the more profound defect in proliferation of CD98hc-deficient B cells.

CD98hc confers a selective advantage on B cells

During T cell–dependent responses, antigen-specific B cell populations expand in germinal centers in competition for limited antigen[33]. The experiments reported above indicated that CD98hc conferred a strong selective advantage during B cell population expansion *in vitro*. To

measure that advantage *in vivo*, we immunized *Slc3a2*$^{f/f}$CD19-Cre^{+} mice with trinitrophenyl–keyhole limpet hemocyanin (TNP-KLH), a T cell–dependent antigen, and analyzed CD98hc expression on splenic B cell subsets. In this experiment, CD98hc was present on less than 10% of resting splenic B cell subsets (**Fig. 8a**). However, during the germinal center response, B cells undergo a proliferative burst and are selected for the ability to bind antigen with high affinity. At this stage, the percentage of CD98hc-expressing cells in the *Slc3a2*$^{f/f}$CD19-Cre^{+} mice increased from less than 10% to 40% (**Fig. 8a**). Furthermore, after class switching, over 99% of plasma cells in *Slc3a2*$^{f/f}$CD19-Cre^{+} mice had detectable surface expression of CD98hc (**Fig. 8a**). Thus, there were no detectable CD98-null plasma cells in *Slc3a2*$^{f/f}$CD19-Cre^{+} mice; these observations are consistent with our *in vitro* finding that CD98hc was required for the rapid proliferation of mature B cells and subsequent formation of plasma cells.

Slc3a2$^{f/f}$CD19-Cre^{+} mice had considerably fewer germinal center B cells and plasma cells than *Slc3a2*$^{f/f}$CD19-Cre^{-} mice had at 1 week after immunization (data not shown), probably because they had far fewer CD98hc-expressing precursor cells able to proliferate in germinal centers and form plasma cells. However, at 2–3 weeks after immunization, titers of antibodies specific for TNP-KLH in *Slc3a2*$^{f/f}$CD19-Cre^{+} mice were similar to those in *Slc3a2*$^{f/f}$CD19-Cre^{-} mice, probably because of germinal center selection for the few pre-existing CD98hc-expressing antigen-specific B cells (**Supplementary Fig. 13** online). This strong selection for CD98hc-expressing B cells can thus account for the relatively modestly lower basal serum IgG concentrations in *Slc3a2*$^{f/f}$CD19-Cre^{+} mice. Immunohistochemical staining for CD98hc in spleens of immunized mice confirmed that, in contrast to the surrounding follicular B cells, germinal center B cells in *Slc3a2*$^{f/f}$CD19-Cre^{+} mice expressed CD98hc (**Fig. 8b**). *In vitro* analysis of B cells purified from *Slc3a2*$^{f/f}$CD19-Cre^{+} mice without depletion of CD98-expressing cells provided further confirmation of the strong selective advantage conferred by CD98hc; after 4 d in culture, 99% of plasma cells expressed CD98hc (**Fig. 8c**).

CD98hc is upregulated 20- to 30-fold after B cell activation, and we have shown here that CD98hc was required for B cells to proliferate and to differentiate into plasma cells. Hence, we propose that upregulation of CD98hc can serve as a checkpoint in the progression to humoral immunity. Consequently, the expression and function of CD98hc are potential targets for the modulation of antibody responses.

DISCUSSION

CD98hc was one of the earliest lymphocyte activation antigens described[3], yet its function in the immune response has remained obscure. Although studies in which T cells were treated with anti-CD98hc *in vitro*[20,21,34] have suggested that CD98hc is involved in T cell activation, the function of CD98hc in lymphocytes *in vivo* has remained unknown. Here we have shown that CD98hc is absolutely required for the rapid B cell clonal proliferation necessary for their subsequent differentiation into antibody-secreting plasma cells. Consequently, higher CD98hc expression provides antigen-stimulated B cells with a profound selective advantage.

The linkage of the integrin-binding function of CD98hc to B cell proliferation suggests a new paradigm for the function of integrin signaling in lymphocytes. In addition to functioning in hematopoiesis, trafficking and the formation of immune synapses[16,35–39], our work has indicated that integrin signaling is involved in clonal proliferation during immune responses. CD98hc serves two cellular functions; the first is amino acid transport, through interaction with one of several CD98 light chains[4,5]. The extracellular domain of CD98hc is responsible for this function, and reconstitution with a chimeric protein containing this domain of CD98hc was not sufficient to restore the proliferation of CD98-null B cells. The second main function of CD98hc is mediating integrin signaling[6,7]. The transmembrane and cytoplasmic domains of CD98hc are necessary for interaction with integrin β-subunits, which leads to pp125^{FAK}-dependent activation of Akt by PI(3)K and p130^{CAS}-mediated activation of the small GTPase Rac[7]. Reconstitution with a chimeric protein that contained only the transmembrane and cytoplasmic portions of CD98hc was sufficient to restore the proliferation of CD98hc-null B cells.

Integrins can act together with immunoreceptors, using similar 'downstream' signaling proteins, to promote lymphocyte proliferation and activation[40]. Thus, our findings establish a nexus of CD98hc-dependent integrin and immunoreceptor signaling pathways that regulate the proliferation of lymphocytes. CD98hc could function by allowing integrins to lower the threshold for cellular activation[41] by efficiently organizing components of the immunological synapse; however, we found that CD98hc was not required for early activation events. Instead, our data support a mechanism whereby CD98h-mediated integrin signals can extend the kinetics of immunoreceptor signals[42] to the point of driving cell division and clonal expansion.

Integrins drive fibroblast proliferation by sustaining Erk activation. Without integrin-mediated adhesion, growth factor signals are transient and are unable to downregulate cyclin-dependent kinase inhibitors such as p27, and cells fail to exit the G1 phase of the cell cycle[26,28,29]. Our data have indicated that a similar mechanism is operative in B cells. CD98hc-deficient B cells were able to generate early B cell antigen receptor signals but could not sustain late Erk1/2 signaling or downregulate p27 and failed to divide. The inability of CD98hc-deficient B cells to spread on integrin-specific antibodies confirmed the integrin signaling defect of CD98hc-deficient B cells. Published work using supported lipid bilayers or plate-bound antibodies[30] to study the formation of immunological synapses has shown that B cells spread rapidly after activation of the B cell antigen receptor in an integrin-dependent way[30,43]; we have now shown that this spreading is CD98hc dependent. Thus, CD98hc could promote integrin-dependent changes in cell shape that might stabilize interactions with antigen-bearing cells.

One implication of our work relates to the origin of the adaptive immune system. CD98hc orthologs first appeared in primitive vertebrates[10], as did sequences in integrin β-cytoplasmic domains that permit CD98hc to interact with integrins[44]. The coincidence of those events with the appearance of adaptive immunity[2,10] suggests that the survival advantage conferred by adaptive immunity was among the factors that favored the maintenance of CD98hc and its ability to mediate integrin signaling. CD98hc is overexpressed in many cancers and mediates tumorigenesis[7,45–47]. In particular, published work has emphasized the importance of integrin signaling[25] in the development and maintenance of epithelial cancers[48,49] and of CD98hc in potentiating the growth of cancer cells[7,47]. Thus, the appearance of CD98hc in vertebrates, which enabled an adaptive immune response, may have led to greater susceptibility to cancer.

METHODS

Mice. Mice with floxed *Slc3a2* were generated by flanking of exons 1 and 2, which encode the transmembrane portion of CD98hc, with *lox*P sites[12]. The neomycin-selection cassette used to select embryonic stem cell clones positive for a floxed *Slc3a2* allele was flanked by Flp sites and thus was excised when mice with floxed *Slc3a2* were bred with human β-actin FLPe deleter mice (Jackson Laboratories). *Slc3a2*$^{f/f}$CD19-Cre^{+} mice were the result of crossing *Slc3a2*$^{f/f}$ with the CD19-Cre^{+} strain[13]. *Slc3a2*$^{f/+}$CD19-Cre^{+} offspring were

identified by PCR and were backcrossed with *Slc3a2*$^{f/f}$ mice to create mice heterozygous for CD19-Cre and homozygous for the *Slc3a2* floxed allele (*Slc3a2*$^{f/f}$CD19-Cre^{-}). This littermate comparison was used wherever possible. For **Supplementary Figures 2** and **4**, the offspring of *Slc3a2*$^{+/-}$ × *Slc3a2*$^{f/f}$ CD19-Cre^{+} matings were used. All mice were housed at the University of California San Diego animal facility, and all experiments were approved by the Institutional Animal Care and Use Committee. 'Pan-integrin'-deficient mice were generated as described[32]. Integrins were ablated by crossing of *Itgb1*^{flf}, *Itgav*^{flf}, *Itgb2*$^{-/-}$ or *Itgb7*$^{-/-}$ mice (deficient in integrin β_1, α_V, β_2 or β_7, respectively) with mice carrying an Mx1-Cre transgene. Cre expression in hematopoietic cells was induced by intraperitoneal injection of 250 μg polyinosinic-polycytidylic acid (Amersham Biosciences); 8 d later, mice were used for B cell–proliferation assays.

Flow cytometry of B cell subsets. Bone marrow cells were prepared by dissection of femur and tibia bones from adult *Slc3a2*$^{f/f}$CD19-Cre^{+} mice (10–20 weeks of age) and flushing with media with a 23-gauge needle. After two passages through the 23-gauge needle, erythrocytes were lysed for 8 min at 25 °C with ammonium chloride–potassium bicarbonate lysis buffer (Biowhittaker). Splenic single-cell suspensions were prepared by dissociation of whole spleens with a 7-ml tissue grinder (Kontes) and lysis of erythrocytes as described for bone marrow. Cells from peritoneal lavage were isolated from adult mice by flushing of the peritoneum with 10 ml complete medium (RPMI medium and 10% (vol/vol) FBS, supplemented with L-glutamine, penicillin and streptomycin) in batches of 1–2 ml. After being counted, bone marrow, spleen, or peritoneal cells were stained in 100 μl staining buffer (0.5% (wt/vol) BSA in PBS) containing fluorochrome-conjugated antibody to mouse B220 (RA3-6B2), IgM (II/41), CD21 (7G6), CD23 (B3B4), CD98hc (RL388), GL7 (GL7), CD138 (281-2) or Fas (Jo2) at optimal concentrations (all from BD Biosciences). After incubation of cells on ice for 30–45 min, followed by three washes in staining buffer, subsets were analyzed by flow cytometry with a FACSAria or FACSCalibur (BD Biosciences).

Immunohistochemistry. For analysis of CD98 selection after immunization, adult *Slc3a2*$^{f/f}$CD19-Cre^{+} mice and littermate control (*Slc3a2*$^{f/f}$CD19-Cre^{-}) mice were immunized intraperitoneally with 100 μg TNP-KLH (Biosearch) emulsified in CFA (250 μl). Then, 7 d later, spleens were embedded in Tissue-Tek optimum cutting temperature compound (Sakura Finetek USA) and were frozen at −80 °C. Sections 8 μm in thickness were mounted on microscope slides, were fixed for 10 min in cold acetone, were blocked for 1 h with blocking buffer (0.5% (wt/vol) BSA in PBS), and were stained for 1 h at 25 °C with fluorescein isothiocyanate–conjugated peanut agglutinin (FL-1071; Vector Labs) and anti-B220 (BRA3-6B2), anti-CD5 (53-7.3), anti-CD3 (145-2C11) or anti-CD98 (RL388; all from BD Biosciences) or anti-MOMA-1 (MOMA-1; BaChem). After being washed with PBS containing 0.5% (vol/vol) Tween, sections were covered with Gel/Mount (Biomeda) and were sealed with glass coverslips. Images were acquired with Zeiss Axiocam M1 microscope (Zeiss) and Slidebook software (Intelligent Imaging Innovations).

Antibody analysis. For antigen-specific antibody responses, adult *Slc3a2*$^{f/f}$ CD19-Cre^{+} and control littermate *Slc3a2*$^{f/f}$CD19-Cre^{-} mice were injected intraperitoneally with 50 μg TNP-LPS (Sigma) in 250 μl PBS (T cell–independent antigen) or 100 μg TNP-KLH (Biosearch) emulsified in 250 μl CFA (T cell–dependent antigen). Blood serum was collected by centrifugation of tail vein blood (100–200 μl with a solution of 1–2 mM EDTA as an anticoagulant) before and 1, 2 and 3 weeks after immunization. Concentrations of TNP-specific antibody in blood sera were assessed by direct enzyme-linked immunosorbent assay (ELISA) with TNP-ovalbumin as the coating antigen and alkaline phosphatase–conjugated polyclonal anti–mouse IgG (A4312; Sigma), polyclonal anti–mouse IgM (A7784; Sigma) or monoclonal anti–mouse IgG3 (R40-82; BD Biosciences) as the detection antibody. Because of inconsistencies in commercially available anti-TNP standards, the ELISA data in **Figure 2** and **Supplementary Figure 13** were quantified by multiplication of the absorbance 'reading out' of three to four dilutions of sample that was in the linear portion of the assay with the dilution factor to obtain the values presented. Concentrations of circulating IgG and IgM from naive mice and from *in vitro* splenic B cell stimulations were measured by sandwich ELISA with polyclonal anti–mouse IgG (715-005-150) or anti–mouse IgM (115-006-020; both from Jackson Immunoresearch), the detection antibodies described for the direct ELISA and standard curves obtained with purified polyclonal IgG or IgM.

***In vitro* proliferation and differentiation of resting B cells.** Resting B cells (defined as CD43^{-}) were purified from spleen cell suspensions of *Slc3a2*$^{f/f}$CD19-Cre^{+}, 'pan-integrin'-deficient or wild-type control mice by depletion of CD43^{+} cells (and depletion of CD98hc^{+} B cells for *Slc3a2*$^{f/f}$ CD19-Cre^{+} mice or depletion of β_1 integrin–positive cells for 'pan-integrin'-deficient mice) with B cell magnetic beads (Dynal). Purity was routinely 95–98%, as assessed by staining with anti-B220 (RA3-6B2) or anti-CD43 (eBioR2-60) and flow cytometry. Resting B cells were plated in 48-well plates at a density of 4 × 10^5 cells per well and were stimulated for 3–5 d with Ultrapure LPS (20 μg/ml; InVivoGen), F(ab′)$_2$ goat anti–mouse IgM (30 μg/ml; Jackson Immunoresearch), anti-CD40 (2 μg/ml; 3/23; BD Biosciences) or recombinant mouse IL-4 (50 ng/ml; Peprotech). Unstimulated resting cells were cultured with medium alone. Staining with anti-CD138 (DL-101; eBioscience), anti-IgG3 (R40-82; BD Biosciences) and anti-B220 (RA3-6B2; eBioscience) and flow cytometry were used to assess class switching and differentiation into plasma cells. For measurement of proliferation, purified resting B cells were labeled with 2 μM CFSE (carboxyfluorescein diacetate succinimidyl ester; Molecular Probes) and were analyzed by flow cytometry at 3–5 d for dilution of fluorescence (cell division). Because the extent of CFSE labeling varied among samples, unstimulated cells were also assessed (**Supplementary Fig. 12**). For some differentiation or proliferation experiments, cells were also stained with anti-CD98 (RL388; eBioscience). Propidium iodide exclusion and automated counting by flow cytometry were used for analysis of the expansion of cell populations. In this *in vitro* culture system, many cells die or are lost during collecting or staining and a smaller subset divides rapidly.

Retroviral infection of mouse bone marrow and transplantation into recipient mice. The bone marrow transplant protocol was from S. Rowland in the lab of R. Pelanda. Donor mice were treated intraperitoneally with 5-fluorouracil (Adrucil; Sicor Pharmaceuticals) in 200 μl PBS at a dose of 4 μg per mouse. Then, 3 d later, EcoPack 293 packaging cells (Imgenex) were transfected with pCl-Eco (Imgenex) and one of four retroviral constructs (C98T98E98, C98T69E98, C98T98E69 or C69T69E69, on a backbone of MSCV-IRES-GFP)[50], followed by culture for 48 h. On day 4, donor mice were killed and bone marrow was cultured overnight in complete medium containing IL-3 (25 ng/ml), IL-6 (50 ng/ml) and stem cell factor (50 ng/ml; all from Peprotech). Viral supernatants were collected from packaging cells on day 5 and were used to 'spin-infect' bone marrow on days 5 and 6 for 90 min at 1,000*g* and at 25 °C. Bone marrow cells were collected on day 7 and were injected intravenously at a dose of 2.5 × 10^5 cells in 100 μl PBS per mouse. Small samples were retained and were stained with antibody to Sca-1 (D7; eBioscience), a marker of stem cells. In all samples, 24–29% of Sca-1^{+} populations were GFP^{+} before injection. At 6–8 weeks after transplantation, resting B cells deficient in mouse CD98hc were purified from spleens of recipient mice, then were labeled and were stimulated with LPS. Proliferation and plasma cell differentiation was assessed as described above but with DiD (1,1′-dioctadecyl-3,3,3′,3′-tetramethylindodicarbocyanine; Molecular Probes), which emits in a range distinct from that of GFP.

Additional methods. Information on hematology, enzyme-linked immunospot assays, spreading assays, signaling and statistical analysis is available in the **Supplementary Methods** online.

Accession code. UCSD-Nature Signaling Gateway (http://www.signaling-gateway.org): A000262.

Note: Supplementary information is available on the Nature Immunology website.

ACKNOWLEDGMENTS

We thank M. Slepak for technical assistance; D. Rose for advice on analyzing antibody responses; M. Cato for advice and protocols for enzyme-linked immunospot assays; and R. Zent (Vanderbilt University) for *Slc3a2*$^{+/-}$ mice. Supported by the National Institutes of Health (AR27214, HL31950 and

HL0780784), the Arthritis Foundation (C.C.F.) and the National Multiple Sclerosis Society (FG1802-A-1 to J.C.).

AUTHOR CONTRIBUTIONS

M.H.G., J.C. and C.C.F. conceived the project with advice and collaboration from R.C.R.; J.C. and M.H.G. wrote the manuscript with editorial input from R.C.R. and C.C.F.; R.C.R. provided CD19-Cre mice; J.C. did experiments except as follows: C.D.B. did immunohistochemical analysis of spleen sections and flow cytometry for B cell subsets, and R.R. tested B cell proliferation in pan integrin-deficient mice.

Published online at http://www.nature.com/natureimmunology/
Reprints and permissions information is available online at http://npg.nature.com/reprintsandpermissions/

1. Burnet, F.M. *The Clonal Selection Theory of Acquired Immunity* 49–68 (Cambridge University Press, Cambridge, 1959).
2. Cooper, M.D. & Alder, M.N. The evolution of adaptive immune systems. *Cell* **124**, 815–822 (2006).
3. Kehrl, J.H. & Fauci, A.S. Identification, purification, and characterization of antigen-activated and antigen-specific human B lymphocytes. *Trans. Assoc. Am. Physicians* **96**, 182–187 (1983).
4. Bertran, J. *et al.* Stimulation of system y^+-like amino acid transport by the heavy chain of human 4F2 surface antigen in *Xenopus laevis* oocytes. *Proc. Natl. Acad. Sci. USA* **89**, 5606–5610 (1992).
5. Torrents, D. *et al.* Identification and characterization of a membrane protein (y^+L amino acid transporter-1) that associates with 4F2hc to encode the amino acid transport activity y^+L. A candidate gene for lysinuric protein intolerance. *J. Biol. Chem.* **273**, 32437–32445 (1998).
6. Fenczik, C.A., Sethi, T., Ramos, J.W., Hughes, P.E. & Ginsberg, M.H. Complementation of dominant suppression implicates CD98 in integrin activation. *Nature* **390**, 81–85 (1997).
7. Feral, C.C. *et al.* CD98hc (SLC3A2) mediates integrin signaling. *Proc. Natl. Acad. Sci. USA* **102**, 355–360 (2005).
8. Abraham, R.T. Mammalian target of rapamycin: immunosuppressive drugs uncover a novel pathway of cytokine receptor signaling. *Curr. Opin. Immunol.* **10**, 330–336 (1998).
9. Mondino, A. & Mueller, D.L. mTOR at the crossroads of T cell proliferation and tolerance. *Semin. Immunol.* **19**, 162–172 (2007).
10. Uinuk-Ool, T. *et al.* Lamprey lymphocyte-like cells express homologs of genes involved in immunologically relevant activities of mammalian lymphocytes. *Proc. Natl. Acad. Sci. USA* **99**, 14356–14361 (2002).
11. Tsumura, H. *et al.* The targeted disruption of the CD98 gene results in embryonic lethality. *Biochem. Biophys. Res. Commun.* **308**, 847–851 (2003).
12. Feral, C.C. *et al.* CD98hc (SLC3A2) participates in fibronectin matrix assembly by mediating integrin signaling. *J. Cell Biol.* **178**, 701–711 (2007).
13. Rickert, R.C., Roes, J. & Rajewsky, K. B lymphocyte-specific, Cre-mediated mutagenesis in mice. *Nucleic Acids Res.* **25**, 1317–1318 (1997).
14. Otero, D.C. & Rickert, R.C. CD19 function in early and late B cell development. II. CD19 facilitates the pro-B/pre-B transition. *J. Immunol.* **171**, 5921–5930 (2003).
15. Brakebusch, C. *et al.* Beta1 integrin is not essential for hematopoiesis but is necessary for the T cell-dependent IgM antibody response. *Immunity* **16**, 465–477 (2002).
16. Lu, T.T. & Cyster, J.G. Integrin-mediated long-term B cell retention in the splenic marginal zone. *Science* **297**, 409–412 (2002).
17. Fenczik, C.A. *et al.* Distinct domains of CD98hc regulate integrins and amino acid transport. *J. Biol. Chem.* **276**, 8746–8752 (2001).
18. Tangye, S.G. & Hodgkin, P.D. Divide and conquer: the importance of cell division in regulating B-cell responses. *Immunology* **112**, 509–520 (2004).
19. Hasbold, J., Corcoran, L.M., Tarlinton, D.M., Tangye, S.G. & Hodgkin, P.D. Evidence from the generation of immunoglobulin G–secreting cells that stochastic mechanisms regulate lymphocyte differentiation. *Nat. Immunol.* **5**, 55–63 (2004).
20. Freidman, A.W., Diaz, L.A., Jr., Moore, S., Schaller, J. & Fox, D.A. The human 4F2 antigen: evidence for cryptic and noncryptic epitopes and for a role of 4F2 in human T lymphocyte activation. *Cell. Immunol.* **154**, 253–263 (1994).
21. Diaz, L.A., Jr. *et al.* Monocyte-dependent regulation of T lymphocyte activation through CD98. *Int. Immunol.* **9**, 1221–1231 (1997).
22. Fernandez-Herrera, J., Sanchez-Madrid, F. & Diez, A.G. Differential expression of the 4F2 activation antigen on human follicular epithelium in hair cycle. *J. Invest. Dermatol.* **92**, 247–250 (1989).
23. Zent, R. *et al.* Class- and splice variant-specific association of CD98 with integrin beta cytoplasmic domains. *J. Biol. Chem.* **275**, 5059–5064 (2000).
24. Proud, C.G. Amino acids and mTOR signalling in anabolic function. *Biochem. Soc. Trans.* **35**, 1187–1190 (2007).
25. Hynes, R.O. Integrins: bidirectional, allosteric signaling machines. *Cell* **110**, 673–687 (2002).
26. Schwartz, M.A. & Assoian, R.K. Integrins and cell proliferation: regulation of cyclin-dependent kinases via cytoplasmic signaling pathways. *J. Cell Sci.* **114**, 2553–2560 (2001).
27. Motti, M.L. *et al.* Loss of p27 expression through RAS→BRAF→MAP kinase-dependent pathway in human thyroid carcinomas. *Cell Cycle* **6**, 2817–2825 (2007).
28. Assoian, R.K. & Schwartz, M.A. Coordinate signaling by integrins and receptor tyrosine kinases in the regulation of G1 phase cell-cycle progression. *Curr. Opin. Genet. Dev.* **11**, 48–53 (2001).
29. Walker, J.L. & Assoian, R.K. Integrin-dependent signal transduction regulating cyclin D1 expression and G1 phase cell cycle progression. *Cancer Metastasis Rev.* **24**, 383–393 (2005).
30. Lin, K.B. *et al.* The rap GTPases regulate B cell morphology, immune-synapse formation, and signaling by particulate B cell receptor ligands. *Immunity* **28**, 75–87 (2008).
31. Arana, E. *et al.* Activation of the small GTPase Rac2 via the B cell receptor regulates B cell adhesion and immunological-synapse formation. *Immunity* **28**, 88–99 (2008).
32. Lammermann, T. *et al.* Rapid leukocyte migration by integrin-independent flowing and squeezing. *Nature* **453**, 51–55 (2008).
33. Wolniak, K.L., Shinall, S.M. & Waldschmidt, T.J. The germinal center response. *Crit. Rev. Immunol.* **24**, 39–65 (2004).
34. Warren, A.P. *et al.* Convergence between CD98 and integrin-mediated T-lymphocyte co-stimulation. *Immunology* **99**, 62–68 (2000).
35. Shimizu, Y., Rose, D.M. & Ginsberg, M.H. Integrins in the immune system. *Adv. Immunol.* **72**, 325–380 (1999).
36. Sims, T.N. & Dustin, M.L. The immunological synapse: integrins take the stage. *Immunol. Rev.* **186**, 100–117 (2002).
37. Cyster, J.G. Homing of antibody secreting cells. *Immunol. Rev.* **194**, 48–60 (2003).
38. Lo, C.G., Lu, T.T. & Cyster, J.G. Integrin-dependence of lymphocyte entry into the splenic white pulp. *J. Exp. Med.* **197**, 353–361 (2003).
39. Rose, D.M., Alon, R. & Ginsberg, M.H. Integrin modulation and signaling in leukocyte adhesion and migration. *Immunol. Rev.* **218**, 126–134 (2007).
40. Abram, C.L. & Lowell, C.A. Convergence of immunoreceptor and integrin signaling. *Immunol. Rev.* **218**, 29–44 (2007).
41. Batista, F.D. *et al.* The role of integrins and coreceptors in refining thresholds for B-cell responses. *Immunol. Rev.* **218**, 197–213 (2007).
42. Roovers, K., Davey, G., Zhu, X., Bottazzi, M.E. & Assoian, R.K. Alpha5beta1 integrin controls cyclin D1 expression by sustaining mitogen-activated protein kinase activity in growth factor-treated cells. *Mol. Biol. Cell* **10**, 3197–3204 (1999).
43. Fleire, S.J. *et al.* B cell ligand discrimination through a spreading and contraction response. *Science* **312**, 738–741 (2006).
44. Prager, G.W., Feral, C.C., Kim, C., Han, J. & Ginsberg, M. H. CD98hc (SLC3a2) interaction with the integrin β subunit cytoplasmic domain mediates adhesive signaling. *J. Biol. Chem.* **282**, 24477–24484 (2007).
45. Esteban, F. *et al.* Relationship of 4F2 antigen with local growth and metastatic potential of squamous cell carcinoma of the larynx. *Cancer* **66**, 1493–1498 (1990).
46. Hara, K., Kudoh, H., Enomoto, T., Hashimoto, Y. & Masuko, T. Malignant transformation of NIH3T3 cells by overexpression of early lymphocyte activation antigen CD98. *Biochem. Biophys. Res. Commun.* **262**, 720–725 (1999).
47. Henderson, N.C. *et al.* CD98hc (SLC3A2) interaction with β1 integrins is required for transformation. *J. Biol. Chem.* **279**, 54731–54741 (2004).
48. White, D.E. *et al.* Targeted disruption of β1-integrin in a transgenic mouse model of human breast cancer reveals an essential role in mammary tumor induction. *Cancer Cell* **6**, 159–170 (2004).
49. Kass, L., Erler, J.T., Dembo, M. & Weaver, V.M. Mammary epithelial cell: influence of extracellular matrix composition and organization during development and tumorigenesis. *Int. J. Biochem. Cell Biol.* **39**, 1987–1994 (2007).
50. Van Parijs, L. *et al.* Uncoupling IL-2 signals that regulate T cell proliferation, survival, and Fas-mediated activation-induced cell death. *Immunity* **11**, 281–288 (1999).

12.10 Paper 10:

The Mechanism of Kindlin-Mediated Activation of Integrin αIIbβ3.

Current Biology 23, 2288–2295, November 18, 2013 http://dx.doi.org/10.1016/j.cub.2013.09.050

Report

The Mechanism of Kindlin-Mediated Activation of Integrin αIIbβ3

Feng Ye,[1] Brian G. Petrich,[1] Praju Anekal,[1] Craig T. Lefort,[2,4] Ana Kasirer-Friede,[1] Sanford J. Shattil,[1] Raphael Ruppert,[3] Markus Moser,[3] Reinhard Fässler,[3] and Mark H. Ginsberg[1,*]
[1]Department of Medicine, University of California, San Diego, La Jolla, CA 92093, USA
[2]La Jolla Institute for Allergy & Immunology, La Jolla, CA 92093, USA
[3]Department of Molecular Medicine, Max Planck Institute of Biochemistry, 82152 Martinsried, Germany

Summary

Increased ligand binding to cellular integrins ("activation") plays important roles in processes such as development, cell migration, extracellular matrix assembly, tumor metastasis, hemostasis, and thrombosis [1–5]. Integrin activation encompasses both increased integrin monomer affinity and increased receptor clustering [6] and depends on integrin-talin interactions [5]. Loss of kindlins results in reduced activation of integrins [7–13]. Kindlins might promote talin binding to integrins through a cooperative mechanism [5, 14–16]; however, kindlins do not increase talin association with integrins [17]. Here, we report that, unlike talin head domain (THD), kindlin-3 has little effect on the affinity of purified monomeric αIIbβ3, and it does not enhance activation by THD. Furthermore, studies with ligands of varying valency show that kindlins primarily increase cellular αIIbβ3 avidity rather than monomer affinity. In platelets or nucleated cells, loss of kindlins markedly reduces αIIbβ3 binding to multivalent but not monovalent ligands. Finally, silencing of kindlins reduces the clustering of ligand-occupied αIIbβ3 as revealed by total internal reflection fluorescence and electron microscopy. Thus, in contrast to talins, kindlins have little primary effect on integrin αIIbβ3 affinity for monovalent ligands and increase multivalent ligand binding by promoting the clustering of talin-activated integrins.

Results

Kindlin-3 Has a Minimal Effect on the Affinity of Monomeric αIIbβ3

To assess the effect of kindlins on individual integrins, we added purified kindlin-3, the isoform in platelets, to monomeric platelet integrin αIIbβ3 inserted in 10–12 nm diameter phospholipid bilayers (nanodiscs) [18]. Since αIIbβ3 clustering cannot occur under these conditions, ligand binding measures the affinity of integrin monomers [18]. Recombinant purified kindlin-3 was monomeric (see Figure S1A available online) and was well folded as judged by a sharp melting point (48°C) in differential scanning calorimetry (data not shown). Kindlin-3, at a concentration that saturated β3 integrin binding [14, 17], was >25-fold less active than talin head domain (THD) in increasing binding of PAC1, an activation-specific antibody, to αIIbβ3 nanodiscs, and it failed to enhance PAC1 binding induced by THD (Figures 1A and S1B). Indeed, kindlin-3 reduced THD-induced PAC1 binding, possibly due to competition between THD and kindlin-3 for binding to the limited lipid surface present in the nanodiscs, rather than to the β3 integrin [14, 17]. Recombinant kindlin-3 bound to the β3 cytoplasmic domain (K_d = 67 ± 9 nM), but not to a kindlin binding-defective β3 mutant [β3(Y759A); Figure S1C]. Kindlin-3 also bound αIIbβ3 nanodiscs (Figure S1D). Thus, in contrast to THD, recombinant kindlin-3 did not increase the ligand-binding affinity of monomeric αIIbβ3 in nanodiscs.

Kindlins Selectively Increase the Binding of Multivalent Ligands to Recombinant Integrin αIIbβ3

The foregoing results suggest that kindlin-3 may regulate ligand binding to integrins by a mechanism other than modulation of monomer affinity. Platelet activation clusters integrin αIIbβ3, and αIIbβ3 dimerization can cooperate with increased monomer affinity to increase the binding of multivalent but not monovalent ligands [6, 20, 21]. These observations led us to compare the effects of kindlins on the binding of multivalent versus monovalent ligands. Kindlin-1 and kindlin-2 are thought to promote αIIbβ3 activation in nonhematopoietic cells via a mechanism similar to that of kindlin-3 in platelets and are thus used to study αIIbβ3 regulation in such cells [11–13, 22]. Kindlin-1 did not synergize with THD to increase monovalent PAC1 Fab binding to integrin αIIbβ3 in HEK293 cells but dramatically increased THD-induced binding of decavalent PAC1 (Figure 1B). To extend this finding, we used the monovalent fibronectin tenth type III repeat (3FN10), an activation-dependent ligand for integrin αIIbβ3 [23], because it can be expressed in prokaryotic systems at the high concentrations required for this experiment, can be directly labeled (e.g., with biotin), and binds to murine αIIbβ3. Again, kindlin-1 did not synergize with THD to increase the specific binding of 3FN10 to integrin αIIbβ3, measured as binding inhibitable by an αIIbβ3-specific antagonist, eptifibatide (Figures 1C and S1E). 3FN10 binding was not maximal in the THD-transfected cells, because addition of Mn^{2+} markedly increased binding (Figure 1C). Mn^{2+} enhanced THD-induced 3FN10 binding, indicating that Mn^{2+} binding to the extracellular domain can synergize with talin to increase integrin monomer affinity. In sharp contrast to results with 3FN10, kindlin-1 markedly synergized [13, 22] with THD in the binding of decavalent PAC1 immunoglobulin M (IgM) (Figures 1C and S1E). The increase of PAC1 binding upon THD expression was greater than that observed with monomeric 3FN10, probably reflecting both the clustering [24] and conformational changes [18] of αIIbβ3 induced by THD.

To directly test the role of ligand valency in 3FN10 binding, we chemically crosslinked 3FN10 and isolated a mixed population of oligomers. In contrast to monovalent 3FN10 or GST-3FN10, kindlin-1 and kindlin-2 markedly increased the capacity of THD to enhance the specific binding of multivalent GST-3FN10 to αIIbβ3 (Figure 1D). Mutation of the RGD sequence in 3FN10 to AAA abolished the binding of both monomeric and oligomeric 3FN10 (Figure S1F), confirming its

[4]Present address: Division of Surgical Research, Alpert Medical School, Brown University, Providence, RI 02903, USA
*Correspondence: mhginsberg@ucsd.edu

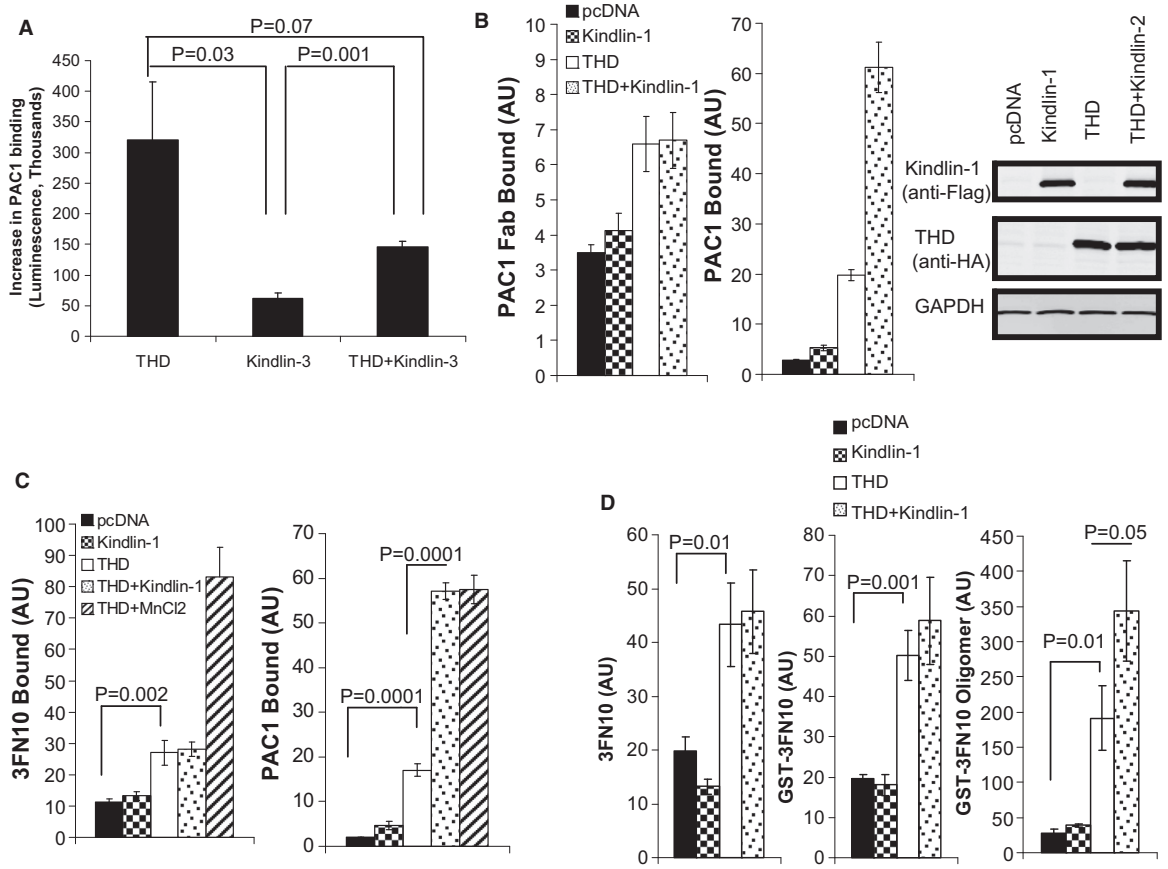

Figure 1. Kindlins Selectively Increase the Binding of Multivalent Ligands to Recombinant Integrin αIIbβ3 Cells, but Not to Monomeric Integrins, in Nanodiscs

(A) Activation of αIIbβ3 in nanodiscs was assayed by PAC1 binding as described in the Supplemental Information. Increase in integrin activation is calculated as (L_i–L_0), where L_i is the eptifibatide-inhibitable PAC1 binding (luminescence) in the presence of THD (2.5 μM), kindlin-3 (2.5 μM), or THD+kindlin-3 and L_0 is PAC1 binding to integrin nanodiscs alone, which was 535,000 arbitrary units. Error bars indicate ±SEM of three independent determinations.

(B) HEK293 cells stably expressing αIIbβ3 were transfected with cDNA encoding kindlin-1, THD, or kindlin-1+THD. Twenty-four hours after transfection, cells were harvested, split into three groups, and stained separately with PAC1, PAC1Fab, or D57 (anti-αIIbβ3). Cells were then fixed in 3.7% formaldehyde. The quantity of PAC1 (decavalent), PAC1Fab (monovalent), or D57 bound was assayed by APC-conjugated anti-IgM (μ chain specific) and anti-IgG and analyzed by flow cytometry. The αIIbβ3-specific ligand binding was calculated as described in the Supplemental Information. The right panel shows the western blots confirming the abundance of expressed proteins in the transfected cells. Error bars indicate ±SEM of three independent experiments. PAC1 Fab was purified by gel filtration to remove protein aggregates and used at a concentration at least 25-fold higher than that used by Bunch [19].

(C) HEK293 cells stably expressing αIIbβ3 were transfected with cDNA encoding kindlin-1, THD, or kindlin-1+THD. The cells were processed as described in (B), and the binding of PAC1 (decavalent), D57, or 3FN10 (GST removed, monovalent) was assayed. The αIIbβ3-specific ligand binding was calculated as described in the Supplemental Information. Error bars indicate ±SEM of four independent experiments.

(D) HEK293 cells stably expressing αIIbβ3 were transfected with cDNA encoding kindlin-1, THD, or kindlin-1+THD. The cells were harvested, and the binding of D57, biotinylated 3FN10 monomer (with GST removed), GST-3FN10, or oligomeric GST-3FN10 was then assayed. Depicted is the αIIbβ3-specific ligand binding as described in the Supplemental Information. Error bars indicate ±SEM of four independent experiments.

specificity. The kindlin-induced increase in multivalent ligand binding was independent of an intact actin cytoskeleton or myosin II-mediated contractility, as latrunculin A, an inhibitor of actin polymerization, or blebbistatin, a myosin II ATPase inhibitor, was without effect (Figure S1G). Thus, kindlins synergized with THD in stimulating the binding of multivalent but not monovalent ligands to αIIbβ3, and this effect required neither an intact actin cytoskeleton nor myosin II-driven contractility.

Silencing of Kindlin-2 Selectively Inhibits the Binding of Multivalent Ligands to Recombinant Integrin αIIbβ3

We then asked whether depletion of kindlins selectively impairs binding of multivalent integrin ligands. HEK293 cells express both kindlin-1 and kindlin-2 [25], making it difficult to perform small interfering RNA (siRNA)-mediated silencing. Thus, we turned to Chinese hamster ovary (CHO) cells, which express only kindlin-2 [13, 17]. In CHO cells expressing an

Current Biology Vol 23 No 22
2290

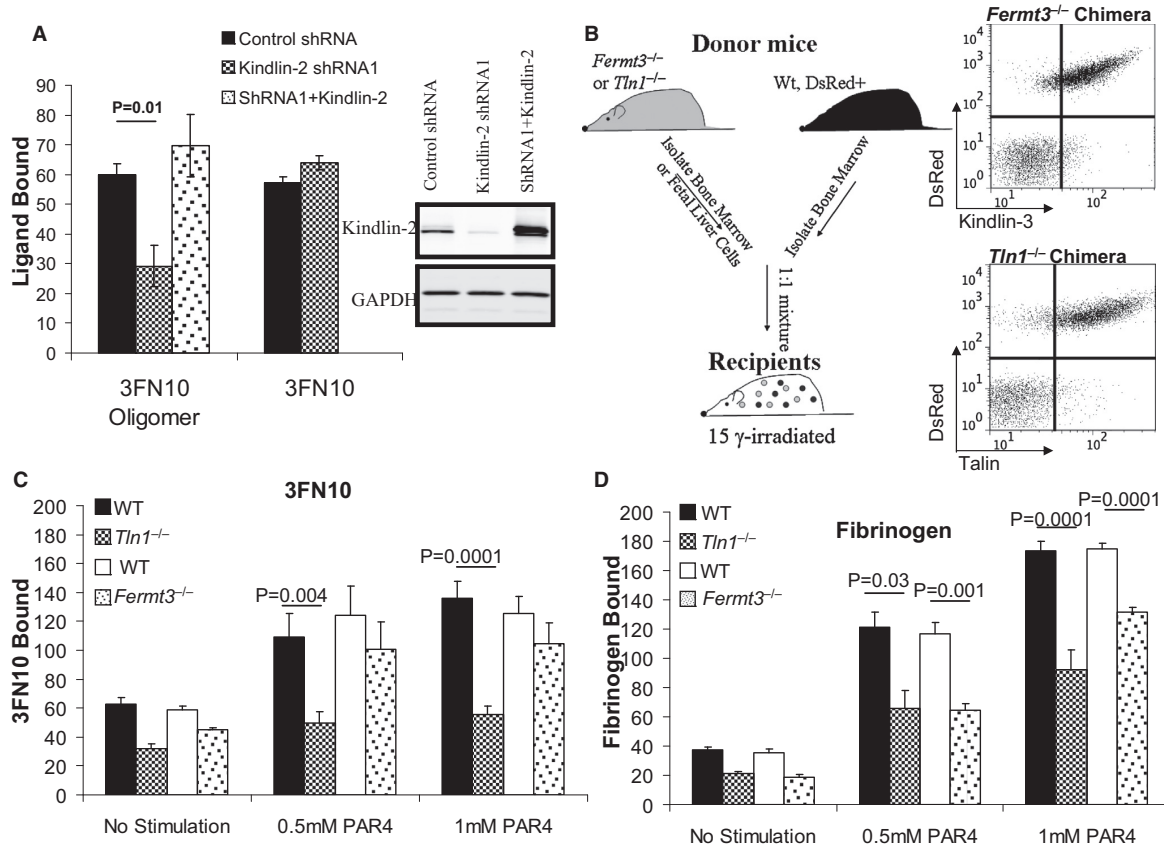

Figure 2. Depletion of Kindlins Primarily Inhibits the Binding of Multivalent Ligands to Integrin αIIbβ3 in Nucleated Cells and in Mouse Platelets

(A) Cells expressing an active αIIbβ3(D723R) mutant were transduced with lentivirus expressing a GFP marker and either a scrambled shRNA (control) or kindlin-2 shRNA1. To confirm the specificity of previously characterized kindlin-2 knockdown constructs [17], we transiently cotransfected shRNA1-transduced cells with a shRNA-resistant human kindlin-2 and tdTomato as a transfection marker (at a 50:1 ratio of kindlin-2:tomato). The cells were then harvested, and binding of anti-αIIbβ3 (D57), monomeric 3FN10 (with GST removed), or GST-3FN10 oligomers was used to measure the αIIbβ3-specific ligand binding as described in the Supplemental Information. Error bars indicate ±SEM of three independent experiments. Kindlin-2 expression level was assessed by immunoblotting as shown in the right panel. The western blot was performed with total cells, whereas the only transduced (GFP-positive) and transfected (tomato-positive) cells were analyzed for ligand binding by flow cytometry.

(B) Generation of chimeric mice as described in the Supplemental Information. For intracellular flow cytometry, platelets were fixed with 2% formaldehyde, permeabilized, and stained with rabbit anti-kindlin-3 polyclonal antibody or biotinylated anti-talin monoclonal antibody (clone 8d4). After washing, bound antibodies were detected with either FITC-anti-rabbit secondary antibody or APC-strepavidin, respectively. The dot plots show the reduced expression of kindlin-3 and talin1 in DsRed-negative *Fermt3*$^{-/-}$ and *Tln1*$^{-/-}$ platelets, respectively.

(C) PAR4-stimulated binding of 3FN10 to platelets. Platelets from irradiated mice reconstituted with mixtures of DsRed-expressing wild-type (WT) and either *Fermt3*$^{-/-}$ or *Tln1*$^{-/-}$ hematopoietic stem cells were incubated in the presence of the indicated concentration of PAR4 agonist peptide or buffer. Eptifibatide-inhibitable specific binding of 3FN10 (with GST removed) to αIIbβ3 on DsRed-negative *Fermt3*$^{-/-}$ or *Tln1*$^{-/-}$ or DsRed-positive wild-type platelets was assessed by fluorescence-activated cell sorting (FACS). Cells were separately stained with anti-CD41 (αIIb) to calculate ligand binding as described in the Supplemental Information. 3FN10 at 100 μg/ml (9.4 μM) was used. In both (C) and (D), error bars indicate SEM (seven chimeric mice for each genotype).

(D) PAR4-stimulated binding of fibrinogen to platelets. In an experiment conducted on the same day as that described in (C), 3FN10 was replaced by FITC-conjugated fibrinogen.

active αIIbβ3(D723R) mutant [26], silencing kindlin-2 inhibited the binding of oligomeric 3FN10, but it had no effect on the binding of monovalent 3FN10. This was a specific effect, as reintroducing small hairpin RNA (shRNA)-resistant kindlin-2 restored the binding of oligomeric 3FN10 (Figure 2A). Moreover, kindlin-2 depletion resulted in similar selective inhibition of oligomeric but not monomeric 3FN10 binding to an active integrin chimera expressed in CHO cells [27, 28](Figure S2A). Furthermore, adhesion of αIIbβ3-expressing CHO cells to surface-bound 3FN10, which is functionally multivalent, was reduced in kindlin-2-silenced cells (Figure S2B). Thus, kindlin-2 silencing inhibits binding of multivalent but not monovalent ligands to αIIbβ3 expressed in nucleated cells.

Kindlin-3-Deficient Platelets Are Primarily Defective in Binding to Multivalent but Not Monovalent αIIbβ3 Ligands

Next, we sought to determine how kindlins function in regulation of αIIbβ3 in platelets. Mice lacking kindlin-3 suffer embryonic and perinatal lethality, recurrent infections, and

erythrocyte defects in addition to reduced αIIbβ3 functions [8, 11, 29]. To examine the consequences of loss of kindlin-3, encoded by the *Fermt3* locus, in healthy adult mice, we reconstituted irradiated mice with kindlin-3 or talin null hematopoietic cells mixed with wild-type hematopoietic cells expressing DsRed (Figure 2B). Intracellular staining of isolated platelets indicated that kindlin-3 or talin was depleted from the respective (DsRed negative) platelet population (Figure 2B).

PAR4 thrombin receptor agonist peptide stimulated similar binding of monovalent 3FN10 to αIIbβ3 in both kindlin-3 null and wild-type platelets, whereas loss of platelet talin-1 significantly inhibited 3FN10 binding (Figure 2C). In contrast, and as expected [11, 30, 31], loss of either kindlin-3 or talin-1 impaired the binding of multivalent fibrinogen, which has at least four potential αIIbβ3 binding sites (Figure 2D). Furthermore, loss of kindlin-3 had little effect on either fibrinogen or 3FN10 binding when platelets were activated exogenously by Mn^{2+}, consistent with previous reports that Mn^{2+} can promote both affinity increase [32, 33] and integrin clustering [24, 34] (Figure S2C). Deletion of talin reduced binding of 3FN10 but not fibrinogen to Mn^{2+}-stimulated platelets (Figure S2C), suggesting that talin binding synergizes with Mn^{2+} in increasing integrin monomer affinity. At higher agonist concentration (1 mM PAR4 peptide), the defect in fibrinogen binding to kindlin-3 null platelets was even less pronounced. To better quantify this result, we examined binding of various concentrations of 3FN10 to wild-type or kindlin-3 null platelets. The binding isotherms of 3FN10 to wild-type and kindlin-3 null platelets virtually overlapped (Figures S2D and S2F), indicating that a lack of kindlin-3 does not change the affinity of 3FN10 for αIIbβ3 on activated platelets or the capacity of a thrombin receptor agonist peptide to stimulate increased binding of a monovalent ligand to αIIbβ3 (Figures S2E and S2F). Therefore, in agonist-stimulated platelets, as in nucleated cells, lack of kindlin-3 has a major effect on the binding of multivalent but not monovalent αIIbβ3 ligands, whereas lack of talin has major effects on both ligand types.

Kindlins Promote Clustering of Occupied Integrins

Integrin clustering increases binding of multivalent ligands without affecting the affinity of integrin αIIbβ3 monomers [6], suggesting that integrin clustering might account for most of kindlins' effects. We used total internal reflection fluorescence (TIRF) microscopy, an established method for studying clustering [24, 35], to measure αIIbβ3 clustering at the submicron scale. Initial cell adhesion to immobilized fibrinogen is αIIbβ3 activation independent [36, 37], possibly due to increased ligand density and altered fibrinogen conformation [38], enabling us to examine effects of kindlins independent of their effects on integrin activation per se. Silencing of kindlin-2 with two different shRNAs significantly reduced both the brightness and size of integrin puncta (Figures 3A, 3B, and 3D), even though it had little or no effect on integrin expression (Figures 3A and 3C). Furthermore, silencing of kindlin-2 by these shRNAs did not affect the distance of the plasma membrane from the substrate, since fluorescence intensity of a membrane-intercalated dye was equal in control and kindlin-2-silenced cells (Figures S3A and S3B) in TIRF images.

To assess integrin clustering at the nanoscale, we used electron microscopy to examine ventral membranes of fibrinogen-adherent αIIbβ3-expressing CHO cells [39]. In control shRNA-transduced cells, we observed numerous clusters, each containing more than five gold particles and usually less than 200 nm in size, i.e., they account for the point sources seen in the TIRF images (Figure 4A, left panel). In sharp contrast, in kindlin-2-silenced cells, gold particles were present; however, there were many fewer clusters (Figures 4A, middle panel, and 4B). The total number of gold particles was also reduced, likely reflecting an overall decreased abundance of integrins in the ventral membrane. Only occasional random gold particles were seen in irrelevant IgG-stained membranes (Figure 4A, right panel). Thus, kindlin-2 promotes the clustering of ligand-occupied αIIbβ3 at the nanoscale.

Kindlins could increase αIIbβ3 clustering either before or after ligand binding. We reasoned that in the latter case, kindlin-dependent increases in ligand binding would be prevented by fixing the cells before addition of ligand. When cells were fixed before adding ligands to αIIbβ3-expressing HEK293 cells, THD induced a near 3-fold increase in PAC1 binding, but kindlin-1 failed to synergize with THD in inducing PAC1 binding (Figure S4A). In contrast, kindlin-1 dramatically increased THD-induced PAC1 binding in cells fixed after ligand addition (Figure S4A). Furthermore, consistent with earlier reports that clustering requires occupancy of the integrin [40], when the ability of αIIbβ3 to bind ligand was blocked by a β3 Asp^{119} mutation, the integrin remained diffusely distributed as judged by TIRF microscopy (Figure S4B). Thus, the effect of kindlins on multivalent ligand binding to integrin αIIbβ3 is mediated by their capacity to promote the clustering of ligand-occupied αIIbβ3.

Discussion

These results pinpoint the locus of kindlin action in mediating integrin αIIbβ3 activation. Earlier studies in invertebrates [41, 42] and cultured cells [43, 44] showed that kindlins mediate formation of integrin-mediated adhesions and foreshadowed studies showing that kindlins regulate the capacity of integrins to bind soluble ligands [7, 8, 10, 11, 13] and to promote integrin signals that regulate the cytoskeleton [12]. Here, we found that the kindlins increase soluble ligand binding to αIIbβ3 primarily by increasing avidity for multivalent ligands due to kindlins' ability to promote clustering of ligand-occupied integrins. Our results now explain why kindlins alone have little apparent effect on soluble ligand binding to cellular integrins in the absence of talin-mediated activation and comport with the finding that kindlin-3 does not induce changes in β3 transmembrane domain topology, which induces integrin αIIbβ3 activation [45].

We utilized 3FN10 as a monovalent ligand because it binds to both murine and human αIIbβ3, and for technical ease of crosslinking. Previous studies showed that kindlin-3 overexpression increased 3FN(7–10) (seventh to tenth type III fibronectin repeats) [11] binding to integrin α5β1 in RAW 264.7 cells. In contrast to 3FN10, 3FN(7–10) contains a free cysteine [46] and two integrin binding sites, one in 3FN9 and the other in 3FN10 [47], and is thus not monovalent. In addition, there may be cell-specific, kindlin-specific, and integrin-specific mechanisms of regulation, as (1) kindlin-1 and kindlin-2 synergize with THD to activate αIIbβ3 but inhibit THD-induced α5β1 activation in CHO cells [22]; (2) overexpressed kindlin-3 is functional in RAW 264.7 cells, but not in CHO cells [11]; and (3) kindlin-3 is required for αLβ2- but not α4β1-increased cell adhesiveness under fluid shear stresses [9]. Secondary antibodies can oligomerize monovalent PAC1 Fab under

Current Biology Vol 23 No 22
2292

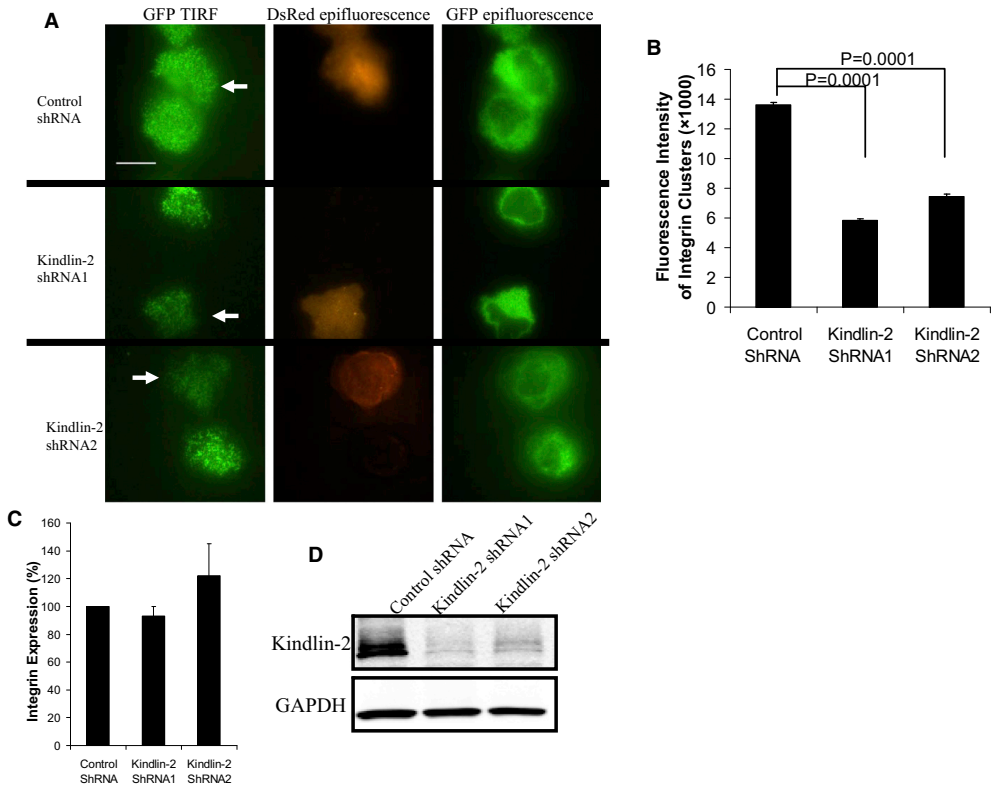

Figure 3. Kindlins Promote Clustering of Occupied Integrins

(A) Cells expressing αIIb-GFPβ3 transduced with lentivirus encoding both kindlin-2 shRNA and DsRed were mixed with uninfected cells and plated on fibrinogen-coated coverslips. The left panels are TIRF images of the distribution of αIIb-GFPβ3 at the cell-substrate interface in uninfected cells (DsRed negative) and shRNA-transduced cells (DsRed positive, white arrows). DsRed epi-illuminated fluorescence images in the middle panel indicate shRNA lentiviral transduction. GFP epi-illuminated fluorescence images in the right panels indicate comparable αIIbβ3 fluorescence in uninfected control cells and kindlin-2 shRNA-expressing cells. Scale bar represents 10 μm.

(B) Fluorescence intensities of integrin puncta were measured and averaged as described in the Supplemental Information. Error bars indicate SEM of n = 1,223, 1,204, and 1,008 puncta in uninfected cells or those transduced with kindlin-2 shRNA1 or shRNA2, respectively.

(C) Cells from the experiment depicted in (A) were stained with anti-αIIbβ3 (D57) and analyzed by FACS to assess αIIbβ3 surface expression. Data are expressed as percent of αIIbβ3 expressed in control shRNA-infected cells. Error bars indicate ±SEM of three independent experiments.

(D) DsRed-positive shRNA-transduced cells were isolated by FACS, and kindlin-2 expression was assessed by western blotting.

appropriate conditions, converting it into a multivalent ligand [19]. We formaldehyde fixed the cells before adding secondary antibody or streptavidin, as recommended by Bunch [19], to avoid potential oligomerization of the 3FN10. Indeed, when highly concentrated PAC1 Fab was used to overcome its low affinity as a monovalent ligand [19], we obtained results comparable to those using 3FN10 (Figure 1B). Thus, when secondary antibody-induced oligomerization is avoided, kindlins have little effect on the binding of an authentic monovalent ligand to integrin αIIbβ3.

Reduced soluble ligand binding alone might not account for the defective platelet aggregation and increased bleeding observed in kindlin-3 null mice and patients. The combined effects of reduced surface integrin expression [11], defective integrin clustering, and impaired integrin outside-in signaling [10–12, 43] may all make important contributions to the hemostatic defect. Similarly, the effect of kindlin-mediated clustering on avidity can be a major contributor to kindlin-3's capacity to support the function of β1 or β2 integrins that mediate increased resistance of leukocytes to detachment under flow [8, 48, 49]. Kindlin-mediated leukocyte arrest is associated with an additional conformational change in αLβ2 that can be driven by shear stress on the integrin [9, 49]. Thus, in addition to effects on soluble ligand binding, it is clear that kindlin-3 makes multiple contributions to the adhesive functions of blood cells.

Integrin-bound kindlins might promote integrin clustering by redistributing integrins between different pools, such as those on the cell surface, in storage pools, and in recycling pathways [50, 51]. Indeed, loss of kindlin-3 is associated with reduced αIIbβ3 surface expression in murine platelets by about 25% ([11] and our unpublished data), and overexpression of kindlins can increase integrin expression in a CHO cell clone [22]. Alternatively, kindlins can recruit migfilin [43] and integrin-linked kinase (ILK) [12] to occupied integrins, thereby enabling the further recruitment of actin-binding proteins such as filamins, PINCHs, and parvins [52] that could promote cooperative integrin clustering. Kindlins can also bind to

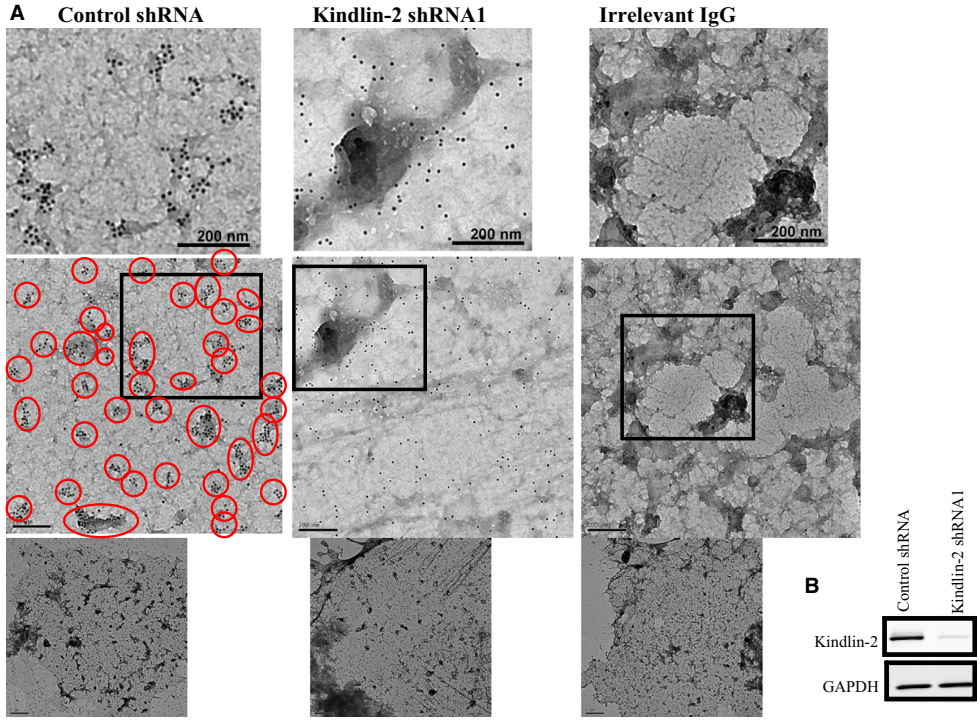

Figure 4. Loss of Kindlin-2 Reduces Clustering of αIIbβ3 Integrins

(A) Electron microscopy (EM) images of colloidal gold-labeled αIIbβ3 in adherent cell ventral membrane. CHO cells stably expressing αIIbβ3 were transduced with lentivirus expressing control shRNA or kindlin-2 shRNA1, adhered to fibrinogen-coated EM grids, swollen in a hypotonic buffer, and subjected to a flow of low-salt buffer to remove the cell body. The remaining ventral membrane sheet was stained with an anti-β3 tail antibody followed by colloidal gold adsorbed 2° antibody. Left, middle, and right columns are control shRNA cells, kindlin-2 knockdown cells, and irrelevant IgG-stained control shRNA cells at differing magnifications. Many clusters of colloidal gold containing more than five particles per cluster are present in control shRNA cells, and such clusters are absent in kindlin-2-silenced cells. Red circles indicate examples of integrin clusters. Scale bars represent 200 nm for the images in top and middle row and 2 μm for the images in bottom row. The images in the middle and lower rows are ventral membranes at different magnifications. Images in the top row show enlarged views of selected areas from those in the middle row.

(B) Cells in (A) were lysed and analyzed with anti-kindlin-2 or anti-GAPDH by western blotting.

polyphosphoinositides [53–56], thereby localizing integrins in membrane domains that might favor clustering. The present work will enable further studies to evaluate the precise roles of kindlin-binding proteins and phospholipids in the capacity of kindlins to increase clustering of integrins, thereby enhancing multivalent ligand binding.

Supplemental Information

Supplemental Information includes four figures and Supplemental Experimental Procedures and can be found with this article online at http://dx.doi.org/10.1016/j.cub.2013.09.050.

Author Contributions

F.Y. and M.H.G. conceived the project and directed the research. F.Y., B.G.P., and P.A. performed experiments. A.K.-F. and S.J.S. provided essential reagents. R.R., M.M., R.F., and C.T.L. provided kindlin-3 null mouse platelets. F.Y. and M.H.G. wrote the paper, which was edited by S.J.S. and R.F.

Acknowledgments

The Institutional Animal Care and Use Committees of the University of California, San Diego; the La Jolla Institute for Allergy & Immunology; and the Max Planck Institute of Biochemistry approved the relevant animal experiments. This work was supported by grants GM 098412 and HL 078784 from the National Institutes of Health.

Received: April 16, 2013
Revised: August 30, 2013
Accepted: September 24, 2013
Published: November 7, 2013

References

1. Haling, J.R., Monkley, S.J., Critchley, D.R., and Petrich, B.G. (2010). Talin-dependent integrin activation is required for fibrin clot retraction by platelets. Blood *117*, 1719–1722.
2. Coller, B.S., and Shattil, S.J. (2008). The GPIIb/IIIa (integrin alphaIIbbeta3) odyssey: a technology-driven saga of a receptor with twists, turns, and even a bend. Blood *112*, 3011–3025.
3. Shattil, S.J., and Newman, P.J. (2004). Integrins: dynamic scaffolds for adhesion and signaling in platelets. Blood *104*, 1606–1615.
4. Hynes, R.O. (2002). Integrins: bidirectional, allosteric signaling machines. Cell *110*, 673–687.
5. Shattil, S.J., Kim, C., and Ginsberg, M.H. (2010). The final steps of integrin activation: the end game. Nat. Rev. Mol. Cell Biol. *11*, 288–300.
6. Hato, T., Pampori, N., and Shattil, S.J. (1998). Complementary roles for receptor clustering and conformational change in the adhesive and signaling functions of integrin alphaIIb beta3. J. Cell Biol. *141*, 1685–1695.

Current Biology Vol 23 No 22
2294

7. Svensson, L., Howarth, K., McDowall, A., Patzak, I., Evans, R., Ussar, S., Moser, M., Metin, A., Fried, M., Tomlinson, I., and Hogg, N. (2009). Leukocyte adhesion deficiency-III is caused by mutations in KINDLIN3 affecting integrin activation. Nat. Med. *15*, 306–312.
8. Moser, M., Bauer, M., Schmid, S., Ruppert, R., Schmidt, S., Sixt, M., Wang, H.V., Sperandio, M., and Fässler, R. (2009). Kindlin-3 is required for beta2 integrin-mediated leukocyte adhesion to endothelial cells. Nat. Med. *15*, 300–305.
9. Manevich-Mendelson, E., Feigelson, S.W., Pasvolsky, R., Aker, M., Grabovsky, V., Shulman, Z., Kilic, S.S., Rosenthal-Allieri, M.A., Ben-Dor, S., Mory, A., et al. (2009). Loss of Kindlin-3 in LAD-III eliminates LFA-1 but not VLA-4 adhesiveness developed under shear flow conditions. Blood *114*, 2344–2353.
10. Malinin, N.L., Zhang, L., Choi, J., Ciocea, A., Razorenova, O., Ma, Y.Q., Podrez, E.A., Tosi, M., Lennon, D.P., Caplan, A.I., et al. (2009). A point mutation in KINDLIN3 ablates activation of three integrin subfamilies in humans. Nat. Med. *15*, 313–318.
11. Moser, M., Nieswandt, B., Ussar, S., Pozgajova, M., and Fässler, R. (2008). Kindlin-3 is essential for integrin activation and platelet aggregation. Nat. Med. *14*, 325–330.
12. Montanez, E., Ussar, S., Schifferer, M., Bösl, M., Zent, R., Moser, M., and Fässler, R. (2008). Kindlin-2 controls bidirectional signaling of integrins. Genes Dev. *22*, 1325–1330.
13. Ma, Y.Q., Qin, J., Wu, C., and Plow, E.F. (2008). Kindlin-2 (Mig-2): a co-activator of beta3 integrins. J. Cell Biol. *181*, 439–446.
14. Bledzka, K., Liu, J., Xu, Z., Perera, H.D., Yadav, S.P., Bialkowska, K., Qin, J., Ma, Y.Q., and Plow, E.F. (2012). Spatial coordination of kindlin-2 with talin head domain in interaction with integrin β cytoplasmic tails. J. Biol. Chem. *287*, 24585–24594.
15. Metcalf, D.G., Moore, D.T., Wu, Y., Kielec, J.M., Molnar, K., Valentine, K.G., Wand, A.J., Bennett, J.S., and DeGrado, W.F. (2010). NMR analysis of the alphaIIb beta3 cytoplasmic interaction suggests a mechanism for integrin regulation. Proc. Natl. Acad. Sci. USA *107*, 22481–22486.
16. Moser, M., Legate, K.R., Zent, R., and Fässler, R. (2009). The tail of integrins, talin, and kindlins. Science *324*, 895–899.
17. Kahner, B.N., Kato, H., Banno, A., Ginsberg, M.H., Shattil, S.J., and Ye, F. (2012). Kindlins, integrin activation and the regulation of talin recruitment to αIIbβ3. PLoS ONE *7*, e34056.
18. Ye, F., Hu, G., Taylor, D., Ratnikov, B., Bobkov, A.A., McLean, M.A., Sligar, S.G., Taylor, K.A., and Ginsberg, M.H. (2010). Recreation of the terminal events in physiological integrin activation. J. Cell Biol. *188*, 157–173.
19. Bunch, T.A. (2010). Integrin alphaIIbbeta3 activation in Chinese hamster ovary cells and platelets increases clustering rather than affinity. J. Biol. Chem. *285*, 1841–1849.
20. Painter, R.G., and Ginsberg, M. (1982). Concanavalin A induces interactions between surface glycoproteins and the platelet cytoskeleton. J. Cell Biol. *92*, 565–573.
21. Polley, M.J., Leung, L.L., Clark, F.Y., and Nachman, R.L. (1981). Thrombin-induced platelet membrane glycoprotein IIb and IIIa complex formation. An electron microscope study. J. Exp. Med. *154*, 1058–1068.
22. Harburger, D.S., Bouaouina, M., and Calderwood, D.A. (2009). Kindlin-1 and -2 directly bind the C-terminal region of beta integrin cytoplasmic tails and exert integrin-specific activation effects. J. Biol. Chem. *284*, 11485–11497.
23. Gardner, J.M., and Hynes, R.O. (1985). Interaction of fibronectin with its receptor on platelets. Cell *42*, 439–448.
24. Saltel, F., Mortier, E., Hytönen, V.P., Jacquier, M.C., Zimmermann, P., Vogel, V., Liu, W., and Wehrle-Haller, B. (2009). New PI(4,5)P2- and membrane proximal integrin-binding motifs in the talin head control beta3-integrin clustering. J. Cell Biol. *187*, 715–731.
25. He, Y., Esser, P., Schacht, V., Bruckner-Tuderman, L., and Has, C. (2011). Role of kindlin-2 in fibroblast functions: implications for wound healing. J. Invest. Dermatol. *131*, 245–256.
26. Hughes, P.E., Diaz-Gonzalez, F., Leong, L., Wu, C., McDonald, J.A., Shattil, S.J., and Ginsberg, M.H. (1996). Breaking the integrin hinge. A defined structural constraint regulates integrin signaling. J. Biol. Chem. *271*, 6571–6574.
27. Tadokoro, S., Shattil, S.J., Eto, K., Tai, V., Liddington, R.C., de Pereda, J.M., Ginsberg, M.H., and Calderwood, D.A. (2003). Talin binding to integrin beta tails: a final common step in integrin activation. Science *302*, 103–106.
28. Han, J., Lim, C.J., Watanabe, N., Soriani, A., Ratnikov, B., Calderwood, D.A., Puzon-McLaughlin, W., Lafuente, E.M., Boussiotis, V.A., Shattil, S.J., and Ginsberg, M.H. (2006). Reconstructing and deconstructing agonist-induced activation of integrin alphaIIbbeta3. Curr. Biol. *16*, 1796–1806.
29. Krüger, M., Moser, M., Ussar, S., Thievessen, I., Luber, C.A., Forner, F., Schmidt, S., Zanivan, S., Fässler, R., and Mann, M. (2008). SILAC mouse for quantitative proteomics uncovers kindlin-3 as an essential factor for red blood cell function. Cell *134*, 353–364.
30. Petrich, B.G., Marchese, P., Ruggeri, Z.M., Spiess, S., Weichert, R.A., Ye, F., Tiedt, R., Skoda, R.C., Monkley, S.J., Critchley, D.R., and Ginsberg, M.H. (2007). Talin is required for integrin-mediated platelet function in hemostasis and thrombosis. J. Exp. Med. *204*, 3103–3111.
31. Nieswandt, B., Moser, M., Pleines, I., Varga-Szabo, D., Monkley, S., Critchley, D., and Fässler, R. (2007). Loss of talin1 in platelets abrogates integrin activation, platelet aggregation, and thrombus formation in vitro and in vivo. J. Exp. Med. *204*, 3113–3118.
32. Kirchhofer, D., Gailit, J., Ruoslahti, E., Grzesiak, J., and Pierschbacher, M.D. (1990). Cation-dependent changes in the binding specificity of the platelet receptor GPIIb/IIIa. J. Biol. Chem. *265*, 18525–18530.
33. Gailit, J., and Ruoslahti, E. (1988). Regulation of the fibronectin receptor affinity by divalent cations. J. Biol. Chem. *263*, 12927–12932.
34. Cluzel, C., Saltel, F., Lussi, J., Paulhe, F., Imhof, B.A., and Wehrle-Haller, B. (2005). The mechanisms and dynamics of (alpha)v(beta)3 integrin clustering in living cells. J. Cell Biol. *171*, 383–392.
35. Yu, C.H., Law, J.B., Suryana, M., Low, H.Y., and Sheetz, M.P. (2011). Early integrin binding to Arg-Gly-Asp peptide activates actin polymerization and contractile movement that stimulates outward translocation. Proc. Natl. Acad. Sci. USA *108*, 20585–20590.
36. Coller, B.S. (1980). Interaction of normal, thrombasthenic, and Bernard-Soulier platelets with immobilized fibrinogen: defective platelet-fibrinogen interaction in thrombasthenia. Blood *55*, 169–178.
37. Blue, R., Li, J., Steinberger, J., Murcia, M., Filizola, M., and Coller, B.S. (2010). Effects of limiting extension at the alphaIIb genu on ligand binding to integrin alphaIIbbeta3. J. Biol. Chem. *285*, 17604–17613.
38. Moskowitz, K.A., Kudryk, B., and Coller, B.S. (1998). Fibrinogen coating density affects the conformation of immobilized fibrinogen: implications for platelet adhesion and spreading. Thromb. Haemost. *79*, 824–831.
39. Carroll-Portillo, A., Spendier, K., Pfeiffer, J., Griffiths, G., Li, H., Lidke, K.A., Oliver, J.M., Lidke, D.S., Thomas, J.L., Wilson, B.S., and Timlin, J.A. (2010). Formation of a mast cell synapse: Fc epsilon RI membrane dynamics upon binding mobile or immobilized ligands on surfaces. J. Immunol. *184*, 1328–1338.
40. Ylänne, J., Chen, Y., O'Toole, T.E., Loftus, J.C., Takada, Y., and Ginsberg, M.H. (1993). Distinct functions of integrin alpha and beta subunit cytoplasmic domains in cell spreading and formation of focal adhesions. J. Cell Biol. *122*, 223–233.
41. Bai, J., Binari, R., Ni, J.Q., Vijayakanthan, M., Li, H.S., and Perrimon, N. (2008). RNA interference screening in Drosophila primary cells for genes involved in muscle assembly and maintenance. Development *135*, 1439–1449.
42. Rogalski, T.M., Mullen, G.P., Gilbert, M.M., Williams, B.D., and Moerman, D.G. (2000). The UNC-112 gene in Caenorhabditis elegans encodes a novel component of cell-matrix adhesion structures required for integrin localization in the muscle cell membrane. J. Cell Biol. *150*, 253–264.
43. Tu, Y., Wu, S., Shi, X., Chen, K., and Wu, C. (2003). Migfilin and Mig-2 link focal adhesions to filamin and the actin cytoskeleton and function in cell shape modulation. Cell *113*, 37–47.
44. Kloeker, S., Major, M.B., Calderwood, D.A., Ginsberg, M.H., Jones, D.A., and Beckerle, M.C. (2004). The Kindler syndrome protein is regulated by transforming growth factor-beta and involved in integrin-mediated adhesion. J. Biol. Chem. *279*, 6824–6833.
45. Kim, C., Ye, F., Hu, X., and Ginsberg, M.H. (2012). Talin activates integrins by altering the topology of the β transmembrane domain. J. Cell Biol. *197*, 605–611.
46. Pankov, R., and Yamada, K.M. (2002). Fibronectin at a glance. J. Cell Sci. *115*, 3861–3863.
47. Bowditch, R.D., Hariharan, M., Tominna, E.F., Smith, J.W., Yamada, K.M., Getzoff, E.D., and Ginsberg, M.H. (1994). Identification of a novel integrin binding site in fibronectin. Differential utilization by beta 3 integrins. J. Biol. Chem. *269*, 10856–10863.

48. Hyduk, S.J., Rullo, J., Cano, A.P., Xiao, H., Chen, M., Moser, M., and Cybulsky, M.I. (2011). Talin-1 and kindlin-3 regulate alpha4beta1 integrin-mediated adhesion stabilization, but not G protein-coupled receptor-induced affinity upregulation. J. Immunol. *187*, 4360–4368.
49. Lefort, C.T., Rossaint, J., Moser, M., Petrich, B.G., Zarbock, A., Monkley, S.J., Critchley, D.R., Ginsberg, M.H., Fässler, R., and Ley, K. (2012). Distinct roles for talin-1 and kindlin-3 in LFA-1 extension and affinity regulation. Blood *119*, 4275–4282.
50. Margadant, C., Kreft, M., de Groot, D.J., Norman, J.C., and Sonnenberg, A. (2012). Distinct roles of talin and kindlin in regulating integrin $\alpha5\beta1$ function and trafficking. Curr. Biol. *22*, 1554–1563.
51. Böttcher, R.T., Stremmel, C., Meves, A., Meyer, H., Widmaier, M., Tseng, H.Y., and Fässler, R. (2012). Sorting nexin 17 prevents lysosomal degradation of $\beta1$ integrins by binding to the $\beta1$-integrin tail. Nat. Cell Biol. *14*, 584–592.
52. Legate, K.R., Montañez, E., Kudlacek, O., and Fässler, R. (2006). ILK, PINCH and parvin: the tIPP of integrin signalling. Nat. Rev. Mol. Cell Biol. *7*, 20–31.
53. Hart, R., Stanley, P., Chakravarty, P., and Hogg, N. (2013). The kindlin 3 pleckstrin homology domain has an essential role in lymphocyte function-associated antigen 1 (LFA-1) integrin-mediated B cell adhesion and migration. J. Biol. Chem. *288*, 14852–14862.
54. Qu, H., Tu, Y., Shi, X., Larjava, H., Saleem, M.A., Shattil, S.J., Fukuda, K., Qin, J., Kretzler, M., and Wu, C. (2011). Kindlin-2 regulates podocyte adhesion and fibronectin matrix deposition through interactions with phosphoinositides and integrins. J. Cell Sci. *124*, 879–891.
55. Perera, H.D., Ma, Y.Q., Yang, J., Hirbawi, J., Plow, E.F., and Qin, J. (2011). Membrane binding of the N-terminal ubiquitin-like domain of kindlin-2 is crucial for its regulation of integrin activation. Structure *19*, 1664–1671.
56. Liu, J., Fukuda, K., Xu, Z., Ma, Y.Q., Hirbawi, J., Mao, X., Wu, C., Plow, E.F., and Qin, J. (2011). Structural basis of phosphoinositide binding to kindlin-2 protein pleckstrin homology domain in regulating integrin activation. J. Biol. Chem. *286*, 43334–43342.

12.11 Paper 11:

Knock-down and knockout of β1-integrin in hepatocytes impairs liver regeneration through inhibition of growth factor signaling.

Knock-down and knockout of β1-integrin in hepatocytes impairs liver regeneration through inhibition of growth factor signalling

Tobias Speicher[1], Beat Siegenthaler[1], Roman L. Bogorad[2], Raphael Ruppert[3], Tobias Petzold[3], Susagna Padrissa-Altes[1], Marc Bachofner[1], Daniel G. Anderson[2,4,5], Victor Koteliansky[2], Reinhard Fässler[3], and Sabine Werner[1*]

[1]Department of Biology, Institute of Molecular Health Sciences, ETH Zürich, 8093 Zurich, Switzerland

[2]David H. Koch Institute for Integrative Cancer Research, [4]Department of Chemical Engineering, and [5]Division of Health Science Technology, Massachusetts Institute of Technology, Cambridge, MA 02139, USA

[3]Max Planck Institute of Biochemistry, Department of Molecular Medicine, 82152 Martinsried, Germany

[6]Skolkovo Institute of Science and Technology, ul. Novaya, d.100, Skolkovo 143025 Russian Federation

*Address for correspondence

Prof. Dr. Sabine Werner, Institute of Molecular Health Sciences

Department of Biology, ETH Zurich, 8093 Zurich, Switzerland

Phone: +41 44 633 3941; Fax: +41 44 633 1174

E-mail: Sabine.werner@biol.ethz.ch

Abstract

The liver has a unique regenerative capability, which involves extensive remodelling of cell-cell and cell-matrix contacts. Surprisingly, however, the roles of different integrins in liver regeneration have not been determined. Here we used Cre/loxP-mediated gene deletion or intravenous delivery of siRNA formulated into nanoparticles to efficiently ablate β1-integrin expression in hepatocytes of mice. While short-term loss of β1-integrin was not detrimental for the non-challenged liver, severe liver necrosis and reduced hepatocyte proliferation were observed after partial hepatectomy. Mechanistically, loss of β1-integrin in hepatocytes impaired the ligand-induced phosphorylation of the epidermal growth factor and hepatocyte growth factor receptors and down-stream signalling *in vitro* and *in vivo*. These results identify a crucial role and novel mechanism of action of β1-integrins in liver regeneration and demonstrate that protein depletion by nanoparticle-based delivery of specific siRNA is a powerful strategy to study gene function in the regenerating liver.

Introduction

Due to the essential functions of the liver in metabolism and compound detoxification, it is pivotal to guarantee a rapid and efficient repair of the organ after injury caused by viruses, toxins or autoimmune attacks as well as after liver transplantation or tumor surgery. The model of two-third partial hepatectomy (PH) in rodents is widely used to study the different stages of liver regeneration, including hepatocyte cell cycle entry, cell proliferation, and termination, which finally result in the restoration of the initial liver mass [1,2]. Growth factors, cytokines and their corresponding receptors control these different stages, and regulate activation, proliferation and survival of liver cells during the regeneration process [3]. Although hepatocytes express multiple adhesion molecules including integrins, surprisingly little is known about their roles in liver regeneration.

Integrins form a large family of transmembrane cell surface receptors, comprising 18 α and 8 β subunits that assemble into 24 non-covalently associated heterodimers with distinct, but overlapping specificities for ligands [4]. Besides their role in cell anchorage via cell-cell and cell-matrix interactions, integrins assemble large signalling hubs that control cell survival, proliferation, differentiation, and migration in normal, injured and cancerous tissues [4-6]. The β1-integrin subunit (Itgb1) associates with at least 10 α subunits, giving rise to the largest integrin subfamily [4]. Interestingly, gene expression profiling revealed that various genes involved in the integrin signalling pathway were regulated during rat liver regeneration [7]. This is obviously of functional relevance, since liver-specific ablation of integrin linked kinase (ILK) interfered with the proper termination of liver regeneration, resulting in enlarged livers after PH [8]. However, the role of individual integrin subunits in liver regeneration has not been determined and their mechanisms of action in the normal and regenerating liver remain to be investigated.

In this study we used a dual approach to study the role of Itgb1 in liver regeneration – inducible Cre/loxP-mediated gene deletion and siRNA-mediated knock-down in hepatocytes *in vivo*. The use of genetically modified mice with gain- or loss-of-function of individual genes is the gold standard to study the involvement of proteins in a biological process *in vivo*. Their use for liver regeneration studies identified the contribution of growth factors and their corresponding receptors to this process. Of particular importance are the hepatocyte growth factor (HGF) receptor c-Met and the epidermal growth factor receptor (EGFR). Inducible deletion of *c-Met* in the liver resulted in reduced hepatocyte proliferation and concomitant impairment of liver regeneration [9]. Constitutive hepatocyte-specific knockout of *c-Met* caused severe liver necrosis after PH and reduced the survival of the animals [10]. Mice lacking the EGFR in the liver showed increased mortality, liver cell damage and reduced hepatocye proliferation resulting from a defective entry into the G1-S phase of the cell cycle [11].

Considerable effort has been directed towards developing effective delivery systems for siRNAs *in vivo* [12-14]. Plasmid-based expression of short hairpin (sh) RNA has been used to study the role(s) of HGF/c-Met and EGFR during liver regeneration in rats [15,16], and stable delivery of pools of shRNAs into mouse livers lead to the identification of the kinase MKK4 as a major regulator of liver regeneration [17]. Additional siRNA delivery systems were invented to improve tissue specificity and low-dose efficacy. In particular, lipid nanoparticle formulations were developed, which efficiently and predominantly delivered siRNA to the liver and allowed knock-down of several genes simultaneously after a single injection of multiple siRNAs [18-20]. Therefore, we used this powerful strategy in combination with a knockout approach to determine the outcome of the loss of β1-integrin in hepatocytes for liver regeneration after PH.

Results

Generation of mice lacking Itgb1 in the liver

Mice with floxed *Itgb1* alleles (Itgb1$^{f/f}$ mice) [21] were mated with MxCre mice, in which Cre expression can be induced by 2 injections of poly-IC with a 2-day interval. This has been shown to result in complete deletion of floxed alleles in the liver and to almost complete deletion in the spleen. By contrast, deletion in other tissues is much less efficient or even absent [22]. The double transgenic progeny was designated Itgb1$^{f/f}$/MxCre mice [23,24]. Mice were injected twice with a 2-day interval with Poly-IC. Already 14 days after the last poly-IC injection, the *Itgb1* alleles were efficiently deleted in the liver of Itgb1$^{f/f}$/MxCre mice as shown by staining for β-galactosidase (β-gal), whose expression is induced upon deletion of the floxed allele [21] (Fig. 1A). No staining was seen in the intestine where recombination had not occurred (Fig. 1B). As expected, a strong reduction in the levels of *Itgb1* mRNA was also seen in the spleen, although to a much lesser extent than in the liver. No reduction was seen in the lung (Fig. 1C). Immunofluorescence staining verified the efficient gene knockout in hepatocytes, whereas PECAM-1 positive endothelial cells were still Itgb1 positive (Fig. 1D,E). In addition, co-staining for Itgb1 and F4/80 or α smooth muscle actin (α-SMA) showed that Kupffer cells and stellate cells also remained Itgb1 positive (Fig. 1F, Suppl. Fig. S1A). Therefore, Mx-Cre-mediated loss of Itgb1 was obviously restricted to hepatocytes. Poly-IC-injected Itgb1$^{f/f}$/MxCre mice did not show obvious health impairments, and a histological analysis of liver tissue showed no gross morphological abnormalities during the first 4 weeks after *Itgb1* deletion (Supplementary Fig. S2A). Furthermore, there were no obvious vascular abnormalities as shown by PECAM-1 staining (Supplementary Fig. S2B). However, despite the normal liver morphology, serum activities of aspartate aminotransferase (AST), alanine aminotransferase (ALT), and lactate dehydrogenase (LDH),

and serum concentrations of bilirubin were increased 14 days after poly-IC injection, indicating initiation of liver damage by knockout of Itgb1 (Supplementary Fig. S2C). By contrast, albumin levels were not affected, suggesting that liver function is not severely compromised (Supplementary Fig. S2C). In line with these findings, all animals survived the observation period.

Itgb1 is required for liver regeneration and survival after PH

Fourteen days after the second poly-IC injection mice were subjected to PH. Our complete treatment scheme, shown schematically in Fig. 2A, caused 47% lethality of Itgb1$^{f/f}$/MxCre mice, but only 7% lethality in control mice within 24-48 hours after PH (Fig. 2B). Since all Itgb1$^{f/f}$/MxCre mice survived the first 24h after surgery, we conclude that a defect in the onset of regeneration and/or metabolic abnormalities rather than acute surgical complications caused the death of the animals.

The liver-to-body-weight ratio was not significantly different between Itgb1$^{f/f}$/MxCre and control mice at 48h after surgery (Fig. 2C). However, we detected a further increase in the activities of ALT, AST, and LDH, enhanced levels of bilirubin, and reduced levels of albumin in the serum of Itgb1$^{f/f}$/MxCre mice 48h after PH, indicating liver damage and impaired liver function (Fig. 2D). Indeed, Itgb1$^{f/f}$/MxCre mice displayed severe liver necrosis 48h after PH (Fig. 2E), which was accompanied by enhanced infiltration of neutrophils (Fig. 1F). The number of apoptotic cells as determined by TUNEL staining (Fig.1G) or staining for cleaved caspase-3 (Supplementary Fig. S2D) was also increased, while the hyperproliferation of hepatocytes that occurred in control mice 48h after PH was strongly reduced in Itgb1$^{f/f}$/MxCre mice (Fig. 1H). Since Poly-IC-induced expression of Cre recombinase also occurs in haematopoietic cells, we generated bone marrow chimeric mice by transplanting

Itgb1$^{f/f}$/MxCre bone marrow into γ-irradiated wild-type mice, and we subsequently induced *Itgb1* deletion in blood cells. Successful transfer of bone marrow and poly-IC-induced knockout after complete engraftment of the recipient mice was verified by the detection of β-galactosidase activity in platelets of bone marrow chimeric mice (Supplementary Fig. S3A). None of the animals showed tissue damage 48h after PH (Supplementary Fig. S3B), indicating that loss of Itgb1 in haematopoietic cells is not the primary reason for the regeneration defect of poly-IC-treated Itgb1$^{f/f}$/MxCre mice. Rather, the regeneration defect in Itgb1$^{f/f}$/MxCre mice results from loss of Itgb1 in hepatocytes.

Knock-down of *Itgb1* in hepatocytes *in vivo*

To further verify the importance of *Itgb1* in hepatocytes for liver regeneration after PH and to compare the outcome after genetic knockout with siRNA-mediated knock-down in hepatocytes *in vivo*, we used lipid-based nanoparticles to deliver *Itgb1* siRNA, which had been optimized for liver specific targeting [19]. A single injection of *Itgb1* siRNA reduced *Itgb1* mRNA levels by more than 85% in comparison to a mock injection with luciferase *(Luc)* siRNA. Importantly, the knock-down was maintained for more than 10 days after a single injection of siRNA (see Bogorad *et al.,* submitted). As a consequence of the *Itgb1* knock-down, adhesion of isolated hepatoctytes on collagen was strongly reduced (Bogorad et al., submitted).

To ensure a prolonged and efficient strong knock-down, we injected siRNA twice within a five day interval. Five days after the last injection the animals were subjected to PH as shown schematically in Fig. 3A. At the time of surgery, the liver tissue showed a more than 90% reduction in *Itgb1* mRNA levels (Fig. 3B). Western blotting revealed an siRNA-mediated reduction of Itgb1 protein in total liver lysates, and a complete loss of Itgb1 protein in

purified primary hepatocytes, indicating that the residual Itgb1 detected in total liver results from expression in non-parenchymal liver cells, which were apparently not efficiently targeted by the nanoparticles (Fig. 3C). Itgb1 immunostaining of the tissue removed during surgery and 48h after PH confirmed the knock-down in hepatocytes (Fig. 3D), while co-staining of Itgb1 with PECAM-1, α-SMA, or F4/80 revealed that endothelial cells, stellate cells and Kupffer cells were still Itgb1 positive (Supplementary Fig. S4A-C).

Consistent with previous findings demonstrating that more than 90% of injected siRNA-loaded lipid nanoparticles accumulated in the liver [25], no reduction in the mRNA levels of *Itgb1* was observed in the lung, kidney, and heart (Supplementary Fig. S5A) or in the adipose tissue (Bogorad et al., submitted). Spleen was the only tissue in which siRNA-loaded nanoparticles reduced *Itgb1* mRNA levels by around 50% (Supplementary Fig.S5A). We assume that the Itgb1 reduction in spleen is unlikely causing phenotypic abnormalities, since a constitutive heterozygous deletion of the *Itgb1* gene in mice lead to no apparent defects [26], and since loss of Itgb1 in haematopoietic cells did not affect the normal liver or the regeneration process after PH (see above).

The siRNA treatment neither induced the expression of interferon γ mRNA under our experimental conditions, nor histological or vascular abnormalities in the liver at day 5 after the second siRNA injection (Supplementary Fig. S5B,C). In contrast to the knockout mice, serum parameters remained normal upon *Itgb1* knock-down (Supplementary Fig. S5D), and all animals survived the observation period.

siRNA-mediated *Itgb1* knock-down leads to a mild regeneration defect

In contrast to Itgb1$^{f/f}$/MxCre mice, the survival of *Itgb1* knock-down animals was not reduced 48h after PH (Fig. 3E). Surprisingly, the animals even showed an increase in liver-to-

body-weight ratio compared to control animals (Fig. 3F). At the histological level, however, we found similar abnormalities in *Itgb1* knock-down and knockout animals, including severe necrotic tissue damage, concomitant neutrophil infiltration (Fig. 3G,H), and reduced proliferation (Fig. 2I). The latter defect in combination with the increased liver/body weight ratio suggested hypertrophy of hepatocytes, and this was indeed confirmed by analysis of cell size upon staining of the actin cytoskeleton (Supplementary Fig. S6A).

To test if the liver necrosis that we observed after PH in mice with Itgb1 knockout or knock-down was due to enhanced sensitivity to the anaesthetic and/or analgesic compounds that we used during PH, we treated Itgb1$^{f/f}$/MxCre mice, Itgb1 knock-down mice, and the corresponding control mice with isoflurane and buprenorphine, similar to the treatment used for PH. 48h later mice were sacrificed, livers were analyzed by H/E staining, and transaminase activities were measured in the serum. Importantly, neither knockout nor knock-down animals showed treatment-induced liver damage (Supplementary Fig. S6B,C). Transaminase activities of Itgb1$^{f/f}$/MxCre mice treated with isoflurane and morphine were in the same range as in untreated Itgb1$^{f/f}$/MxCre mice (Supplementary Fig. S2C).

Due to the better health status of the knock-down compared to the knockout mice and their survival post 48h PH, we were able to analyze later stages of the regeneration process. Therefore, we next analyzed the effect of *Itgb1* knock-down 5d after PH. The lasting knock-down at the 5-day time point was confirmed by qRT-PCR (Fig. 4A) and immunofluorescence staining (Fig. 4B). We also analyzed an early time point (6h after PH) and found no tissue damage in animals treated with siRNA either against luciferase or Itgb1 (Fig. 4C). Five days post PH we still observed some necrotic tissue in the *Itgb1* knock-down animals (Fig. 4C), but to a much lesser extent than 48 post PH (Fig. 3G). Proliferation of hepatocytes had declined to almost basal levels in knock-down and control mice, and the liver-to-body-

weight was also similar at this late time point, demonstrating that regeneration can occur under these conditions (Fig. 4D,E). Since we observed a uniform knock-down of Itgb1 even 5 days after PH, it seems unlikely that cells with inefficient knock-down preferentially contributed to regeneration. Taken together, these data reveal that Itgb1 knock-down impairs liver regeneration, but does not prevent it.

Itgb1 controls c-Met and EGFR activation

Since EGFR ligands and HGF are major mitogens for hepatocytes in the regenerating liver [1,3] and since mice lacking EGFR or the HGFR c-Met in the liver revealed similar regeneration abnormalities as the Itgb1$^{f/f}$/MxCre and *Itgb1* knock-down mice [9-11], we tested a possible involvement of impaired EGFR and/or c-Met signalling in the proliferation and survival defect of Itgb1-deficient hepatocytes. Levels of phosphorylated c-Met (Tyr1003) and EGFR (Tyr1068) were indeed reduced in *Itgb1* knockout animals 0h and 48h post PH (Fig. 5A), and reduced phosphorylation of EGFR was also observed in mice with *Itgb1* knock-down 48h after PH (Fig 5B). Levels of total and phosphorylated focal adhesion kinase (FAK), a major relay of integrin signalling, were not affected by loss of Itgb1 (Fig. 5A).

To test if Itgb1 directly controls hepatic EGFR signalling, we injected EGF intraperitoneally into mice with *Itgb1* knockout or knock-down and analyzed EGFR activation. 15 min after EGF injection we observed strong phosphorylation of the EGFR in control animals, but not in knockout animals (Fig. 6A). *Itgb1* knock-down mice showed increased levels of phosphorylated EGFR in unstimulated conditions, which, however, only mildly increased upon EGF injection (Fig. 6B). To determine if the inhibition of EGFR and c-Met signalling upon loss of Itgb1 is a cell autonomous effect, primary hepatocytes were cultured after siRNA-mediated knock-down *in vivo*. Efficient knock-down of Itgb1 in cultured hepatocytes

was confirmed by immunostaining and western blotting (Fig. 6C,D). Interestingly, EGF-induced EGFR phosphorylation was also abolished in cultured hepatocytes with *Itgb1* knock-down (Fig. 6D). In contrast to the *in vivo* situation, basal levels of pEGFR were not increased upon *Itgb1* knock-down *in vitro*, indicating that the enhanced levels *in vivo* result from cell types other than hepatocytes. Concomitant with the impaired receptor phosphorylation, EGF-induced phosphorylation of Erk was strongly reduced and phosphorylation of Akt was abolished in cultured *Itgb1* knock-down hepatocytes (Fig 6D). HGF-induced phosphorylation of c-Met and Erk1/2 activation were also impaired in *Itgb1* knock-down hepatocytes (Fig. 6E). In addition, internalization of fluorophor-labelled EGF was significantly diminished (Fig. 6F). Taken together, these findings demonstrate that loss of Itgb1 impaired EGFR and c-Met phosphorylation, EGFR internalization, and activation of mitogenic signalling pathways downstream of EGFR and c-Met. These abnormalities in growth factor signalling provide a plausible explanation for the impaired hepatocyte proliferation in the *Itgb1* knock-down and knockout mice.

Discussion

In this study we demonstrate (i) that β1-integrins in hepatocytes are essential for liver regeneration, (ii) that they execute the regeneration promoting function by cooperating with growth factor signalling, and (iii) that siRNA-mediated knock-down in hepatocytes is a potent strategy to study gene function in the regenerating liver *in vivo*.

The generation of knockout mice guarantees a complete loss of a protein, but it is time- and cost-intensive, and permits to delete only a few genes in a mouse. Furthermore, many abnormalities in humans do not result from a complete loss of a gene, but rather from reduced levels of (a) protein(s). Therefore, a knock-down approach can sometimes reflect more closely the situation that occurs in human diseases. In this study we describe the first phenotypic comparison of a genetic knockout with siRNA-mediated knock-down *in vivo* in a tissue regeneration model within one species. The similar phenotypes that we observed in knock-down and knockout mice highlight the usefulness of the siRNA approach. The slightly milder phenotype of the knock-down animals prevented the lethality associated with the knockout and thus allowed us to extend mechanistic studies.

We chose to deplete Itgb1, since there is as yet little information on the role of individual integrins in liver regeneration. This is surprising, given their high expression level on hepatocytes and the extensive matrix remodelling that occurs early after PH, which was suggested to promote the onset of hepatocyte proliferation [27,28]. However, the consequences of the loss of individual integrin subunits for liver regeneration had previously not been determined. Our results revealed that complete loss of Itgb1 using the loxP/Cre approach still enabled liver homeostasis for a limited period of time, but was detrimental

for liver regeneration as reflected by the strongly enhanced lethality observed between 24 and 48h after PH in knockout mice. As the underlying mechanism we identified severe liver necrosis and strongly impaired hepatocyte proliferation. This defect was recapitulated after *Itgb1* knock-down, although without lethality. This difference is not surprising, since – in contrast to a knockout – a knock-down approach never leads to a complete loss of the expression of a gene. Thus, very low levels of Itgb1 in hepatocytes already prevent lethality. It is also possible that remnants of type I interferons induced by the poly-IC treatment represent a further challenge for the liver, resulting in more severe liver damage in *Itgb1* knockout mice.

Although neither the knockout nor the knock-down approach that we used resulted in specific deletion of Itgb1 in hepatocytes, several results obtained in this study strongly suggest that the loss of Itgb1 in these cells is responsible for the phenotype: (1) Liver was the only tissue where an efficient knockout and knock-down was achieved, (2) co-stainings of liver sections for Itgb1 and cell-type specific markers revealed that hepatic endothelial cells, stellate cells and Kupffer cells retained Itgb1 expression in the knockout and knock-down mice, (3) loss of Itgb1 in haematopoietic cells did not affect liver regeneration, and (4) the impairment in growth factor signalling in the absence of Itgb1 was observed in cultured primary hepatocytes, demonstrating that this is a cell autonomous effect. Finally, the data presented in the accompanying manuscript demonstrate that loss of Itgb1 in hepatoma cells alone is sufficient to inhibit liver tumorigenesis (Bogorad et al., submitted).

Integrins assemble a large number of signalling and adaptor proteins at the adhesion site, which transduce integrin signals to various subcellular compartments. Integrin-linked kinase

(ILK) is a major adaptor that directly binds the β1-integrin tail and plays essential roles in integrin-mediated actin reorganization and growth factor signalling. Therefore, it was unexpected that our phenotype markedly differed from the abnormalities observed in mice lacking ILK in hepatocytes [8]. The only similarities were the enhanced liver/body weight ratio, which was, however, much more pronounced in the ILK-deficient mice. By contrast, hepatocyte-specific *Ilk* gene disruption in mice resulted in excessive rather than delayed/impaired regeneration through sustained hepatocyte proliferation and inappropriate termination of the PH-induced regeneration process. This resulted in severe liver enlargement [8]. Our data suggest that Itgb1 controls negative regulators, such as ILK, as well as positive regulators, and the latter seem to dominate during liver regeneration in our mouse models.

The liver regeneration phenotype that we observed in *Itgb1* knock-down and knockout mice is remarkably reminiscent of the abnormalities seen in mice lacking c-Met or EGFR in hepatocytes, suggesting that Itgb1 signalling is required for signalling by these receptors. This hypothesis is strongly supported by several results obtained in this study: (i) Levels of phosphorylated EGFR and c-Met were reduced after knockout or knock-down of *Itgb1* in hepatocytes in the regenerating liver, (ii) EGF-induced receptor phosphorylation was diminished after knockout or knock-down of *Itgb1* in hepatocytes *in vivo*, (iii) EGF- and HGF-induced receptor phosphorylation and subsequent Erk1/2 activation were decreased in primary hepatocytes after *Itgb1* knock-down, and (iv) EGF internalization was reduced after *Itgb1* knock-down in primary hepatocytes. Taken together, these data strongly suggest that loss of Itgb1 in hepatocytes impairs EGFR and c-Met activation on the cell surface and/or after internalization on endosomes, resulting in attenuated intracellular signalling. These

results are consistent with previous findings that demonstrated the importance of integrins for EGFR activation and signalling, whereby the interaction can occur at various levels [28-30]. For example, it has been reported that integrin-mediated EGFR phosphorylation may occur in the absence of EGF [31], and that *Itgb1* knock-down affects EGFR signalling and subsequent cell proliferation in human lung cancer cells through impairment of EGFR turnover at the cell membrane [32]. However, an effect of integrins on ligand-induced phosphorylation of EGFR and the subsequent receptor internalization as shown in our study has not been demonstrated yet. Most importantly, loss of Itgb1 not only affected the EGFR, but also c-Met, a second key player in liver regeneration. Therefore, our findings unravel a more general role of Itgb1 in the growth factor receptor signalling cross-talk in hepatocytes.

The impaired EGFR and c-Met signalling provides an obvious explanation for the proliferation defect that we observed in *Itgb1* knockout and knock-down mice. This hypothesis is further supported by the similar regeneration abnormalities of mice lacking EGFR or c-Met in the liver, which also suffered from delayed proliferation and enhanced necrosis, resulting in increased mortality after PH [9-11]. The extensive necrosis and apoptosis is most likely a consequence of the failure to restore the liver mass required for efficient detoxification of exogenous and endogenous compounds. In addition, the loss of the pro-survival activity of the Itgb1/EGFR/c-Met axis may further contribute to the phenotype as suggested by the reduced EGF-mediated activation Akt in the absence of Itgb1. These results highlight the importance of the cross-talk between growth factor and integrin signalling and suggest that proper activation of growth factor receptors is a major role of integrins in regenerating tissues.

Methods

Animals

Mouse maintenance and experiments had been approved by the local veterinary authorities (Kantonales Veterinäramt Zürich or Regierung von Oberbayern, respectively). The animals were free of pathogens, including mouse hepatitis virus. Mice with floxed *Itgb1* alleles [21] were mated with MxCre mice [22], which allow activation of Cre recombinase upon treatment with poly-IC. Single and double mutant mice were injected intraperitoneally (i.p.) twice with poly-IC (250mg/animal poly-IC, Amersham Biosciences, Piscataway, NJ) with a time interval of 2 days. After additional 14 days mice were used for experiments.

siRNA-mediated knockdown

The following siRNAs were used:

Itgb1	Sense 5'-AGAuGAGGuucAAuuuGAAdTsdT-3'
	Antisense 5'-UUcAAAUUGAACCUcAUCUdTsdT-3'
control	Sense 5'-cuuAcGcuGAGuAcuucGAdTsdT-3'
	Antisense 5'-UCGAAGuACUcAGCGuAAGdTsdT-3'

2'-OMe modified nucleotides are in lower case, and phosphorothioate linkages are indicated by 's'. siRNAs were formulated in lipid nanoparticles (C12-200 lipoids) [19]. Seven week-old C57BL/6 male mice received formulated siRNA directed against luciferase or Itgb1 (0.5mg/kg) via tail vein injection in a volume of 5ml/kg body weight at day 1 and day 5. At day 10, the knock-down efficiency was determined in the liver tissue that was removed during PH (0h time point).

Generation of bone marrow chimeric mice

Bone marrow chimeras were generated by injecting $6x10^6$ bone marrow cells from Itgb1$^{f/f}$/MxCre mice into the tail vein of lethally irradiated 8 week-old C57BL/6 mice [33]. Six weeks after bone marrow transfer, Cre expression in the haematopoietic system was induced by poly-IC as described above.

Partial hepatectomy

Eight- to ten-week-old male mice, which received food and water *ad libitum* before surgery, were anaesthetized by inhalation of isoflurane (2%). PH was performed in the morning between 8 and 12 a.m. as previously described [34]. After surgery, mice were injected with buprenorphine for analgesia (Temgesic; Essex Chemie AG, Luzern, Switzerland; 0.1mg/kg of body weight). They were euthanized by CO_2 inhalation, and the remaining liver was harvested at different time points after PH for further analysis.

Histology and histomorphometry

Liver samples were fixed in 4% paraformaldehyde (PFA) in PBS or in 95% ethanol/1% acetic acid and embedded in paraffin. Sections (3.5µm) were stained with haematoxylin/eosin (H&E) and photographed (3–5 pictures per animal); the necrotic area was determined morphometrically. For the identification of cell size, unfixed cryosections (10µm) were fixed in 4% PFA/PBS and permeabilized for 5min in 0.1% Triton-X100 in PBS. Unspecific binding sites were then blocked with 3% BSA/PBS for 30 min at RT. Rhodamine-coupled phalloidin (Life Technologies, Carlsbad, CA) was applied to stain the actin cytoskeleton and incubated overnight at 4°C. Nuclei were counterstained with 4',6-diamidino-2-phenylindole (DAPI). Sections were mounted with Mowiol.

Identification of proliferating cells

Proliferating cells were identified by 5-bromo-2`-deoxyuridine (BrdU) labelling 2h before livers were harvested and subsequent staining of sections with a BrdU antibody [35]. BrdU positive cells were counted in 4 independent microscopic fields (200x magnification) per animal.

Terminal dUTP nick-end Labeling (TUNEL)

The *In Situ Cell Death Detection Kit* (Roche, Basel, Switzerland) was used for the detection of apoptotic cells.

LacZ staining and activity assay

Non-fixed cryo-sections (10μm) were stained with lacZ for detection of β-galactosidase activity [29]. For detection of β-galactosidase activity in platelets, lysates were incubated at 37°C in assay buffer overnight and absorbance was monitored photometrically at 420 nm.

Serum collection and analysis

Mice were euthanized by CO_2 inhalation, and blood was taken by heart punctuation. After coagulation, serum was harvested and snap-frozen. It was analyzed using a Cobas Integra 400 Chemistry Analyzer (GMI, Ramsey, MN) and the corresponding reagents (Roche).

Injection of EGF into mice

Murine EGF (Peprotech, Rocky Hill, NJ; 0.05mg/kg body weight in 0.1% BSA in isotonic saline) was injected i.p. into mice.

Establishment and growth factor treatment of primary mouse hepatocytes

Murine hepatocytes were isolated as described [36], plated on 6-well dishes coated with collagen R (Serva, Heidelberg, Germany; 0.2mg/mL) in RPMI medium at a density of 4 x

10^5 cells/well, and left to adhere for 3h. The medium was changed to remove non-attached cells, and after 30min 10ng/ml murine EGF or HGF were added. Cells were lysed at different time points after growth factor addition and analyzed by western blotting.

EGF internalization

Internalization of EGF was determined as previously described [37]. Briefly, after adherence of hepatocytes for 3h, the medium was replaced by ice-cold medium containing 10ng/ml fluorescein-conjugated EGF (Life Technologies) and incubated for 30min to allow efficient ligand binding. Cells were washed with ice-cold PBS, prewarmed RPMI was added, and plates were incubated at 37°C for 5min to adjust the temperature. Internalization was stopped at different time points by placing samples on ice and washing for 5min with 0.2M acetic acid, 500mM NaCl, pH2.8. Cells were then washed with ice-cold PBS, scraped off the dish, transferred into tubes in 1% PFA, 110mM glucose, 50mM sodium acide in PBS, and fixed for 20min. After centrifugation, they were resuspended in 2.5mM EDTA, 0.1% BSA, 15mM sodium acide in PBS and analyzed by FACS using FloJo software (TreeStar Inc., Ashland, OR).

Identification of neutrophils by immunohistochemistry

Paraffin sections of tissue fixed with 95% ethanol/1% acetic acid were incubated for 30min in 12% BSA in PBS/0.025% NP-40 to block unspecific binding sites. The primary antibody (anti-Ly6G; BD Pharmingen, Allschwil, Switzerland) was diluted in blocking buffer and incubated overnight at 4°C. Sections were stained using the ABC Vectastain Peroxidase Kit (Vector Laboratories, Burlingame, CA) according to the manufacturer`s protocol, counterstained with haematoxylin, rehydrated, and mounted.

Detection of Itgb1 by immunofluorescence

Unfixed cryosections (10µm) were dried 30min at RT, fixed for 20min at RT in 4% PFA/PBS, permeabilized for 5 min in 0.1% Triton-X100 in PBS, and unspecific binding sites were blocked in 3% BSA/PBS for 30min at RT. A rat monoclonal antibody against Itgb1 (Millipore, Zug, Switzerland), was applied and incubated overnight at 4°C. Sections were incubated with Cy3-conjugated secondary antibody (Jackson ImmunoResearch Laboratories, West Grove, PA) diluted in 3%BSA/PBS and Hoechst (Molecular Probes, Basel, Switzerland) to counterstain the nuclei, and mounted with Mowiol.

Co-immunofluorescence staining of Itgb1 and F4/80

Unfixed cryosections (10µm) were equilibrated at RT, fixed for 10min in -20°C cold acetone, dried on air and rehydrated with PBS. After blocking for 1h with Dako blocking solution, primary antibodies were applied for 1h (rat monoclonal Itgb1 antibody labeled with DyLight647 and F4/80 (BM8, Biolegend, San Diego, CA) conjugated with Alexa488). Nuclei were counterstained with Hoechst. Images were taken using a Zeiss LSM 700 laser scanning confocal microscope.

Co-immunofluorescence staining of Itgb1 and α-SMA or PECAM-1

Unfixed cryosections (10µm) were dried 30min at RT, fixed for 5min at 4°C in methanol, permeabilized for 5min on ice in 0.1% Triton-X100/PBS, washed once in PBS and unspecific binding sites were blocked in 0.7% fish gelatin, 3% BSA, donkey serum 1:20 in PBS for 2h at RT. After washing in PBS the primary antibodies anti-Itgb1 (Cell Signaling, Danvers, MA) and anti-α-SMA-Cy3 (Sigma, Buchs, Switzerland) or anti-PECAM-1 (Milipore, Zug, Switzerland)

were applied overnight at 4°C. After washing, anti-rat-Alexa 488 (Jackson), anti-hamster-Cy3 and Hoechst were applied for 1h at RT. After washing in PBS the samples were mounted.

Staining for cleaved caspase-3

Unfixed cryosections (10µm) were dried 30min at RT, fixed for 15min at 4°C in methanol, washed once in PBS and unspecific binding sites were blocked in 3% BSA/PBS. After washing in PBS, anti-cleaved caspase-3 antibody (Cell Signaling) was applied overnight at 4°C. After washing in PBS, anti-rabbit-Cy3 antibody (Jackson) and Hoechst (Molecular Probes) were applied for 1h at RT, followed by washing in PBS and mounting.

RNA isolation and qRT–PCR analysis

Total cellular RNA was isolated from liver tissue as described [38], including a DNase digest (Promega, Dübendorf, Switzerland). cDNA synthesis and qRT-PCR were carried out as described previously [34]. The following primers were used: *Gapdh*: 5'-TCG TGG ATC TGA CGT GCC GCC TG-3` and 5`- CAC CAC CCT GTT GCT GTA GCC GTA T-3`; Itgb1 5'- ATG CCA AAT CTT GCG GAG AAT-3 and 5'- TTT GCT GCG ATT GGT GAC ATT-3`.

Preparation of protein lysates and Western blot analysis

Frozen tissue was homogenized in T-PER tissue protein extraction reagent (Pierce, Rockford, IL) containing Complete Protease Inhibitor Cocktail and PhosSTOP Phosphatase Inhibitor Cocktail (Roche). Lysates were cleared by sonication and centrifugation (13 000rpm, 30min, 4°C), snap frozen, and stored at -80°C. The protein concentration was determined using the BCA Protein assay (Pierce). Proteins were separated by SDS-PAGE and transferred onto nitrocellulose membranes. The following antibodies were used: anti-P-ERK1/2, anti-total

ERK1/2, anti-P-FAK Y379 (Life Technologies), anti-total FAK (BD Biosciences, San Jose, CA), anti-P-EGFR (Tyr1068), anti-Itgb1 (all from Cell Signaling), anti-P-FAK (Tyr379), anti-total EGFR, anti-total c-Met (all from Santa Cruz, Santa Cruz, CA), anti-GAPDH (HyTest, Turku, Finland), anti-P-c-Met, (Tyr 1003) (Sigma), and anti-ASGPR2 (Abcam, Cambridge UK).

Statistical analysis

Statistical analysis was performed using the Prism4 software (GraphPad Software Inc, San Diego, CA). Quantitative data are expressed as mean ± SEM. Significance was calculated with the Mann–Whitney *U* test; **P* ≤0.05, ***P* ≤0.01, and ****P* ≤0.001.

Acknowledgements

We thank Dr. Katharina Birkner for help with the animal experiments, Dr. Satya Kuchimanchi and Dr. Lubomir Nechev for synthesis of siRNAs, Dr. Brian Bettencourt for design of siRNA, and Dr. Akin Akinc for help with the siRNA formulation. This work was supported by the Swiss National Science Foundation (310030_132884/1 to S.W), a postdoctoral fellowship from the Deutsche Forschungsgemeinschaft (to T.S.), and a predoctoral fellowship from the Janggen-Pöhn Stiftung (to M.B.).

Author contributions:

T.S. performed experiments, analyzed data and wrote the manuscript together with S.W.

B.S., R.L.B., R. R., T.P., S.P., and M.B. performed experiments and analyzed data

D.G.A. provided technology for nanoparticle-based delivery of siRNA

V.K. led the development of Itgb1-specific siRNA for *in vivo* studies

R.F. provided *Itgb1* knockout mice

S.W., R.F., and V.K. initiated the study

S.W. designed the study and wrote the manuscript together with T.S.

All co-authors made important suggestions to the manuscript.

Conflict of interest: None of the authors has a conflict of interest

References

1 Michalopoulos, G. K. Liver regeneration. *J. Cell. Physiol.* **213**, 286-300 (2007).

2 Taub, R. Liver regeneration: from myth to mechanism. *Nat. Rev. Mol. Cell Biol.* **5**, 836-847 (2004).

3 Bohm, F., Kohler, U. A., Speicher, T. & Werner, S. Regulation of liver regeneration by growth factors and cytokines. *EMBO Mol. Med.* **2**, 294-305 (2010).

4 Hynes, R. O. Integrins: bidirectional, allosteric signaling machines. *Cell* **110**, 673-687 (2002).

5 Desgrosellier, J. S. & Cheresh, D. A. Integrins in cancer: biological implications and therapeutic opportunities. *Nat. Rev. Cancer* **10**, 9-22 (2010).

6 Brakebusch, C. & Fassler, R. beta 1 integrin function in vivo: adhesion, migration and more. *Cancer Metastasis Rev.* **24**, 403-411 (2005).

7 Xu, C., Yang, Y., Yang, J., Chen, X. & Wang, G. Analysis of the role of the integrin signaling pathway in hepatocytes during rat liver regeneration. *Cell Mol. Biol. Lett.* **17**, 274-288 (2012).

8 Apte, U. *et al.* Enhanced liver regeneration following changes induced by hepatocyte-specific genetic ablation of integrin-linked kinase. *Hepatology* **50**, 844-851 (2009).

9 Borowiak, M. *et al.* Met provides essential signals for liver regeneration. *Proc. Natl Acad. Sci.USA* **101** (2004).

10 Huh, C. G. *et al.* Hepatocyte growth factor/c-met signaling pathway is required for efficient liver regeneration and repair. *Proc. Natl Acad. Sci.USA* **101** (2004).

11 Natarajan, A., Wagner, B. & Sibilia, M. The EGF receptor is required for efficient liver regeneration. *Proc. Natl Acad. Sci.USA* **104** (2007).

12 Musacchio, T. & Torchilin, V. P. siRNA delivery: from basics to therapeutic applications. *Front. Biosci. (Landmark Ed)* **18**, 58-79 (2013).

13 Rettig, G. R. & Behlke, M. A. Progress toward in vivo use of siRNAs-II. *Mol. Ther.* **20**, 483-512 (2012).

14 Shim, M. S. & Kwon, Y. J. Efficient and targeted delivery of siRNA in vivo. *FEBS J.* **277**, 4814-4827 (2010).

15 Paranjpe, S. *et al.* Cell cycle effects resulting from inhibition of hepatocyte growth factor and its receptor c-Met in regenerating rat livers by RNA interference. *Hepatology* **45**, 1471-1477 (2007).

16 Paranjpe, S. *et al.* RNA interference against hepatic epidermal growth factor receptor has suppressive effects on liver regeneration in rats. *Am. J. Pathol.* **176**, 2669-2681 (2010).

17 Wuestefeld, T. *et al.* A Direct In Vivo RNAi Screen Identifies MKK4 as a Key Regulator of Liver Regeneration. *Cell* **153**, 389-401 (2013).

18 Zeigerer, A. *et al.* Rab5 is necessary for the biogenesis of the endolysosomal system in vivo. *Nature* **485**, 465-470 (2012).

19 Love, K. T. *et al.* Lipid-like materials for low-dose, in vivo gene silencing. *Proc. Natl Acad. Sci.USA* **107**, 1864-1869 (2010).

20 Querbes, W. *et al.* Treatment of erythropoietin deficiency in mice with systemically administered siRNA. *Blood* **120**, 1916-1922 (2012).

21 Brakebusch, C. *et al.* Skin and hair follicle integrity is crucially dependent on beta 1 integrin expression on keratinocytes. *EMBO J.* **19**, 3990-4003 (2000).

22 Kuhn, R., Schwenk, F., Aguet, M. & Rajewsky, K. Inducible gene targeting in mice. *Science* **269**, 1427-1429 (1995).

23 Brakebusch, C. *et al.* Beta1 integrin is not essential for hematopoiesis but is necessary for the T cell-dependent IgM antibody response. *Immunity* **16**, 465-477 (2002).

24 Potocnik, A. J., Brakebusch, C. & Fassler, R. Fetal and adult hematopoietic stem cells require beta1 integrin function for colonizing fetal liver, spleen, and bone marrow. *Immunity* **12**, 653-663 (2000).

25 Akinc, A. *et al.* Development of lipidoid-siRNA formulations for systemic delivery to the liver. *Mol. Ther.* **17**, 872-879 (2009).

26 Fassler, R. & Meyer, M. Consequences of lack of beta 1 integrin gene expression in mice. *Genes. Dev.* **9**, 1896-1908 (1995).

27 Kim, T. H., Mars, W. M., Stolz, D. B., Petersen, B. E. & Michalopoulos, G. K. Extracellular matrix remodeling at the early stages of liver regeneration in the rat. *Hepatology* **26**, 896-904 (1997).

28 Ivaska, J. & Heino, J. Cooperation between integrins and growth factor receptors in signaling and endocytosis. *Annu. Rev. Cell Dev. Biol.* **27**, 291-320 (2011).

29 Piwko-Czuchra, A. *et al.* Beta1 integrin-mediated adhesion signalling is essential for epidermal progenitor cell expansion. *PloS One* **4** (2009).

30 Streuli, C. H. & Akhtar, N. Signal co-operation between integrins and other receptor systems. *Biochem. J.* **418**, 491-506 (2009).

31 Moro, L. *et al.* Integrins induce activation of EGF receptor: role in MAP kinase induction and adhesion-dependent cell survival. *EMBO J.* **17**, 6622-6632 (1998).

32 Morello, V. *et al.* beta1 integrin controls EGFR signaling and tumorigenic properties of lung cancer cells. *Oncogene* **30**, 4087-4096 (2011).

33 Bauer, M. *et al.* Beta1 integrins differentially control extravasation of inflammatory cell subsets into the CNS during autoimmunity. *Proc. Natl Acad. Sci. USA* **106**, 1920-1925 (2009).

34 Bohm, F. *et al.* FGF receptors 1 and 2 control chemically induced injury and compound detoxification in regenerating livers of mice. *Gastroenterology* **139**, 1385-1396 (2010).

35 Beyer, T. A. *et al.* Impaired liver regeneration in Nrf2 knockout mice: role of ROS-mediated insulin/IGF-1 resistance. *EMBO J.* **27**, 212-223 (2008).

36 Latta, M., Kunstle, G., Leist, M. & Wendel, A. Metabolic depletion of ATP by fructose inversely controls CD95- and tumor necrosis factor receptor 1-mediated hepatic apoptosis. *J. Exp. Med.* **191**, 1975-1985 (2000).

37 Azimifar, S. B. *et al.* Induction of membrane circular dorsal ruffles requires co-signalling of integrin-ILK-complex and EGF receptor. *J. Cell Sci.* **125**, 435-448 (2012).

38 Chomczynski, P. & Sacchi, N. Single-step method of RNA isolation by acid guanidinium thiocyanate-phenol-chloroform extraction. *Anal. Biochem.* **162**, 156-159 (1987).

Figure legends

Fig. 1. Mx-Cre-mediated knockout of Itgb1 occurs predominantly in hepatocytes. Cre-mediated deletion of the *Itgb1* alleles, resulting in knockout of *Itgb1* and concomitant expression of β-galactosidase, was analyzed by lacZ staining on liver (A) and intestine (B) from poly-IC-treated *Itgb1$^{f/f}$/MxCre* mice (Itgb1 ko) and control littermates (ctrl). (C) *Itgb1* mRNA levels relative to *Gapdh* were analyzed by qRT-PCR using RNAs from liver, spleen and lung. N ≥ 3 per genotype. (D) Immunofluorescence staining for Itgb1 (red) was performed on liver sections from *Itgb1$^{f/f}$/MxCre* mice (Itgb1 ko) and control littermates (ctrl). (E,F) Co-staining for Itgb1 (red) and PECAM-1 (green) (E) or F4/80 (green) (F) of liver sections from poly-IC-treated Itgb1$^{f/f}$/MxCre and MxCre control mice. Nuclei were stained with Hoechst (blue). (N≥3) Representative pictures were chosen. Scale bars represent 100 µm (A-E) and 20 µm (F) . Bars in (D) represent SEM.

Fig. 2. Loss of Itgb1 in the liver reduces survival, enhances tissue damage, and impairs hepatocyte proliferation after PH. (A) Scheme of Poly-IC-induced knockout of *Itgb1*. (B) Survival index 48h after PH (N≥16 mice per), (C) liver-to-body-weight ratio, (D) AST, and ALT activities, bilirubin, and albumin levels in the serum 48h after PH of control (white bars) and Itgb1$^{f/f}$/MxCre mice (black bars) (N≥8 per genotype). (E) Representative pictures of liver tissue and quantification of necrotic area (N≥10 per genotype), (F) immunostaining for neutrophils and quantification (N≥3), positive cells are indicated by arrows, (G) TUNEL staining of apoptotic cells and quantification (N≥7), positive nuclei are indicated by arrows, and (H) BrdU immunostaining and quantification (N≥5), positive nuclei are indicated by arrows, 48h after PH of poly-IC-treated control (white bars) and Itgb1$^{f/f}$/MxCre mice (black

bars). Scale bars in (E-H) represent 100 μm. Bars in (B-H) represent mean ± SEM. *P ≤0.05, **P ≤0.01, and ***P ≤0.001 (Mann-Whitney U-test).

Fig. 3. siRNA-mediated knock-down of *Itgb1* phenocopies *Itgb1* knockout

(A) Scheme of siRNA-mediated *Itgb1* knock-down and the following PH experiment. Mice were treated twice with siRNA against luciferase (*Luc*) or Itgb1 (*Itgb1*) with a time interval of 5 days. After additional 5 days animals were used for experiments. (B) Verification of siRNA-mediated knock-down of *Itgb1* mRNA in the liver by qRT-PCR (normalized to *Gapdh*) 5 days after the second siRNA injection (N≥8 per treatment group). (C) Immunoblotting of Itgb1 and asialoglycoprotein receptor (ASGPR2) as loading control using total liver homogenates or lysates from isolated primary hepatocytes after siRNA-mediated knock-down *in vivo*. (D) Immunostaining for Itgb1 (red) and DAPI nuclear counterstain (blue) on cryosections of tissue removed during PH and 48h after PH. (E) Survival index (N≥12) 48 after PH and (F) liver-to-body-weight ratio (N≥12) 48h after PH. (G) Necrosis (N≥12), (H) neutrophils (N≥5), positive cells are indicated by arrows and (I) BrdU-positive cells, (N≥11) 48h after PH, positive nuclei are indicated by arrows. Scale bars in (D-I) represent 100 μm. Bars in (B) and (E-I) represent mean ± SEM. **P ≤0.01, and ***P ≤0.001 (Mann-Whitney U-test).

Fig. 4. Effect of siRNA-mediated *Itgb1* knock-down 6h and 5d after PH

(A) Verification of siRNA-mediated knock-down of *Itgb1* mRNA by qRT-PCR (normalized to *Gapdh*) (N≥5 per treatment group and time point) and (B) immunostaining for Itgb1 (red) and DAPI nuclear counterstain (blue) on cryosections of tissue removed 5d after PH. (C) Necrotic area 6h and 5d after PH (N≥5 per genotype and time point), (D) BrdU-positive cells 5d after PH (N≥5), and (E) liver-to-body-weight ratio of *Luc* and *Itgb1* siRNA treated animals

6h and 5d after PH (N≥5). Scale bars in (B) represent 100 μm. Bars in (A) and (C-E) represent mean ± SEM. *$P \leq 0.05$, and **$P \leq 0.01$ (Mann-Whitney U-test).

Fig. 5. Loss of Itgb1 affects phosphorylation of c-Met and EGFR during liver regeneration

(A) Immunoblotting of Itgb1, phosphorylated and total c-Met, EGFR, and FAK and of GAPDH (loading control) using homogenates from livers of three poly-IC-treated control and Itgb1$^{f/f}$/MxCre mice removed during surgery (0h) and 48h after PH. Densitometric analysis was performed for phosphorylated EGFR and c-Met. (B) Immunoblotting of Itgb1, phosphorylated and total EGFR and GAPDH using homogenates from livers of three *Luc* or *Itgb1* siRNA pre-treated animals removed during PH (0h) and after 48h. Densitometric analysis was performed for phosphorylated EGFR. Bars represent mean ± SEM.

Fig. 6. Itgb1 controls growth factor receptor activation in hepatocytes *in vitro* and *in vivo*

Liver lysates from poly-IC-injected control and Itgb1$^{f/f}$/MxCre mice (A) and from knock-down mice (B) 15min after i.p. injection of EGF or vehicle were analyzed by immunoblotting for Itgb1, phosphorylated and total EGFR and GAPDH (loading control). Densitometric analysis was performed for phosphorylated EGFR. C) Itgb1 knock-down in primary hepatocytes prepared from *Luc* or *Itgb1* siRNA pre-treated mice was confirmed by immunostaining for Itgb1 (red). Nuclei were countersained with DAPI (blue). (D,E) Primary hepatocytes were incubated for 15min with EGF (D) or for the indicated periods with HGF (E). Lysates were used for immunoblotting of Itgb1, phosphorylated and total EGFR, c-Met, Erk, Akt and as loading control for GAPDH. Densitometric analysis was performed for phosphorylated EGFR and c-Met. (F) EGFR internalization upon stimulation with EGF was monitored by FACS

analysis in primary hepatocytes from *Luc* or *Itgb1* siRNA pre-treated mice (N≥3 per treatment group and time point). Bars in (A) and (B) represent mean ± SEM.

Speicher et al.
Fig. 1

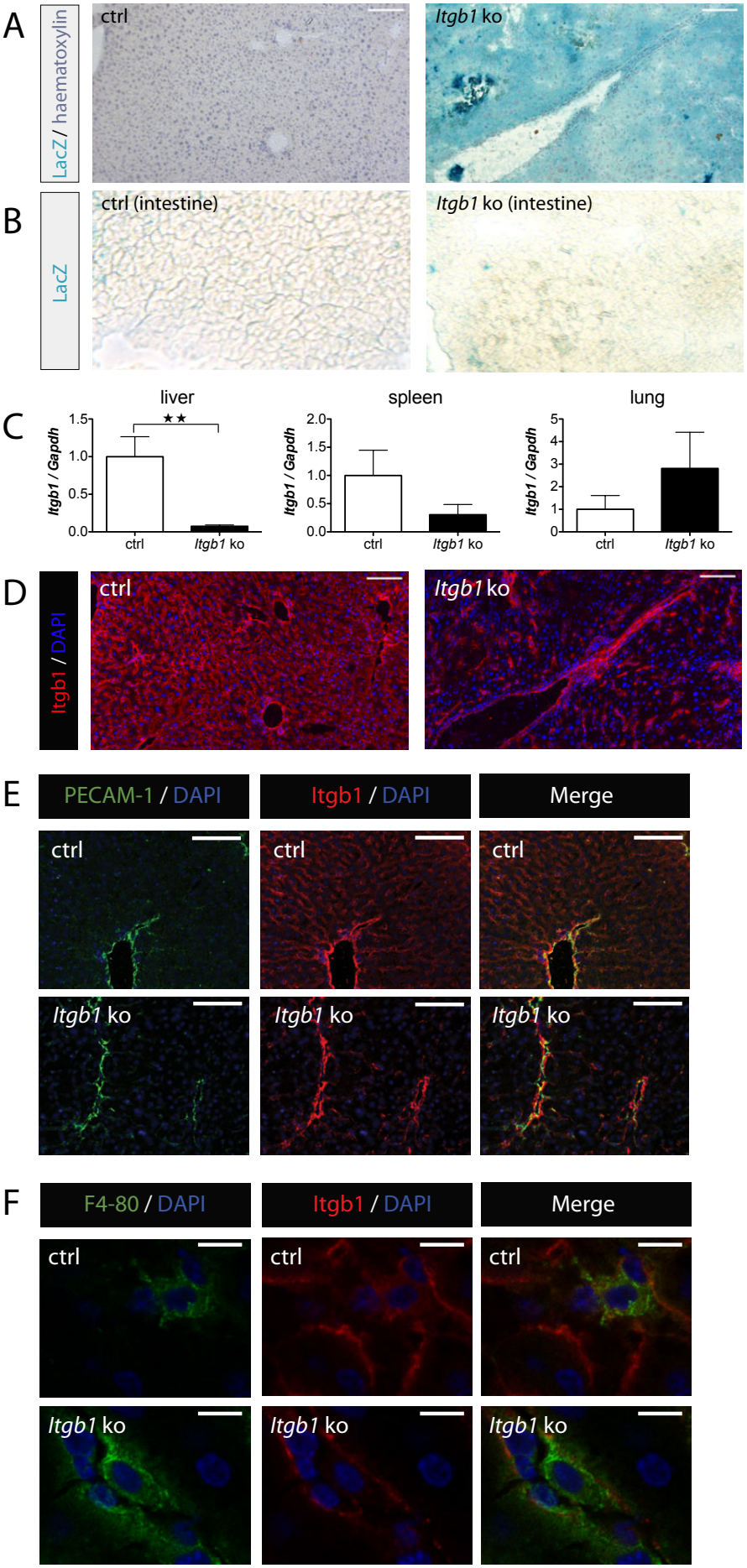

Speicher et al.
Fig. 2

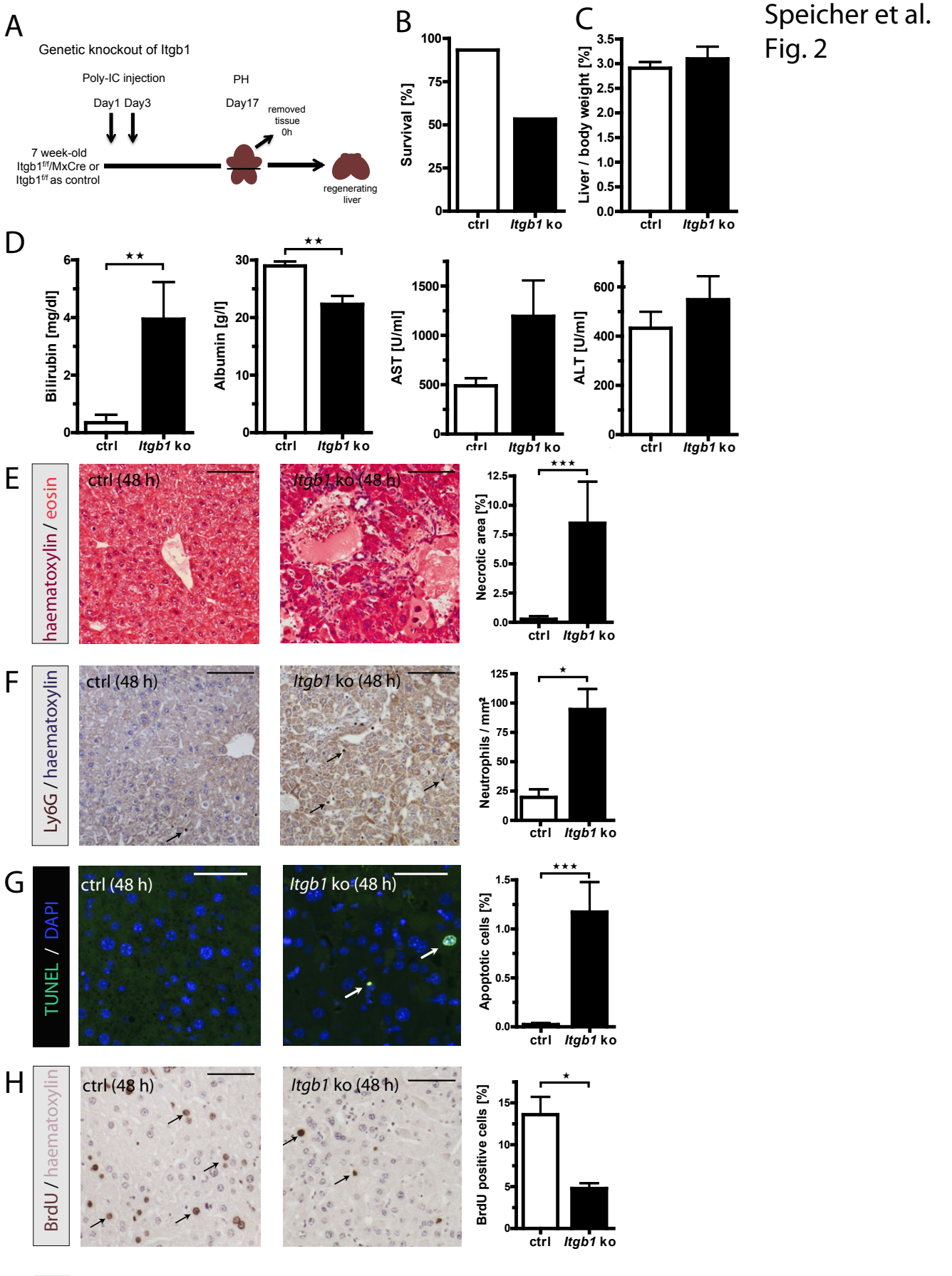

Speicher et al.
Fig. 3

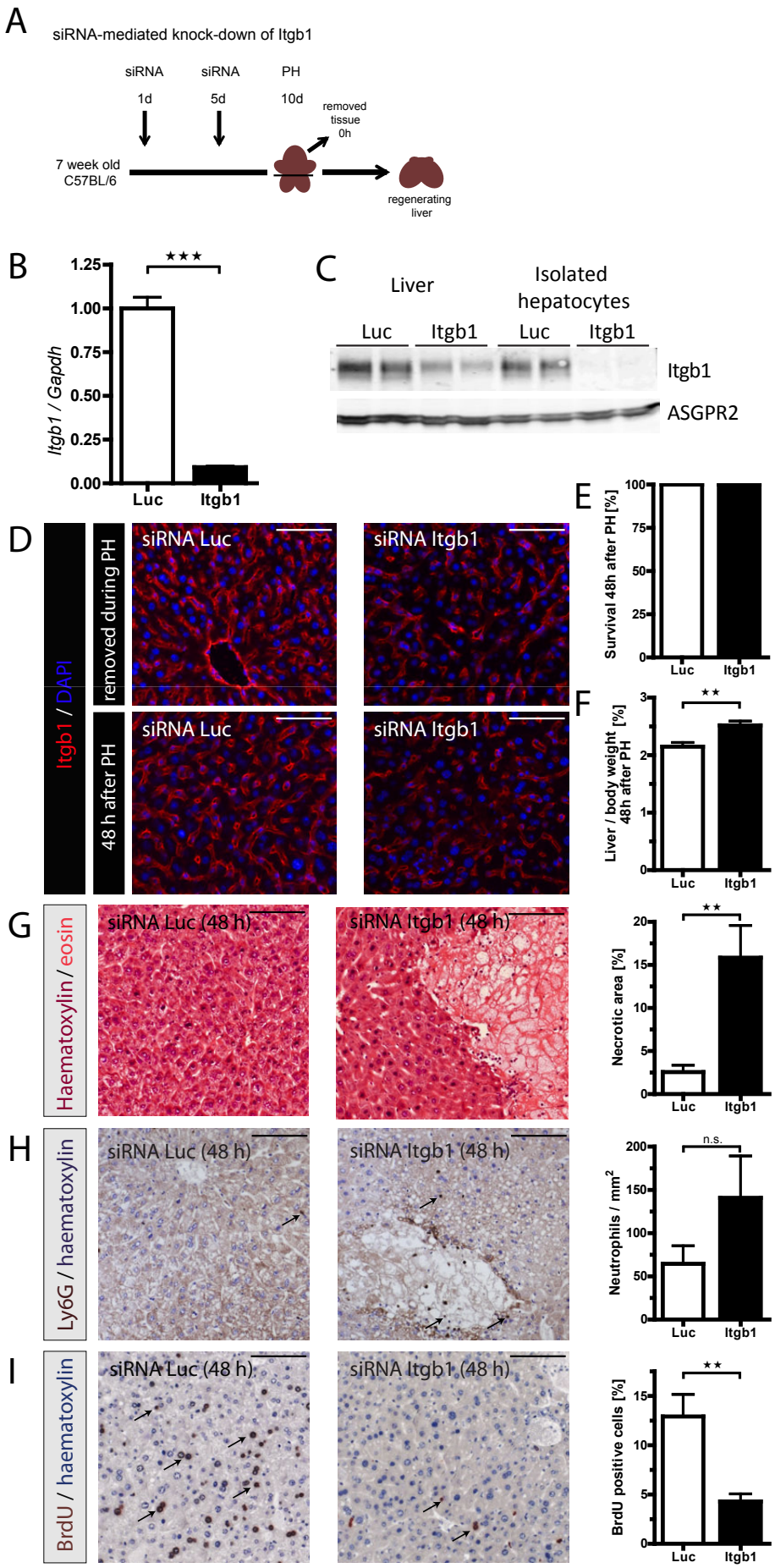

Speicher et al.
Fig. 4

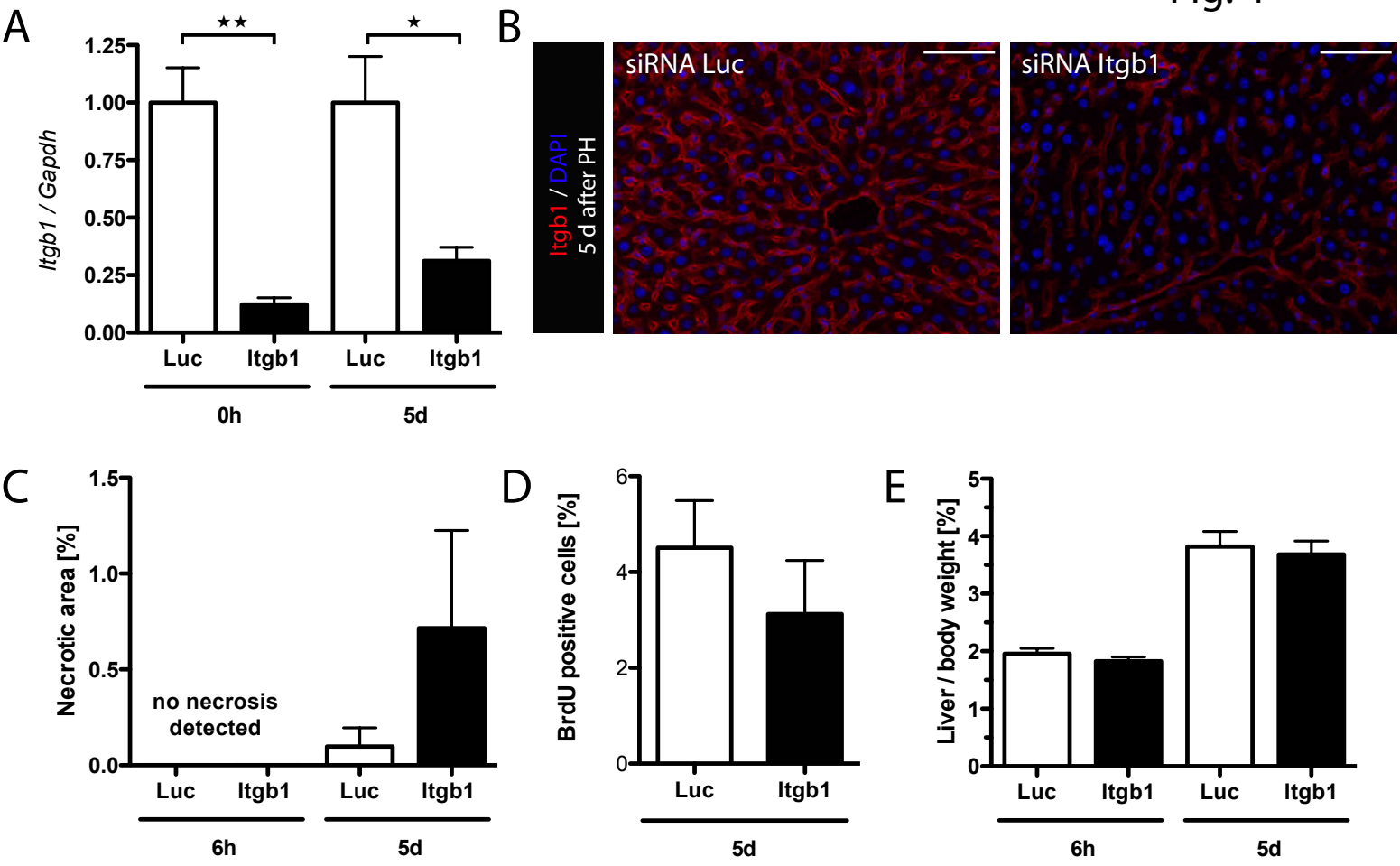

Speicher et al.
Fig. 5

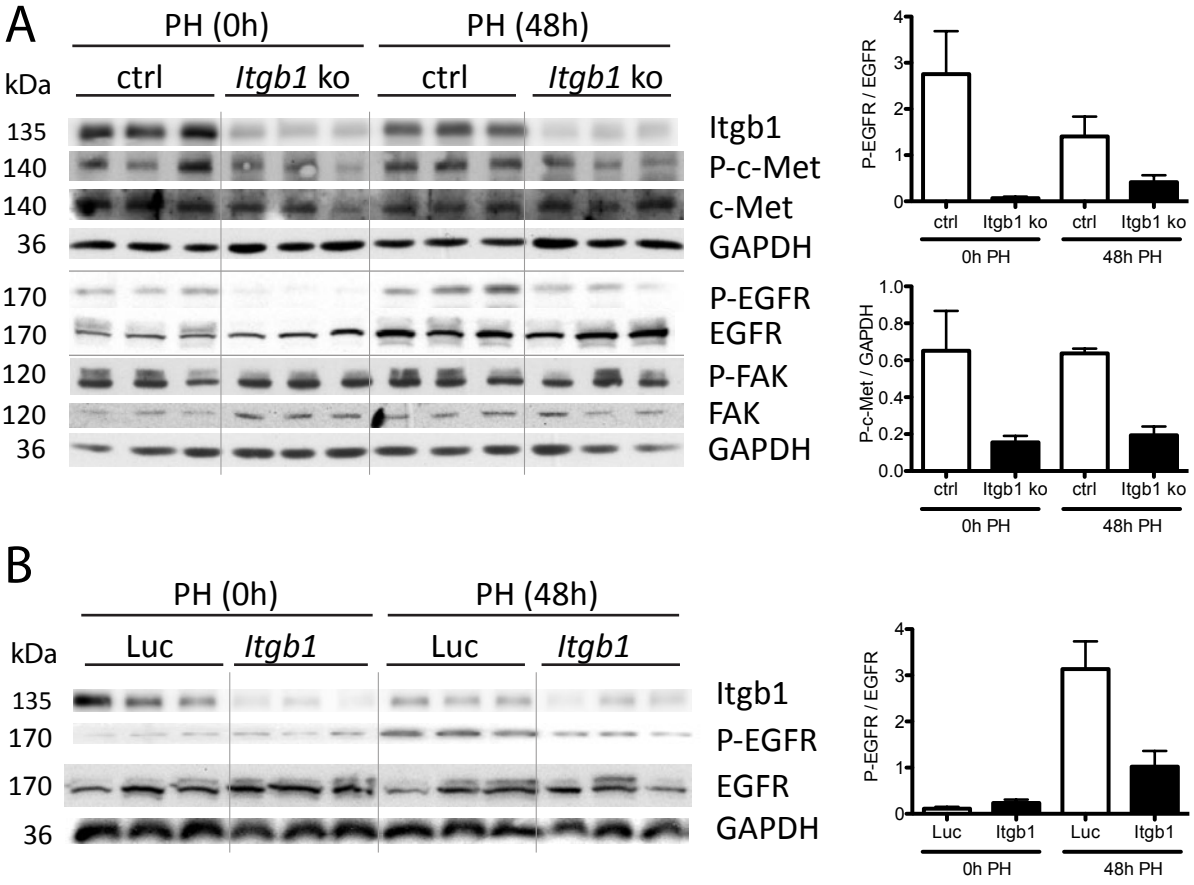

Speicher et al.
Fig. 6

A

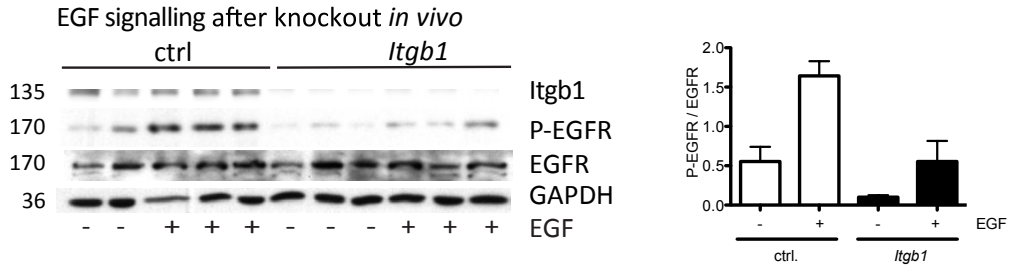

B

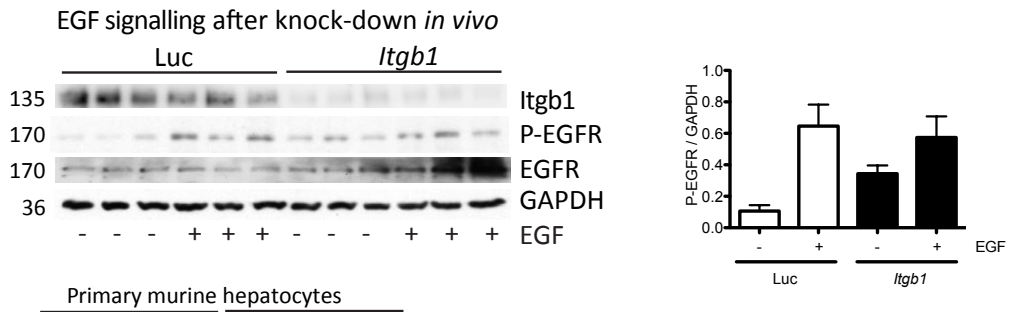

C

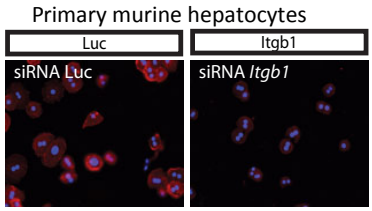

D

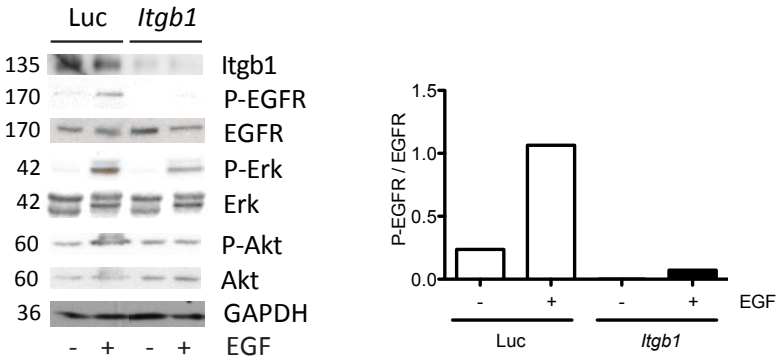

E

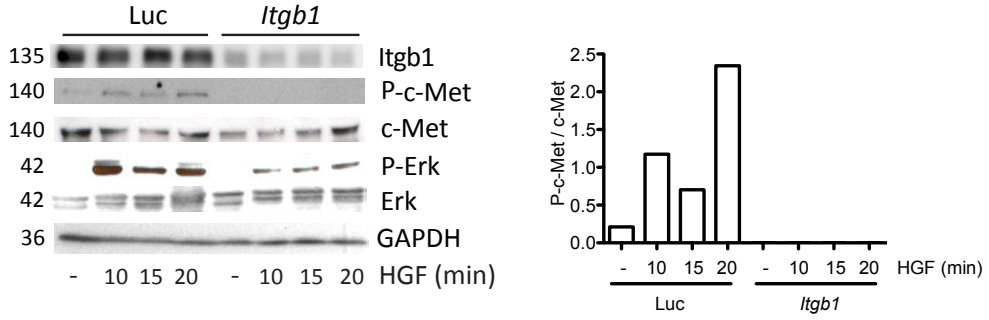

F